BALTEX

Baltic Sea Experiment

World Climate Research Programme / Global Energy and Water Cycle Experiment
WCRP GEWEX

Third Study Conference on BALTEX

Assembly Hall of the Ålands Parliament Building
Mariehamn, Åland, Finland

2-6 July 2001

Conference Proceedings

Editor: Jens Meywerk

Jointly organized by
Finnish Meteorological Institute
and GKSS Research Centre

International BALTEX Secretariat
Publication No. 20
July 2001

International BALTEX Secretariat
GKSS Research Center
Max Planck Straße
D-21502 Geesthacht
Germany
Phone: +49 4152 87 1536
Fax: +49 4152 87 2020
e-mail: baltex@gkss.de

Third Study Conference on BALTEX

Assembly Hall of the Ålands Parliament Building
Mariehamn, Åland, Finland

2-6 July 2001

Conference Proceedings

Editor: Jens Meywerk

Jointly organized by
Finnish Meteorological Institute
and GKSS Research Centre

Sponsors of the Conference are:

European Commission through their 5th Framework Programme, Contract No. EVK2-CT-2001-60003

Finnish Institute of Marine Research

Finnish Meteorological Institute

FINNISH METEOROLOGICAL INSTITUTE

Gesellschaft zur Förderung des GKSS Forschungszentrums e.V.

GKSS Research Centre

GKSS FORSCHUNGSZENTRUM

Max-Planck Institute for Meteorology

Max Planck Institute for Meteorology

Table of Abstracts

Author Index

Radar profiles of rain rate, reflectivity and fall speed of precipitation particles

Tage Andersson, Gerhard Peters and Bernd Fischer

Meteorologisches Institut, Universität Hamburg, Bundesstr. 55, 20146 Hamburg, Germany

1. Introduction

The MRR2 is a low cost 24 GHz FM-CW-Doppler radar rain profiler, *Klugmann et al., 1995, Löffler-Mang et al., 1999.* It measures the fall velocities of the precipitation particles and deduces the rain rate from their fall velocity spectra. From these measurements rain rates, liquid water contents and drop size spectra can be derived. One apparent problem then is that during parts of the year in temperate climates and in the free atmosphere the precipitation appears in the solid phase (ice crystals, snow flakes, graupel or hail). Other difficulties are the attenuation in precipitation, which is large in this frequency band, and the vertical velocity of the ambient air, which affects the fall speed of the drops. The MRR2 also measures the intensity of the return signal.

For radar analysis and forecasting of precipitation the vertical reflectivity profile of the lower atmosphere (generally the ordinary weather radar beam is above due to the topography and the curvature of the earth) is very important, see for instance *Löffler-Mang et al., 1999*, and the MRR2 produces just such profiles.

The usefulness of this type of instruments is also exploited in other applications. It is a precipitation sensor candidate for present weather sensors. It is used as a precipitation indicator by customers as different as the Häkkinen Formula 1 Racing Team and the Onsala Space Observatory, *Gradinarsky et al., 1999.*

2. The radar signature of the Bright Band

According to our experience the Bright Band, BB, is a common feature in temperate climates when the 0° C isotherm is above the ground. Since the BB and the vertical reflectivity profile have a large impact upon the radar mapping and forecasting of precipitation we will discuss its radar signature. Traditionally, the BB is depicted in vertical reflectivity profiles as a pronounced maximum or 'nose', and so it appears also on the MRR2, Fig. 1. However, it is more evident on the MRR2 rain rate profile, where it also occurs somewhat higher.

Fig. 2 shows fall velocity spectra above, in and below a BB. Above the BB the dominant peak is at about 2 m/s, the fall speed of the ice crystals/snow flakes. Their spectra are fairly narrow, as also other researchers have found, see for instance *Gossard et al, 1990,* and *Duvernoy et al, 1996.* In this region there is also a broad maximum, centered at about 6 m/s. Such a bimodal spectrum appears often, though not always, above the BB. Descending through the BB the ice crystal peak is displaced toward higher velocities and together with the 6 m/s peak forms a broad spectrum. Below the BB there is a fairly broad raindrop spectrum with the peak at about 7 m/s.

3. The vertical velocity of the ambient air

Since the vertical movement of the air affects the fall velocities of the rain drops, the rain rate retrieval, based on fall velocities in quiet air, becomes erroneous. The vertical wind error is probably the most serious limitation of this

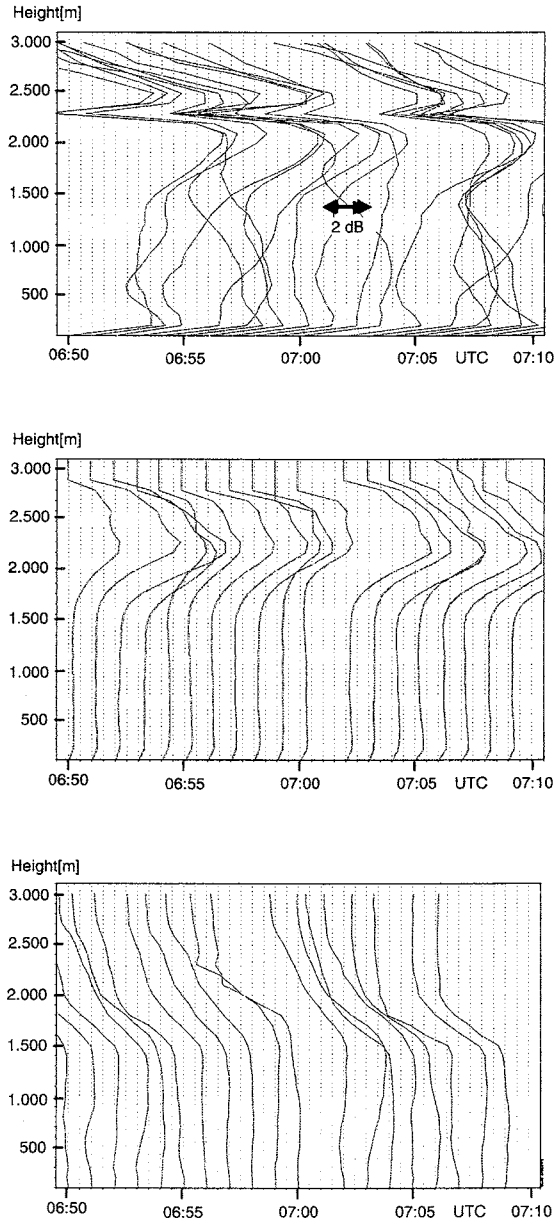

Figure 1: Vertical time cross sections of reflectivity (uppermost Fig.), rain rate (middle Fig.) and fall speed of the precipitation particles (lowest Fig.). The Figures show how the BB appears in these 3 parameters. In the reflectivity image there is an artefact at 2300 m height. A later version of the instrument has eliminated this artefact. Christiansö, 7 Nov. 1999, 06:50-07:10 UTC.

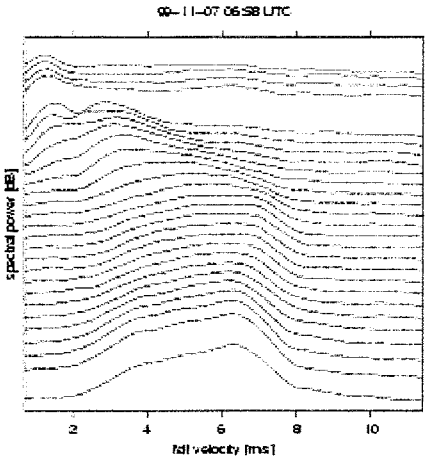

Figure 2: Radar reflectivity spectra for Christiansö, 7 Nov. 1999, 06:58 UTC. The spectra are stacked in range, that is height, above the radar antenna. Vertical scale is the reflectivity factor in dB. The range spacing is 100 m. The BB occupies mainly the interval 1800-2200 m. Three range gates, 2400-2600 m, are omitted due to an artefact at these levels, which appears in Fig. 1.

technique. So far correction schemes as suggested for example by *Probert-Jones et al. 1962, Hauser et al.1984, Klaasen 1988* have not been applied, because their efficiency is difficult to assess in our application. For small deviations from zero ($|w| < 0.5$ m/s) the retrieval error is about $\frac{\Delta R}{R}(w) \approx 1\%/(1\text{ cm/s})$ (*Richter, 1993*). The error is not linear with respect to the vertical wind, with the consequence of some mean bias also for $\overline{w} = 0$. We estimate that the w-induced standard deviation is less than 20% in stratiform rain, which can be inferred from comparison of rainrates, derived from radar reflectivity (not affected by vertical wind) and from Doppler spectra, Fig. 3.

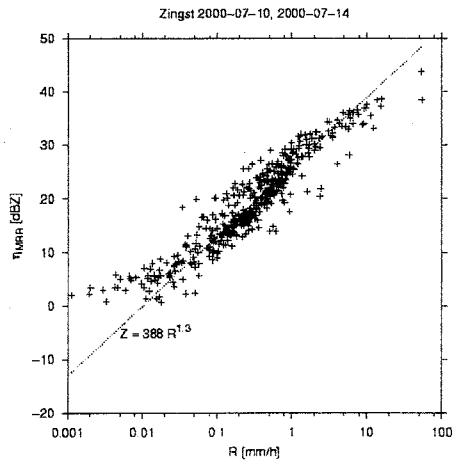

Figure 3: Rain rates computed with the ordinary Z-R relation versus the method used by the MRR2.

4. An attenuation experiment

Since the rain attenuation is severe in this frequency band and since the available literature data is fairly old, a special experiment was performed to get empirical attenuation data. Two MRR2 were mounted horizontally, one on the roof of the building of the Umweltbundesamt in Zingst (10 m above the ground) and one on the roof of the Meteorological Institute in Hamburg (60 m above the ground). Assuming that the longterm precipitation rate is constant over the measuring range (about 1 km) and applying the geometrical range correction, the scattering cross section should be constant with range, if there was no rain attenuation. Longterm measurements showed an attenuation that was appreciable, Fig. 4., a factor of about 10 larger than the attenuation given in the literature,

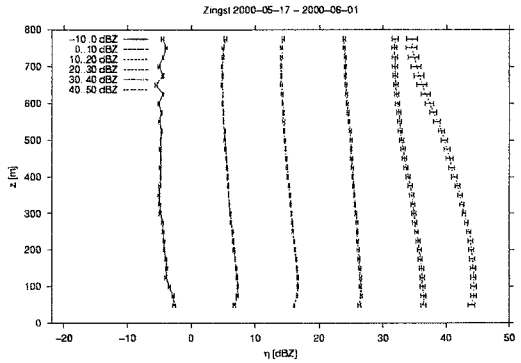

Figure 4: Relectivity against range from a horizontally mounted MRR2 antenna.

References

Duvernoy, J. and J.L. Gaumet, Precipitating Hydrometeor Characterization by a CW Doppler Radar. *J. Atmosph. Ocean. Techn.*, Vol. 13, 620-629, 1996.

Gossard, E.E., R.G. Strauch and R.R. Rogers, Evaluation of Dropsize Distributions in Liquid Precipitation Observed by Ground-Based Doppler Radar. *J. Atmosph. Ocean. Techn.*, Vol. 7, 815-828, 1990.

Gradinarsky, L., G. Elgered and Y. Xuie, Using a micro-rain radar to assess the editing of ground-based microwave radiometer data. *Microwave Radiometry and Remote Sensing of the Earth's Surface and Atmosphere. Proc. of the 6-th Specialist Meeting on Microwave Radiometry and Remote Sensing of the Environment,* Eds P. Pampalini and S. Paloscia, pp. 183-191, 16-18 March 1999, Firenze, Italy.

Hauser, D., and P. Amayenc, Raindrop-size distributions and vertical air motions as inferred from zenith pointing Doppler radar with the RONSARD system. *Radio Sci.*, Vol. 19, 185-192, 1984.

Klaasen, W., Radar observations and simulation of the melting layer of precipitation. *J. Atmos. Sci.*, Vol. 45, 3741-3753, 1988.

Klugmann, D., K. Heinsohn and H.-J. Kirtzel, A Low Cost 24 GHz FM-CW-Doppler Radar Rain Profiler. *Contributions to Atmos. Physics,* Vol. 69, 247-253, 1996.

Löffler-Mang, M. and M. Kunz, On the Performance of a Low-Cost K-Band Doppler Radar for Quantitative Rain Measurements. *J. Atmos. Ocean. Techn.*, Vol. 16, 379-387, 1999.

Probert-Jones, J. and W. Harper, Vertical air motion in showers as revealed by Doppler radar. *9th Weather Radar Conf.*, Amer. Meteor. Soc., 225-232, 1962.

Richter, C., Niederschlagsmessungen mit dem vertikal ausgerichteten FM-CW-Dopplerradar-RASS-System, Validierung und Anwendung, *Dissertation Universität Hamburg*, 143 pp., 1993.

Reanalysis of BRIDGE. An estimation of the water and heat budgets over the Baltic Sea drainage basin through variational data assimilation

Ulf Andræ[1], Carl Fortelius[2]

[1] SMHI, SE-601 76 Norrköping, Sweden.
[2] FMI, P.O.Box 503, FIN-00101 Helsinki, Finland.

1. Introduction

The main purpose of BALTEX is to calculate the water and heat budgets of the Baltic Sea. Several groups have presented model and measured estimates, however a system that fully takes advantage of the observations and models available has not yet been presented. The HIRLAM-BALTEX data assimilation project uses a special version of the HIRLAM system that is specially designed for quantifying the water and energy budgets of the area relevant to BALTEX. Data assimilation has been used for decades to provide initial states for numerical weather prediction. A more recent application is in climate research, where data assimilation is used to provide archives of the physical history of the climate system, consisting of the atmosphere, oceans and land surface (e.g. *Kalnay et al.*, 1996).

The HIRLAM-BALTEX data assimilation is organized by the meteorological services of Finland and Sweden. The project has its own web site, http:\\hirlam.fmi.fi/bridge, which is linked to the site of the BALTEX project. This site describes the assimilation system, the data archive and progress of the work. We will present a reanalysis of one year of the BRIDGE period (October 1999 – October 2000) with special emphasis on the quality of the reanalysis and the components crucial for the water and heat budgets.

2. BRIDGE assimilation system

The atmospheric forecast model is a hydrostatic two time level, semi-lagrangian, semi-implicit limited area grid point model (*Källen*, 1996). Prognostic variables are surface pressure, horizontal wind, temperature, specific humidity, specific cloud condensate and turbulent kinetic energy (TKE). Model components directly related to the water and energy balance have received special attention in the configuration used for the BALTEX assimilations. The parameterization of large scale condensation is based on *Rasch & Kristjansson* (1998) and the convection of *Kain & Fritsch* (1998). The convective part uses TKE as a closure for shallow convection and is closely connected to the turbulence scheme which is based on the TKE as a prognostic variable (*Cuxart et al.*,2000). Radiation is treated according to *Savijärvi* (1989). At the surface each grid box consists of a certain fraction of land, sea or ice. The land points are further divided in forest and open land. Fluxes of heat and momentum at the surface are computed for each surface type, and averaged over each grid box. The evaporation from land surfaces includes transpiration from the vegetation, evaporation of water intercepted on the canopy, and evaporation from bare ground soil. Parameterization of soil moisture and runoff is based on soil moisture variability functions traditionally used in hydrological models (*Bergström*, 1998).

At the lateral boundaries the model is forced with ECMWF operational analyses updated every three hours. The frequency of the boundary update is important for reproducing the semi-diurnal tidal motions in the atmosphere.

The assimilated observations comes from the archives of the ECMWF. During the BRIDGE period SMHI and FMI have also reported climate SYNOP stations and thereby strenghend the observation amount.

The analysis of atmospheric variables is based on a variational formulation (3DVAR). It minimizes a cost function measuring the distance between the model state and a background field and the model state and the observations respectively (*Gustafsson et al.*,2001, *Lindskog et al.*, 2001). The time evolution of the analyzed atmospheric state is filtered with respect to gravity waves using a diabatic digital filter to get a balanced initial field for the prognostic model. The analysis of surface variables includes assimilation of snow and sea surface temperature (SST) observations. The SST and ice evolution in the Baltic Sea is described with a coupled ice-ocean model (*Gustafsson et al.*, 1998). The model SST is adjusted through a nudging process with observations from the SMHI marine service twice a week. The numerous inland lakes in Scandinavia are described with slab and 1-D lake model (*Ljungemyr*, 1996). The lake model as well as the Baltic Sea model are forced with atmospheric data from the forecast model, and are coupled back through the updated temperature and ice fields. The assimilation cycle is 6 h and at every cycle a 30 h forecast is run.

3. Budget components

The BALTEX BRIDGE data assimilation archive describes the physical evolution of the climate system as analyzed and predicted by HIRLAM. Snapshots of atmospheric motion, temperature, specific humidity, specific cloud condensate, turbulent kinetic energy, diagnostic cloud cover, and surface pressure are available every six hours on the grid of the forecast model. The sea surface is described by the sea surface temperature, ice cover, and roughness, while the snowpack, soil temperature and soil water content are available over land. In addition physiographical data on orography, distribution of land and sea etc. are available, as are diagnostic variables like temperature and moisture at screen level, wind at 10 metres above ground, and cloud cover.

The snapshots are augmented with the cumulative effects of parameterized physical processes. These include two-dimensional fields of radiative fluxes at the top of the atmosphere and at the surface, surface fluxes of sensible heat, latent heat, and momentum, as well as precipitation, evaporation, and local runoff. In addition, three-dimensional distributions of the flux of precipitating water, the local cumulative tendencies of temperature, humidity, and cloud condensate due to turbulence alone and to all parameterized processes together, and the temperature tendency by radiation, are stored on a sub set of the model grid, covering the catchment basin of the Baltic Sea. Other processes of interest, such as the net condensation of water vapour or the convective fluxes of sensible and latent heat can be studied by forming linear combinations of the stored fields. Like the snapshots, the cumulative fields have a temporal resolution of six hours,

but a selection of two-dimensional fields is available every hour.

4. Preliminary Result

The first impression of the performance of the system is given in the verification of analyses and forecasts against observations in Figure 1. The system has a slightly positive bias in low level wind and temperature and negative bias in the cloud cover and the low level relative humidity. Examples of monthly budgets for September and October 1999 are given in Table 1 and 2. The budgets are accumulated from consecutive 6 to 12 hour forecasts. The net precipitation (P-E) is positive over the drainage basing during the two months, but negative over the sea. This means that there is a net inflow of water in the atmosphere over the Baltic area. In October the Baltic Sea is a considerable heat source through the latent heat flux with a net loss of 117 W/m^2. A budget over the whole BRIDGE period including river runoff will allow us to close the water cycle during a year.

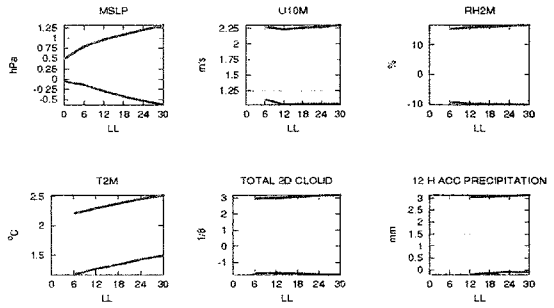

Figure 1: Verification of SYNOP observations over Europe during September and October 1999. Shown are RMS and bias against forecast length in hours.

Table 1: The mean water balance for the atmosphere over the Baltic Sea catchment area in mm/month. The flows are denoted by: Precipitation (**P**), Evaporation (**E**), Atmospheric convergence (**C**), Atmospheric change (**dQ**). Negative values means a sink in the atmosphere.

	P	E	C	dQ
			199909	
Land	-42.9	30.2	6.4	-6.2
Sea	-37.4	68.9	-30.2	1.2
All	-41.6	38.9	-1.8	-4.5
			199910	
Land	-70.0	14.5	48.3	-7.2
Sea	-72.4	102.2	-34.6	-4.7
All	-70.5	34.2	29.6	-6.6

Table 2: The mean heat balance at the surface over the Baltic Sea catchment area in W/m^2. The flows are denoted by: Net short wave radiation (**SW**), Net long wave radiation (**LW**), Sensible heat flux (**S**), Latent heat flux (**L**), Net loss/gain of heat at surface (**dH**). Negative values means flux from surface.

	SW	LW	S	L	dH
			199909		
Land	120.0	-61.2	-22.6	-29.2	7.1
Sea	139.0	-65.8	-4.4	-66.4	2.3
All	124.3	-62.2	-18.5	-37.6	6.0
			199910		
Land	53.3	-47.3	1.2	-13.5	6.3
Sea	63.2	-63.0	-21.9	-95.5	-117.1
All	55.5	-50.8	-4.0	-32.0	-31.2

References

Bergström, S., P. Graham, On the scale problem in hydrological modeling., *J. Hydrol.*, 211, 253-265, 1998

Cuxart, J., P. Bougeault, J. L. Redelsperger, A turbulence scheme allowing for mesoscale and large-eddy simulations., *Q.J.R. Meteor. Soc.*, 126,562,1-30, 2001

Gustafsson, N., L. Berre, S. Hörnqvist, X.-Y. Huang, M. Lindskog, B.Navascue, K. S. Mogensen, S. Thorsteinsson, Three-dimensional variational data assimilation for a limited area model. Part I: General formulation and the background error constraint., *Tellus*, in press, 2001

Gustafsson, N., L. Nyberg, A. Omstedt, Coupling of a high-resolution atmospheric model and an ocean model for the Baltic Sea., *Mon. Wea.. Rev.*, 126,11,2822-2846, 1998

Kain, J. S., M. J. Fritsch, Multiscale convective overturning in mesoscale convective systems: Reconciling observations, simulations and theory., *Mon. Wea. Rev.*, 126,8, 2254-2273, 1998

Kalnay, E., M. Kanamitsu, R. Kistler, W. Collins, D. Deaven, L. Gandin, M. Iredell, S. Saha, G. White, J. Woollen, Y. Zhu, M. Chelliah,W. Ebisuzaki, W. Higgins, J. Janowiak, K.C. Mo,C. Ropelewski, J. Wang, A. Leetmaa, R. Reynolds, R. Jenne, D. Joseph, The NCEP/NCAR 40-year reanalysis project. *Bull. Amer. Meteor. Soc.*, 77, 437-471, 1996

Källen, E, 1996: HIRLAM documentation manual. System 2.5, Technical report, HIRLAM project

Lindskog, M., N. Gustafsson, K. S. Mogensen, X.-Y. Huang, X. Yang, U. Andræ, L. Berre, S. Thorsteinsson, J. Rantakokko, Three-dimensional variational data assimilation for a limited area model. Part II: Observation handling and assimilation experiments., *Tellus*, in press, 2001

Ljungemyr, P., N. Gustafsson, A. Omstedt, Parameterization of Lake thermodynamics in a high resolution weather-forecasting model., *Tellus*, 48A, 608-621, 1996

Rasch, P. J., J. E. Kristjansson, A comparison of the CCM3 Model climate using diagnosed and predicted condensate parameterizations., *J.Climate*, 11,7,1587-1614, 1998

Savijärvi, H., Fast radiation parameterization schemes for mesoscale3 an short-range forecast models., *J. Appl. Meteor*, 29, 437-447, 1989

Mean circulation, exchange, retention and renewal time of water masses in the Gulf of Finland.

Oleg Andrejev, [1] Kai Myrberg,[1,2] Pekka Alenius,[1] and Peter A. Lundberg[2]

[1] Finnish Institute of Marine Research, P.O.Box 33, FIN-00931, Helsinki, Finland, Tel: +358 9 613 941, Fax: +358 9 613 94 494, email:Andrejev@fimr.fi

[2] Department of Meteorology, University of Stockholm, S-10691, Stockholm, Sweden

Abstract

A three-dimensional baroclinic prognostic model has been is applied to study the mean circulation, water exchange and retention and renewal time of water masses in the Gulf of Finland.

A five-year simulation for 1987-1992 was carried out using a nested grid approach, where a high-resolution sub-model of the Gulf of Finland was forced by a large-scale Baltic Sea model at the open boundary. Realistic meteorological forcing for the period under study was used.

Even if the mean circulation is a statistic artefact, which does not reflect a true physical situation, it can be used to estimate e.g. the average distribution of pollutants or nutrients released from point sources. Practical activities, like shipping and coastal construction, need information concerning the mean circulation and persistency. Refined estimates are needed in order to study the water balance of the gulf in detail. Calculation of the retention time of water masses is based on using an advection-diffusion equation. The overall dynamics of the system serves as the source term which adds the "age" to water parcels present in the modelled area.. The retention time thus provides a possibility to understand over which time-scales the pollutants are gradually mixed with the Baltic Sea water. The retention time is a non-homogeneous and non -stationary quantity due to the variability of currents and stratification, and cannot be described by a simple measure. Hence retention time may be regarded as a more subtle distinguishing trait, which should be employed when evaluating the spatial variability of the water "age" and the related state of the marine environment.

The mean surface circulation of the gulf was found to take place in the form of a strong outflow adjacent to the Finnish coast compensated by an inflow at the Estonian coast, a circulation which is highly dependent on depth. The water exchange between the gulf and the Baltic proper appears to be stronger than previously estimated. The retention time ("age") of the water masses in the gulf is strongly dependent on space and time; the largest values of this quantity found in the eastern part of the central gulf were around 2 years, whereas very short retention times proved to characterise the inflow and river mouths regions. The complete renewal of the gulf water masses was found to take about 5 years, which implies that the improvement of the ecological state of the gulf is a relatively slow process; even in case of a drastic decrease of the antropogenic loading the state can be expected to improve, only after the entire water mass has been renewed. Additionally, the possible reductions should be focused on the areas characterised by the longest retention times, since the accumulation of settled particles most likely takes place there.

Verification of HIRLAM marine wind forecasts in the Baltic

Ivar Ansper[1], Carl Fortelius[2]

[1] EMHI, 10143 Rävala 8, Tallinn, Estonia; e-mail: Ivar.Ansper@solo.ee
[2] FMI, P.O.Box 503, FIN-00101, Helsinki, Finland; e-mail: carl.fortelius@fmi.fi

1. Introduction

This study deals with verification of marine surface wind forecasts being based on a numerical weather prediction system. Such forecasts are used directly by the shipping in the Baltic Sea and serve as an input to wave models. The winds near the surface are also needed for calculating the surface fluxes of heat and momentum in the model.

2. Model

Model data were extracted from operational forecasts by the HIRLAM version 4.6.2, run at FMI with a horizontal resolution of 0.2 degrees and 31 levels. The surface layer parameterization was based on Monin-Obukhov theory of similarity which assumed that the fluxes of momentum and heat were nearly constant with height in the surface layer. A prognostic equation for the turbulent kinetic energy was used together with conservative variables for the non-precipitating processes (Cuxart et. al., 2000).
Over the open sea the roughness length depends on wind speed, over land and ice roughness is constant in time. Profiles of wind speed as well as temperature and humidity are computed in the surface layer diagnostically using data from the lowest model level and the surface. In grid squares containing, both land and sea the characteristics of the dominating surface type are used (Tisler and Fortelius, 1999).

3. Observations

Observational data were gathered from meteorological towers and stations. Towers locate at the open sea and their height is over 25 m from the sea level. They can be influenced by ice and close coast. Stations are situated on the coast or on the island and their height is under 25 m from the sea level. They are more influenced by the land and obstacles at different directions.
There are used 4 Finnish towers/stations (Kalbådagrund (the anemometer height from the sea level is 31.6 m), Kemi (26.0 m), Nahkiainen (31.8 m), Märket (20.0 m)) and 3 Estonian stations (Kunda (11.7 m), Sõrve (14.8 m), Vilsandi (16.4 m)) (Figure 1.).

4. Methods

Finnish towers and station (Märket) were compared at the lowest model level (32 m). For Estonian stations the model data were derived from the lowest model level to the comparison level at 10 m. height. In this way better results were received for each station/tower.
When the wind is blowing from the land to sea, it takes considerable distance before marine wind profile is established. Validation of marine winds should therefore ideally be based on offshore measurements uninfluenced by land and islands. In practice, such influences are felt for some wind directions at nearly all observing sites. In addition local obstacles (trees, buildings etc.) also tend to influence the measurements. (Heiskanen and Frisk, 1998)

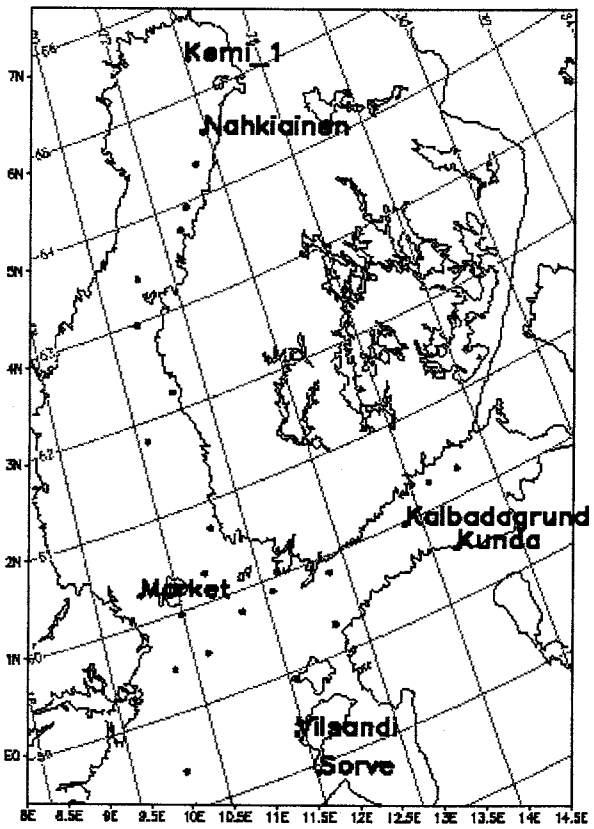

Figure 1: Observational stations and towers.

The observations at different stations are made at different times. For Finnish towers and station the closest 10 min. average wind speed and direction in the period of 3 hours to model results were used. For Estonian stations the 10 min. average data were used at every synoptic observation. Also there was limited accuracy at Estonian stations where the wind speed was given with accuracy 1 m/s and the direction with accuracy 10 deg.
The comparison of observational data was carried out with the forecasts of different lenght (06fc (6-hour forecast), 12fc, 18fc, 24fc, 30fc, 36fc, 42fc, 48fc), during the period 01.11.1999 to 31.01.2000 (November, December, January).
In assessing of forecasts two different measures of quality were computed: forecasts reliability and accuracy. For reliability mean error (ME) and for accuracy root mean square error (RMSE) was used.
Each wind speed was additionally studied in different wind directions. The usual wind directions were chosen: N, NW, W, SW, S, SE, E, NE. In addition winds were divided into two groups: winds blowing from the open sea and winds blowing from the land, island(s) and ice-areas.

5. Results

Following conclusions were made:

1. Comparison of observed wind speed with forecasts allows to discover linear increase of RMSE for Finnish and exponential increase for Estonian stations (Figure 2.). The same tendency was discovered in wind direction;

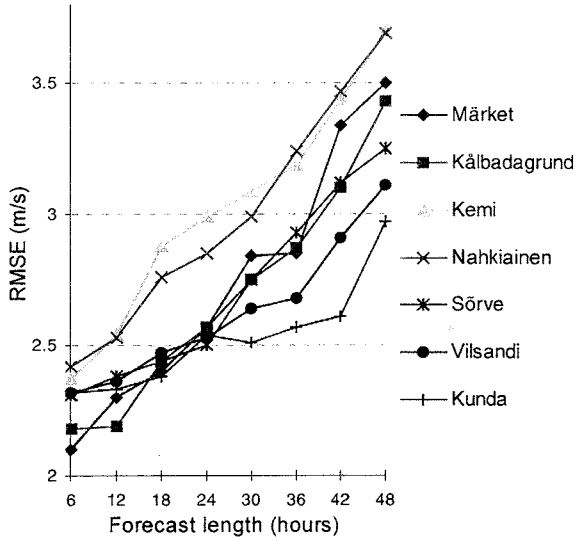

Figure 2: Root Mean Square Error (RMSE) of HIRLAM wind speed forecasts at different stations and towers.

2. HIRLAM-model predicts wind speed and direction more reliably at the open sea areas. The best results occur at the towers (Kalbådagrund, Kemi, Nahkiainen). Quite little mean errors are found for Sõrve surrounded from the most sides by the sea (Figure 3.);

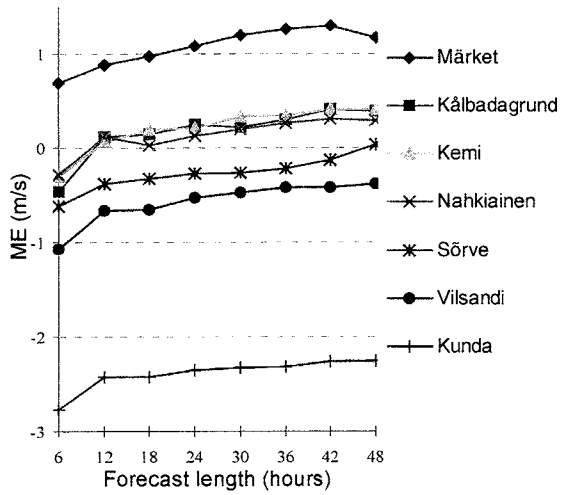

Figure 3: Mean error (ME) of HIRLAM wind speed forecasts at different stations and towers. If ME has a minus sign, model overpredicts and if a plus sign, it underpredicts wind speed.

3. In forecasts were discovered underprediction up to 10 degrees of wind direction for all sites. It means that model overestimates frictional turning. Therefore cyclones fill faster as compared with the real situation and wind speed is also estimated wrongly. Especially it is noticeable at the stations;
4. Model over-predicts the winds blowing from open sea to the direction of the towers. At the stations (Kunda, Sõrve, Vilsandi) the situation was opposite, the winds blowing from the land were overpredicted;
5. Model used to overpredict the strong winds (> 15 m/s) at the towers. At the stations it wasn't so noticeable;
6. Ice conditions that were forecasted wrongly by the model influenced strongly predicted wind speed and directions (Kemi, Nahkianen);

References

Cuxart, J. Bougeault, P. Redelsperger, J.-L., A turbulence scheme allowing for mesoscale and large-eddy simulations – *Quarterly Journal of the Royal Meteorological Society*, 2000

Heiskanen, M. Frisk, M., EndWind and Wind Speed Corrections, 1998

Tisler, P. Fortelius, C., Verification of HIRLAM marine boundary layer winds – *MERI – report of series of the Finnish Institute of Marine Research*, 1999

Trends in the hydrological cycle over the Baltex area, simulated and observed

Klaus Arpe and Stefan Hagemann

Max-Planck-Institute for Meteorology, Bundesstr. 55, 20146 Hamburg, Germany, e-mail: arpe@dkrz.de

Introduction

Simulations with different models using CO2 doubling scenarios have shown a strong increase of precipitation during winter in the 21st century (Arpe and Roeckner, 1999) over the Baltex area. During the 20th century an increase has already been observed (Schönwiese and Rapp, 1997). It will be shown in section 3, how far different simulations and observational data sets support each other in showing trends in the precipitation. Trends in the evaporation can only be investigated from model output, simulations or reanalyses, because there are hardly any direct observations available. But on a long time scale the difference between precipitation and evaporation can be compared with river discharge observations which will be discussed in section 4. First the ability of the model used for the climate simulations to produce a reasonable hydrological cycle over the Baltex area will be shown in section 2.

Performance of the ECHAM model

The 20th century climate simulations are carried out with the ECHAM4 model (Roeckner et al., 1996a) forced by observed SSTs (Rayner et al., 1996). These are compared with simulations using the same atmospheric model but coupled interactively to the ocean model OPYC (Roeckner et al., 1996b). In the Baltex area the simulated precipitation for the present climate is generally overestimated in winter and underestimated in summer, however, there is a good simulation of the patterns in both seasons. It is hoped that the biases in summer and winter are of a minor importance for the investigations below, where we are interested in trends due to changes in the concentration of greenhouse gases and less in absolute values. This expectation is supported by the fact that simulations of the Hadley Centre exhibit similar trends but without having such a bias for the present climate.

Trends in the precipitation (observed and simulated)

When investigating trends in the climate system, one is looking for areas and seasons with a strong and steady signal. In scenario simulations such clear trends can be found in the precipitation during winter in the northern hemisphere north of about 50°N. This is especially true for the Scandinavian area. For this area one can find similar trends also in simulations with the Hadley Centre climate model (Arpe et al., 2000). These trends are mainly simulated for the future while there are only weak trends simulated for the last 100 years.

For the validation of these weak trends, we have several data sets available. In Figure 1 the winter precipitation averaged over the BALTEX area is compared between the simulations assuming an increase of greenhouse gases according to IPCC IS92a with the coupled MPI model (scen) and the same model but keeping a constant greenhouse gas concentration (ctrl). It is further compared with simulations (mean of 4 runs) using the same atmospheric model but forced with observed SSTs provided by Rayner et al. (1996) (AGCM) and another simulation with the same model but using a more recent SST analysis by the Hadley Centre (HadT). Finally observed precipitation values prepared by New et al. (2000) (CRU) are shown as well. All data have been smoothed by applying a 19 year running mean. The observational data by New et al. (2000) have a strong bias compared to analyses by GPCP (Huffman et al., 1996) and others, probably because they have not been corrected for observational errors. Therefore the CRU values have been multiplied by a factor 1.34 in Figure 1. This factor is the one used by GPCP. Nevertheless a bias in the model values mentioned above can be recognized.

From the comparison between the "scen" and the "ctrl" run it can be seen that the model on its own is stable and that the trend in the scenario run is only resulting from the forcing by increased greenhouse gases. Further a strong interdecadal variability in both simulations is obvious, suggesting that there is no defined short time span when the increase occurs such as for global mean surface temperatures. Nevertheless one can already recognize a modest increase of precipitation in the 20th century scenario run during winter. Such an increase can also be seen in the AGCM and HadT simulation and in the observation (CRU). This agrees with the analysis by Schönwiese and Rapp (1997). This trend is most consistent for southern Sweden, where all observed station values of precipitation provide the same signal. Applying a laborious correction of the station values, the trends may become even stronger as shown by Hansen-Bauer (1994).

For summer (not shown) the scenario simulation shows a weak decrease in the 21st century while it is hard to see any trend for the 20th century in all simulations and the observation. For the annual mean values the winter increase is dominating and in this respect the scenario simulation resembles the observations to a high degree.

Trends in the observed river discharge in comparison with simulated precipitation minus evaporation

Trends in the evaporation can only be investigated from model output, simulations or reanalyses, because there are hardly any direct observations available. But on a long time scale the difference between precipitation and evaporation can be compared with river discharge observations. Such a comparison can presently best be done by investigating annual means as the annual cycle of river discharge is governed by the snowmelt for a natural river which is difficult to simulate but most rivers are regulated and their annual cycle is governed by the energy consumption, which is not addressed by the models.

Evaporation anomalies are strongly influenced by the availability of water and energy in the ground. Because of an increased precipitation there would be more water available in the ground in a future climate and because of increased temperatures one can expect some increase of evaporation. This applies mainly to the winter season while in summer the effect of reduced availability of water due to less precipitation is counteracting the effect of increased temperatures. In fact this expectation is fulfilled by the simulations.

Table 1: Changes from 2000 to 2100 in the precipitation, evaporation and their differences (P-E) (mm/month) in the BALTEX area as simulated with the scenario run. 30 year means at the ends of the centuries are given.

	DJF		JJA		Year	
	2000	2100	2000	2100	2000	2100
precip	70	83	43	36	59	64
evap	27	33	38	39	33	38
P-E	43	50	5	-4	24	26

Table 1 gives an overview of the effect of increased greenhouse gas concentration on different components of the hydrological cycle. On the whole the simulations do not suggest much of a trend in the river discharge because the influence on precipitation is compensated by induced changes in evaporation. The long-term variations are larger than a possible trend.

Conclusion

Scenario simulations with increased greenhouse gas concentrations show a clear increase of precipitation in winter and some decrease in summer. These trends can already be seen during the last 100 years in model simulations and observations. Because of counter effects by evaporation the simulation does not suggest clear trends for the river discharge.

References

Arpe K., U. Cubasch, R. Voss, Use of climate models for climate change investigations. In: Proc. 1st Solar & Space Weather Euroconference.'The Solar Cycle and Terrestrial Climate', Santa Cruz de Tenerife, Tenerife, Spain, 25-29 September 2000 (ESA SP-463, December 2000), 233-241, 2000

Arpe, K., E. Roeckner, Simulation of the hydrological cycle over Europe: Model validation and impacts of increasing greenhouse gases. Advances in Water Resources, 23, 105-119, 1999

Hansen-Bauer, I., Regional trends in Norwegian precipitation series. In: Heino, R. (ed.). Climate variations in Europe. Proceedings of the European Workshop on Climate Variations. Kirkkonummi, Finland, May 1994, Publications of the Academy of Finland, 3/94, Helsinki, 1994

Huffman, G.J., R.F. Adler, P.A. Arkin, A. Chang, R. Ferraro, A. Gruber, J. Janowiak, R.J. Joyce, A. McNab, B. Rudolf, U. Schneider, P. Xie, The Global Precipitation Climatology Project (GPCP) combined precipitation data set. Bull. Amer. Meteor. Soc., 78, 5-20, 1996

New, M., M. Hulme, P. Jones, Representing twentieth-century space-time climate variability. Part II: Development of 1901-96 monthly grids of terrestrial surface climate. Journ. of Climate 13, 2217-2238, 2000

Rayner, N.A., E.B. Hearten, D.E. Parker, C.K. Folland, R.B. Hacked, Version 2.2 of the global sea-ice and sea surface temperature data set, 1903-1994. (Climate Research Technical Note CRTN74, Bracknell, UK) 1996

Roeckner, E. et al., The atmospheric general circulation model ECHAM-4: Model description and simulation of present-day climate (Max-Planck Institute for Meteorology, Hamburg, Report no. 218, 1996a

Roeckner, E., J.M. Oberhuber, A. Bacher, M. Christoph, I. Kircher, ENSO variability and atmospheric response in a global coupled atmosphere-ocean GCM, Clim. Dyn., 12, 737-754, 1996b

Schönwiese C.-D., J. Rapp, Climate Trend Atlas Europe. Based on Observations 1891-1990. Kluwer, Dordrecht, 228 pp, 1997

Xie, P., P. Arkin, Global Precipitation: A 17-Year Monthly Analysis Based on Gauge Observations, Satellite Estimates and Numerical Model Outputs. Bull. Amer. Meteor. Soc., 78, 2539-2558, 1997

The Height of the Marine Boundary Layer over the Baltic Sea: Measurements and Modelling

Ekaterina Batchvarova[1,2] and Sven-Erik Gryning[1]

[1] Risø National Laboratory, DK-4000 Roskilde Denmark
[2] National Institute of Meteorology and Hydrology, Bulgarian Academy of Sciences, Sofia, Bulgaria

1. Summary

Two-weeks of measurements of the boundary-layer height over the small island of Christiansø in the Baltic Sea are discussed. Here we give an overview, details can be found in Gryning and Batchvarova (2002). The meteorological conditions are characterised by high wind speed and positive heat flux over the sea. The boundary-layer height was simulated with two models, a simple applied high-resolution (2 km times 2 km) model, and the operational numerical weather prediction model HIRLAM (grid resolution of 22.5 km times 22.2 km). For south-westerly winds it was found that the boundary-layer height is influenced by a relatively large island (Bornholm) lying 20 km upwind of the measuring site. In this situation the high-resolution simple applied model reproduces the characteristics of the boundary-layer height over the measuring site. Richardson-number based methods using data from simulations with the HIRLAM model, most likely fail because the island and the water fetch to the measuring site are about the size of the grid resolution of the HIRLAM model and therefore poorly resolved. For northerly wind the water fetch to the measuring site is about 100 km. Both models reproduce the characteristics of the height of the marine boundary layer. This suggests that the HIRLAM model adequately resolves a water fetch of 100 km with respect to predictions of the height of the marine boundary layer.

2. Measurements

The measuring activities were concentrated at a cluster of small islands in the Baltic Sea known as Christiansø. Figure 1 shows a map of the Baltic Proper with Christiansø marked by a cross. For wind directions in the sector 190 to 270 Christiansø lies about 20 km downwind of Bornholm, Figure 2. In the sector 270 to 45 degrees the water fetch to the Swedish coast is about 100 km, Figure 1.

Long term measurements (April 1998 through December 1999) of atmospheric turbulence and evaporation were carried out at an 8-meter mast with an open sector to the sea of 120° to 300° through south. The measurements of heat and momentum fluxes were performed with a Kaijo-Denki DAT/TR-61B three-dimensional sonic anemometer. The fluctuations of water vapour content in the air were measured with an open path infrared optical hygrometer.

During an extensive observation period from 24 October to 5 November 1998 the measurement programme was extended with radiosoundings, with a total of 24 radiosondes released at Christiansø. The depth of the boundary layer was subjectively estimated from the soundings, based mainly on the profile of the potential temperature, and taken as the height where the potential temperature starts to increase.

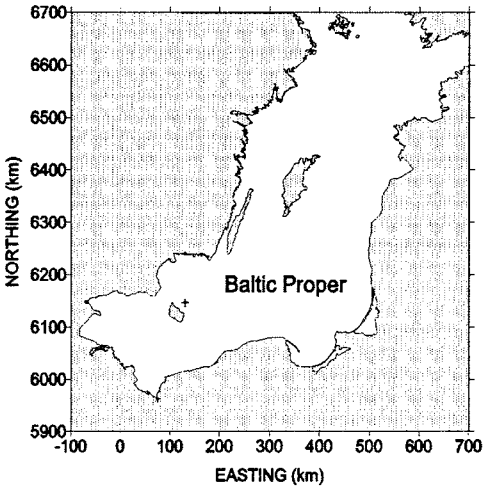

Figure 1: Map of the Baltic Proper with land surfaces and islands dotted. A cross shows the location of Christiansø east of Bornholm The co-ordinate system refers to UTM34.

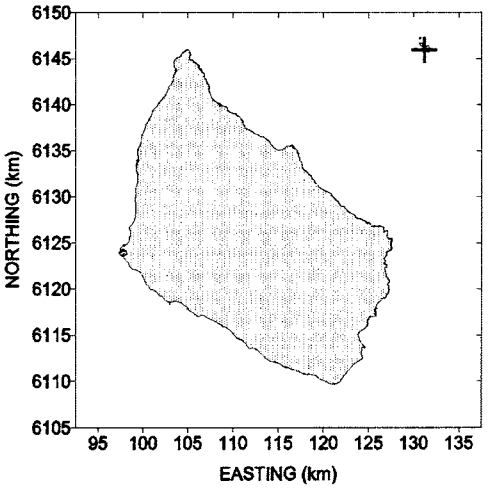

Figure 2: The island of Bornholm. Christiansø is marked by a cross. The co-ordinate systems refer to UTM34.

3. Meteorological conditions

During the experiment the water was generally warmer than the air which is a very typical feature for the Baltic Sea during the late summer, autumn and early winter. This results in a generally positive sensible heat flux to the atmosphere and the generation of a convectively driven boundary layer over the water. The experimental period covers wind speed in the range from calm to 19 ms^{-1}. The period from 26 October until midday 1 November 1998 is characterised by winds about 10 ms^{-1} from south-west to west. This corresponds to the period until hour 160 on Figures 3 and 4. In this sector Christiansø is downwind of

Bornholm with a water fetch of about 20 km. Following a wind direction shift on 1 November 1998 to north-west and north, roughly corresponding to 160 hours on Figures 3 and 4, the wind ceased to about 4 ms^{-1} . Then Christiansø is not downwind of Bornholm and the over water fetch from the Swedish coast is of about 100 km.

4. Models

The height of the boundary layer during the period with intensive measurements was modelled by a simple applied model *Gryning and Batchvarova (1996)*, and by data from the operational numerical weather prediction model HIRLAM. The model domain of the simple applied model is shown in Figure 1. A grid resolution of 2 km and a time step of 15 seconds were used in the simulation. The version of the HIRLAM model that was applied in this study has a horizontal grid resolution is 22.5 times 22.5 km and 31 vertical levels. Both models were applied for the period 26 October to 2 November 1998.

The interpolated wind speed and direction predicted by the HIRLAM model during the intensive period agrees well with the measured values at Christiansø. The agreement between modelled and measured wind speeds and direction is typically 20 degrees and 2 ms^{-1}.

The boundary-layer heights were derived each hour from output of the Numerical Weather Prediction model HIRLAM, applying the Richardson-number methods suggested by *Sorensen (1998)* and *Vogelezang and Holtslag (1996)*, Figure. 3.

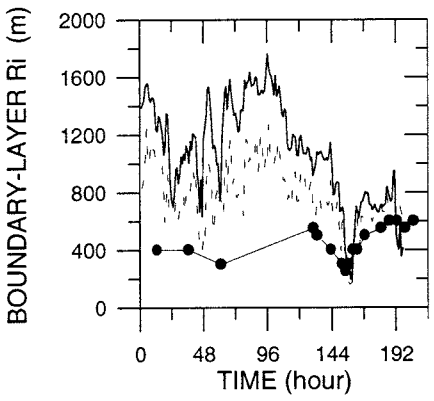

Figure 3: Boundary-layer height over Christiansø during the extensive observation period, estimated from the HIRLAM model. The full line shows the results using the Richardson number suggested by *Sorensen (1998)*, the dashed line when using *Vogelezang and Holtslag (1996)*. Bullets show measurements.

The simulation of the boundary-layer height with the simple applied model was based on the wind field from the HIRLAM model. Interpolated wind field component at each grid point in the 2 km grid are derived for the whole model domain by inverse square interpolation between the wind predictions at the HIRLAM grid points. The sensible heat flux and the friction velocity measured at Christiansø were taken as the basis for the simulations. Figure 4 shows the evolution of the simulated boundary-layer height over Christiansø.

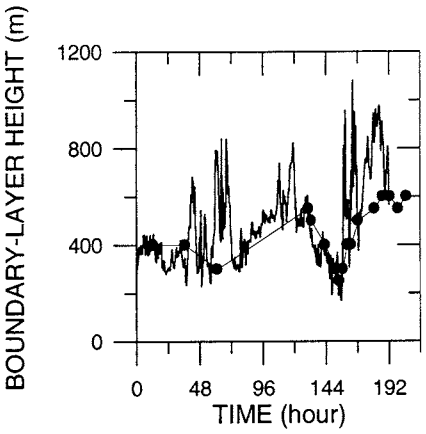

Figure 4: Simulation with the simple applied model of the evolution of the boundary-layer height over Christiansø during the extensive observation period. Bullets show measurements.

5. Discussion

The model simulations suggest that during the first period the island of Bornholm controls the boundary layer over Christiansø. The high-resolution simple applied model successfully predicts the boundary-layer height over Christiansø. The boundary-layer height that was estimated from the HIRLAM data by use of the Richardson-number methods is higher than the measured one, which suggests that the water fetch to Bornholm and Bornholm itself is not adequately resolved by the HIRLAM model and therefore HIRLAM does not provide a realistic prediction of the boundary-layer height over Christiansø.

During the last period of the experiment the wind was northerly. The air that reached Christiansø did not pass Bornholm on its way, but the water fetch to the nearest coast was about 100 km. For this case good agreement between measured and simulated boundary-layer heights was found for all the model simulations.

Acknowledgements

We thank the Swedish Meteorological and Hydrological Institute and Anna Rutgersson for generously providing the data from the HIRLAM simulations. The European Union supported the project, ENVC4-CT97-0484.

References

Gryning, S.-E. and E. Batchvarova, A model for the height of the internal boundary layer over an area with a irregular coastline, *Boundary-Layer Meteorology*, Vol. 78 , 405-413, 1996

Gryning S.-E. and E. Batchvarova, Marine boundary layer and turbulent fluxes over the Baltic Sea at high wind speed conditions: measurements and modelling, *Boundary-Layer Meteorology*, Submitted, 2002

Sørensen, J. H., Sensitivity of the DERMA long-range Gaussian dispersion model to meteorological input and diffusion parameters, *Atmospheric Environment* Vol. 24, 4195-4206, 1998

Vogelezang, D. H. P. and A. A. M. Holtslag, Evaluation and model impacts of alternative boundary-layer height formulations, *Boundary-Layer Meteorology* Vol. 81, 245-269, 1996

Precipitation classification and analysis from remote sensing observations

Ralf Bennartz[1], Anke Thoss[2], Adam Dybbroe[2], Daniel Michelson[2]

[1] University of Kansas, Dept Physics & Astronomy, Lawrence, KS 66045, USA
and Free University of Berlin, Inst. For Space Sciences, e-mail: bennnartz@ukans.edu
[2] Swedish Meteorological and Hydrological Institute (SMHI), Norrkoeping, Sweden

1. Introduction

A method to classify precipitation type based on the combination of satellite and ground-based radar data has been developed. This method (1) removes systematic errors in satellite-based precipitation estimates and (2) reduces the uncertainty associated with the spaceborne precipitation estimates. It allows to consistently describe the passive microwave optical properties and at the same the radar backscatter characteristics of frozen and liquid precipitation (Bennartz and Petty, 2001). We apply the new method to different precipitation events and evaluate the relative impact of ice particle size and density on precipitation retrieval. We find high correlations (0.8-0.9) between passive microwave and radar-derived precipitation intensity. Subsequently, we give a short discussion on an operational algorithm developed at SMHI in the framework of EUMETSAT's to derive precipitation information from the Advanced Microwave Sounding Unit (AMSU).

In the next years we will use this technique to further evaluate precipitation statistics over the Baltic region. These studies will be performed in the framework of the German BALTIMOS-project. The main emphasis of our project will be the discrimination of different types of precipitation events and the determination of their respective contribution to the total amount of precipitation in the Baltic area based on a dataset covering the entire BRIDGE period.

2. Development Dataset

The algorithm development was performed using an eight month dataset (April 1999 to November 1999) of NOAA-15 AMSU-A/B and AVHRR data. The data was co-located with radar data from the BALTEX Radar Data Centre (BRDC) for the entire Baltic region covered by 13 radars (Michelson et al, 2000). The precipitation amount of the radar data was gauge adjusted using a technique described in (Michelson and Koistinen, 2000).

3. Algorithm

The algorithm is giving the likelihood of precipitation in four intensity intervals under the constraint, that the total likelihood has to be 100%. Intensity classes are defined as follows:

Class 1: Precipitation-free rain rate 0.0 to 0.1 mm/h
Class 2: Risk for or very light precipitation rain rate 0.1 to 0.5 mm/h
Class 3: Light/moderate precipitation rain rate 0.5 to 5.0 mm/h
Class 4: Intensive precipitation rain rate greater 5.0 mm/h

Separate estimates of precipitation likelihood are performed from AMSU and AVHRR and finally blended into a joint estimate.

Most information of the precipitation product is derived from microwave frequencies. When developing a precipitation algorithm for AMSU, we had to consider whether to concentrate on an emission or scattering based algorithm. Whereas the emission signal from precipitation for frequencies below 50 GHz is more directly linked to precipitation, it can only be retrieved over water surfaces, which give a radiatively cold background because of their low surface emissivity. For frequencies higher than 50 GHz it is possible to derive precipitation algorithms based on the scattering signature of frozen precipitation sized particles over both land and sea (Bennartz and Petty, 2001). Since it was desirable to also make use of MW data over land, we developed a scattering based algorithm using AMSU-A and AMSU-B window channels. This enabled us to also take advantage of the higher spatial resolution of AMSU-B of 1.1° (corresponding to 16 km at nadir) as compared to AMSU-A with 3.3° resolution.

The scattering index makes use of a predicted brightness temperature T^* in the absence of scattering, which is derived from low frequency channels. The functional relationship between the low frequency brightness temperature and T^* can either be found by inverse radiative transfer modelling, or by global brightness temperature statistics. From T^* the high frequency brightness temperature is subtracted:

$$SI = T^*(T_{low}) - T_{high}$$

with SI being the scattering index, T_{low}, T_{high} being the observed low and high frequency brightness temperature respectively. The scattering index has been found to be a linear measure for precipitation intensity. In the algorithm described here, T^* is determined statistically as:

$$T^* = T_{low} - CORR$$

where CORR includes a statistical correction for scan position effects and a statistical offset for non-scattering situations. For algorithm development, it is necessary to take into account the surface properties of the scene viewed. Scene specifications will influence the channel selection and will also necessitate separate tuning of the correction coefficient. According to the scene viewed, our algorithm specifies three separate cases for FOV's covered with land or water:

- AMSU-A land (and AMSU-B land):
  $SI_{land1} = T23 - CORR - T150$
- AMSU-A water or coast, AMSU-B Land:
  $SI_{land2} = T89 - CORR - T150$
- AMSU-B water:
  $SI_{sea} = T89 - CORR - T150$

In the case of the water algorithm, the offset for non-scattering situations is adjusted dynamically for each scene processed.

Coastal estimates have to be treated separately. A linear dependence exists between the MW brightness temperatures and the land fraction within the FOV, as illustrated for the 23GHz channel in figure 1. Thus the scattering index for coastal scenes can be estimated as a linear combination of the land and sea scattering index, taking into account the land fraction within the FOV:

$$SI_{coast} = (1 - N_{land}) * SI_{sea} + N_{land} * SI_{land}$$

with N_{land} being the land fraction and SI_{land} and SI_{sea} being the scattering indices for land and sea respectively. Due to

the high sensitivity of scene coverage within the FOV it is necessary to properly convolve a high resolution land/sea mask to the AMSU FOV, as well as to properly convolve AMSU-B to AMSU-A. We used a Backus-Gilbert convolution described by Bennartz (2000) for this purpose.

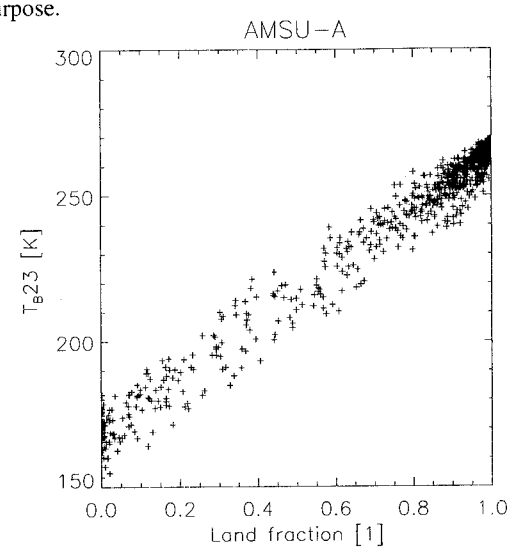

Figure 1: Dependence of AMSU-A brightness temperature at 23GHz on the fraction of land surface within the footprint.

The scattering indices are matched with gauge corrected radar rain rates, which have been convolved to the AMSU-B field of view. Frequency distributions of scattering indices have been derived for each of the four precipitation classes defined above. For each scattering index the probability that the observation falls within a certain precipitation class is determined under the constraint that the total probability has to sum up to 100%. It could be shown that the 23GHz-150GHz scattering index gives a better discrimination of precipitation over land than the 23GHz-89GHz scattering index (figures 2 and 3). The probability distribution of the scattering indices for the four precipitation classes is given in figure 3 for land and in figure 4 for sea. Whereas it is possible to clearly discriminate non-precipitating situations from strong precipitation, there is some overlap of the very light and the light/moderate precipitation classes with both the high and non-precipitation classes. The two intermediate classes overlap substantially with each other. In this light it seems even more valid, to express the precipitation estimate as probabilities.

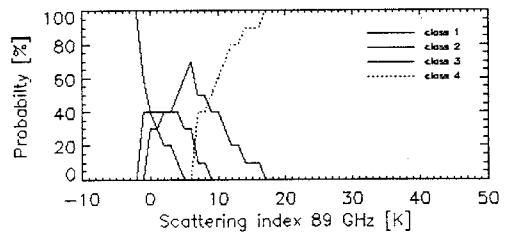

Figure 2: Probability that the Scattering Index belongs to a certain precipitation class for the **23GHz-89GHz index over land**. Peaking from left to right: no rain, very light rain, light to moderate rain, heavy rain.

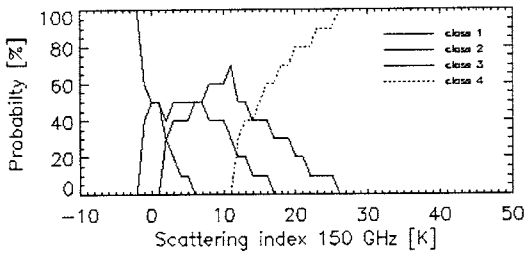

Figure 3: Probability that the Scattering Index belongs to a certain precipitation class for the **23GHz-150GHz index over land**. Peaking from left to right: no rain, very light rain, light to moderate rain, heavy rain

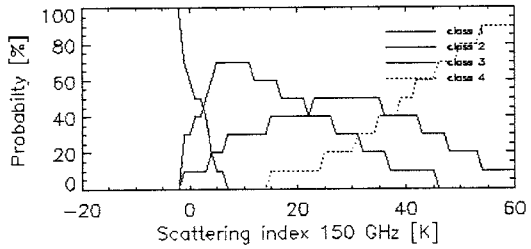

Figure 4: Probability that the Scattering Index belongs to a certain precipitation class for the **89GHz-150GHz index over sea**. Peaking from left to right: no rain, very light rain, light to moderate rain, heavy rain

References

Bennartz, R. and G.W. Petty: The sensitivity of microwave remote sensing observations of precipitation to ice particle size distributions. J. Applied Meteorology, Vol. 40, No. 3, 345-364, 2001.

Bennartz, R., 2000: Optimal convolution of AMSU-B to AMSU-A. J. Atmos. Oceanic Technology, Vol. 47, No. 9, 1215-1225.

Dybbroe, A., K.-G. Karlsson and A. Thoss, 2000:Scientific report of the SAFNWC Mid Term Review, http://www.smhi.se/saf.

Grody et al., 2000: MSPPS science algorithms. http://orbit18i.nesdis.noaa.gov/html/algorithm.html

Michelson, D.B., T. Andersson,J. Koistinen, C.G. Collier, J. Riedl,J. Sztuurz, U.Gjertsen, A. Nielsen, S. 'Overgaard, 2000: BALTEX RadarData Centre – Products and their Methodologies. SMHI Reports Meteorology and Climatology, No. 90. Publ. SMHI.

Michelson, D.B. and J. Koistinen, 2000: Gauge-radar network adjustment for the Baltic Sea Experiment. Phys. Chem. Earth (B), Vol.25, No10-12, pp. 915-920.

Surface Radiant and Energy Flux Densities inferred from Satellite Data for different BALTEX periods

Franz H. Berger[1] and Thomas Halecker[2]

[1] Dresden University of Technology, Institute of Hydrology and Meteorolgy
[2] Department of Meteorology, Piennerstr. 9, D-01737 Tharandt, Germany

Introduction

To improve our knowledge in climate and weather prediction, all processes must be clearly understood. One primary goal is the investigation of the energy and water cycle at different scales, reaching from global to local with adequate temporal scales from months to seconds (*Chahine, 1992*). The water cycle itself influences climate and weather in different ways. The exchange of energy and humidity between the Earth surface and the atmosphere influences dynamics and thermodynamics in the weather and climate regime. As water vapour, clouds, precipitation, ice and snow, water play a significant role in heating or cooling of the Earth/atmosphere system. Thus, a large fraction in cooling of the Earth surface is due to evapotranspiration at the surface. The water cycle is together with the energy cycle an important component in the processes within the Earth atmosphere. These processes will be studied in the context of large hydrological experiments, like GEWEX (Global Energy and Water cycle EXperiment; *WMO, 1990*).
Therefore the task of this investigation was the development of an analysis scheme to infer surface radiant and energy fluxes from remotely sensed data for individual atmospheric conditions, from clear-sky to totally overcast.

1. Analysis Scheme

Determining surface radiant and energy flux densities from remotely sensed data, a modular analysis scheme, named SESAT (*Strahlungs- und Energieflüsse aus SATellitendaten*), could be developed for different meteorological satellite data, such as NOAA-AVHRR, ERS-1/2 ATSR, Envisat AATSR as well as for MSG (*Berger, 2000*).
SESAT contains several modules, where additional information must also be taken into account. Thus, a detailed topography (GTOPO30 / 1 km resolution), a landuse classification (USGS / 1 km resolution) as well as synoptic observations are considered. The synoptic observations are used to characterize the aerosol content and the relative humidity within the atmospheric boundary layer (*Berger et al, 2001*). Concerning the free atmosphere, standard conditions are used.
To infer surface fluxes for varying atmospheric conditions, within one module a detailed cloud classification to define cloud types, and the determination of cloud optical (cloud optical depth) and microphysical (effective cloud droplet radius) properties could be used. Within another module surface reflectances and emissivities for clear-sky conditions could be determined. For cloudy conditions, a multi-day sampling of satellite data provides the needed information about surface properties. Applying an inverse remote sensing technique, which includes intensive radiative transfer simulations (Two-Stream and Streamer) for a large set of look-up tables (for various atmospheric and viewing conditions), surface radiant flux components could be calculated for individual pixels. Concerning the insolation at the surface, the topography is additionally considered leading to a modified surface insolation. For the longwave, an empirical relationship could be developed to quantify the influence of clouds on both, back radiation and outgoing longwave radiation at the surface.
Based on surface net radiation and additional land surface properties, like leaf area index or roughness length – all determined using passive remotely sensed data – surface energy flux densities could be inferred for each individual pixel at a given resolution, like 1 km^2. This includes the storage of heat within a soil layer or within a soil and a canopy layer, and the sensible and latent heat flux densities (potential and actual evaporation).

2. Application of SESAT

SESAT could be applied to a large variety of NOAA AVHRR data for the Baltic Sea region, where several months are considered: May and June 1993, August and September 1995, September and October 2000. For various conditions (dry and wet months, for long clear as well as cloudy periods), temporal and spatial variabilities of radiant and energy flux densities could be inferred. Comparisons with surface based observations and with model simulations (REMO) show the potential of SESAT, where in general the solar radiant fluxes are overestimated (due to the heterogeneity of landsurface characteristics and due to calibration effects). In the longwave realistic flux densities could be calculated. Due to the assumptions in determining the energy flux densities, less accurate results could be achieved. Nevertheless, the results allow a first estimate in the spatially highly variable evaporation within the Baltic Sea watershed. The results show a high dependence on the used landuse classification, which is further related to the different applied parameterizations.

3. Outlook

Using future studies within the BALTEX framework (EVA-GRIPS) improvements of SESAT will be carried out, where specific emphasis will be given to better parameterizations for various landsurface types (forests, agricultural landscapes, mixed areas), to an improved landuse classification and to the estimate of subpixel effects. The improvements will further be tested applying surface measurements at different measuring sites, where these results will also be used to quantify the achievable accuracies.

References

Berger, F.H.: *Bestimmung des Energiehaushaltes am Erdboden mit Hilfe von Satellitendaten.* Habilitationsschrift an der TU Dresden, Juli 2000.

Berger, F.H., Halecker, Th. and Podlasly, C.: *Zeitliche Variabilität der Energieflüsse in einem heterogenen Gelände, abgeleitet aus Satellitendaten.* Abschlußbericht BMBF AKA Forschungsvorhaben 01 LA 9836/6, 2001.

Chahine, M.T.: The hydrological cycle and its influence on climate. *Nature*, 359, 373-380, 1992.

WMO: *Scientific Plan for the Global Energy and Water Cycle Experiment.* Tech. Rep. WCRP-40, WMO/TD-No. 376, International Council of Scientific Unions and World Meteorological Organization, 1990.

Climate change impacts on the hydrology of the Baltic Basin

Sten Bergström, L. Phil Graham and Marie Gardelin

Swedish Meteorological and Hydrological Institute, SE-60176 Norrköping, Sweden

1. Introduction

Analysis of the climate change impacts on the hydrology of the Baltic Basin are carried out at two different scales within the Swedish Regional Climate Modelling Programme (SWECLIM, Rummukainen et al., 2000). Hydrological modelling at large scale simulates trends for impacts to the entire Baltic Basin and at smaller basin scales simulates local impacts in Sweden (Bergström et al., 2001; Graham et al., 2001).

The climate change signal used for hydrological simulations comes from the Rossby Centre Regional Atmospheric Climate Model (RCA, Rummukainen et al., 2001)), which is applied over Northern Europe. Two different GCMs have thus far been used to provide boundary conditions to the regional model—HadCM2 (Mitchell and Johns, 1997) and ECHAM4/OPYC3 (Roeckner et al., 1998). A combination of different GCMs, different model versions of RCA, and variations to the hydrological impact model provides a range of hydrological scenarios, as presented below.

2. Interface Between Climate and Impact Models

As direct input of climate model results into hydrological models has shown to result in inaccurate estimates of river discharge (Graham and Jacob, 2000), an interface between RCA and the hydrological models is required. The interface is essentially an analysis of the climate change signal to precipitation and temperature, which is used to perturb a database of present climate observations that in turn drives the hydrological models. In some instances, the specific climate change signal to evapotranspiration is also extracted for use in the hydrological impact models. This process of extracting the climate change signal and modifying an observational database can also be referred to as the "delta change approach."

Variations in the way that the changed climate signal is extracted from climate model simulations have shown to have a significant effect on the outcome of impact studies (Gardelin et al., 2001). The latest scenarios from SWECLIM included consideration for the fact that the climate change signal proved to be strongest for low temperatures (i.e. below 0°C). Inclusion of this in the interface served to reduce the climate change impact on the snow regime and thus on spring runoff, particularly in northern basins. For example, even large changes in temperature have no effect on snowmelt if the baseline temperature is -15°C.

3. Impacts on Water Resources in the Baltic Basin

For large-scale simulations, the existing large-scale hydrological model, HBV-Baltic (Graham, 1999), was used. Results are shown in Figure 1, which contains seven different realizations of climate change for the five main Baltic Sea drainage basins. Although they are not specifically labeled, the different realizations cover combinations of the two GCM driving scenarios, the RCA model applied at different resolutions and with further developments in parameterization, and differences in how the climate change interface is carried out.

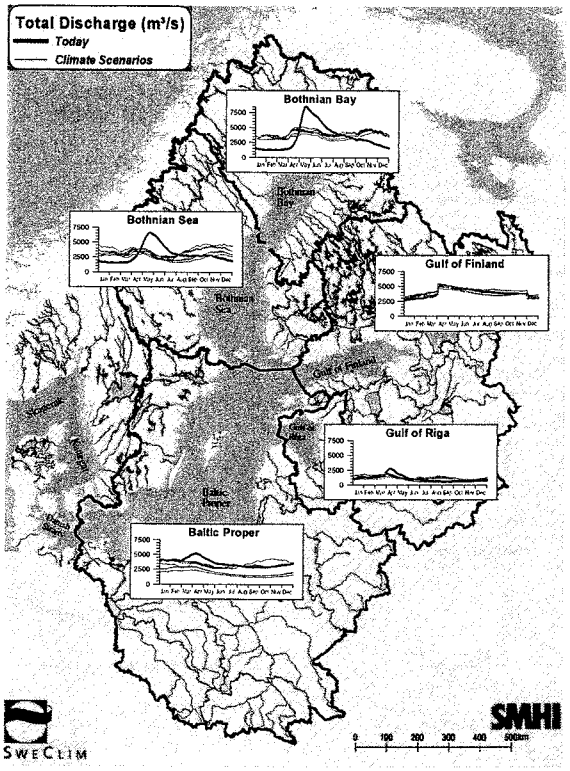

Figure 1: Modelled average seasonal river runoff to the Baltic Sea for present and future conditions. The observational database used is for 1980-1998.

4. Impacts on Water Resources in Sweden

For local impact studies in Sweden, hydrological HBV model simulations of a selected group of six smaller basins distributed over the country were used (Bergström et al., 2001). Results are shown in Figure 2, which contains eight different realizations of climate change for these basins. In addition to the different scenarios mentioned above for the Baltic Basin, these results also include realizations where different methods for simulating future evapotranspiration were applied. For these realizations, modelling of the evapotranspiration in the hydrological models was adjusted so that the change between present and future conditions matched the change produced by the climate model.

5. Conclusions

The most obvious effects apparent from these simulations are the changes in runoff due to changes in the snow regime. This is particularly pronounced in the northern basins of the Baltic Basin studies where the spring runoff peaks disappear under the future climate scenarios. Looking at the local impact studies, more variation is apparent from basin to basin and the small northernmost mountain basins show only mild effects. Yet, further south and at lower elevations, effects become as pronounced as

displayed on the large scale. The range of the different curves shown in Figures 1 and 2 represent to some extent the uncertainties that are inherent in this type of application. The large range of difference for the Baltic Proper basin in Figure 1 primarily reflects the fact that differences between the HadCM2 and ECHAM4/OPYC3 transient scenarios are largest in the south as one nears Central Europe. Future impact studies will focus on increasing the representation of climate variability in the interface between climate models and impact models.

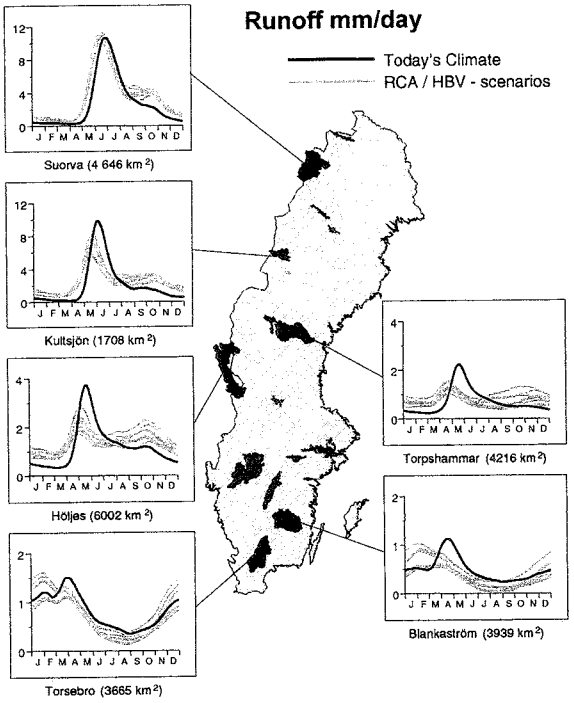

Figure 2: Modelled average seasonal river runoff to six Swedish basins for present and future conditions. The observational database used is for 1967-1997.

References

Bergström, S., Carlsson, B., Gardelin, M., Lindström, G., Pettersson, A. and Rummukainen, M., 2001. Climate change impacts on runoff in Sweden - assessments by global climate models, dynamical downscaling and hydrological modelling. *Climate Research* 16, 101-112.

Gardelin, M., Bergström, S., Carlsson, B., Graham, L.P. and Lindström, G., 2001. Climate Change and Water Resources in Sweden - Analysis of Uncertainties. In: M. Beniston (ed.), *Climatic Change: Implications for the Hydrological Cycle and for Water Management.* Advances in Global Change Research. Kluwer Academic Publishers, Dordrecht, (accepted).

Graham, L.P., 1999. Modeling runoff to the Baltic Sea. *Ambio* 28, 328-334.

Graham, L.P. and Jacob, D., 2000. Using large-scale hydrologic modeling to review runoff generation processes in GCM climate models. *Meteorol. Z.* 9, 49-57.

Graham, L.P., Rummukainen, M., Gardelin, M. and Bergström, S., 2001. Modelling Climate Change Impacts on Water Resources in the Swedish Regional Climate Modelling Programme. In: M. Brunet and D. López (eds.), *Detecting and Modelling Regional Climate Change and Associated Impacts.* Springer-Verlag, Berlin Heidelberg New York, (in press).

Mitchell, J.F.B. and Johns, T.C., 1997. On modification of global warming by sulphate aerosols. *J. Climate* 10, 245-267.

Roeckner, E., Bengtsson, L., Feichter, J., Lelieveld, J. and Rodhe, H., 1998. *Transient climate change simulations with a coupled atmosphere-ocean GCM including the tropospheric sulfur cycle.* Report No. 266, Max-Planck-Institute for Meteorology, Hamburg, 48 pp.

Rummukainen, M., Bergström, S., Källén, E., Moen, L., Rodhe, J. and Tjernström, M., 2000. *SWECLIM - The First Three Years.* SMHI Reports RMK, No.94, Swedish Meteorological and Hydrological Institute, Norrköping, 87 pp.

Rummukainen, M., Räisänen, J., Bringfelt, B., Ullerstig, A., Omstedt, A., Willén, U., Hansson, U. and Jones, C., 2001. A regional climate model for northern Europe: model description and results from the downscaling of two GCM control simulations. *Clim. Dynamics* 17, 339-359.

A Swedish perspective on recent wet years in the Baltic basin

Sten Bergström and Göran Lindström

Swedish Meteorological and Hydrological Institute, SE-601 76 Norrköping, Sweden

1. Introduction

The last 15 years have been remarkable in Sweden and Norway with extraordinary production of hydroelectric power and several floods. In fact the year 2000 turned out to be one of the wettest on record in Sweden with three spectacular flood events and one of he most extensive rescue actions ever performed in connection to inundations - the flood in Arvika. The Baltic perspective is even more dramatic. The year 1997, with the flooding of River Odra, stands out as the one with the greatest flood disaster in modern times in the area.

In Sweden the need for a balanced perspective on the recent years has become obvious as speculations and questions on long-term river flow, flood risks and climate change are growing. This has led to the initiation of the Swedish project "Long term water balance" financed jointly by the hydropower industry through its research organisation ELFORSK and the Swedish dam safety authority hosted by Svenska Kraftnät. The project is run by the research unit of SMHI.

2. Mean annual river flow

The work within the project "Long term water balance" has concentrated on quality control and joint analysis of the longest runoff records in Sweden. Figure 1 shows sums of the mean annual river flow in 8 of the main rivers in the northern parts of Sweden (Torneälven, Luleälven, Skellefteälven, Vindelälven, Ångermanälven, Indalsälven, Ljungan and Dalälven) and 3 from the southern parts (Göta Älv, Motala Ström and the outlet of Lake Mälaren in Stockholm). It confirms that the recent years have been wet, although the trends are far from dramatic in a 100-year perspective. Figure 2 shows the longest runoff records of the Swedish archives, River Dalälven, River Motala Ström and the outlet of Lake Vänern. As can be seen, most signs of increasing trends disappear, when we look back as far as to the beginning of the 19th century, as is the case for Lake Vänern. There must have been some spectacular floods in the 19th century and at least the one in 1860 is relatively well documented.

3. Extremes

Due to effects of river regulation it is not feasible to use the above records for analyses of extreme peak flows in more detail. Therefore a new set of smaller basins, not effected by reservoirs, has been selected. A yearly flood index has been defined as the average for these basins of the relation between peak flow and average peak flow for each year. This gives a joint picture of the severity as concerns floods. The index has been computed separately for spring floods, dominated by snowmelt, and summer and autumn floods, where rainfall dominates as flood generating process.

Analysis shows that spring flood severity seems to be fairly stable for the 31 selected stations in northern Sweden although the year 1995 is outstanding with the spring flood of the century. The summer and autumn flood index for northern Sweden shows a lot more variation. This is really interesting, as these floods are very significant for the safety of dams and risks of downstream flooding. They often occur when the reservoirs are full and the spillways have to be activated. A short-term increasing trend from the late 1960s may explain some of the debate on increasing flood problems in regulated rivers. This period started when we had a fully developed hydropower system in the country. Thus the pressure on hydropower operators as concerns flood management has increased drastically.

For southern Sweden the long term flood index does not show any tendency to increase. The worst year is 1951 but a few autumns in the 1910s and 1920s are also very wet.

4. Inflow to the Baltic Sea

Thanks to the recent work on the HELCOM Fourth Periodic Assessment of the environmental state of the Baltic Sea it has been possible to update the database on river flow to the Baltic Sea until 1998. The wetness of the recent years may be distinguished also in these data, although not as pronounced as in northern Scandinavia. 1998 was the second wettest year in this record, but it has to be remembered that the number of rivers in this database is small before 1950. The inflow figure for the highest year on record, 1924, is therefore rather uncertain.

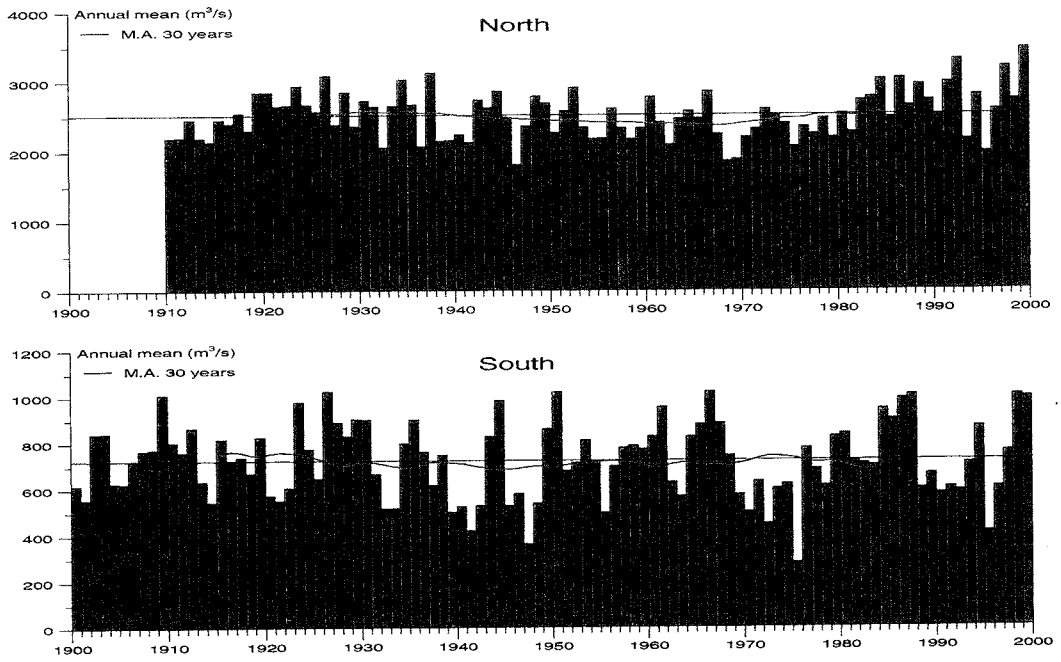

Figure 1: Time series of sums of mean annual flow for 8 rives in northern Sweden (upper) and 3 rivers in the south (lower).

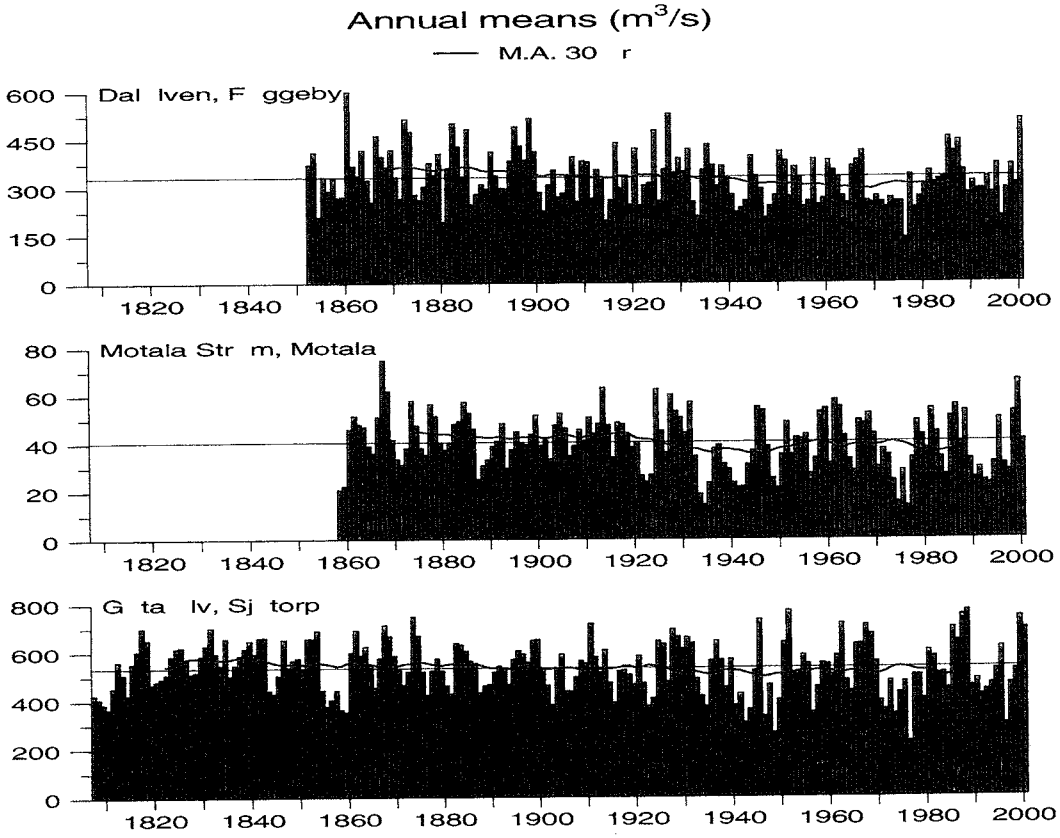

Figure 2: The longest Swedish records of mean annual river flow. Motala is the outlet of Lake Vättern and the observations at Sjötorp are representative for the outlet of Lake Vänern.

Energy and Water cycle components over a heterogeneous land surface: Status and Results from LITFASS

Frank Beyrich [1,*], Henk deBruin [2], Horst Lohse [3], Sieghard H. Richter [1], and Ulrich Weisensee [1]

[1] Deutscher Wetterdienst, Meteorologisches Observatorium Lindenberg, D-15864 Lindenberg
[2] Wageningen University, Meteorology and Air Quality Group, NL-6701 AP Wageningen
[3] GKSS Forschungszentrum Geesthacht, Institut für Atmosphärenphysik, D-21502 Geesthacht
[*)] email-adress: frank.beyrich@dwd.de

1. Background

Climate and numerical weather prediction models are more and more developing towards a simulation of mesoscale structures and phenomena. This is associated with a reduction in the size of the horizontal grid cell, with an increased vertical resolution, especially in the boundary layer, and with the use of more detailed physical parameterization schemes. Models thus become more sensitive to a proper description of the land surface - atmosphere interaction processes forming their lower boundary condition. In particular, parameterization schemes have to consider the subgrid-scale heterogeneity of the land surface which is typical for large parts of Europe. The German Weather Service (DWD) currently runs a research project (LITFASS = **L**indenberg **I**nhomogeneous **T**errain - **F**luxes between **A**tmosphere and **S**urface: a Long-term **S**tudy') in order to develop and to test a strategy for the determination of the area-averaged turbulent fluxes of heat, momentum, and water vapour over a heterogeneous landscape. The fluxes shall be representative for a horizontal scale of about 10 km (while the typical patch scale is between 10^2 to 10^3 m).
LITFASS consists of three components:

- the development of an LES-type non-hydrostatic micro-α-scale model (the LITFASS local model - LLM) with a grid resolution of 100 m driven from observations,
- experimental investigations of land surface - atmosphere exchange processes and boundary layer structure within a 20 x 20 km^2 area around the Meteorological Observatory Lindenberg (MOL),
- operation of a data base as an interface between measurement and modeling activities.

The landuse in the LITFASS area is characterized by about 46 % of agricultural farmland and meadows, 42 % of forest, and 7 % of open water (lakes), the rest goes on settlements (4 %) and others (1%). Such kind of landscape is typical for large parts of the southern BALTEX region.
The measurement strategy includes i.a. the operation of

- a wind profiler / RASS, a sodar / RASS and a microwave radiometer profiler for continuous profile measurements of wind, temperature and humidity,
- a special boundary layer field site (with a 99 m tower),
- micrometeorological stations (energy budget stations - EBS) over different types of landuse in the area,
- a large-aperture scintillometer (LAS) over a path of 4.7 km allowing to estimate the area-averaged sensible heat flux during daytime,
- a precipitation (up to 15 sites) and global radiation (up to 5 sites) network

2. Status of LITFASS

The overall project strategy has been tested over a three weeks period in June 1998 during the LITFASS-98 field experiment. Different techniques including eddy-correlation and profile measurements, different types of scintillometers, budget methods, and airborne flux measurements have been employed in order to determine the turbulent fluxes both locally over different types of landuse (grassland, agricultural land, forest, lake) and as area representative values. In the meantime, major parts of the LITFASS measurement strategy have been set into permanent operation, an overview on the status of the LITFASS related components of the MOL measurement program since the beginning of BALTEX-BRIDGE is shown in Figure 1.

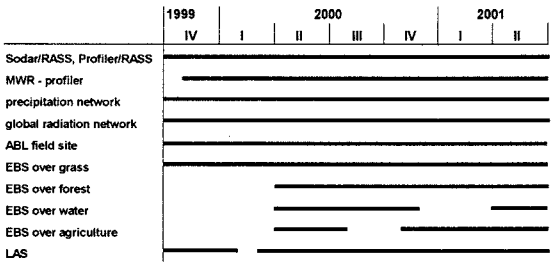

Figure 1: Overview on measurements in the Lindenberg area related to LITFASS and BALTEX – BRIDGE.

3. Selected Results

The areal distribution of rain

It is well known that large differences in the amount of precipitation can occur during certain weather situations (showers, thunderstorms) even over short distances. Such differences are of special relevance for the local forcing of the turbulent exchange processes, in particular for the partitioning of available energy between the sensible and latent heat fluxes.

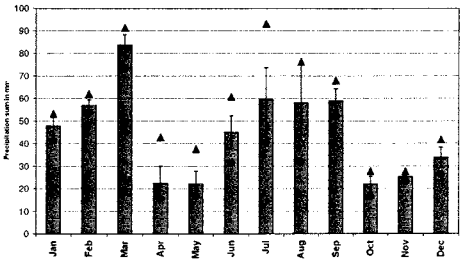

Figure 2: Variability of monthly precipitation in the LITFASS area over the year 2000: arithmetic mean, standard deviation, maximum and minimum values.

Considerable differences across the LITFASS area have been found in the precipitation sum even over longer time scales (months, year, see Figure 2).They easily amount to a factor of two for monthly values in summer, and even the total annual precipitation differs by about 15 % between the sites in the area.

LITFASS-98

The diurnal cycle of the sensible heat flux as derived from local eddy correlation or profile measurements over different types of landuse in the LITFASS area on June 04, 1998, is shown in Figure 3.

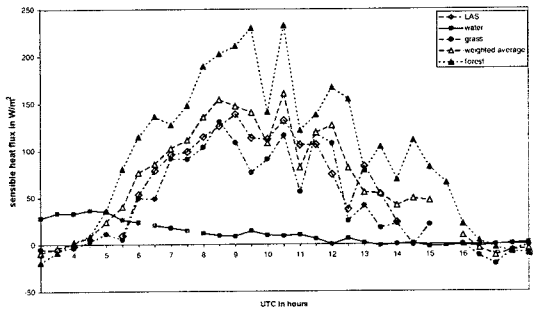

Figure 3: Daytime evolution of the sensible heat flux in the LITFASS area on June 04, 1998.

Highest heat fluxes have been usually found over the forest. Minor differences were observed between the different types of low vegetation. The heat flux over the lake is determined by the thermal inertia of the water which was warmer than the air over large periods of the experiment. An area-representative heat flux has been estimated by computing a landuse-weighted average of the fluxes over forest, grassland and water. For daytime conditions, the resulting heat flux has been compared with the sensible heat flux estimated from the LAS measurements. Reasonable agreement has been found indicating the tile approach to be a feasible concept for heat flux averaging in the LITFASS area.

A winter day

Remarkable differences in the local energy budget over different types of vegetation can be observed during winter under conditions of partial / temporal snow cover. This is illustrated in Figure 4, showing the diurnal cycle of single components of the energy budget over grass and over forest, respectively, on January 23, 2000. A thin snow cover was present on that day at the fields, while the snow from the trees had already disappeared. Global radiation on that clear day did reach a maximum of between 300 and 350 W/m^2. Over grass, the albedo was high resulting in a negative net radiation and in a downward heat flux, consequently. On contrary, low albedo over the forest resulted in a positive net radiation, and there was enough energy available to initiate an upward heat flux of about 50 to 60 W/m^2. The question arises, what area-averaged flux will result from these local flux contributions of different sign. The LAS measurements gave a value of about 30 W/m^2 around noon.

4. Conclusions and Perspectives

The LITFASS experimental strategy has been proven to provide valuable data on land surface - atmosphere interaction processes over heterogeneous terrain. Basic components of the measurement program will be continued during the whole period of BALTEX - BRIDGE

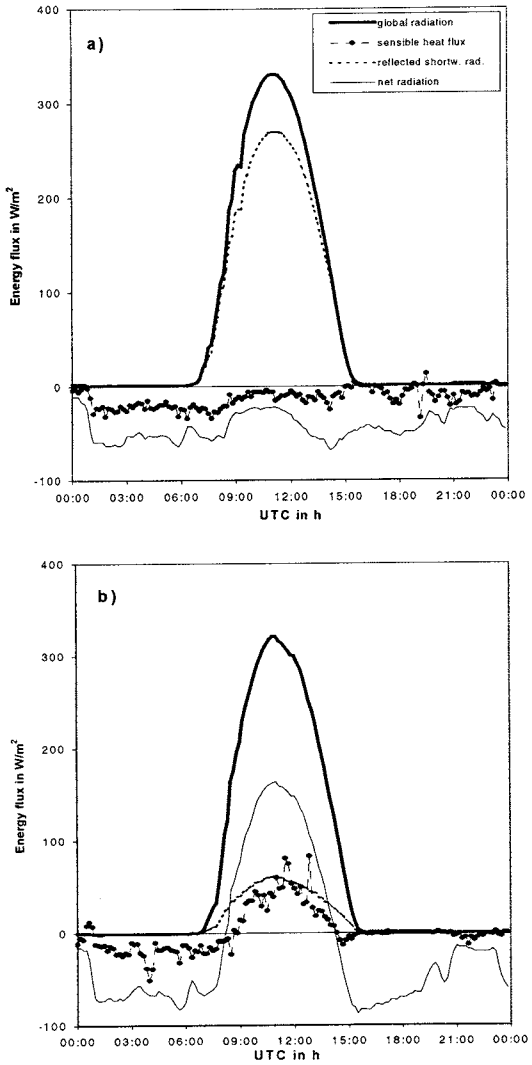

Figure 4: Diurnal cycle of selected components of the energy and radiation budget over grass (a) and over forest (b) on January 23, 2000.

and during GEWEX - CEOP. Harmonization of the measurement program, data quality control, and data formats between different sites in Europe (Sodankylä, Marsta-Norunda, Cabauw, Valladolid) running similar measurements programs is under discussion. Data are collected in order to study the local flux differences and the formation of area-averaged fluxes for a variety of weather conditions and on seasonal time scales. The LLM will, in addition, be used to compute the area averaged turbulent fluxes and boundary layer characteristics and to investigate the possible contribution from mesoscale circulations or the advection of turbulence. Results from both the measurements and the LLM simulations serve to validate and to improve the boundary layer parameterization scheme in the operational NWP models.

Climate Monitoring Using GPS: Statistical analysis in space and time of the Estimated Amounts of Water Vapour from the Swedish and Finnish Permanent GPS Networks

Harald R. Bouma and Lubomir P. Gradinarsky

Chalmers Center of Astrophysics and Space Science, Onsala Space Observatory, SE-439 92 Onsala, Sweden

1. The Swedish and Finnish GPS networks

The Swedish GPS network consists of 25 stations (Fig. 1)

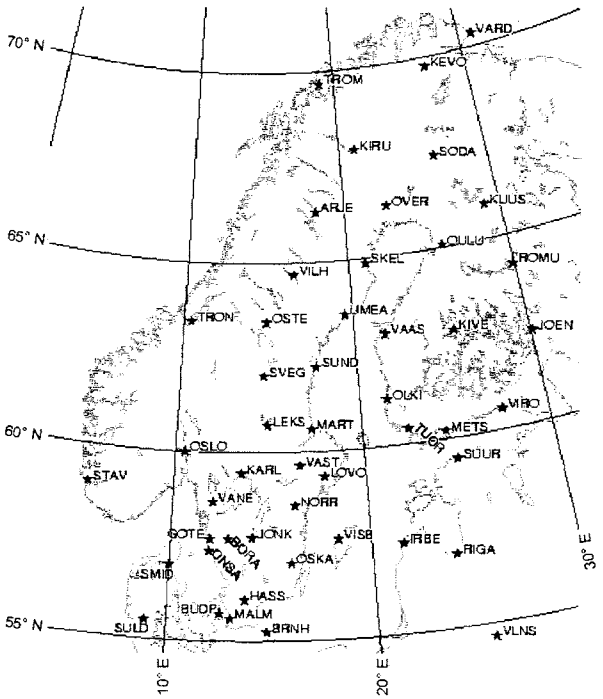

Figure 1: The Swedish (SWEPOS) and Finnish (FinnRef) permanent GPS networks.

with an average baseline length of 200 km. Most of the stations came in operation during the years of 1993 and 1994. The Finnish GPS network has 12 stations (Fig.2) and came into operation 1995–1996.

Apart from the navigation application, GPS established itself as an excellent technique for high precision (mm-level) geodetic measurements. The atmospheric water vapour introduces additional delay to the primary GPS observable – the radio wave propagation time (*Businger et al.* 1996). Precise estimation of the excess propagation delay for increased geodetic precision introduced an additional GPS application, namely the remote sensing of the atmospheric water vapour. The total delay can be divided into a hydrostatic (dry) term mainly caused by the dry gases in the atmosphere and a wet term caused by the refractivity due to water vapour. GPS measurements provide estimates of the total delay comprising both terms.

By using ground based pressure measurements, an accurate estimate of the hydrostatic delay term can be obtained. Subtracting the hydrostatic delay component from the estimated total delay gives the wet delay estimate, from which we are able to infer the integrated water vapour content. In the data processing of both networks estimates of the integrated water vapour content are updated every five minutes.

2. Methods and Results

Time series analysis in order to identify possible trends in the amounts of water vapour has been performed. To model also the annual variations we used a 4 parameter model, having an initial offset parameter, a trend and 2 annual terms (amplitude and phase). Comparing our results with the results of radiosonde (RS) and radiometer (WVR) technique *Elgered* (1998), the trend from the GPS measurements was in good agreement (Table 1).

Table 1: Trends in integrated water vapour for three different techniques at the Onsala site, Sweden

Site	Onsala		
Technique	RS	WVR	GPS
Trend mm/year	0.28	0.24	0.28

Preliminary results of the spatial analysis show a positive trend for the southern part of Sweden and Finland while in the north we see indications that the trend is negative. This analysis is done over a time period 1996-2001. Looking at a longer time period (1994-2001) the trend is positive over the whole of Sweden. For this time period too few data are available from the Finnish network.

References

Businger, S., S. R. Chiswell, M. Bevis, J. Duan, R. A. Anthes, C. Rocken, R. H. Ware, M. Exner, T. VanHove, and F. S. Solheim, The Promise of GPS in Atmospheric Monitoring, *Bull. Amer. Meteor. Soc.*, Vol.77, No.1, 1996

Elgered, G., and P. O. J. Jarlemark, Ground-based microwave radiometry and long-term observations of atmospheric water vapour, *Radio Sci.*, Vol.33, No.3, 707-717, 1998

Land-surface parameterizations in northern regions: preliminary results from the PILPS 2e model intercomparison

Laura Bowling, Dennis Lettenmaier and Phil Graham

[1] University of Washington, Department of Civil and Environmental Engineering, Box 352700, Seattle, WA, USA, 98125

[2] Rossby Centre, Swedish Meteorological and Hydrological Institute, SE-601, 76 Norrköping, Sweden

1. Background

The potential sensitivity of land-atmospheric interactions to projected climate warming at high latitudes has motivated improvements to parameterizations of cold region processes in land surface schemes used in numerical weather prediction and climate models. Phase 1 of the PILPS (Project for Intercomparison of Land surface Parameterization Schemes) Experiment 2e (PILPS-2e) was designed to evaluate the performance of uncoupled land surface parameterizations in high latitudes, in a context that allows evaluation of their ability to capture key processes spatially. The Arctic Climate System Study (ACSYS) and the Global Energy and Water balance Experiment (GEWEX) Hydrometeorological Panel (GHP) are sponsoring the model intercomparison under the direction of PILPS. Data exchange protocols and quality control were coordinated with the Assistance for Land Surface Modelers (ALMA) program, a newly initiated project which is part of the GEWEX Global Land Atmosphere System Study (GLASS).

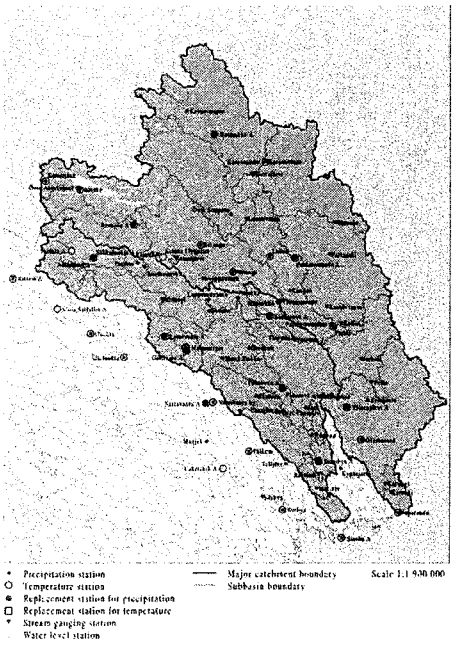

Figure 1: Location map for the Torne and Kalix Rivers.

2. Experiment Design

The Torne/Kalix River system in northern Scandinavia was selected for the first stage of the project (Figure 1). As part of the BALTEX domain, the Torne/Kalix is a small, well-instrumented catchment in comparison with the larger, less well-instrumented north flowing rivers, while still exhibiting
the unique 'northern' features of interest. The 58,000 km^2 basin is represented by 218 grid boxes at 1/4 degree spatial resolution for the ten-year period 1989-1998. Participants were asked to calibrate their models to observed streamflow for two small sub-catchments, prior to running models over the entire domain. Streamflow at the basin mouth(s) was not provided.

Radiative and moisture fluxes were constructed from station data provided by the Swedish Meteorological and Hydrological Institute (SMHI), as follows:

- Precipitation and temperature were gridded from station data, after accounting for elevation and gauge undercatch;
- Pressure, specific humidity and cloud cover were interpolated from 1° SMHI dataset optimally interpolated from station data; and
- Longwave radiation was estimated using observed cloud cover and temperature.
- Shortwave transmissivity was originally estimated using the Tennessee Valley Authority (1972) method. Subsequent analysis indicated that this resulted in a low bias and transmissivity was estimated from point station data for the model re-runs.

Daily wind velocities were taken from the NCEP/NCAR reanalysis surface wind fields.

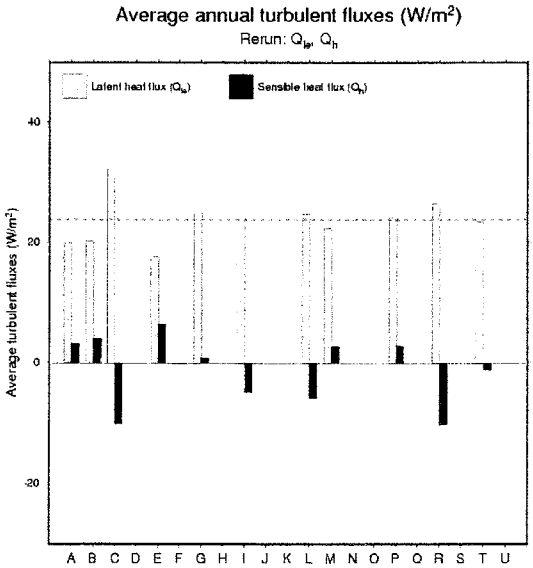

Figure 2: Annual average sensible and latent heat fluxes for the PILPs 2e model reruns.

3. Preliminary Results

Twenty-one models participated in the original intercomparison, and 12 models have currently completed the re-runs. As shown in Figure 2, net radiation for all models is very low for this high latitude domain, varying

between 15 and 28 W/m^2. Most models cluster within a few
W/m^2 of the 23 W/m^2 estimated from the annual water balance. The high outliers correspond with models with high values of sublimation.

Sublimation from the snow pack explains much of the underprediction of annual runoff exhibited by models 'C', 'E' and 'R' in Figure 3. Figure 3 also indicates that increases in the quantity of snow meltwater that infiltrates into the ground or is captured by lake storage, increases the ratio of subsurface to surface runoff, but has little effect on annual runoff volume.

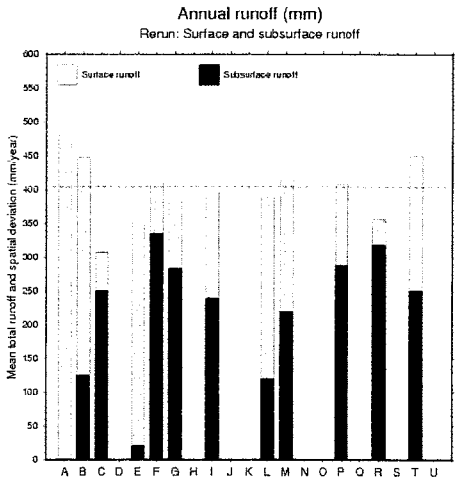

Figure 3: Annual average surface and subsurface runoff for the PILPs 2e reruns.

4. Conclusions

The preliminary results from the PILPS 2e experiment indicate the following:

- Limited net radiation in this high latitude environment provides a lower bound on runoff generation. Although seasonal runoff is dominated by snowmelt, annual runoff volume is controlled in large part by sublimation.
- An increase in net radiation, as supplied by a re-estimate of the incoming solar radiation, results in relatively larger changes in sensible heat than latent heat.
- Hydrologic parameters that effect storage (either through calibration or changes to model structure) primarily change runoff timing, not volume.

References

TVA, 1972. Heat and mass transfer between a water surface and the atmopshere. Water Resources Report No. 0-6803 14. Tennessess Valley Authority.

Winter field campaign BASIS / BALTIMOS over the Bay of Bothnia

Burghard Brümmer[1], Gerd Müller[1], David Schröder[1], and Timo Vihma[2]

[1] Meteorological Instiute, University of Hamburg, Bundesstrasse 55, D-20146 Hamburg, Germany
[2] Finnish Instiute of Marine Research, P.O. Box 33, FIN-00931 Helsinki, Finland

As part of the BALTEX-BRIDGE field phase, the joint Finnish/German field campaign BASIS/BALTIMOS took place over the northern, ice-covered part of the Bay of Bothnia during the period 12-23 February 2001 (BASIS = Baltex Air Sea Ice Study; BALTIMOS = Baltex Integrated Model System). The main objective of the field campaign was to collect an atmosphere-ice-ocean data set in order to study the interaction processes between these three media and to validate the integrated model system BALTIMOS. The main focus will be on the turbulent fluxes of heat, moisture and momentum under different ice conditions and on the structure of the atmospheric boundary layer and the interaction between temperature inversion and low-level jet.

Four kinds of platforms were involved (see Figure 1). The Finnish research vessel Aranda was positioned in the land-fast ice at 65.52°N, 24.56°E where regular measurements of sea ice properties, turbulent and radiation fluxes in the atmospheric surface layer, and radiosondes were made. A surface station was installed (on land-fast ice) about 200 m off the coast of the island of Hailuoto close to the village of Marjaniemi (65.03°N, 24.56°E). Here, also turbulent and radiation fluxes in the atmospheric surface layer were measured, as well as precipitation and cloud base height. In order to monitor mesoscale fields of pressure, wind, temperature and humidity, two automatic surface stations which transmitted the data via the ARGOS satellite system were deployed at the tips of the Peninsulas close to Kuivaniemi (65.55°N, 24.12°E) and Haparanda Hamn (65.76°N, 23.93°E). In and beyond the area of the four surface stations, the German research aircraft DO-128 performed in total ten flight missions in the atmospheric boundary layer between 10 m and 2000 m height. The aircraft operated from the airport Oulu.

Ice conditions in the Bay of Bothnia were characterized by an about 20 km broad stripe of land-fast ice around the northern coast and by drift ice of different concentration and thickness in the interior which was shifted depending on the wind direction between Finland and Sweden. Weather conditions were very variable due to frequent passages of synoptic weather systems. The air temperature ranged from + 4°C to - 25°C and the surface layer wind from 1 to 15 m/s. The surface layer was predominantly stably stratified. The boundary layer was shallow; often a surface-based or slightly elevated inversion was present. A low level jet was typical phenomenon of the stable boundary layer. As an extremum a low-level jet of 27 m/s was observed at 200 m height.

Taken together, the measurements during BASIS/BALTIMOS were very successful and covered a wide range of the atmospheric parameter space. They are a continuation of the field campaign BASIS 1998 and represent a unique data set for process studies and model validation. First results on the turbulent fluxes for different ice conditions and on the wind structure in the atmospheric boundary layer are presented.

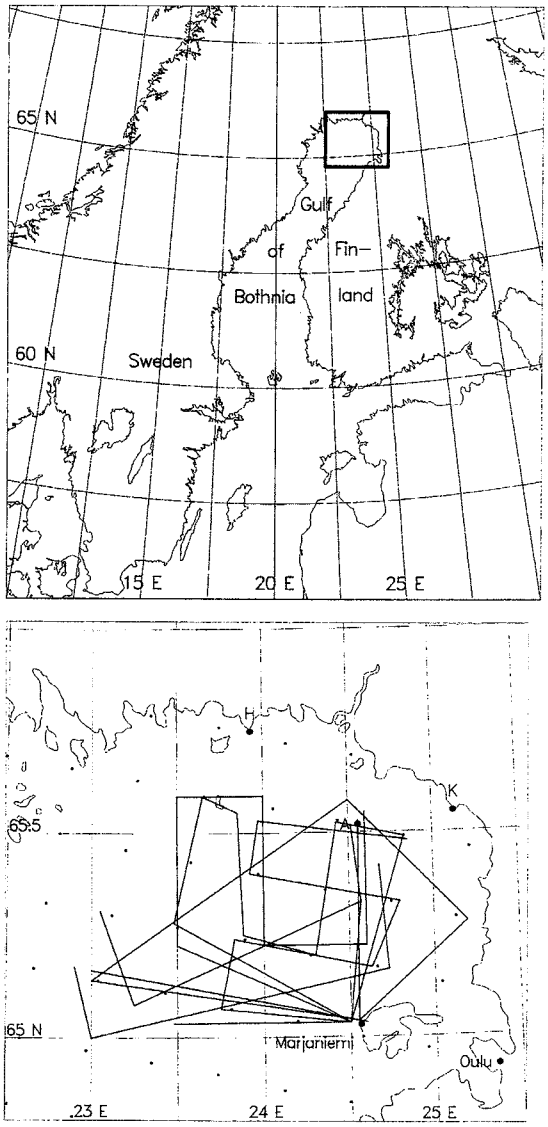

Figure 1: Experimental area of BASIS/BALTIMOS in the Gulf of Bothnia (top). Experimental area in detail (bottom) with locations of research ice-breaker Aranda (A), surface station Marjaniemi, automatic Argos stations at Kuivaniemi (K), and Haparanda Hamn (H), airport Oulu and flight patterns of the ten aircraft missions

The Flood Events on the Daugava River

Mira Butina and Irena Nikolushkina

Latvian Hydrometeorological Agency, 165, Maskavas str., Riga, LV-1019 Latvia, e-mail: hydro.fcst@meteo.lv

1. Introduction

Floods are among the few natural disasters Latvia has been exposed to. Flood risks in Latvia are related to a combination of spring flood and ice jamming. Flood-risk areas are middle sections of the main Latvian rivers, Daugava and Lielupe, and downstream sections of the Daugava's tributaries, Aiviekste and Ogre. Downstream of rivers which inflow the sea, the critical water level may be caused by spring flood, ice jams, as well as wind-induced surges.

2. Hydrological regime of the Daugava River

Daugava River is the largest river in Latvia and one of the largest international rivers in the Baltic region (Fig.1). Its drainage basin stretches from the Valday Massive, Russia, to the Gulf of Riga (Ziverts and Jauja 1998). The total area covered by the Daugava's basin exceeds 87,900 km2, with 24,700 km2 in the territory of Latvia. The Daugava is the most important river in Latvia with respect to hydropower production, water supply, and fishery. In the upper and middle parts, the river is not regulated. The lower parts of the river basin are well regulated: there are three hydropower stations close to the mouth of the Daugava River.

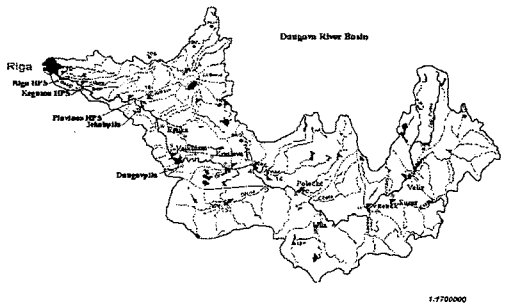

Figure 1: The basin of Daugava River

The proximity of the Atlantic Ocean determines the climatic conditions, moderately mild and moist. The Latvian rivers have a hydrological regime typical of the most Eastern-European rivers: a relatively high and fast spring flood and relatively low summer and winter runoff. Rains may cause increase of runoff during summer and autumn and thaws - in winter. Approximately 50% of annual runoff in Daugava River are formed in the period of the spring flood that is formed mainly by water reserves in snow. The spring snowmelt begins mostly in March and the maximum flood level usually is observed in the middle of April. Spring flood lasts 60 days on average.

High spring flow usually is formed after a long cold winter with abundant snow. Largest ice jams and critical water levels occur in spring with an abrupt increase in air temperature and snow melt with rainfall. Ice and slush jams with extremely high water level are recorded during warm winters with unstable ice cover as well.

3. Floods risk areas on the Daugava River

Flood-risk areas on the Daugava River are a section between the cities of Plavinas and Daugavpils and Daugava's tributaries Aiviekste and Ogre.

The Daugava River near Jekabpils is a 'hydrological hot spot' (Fig.2).

The hydrological observations in the river near Jekabpils (catchment area of 70,500 km^2) started in 1907. Annual mean discharge is 515 m^3/s near Jekabpils and 678 m^3/s in the river mouth. The mean duration of ice cover is 97 days. The mean date of ice-cover formation is the 20th of December and the mean date of the ice break-up is the 30th of March.

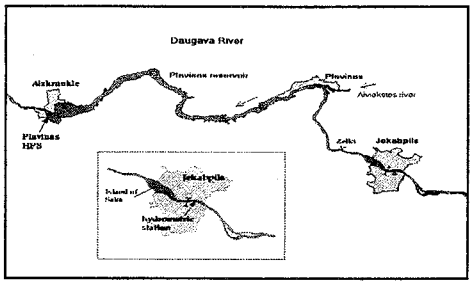

Figure 2: Scheme of Daugava near Plavinas HPS

The Plavinas Hydropower Station was constructed in 1965. It is situated some 149 km from the Daugava's mouth. The Plavinas reservoir of a length of 57 km and a maximum width of 3 km stretches from Aizkraukle to the Zelki village.

The HPS has changed the hydrological regime in the Daugava River:

- Before the construction of HPS these sections of river had high flow velocities and were not covered with ice during the winter months. Ice and slush jams had occurred relatively rarely during the winter-spring periods.
- After the construction of the Plavinas HPS and the reservoir, intensive accumulation of ice material and ice jams and, as a result, extremely high water levels have occurred more often than in previous years.

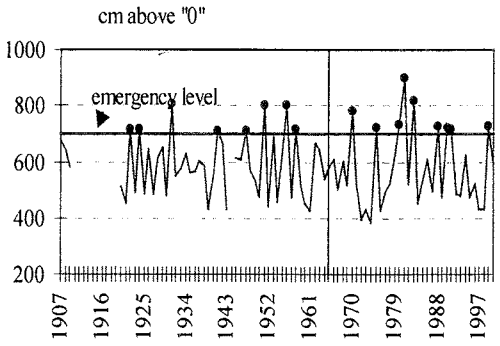

Figure 3: Maximum water level, Daugava-Jekabpils

Figure 3 demonstrates variation of maximum water level in Daugava near the city of Jekabpils during the whole period of observation. Maximum spring runoff on the Daugava River was observed in 1931. That winter was

characterised by abundant snow in the river basin. The maximum discharge was 7470 m3/s in the river near Jekabpils and 9460 m^3/s in the river mouth. The extremely high level in 1931 was caused by an intensive snow melting.

After the construction of HPS (1965), the maximum level measured 897 cm in 1981 and was caused by ice and ush jam.

What can be expected in future? Due to the changing climatic conditions on global scale, during the last two decades, winters have become warmer with frequent thaws, flood time has shifted to an earlier period and the duration of spring floods has increased (Butina at al. 1998).

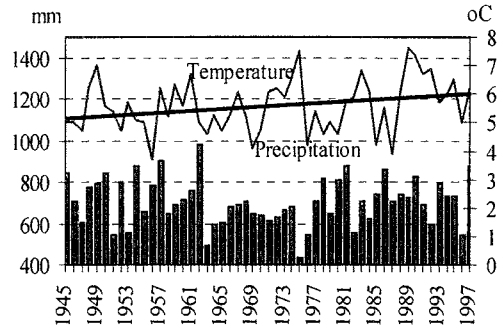

Figure 4: Mean annual temperature and precipitation. Skriveri station.

The increasing air temperature, especially in the winter season can aggravate the flood-related problems in river basins, and cause inundation of flood-risk territories (Fig.4, 5).

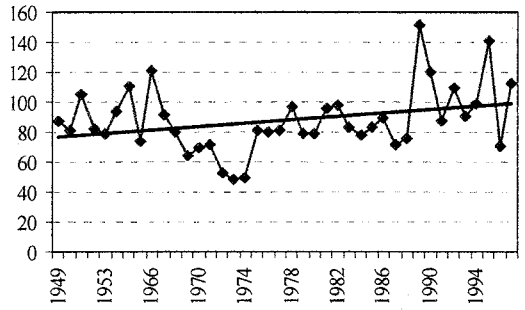

Figure 5: Duration of spring flood. Daugava-Jekabpils

To meet the challenge, a strong comprehensive flood protection strategy is needed.

4. Conclusions

Flood events and as a result inundation of lands is a significant problem in Latvia.

Flood risk is usually related to a combination of spring flood and ice jams, and downstream of rivers - to wind-induced surges as well. Due to the changing climatic conditions winters have become warmer, flood time has shifted to an earlier period and the duration of spring floods has increased. In future, climate change can aggravate flood-related problems in river basins.

Modernization of the hydrological network and the implementation of the new hydrological programs and models will allow to produce more accurate hydrological forecasts and flood warnings.

References

Butina,M., Melnikova,G. and Stikute,I., "Potential impact of climate change on the hydrological regime in Latvia", in Second Study Conference on BALTEX proceedings, Germany, pp 30-32, 1998.

Ziverts,A., Jauja,I.,"Simulation of actual evapotranspiration and runoff from the Daugava River basin". Second Study Conference on BALTEX proceedings. Germany, 250-251, 1998.

The BALTEX Hydrological Data Centre

Bengt Carlsson

Swedish Meteorological and Hydrological Institute, SE - 60176 Norrköping, Sweden

1. The BALTEX HDC

SMHI in Norrköping, Sweden, hosts the BALTEX Hydrological Data Centre. The main objective is to concentrate specific types of hydrological data and information about this data at one location. http://www.smhi.se/bhdc gives you all necessarily information about what data is available and how to receive data from the BHDC

The BHDC data base today consists of:

- **Daily runoff data** from runoff stations, Figure 1.
- **Monthly runoff data** from coast sections, Figure 2.
- **Gridded meteorological data** (1 deg. lat x 1 deg. long.) interpolated from synoptic stations, Figure 3.
- **Hydrological and meteorological data** from the special study Torne River basin and runoff data from the special study basins of the Daugava and Odra rivers.

2. Data policy

The regulations for the use of data are set through agreements between SMHI - BALTEX HDC and the providing institute, and user of the data and the SMHI - BALTEX HDC

Data delivery by the BALTEX HDC is strictly limited to groups of scientists which are officially registered as BALTEX Data Users. The delivery of data from the supplying institute will be free of charge. The distribution costs at the BALTEX HDC will be covered by the user.

3. Data management

The data collected by the BHDC is supplied mainly by the different national institutes in the countries participating in BALTEX. The structure of the daily runoff data base is identical to the one that SMHI currently uses for the Swedish national runoff network. In that way BHDC can benefit from any progress being made to the current data base structure at SMHI. Meta data and other hydrological data are stored in different data bases designed solely for these purposes. Data from the data base will be provided to BALTEX Data Users upon request.

4. Time periods of data

The Warsaw hydrology workshop suggested including daily runoff data for the period 1980 and onwards in the archives of BHDC. The Status report 2001 describes the status of the data base today.

Monthly runoff data is collected from 1950 and onwards.

Other hydrological data will be collected depending on their availability and specific requirements from the BALTEX modelling community. Most of these data are not measured routinely and are only available from specific experiments.

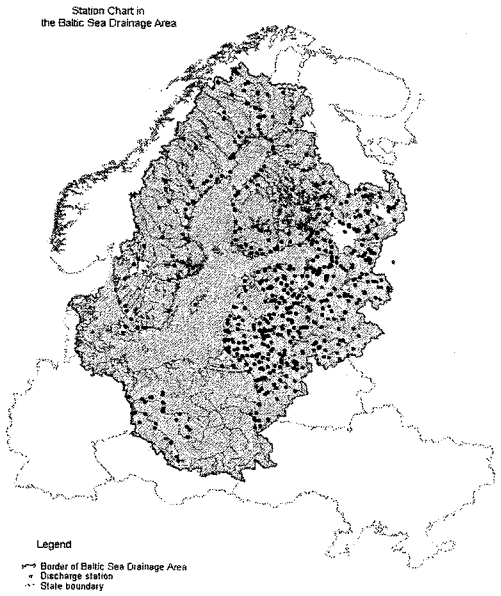

Figure 1: Daily Runoff Stations in the Baltic Sea Drainage Basin

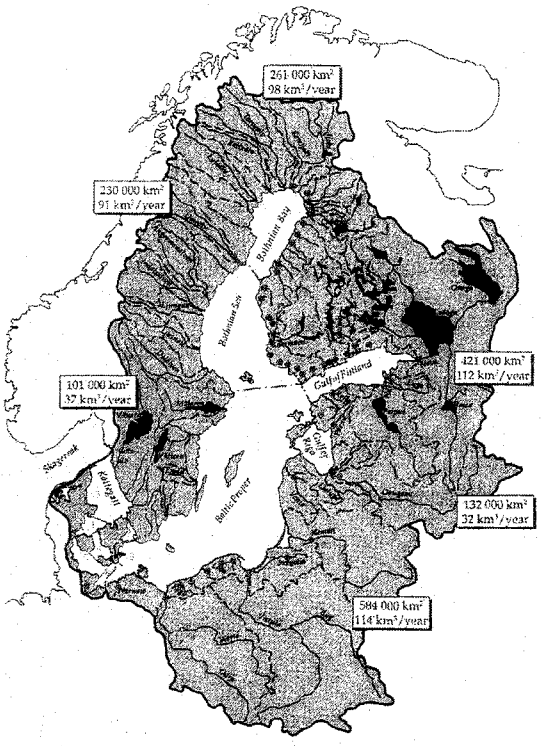

Figure 2: . Monthly runoff from Finland, Russia, Estonia, Latvia, Lithuania, Poland and Germany to the Baltic Sea are calculated from measurements at the stations near the coast. The stations are marked with dots in Runoff from Sweden is calculated with use of all stations near the coast (>100), and divided in 40 coast sections. The Danish calculations are made with a similar method resulting in nine sections. As a whole more then 200 stations are used and about 86% of the total area is covered by measurements.

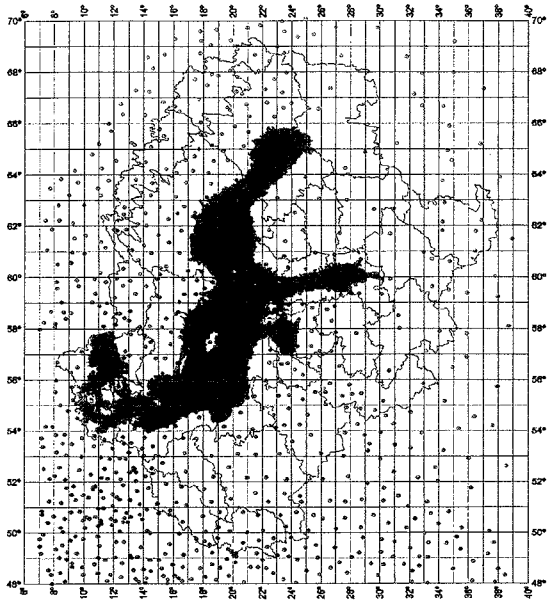

Figure 3: The synoptic meteorological data set covers the whole Baltic Sea drainage basin with a grid of (1×1)° squares. The grid extends over the area: Latitude N 49.5° - 71.5°, Longitude E 7.5° - 39.5°. Time resolution: UTC 00, 03, 06, 09, 12, 15, 18, 21. The present available time period is from 1979 to 1999. This Figure shows the synoptic stations reporting on December 1999.

Reference

Carlsson,B , Hydrological Data Centre for Baltex, Status Report 2001. Swedish Meteorological and Hydrological Institute, 2001.

Floods in the Pripyat transboundary river basins

Grigory Chekan[1], Alexander Stankevich[2]

[1] State Committee on Hydrometeorology of the Republic of Belarus
[2] Central Research Institute for Complex Development of Water Resources
(The Ministry of Natural Resources and Environmental Protection of the Republic of Belarus)

The river Pripyat is one of the most lengthy and water river of the Republic of Belarus. Length of the river is about 761 km, catchment area is about 121000 km^2. Pripyat and its tributaries flow through the territories of Belarus and Ukraine. Catchment area including main tributaries which related to Belarus territory is about 51370 km^2 which include more then 25% from whole territory of country. In Pripyat river basin took place 12 severe floods for last 50 years which were resulting in huge damages. Tacking into account intensification of economic activity, the extension of the list of embankments and melioration activities the tendency of magnification of damages from flooding is increase. In the modern scientific literature the paradoxical fact are observe - together with investments activities in construction of dams and other structures is observed the magnification of damage from floods. For variation of this tendency a scientists offers to reconsider approaches to a problem of floods and the main idea is to find a means to search of ways to adaptation to flood, but not protection against them [1].

The inventory of modern situation with floods regulation in USA demonstrates that the center of gravity in floods control was displaced from engineering activities to not engineering: forecasting of floods on the basis of the improved computer method of modeling, creation of early warning notification systems, good economic policy on flooded grounds tacking into account a factor of the damage from floods is minimum.

All given facts allow to make a conclusion that at the present stage for decreasing of damage from floods it is necessary to point major attention to creation of the floods forecasting systems.

The river Pripyat and its tributaries are characterized by the extremely unfavorable hydrological regime. Floods took place in average about 9 times per 10 years.

More then 800 water objects exist to the catchment area of the Pripyat river basin. Greatest of them: Stochod, Styr, Pina, Iaselda, Bobryk, Lan, Goryn, Cna, Ubort, Ptich. Some tributaries have comparable water discharges with river Pripyat in the separate moments. It conclusion essentially related to Goryn, peak discharge of a catastrophic flood of 1% of probability of excess constitutes 3167 m^3/s.

Twenty years ago the realization of the projects on Pripyat and its tributaries high-water bed protection was began. By 1998 approximately 50 % of this project was made. 1166 km of dams were projected. 517 km are constructed approximately. Basically These dams are constructed in upper and mid part of the river Pripyat.

However all these activities could not completely solve the problem of protection a territories and populations from submergence. The damage from flooding which took place in the of 1993 has estimated about 100 million US dollars (base on official information which Republic of Belarus are presented in UN). The submergence have repeated in February - March 1994 once again. The most damages from flood also was observed in 1998, specially in Gytckovichy region. In 1999 y high levels of water in flat bed was observed in the river Pripyat and its tributaries.

State Committee on Hydrometeorology of the Republic of Belarus make regular observations of water levels and water discharges in base points of the river Pripyat and its tributaries.

The observing data's exchange is realized with the Ukrainian party for left tributaries which basically situated in the territory of Ukraine - Stochod, Styr, Goryn, Slovechna etc. (see the figure below)

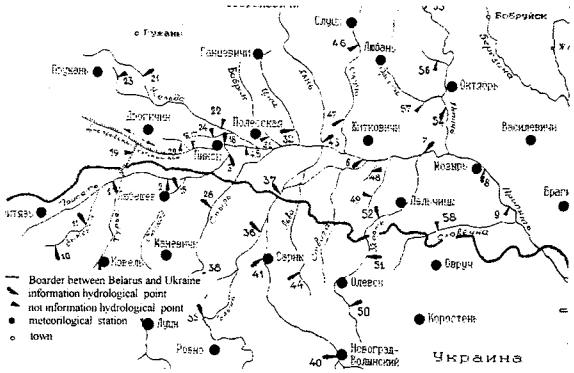

State Committee on Hydrometeorology of the Republic of Belarus has developed the prognosis of maximum levels of a Spring flood annually. The method of application of the prognostic maximum water levels calculation for stationary observation stations is founded on the information which include:

1. Data's about maximum water levels (discharges) of spring flood for the previous years of observation.
2. The data's about an air temperature regime and precipitation's which have received from hydro-meteorological stations and observations posts which are situated in Pripyat river basin and near to its borders.
3. Data's about a snow depth.
4. Data's about a depth of ground freezing.
5. Data's about relative moisture of an air.

On the basis of this data's and a method of water balance the prognostic functional characteristics for maximum water levels are defined [2,3]. The long-term and short-term methods forecasts of maximum levels of the river Pripyat and its tributaries has developed also. In accordance with accruing of the current operating information about a regime of flood clarification of parameters prognostic dependence's and the prognosis have updated.

Amount of stationary point of observation in the Pripyat river basin is limited. Four regions of cities Pinsk, Gytkovichy, Stolyn, Luninec are situated on site with length about 186 km between points observation of the cities Pinsk and Chernichy. Regular submergence take place in these regions. On the basis of financial problems at present time it is impossible to open a additional

stationary hydrological points of observations in these regions.

At the same time, for the purposes of operational monitoring and forecasting of flood zones the knowledge of water levels of the river Pripyat is necessary with a step on length in some km.

For a decision of this problem it is proposed to use a mathematical model of unsteady movement of the flooding surge in the water streams systems of the river Pripyat [4]. This model is founded on a decision of the generalized equations such as Sean-Venan which one take into account features of the movement of water deluge at an exit on flood bed.

The given approach to modeling of movement of water stream on floodplain is significant for the river Pripyat because the river has small underwater and stream gradient. At passing of the flood-float on a floodplain she is flooded on a large distance from river bed.

Data's which necessary for this mathematical model of movement of water in the system of the Pripyat river basin water streams there are observed water discharges and (or) water levels in a boundary points of system, which one coincide with stationary points of observations of the State Committee on Hydrometeorology.

The model allow to determine calculated water discharges and water levels for all given points of the river Pripyat and its basic tributaries.

For executing an error estimation of modeling of a water regime the calculations of the flood float for the real situation which took place in 1998 are made.

Inaccuracy of mathematical model is about 0,04 m in average and do not exceed 0,12 m for whole system of water stream of the river Pripyat. This estimation was received as a result of comparison of the calculated water levels with observed water levels received from stationary hydrological stations.

References

Kundewicz Z.W., Takeuchi K. Flood protection and management:. Quo vadimus ? // Hydrol.Sci.J. 1999 - 44. № 3 , p. 417-432

Rutkovsy P., Chekan G. Floods in Polesie-region and means of decreasing of their negative consequences. The journal of water resources. No. 6 Minsk 1999

Faschevscy B, Shulika L, Chekan G. Features of floods forming in Polesie-region and prognoses of water levels. International Conference "Modern problems of study, usage and protection of natural recourses of Polesie-region". 22-25 of September, 1998, Minsk, pp.118-119

Korneev, V., Rogunovic, V., Stankevich, A. Water regime of the river Pripyat and its tributaries at incomplete realization of the project of protection of basin from submergence. International Conference "Modern problems of study, usage and protection of natural recourses of Polesie-region". 22-25 of September, 1998, Minsk, p.120

Modelling of Superimposed Ice Formation in the Baltic Sea

Bin Cheng, Jouko Launiainen and Timo Vihma

Finnish Institute of Marine Research, P.O. Box-33 FIN-00931, Helsinki, Finland

1. Introduction

In thermodynamic sea ice models, the ice formation is usually considered as the ice bottom accretion. However, snow layered on the top of the ice may partly transfer to snow-ice due to ocean flooding or refreeze to form superimposed ice due to surface melting. This is particularly true in the Baltic Sea region where the incoming snow-fall was accounted on a average of 25-45 mm equivalent water per month from December to February. Hance the snow may contribute to some 1/3 of the total ice thickness (Leppäranta and Seinä, 1982). The first attempt to model the snow-ice formation in the Baltic Sea was made by Leppäranta (1983). A recent study of modelling the evolution of snow-ice formation in the Baltic Sea was given by Saloranta (2000). Those studies were focused on the climatological scale, i.e. the seasonal snow-ice evolution. Observations and modelling of superimposed ice formation in a synoptic scale are presented in this paper. The results indicate that the ice formation is mainly occurred at the snow ice interface via refrozen of the surface or near surface internal melting water during the ice thermal equilibrium stage. The re-freezing water originated more likely from the surface than from the ocean below.

2. Observations and the ice model

Observations were performed during the BALTEX-BASIS field campaign in the northern Baltic Sea in 1998. Observations of wind speed, air temperature and relative humidity were made from a sea ice weather mast. The 10-minute averages of these quantities served as the forcing data for the ice model. The cloudiness was observed visually every 3 hours. Downward and upward short-wave radiation and the derived surface albedo served as other important external model forcing data. A sonic anemometer was also deployed, and eddy fluxes of sensible heat and momentum were measured. The heat transfer coefficient and temperature roughness length applied to the ice model were those based on the analysis of the turbulent surface fluxes (Launiainen et al., 2001). A thermistor string with 11 sensors was deployed vertically through the snow and ice. The temperatures of near-surface air, snow, ice, and sea water near the ice bottom were measured at various levels. The thermistor string and its sensors are shown schematically in Figure 1, indicating the initial and final stages in the ice. Snow and ice thickness were measured manually once a day at 10 locations near the thermistor string. The daily means of snow thickness were interpolated linearly and used as model input. The model parameters were specified to correspond to the BASIS field characteristics. Eddy flux measurements performed in the water near the ice bottom suggested that there was, on average, a small upward heat flux during BASIS. Its small magnitude ($\approx$ 1.0 W m^{-2}) is explained by the strong water stratification below the ice.

The ice model was the one given by Launiainen and Cheng (1998) and Cheng and Launiainen (1998). The numerical integration of the vertical heat conduction equation is considered as an essential part of the model, which resembles those of Maykut and Untersteiner (1971) and Gabison (1987). The boundary conditions of the heat conduction equation are, however, well considered and specified compared with those older models. The main physical processes expressed in the model involve the air-ice coupling, heat fluxes and heat balance at the surface and the ice bottom, heat conduction in the multi-layer snow and ice, and mass balances at the surface and the bottom, for each time step.

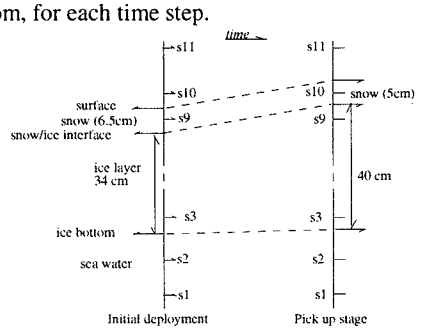

Figure 1: Geometric location of sensors attached to an ice thermistor string in the air/snow surface, snow/ice interface and ice/water. At the beginning, sensor s10 was 1.5 cm above the surface. The snow depth was 6.5 cm (3 cm soft snow + 3.5 cm hard snow) measured from the surface of the ice. The ice thickness was 34 cm. S3 was 5 cm from the ice bottom. At the end of BASIS, s10 was situated 3.5 cm below the snow surface. The snow-ice interface was 1.5 cm below s10 and the total ice thickness was 40 cm. A 4.5 cm distance in depth between s3 and the ice bottom was measured.

3. Results and discussion

The measured snow and ice and modelled ice thickness variations are given in Figure 2. The measurements of snow and ice show distinct areal and temporal variations in the test area, due to the highly variable weather during the BASIS experiment. The surface melting largely occurred when the measured air temperatures were well (2-3 °C) above freezing. Figure 2b shows the time series of the modelled surface melting, producing a cumulative snow thickness change of about 12 cm. Figure 2c gives the modelled ice growth at the ice bottom, leading to an increase in thickness of 3 cm. Figure 2d shows the simulated ice thickness compared with the measurements. Assuming the surface melt-water is totally refrozen, and the density ratio between the snow and sea ice is 0.35, the above modelled melting would correspond roughly to about 5 cm of superimposed ice formation. In practice, however, instead of immediately re-freezing, melting water percolates into the snow/ice interface and may be mixed with snow forming a slush layer, which later will be refrozen under the proper weather conditions. Such a layer of slush will affect the heat conduction and heat flux through the whole ice layer. These uncertainties may cause discrepancies between the measurements and modelling of ice temperature and ice thickness.

The ocean flooding is another source for slush layer and snow-ice formation. In general, the ocean flooding depends on the density of sea water (ρ_{sw}), sea ice (ρ_{si}), and

snow (ρ_s), as well as the depth of snow h_s and ice H_i . Assuming that $\rho_{si} \approx 0.9\ \rho_{sw}$ (Baltic Sea is almost fresh water body, since the average salinity is low), according to the Archimedes law, the criterion (ice surface start to merge below water level) for ocean flooding would be a) $h_s \geq 0.6\ H_i$ for very fresh (soft) snow, i.e. $\rho_s < 0.15\ \rho_{sw}$; b) $h_s \geq 0.2\ H_i$ for very old (hard) snow, i.e. $\rho_s < 0.5\ \rho_{sw}$. In this study, we assumed that the snow density was about $0.3\ \rho_{sw}$, and h_s should accordingly be larger than approximately $0.3\ H_i$ for ocean flooding. During BASIS experiment, in addition to the snow and ice thickness measurement, the water level was also measured from the ice holes in order to see if the snow loading was heavy enough for ocean flooding. The individual measurements indicated that there were few data with (b) satisfied and the water level simultaneous positive, i.e. water above ice surface. For most data of water level positive, the snow thickness matched neither (a) nor (b). We further looked at the weather data and found that the air temperature were above or close to zero during these water flooding measurements indicating that the water may have come due to the surface melting. The measured average snow thickness did not reach the range from $0.2\ H_i$ to $0.6\ H_i$, and the average water level was positive only for the period of days 52-54 when the air temperature was above zero. If we look at the temperature gradient (Fig. 3), the measurement and model calculation both indicated a downward heat flux during the period of these single water flooding events. This downward heat flux may be considered as a result of a warm surface, i.e. surface melting. The overall effect of ocean flooding is important in understanding sea ice thermodynamics. According to our analyses, it seems that its contribution to snow-ice formation in this study was minor.

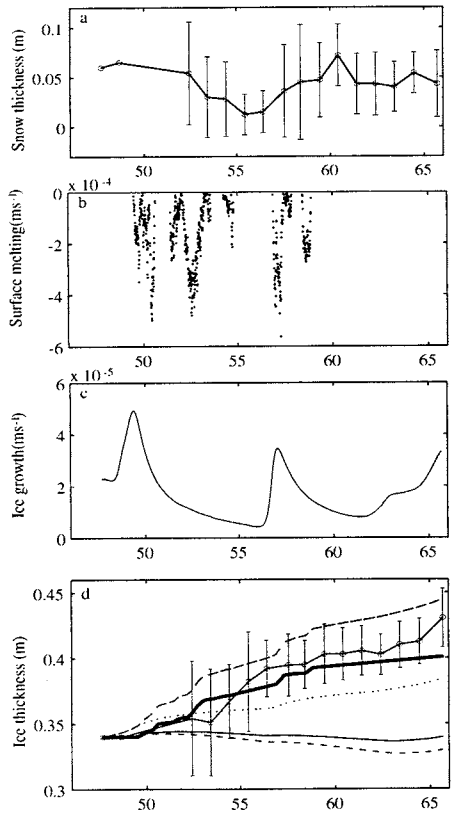

Figure 2: Observed mean snow thickness (circle-connected line) with ± standard deviation (vertical bars). b) Modelled melting rate at the surface. c) Modelled freezing at the ice bottom. d) Observed mean ice thickness (circle-connected line) with ± standard deviation (vertical bars) The dotted line gives the modelled ice growth at the bottom, and the thick line gives the ice growth solely due to snow-ice transformation. The broken line on top is the cumulative ice growth. The lowermost two lines (solid and broken) give the ice thickness variation calculated from the ice bottom heat mass balance using thermistor string temperature data with an assumed average oceanic heat flux of 1 and 2 W m^{-2}, respectively.

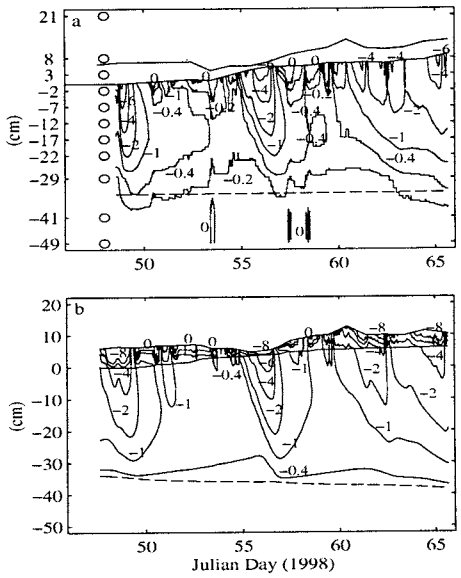

Figure 3: Intra ice temperatures (°C) during the BASIS experiment. a) Observed in-ice temperatures. Circles indicate the locations of sensors attached to the thermistor string. b) In-ice temperatures calculated by the ice model. The three horizontal lines show the average observed (a) and modelled (b) evolution of the height/depth of the snow surface, the snow/ice interface and the ice bottom.

References

Cheng, B. and J. Launiainen. A one-dimensional thermodynamic air -ice -water model: technical and algorithm description report. *MERI-Report series of the Finn. Inst. of Mari. Res.*, 37, 15-36, 1998.

Gabison R. 1987. A thermodynamic model of the formation growth and decay of first-year sea ice. *J. Glaciol.* 33(113), 105-109, 1987.

Launiainen, J., B. Cheng. J. Uotila, and T. Vihma. Turbulent surface fluxes and air-ice coupling in BASIS. *Ann. Glaciol.*, 33 in press, 2001.

Launiainen, J. and B. Cheng. Modelling of ice thermodynamics in natural water bodies. *Cold Reg. Sci. Technol.*, 27(3), 153-178, 1998.

Leppäranta. M., A growth model for black ice snow ice and snow thickness in subarctic basins. *Nordic Hydrology*, 14, 2, 59-70, 1983.

Leppäramta, M.,Seinä,A. Statistics of fast ice thickness along the finnish coast, *Finnish Mar. Res.*, 249, 62-71. 1982.

Maykut, G.A. and N. Untersteiner. Some results from a time dependent thermodynamic model of sea ice. *J. Geophys. Res.*, 76(6). 1550-1575, 1971.

Saloranta, T., Modelling the evolution of snow, snow ice and ice in the Baltic Sea, *Tellus*, 52A, 93-108, 2000.

Aerosol emission by breaking waves

Maria Chomka and Tomasz Petelski

Polish Academy of Sciences, Institute of Oceanology Powstancow Warszawy 55 81-712 Sopot, Poland
e-mail: chomka@iopan.gda.pl

1. Introduction

Aerosol emission from the sea surface is one of the most interesting phenomena characterizing the marine boundary layer. The sea aerosol effects nearly every physical process taking place in that layer *(Garbalewski, 1999).* The fluxes of aerosol participate in the mass and heat transfer between the sea and the atmosphere *(Andreas et al, 1995)* and they can affect turbulent fluxes considerably greater than themselves *(Petelski, 1996).* More and more attention has been recently attached to the aerosol as a factor determining climate through its influence on optical properties of the atmosphere *(Wright, 2000).* Development of the satellite detection methods caused greater interest in the sea aerosol. Several aegfrosol models *(Gonng et al, 1997),* which are used in the optics of the atmosphere, have been created. However the problem of parameterisation of the aerosol emission from the sea surface is still far from solved. *Monahan et al. (1989)* determined the aerosol emission fluxes, using the findings of whitecap simulation in the open sea. There are no papers describing the emission based on the data obtained from direct natural measurements due to difficulties in measurement. Most of the references cited deal with the mean macro scale emission fluxes calculated on the basis of marigenic aerosol concentration values in the atmosphere. *Petelski and Chomka (1996)* presented a method of calculation of mean fluxes of emission from the coastal zone based on the balance of the aerosol over that zone in the paper. The emission fluxes were calculated according to the method using the data obtained during the BAEX experiment. The results allowed to create the equations of the aerosol emission from the coastal zone, *Chomka* and *Petelski (1997).* The model relates the aerosol emission flux and wave energy dissipation. It was shown that the aerosol emission is proportional to the dissipation of wave energy to the power of 3/4. However the amount of data used was rather small. That is why it was necessary to prove the relation for the data from other experiments. Therefore the aim of the work is to prove that the relation between the aerosol emission flux and energy dissipation to the power of 3/4 is universal, correct not only for the conditions during the BAEX experiment. The results of measurements of sea salt gradients in the TABEX experiments (TABEX'97, TABEX98', TABEX'99) have been presented herein and the emission fluxes have been calculated using those data. The aerosol emission fluxes were correlated with the amount of wave energy dissipation within the coastal zone.

2. Results

The obtained emission fluxes were correlated with the mean values of wave energy dissipation. The values of wave energy dissipation were calculated from the numerical model based on the equation of wave energy transporting within the coastal zone *(Thornton and Guza, 1983; Chomka and Petelski, 1997).* The model enables to calculate the magnitude of wave energy dissipation in the profile perpendicular to the shore in relation to the depth. Wave parameters obtained from the empirical equations *(Paszkiewicz, 1989)* and based on the meteorological conditions of the ship were used as initial conditions for the calculations. Real bathymetry of the bottom in Prelija was used in the model.

The average wave energy per sea surface unit was calculated on the assumption that energy is lost evenly throughout the entire breaker zone.

The relation between the aerosol emission flux and the mean wave energy dissipation is described by the following equation:

$$F_E = 90.5\langle dE\rangle^{3/4} + 12.6,$$

which represent the data obtained during TABEX experiments and

$$F_E = 99.4\langle dE\rangle^{3/4} + 3.5$$

for BAEX data.

The emission coefficient A_p = 90.5 is slightly, by 10%, lower than the one calculated with the data of BAEX (A_p=99.4). The difference is equal to the measurement error. Another experiment will increase the size of the data set in various meteorological conditions, which will consequently allow to calculate accurately that values of the emission coefficient.

The presented analysis of the data on sea aerosol over the coastal zone obtained during TABEX and BAEX experiments indicates that the zone plays a considerable role in the aerosol emission. The fluxes of aerosol emission from the wave breaking zone do not directly depend on the wind velocity, but on wave energy dissipation.

Emission fluxes calculated for the distribution of aerosol concentration are proportional to dissipation of wave energy to the power of 3/4. That relation, for the first time obtained for the BAEX experiment data was confirmed within TABEX experiments. Both regression equations and correlation coefficients are very close. Therefore it can be said that aerosol emission within the coastal zone is proportional to dissipation of wave energy.

The relation was proved for different weather conditions as well as coastal zones (Lubiatowo, Prerija). It can be statedthat it is a universal rule which should apply to all coastal zones.

References

Andreas L.E., Edson J.B., Monachan E.C., Roualt Mu P., Smith S.D., 1995, The Spray Contribution To Net Evaporation From The Sea: A Review of Recent Progress, *Boundary - Layer Meteorology* 72, 3-52.

Carruthers D.J., Choularton T.C., 1986, The microstructure of hill cap clouds, *Quart. J. R. Met. Soc.*, 1/2, 113-129.

Chomka M., Petelski T., 1997, Modelling of the sea aerosol emission by the coastal zone, *Oceanologia,* no. 39 (3).

Garbalewski C.,1999, Fizyka Aerozolowej Aktywności Morza, *IO PAN Rozprawy i monografie* 12.

Gonng S.L., Barrie L.A., Blanchet J.P., 1997, Modeling sea-salt aerosols in the atmosphere, *Journal of Geophisical Research.* Vol. 102, No.D3, 3805-3818.

Monahan E.C., Van Patten M. A., Editors, 1989, The Climate and Health Implications of Bubble - Mediated Sea-Air Exchange.

Paszkiewicz C., 1989, Falowanie wiatrowe Morza Bałtyckiego, PAN, KBM, *Zakład Narodowy Imienia Ossolińskich*, 206.

Petelski T., 1996, Emission of Sea Sprays and Heat Exchange between the Sea and Atmosphere, *Water Resources* Vol.23, No2, 145-148.

Petelski T., Chomka M., 1996a, The Role of Sea Spray Emission in the Mass Exchange in the Coastal Zone, *Atmospheric Physics* 18 No1, 35- 39.

Petelski T., Chomka M., 1996b, Marine aerosol fluxes in the coastal zone - BAEX experimental data, *Oceanologia* No38 (4), 1-17.

Thornton E.B., Guza R.T., 1983, Transformation of wave height distribution, *Journal of Geophisical Research.* 88, 5925-5938.

Wright D.L. 2000, Retrieval of Optical Properties of Atmospheric Aerosols from Moments of The Particle Size Distribution, *Journal of Aerosol Sciences*, 124-129.

Baltic Sea – Vistula Lagoon Water-Exchange: Annual inflow-outflow dynamics simulation (numerical model MIKE21)

Irina P.Chubarenko

Laboratory for Coastal Systems Study P.P.Shirshov Institute of Oceanology of Russian Academy of Sciences, Atlantic Branch, prospect Mira,1,Kaliningrad 236000 Russia E-mail: irina@ioran.gazinter.net

The shallow Vistula Lagoon (Baltic Sea) has an average depth of 2.7 m (maximum is 5.2 m). The surface area and the volume of the Lagoon are 838 km^2 and 2.3 km^3 respectively. The Baltiysk strait of width equal to 400 m is the only connection between the Lagoon and the Baltic sea; it has a navigable ship channel in width of about 100 m and in depth of 12 m. Water exchange through Baltiyst strait is very complicated: 44 % outflow, 21 % inflow, 28 % two-streams and 7% two-layers currents were observed [Lazarenko et al (1971)].

The numerical model MIKE21 of Danish Hydraulic Institute together with original computing tools were used for the estimations of discharges through Baltiysk strait during the whole year. The hydrodynamic part (MIKE 21 HD) simulates unsteady two-dimensional flows in one layer (vertically homogeneous) fluids and has been applied in a large number of studies. Salinity variations were simulated by MIKE 21 AD (Advection-Dispersion module) which solves advection-dispersion equation for dissolved or suspended substances in two dimensions (the mass-conservation equations).

The model was initially fed by real data (bathymetry, 21 river discharges and 7 point sources) and calibrated with data from the 1994 field study held during the Danish-Russian-Polish project "Vistula Lagoon". It was found that MIKE21 model simulates adequately levels and fluxes in the Vistula Lagoon, and effectively represents the features of time and space variations in salinity field. The following values for calibrating coefficients were used in simulations: the wind friction factor f = 0.0017; the Chezy coefficient C = 32 ($m^{0.5}/s$); horizontal eddy viscosity coefficient E = 20 m^2/s, horizontal dispersion coefficient D = 45 m^2/s. The circulation and salinity field throughout the entire 1994 year were modelled using a grid with 1000x1000m meshes. The computational time step was equal to five minutes. Real wind and level variation data measured with the time step 6 hours during the whole year near the Lagoon entrance (Baltiysk station) were used. The salinity at the open boundary (Baltiysk) was specified as 6.5 psu, initial salinity in the Lagoon - 4.5 psu, and the ice-coverage (no wind) was taken to be 56 days - as in the winter 1994/95.

The results of simulations are presented in table 1.

	Sum, cub.km	Inflow, cub.km	Outflow, cub.km
January	-0.221	2.313	-2.532
February	-0.993	0.927	-1.917
March	-0.951	1.689	-2.643
April	-1.083	0.999	-2.082
May	-0.256	1.224	-1.479
June	0.082	1.839	-1.758
July	-0.293	0.837	-1.128
August	-0.018	1.302	-1.320
September	-0.004	1.569	-1.572
October	-0.201	1.587	-1.968
November	-0.044	2.163	-2.208
December	-0.255	1.677	-1.932
Total	-4.237	18.126	-22.539

Total outflow of the Vistula Lagoon waters to the Baltic Sea was found to be equal to 22.5 cub.km, total inflow of marine water to the Lagoon – 18.1 cub.km during the simulated 1994 year. General water-exchange has not obvious seasonal course, but is rather small in summer. In June the sea water income to the Lagoon exceeds a little (0.08 cub.km) outflow to the sea.

The results of numerical simulations were found in good agreement both with field data available (salinity fields in the Lagoon in 1994, general behavior of currents observed in Baltiysk strait) and previous published water-exchange estimations. Simulated 1994 year was treated like typical from the point of view of hydrological conditions.

The contribution of different forcing factors to water-exchange was also investigated. It was estimated that total annual sea water income/outcome due to boundary level variations only amounts 17.5 cub.km., due to wind forcing only – 11 cub.km

Reference

Lazarenko N. and Maevskiy A. (editors), 1971, Hydrometeorological regime of the Vistula Lagoon, pp.280 (in Russian.)

Precipitation fields over the Baltic Sea derived from ship rain gauge measurements on merchant ships

Marco Clemens and Karl Bumke

Institut für Meereskunde, FB 1, Maritime Meteorologie, Düsternbrooker Weg 20, 24105 Kiel, Germany

1. Introduction

Precipitation is one of the main components of the hydrological cycle and intimately linked with almost all aspects of climate change. Thus, precipitation data are of primary importance for hydrological calculations. To measure precipitation over the Baltic Sea several merchant ships have been equipped with ship rain gauges (SRGs). An interpolation scheme based on the Kriging method (Karnieli and Gurion, 1990) has been adopted to the data to estimate precipitation fields along the shipping routes over the Baltic Sea.

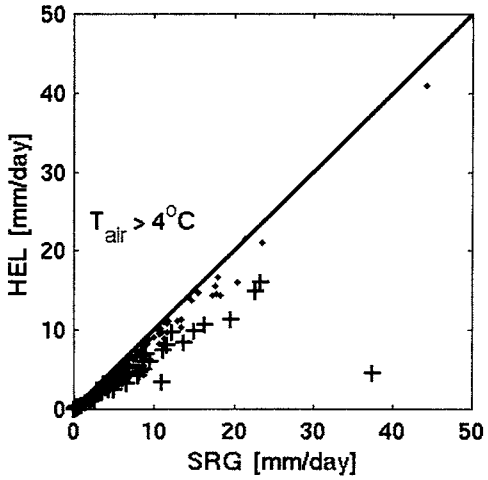

Figure 1: Comparison of daily precipitation sums (06 to 06 UTC) measured with a Hellman rain gauge and a SRG on the roof of the institute's building. Dots indicate mean wind speeds < 4ms^{-1}, crosses mean wind speeds > 6ms^{-1} during precipitation events.

2. Ship rain gauge measurements

The SRG is designed to measure rain under high wind speeds as they are typical for conditions over sea or in coastal areas. A unique feature of the SRG is an additional lateral collector, which is effective under high wind speeds (Hasse et al. 1998). The calibration of the SRG was performed by simultaneous measurements with an optical disdrometer (Großklaus et al. 1998) onboard the R/V ALKOR. So losses by wetting and evaporation are taken into account by the calibration.

Beginning in 1994 at least five merchant ships have been equipped with SRGs, which are travelling from Germany to Finland. All measurements are stored as 8 minutes averages. The number of measurements exceeds 25000 in several months.

Measurements with a SRG mounted on the roof of the institute's building have been compared for a three year period with measurements of a Hellman rain gauge. Figure 1 shows that especially under high wind speeds the Hellman measurements underestimate precipitation rates compared with measurements of the SRG.

3. Interpolation scheme

Interpolation has been performed by applying the Kriging method (Karnieli and Gurion, 1990). Kriging can be regarded as prediction of a value x_0 at a location P_0 by using information from measurements in the surroundings:

$$x_0 = \sum_{i=1}^{n} w_i (x_i + \Delta x_i),$$

where the x_i are the SRG measurements averaged over the i^{th} grid box, here of a 1°x 1° grid, and the w_i are the weights. A minimizing of

$$\sum_{j=1}^{m} \left(x_0 - \sum_{i=1}^{n} w_i (x_i + \Delta x_i)\right) = \min,$$

over all grid boxes j gives the covariance matrix. An example of the estimated covariance function is given in figure 2.

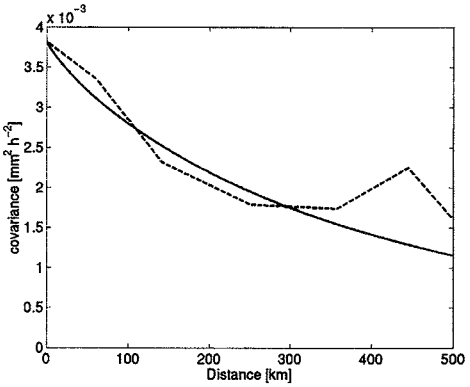

Figure 2: Estimated monthly covariance function (JJA 1996/98). The dashed line gives the empirical function, the full line denotes the theoretical function.

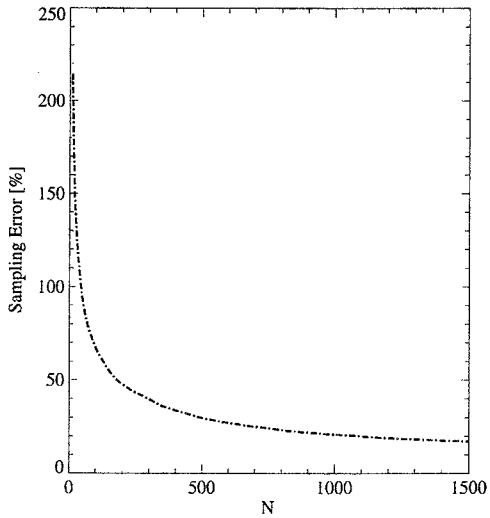

Figure 3: Sampling error as a function of the number of observations N for August 1998.

The error of the calculated mean value of each grid box depends on the number of observations available for analysis. The error variance is given by

$$err = \frac{1}{a \cdot N^b} + c,$$

where a, b, and c are empirical coefficients. An example of the resulting sampling error is given in figure 3.

4. Precipitation fields

The number of observations is sufficient to compute precipitation fields for 1^ox 1^o grid on a seasonal base, sometimes even on a monthly base. This depends on the precipitation frequency, which determines the sampling error. The precipitation field for August 1998 is depicted in figure 4. The number of observations of each grid box for August 1998 ranges from about 200 to more than 1000. This corresponds to a sampling error of 20 to 45% (figure 3). It should be noted that the sampling error is reduced for seasonal precipitation fields due to increasing observation numbers.

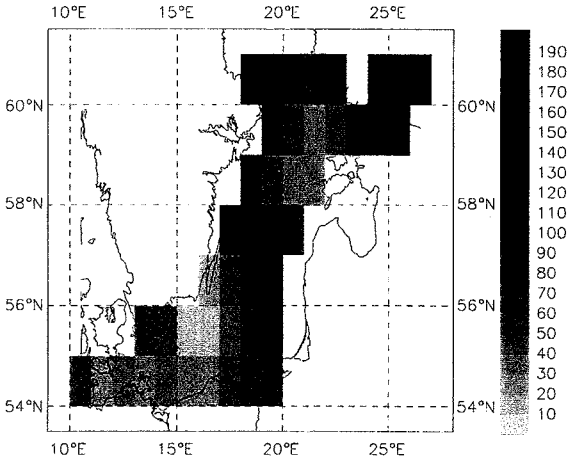

Figure 4: Precipitation field for August 1998. Units are mm month^{-1}

The estimated precipitation fields were compared to synoptic measurements of precipitation at coastal stations and on islands. These measurements were corrected by F. Rubel to take the wind speed induced error, wetting and evaporation losses into account (Rubel and Hantel 1999). The comparison was done between all synoptic stations, which are closer than 25km to the centre of an analysed grid box. The bias of less 3 mm month^{-1} compared to mean values of about 60 mm month^{-1} indicate that the chosen method to estimate precipitation over sea gives reliable results.

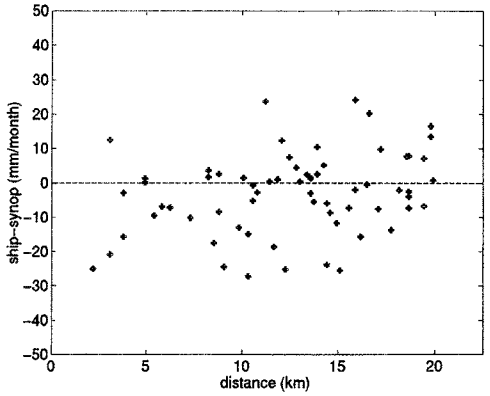

Figure 5: Comparison between analysed precipitation fields and those precipitation measurements at synoptic stations, which are closer than 25km to the centre of an analysed grid cell. Precipitation measurements at synoptic stations were corrected for measurement errors by Rubel (Rubel and Hantel 1999).

References

Großklaus, M., K. Uhlig, and L. Hasse, An optical disdrometer for use in high wind speeds, J. Atm. Technol., 15, 1051-1059, 1998

Hasse, L., M. Großklaus, K. Uhlig, and P. Timm, A ship rain gauge for use in high wind speeds, J. Atmos. Oceanic. Thechnol., 380-386, 1998

Karnieli, A. and B. Gurion, Application of the Kriging technique to areal precipitation mapping in Arizona, GeoJournal 22.4, 391-398, 1990

Rubel,F. and M. Hantel, Correction of daily rain gauge measurements in the Baltic Sea drainage basin, Nordic Hydrology, 30, 191-208, 1999

Cloud Observations from the Ground-Based CLIWA-NET Network I (CNN I) during BRIDGE EOP I

Susanne Crewell[1], Matthias Drusch[1], Ulrich Löhnert[1], Clemens Simmer[1] and Andre Van Lammeren[2] and the CLIWA-NET Project Team

[1] Meteorological Institute, Bonn University, Bonn, Germany
[2] Royal Netherlands Meteorological Institute, KNMI, De Bilt, The Netherlands

1. Introduction

Within the EU-project CLIWA-NET (BALTEX Cloud Liquid Water Network) (Van Lammeren, 2001) one objective is to establish a prototype of a European Cloud Observation Network (ECON), which can provide data almost in real time to a broad community. Another objective is to use this data together with satellite measurements to evaluate/improve cloud parameterizations in weather forecast and climate models. The most important parameter linking dynamics to clouds, in both the real world and in forecast models, is the water content of clouds, which is, unfortunately, difficult to measure. The most accurate method to determine the liquid water path (LWP) is groundbased passive microwave radiometry. However, for many applications it is also crucial to know at which altitudes the water is located. To determine the cloud base height several instruments can be used (e.g. cloud radars, cloud lidar ceilometers and IR-radiometers), while for the profiles of the liquid water content (LWC) the combination of passive microwave and cloud radar measurements is promising (*Löhnert et al.*, 2001).
A prototype of ECON is achieved within CLIWA-NET by co-ordinating the use of existing, mostly operational, groundbased passive microwave radiometers and profiling instruments. This network feeds high quality cloud information with high temporal resolution but poor spatial coverage into the calibration of satellite-based estimates of cloud water content with large spatial coverage. The network was and will be operated during the two continental scale measurement campaigns CNN I (August/September 2000) and CNN II (April/May 2001). Both periods correspond to BALTEX/BRIDGE enhanced observation periods (EOP I and III). Here we will report on the first results from CNN I.

2. Instrumentation

During CNN I eleven stations (Table 1) within the BALTEX modeling area were operated by the University of Bern (UNIBE), Royal Netherlands Meteorological Institute (KNMI), Rutherford Appleton Laboratory (CCLRC), GKSS-Research Center, Geesthacht (GKSS), Helsinki University of Technology (HUT), Chalmers University of Technology (Chalmers), Centre des Environnements Terrestre et Planetaires (CNRS), Deutscher Wetterdienst (DWD) and the Institute of Radio Engineering and Electronics, Moscow (IRE). Additional sensors from the Institut für Meereskunde, Kiel (IFM), the Meteorological Institute Bonn (MIUB), KNMI and Vaisala were distributed to some of the stations. For an overview see Table 1.
The basic instrument for the observation of the liquid water path is a passive microwave radiometer (MWR). Several types of these MWR were used during CNN I. Some are commercially available and some were built by the partners and therefore comprise different frequencies, bandwidths, viewing geometries, opening angles and integration times. Nearly all stations were equipped with infrared radiometer and lidar ceilometer. This combination is quite useful in characterizing cloud height (derived with an accuracy of ~30 m from ceilometer measurements) and cloud base temperature as shown by Feijt and Van Lammeren (1996) (derived from the infrared sky temperature after subtracting the atmospheric contribution). At three stations cloud radars were operated. Seven stations are covered by the BALTRAD network and time series at these stations are available. The delivered data products were quality checked and processed for www applications on a weekly basis. The measurements as daily plots are shown on the central CLIWA-NET web site at http://www.knmi.nl/samenw/cliwa-net.

3. Analysis

To retrieve the LWP and the integrated water vapor (IWV) (as a bye-product) statistical algorithms were developed for each station based on a ten year data set of European radiosondes. The LWP accuracy for the different stations ranges between 15 and 35 gm^{-2}, and the IWV accuracy between 1 and 1.5 kgm^{-2} due to the different instrument

Table 1: Stations and instrumentation during CNN I. Crosses (x) indicate instruments already present at stations and circles (o) the instruments (and their owners), which will be moved to the station.

	Station	Operator	Latitude / Longitude	Microwave Radiometer	Infrared Radiometer	Lidar Ceilometer	Cloud Radar	BALTRAD Coverage
BE	Bern	UNIBE	46.9 N / 7.7 E	x	x			
CA	Cabauw	KNMI	51.9 N / 4.9 E		x	x		
CH	Chilbolton	CLRC	51.1 N / 1.4 W	x	o KNMI	x	3, 94 GHz	
GE	Geesthacht	GKSS	53.4 N / 10.4 E	o MIUB	x	x	95 GHz	x
HE	Helsinki	HUT	60.2 N / 24.8 E	x	o KNMI	o Vaisala		x
KI	Kiruna	Chalmers	67.9 N / 21.1 E	o Chalmers	o KNMI	o MIUB		x
LI	Lindenberg	DWD	52.2 N / 14.1 E	x	xo KNMI	x		x
ON	Onsala	Chalmers	57.4 N / 11.9 E	x	o KNMI	o IFM		x
PA	Paris	CETP	48.7 N / 2.2 E	x	o KNMI			
PO	Potsdam	DWD	52.4 N / 13.1 E	x	o KNMI	x		x
SP	St. Petersburg	KNMI/IRE	59.9 N / 30.7 E	x	o KNMI		3, 9.6 GHz	x

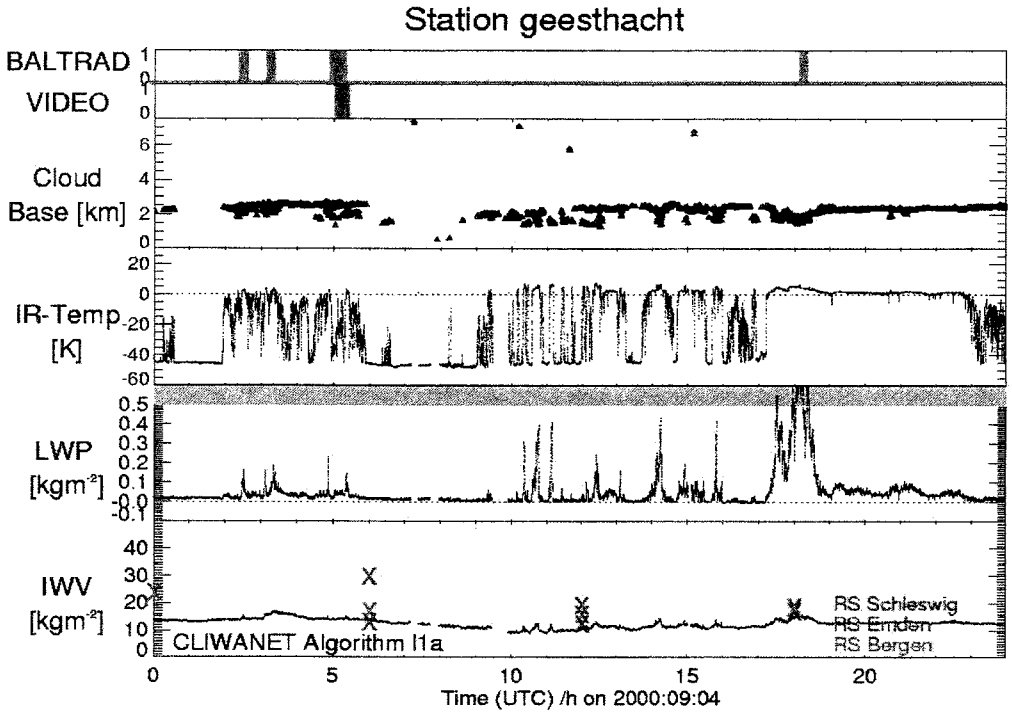

Figure 1: Time series of LWP and IWV derived from microwave radiometers, ceilometer and infrared radiometer measurement on September 4, 2000 at Geesthacht as an example for one daily plot at one station.

specifications. However, these values are derived solely from theory. A first indirect assessment of the LWP quality has been performed by comparing the IWV with the values measured by the closest radiosondes. This has shown a good performance for most stations, however at two stations (Bern and Chilbolton) the microwave radiometer suffered from malfunction and the data should be handled with care.

An important aspect are precipitation events; for studies on the hydrological cycle the onset and duration of precipitation is quite relevant. However, most of the instruments do not execute useful measurements during rain because the antenna/lens is affected by rain drops. Therefore a precipitation index from different sources (BALTRAD data, ceilometer, rain gauges, video) was derived to identify periods of rain. During CNN I a comprehensive data set from the groundbased network was created. The final version of the level 1a products has been produced and can be accessed from the CLIWA-NET central web site or http://r203d.meteo.uni-bonn.de/CLIWANET/CNN_level1a.html (see Fig. 1 as an example).

1. Future Work

Current work focuses on the validation of the data, e.g. the specification of the data accuracy. Here we want to make use of the synergy of the different sensors. Lidar ceilometer and infrared radiometer allow the identification of cloud free scenes. Because the derived LWP should be zero during these times the LWP derived from the microwave radiometer measurements can be evaluated regarding offset errors and noise. A detailed intercomparison of several microwave radiometer will be performed during the BALTEX Bridge Campaign (BBC) in August/September 2001 in Cabauw, Netherlands.

The two month time series of LWP, most with a resolution of better than 10 s allow to study several cloud processes.

- The synergy of cloud radar measurements, lidar ceilometer and microwave radiometer will be used to develop procedures for detecting icing conditions.
- Scaling properties of LWP will be investigated using structure functions and wavelets.
- It will be studied if a LWP threshold which determines the onset of precipitation eventually exists depending on location, cloud type, etc.

We will present first results on these issues in our contribution.

Acknowledgements.

We gratefuly acknowledge the measurements performed within the CNN I network by Christian Mätzler (UNIBE), Hannelore Bloemink (KNMI), Charles Wrench (CCLRC), Henriette Lemke, Markus Quante (GKSS), Martti Hallikainen (HUT), Gunnar Elgered (Chalmers), Cecille Mallet (CNRS), Jürgen Güldner (DWD), Boris Kutuza (IRE) and Daniel Michelson (SMHI).

References

Feijt, A. and A. van Lammeren, Ground-based and satellite observations of cloud fields in the Netherlands, *Monthly Weather Review*, Vol. 124, 1914-1923, 1996.

Löhnert, U., S. Crewell, A. Macke and C. Simmer, Profiling cloud liquid water by combining active and passive microwave measurements with cloud model statistics, *Journal of Atmospheric and Oceanic Technology*. 2001, (accepted)

Van Lammeren et al., The Baltex BRIDGE cloud liquid water network project: CLIWA-NET. *This conference*. 2001.

The development of the coupled ocean-atmosphere model RCAO

Ralf Döscher, Ulf Hansson, Colin Jones, Markus Meier, Anna Rutgersson and Ulrika Willén

Rossby Centre/SMHI, SE-60176 Norrköping, Sweden

1. Why coupling?

Coupled ocean-atmosphere modelling in the Baltic area opens new possibilities, e.g. better surface fluxes, higher resolution in forcing acting on the ocean, and a better description of coupled interactive effects. Budgets for heat and freshwater can be accessed more directly (even better with hydrology and river routing included). Moreover, a coupled system provides a basis for biogeochemistry studies and pollutant prediction capabilities. The necessity of a proper description for the Baltic Sea for describing atmospheric climate has been shown by Räisänen et al. (2000). A coupled 3-dimensional ocean-atmosphere model for the Baltic area has been developed at SMHI's Rossby Centre.

2. Model development

The previously existing models for Baltic Sea (RCO, see Meier et al., 1999 and Meier and Faxén) and atmosphere (RCA, see Rummukainen et al., 2000) have been coupled by means of the OASIS coupler (Valcke, 2000). Different coupling strategies have been tested, ranging from a weakly coupled system to a fully flux coupled system. Thereby, weak coupling means to pass only state variables. The component models use their own ocean-only and atmosphere-only algorithms to calculate individual fluxes. As a result, we get a positive trend in sea surface temperature. The reason is a mismatch of the forcing provided by the atmosphere model and observed forcing to which the ocean model is adjusted with parameters within the range of best knowledge. Satellite observations show a clear land-sea contrast in cloudiness over the central Baltic during summer. Karlsson (1996) found 40-60% cloudiness over sea and 50-80% over land during summer 1993. This pattern is reproduced by the coupled model. On the other hand, the standalone ocean model's radiative forcing works fine with cloud observations from the SMHI database, which are likely biased to land values. As the ocean model's radiative formulation for standalone runs is used in the weakly coupled system, the downward radiation is overestimated by this weakly coupled system due to correctly reduced cloud cover. This can explain the unrealistically high SST in the weakly coupled system.

In a fully flux coupled system, ocean surface quantities are passed to the atmosphere and atmosphere-ocean fluxes are passed back to the ocean. This scheme works in general. However, the finer resolution of the ocean model (10km) compared to the coarser resolution of the atmosphere (44km) has to be taken into account. Isolated ocean points such as small shallow bays which heat up rapidly in spring need the application of longwave upward radiation directly on the fine ocean grid. Otherwise "hot spots" might occur in the ocean. Thus, longwave upward radiation is calculated on the ocean grid and passed to the atmosphere. As most fluxes show some sensitivity on the ocean gridscale surface structure, we aim to calculate more fluxes on a fine "flux" grid.

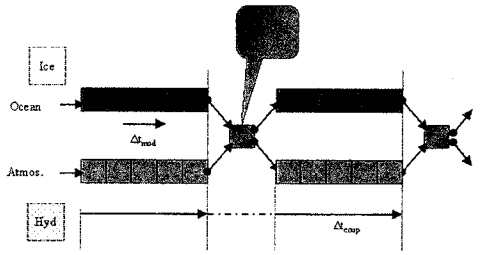

Figure 1: Coupling scheme: ocean and atmosphere run in parallel. Both are linked via the OASIS coupler.

3. First results

Sea surface temperature and sea ice extent are used as integral quantities to monitor the coupled systems simulation capabilities. First coupled runs show a good agreement between observed and simulated SST's at selected stations (Fig. 2). Generally, the SST is too low. Comparison of radiative fluxes at coastal observational stations suggest a lack of shortwave and longwave radiation reaching the sea level within the atmosphere model.

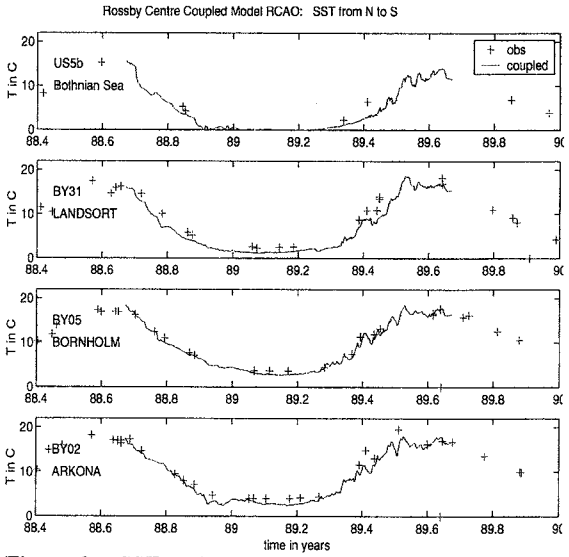

Figure 2: SST timeseries for selected stations: observations and simulations from the coupled system

Modifications to the atmospheric parameterization of radiation and clouds within the limits of observational uncertainty have been tested. Improvements result from a revised treatment of clouds within the model's columns, cloudwater treatment and pollutants over the Baltic. Recent improvements are discussed by Willén et al. during this BALTEX meeting. Results from first multi-annual runs will be presented.

References

Karlsson, K-G, Validation of modelled cloudiness using satellite-estimated cloud climatologies. Tellus (1996), 48A, 767-785.

Meier, H.E.M., R. Döscher, A.C. Coward, J. Nycander and C. Döös, RCO - Rossby Centre regional Ocean climate model description (version 1.0) and first results from the hindcast period 1992/1993. SMHI Reports Oceanography, No. 26, 1999.

Räisänen, J., M. Rummukainen and A. Ullerstig, Downscaling of greenhouse gas included climate change in two GCM's with the Rossby Centre regional climate model for northern Europe. Submitted to Tellus, 2000.

Rummukainen, M., J. Räisäanen, A. Ullerstig, B. Bringfelt, U. Hansson, P. Graham and U. Will\'en , RCA - Rossby Centre regional Atmospheric climate model: model description and results from the first multi-year simulation. SMHI Reports No. 83, 1998.

Valcke, S., L. Terray, and A. Piacentini, Oasis 2.4, Ocean atmosphere sea ice soil: user's guide. Technical Report TR/CMGC/00/10, 2000, CERFACS, Toulouse, France.

AMSR – E Soil Moisture Retrieval: An Observation System Simulation Experiment for GCIP.

Matthias Drusch [1], Wade T. Crow [2] and Eric F. Wood [2]

[1] Meteorological Institute, Bonn University, Bonn, Germany
[2] Dept. of Civil and Environmental Eng., Princeton University, NJ, USA

1. Introduction

Recent studies in the fields of climate modeling, regional climate modeling, and numerical weather prediction stress the importance of soil moisture. Soil moisture influences the latent and sensible heat fluxes and therefore the exchange of water and energy between the land surface and the atmosphere. In addition, soil moisture drives the decomposition processes of dead organisms in the soil through microbes and therefore the release of CO_2 into the atmosphere.

Only satellite remote sensing can provide independent soil moisture estimates for long periods and continental or global scales. Passive microwave remote sensing at frequencies ranging from 1.4 to 6.9 GHz has probably the highest potential for large scale surface soil moisture retrievals. Due to the lack of L - band radiometers in space the Advanced Microwave Sensing Radiometer (AMSR – E) 6.9 GHz channels, which will be operational in summer 2001 onboard EOS - PM (AQUA), are most promising and of particular interest. However, due to the poor spatial resolution of approximately 75 × 43 km at –3 dB non-linearities in the radiative transfer, in the radiometer's antenna sampling and in the hydrological processes will limit the accuracy of a satellite derived soil moisture product over heterogeneous land surfaces.

In this study an Observation System Simulation Experiment (OSSE) was carried out over the entire 575,000 km^2 Red-Arkansas River Basin to quantify the accuracy of a future gridded AMSR - E soil moisture product. The complete OSSE experiment consisted of four parts: a simulation of surface conditions based on hydrologic modeling, forward land surface microwave emission modeling, a simulation of the AMSR – E retrieval and gridding of brightness temperature products, and backwards land surface microwave emission modeling of the simulated AMSR – E brightness temperature products. A detailed description of this study can be found in Crow et al. (2000).

2. TOPLATS hydrologic modeling

The hydrological model TOPLATS (TOPMODEL-based Land-Surface-Atmosphere Scheme) was run on a 1 km grid over the entire Red-Arkansas River Basin in the south- central United States from April 1 to July 31, 1994. For more information regarding TOPLATS the reader is referred to Beven and Kirkby (1979) or Peters-Lidard et al. (1997).

Forcing data were derived from a number of high resolution data sets: 4 km WSR-88D (NEXRAD) precipitation imagery, 1 km GOES solar radiation imagery, spatially interpolated NCDC surface airways meteorology data, and 1 km soil and vegetation classifications derived from the STATSGO data set and AVHRR measurements, respectively. The model was calibrated using naturalized stream flow data for 5 sub-catchments of the Red-Arkansas River Basin, the initial conditions were calculated by running a low-resolution version of TOPLATS over 314 sub-catchments of the Red-Arkansas Basin from April 1992 to April 1994. The energy and water balance components of TOPLATS have been validated at the point scale (Peters-Lidard, 1997), with soil moisture data from the Southern Great Plain Hydrology Experiment (SGP97) and with spatially averaged flux tower measurements from the 360^2 km^2 ARM-CART study site.

3. Land-surface microwave emission modeling

The land-surface microwave emission model (LSMEM) was used to calculate 6.9 GHz brightness temperatures at the top of the canopy layer. The atmospheric contribution was neglected since the influence of atmospheric water vapor and cloud liquid water at this frequency is small (Drusch et al., 2001). A description of the model can be found in Kerr and Njoku (1990) or Drusch et al. (1999b). The simulations for the OSSE were based on noon time soil moisture and surface temperature calculations from TOPLATS. Additional information on the parameter selection for the soil and vegetation are given in Crow et al. (2000).

Since soil roughness, which has a strong influence on the calculated brightness temperatures, is generally not available, SMMR 6.6 GHz measurements were used to calibrate the radiative transfer model. A strict validation of the radiative transfer model is impossible, since there is always a limited number of unknown parameters. However, the individual parameterizations are state-of-the-art components, which have been tested in various studies.

4. Sampling and inversion procedure

A synthetic satellite data set for the observation period was produced using the sun-synchronous orbit of the future EOS-AQUA platform and the exact scan geometry of the AMSR-E sensor. The simulated 1 km brightness temperatures were aggregated to the actual radiometer's footprint size using a Gauss function approximation to the exact antenna gain function (Drusch et al., 1999b). A 25^2 km^2 grid product was calculated from every footprint, which was centered within a specific 25^2 km^2 grid box, as proposed in the preliminary data product plan. An iterative root finder was then used to numerically invert the LSMEM and convert the gridded brightness temperatures fields back to soil moisture. It has to be noted up front that the 25^2 km^2 values should not be used for any comparisons, since gridded satellite products, e.g. the NSIDC EASE 25^2 km^2 grid products, are not designed to enhance the resolution of the original measurements, but to provide handy data sets for a broad community. Therefore, any comparisons presented in the following section were performed at the 50^2 km^2 scale, which is comparable to the radiometer's original resolution.

5. Results and discussion

The satellite derived 50^2 km^2 soil moisture product was compared with the 'true' 50^2 km^2 value, which is defined as the linear average of the 1 km TOPLATS soil moisture. The difference between both products is expressed as an

rms error. A detailed discussion of the results is given in Crow et al. 2000.

The sensitivity to spatial heterogeneity is positively correlated with the density of vegetation. For dense canopy layers with vegetation water contents exceeding 1.5 kg m^{-2} the rms error was found to be 2.4 and 3.7 % (0.03 cm^3_{water} / cm^3_{soil}) volumetric soil moisture, depending on how failed retrievals were processed. The lower value was obtained when failed retrievals were set to regional mean, a value of 3.7 % was obtained when failed retrievals were set to residual or saturation. However, the maximum errors for individual 50^2 km^2 boxes exceeded 30 %. If only sparse vegetation was taken in account (vegetation water content below 0.75 kg m^{-2}) the rms error in soil moisture is 1.7 %. The errors given above are comprised of two separate components: sampling errors caused by the non-linear antenna gain function and aggregation errors associated with the non-linearities in radiative transfer. It was found that for 6.9 GHz the errors related to the non-linear antenna gain dominate the total rms error of 1.7 %. These results are consistent with results from previous studies (Drusch et al., 1999a, Galantowicz et al., 2000).

Under the assumption that the individual 1 km soil moisture values from the TOPLATS calculations represent the field scale soil moisture, which may be obtained by in-situ measurements, sampling strategies for validation experiments can be studied. An rms error of 4 % was found when one randomly chosen 1 km element was compared to the corresponding 50^2 km^2 AMSR value. This value can be reduced to 2.5 and 1.8 % if 4 and 16 elements were averaged. Current operational soil moisture networks, e.g. the Illinois Water Survey Network or the Oklahoma Mesonet Network, will not provide this spacing. However, within specialized soil moisture networks or during field experiments these dense sampling strategies may be feasible.

Temporal aggregation of the soil moisture products did not decrease the corresponding rms errors significantly. Despite sampling a number of consecutive rainfall and drydown events the error in the 25^2 km^2 AMSR product and the field scale product retained the same sign for the aggregation period.

It has to be stressed again that this OSSE investigated the effect of land surface heterogeneity on the soil moisture retrieval only. Several effects, which were not taken into account in this study, will certainly increase the rms errors. Soil roughness and the vegetation structure coefficient exhibit a strong non-linear relationship with brightness temperature. Due to the lack of appropriate data both values were kept constant in this study. In addition, the same geophysical parameters and model were used for the forward and backward radiative transfer calculations. In 'reality' the inversion of the radiative transfer will be based on an incomplete approximation of the forward process. The vegetation and soil parameters, e.g. soil texture and roughness, vegetation water content or fractional vegetation cover, will be poor estimates for large parts of the globe.

The results from this study indicate that the accuracy goal of 6 % volumetric soil moisture for an AMSR – E data set will be hard to meet even for sparsely vegetated areas, especially since the uncertainty of probes or spatula measurements is ~ 3 %. The persistence of a relatively constant bias in simulated AMSR – E retrievals suggests that spatial heterogeneity will not prevent validation and retrieval products from accurately representing temporal fluctuations in coarse scale soil moisture. Such a simplistic temporal error structure may lend itself to correction through either calibration adjustments in the retrieval process or assimilation techniques that combine model predictions of surface soil moisture with AMSR – E retrievals.

Acknowledgments

The authors would like to thank Dr. Eni Njoku of JPL/NASA for providing the software to simulate the orbital and scanning characteristics of EOS AQUA and AMSR – E, respectively. The work was funded from NASA grants NAG8-1517, NAG5-6494 and NOAA grant NA96GP0413.

References

Beven, K.J., M.J. Kirkby, A physically based, variable contributing area model of basin hydrology, *Hydrol. Sci. Bull.*, Vol. 24(1), 43-69, 1979

Crow, W.T., M. Drusch, E.F. Wood, An Observation System Simulation Experiment for the impact of land surface heterogeneity on AMSR-E soil moisture retrieval, *submitted to IEEE Trans. Geosc. Rem. Sens.*, 2000

Drusch, M., C. Simmer, E.F. Wood, Up-scaling effeccts in passive microwave remote sensing: ESTAR 1.4 GHz measurements during SGP97, *Geophys. Res. Let.*, Vol. 26, 879-882, 1999a

Drusch, M., R. Lindau, E.F. Wood, The impact of the SSM/I antenna gain function on land surface parameter retrieval, *Geophys. Res. Let.*, Vol. 26(23), 3481-3484, 1999b

Drusch, M, T.J. Jackson, E.F. Wood, Vegetative and atmospheric corrections for the soil moisture retrieval from passive microwave remote sensing data: results from the Southern Great Plains Hydrology Experiment 1997, *J. Hydromet.*, Vol. 2(2), 181-192, 2001

Galantowicz, J.F., D. Entekhabi, E.G. Njoku, Estimation of soil type heterogeneity effects in the retrieval of soil moisture from radiobrightness, *IEEE Trans. Geosc. Rem. Sens.*, Vol. 38, 312-316, 2000

Kerr, Y.H., E.G. Njoku, A semiempirical model for interpreting microwave emission from semiarid land surfaces as seen from space, *IEEE Trans. Geosc. Rem. Sens.*, Vol. 28(3), 384-393, 1990

Peters-Lidard, C., M.S. Zion, E.F. Wood, A soil-vegetation-atmosphere transfer scheme for modeling spatially variable water and energy balance processes, *J. Geophys. Res.*, Vol. 102 (D4), 4303-4324, 1997

The condition of water resources of the Odra basin and the tendencies of their changes

Alfred Dubicki, Zenon Wozniak

Institute of Meteorology and Water Management, Branch in Wroclaw, ul. Parkowa 30, 51-616 Wroclaw, Poland

1. Introduction

In his message „Water in 21st Century" the Secretary General of the World Meteorological Organisation said that due to the limits of its resources, fresh water will be as much of a problem in future as it was in the past. Out of 2.5% of fresh water on the Earth, 2.24% is entrapped in glaciers of Antarctic and Greenland and in deep underground pools. Within the declaration of the meeting which was held in 1998 in Paris, it was indicated that it is necessary to take into account the using of water resources and integrated ecosystems management. Due to its little water resources, Poland supports all activities which aim at the effective management and usage of water resources in the basin, especially when such resources are small.

2. Recent water resources

The world renewable water resources are estimated at the level of about 40673.0 km^3, the European ones of 2321 km^3. When compared to the Polish water resources of (57,1 km^3), they are much higher. Poland is in the group of very little water resources, i.e. 1000-2000 m^3/inhabitant/year. In the years 1985-1997 the water resources in the area of Poland ranged from 43,4 km^3 in 1990 to 67,1 km^3 in 1997. They were also territorially differentiated in the area of the whole country.

The space changes of water resources are determined by two groups of factors: the area's orography, which shapes the water capacity of the basin and the conditions of the outflow, and the meteorological factors, especially precipitation, its height, distribution in time and in area of the basin, and those which are decisive for the volume of losses.

In about 80% of the area of the Odra basin the precipitation ranges within 500-700 mm. Only in the mountains is it higher than 700 mm, which do not make up more than 20% of the area of upper and middle Odra basin. Especially important to the water balance is the fact that the areas north of Wrocław are characterized by a negative climatic balance, where evaporation is higher than precipitation.

Occurring since the mid 60s process of systematic diminishing of precipitation turned out to be unfavorable for water resources. Altogether, in the period of 1965-1990, especially in the west and south, the Odra basin received locally about 1500 m less of precipitation, *Dubicki, Tomczyński* (1998).

The accumulation of unfavorable for the river outflow processes, such as negative climatic balance, drop in the amount of precipitation and increase of temperature, as well as the size of the Silesian Lowland which is characterized by small slopes and big soil permeability caused that the unit run-offs in the basin are small in the majority of the area and they range from 2.5 to 7.5 l/s/km^2. Higher values are present merely in the mountains and piedmont areas.

3. Tendencies of changes of water resources in the Odra basin in the 21st century

Present knowledge based on reliable research results of IMGW confirm the tendency of temperature increase, descrease in the amount of precipitation and flow-off, *Gutry-Korycka* (1999).

In many-years course of temperature and precipitation, based on over 120-years long observations on the Śnieżka Mountain, an increase has been observed by 0,2°C in 100 years. Also, decrease of daily and annual amplitude of temperature was observed. In the distribution of precipitation in the area of the Odra basin, based on the 50-years' measurement courses, apart from normal oscillation negative tendencies of the trend lines have been observed. Negative tendencies of the trend lines for precipitation (annual sums) concern both mountain and lowland areas (Fig. 1). The slope factors of the precipitation trend line have been specified for the mountain areas – 0.0262, for lowland areas – 0.6765 and for the whole of the middle and upper Odra basin – 0.2142. Negative slope factors trend lines have been calculated also for 50-years' collection of average annual flow. An example of mountain rivers is Nysa Kłodzka, whose slope line factor has been specified as – 0.6582, and of the lowland rivers - Widawa, with 0.0104 (Fig. 1).

Changes have been observed also in the flow from melting snow. Also a shift from april to March has been observed for the maximal spring flows.

Unfavorable hydrological-meteorological changes are accompanied by useful phenomena, such as diminishing amount of sewage dumped and water intake. However, a possibility of breakdown of this favorable tendency in water management can be expected along with renewed increased trend in the industrial and agricultural production. According to the forecasts, the demand for water for people, industry and agriculture will increase by 27,3% from 1990 to 2020, and in year 2050 by 39,4%.

The necessary for the planned level of industrial water intake in year 2050 can reach again the condition of the year 1990, i.e. about 2550 km^3. Assuming a minimal decreasing tendency of water resources at 10-15% and a rational water management with good water quality maintained, it is expected that the needs of industry will be satisified for the nearest 50 years, *Kaczmarek, Napiórkowski* (1997).

In order to fulfil the condition of maintained good quality of water in the Odra basin the „Program of Immediate Action for the Odra River Protection against Pollution" must be consequently realised. This program, with its implementation period of 1997-2002, will be the first stage of improvement of water purity. It assumes a decrease in the Odra river of the BZT_5 load by 84776tO_2/a, total Nitrogen by 6856tN/a and total phosphorus by 22756tP/a and the load of CZT-Cr by 10311tO_2/a. It includes building, modernising and restructuring 138 water treatment plants, including 86 municipally owned and 52 industrial. In the first three-years-long period of (1997-1999) the program realisation 41 municipal and 20

industrial water treatment plants were built and started to work.

In the newly built municipal water treatment plants reduced were 14606tO_2/a BZT_5, 3397tN/a of total Nitrogen and 541tP/a of total phosphorus and 4587tO_2/a of CZT-Cr load.

References

Gutry-Korycka M., Extreme conditions of hydrological system in the perspective of climate warming, National Polish Scientific Conference in Lódz, November 1999 „Changes and changeability of Polish climate", 1999.

Dubicki A., K. Tomczynski., Atmospheric precipitation shortage in the Izerskie Mountains, Karkonosze Mountains and their foregrounds, *Geoecological Problems of the Karkonosze Mountains*, Wyd. Acorus, Poznan, 1998.

Kaczmarek Z., J. Napiórkowski , Impact of climate change on water resources in Poland, *Publications of the Institute of Geophysics Polish* Academy of Sciences, Warszawa, 1997.

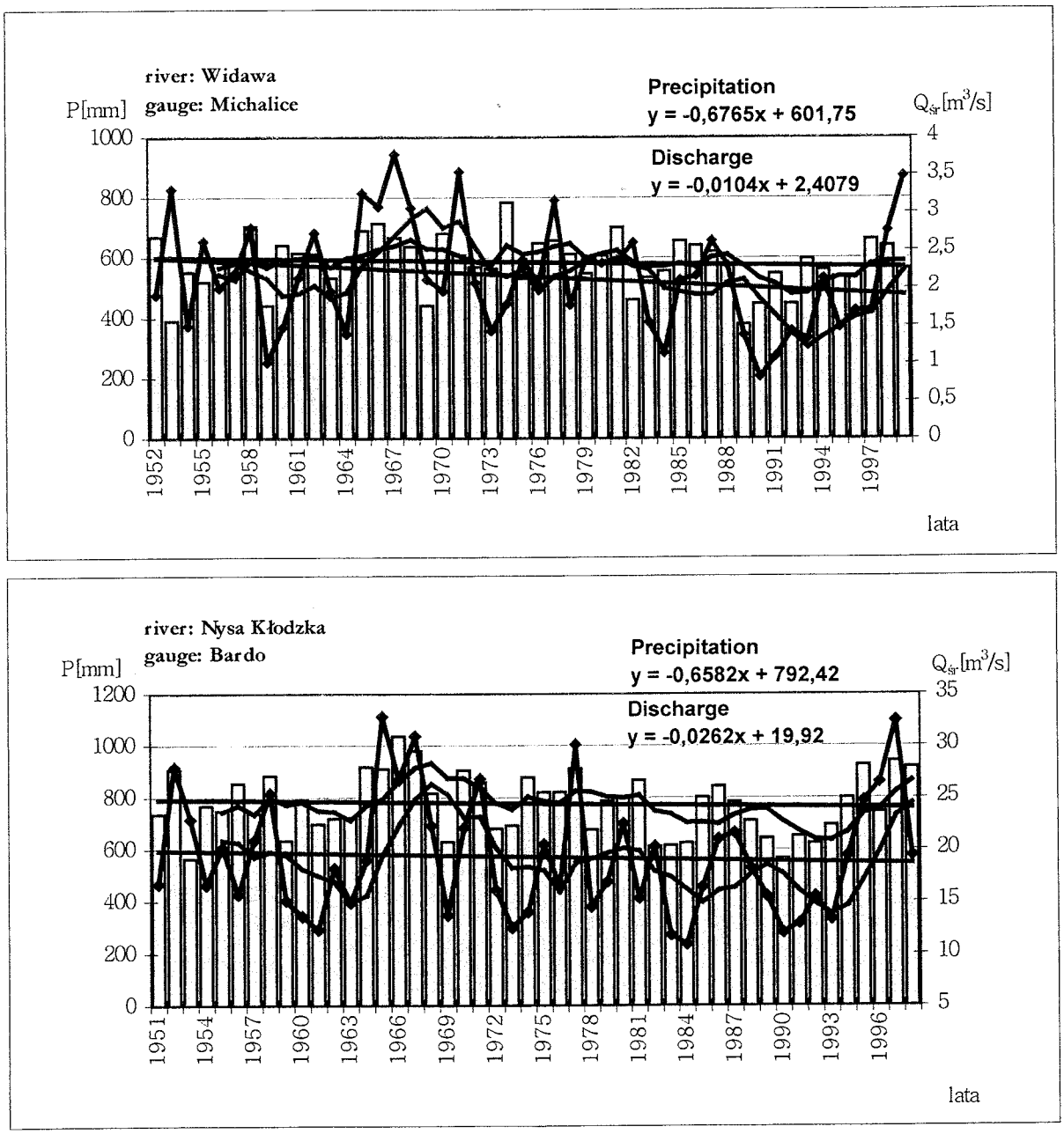

Figure 1: Annual precipitation sums, average annual flows and 5-years' consecutive and straight slopes of trends of these elements.

Mean Cloudiness Derived from Satellite Data over the Baltic Sea Drainage Basin During CLIWA-NET Campaigns

Adam Dybbroe, Anke Thoss and Karl-Göran Karlsson

Research and Development, SMHI, SE-60176 Norrköping, Sweden

1. Introduction

SMHI is responsible for the derivation of the basic cloud parameters Cloud Mask and Cloud Type from satellite data, for the two intensive observing periods (CNN1 & CNN2) of the Framework 5 project CLIWA-NET.

The Cloud Mask and Cloud Type parameters are important input for the derivation of other cloud parameters from satellite data, like the cloud top temperature or the total liquid water path. But they also provide fairly independent means to validate cloud parameterization schemes of Numerical Weather Prediction (NWP) or Climate Models. See *Jones et al.* (2001).

2. The Nowcasting SAF Cloud Mask and Type

In the framework of the EUMETSAT Satellite Application Facility (SAFs) to support Nowcasting and very short range forecasting (SAFNWC) and for Ocean and Sea Ice applications (SAFOSI), SMHI is developing new methods and software to retrieve cloud and precipitation information from present and the coming generation of meteorological satellites (MSG and EPS/NOAA).

The main delivery of SMHI within the SAFNWC will be a software package for the extraction of four high latitude cloud and precipitation products based on AVHRR and AMSU/MHS data. It is planned to release the programme package with the initial capability to process NOAA data during 2002/2003.

The EPS Package will contain four products: Cloud Mask, Cloud Type, Cloud Top Temperature and Height and Precipitating Cloud. See *Dybbroe et al.* (2000a) and *Dybbroe et al.* (2000b) for details.

The Cloud Mask scheme is a multi-spectral thresholding algorithm taking AVHRR data as input. The scheme employs smoothly varying thresholds, separating cloudy and snow cover from cloud free conditions. Tabulated thresholds as a function of the state of the atmosphere and earth surface and the satellite-sun viewing geometry have been derived from off-line radiative transfer model (RTM) simulations, and adapted to the spectral characteristics of the AVHRR channels.

The processing is divided in two steps. In order to minimise the delay of the final product everything not dependent on satellite data is carried out prior to the local reception. The dynamical thresholds are derived in the pre-processing step using the pre-calculated tables and short range forecasted temperatures and integrated water vapour, from a NWP model, 1 km digital elevation model and land use data, and satellite and sun viewing angles.

After the reception of the satellite data, a sequence of tests is performed utilising the dynamical thresholds and a set of spectral and textural features.

The Cloud Type classification is a multi-spectral thresholding algorithm applied to all cloudy pixels as provided by the Cloud Mask. The main approach is that IR and short-wave IR imagery may be used to separate opaque from semi-transparent or fractional clouds, and that opaque clouds may be vertically sub-divided by use of 11 μm imagery.

3. Comparison with SCANDIA

The AVHRR Cloud Mask and Type of the SAFNWC can be seen as the follow-on to the current operational cloud classification scheme at SMHI, SCANDIA, which was developed in the late 1980', Karlsson (1996).

SCANDIA is an empirical thresholding scheme, well tuned for Scandinavian conditions, but is not easily adapted to other environments. The SAFNWC algorithms employ to a large extent RTM calculations and auxillary information, like landuse and DEM data, and account for the sun-satellite viewing geometry.

The SAFNWC Cloud Mask has been validated against 2 years of Synop reports, mainly over Scandinavia and northern Europe, collocated with the satellite data in time and space. Only overpasses withing 1 hour of the Synop is accepted and the cloudiness from satellite is derived from a 32 by 32 pixel square around each Synop.

A number of verification scores have been derived, and the results show an overall improvement over the SCANDIA model (table 1). The Ranked Probability Score (RPS) shown in the table, is derived by assuming the Synop to give the true cloud cover. A completely perfect (in the respect of reproducing the Synop report perfectly) cloud algorithm would have an RPS of 0, and a completely imperfect model would have an RPS of 9.

Table 1: Ranked Probability score, for the SAFNWC Cloud Mask and SCANDIA, for all stations in the database, as well as for five individual stations representing *arctic inland*, *nordic inland*, *coastal*, *open sea*, and *northern European continental* conditions. Derived from Synop-satellite matchups from June 1998 till May 2000. The Synop report is here assumed to be the truth.

	RPS Cloud Mask	RPS Scandia	N
Sodankylä	1.416	1.612	1085
Malmslätt	1.296	1.377	1684
Rønne	1.536	1.515	1272
Ekofisk	1.476	1.619	63
Gorzow	0.867	0.944	143
All stations	**1.685**	**1.725**	**51508**

4. Results from CNN1

From the high resolution (1km) SAFNWC Cloud Type we have derived a coarse resolution product giving the frequency of each cloud type within a 10km by 10km box. This step both reduces the amount of data and creates a parameter more suitable for validation against NWP or Climate models, with typical grid-point distances of 10-40 km, or more.

From the CNN1 dataset of August till September 2000 it is possible to extract a number of mean cloudiness parameters. In figure 1 we present the mean total cloud cover for all morning passes, and all afternoon passes over the BALTEX study region for August and September.

Unfortunately the available NOAA satellite data during CNN1 did not provide the optimal conditions for the analysis of the diurnal cycle, as seen from table 2. The NOAA15 AVHRR stopped giving useful data on July 10th, the launch of NOAA16 was delayed, and maybe more important the NOAA12 and NOAA14 have both drifted so as to have almost the same local overpass times (early morning and early afternoon).

Table 2: Number of utilized scenes and their average overpass time during CNN1.

	Number of scenes	Average overpass time (UTC)
August-Morning	64	04:23
August.Afternoon	81	14:22
September-Morning	30	05:00
September-Afternoon	70	14:30

Despite these poor conditions, a clear increase in cloud cover from morning till afternoon can be seen in August, which was dominated by low-pressure systems passing over southern Scandinavia from the west. The increase in cloud cover is observed over the whole area regardless of the underlying surface (sea or land) as expected from the ruling weather patterns.

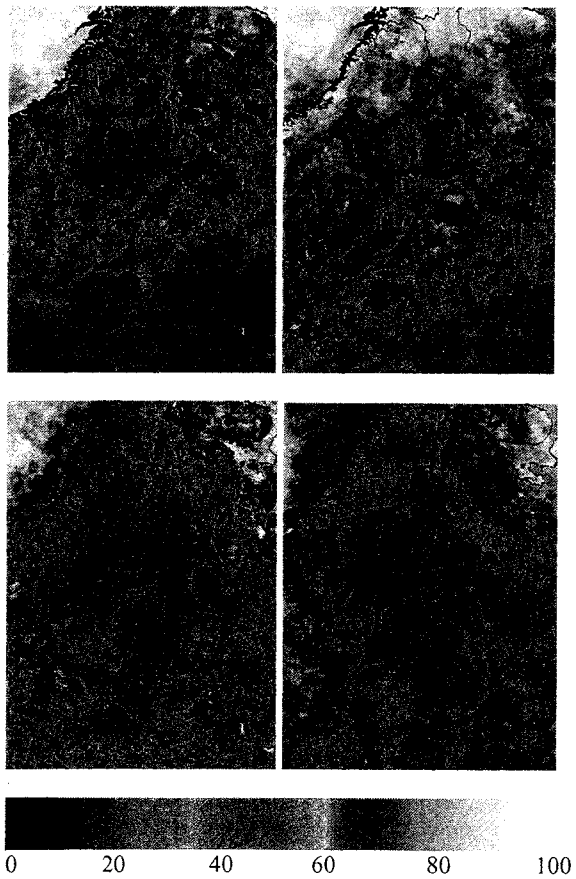

Figure 1: Mean total cloudiness for the BALTEX study area, for morning (left panels) and afternoon (right panels) August (upper panels) and September (lower panels) 2000.

During September, for which a large part was dominated by a stationary high pressure in the center of the area, there is less of a diurnal variation in cloudiness to be observed from these data. The stationary high and the fairly low surface temperatures and the lower insolation prevented strong convection to build up.

References

Dybbroe, A., Moberg, M., Karlsson, K.-G., Thoss, A. Scientific report for the SAFNWC Mid Term Review, *Report available from http://www.smhi.se/saf/*, 2000a.

Dybbroe, A., Thoss, A., and Karlsson, K.-G. The AVHRR & AMSU/MHS Products of the Nowcasting SAF, *Proceedings of The 2000 EUMETSAT Meteorological Satellite DATA Users''Conference, Bologna May 29th - June 2nd*, pp. 729-736, 2000b.

Jones, C., Willen, U., Michelson, D., Karlsson, K.-G. The diurnal Cycle of Clouds and Precipitation, *this pre-print volume*, 2001.

Karlsson, K.-G. Cloud Classification with the SCANDIA Model, *Reports Meteorology and Climatology*, SMHI, 36 pp., 1996.

Mixing and water exchange in the Baltic Sea

Jüri Elken

Estonian Marine Institute, Paldiski St 1, 10137 Tallinn, Estonia

1. Introduction

Depending on the scales of interest, the Baltic Sea may be considered as a huge estuary, large lake or small ocean. Water exchange and mixing may be quantified by models of different complexity (*Omstedt and Axell,* 1998; *Gustafsson,* 2000; *Lehmann and Hinrichsen,* 2000; *Meier,* 2000). Recent advances in understanding the mechanisms are given below.

2. Inter-basin processes

The steady Knudsen budget for the deep water (*Kõuts and Omstedt,* 1993) has established its downstream dilution by entraining the waters above the permanent halocline, with average flow increasing by 28% in the Stolpe Channel and by 14% in the Farö Channel. Stigebrandt introduced in the eighties the rotating hydraulic theory by Whitehead, where baroclinic transports in the Baltic deep channels are determined by the stratification of upstream basin relative to the sill depth (recently re-used by *Omstedt and Axell,* 1998). *Laanearu and Lundberg* (2000) considered also horizontal constriction of the channel and got that either the sill or the smallest width section serves as a control with unidirectional flow. In such flow models, the wind component of the transport is usually ignored. *Gustafsson* (2000) has accounted the Ekman transport in the upper layer only. Following the model results by Krauss and Brügge with a constant wind forcing, *Elken* (1996) and *Jakobsen* (1996) showed that barotropic flow component in the Stolpe Channel may be empirically described as a function of time-dependent wind stress whereas barotropic-baroclinic coupling is weak. An assumption on wind-dependent flow reversal in the Stolpe Channel was confirmed by measurements in autumn 1998 when westward transport in the deep layer was opposed to the wind direction (*Golenko et al.,* 1999). The flow of higher-salinity water over the Stolpe Sill has frequently a splash-like nature while the observed thermohaline structure often reflects the hydraulically controlled transport over the sill (*Piechura et al., 1997*).

The Gulf of Riga is connected with the Baltic Proper by the Irbe Strait where bidirectional currents of different salinity feed migrating S-shaped salinity front against mixing. The flow is roughly in a geostrophic balance with cross-strait density and sea level gradients (*Lilover et al.,* 1998). In the much narrower northern strait, unidirectional currents are modelled well by a combination of barotropic Helmholtz oscillators (*Astok et al.*, 1999). Properties of exchanging water depend on the behavior of the Moonsund front that is usually located in the buffering archipelago sea but takes longer excursions than the Irbe front.

The Gulf of Finland does not have a sill or horizontal constriction. Despite the low stability of estuarine currents under wind forcing (*Alenius et al.,* 1998), converging flows give rise to a quasipermanent front in the entrance area (*Pavelson et al.,* 1997).

1. Intra-basin processes

Spreading of juvenile freshwater adventing from the spring maximum of river discharge is much faster than it can be expected from the quite slow mean circulation in the Baltic Proper (*Eilola and Stigebrandt*, 1998). Also in the Gulf of Riga, a buoyant plume of mixed river water spreads from the southern part to the central and northern areas within one or two months (*Stipa et al.,* 1999). *Lehmann and Hinrichsen* (2000) have shown that under realistic wind forcing stable current bands exist in the Baltic Proper and the Bothnian Sea. Reanalysis of Estonian mesoscale CTD database confirms these current loops in the Eastern Gotland Basin.

Fluctuating winds induce transient Kelvin waves and coastal-trapped waves in the Western Baltic (*Fennel and Seifert*, 1995), the Gulf of Finland (*Raudsepp*, 1998) and west of Gotland (*Pizarro and Shaffer*, 1998). For the latter case, large low-frequency fluctuations were found in alongshore flow and isopycnal displacements. They were significantly correlated with winds whereas the best correlations were found with winds from the island's southern tip rather than with local winds. Signature of basin scale topographic wave is well observed in the deep water of the Gulf of Riga and nearly absent in the shallow water (*Raudsepp et al.*, submitted). The two-cell circulation pattern excited by a storm pulse rotates at calm winds and completes about 3/4 cycle during 5 days. Under realistic wind forcing, the two-cell topographic mode is generated by cyclonically rotating wind and destroyed by anticyclonically rotating wind.

Hydrodynamic instability of coastal current, appearing also without wind forcing, has been demonstrated along the northern coast of the Gulf of Finland (*Stipa*, 1999) where river discharge induces initial vorticity of the flow.

The 1993/1994 major inflow allowed excellent scenario to study the behavior of large intruding dense water mass. A dense bottom pool was formed in the Arkona Sea including the baroclinic geostrophic boundary current responsible for downstream leaking of dense water (*Liljebladh and Stigebrand,* 1996). In the Bornholm Basin the intruding dense water passed through the southern part of the basin (*Jakobsen*, 1996). Further downstream, a well-defined front of the intrusive region was found to be propagating north from the Stolpe Channel to the Gotland Deep with a speed of 2 cm s^{-1} or more. A substantial horizontal intermittence of intrusion intensity, related to mesoscale eddies, was observed behind the front. A strongly nonlinear cyclonic eddy, undetectable on the sea surface, was found in the halocline (*Zhurbas and Paka,* 1997).

Within and below the halocline, both the currents and the mixing are concentrated in the Eastern Gotland Basin near the slopes where halocline intersects the bottom. This process is seasonally intensified during late autumn and winter (Elken, 1996). Several authors have pointed to the importance of internal wave breaking above sloping bottom.

3. Mixing parameterization

According to numerous estimates, the turbulent diffusion coefficients vary in a wide range. It is found that the wind is an essential source of energy for the mixing. However, F.Schott has shown in 1978 that increase of mixing coefficients in the surface layer depend more on the surface wave height than on the wind stress.

Recent investigations at the entrance to the Gulf of Finland by microstructure probe have shown that below the thermocline Richardson number dependence of

vertical eddy diffusivity does not give good correlation with direct estimates based on the Osborn model, assuming local production-dissipation balance for turbulent energy (*Lilover*, 2001). According to *Zülicke et al.*, 1998, in the shallow region most of the dissipation results from local production of turbulent kinetic energy, caused by Reynolds stress in the coastal jet.

If the most advanced $k-\varepsilon$ model for turbulence closure is used in the connected basin model (*Omstedt and Axell*, 1998) or 3D circulation model (*Meier*, 2000) then reproduction of stratification changes is improved considerably. Below the halocline the $k-\varepsilon$ model produces too low mixing that is overcome by adding the stability-dependent mixing coefficient $K_v = \alpha N^{-1}$, with generally speaking, variable α. In the deep stagnant layers of the Gotland Deep, *Axell* (1998) estimated diagnostically from the hydrographic data series a 5-fold increase of K_v from 0.05 cm^2/s during spring to 0.25 cm^2/s during fall. This increase was found in agreement with the seasonal course of synoptic wind speed cubed, a measure of vertical energy flux for mixing via inertial currents and internal waves. The value of K_v also increases from the basin interior towards the coastal slope region. In the coastal boundary layer, the expected flux density of energy from the local wind cannot explain the observed rate of work against the buoyancy forces. *Axell* (1998) proposes that the active coastal boundary layer plays a central role in the transfer of energy to mixing processes in the deep water. This diagnostically derived statement is compared with available results from process observations.

References

Alenius, P., K. Myrberg, A. Nekrasov, The physical oceanography of the Gulf of Finland: a review, *Boreal Env. Res.*, 97-125.

Astok, V., M. Otsmann, Ü. Suursaar, Water exchange as the main physical process in semi-enclosed marine systems: the Gulf of Riga case. *Hydrobiologia*, 393, 11-18, 1999.

Axell, L.B., On the variability of Baltic Sea deepwater mixing, *J. Geophys. Res.*, Vol. 103, No. C10, 21,667-21,682, 1998.

Eilola, K., A. Stigebrandt, Spreading of juvenile freshwater in the Baltic proper, *J. Geophys. Res.*, Vol. 103, No. C12, 27,795-27,807, 1998.

Elken, J., Deep water overflow, circulation and vertical exchange in the Baltic proper, *Estonian Marine Institute Report Series*, No. 6, 91 pp, 1996.

Fennel, W., T. Seifert, Kelvin wave controlled upwelling in the western Baltic, *J. Mar. Syst.*, No. 6, 289-300, 1995.

Golenko, N.N., A. Beszczynska-Möller, J. Piechura, W. Walczowski, A. Ameryk, Some results of research on internal waves in the Stolpe Sill area, *Oceanologia (Sopot)*, Vol. 41, No. 4, 537-551, 1999.

Gustafsson, B.G., Time-Dependent Modeling of the Baltic Entrance Area. 1. Quantification of Circulation and Residence Times in the Kattegat and the Straits of the Baltic Sill, *Estuaries*, Vol. 23, No. 2, 231-252, 2000.

Jakobsen, F., The dense water exchange of the Bornholm Basin in the Baltic Sea, *Dt. Hydrogr. Z.*, Vol. 48, No. 2, 133-145.

Kõuts, T., A. Omstedt, Deep water exchange in the Baltic Proper, *Tellus*, Vol. 45A, No. 4, 311-324, 1993.

Laanearu, J., P. Lundberg, Topographic control of a rotating deep water flow through the combination of a sill and horizontal constriction, *J. Geophys. Res.*, Vol. 105, No. C12, 28,663-28,669, 2000.

Lehmann, A., H.-H. Hinrichsen, On the Wind Driven and Thermohaline Circulation of the Baltic Sea, *Phys. Chem. Earth (B)*, Vol. 25, No. 2, 183-189, 2000.

Liljebladh, B., A. Stigebrandt, Observations of deepwater flow into the Baltic Sea, *J. Geophys. Res.*, Vol. 101, No. C4, 8895-8911, 1996.

Lilover, M.-J., Improved Microstructure Measurement Technologies for Marine near Surface Flux Studies (MITEC): Scientific Data Report, Part I CYANO98, Space Applications Institute, Ispra, *EUR 19816 EN*, 2001.

Lilover, M-J., U. Lips, J. Laanearu, B. Liljebladh, Flow regime in the Irbe Strait, *Aquatic Sciences*, Vol. 60, No. 3, 253-265, 1998.

Meier H.E..M., The use of the $k-\varepsilon$ turbulence model within the Rossby Centre regional ocean climate model: parameterization development and results, *SMHI Reports Oceanography*, No. 28, 2000.

Pavelson, J., J. Laanemets, K. Kononen, S. Nõmmann, Quasi-permanent density front at the entrance to the Gulf of Finland: Response to wind forcing. *Cont. Shelf Res.*, Vol. 17, No. 3, 253-265, 1997.

Piechura, J., W. Walczowski, A. Beszczynska-Möller. On the structure and dynamics of the water in the Slupsk Furrow. *Oceanologia (Sopot)*, Vol. 39, No. 1, 35-54, 1997.

Pizarro, O., G. Shaffer. Wind-Driven, Coastal-Trapped Waves off the Island of Gotland, Baltic Sea. *J. Phys. Oceanogr.*, Vol. 28, No. 11, 2117-2129, 1998.

Raudsepp, U., Current Dynamics of Estuarine Circulation in the Lateral Boundary Layer, *Estuarine, Coastal and Shelf Science*, Vol. 47, 715-730, 1998.

Raudsepp U., D. Beletsky, D.J. Schwab. Basin scale topographic waves in the Gulf of Riga. Submitted to *J. Phys. Oceanogr.*

Omstedt, A., L.B. Axell, Modelling the seasonal, interannual, and long-term variations of salinity and temperature in the Baltic proper, *Tellus*, Vol. 50A, No. 5, 637-652, 1998.

Stipa, T., T. Tamminen, J. Seppälä, On the creation and maintenance of stratification in the Gulf of Riga. *J. Mar. Syst.*, 23: 27-46, 1999.

Stipa, T., Instabilities and along-shore variability in the Finnish coastal current, Fourth Workshop on Physical Processes in Natural Waters, *Estonian Marine Institute Report Series*, No. 10, 62-66, 1999.

Zhurbas, V.M., V.T. Paka. Mesoscale thermohaline variability in the Eastern Gotland Basin following the 1993 major Baltic inflow. *J. Geophys. Res.*, Vol. 102, No. C9, 20,917-20,926, 1997.

Zülicke, C., E. Hagen, A. Stips, Dissipation and mixing in a coastal jet: A Baltic Sea case study, *Aquatic Sciences*, Vol. 60, No. 3, 220-235, 1998.

The Lindenberg SODAR/RASS Experiment LINEX-2000: Concept and First Results

Dirk A.M. Engelbart and Hans Steinhagen

Lindenberg Observatory, German Meteorological Service (DWD), Am Observatorium 12, 15864 Lindenberg, Germany, e-mail: Dirk.Engelbart@dwd.de

1. Introduction

Vertical profiles of mean and turbulent quantities in the atmospheric boundary layer are essentially influenced in its lower heights by footprints of local characteristics of the underlying surface. Hence, a priori there is no answer about the question whether such a vertical profile is representative for a meso-scale surrounding, and so e.g. for the characteris-tic length scale of the former operational meso-scale model of the German Meteorological Service (DWD), which is about 15 x 15 km^2. The heterogeneity of the earth's surface in this Lindenberg grid element (LGE) suggests a certain variability of the average as well as of the turbulent structure of the atmospheric boundary layer as a function of the characteristics of the surface. This is to be considered both, for model forcing and for validation of flux data if necessary. Therefore, a contribution is to be made with the SODAR/RASS experiment LINEX 2000 for clarifying the representativness of local profile measurements in the boundary layer.

Generally, the LINEX-2000 campaign is designed as the experimental component of a German-Russian cooperative research project, where the main objective is the development and test of methods for the determination of turbulent flux profiles in the boundary layer.

Beyond that, the experiment is a component of the intensified measuring period EOP-1 of the BALTEX experiment *„BRIDGE"*, for which a comprehensive experimental data set will be made available concerning the measuring activities performed at the Meteorological Observatory Lindenberg.

Apart from the experimental design of the campaign, this paper will show some first results of the experiment, in particular regarding an assessment of the horizontal inhomo-geneity of mean wind and temperature profiles within the LGE, as well as case studies for the determination of heat and momentum fluxes derived from SODAR/RASS.

2. Experimental design of the campaign

The core objective of the above German-Russian project is the development of a reliable and operationally applicable method for the determination of turbulent fluxes from SODAR/RASS measurements. This method is based on the transilient turbulence theory (Stull, 1993), which only requi-res measurements of the averaged profiles of wind and tem-perature (Engelbart, 1998). The efficiency of this new me-thod is to be examined in the context of the experiment.

All investigations will be realised on the base of simulta-neous measurements of several SODAR/RASS in the LGE, and evaluated as a function of the respective surface charac-teristics (grassland, low farmland vegetation, forests, and lakes) and flow direction. This is not only of interest for the determination and interpretation of vertical flux profiles but also in the context of the project LITFASS for the forcing of the *LITFASS Local Model* (LLM), implemented on the basis of measured data from tower sensors, SODAR/RASS and two wind profiler/RASS as well as a microwave radiometer profiler for humidity profiling (Görsdorf et al., 2000): In the current realisation, one locally measured vertical profile in the "LITFASS area" is assumed to be representative for the whole 'grid point' region, i.e. for the total LGE around Lindenberg Observatory. This single profile is currently used for the model forcing at all boundaries. Thus, differences of vertical profiles as a function of orographic and surface conditions occurring in the lowest hectometres are neglected. Beyond that, temporal differences between the individual boundaries of the LGE are neglected similarly.

To assess the influence of this simplification, all simultaneously-measured vertical profiles during the SODAR/RASS experiment, which are shaped by the local characteristics of the surrounding land surface are inten-ded to be used for validation of results from standard LLM runs, assuming horizontal homogeneity within the LGE atmosphere above 30m height.

In summary, the key aspects of the experiment *LINEX-2000* are characterised by the following:

- Description of the horizontal heterogeneity on the basis of averaged vertical profiles of wind and virtual temperature from spatially distributed SODAR/RASS in the LGE;
- determination of vertical profiles of the turbulent fluxes of momentum and heat (buoyancy) as well as interpretation of the horizontal variability of these quantities from SODAR/RASS and wind profiler/ RASS (WPR/RASS) measurements within the LGE;
- comparison of remotely-sensed vertical flux profiles of momentum and heat with directly-measured values in the Prandtl layer as well as with directly-measured values from the 99m tower sensors;
- comparison of remotely-sensed vertical flux profiles with corresponding values of the micro-α scale model simulations with the *LLM*;
- determination of boundary-layer heights from SODAR- and WPR/RASS-measurements for valida-tion of a parameterisation for the determination of mix-ing heights, in cases when mixing heights exceed the maximum vertical range of SODARs.

In order to reach the scientific objectives, and in particular to be able to interpret deviations between different systems, quality targets have been defined which should be met by all participating SODAR and RASS.

For quality assurance of each system, a two-weeks intercomparison prior to the real experiment had been designed, where all systems were compared versus reference systems.

3. First results from the campaign

As a first step for the investigation into homogeneity of vertical profiles some parameters from comparative

statistics have been calculated for the different SODAR sites. In preparing these calculations each systems' data have been smoothed with respect to time (hourly average) and to the vertical (50-400m agl). Figure-1 reveals the vertical range of the influence of surface characteristics at various sites in a meso-scale surrounding by means of the vertical profile of the bias of three different SODAR/RASS versus the reference system "SDR" (Engelbart et al., 1999).

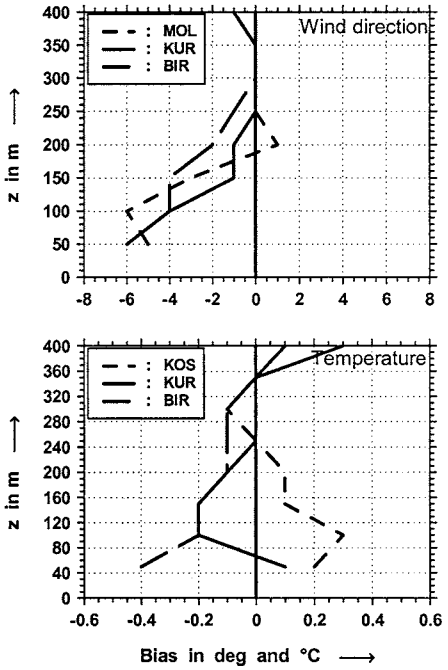

Figure 1: Mean profiles of the bias against the reference system "SDR" for wind direction and temperature from three different SODAR/RASS sites within the 'LGE': The averaging refers to the period Sep 14-25, 2000

The figure makes clear that the inhomogeneity in this scale ranges up to about 200-300m with respect to wind direction as well as virtual temperature. The different sign in the profiles of temperature bias furthermore reflects the surface conditions, i.e. the positive bias (reference - test system) refers to the cooler footprint of a larger lake.

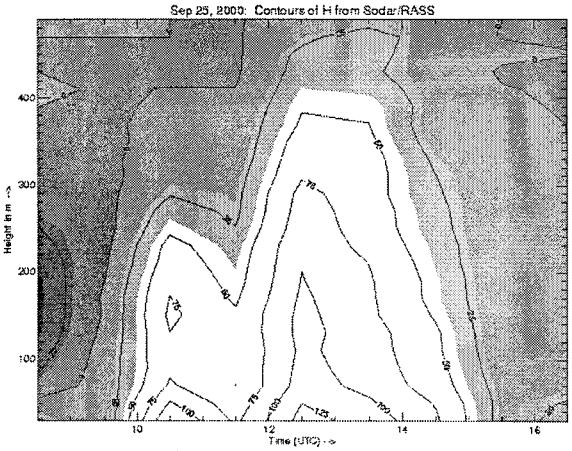

Figure 2: Time-height cross section of the buoyancy heat flux at Sep 25, 2000 from SODAR/RASS data using '*TTP' (high values=light)*

With respect to the determination of turbulent fluxes, figure-2 and 3 demonstrate a case study for the determination of heat and momentum fluxes using the transilient turbulence parameterization (*TTP*) applied on remotely-sensed data from SODAR/RASS.

For verification of the parameterized (virtual) heat fluxes, directly-measured profiles from a 482 MHz WPR/RASS have been compared. Although the height range of the WPR/RASS does not cover the SODAR height range but starts in an altitude of about 470m, these eddy-correlation-derived fluxes agree reasonably well with those of the uppermost SODAR/RASS range gates. In conclusion, the *TTP*-derived heat fluxes show this conformity with eddy-correlation fluxes not only with respect to the time of maximum heat fluxes but also with respect to its absolute values. A discrepancy of about 40 W/m^2 in 400-500m maybe explained by the horizontal distance of about 10km between the WPR/RASS and the SODAR/RASS used here and additionally by the somewhat more forested surrounding at the WPR/RASS site.

The reasonability of the *TTP*-derived heat fluxes from SODAR/RASS can also be derived for momentum fluxes (Fig.-3). So, apart from a sensible diurnal cycle of the momentum flux, the late morning and early evening structures in this figure fit well to some dissolving/evolving low-level jet and the elevated maximum at early afternoon exhibits the typical structure of a convective boundary-layer.

For a verification of the lowest heights, a comparison with Sonic anemometer data fits also well to the *TTP*-derived fluxes.

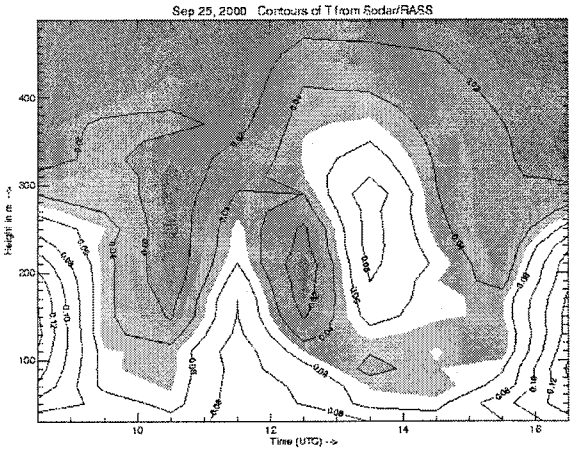

Figure 3: Time-height cross section of the momentum flux at Sep 25, 2000 from SODAR/RASS data using *TTP (high values=light)*

References

Engelbart, D., 1998, 'Determination of boundary-layer parameters using windprofiler/RASS and SODAR/RASS', *Proc. 9th Intl. Symp. Acoust. Rem. Sens.*, Vienna, 192-195.

Engelbart, D., Steinhagen, H., Görsdorf, U., Neisser, J., Kirtzel, H.-J., and Peters, G., 1999, 'First results of measurements with a newly-designed phased-array Sodar with RASS', *Meteorol. Atmos. Phys.* **71**, 61-68.

Görsdorf, U., Beyrich, F., Dier, H., Güldner, J., Leiterer, U., and Herzog, H.J., 2000 , 'Composite vertical profiles of wind, temperature and humidity for use in numerical modeling', *5th Intl.Symp.Troposph.Profiling, Dec.4-8, 2000,* Adelaide, Australia, 179-182.

Stull, R.B., 1993, 'Review of non-local mixing in turbulent atmospheres: Transilient turbulence theory', *Bound.-Lay. Meteorol.* **62**, 21-96.

Comparison of Radiosonde Data and HIRLAM Model Results for the BALTEX-BASIS Experiment.

Dieter Etling, and Anette Ganske

Institut of Meteorology and Climatology, University Hannover, Herrenhäuser Str. 2, D-30419 Hannover, Germany

1. Introduction

Within the BALTEX-BASIS project, a field experiment was performed in the period 18 February to 7 March, 1998 in the Baltic Sea. Among other measurements, radiosondes were launched every 6 hours at the stations Aranda, Kokkola, Merikarvia and Umea. These provided vertical profiles of wind, temperature and moisture up to 10km height. Details of the field experiments and the radiosonde data can be found in Launiainien (1999).
For the period of the BASIS experiments also runs with the operational mesoscale model HIRLAM were performed by SMHI. This gave the opportunity to compare the model results with observed radiosonde data, which were not taken into account for the model initialization.

2. Results of Radiosonde Comparison

The radiosonde observations were compared to the reanalysis and 24-hour forecast data for the grid point in the HIRLAM model which was nearest to the radiosonde station. As an example, air temperature and wind speed near the surface (level 31) obtained from the HIRLAM reanalysis and the 24-hours forecast is compared with the observations at the radiosonde stations in Fig. 1 and Fig.2.

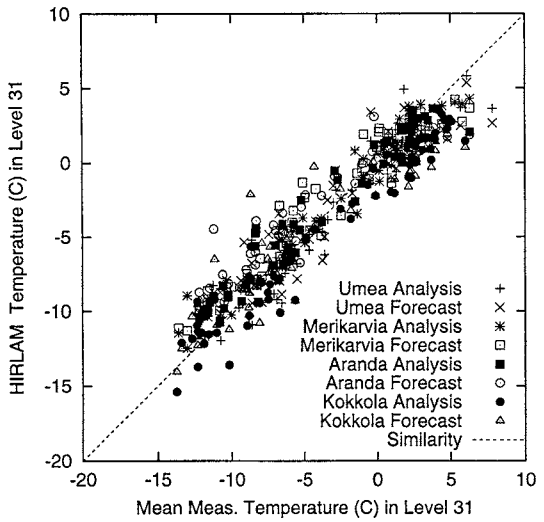

Figure 1: Comparison of near surface air temperature as obtained at the radiosonde stations Umea, Merikarvia, Aranda and Kokkola with HIRLAM reanalysis and 24-hour forecast for the whole period of the BASIS field experiment.

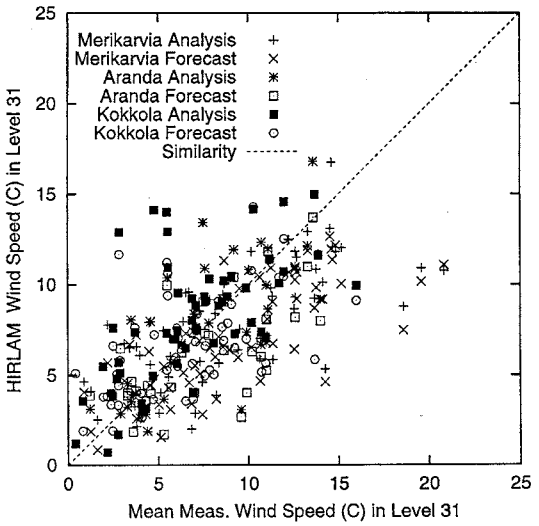

Figure 2: Same as Fig. 1 but for the near surface wind speed.

In summary it can be said, that there was a reasonable agreement between field observations and HIRLAM simulations. However, strong temporal variations in wind and temperature due to the passage of fronts were captured by the model only with some time lag. Also vertical gradients of wind and temperature were often underestimated by the model. Hence temperature in versions and low level wind maxima (low level jets) were not captured in full strength. Most differences between observations and simulations were found in the lower part of the atmospheric boundary layer. This could be possible due to the turbulence parameterization used in the HIRLAM model.
More details on the evaluation of radiosonde data and comparison with HIRLAM model results can be found in Ganske et al. (2001).

References

Ganske, A., D. Etling, D. Schroeder, Evaluation of radiosounding data and aircraft observations in compararison to HIRLAM model results. In. *Launiainien, J., T. Vihma (Eds.): BALTEX-BASIS Final Report. BALTEX Publ., 2001.*

Launiainien, J. (Ed.), BALTEX-BASIS Data Report 1998. *BALTEX Publ.* No. 14, 1999.

Quantitative Cloud Analysis using AVHRR for CLIWA-NET

Arnout Feijt, Dominique Jolivet, Rob Roebeling and Rose Dlhopolosky

KNMI, NL-3730 AE, De Bilt, Netherlands

Satellite data analysis

In the framework of CLIWA-NET, liquid water path fields will be compiled from a network of ground based microwave radiometers and satellite based AVHRR and AMSU (Van Lammeren, 2001). Cloud analysis from the AVHRR and AMSU instruments onboard of the NOAA satellites is a joint effort of KNMI, SMHI and IfM. KNMI is responsible for the retrieval of physical cloud properties from AVHRR. SMHI produces a meteorological cloud type classification of the cloud fields in about 10 classes. IfM retrieves liquid water path (LWP) from AMSU and investigates the correlation between LWP derived from AMSU, AVHRR and ground based microwave radiometers. The KNMI contribution is described in this abstract.

KLAROS

KNMI has developed an operational and automated cloud detection and cloud property retrieval scheme, referred to as KLAROS (KNMI's Local implementation of APOLLO Retrievals in an Operational System). The APOLLO cloud detection scheme is applied to discriminate cloudy from cloud free pixels (Saunders and Kriebel, 1988). The scheme is adapted and extended to include variable thresholds from atmospheric profiles and NWP surface temperature fields that operate automatically. Moreover, the scheme allows the determination of the following cloud properties: optical thickness, cloud emissivity, cloud top temperature and cloud liquid water path. Figure 1 shows a schematic representation of the steps involved in the retrieval of KLAROS optical thickness and cloud top temperature.

The properties of clouds are determined on a pixel by pixel basis for pixels that are flagged cloudy. The visible optical thickness is derived from the 0.6μm reflectivity. A radiative transfer model, Doubling Adding KNMI (DAK), is used to simulate both the atmospheric absorption/scattering and the cloud scattering properties (Stammes, 1994). With DAK the top of the atmosphere reflectivity is calculated for plane parallel clouds with different optical thickness, as a function of surface albedo, solar zenith angle, viewing zenith angle, relative azimuth angle and cloud thermodynamic phase. The scattering phase function for a size distribution of liquid water droplets has been calculated using Mie theory. The scattering phase function for a size distribution of ice crystals has been calculated by ray-tracing, assuming the imperfect hexagonal shape (Hess et al., 1998, Knap et al., 1999). Figure 2 is an example of a retrieved optical depth field for a frontal zone during the CLARA96 observational campaigns in April 1996 (Dlhopolsky et al., 2000). The cloud consists of ice crystals at about 230K. At the edge of the cloud field the optical thickness is low. The KLAROS derived cloud properties have been validated with radar and lidar data (Feijt, 2000).

For semi-transparent clouds the signal in the 10.8μm channel consists of radiation from the clouds, but also radiation from the surface that is transmitted through the cloud. As a result, the equivalent brightness temperature as measured from the 10.8μm channel, is not representative

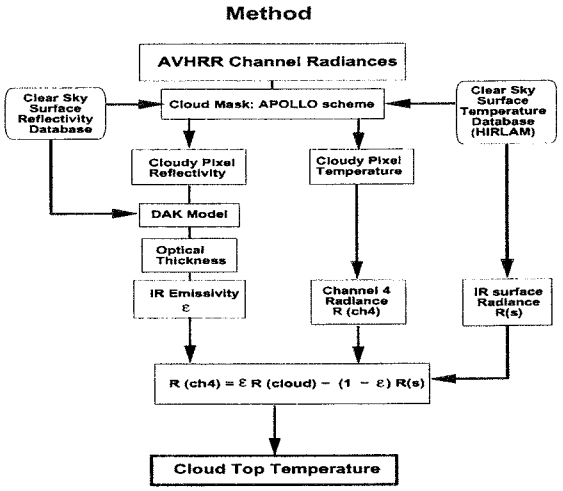

Figure 1: Flow diagram of KLAROS for cloud detection and cloud property retrieval

for the cloud thermodynamic temperature. KLAROS includes a method to retrieve the thermodynamic temperature. The method uses the optical depth as derived from the 0.6μm channel. The optical thickness is used to retrieve cloud emissivity at 10.8μm. When the surface temperature is known this enables the retrieval of the thermodynamic cloud temperature using the equation of Figure 1. The HIRLAM NWP model is employed to obtain an estimate of the surface temperature.

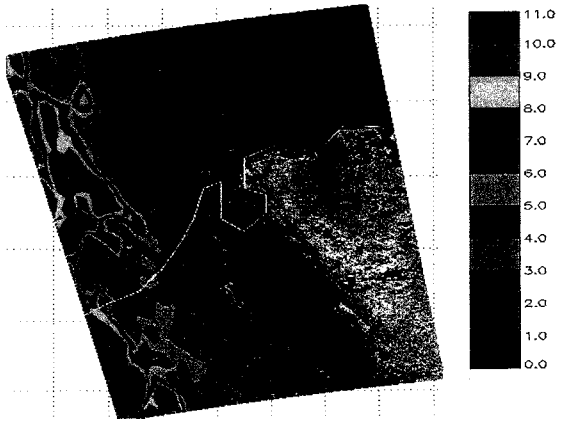

Figure 2: Spatial distribution of cloud optical depth at 0.6μm for 17 April 1996 13UT over the Netherlands

An estimate of the LWP can be obtained from the optical thickness assuming a droplet size distribution (Roebeling et al, 2000). In the current KLAROS implementation the effective radius of the drop size distribution is assumed to be 10μm. During CLIWANET KLAROS will be extended to include the use of the 1.6μm channel to obtain an estimate of the droplet size of the top of the cloud. This is believed to improve the LWP retrieval. The theoretical relation between reflectivities at 0.6 and 1.6μm for various

optical thickness and drop size values is shown in figure 3 (Jolivet et al., 2000).

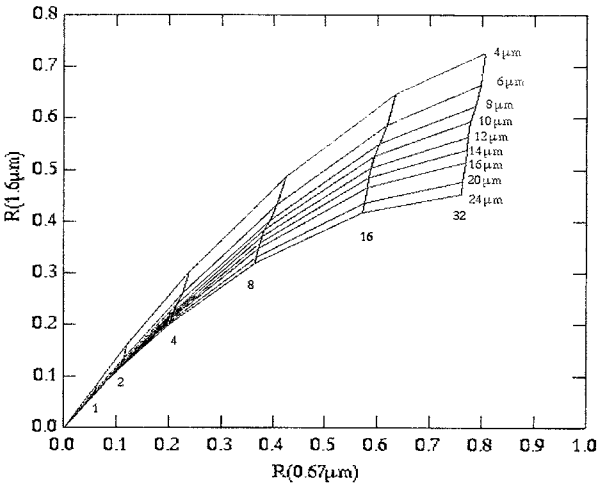

Figure 3: Reflectivity at 0.67 versus 1.6μm for water clouds.

The retrieval of optical thickness and liquid water path values from AVHRR is based on a large number of assumptions and therefore the quality is uncertain. In order to optimize the estimate of LWP values the AVHRR products will be compared and brought into accordance with measurements from a network of ground based microwave radiometers. We expect that this will: a) give a measure of the quality in individual cases; b) enhance the quality of the derived LWP fields from AVHRR.
The comparison of time series of ground based microwave radiometer and the instantaneous spatial distribution of LWP from satellite is a challenge in itself, because clouds are highly variable in time and space. The results from the BBC intensive measurement campaigns will be used to optimize the methods to bring LWP values from AVHRR and ground based microwave radiometer into accordance. During the BBC the additional ground based and aircraft measurements on macro- and microphysical cloud properties will be used to identify keyparameters in the satellite retrieval of LWP. The comparison of microwave and AVHRR results in relation to microphysical cloud properties, which can be retrieved from satellite, will be studied. The knowledge obtained from the BBC will be used to reprocess the measurements from the BALTEX BRIDGE period to obtain optimal estimates of liquid water fields.

References

Dlhopolsky R., Feijt A.J. and Koelemeijer R., 2000: Cloud properties of frontal zone cirrus: AVHRR derived cloud properties and CLARA ground based validation, Proc. The 2000 EUMETSAT Meteorological Satellite Data User's Conference, Bologna, Italy, 2000, 284-298.

Feijt A.J., 2000: Quantitative Cloud Analysis using Meteorological Satellites, Thesis, KNMI, De Bilt.

Hess, M., Koelemeijer, R., Stammes, P., 1998: Scattering Matrices of Imperfect Hexagonal Ice Crystals, J. Quant. Spectrosc. Radiat. transfer, 60, 301-308.

Jolivet D., Feijt A., Watts P., 2000: Requirements for synergetic use of the ERM imager, ESA Contract RFQ/3-9439/98/NL/GD.

Knap, W.H., Hess, M., Stammes, P., Koelemeijer, R.B.A., and Watts, P.D., 1999: Cirrus optical thickness and crystal size retrieval from ATSR-2 data using phase functions of imperfect hexagonal ice crystals, J. Geophys. Res., 104, 31,721-31,730.

Lammeren A.C.A.P., 2001: CLIWA-NET an overview, this abstract book.

Roebeling. R, D. Jolivet, R. Dlhopolsky and A. Feijt, 2000: Determination of cloud optical thickness and cloud liquid water path using multi-spectral NOAA-AVHRR or MSG data, Proc.

Saunders R.W. and Kriebel K.T., 1989, An improved method for detecting clear sky and cloudy radiances from AVHRR data, Int. J. of Remote Sensing, 9, 123-150.

Stammes, P., 1994: Errors in UV reflectivity and albedo calculations due to neglecting polarization, SPIE 2311, 227-235.

The GEWEX Americas Prediction Project (GAPP)

Benjamin Felzer, Rick Lawford

NOAA/OGP 1100 Wayne Ave. Suite 1210, Silver Spring, MD 20910

Theme: Water Cycle, Water Resources, Water Security

In recognition of the increasing stresses and demands on limited water resources and the emerging capabilities to make seasonal predictions, the U.S. has embarked on the new GAPP (GEWEX [Global Energy and Water Cycle Experiment] Americas Prediction Project) initiative. While the goal of GAPP continues to be to demonstrate skill in predicting changes in water resources on time scales up to seasonal and annual as an integral part of the climate system, the objectives are meant to build on GCIP accomplishments to develop a more comprehensive prediction capability. GAPP objectives are to make monthly to seasonal predictions of the hydrological cycle and to use these improved predictions for better water resources management. The first objective largely involves improving the land surface, hydrology, and boundary layer representations of models used for climate prediction through improved understanding of the hydrological processes, feedbacks between the land and atmosphere, model transferability, and development of a comprehensive modeling system. The second objective involves scaling the climate model output to make it useful for water resource managers, improved understanding of the links between hydrologic predictions and water resources management, including the use of demonstration projects, and better understanding of the effects of land surface changes on the regional hydrology. Two major new initiatives will be the effect of orography on the hydrological cycle of the Western Cordillera and the predictability of the North American Monsoon (NAM) and its effects on summer precipitation over the USA. The other components all relate to improving the predictability of the hydrological cycle with special regards to the land surface and the role of predictions for water resources management.

GAPP is a follow-on to the GEWEX Continental-Scale International Project (GCIP), which concentrated on similar issues for the Mississippi River Basin, with an emphasis on closing the water budget within the basin. GCIP research has produced many in-situ and satellite datasets of variables like precipitation, water and energy fluxes, vegetation, snow, and soil moisture. Computer modeling efforts have included data assimilation, model initialization, and validation. A new Land Data Assimilation System (LDAS) has provided an operational mechanism for incorporating observational land-surface data from satellite and surface based measurements into a real-time land surface modeling system for the continental U.S. The GAPP program was initiated in 2001 with funding from NOAA and NASA and is expected to continue until 2007. Further information is available at: http://www.ogp.noaa.gov/mpe/gapp.

Intercomparison of precipitation from BALTRAD and HIRLAM

Carl Fortelius

Finnish Meteorological Institute, P.O.Box 503, FIN-00101, FINLAND

1. Introduction

The verification of numerical precipitation forecasts is made difficult by the huge variability of precipitation in time and space. In general a large number of in situ measurements is needed to estimate the average precipitation flux over a model grid box measuring typically some hundreds of km^2.

A network of radars provides virtually continuous observations, but obtaining accurate estimates of the precipitation at the surface is problematic using radars alone. The BALTRAD data base of the BALTEX Radar Data Centre combines corrected rain gauge data with radar measurements over the catchment basin of the Baltic Sea. In the present study the BALTRAD data are compared with predicted precipitation by the HIRLAM numerical weather prediction system. The periods of December 1999 and July 2000 are examined.

2. The BALTRAD data

Products and methodologies of the BALTEX Radar Data Centre are described in Michelson et al. (2000). The BALTRAD data used here consists of gridded consecutive 12-hourly precipitation sums with a horizontal resolution of 2 km. For the purpose of this study, the BALTRAD data are transformed by box-averaging to the HIRLAM-grid having a grid length of 22 km. The entire radar network is shown in figure 1, but the present study is restricted to the quadrilateral area covering southern Finland and surrounding seas, where the radar network is homogeneous, and the terrain rather flat. This restriction is made in order to avoid some problematic regions, where the BALTRAD data is obviously unrealistic.

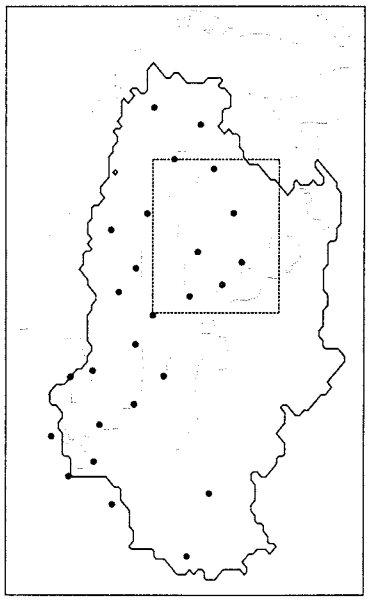

Figure 1: The radars of the BALTRAD network, and the catchment basin of the Baltic Sea. Results will be shown for the quadrilateral area covering southern Finland and surrounding seas.

3. The HIRLAM data

HIRLAM is a complete limited area numerical weather prediction system with hydrostatic dynamics and including parameterizations of radiative transfer, grid scale and sub-grid scale precipitation processes, turbulent mixing, and surface interactions. Within BALTEX, a special version of HIRLAM is used for quantifying climatic energy and water cycles through data assimilation. The system is described in Andrae and Fortelius (the present volume). Forecasts are initiated four times daily on 31 levels with a horizontal resolution of 22 km. The results presented here are based on hours 6 to 12 in each forecast in order to avoid initial spin up in the precipitation while yet minimizing the random forecast error.

4. Findings

Figure 2 shows the semi diurnal precipitation over the control area shown in fig. 1. December 1999 (upper panel) was a stormy month with abundant precipitation associated with many frontal systems passing over the region. The correlation between HIRLAM and BALTRAD is very high, but the model gives higher amounts of precipitation. July 2000 (lower panel) was also a wet month, with even severe flooding over central Sweden. Compared with the winter month, a much larger fraction of the rainfall was of a convective nature. The correlation between HIRLAM and BALTRAD is inferior to the winter case, but still good.

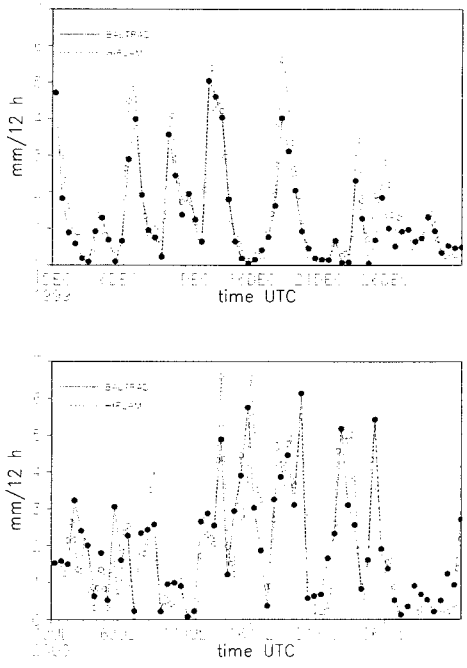

Figure 2: Semi-diurnal areal precipitation amounts for the control area shown in Fig. 1.

Table 1 summarizes monthly mean areal precipitation over land and water for both of the periods. In December 1999 HIRLAM gives significantly more precipitation than BALTRAD. Both systems show higher values over sea

than over land, but the contrast is stronger in the model data.
In July 2000 the mean difference is very small over land, but again HIRLAM shows a much larger contrast between land and sea than does BLATRAD. However, the difference between land and sea is now the opposite to the one in December, with a minimum over sea. It may be, that the model responds too strongly to the thermal contrast between land and see.

Table 1: Monthly accumulated precipitation (mm) in December 1999 and July 2000 over the control area shown in fig. 1.

		Total	Land	Sea
December	HIRLAM	92	85	105
	BALTRAD	76	73	84
July	HIRLAM	116	128	94
	BALTRAD	123	125	119

5. Conclusions

A remarkable correspondence was found between the totally independent estimates of areal precipitation amounts by HIRLAM and BALTRAD. The latter data is thus likely to be valuable for forecast verification and model validation in general. The results add confidence in the ability of a limited area weather prediction system to produce realistic estimates of the precipitation, which is a prerequisite for reproducing the hydrological cycle.
It was also found, however, that in their present state of development, neither HIRLAM or BALTRAD is likely to yield completely reliable estimates of precipitation over the whole catchment basin of the Baltic Sea. In the winter case, HIRLAM gave significantly more precipitation than BALTRAD, and during both of the periods studied the BALTRAD data contained isolated areas of doubtful reliability.

References

Andrae, U., and C. Fortelius (the present volume): Reanalysis of BRIDGE. An estimation of the water and heat budgets over the Baltic Sea drainage basin through variational data assimilation.

Michelson, D. B., T. Andersson, J. Koistinen, C. G. Collier, J. Riedl, J. Szturc, U. Gjertsen, A. Nielsen, S. Overgaard, BALTEX Radar Data Centre Products and their methodologies. Reports Meteorology and Climatology, No 90, 76 pp., 2000

Long-term changes of river discharge in Latvia

Tom Frisk[2], Maris Klavins[1], Agrita Briede[1], Ilga Kokorite[1]

[1] University of Latvia, Department of Environmental Sciences, Raina blvd. 19, LV 1586, Riga, Latvia
[2] Pirkanmaa regional Environmental Centre, Tampere, Finland

Considering the increasing human impact on the environment, studies of environmental changes are of utmost importance. Long-term observations of hydrologic systems provide time series of evapotranspiration, precipitation and river discharge. These data series can be analysed from different points of view. For example, the study of the hydrological cycle is important in investigation of climatic variation and in hydrological applications. Considerable attention has been paid to the study of global climate change, to relations between global processes of atmospheric circulation (NAO, ENSO) and the hydrological cycle, and as to the regional impacts of global climatic changes. River discharge time series have been extensively studied world-wide. The relevant trends regarding global climate changes have been identified in Nordic countries (Kite 1993, Rosenberg et al. 1999, Vehvilainen and Lohvansuu 1991). Extensive study of river discharge trends in USA identified that USA is becoming wetter with less extreme events. Commonly, river discharge patterns have been studied in terms of linear trend analysis, while they can be much more complex. Such linear trend analysis is not suitable for the Baltic countries, which are located in a climatic region directly influenced both by atmospheric processes in the Northern Atlantic and by continental impacts from Eurasia.

The earliest observations of river discharge in Latvia can be dated back to the 19th century for the Daugava River, and a long series of data has since been accumulated. Studies conducted on river discharge trends in Estonia confirm the importance of such analysis (Jaagus et al. 1998). Long-term stream flow analysis is essential for effective water resource management and therefore has immense socio-economic significance. Also, discharge analysis in respect to global climatic changes is presently important considering the predicted changes in this region. The aim of the present study is to analyse long-term changes of river discharge in Latvia.

The climatic conditions for Latvia are dominated by transport of cyclonic air masses from the Atlantic Ocean, leading to comparatively high humidity, uneven distribution of atmospheric precipitation through the year, mild winters and moist summers. In general, the spatial heterogeneity of the climate of Latvia is determined by physiogeographical features, such as upland relief, distance to the Baltic Sea, and coverage of forests and mires. More precipitation is common for uplands (> 200 m from sea level), and differences between regions can reach up to 250 mm annually. Differences in annual precipitation between selected stations ranges from 63 % to 150 % in comparison with the mean values. More precipitation occurs in the warm period of the year, reaching 63 – 70 % of the annual total. Mean air temperature decreases in the direction from the West to the East. Interannual temperature variability (mean value 22-23°, maximum 34°), as well as intraannual variability has comparatively minor significance. Mean climatic characteristics included in Table 3 are based on observations for the last 36 –55 years. Analysis of observations from a longer period can provide information regarding long-term changes of meteorological parameters. However, using statistical methods, it is possible to evaluate the characteristics of processes affecting regional climate and their variability, and to identify cyclic patterns.

Past changes in river discharge were determined using linear trend analysis, the most widely used approach in the study of river discharge. Figure 3 and Table 4 show that the discharge trends in rivers of Latvia and the north-eastern part of the Baltic Sea North are minimal: the discharge has significantly increased for River Venta, but the changes are insignificant and decreasing for all of the other studied rivers (Daugava and Lielupe in Latvia, and for comparison, also Neman, Narva and Neva). The trends do not shown common changes of water discharge regime for Latvia and rather they illustrate differences in river discharge between hydrological regions of Latvia.

The average annual runoff of rivers is about 35 km^3, of which more than 50 % forms in neighbouring countries. The trends for precipitation, temperature and river discharge are similar for the II, III, IV hydrological regions. Regarding the River Venta, located in the type I hydrological region, a positive trend of discharge is more expressed.

Using moving average values (in this case with step 10 years), good coherence is seen between changes in annual precipitation at the Meteorological Station Riga-University and discharges of the largest rivers (Daugava and Nemunas Rivers) flowing into the eastern coast of the Baltic Sea (Figure). The Figure also indicates periods with low- and high-water levels, and the presence of regular cyclic processes. Close relationships between meteorological data and discharge can be found when studied for periods longer than 60 years

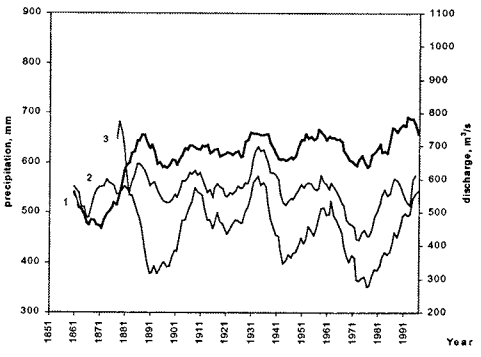

Figure 1: Changes (10-year step moving mean) of annual discharge and precipitation (1851-1996):1 – precipitation (Station Rīga-University); 2 - Nemunas River; 3 - Daugava River

The use of integral curves allows to better identify oscillation patterns. Integral curves for water discharge in the 5 largest rivers in Latvia shows differences are seen

between Lielupe and the other four rivers in Latvia, and in all rivers there is an apparent difference between observations before and after 1920. For example, in the River Lielupe, water discharge decreased from 1986 to 2000, in contrast to the other rivers which showed stable increasing trends of water followed by a very recent trend (presently a high-flow regime is changing to a low-flow regime). We presume that a new cycle of water flow began in 1996, when the water discharge reached the lowest value during the last ten years rivers in Latvia The differences between river Lielupe and other rivers in Latvia can be done also considering that the sampling station in Lielupe, which is situated quite upstream (110 km) and thus can reflects slightly more than 50 % of the total river discharges. The Lielupe River basin is intensively affected by melioration and by construction of various hydrotechnical obstructions (dams, ponds etc.). Also agricultural activities influence the water flow regime in this river.

General patterns of the periodicity of water flow regime in several major rivers in Latvia and in neighbouring countries are summarised in Table 5. The duration of the high water flow period for the last half of century was 27 years in the case of the Daugava River and up to 33 years for the rivers Salaca, Venta and Gauja. The number of low water-flow periods has been correspondingly 23 and 17 years for the Daugava and the other rivers. During the same time period in the Lielupe River, duration of the high water flow period was 21 years and the low water flow periodicity was 29 years.

Spectral analysis was applied for the river streamflow data. Figure 8 shows the spectrum of the normalised time series (Tukey window 20). A low-order harmonics at frequencies of 0.05 and 0.07 cycles/year, corresponding to a period of about 20 and 13 years, dominate for the spectrum. The pronounced power has been obtained also for about 2 and 4 years (i.e. frequencies of 0.26, 0.43 respectively). A periodicity of 2.1 years is more expressed than for 4 years. The spectral analysis confirms the suggested oscillations of river discharge.

Goudie (1992) described sinusoidal changes of river discharge in Eastern Europe. Short-term fluctuations with mean duration 4-6 years have been previously found in Estonia and Finland (Jagus 1995). An approximately 20-year periodicity has been suggested in earlier studies for rivers in the Baltic region and Eastern Europe, along with a period of about 20 to 50 years for monthly mean precipitation and water level which may be the result of interference of the precipitation and temperature regimes. In previous studies, a 26 year periodicity of Daugava River flow was considering as the main period, which includes 2-, 6- and 13- year smaller cycles. The shorter-period oscillations of river stream flow may be explained by changes in solar activity, and the longer-period oscillations by circulation patterns of air masses in the Northern Hemisphere.

The study showed that, due to the oscillation of water discharge, cyclic processes should be considered rather analysis in terms of linear trends.

References

Goudie, A., (1992) Environmental change, Clarendon Press: Oxford

Jaagus J., Järvet A., Roosaare J. (1998) Modelling the climate change impact on river runoff in Estonia. In:Climate change studies in Estonia (Eds. T.Kallaste, P.Kuldna), Stockholm Environment Institute Tallinn Centre: Tallinn, pp.117-127

Kite, G. (1993) Analysing hydrometeorological time series for evidence of climatic change, Nordic. Hydrol., Vol. 24, pp. 135-150

Rosenberg, N.L., Epstein, D.J., Wang D., Vail, L., Srinivasan, R., Arnold, J.G. (1999) Possible impacts of global warming on the hydrology of the Ogallala aquifer region, Climatic change, , Vol, 42, pp.677-692

Vehvilainen, B., Lohvansuu, J. (1991) The effects of climate change on discharges and snow cover in Finland, J. Hydrol. Sci., Vol. 36 (2), pp.109-121

Zeng, N. (1999) Seasonal cycle and interannual variability in the Amazon hydrologic cycle, J.Geophys. Res., Vol. 104 (d8, pp. 9097-9106

Joint Analysis of the Satellite Imagery and High Resolution U-tow CTD Transects in the Baltic Sea

Nikolay Golenko[1], Vadim Paka[1], Yuri Kravtsov[2], Olga Lavrova[2], Konstantin Litovchenko[2], Yuri Trokhimovsky[2]

[1] Atlantic Branch of Shirshov Institute of Oceanology, Prosp. Mira,1, 236000 Kaliningrad, Russia
[2] Space Research Institute, Profsoyuznaya Str. 84/32, 117810 Moscow, Russia

The Atlantic Branch of the Shirshov Institute of Oceanology realizes the mesoscale water structure monitoring in the Baltic Sea by means of repeated U-tow CTD transects. In 1997-2000 several cruises of RV "Professor Shtokman" were performed with such aim, and a wide variety of mesoscale features, which originated from local subsurface currents, by inflows, by internal waves, *etc.* were detected. There is a problem to conduct field measurements permanently. The SAR images give the unique opportunity to observe subsurface motion and some other effects on a regular basis with no respect to daylight and weather conditions. The joint analysis of SAR, infrared NOAA imagery and *in situ* data shows that current features observed by SAR are in reliable agreement with SST variations measured from IR data on the one hand and temperature/salinity distribution measured by the towed undulating probe. The joint analysis of oceanographic and satellite data allows the improvement of ship operations and leads to a better understanding of the dynamics of the Baltic Sea.

In Figure 1 a portion on ERS SAR image of the area with the Stolpe Sill in the centre dated 18.06.99 is presented. Added curves are isobaths (meters). Strength of return pulses from smooth or rough areas of sea surface is low (dark) or high (light), respectively. The image looses contrast in the right part of the area probably due to high sea states and in the dark patch in the center of the picture probably due to high sea surface contamination. Potentially retrievable oceanographic parameters are internal waves and any other internal motion, which create convergence or divergence at the surface. At moderate sea surface roughness and typical content of natural wedging agents provide the dependence of roughness and wedging agents distribution concentration uniform along surface currents and changing along their gradients, thus the pattern of surface currents becomes visible. In the deep part of the Bornholm Basin dark uniform tint testifies weak dynamics. The pattern generated apparently by internal waves stretched parallel to isobaths is visible above the slopes of the Bornholm Deep. The most complicated pattern is adjacent to the sill.

Figure 2 presents four joined temperature transects, the positions of two of them in the middle are shown by solid lines in fig. 1. These transects were made during a week after the ERS flight. The upper layer temperature is almost uniform within two neighboring sub-basins, but properties of intermediate and bottom layers change sharply above the sill.

It could be concluded from comparison of the independent measurements that the complexity of SAR image above the Stolpe Sill is linked with the subsurface motion.

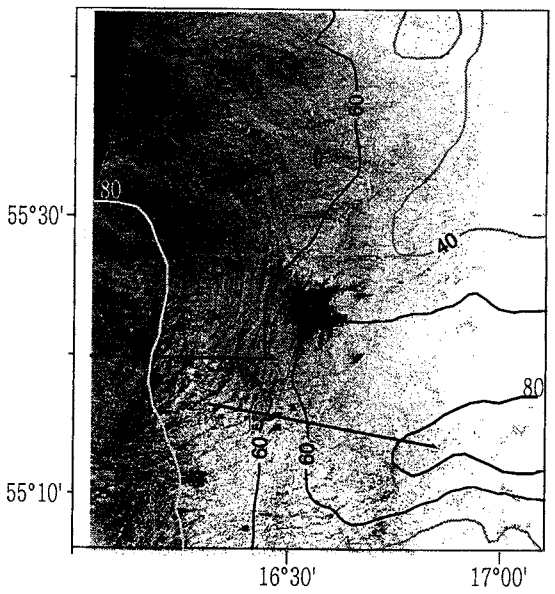

Figure 1: ERS SAR image of sea surface roughness obtained on 18.06.99 in the Baltic Sea, in the area including the eastern part of the Bornholm Deep and the western part of the Stolpe Furrow. Solid curves are isobaths, solid lines show positions of two transects, which are presented in the middle of fig. 2.

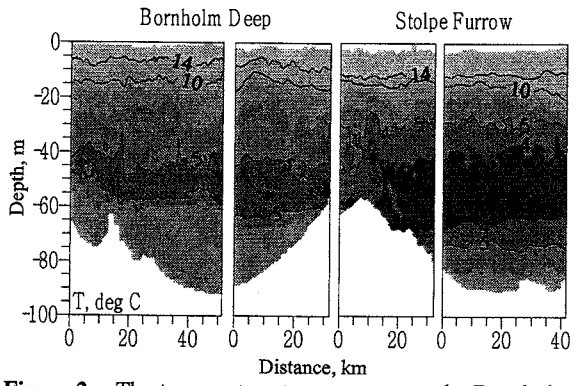

Figure 2: The temperature transects across the Bornholm Deep (left) and the Stolpe Furrow (right), with the Stolpe Sill in the middle.

On hypothesis of inertial wave ray structure in region of the Stolpen Sill and the Stolpen Furrow

Nikolay Golenko[1] and Agnieszka Beszczynska-Möller[2]

[1] Atlantic Branch of Shirshov Institute of Oceanology, 23600 Kaliningrad, Russia, golenko@ioran.gazinter.net
[2] Institute of Oceanology, 81-712 Sopot, Poland, abesz@iopan.gda.pl

1. Introduction

Measurements of thermohaline structure, conducted in last years with use of scanning CTD probe, allow to describe variability with scales from hundreds km to hundreds meters. Thereby structure peculiarities of internal waves may be included in consideration. Since 1995 the regular measurements have been performed by Polish and Russian scientific groups (*Paka* (1996), *Piechura et al.*(1997)) along a track from the Bornholm besin across the Stolpe Sill and along the whole Stolpe Channel (Fig.1).

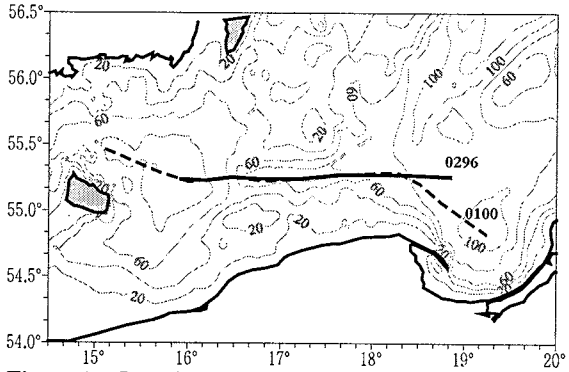

Figure 1: Locations of transects done with an undulated CTD probe in February 1996 (0296) and January 2000 (0100).

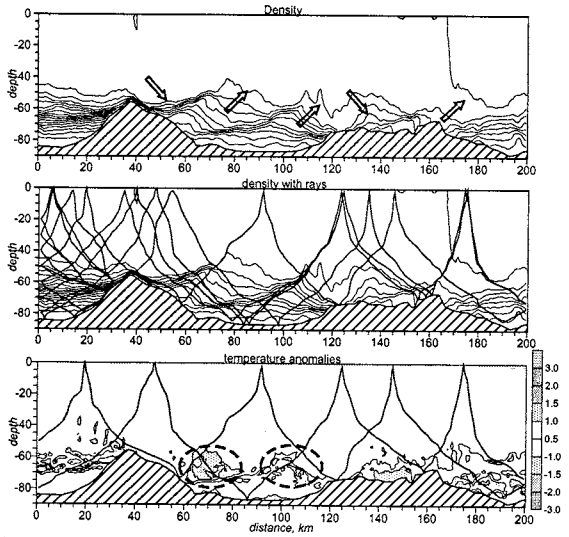

Figure 2: Transects in density field (upper two) and in temperature anomalies (lower one) for February 1996. Rays of QIIW are superimposed. Arrows shows supposed directions of group velocity vectors. Large temperature anomalies on rays crossing are marked out with ovals.

Numerous transects just along this track were analyzed. Pronounced oscillations with spatial scales of tens km were regularly observed. Example of such wave structure is presented on Fig.2.

Oscillations with distinctive phase shifts along some inclined directions were observed at almost all transects. Spatial structure of these oscillations is very similar to one of internal waves which energy radiates along some angle to horizon. Supposed directions of group velocities are shown at density distribution (Fig.2). Approximate evaluations of group velocity vector inclination give angle *ca* 0.1 degree. According to dispersing equation this value correspond to near inertial frequencies, so observed features in termohaline structure may caused internal waves of near-inertial frequency or quasi-inertial internal waves (QIIW). The objective of the presented work is in basing of this hypothesis.

2. Ray calculations

Numerical calculations of ray trajectories were based on the following equation:

$$dz/dx = \pm\sqrt{\frac{\omega^2 - f^2}{N^2 - \omega^2}}\,.$$

This equation was integrated numerically on the net with vertical step 1 m and horizontal step 500 m. The vertical density gradients, needed for N^2 evaluation, calculated from density data of high resolved transects. Preliminarily density data were interpolated in cross-points of a grid. When the calculated ray trajectory reached the upper surface or the bottom the sine before radical changed to the opposite one. It corresponds ray reflection events.

On the first step of investigation the equation was solved for variety of frequencies ω. It turned out that inclined lines along which the shifts of oscillation were observed, corresponded frequencies of ω=0.96-0.98 f, differing from a local inertial frequency on 2-4%. The further analysis was curried out with rays calculated for the frequency ω=0.96 f. For each transect a series of rays was calculated. The rays were launched from western boundary of each considered transect through the intervals 10 m from 20 m. Results of ray calculations which were putting over on density fields and temperature fields are presented on fig.2 (transect 0296) and fig.3 (transect 0100).

3. Temperature anomalies

For examination of a question about possible influence of inertial waves on temperature inhomogeneities, temperature anomalies were considered on isopycnal surfaces. These data for transect 0296, executed accordingly in February 1996, are submitted as transects at Fig. 2.

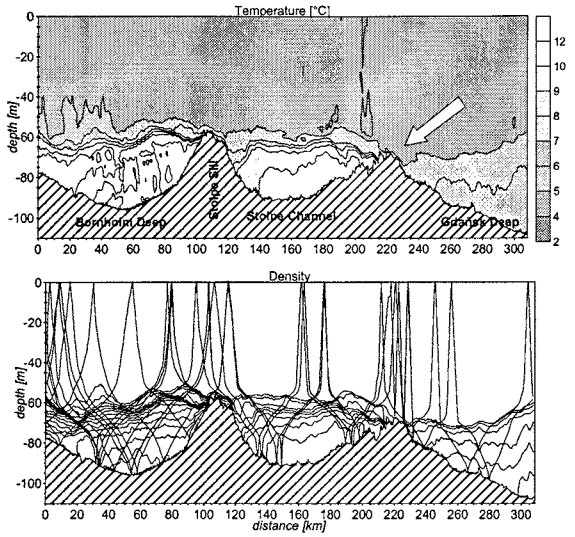

Figure 3: Transects of temperature (upper figure) and density field (lower figure) for January 2000. Rays of QIIW are superimposed. Arrow shows the place with deep convection until near bottom layer.

4. Discussion and conclusions

The summary results of performed analysis lead to the following conclusions:

1. The strains in oscillatins, specific for rays structure appear laying on the same beam of QIIW (Fig.2 and Fig.3).

2. Beams of QIIW, which have been started from various points of the Bornholm Deep, concentrate in the region of the Stolpen Sill. This effect was observed for all cases. Two groups of beams are usually shaped. Specific strains in the salinity/density fields are observed in places where the beams focus in to these two groups.

3. Sometimes temperature inhomogeneities developed in areas of beams crossing. It is clear that maximum velocity shear has there. Therefore temperature inhomogeneities with shear instability of QIIW develop with greater probability just in the areas of beams crossing. Observation of temperature inhomogeneities in these locations is an evidence that QIIW can form critical velocity shear, influencing on diapycnal exchange in the Baltic Sea.

4. An event of mixing throughout the whole water column from the upper layer to the bottom observed in January 2000 near the east border of the Stolpe Sill present the special interest, because concentration of QIIW beams occurred in the area of intensified mixing (Fig.3). Concentration of incident and reflected rays was clearly manifested within rather narrow horizontal interval. Obviously that halocline erosion within this area might occur not owing convection, which disturbs halocline from above, but due to turbulence generated by QIIW within the area of closely passing incident and reflected rays. Authors consider that a mechanism of positive feed-back between QIIW and convection functioned in this area. Convection makes the upper layer more homogeneous, so incident and reflected rays of QIIW becomes more vertical and more close to each other. At the same time shear instability due to superposition of several beams and subsequent turbulence generation occurred and stimulated further mixing. Mixing processes cause rays to be bent on closely and furthermore provoke instability and mixing. Note that described mechanism can develop not only at the upper boundary of the halocline as it takes place in case of convection, but mainly near the bottom , where incident and reflected rays are in a closest position. Naturally this effect occurs only during a cold season when the wide enough quasi homogeneous upper layer is already formed.

References

Paka, V. T. Thermohaline structure on transects in the Slupsk Furrow of the Baltic Sea in spring 1993, *Oceanologia (Russian)*, V.36, N 2, 207-217, 1996.

Piechura, J., W. Walczowski, A. Beszczynska-Moller. On the structure and dynamics of the water in the Slupsk Furrow, *Oceanologia (Polish)*, 39 (1), 35-54, 1997.

Towards improved modelling of runoff in climate models

L. Phil Graham and Björn Bringfelt

Rossby Centre, Swedish Meteorological and Hydrological Institute, SE-60176 Norrköping, Sweden

Introduction

As models continue to develop and coupled modelling between the atmosphere and the ocean evolves, the importance of accurate representation of runoff in climate models becomes more apparent. Not only should the overall water balance be resolved in time and space, but also the lateral transport of water from land to the sea should be adequately accounted for.

Such work is ongoing within the Swedish Regional Climate Modelling Programme (SWECLIM, Rummukainen et al., 2000) with further development of the Rossby Centre Regional Atmospheric Climate Model (RCA, Rummukainen et al., 2001) based on the HIRLAM weather forecast model (Källén, 1996). Development of better runoff in RCA is one result of cooperation between meteorological and hydrological modellers working in the Baltic Basin (Graham and Bergström, 2000; Graham and Bergström, 2001; Graham and Jacob, 2000). Concepts from hydrological modelling, and specifically the HBV model (Bergström, 1995; Lindström et al., 1997), have been incorporated into the climate model as described below.

Modelling Runoff Variability in RCA

Some of the components for generating runoff in the land surface parameterization of RCA are shown in Figure 1. For simplicity, the evapotranspiration components are not shown. Soil moisture is represented in two soil layers, a shallow surface layer, w_s, and a deeper layer, w_d. The HBV hydrological model approach to soil moisture and runoff was incorporated into these layers. Snow depth, SN, accumulates as a single layer on top of the uppermost soil layer.

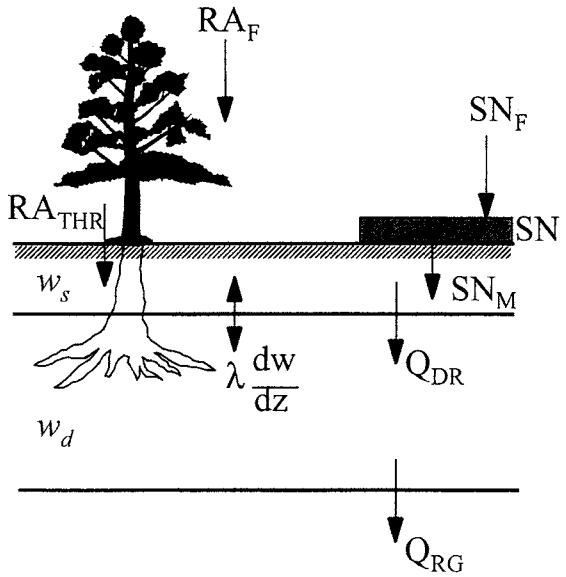

Figure 1: Runoff components of the surface parameterization scheme in RCA. (Evapotranspiration components are not shown.)

RCA uses modifications of the HBV model equations to give the fraction of rainfall plus snowmelt used for drainage flow, Q_{DR}, from the surface to the deep soil layer and for total runoff generation from the deep layer, Q_{RG}, as shown in equations 1 and 2 below,

$$Q_{DR} = (RA_{THR} + SN_M) \cdot \left(\frac{w_s}{w_{FCs}} \right)^{\beta_s} \qquad (1)$$

$$Q_{RG} = Q_{DR} \cdot \left(\frac{w_d}{w_{FCd}} \right)^{\beta_d} \qquad (2)$$

where, RA_{THR} is throughfall (rainfall, RA_F, minus interception), SN_M is snowmelt, w_s and w_d are soil moisture in the surface and deep layers, w_{FCs} and w_{FCd} are model field capacity for the surface and deep soil layers, and β_s and β_d are the index of heterogeneity for the surface and deep layers.

The exponents β_s and β_d reflect the areal variability of soil moisture. Thus, in contrast to many climate models, runoff can occur even if the area averages w_s and w_d are below field capacity, w_{FC}. These equations provide a much stronger relationship between runoff and soil moisture than those in the original HIRLAM model. As in nature, runoff response to infiltration increases (or decreases) nonlinearly as soil moisture increases (or decreases). The diffusive flux-gradient relationship for soil moisture, $\lambda\, dw/dz$, was retained to allow for more effective drainage of soil water as the top layer dries out (λ is hydraulic conductivity). However, most moisture transport from the surface to the deep layer occurs via Q_{DR}. Further detail on the RCA land surface parameterization is documented by Bringfelt et al. (2001).

Routing Runoff in RCA

Runoff generation, Q_{RG}, from the RCA soil moisture parameterization is instantaneous excess water per grid square, without any translation or transformation for either groundwater, lake and channel storage, or transport time. Further manipulation of this quantity is required to produce river discharge at river mouths into the Baltic Sea. This was accomplished by adapting the runoff response routine of the HBV model for use in RCA. A schematic of this approach is shown in Figure 2; the equations are,

$$Q_{UZ} = K_{UZ} \cdot UZ^{(1+\alpha)} \qquad (3)$$

$$Q_{LZ} = K_{LZ} \cdot LZ \qquad (4)$$

$$Q_{total} = Q_{UZ} + Q_{LZ} \qquad (5)$$

where, UZ and LZ are storage in the upper and lower runoff response zones, Q_{UZ} and Q_{LZ} are the discharge components from the upper and lower zones and Q_{total} is the total river discharge from the subbasin. K_{UZ}, K_{LZ} and α are recession parameters. The upper zone represents quick flow response, whereas the lower zone represents a slower baseflow type of response. $PERC$ is a constant percolation rate from the upper zone to the lower zone.

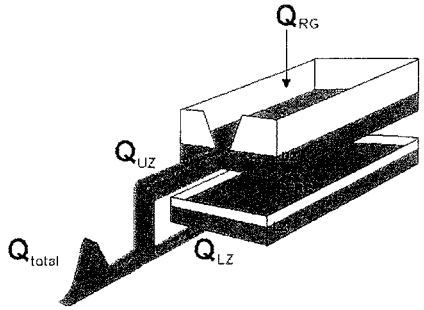

Figure 2: The runoff response routine for RCA.

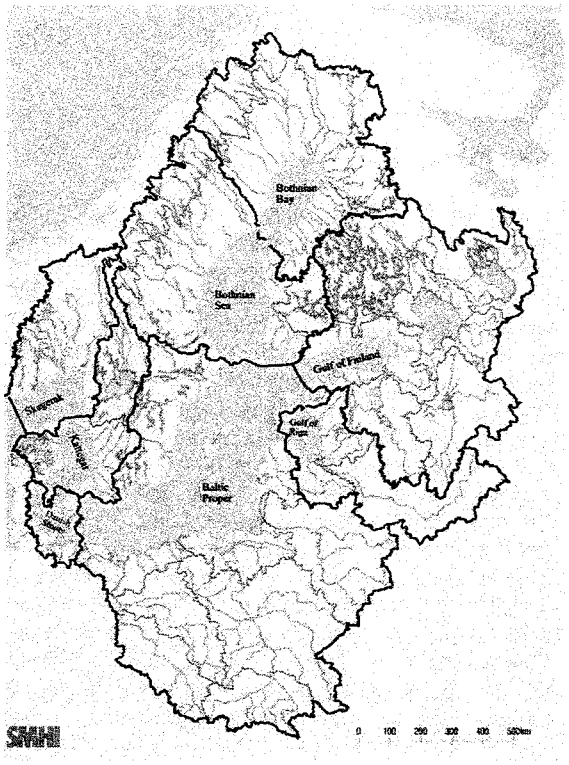

Figure 3: Subbasin map for RCA routing over the Baltic Basin.

As a first effort to produce river flow into the Baltic Sea directly from RCA, the routed runoff was setup with the same subbasin delineation used for the existing large-scale hydrological model, HBV-Baltic (Bergström and Graham, 1998; Graham, 1999). Figure 3 shows the division of subbasins used. In this way, the calibrated flow recession parameters from HBV-Baltic could be used as input parameters for the routing routine in RCA. The average runoff generation, Q_{RG}, from grid squares within each of the subbasins is the input to the routing routine and total river discharge from the subbasin is the output. For the case where upstream subbasins connect to a downstream subbasin before reaching the sea, lag times were applied. These lag times were also taken from HBV-Baltic. The final result is daily average river discharge in m^3s^{-1} to the sea from the respective coastal subbasins.

Conclusions

With the above modifications in RCA, the climate model is now better equipped to produce runoff that is more consistent with the variability of soil moisture that occurs in each grid square. Moreover, RCA now has the capability to directly provide river discharge to the sea, which previously required the use of an offline large-scale hydrological model. Although this by itself does not mean that the model will always provide the correct river inputs to the sea, it is a step in the right direction. Future testing and development will continue to include offline hydrological models, but we now have the means to better use the runoff that comes out of the RCA model. River discharge will be a diagnostic variable in coming SWECLIM climate scenario runs, both for coupling to ocean models and for large-scale impact studies.

References

Bergström, S., 1995. The HBV Model. In: V.P. Singh (ed.), *Computer Models of Watershed Hydrology*. Water Resources Publications, Highlands Ranch, Colorado, pp. 443-476.

Bergström, S. and Graham, L.P., 1998. On the scale problem in hydrological modelling. *J. Hydrol.* 211, 253-265.

Bringfelt, B., Räisänen, J., Gollvik, S., Lindström, G., Graham, L.P. and Ullerstig, A., 2001. *The Land Surface Treatment for the Rossby Centre Regional Atmospheric Climate Model - Version 2 (RCA2)*. SMHI Reports RMK, Swedish Meteorological and Hydrological Institute, Norrköping, (in press).

Graham, L.P., 1999. Modeling runoff to the Baltic Sea. *Ambio* 28, 328-334.

Graham, L.P. and Bergström, S., 2000. Land surface modeling in hydrology and meteorology - lessons learned from the Baltic Basin. *Hydrol. Earth Sys. Sci.* 4, 13-22.

Graham, L.P. and Bergström, S., 2001. Water balance modelling in the Baltic Sea Drainage Basin - analysis of meteorological and hydrological approaches. *Meteorol. Atmos. Phys.* (in press).

Graham, L.P. and Jacob, D., 2000. Using large-scale hydrologic modeling to review runoff generation processes in GCM climate models. *Meteorol. Z.* 9, 49-57.

Källén, E. (ed.), 1996. *HIRLAM Documentation Manual System 2.5*. Swedish Meteorological and Hydrological Institute, Norrköping, 178 pp.

Lindström, G., Johansson, B., Persson, M., Gardelin, M. and Bergström, S., 1997. Development and test of the distributed HBV-96 model. *J. Hydrol.* 201, 272-288.

Rummukainen, M., Bergström, S., Källén, E., Moen, L., Rodhe, J. and Tjernström, M., 2000. *SWECLIM - The First Three Years*. SMHI Reports RMK, No.94, Swedish Meteorological and Hydrological Institute, Norrköping, 87 pp.

Rummukainen, M., Räisänen, J., Bringfelt, B., Ullerstig, A., Omstedt, A., Willén, U., Hansson, U. and Jones, C., 2001. A regional climate model for northern Europe: model description and results from the downscaling of two GCM control simulations. *Clim. Dynamics* 17, 339-359.

The NOPEX Project, challenges and some recent scientific results

Sven-Erik Gryning[1], Sven Halldin[2] and Anders Lindroth[3]

[1] Risø National Laboratory, DK-4000 Roskilde Denmark
[2] Department of Earth Sciences/Hydrology, Uppsala University, Uppsala, Sweden
[3] Department of Physical Geography, Lund University, Lund, Sweden

1. The NOPEX project

NOPEX (NOrthern hemisphere climate-Processes land-surface EXperiment) is devoted to studying land-surface-atmosphere interaction in northern European forest-dominated landscapes. In NOPEX equal weight is put on long-term measurements and time-limited, areally extended concentrated field efforts. The original NOPEX study region represents the southern part of the boreal zone, situated in the Baltic Sea drainage basin near Uppsala, Sweden. A northern study region, centred on the Sodankylä Meteorological Observatory (SMO) in north Finland, was introduced 1996 in connection to winter-time studies. SMO represents the northern part of the boreal-forest zone.

NOPEX is specifically aiming at investigating fluxes of energy, momentum, water, and CO_2 between the soil, the vegetation and the atmosphere, between lakes and the atmosphere as well as within the soil and the atmosphere on local to regional scales ranging from centimetres to tens of kilometres.

Here we present selected results from the concentrated field efforts in 1994, 1995 (NOPEX-summer) and 1997 (NOPEX-winter). Main results from NOPEX-summer is presented in a special issue of *AgForMet*, similarly for NOPEX-winter in *Theoretical and Applied Climatology*. Both issues include a CD with the measurements from the campaigns. Further articles on NOPEX-winter can be found in *Boundary-Layer Meteorology*. See reference list for complete information. The references in this report can be found in the volumes in the reference list. Presently the NOPEX project has resulted in 8 PhD dissertations.

2. NOPEX-summer

The first phase of NOPEX dealt with processes governing states and fluxes at the boreal-forest land-surface-atmosphere interface during spring and summer conditions. Here we report main results from regional-scale studies. For results from local-scale studies focusing on small-scale processes, including lakes, and the long-term monitoring programme please consult the *AgForMet* special issue.

2.1. Surface-atmosphere exchange-regional scale

Spatial integration of land-surface parameters over non-homogeneous surfaces is a central issue for NOPEX as well as for BALTEX. Direct assessment of mesoscale fluxes were primarily performed with experimental aircraft and balloon sounding. These measurements were complemented with a network of groundbased stations measuring both fluxes and states at the surface.

Gottschalk et al. (1999) compare fluxes of sensible and latent heat over the NOPEX region calculated with five methods (airborne and balloon-sounding measurements, weighted mast measurements, and two models) and found rather large differences between some of them. The aircraft measurements of sensible heat fluxes were generally lower than those obtained from ground measurements whereas latent heat fluxes showed a fair agreement. Good agreement was found between all the different methods when it came to evaporation fluxes. This indicates that evaporation fluxes can be aggregated from land-use-weighted mast fluxes in this boreal-forest region. Tests with a new parameterisation scheme in HIRLAM (*Bringfelt et al., 1999*) confirmed the conclusion that straightforward area-weighted flux averaging gave results as good as more complex aggregation schemes.

Frech and Jochum (1999) evaluated flux-aggregation methods from aircraft measurements and found different behaviour for momentum and scalar transfer. It seems as if the momentum transfer is governed by the roughest elements (the forest) whereas the sensible heat flux is determined by the predominant land-cover type in a given grid cell or aircraft run segment.

The radiosonde data have been used to deduce regional fluxes. *Hiyama et al. (1999)* explore two methods to determine regional momentum flux. *Gryning and Batchvarova (1999)* deduce the regional sensible heat flux over the NOPEX region for three days in 1994. The regional flux was lower than that over forests and higher than that over agricultural land. The regional flux agreed well with land-use-weighted average heat flux.

The regional CO_2 flux was determined by *Levy et al. (1999)* with a boundary-layer-budget method. The regional fluxes were compared with ecosystem-scale fluxes and good agreement was found on days when the airmass was of maritime origin, and the CO_2 mixing ratio above the convective boundary layer could be assumed to be equivalent to values measured at oceanic sites. Poor agreement was found on days when this assumption did not hold.

2.2. Surface and subsurface water

Data from the synoptic and long-term catchment studies have been combined with standard hydrological data from central Sweden to develop and assess hydrological models. Evaluation of precipitation data both from weather radar and from new and old rain gauges has been emphasised.

The ECOMAG hydrological model was further developed as a combined prediction and assimilation tool for the NOPEX region (*Motovilov et al., 1999*) and was used as a first step towards a fully coupled hydrological-atmospheric model. The HBV model, another conceptual precipitation-runoff model used operationally in Sweden, was applied to 11 different catchments within the NOPEX region with the aim to relate the parameter values to independently measurable catchment characteristics (*Seibert, 1999*). After Monte-Carlo calibration with a two-criteria optimisation procedure good runoff simulations were achieved.

Beldring et al. (1999) found that measured soil-moisture content and groundwater levels show a characteristic pattern which are closely related to the landscape elements in the region. The variability of average values between

areas decreases to a minimum for landscape elements of around 1 km^2.
Precipitation is difficult to measure with accuracy and precision. *Seibert and Morén (1999)* show how the systematic errors in traditional rain gauging was reduced with a new type of gauge used in NOPEX. Average wind losses were reduced by 3% and wetting losses by 0.25 mm per rain event. Ground-based precipitation measurements were used as validation for the application of the threshold method for estimating areal rainfall over the NOPEX region from weather-radar data (*Crochet, 1999*).

2.3 Remote sensing
The ultimate objective of the remote-sensing studies was to supply hydrological and meteorological models with input and validation data. The studies have been based on satellite, airborne scenes and ground-based observations.
Van de Griend and Seyhan (1999) used seven acquisitions from ERS-1/SAR during 1994 and 1995 to determine the potential of the C-band VV-polarised backscattering data to discriminate different surface types within the NOPEX region. The seven scenes were evaluated against forest-density classes derived from aerial photos and a fully polarimetric EMISAR C-band image and it was found that they could be used to discriminate between forests of different density throughout the season. The same images were also evaluated to find out if it was possible to determine if the backscattering properties of lakes depended on regional wind speeds. The results supported the potential of monitoring regional-scale wind fields from radar observations of boreal lake surfaces.

3. NOPEX-winter (WINTEX)

The high latitudes are snow covered for as much as nine months of the year. The difference between open snow fields and forests is probably the largest land surface contrast found in the terrestrial biosphere. The presence of a snow cover radically alters the surface radiation budget, reflecting as much as 90% of the incoming solar radiation. It also changes the surface aerodynamic characteristics and insulates the ground preventing very cold air temperatures propagating into the soil. The contrasts between the northern and the southern NOPEX sites are significant because the southern site is at the southern boundary of the boreal forest zone whereas the northern region represents the northern boundary of the boreal forest.

3.1 Surface atmosphere exchange
During the winter transpiration rates are small, due to the cold, often frozen soils. The substantial solar radiation input to the canopy in spring is balanced by a substantial upward sensible heat flux, leading to unstable boundary layer above the forest (*Gryning et al. 2001*, *Batchvarova et al. 2001*). These exchanges can be simulated with a combination of a simple geometric radiation model and a two source energy exchange model such as that described by *Shuttleworth and Wallace 1985* (*Gryning et al. 2001* and *Melas et al. 2001*).
The importance of the snow model within a Numerical Weather Prediction (NWP) model is illustrated in *Savijärvi and Kauhanen (2001)*. The data set produced at the WINTEX site at Sodankylä was used to test the FMI HIRLAM model. In the case study presented the night-time air temperature were under-predicted by between 12 and 15°C. The thermal properties of the snow surface appeared crucial. A layer of snow of very low density was present on the night of the case study, this tended to insulate the surface and helped the surface to cool strongly overnight. *Savijärvi and Kauhanen* conclude that realistic parameterisations of all the main processes (surface exchanges, snow/soil physics, turbulence, radiation etc) are necessary to achieve a good simulation of the nocturnal inversion.

3.2 Numerical simulations
A comparison between surface and aircraft observations and numerical simulations (*Savijärvi and Amnell 2001*, *Melas et al. 2001*, *Batchvarova et al. 2001*) showed good agreement. These studies also illustrated the high sensible heat flux from the forested areas, leading to the development of a convective atmospheric boundary layer. The rougher forest patches also dominate the momentum flux from the landscape, *Batchvarova et al. (2001)*. A simulation for 4 days during March showed the importance of the correct parameterisation of the absorption of solar radiation by the sparse boreal forest (*Melas et al. 2001*). The combination of sparse forest and snow on the ground (i.e. a considerable contrast in the net radiation between the ground surface and the vegetation) results in a strong dependence of the aggregate albedo on the sun angle and leads to a high interception of radiation by the vegetation at low sun angles (*Gryning et al. 2001*). The correct simulation of the measured surface day-time sensible heat fluxes and boundary layer properties depends on the accurate parameterisation of this radiation exchange. The simulation of the near surface temperature also depends on the inclusion of new parameterisation of heat storage in the forest canopy. All these modelling studies show the importance of the snow-vegetation-atmosphere interface to the atmosphere. The improvements in the parameterisations of the fluxes across this interface substantially improved the simulations of the atmospheric boundary layer. These improvements will certainly lead to improved performance of NWP and climate models in high latitude regions.

3.3 Remote sensing
Satellite measurements provide a methodology to extrapolate from the point to the landscape or catchment scale. A comparison of surface reflectance patterns over the snow-covered forested landscape of northern Finland showed good agreement between aircraft and satellite measurements (*Kangas et al. 2001*) and illustrates the substantial variation between the forested and non-forested regions. During the winter frequent changes in reflectance patterns are to be expected due to snowfall and the rapid development of snow intercepted on the trees. The study of reflectance distributions from the aircraft observations for the main land cover types and the comparison with satellite measurements suggests that real-time satellite-based estimates could be used to monitor the day-to day variation in surface reflectance as an input to NWP models.

References:

Halldin, S., Gryning, S.-E., Gottschalk, L., Jochum A. A. van de Griend. Boreal Forest and Climate, Special issue. *Agricultural and Forest Meteorology.* Vol. 98-99., 1999

Halldin, S., Gryning, S.-E., Lloyd, C. R. Land-surface/atmosphere exchange in high-latitude landscapes. Special issue. *Theoretical and Applied Climatology.* In print. 2001

Roughness length over the Baltic Sea

Xiaoli Guo-Larsén and Ann-Sofi Smedman

Department of Earth Sciences, Meteorology, Uppsala University, Sweden

1. Introduction

The air-sea momentum transfer is proportional to the roughness of the waves. For decades people have been exploring with lab and field data the roughness length over water in terms of wave age c_0/u_* and the root-mean-squared (rms) surface elevation (refer to e.g. *Donelan* (1990)) A simple regression formula of roughness length is given for fully rough flow:

$$z_0/\sigma = \alpha\,(u_*/c_0)^{\beta} \qquad (1)$$

where z_0 is the roughness length, σ the rms. surface elevation, u_* the surface friction velocity, and c_0 the wave phase velocity. Coefficients α and β vary from experiment to experiment.

Addressing this problem, *Drennan et al* (2000) selected data from five recent field campaigns for pure wind sea, deep water, and fully rough flow, and eliminated the self-correlation between the left and right hand side of equation (1). *Dobson et al* (1994) also tried to delete swell from the wave spectra in order to produce a sea state/wind stress relation for not only the pure wind sea but also swell cases. It was stated that for their data equation (1) is not significantly affected by the relative contribution of sea waves and swell.

In this research the roughness length over the Baltic Sea is investigated. Firstly we focus on cases of the pure wind sea, deep water and fully rough flow, and secondly swell condition is studied.

2. Measurement and Data Analysis

Data contain one-hour averages of profile, turbulence and wave data. Profile and turbulence were measured at Östergarnsholm, a flat island in the Baltic Sea, where a 30m high tower is instrumented by slow response sensors for profiles, and SOLENT 1012R2 sonic anemometers to record turbulent fluctuations. Wave spectra and water temperature were measured by a Directional Wave-rider Buoy (run and owned by the Finnish Institute for marine Research). The buoy is moored 5 km south-southeast of the tower at a site with water depth about 40 m. Detailed description of measurements can be found in *Smedman et al* (1999).

The data set consists of whole year data of 1998, 1999, and several periods in 1995-06, 1995-09, 1996-09 and 1997-05.

We select data with airflow from the undisturbed water fetch, i.e. with wind coming from 80° to 220°, and require direction difference between wind and wave propagation less than 40°.

Data are classified into two classes, class 1 is restricted to pure wind sea, deep water and fully rough flow, and class 2 is swell condition. According to *Vickers and Mahrt* (1997), for deep water we require the dominating wave length $\lambda_0<4H$, where H is the water depth. According to *Drennan et al* (2000) for rough flow we require the roughness Reynold's number $u_*z_0/\nu > 2.3$, where ν is the kinematic viscosity of air. For pure wind sea we require the integrated spectral swell and wind sea energy E_1 and E_2 satisfying $E_1/E_2<0.2$, where

$$E_1 = \int_{n_{start}}^{n1} S(n)dn \qquad (2)$$

$$E_2 = \int_{n1}^{n_{end}} S(n)dn \qquad (3)$$

In the wave spectrum, S is the spectral energy density plotted as a function of frequency n; n1 is the frequency at which wave phase velocity matches the wind speed at a height of wave length order (here 8 m is used); n_{start} and n_{end} are the first and last sampling frequencies respectively.

The roughness length is calculated as:

$$z_0 = z\cdot\exp\left(-\frac{\kappa}{\sqrt{C_{DN}}}\right) \qquad (4)$$

where κ the von Kármán constant ≈ 0.4, z is the height where turbulence is measured. It is adjusted to the mean water level of the Baltic Sea supplied by the Visby Harbour, see *Sjöblom A and Smedman* (2001), and it varies between 9.88– 10.79 m. The 10 neutral drag coefficient is defined as:

$$C_{DN} = u_*^2/U_{N10}^2 \qquad (5)$$

and

$$U_{N10}=U_{10}+(u_*/\kappa)\psi_M \qquad (6)$$

ψ_M is the integrated analytical form of the non-dimensional gradients for momentum.

In order to avoid substantial corrections for stability and make variables less dependent on the stability functions, we restrict data to essentially neutral cases by requiring $|\langle w'\theta'_{10}\rangle| < 0.01$ for swell cases.

3. Results

In Fig. 1 the dimensionless roughness is plotted versus inverse wave age for pure wind sea, deep water and fully rough flow. Data are grouped into five groups according to u_*. In doing so, almost all the change in wave age is in the wave phase velocity, so that the influence of self-correlation between the two variables is eliminated. The regression curve for each group is very close to each other for each wave age region except for the last group which has very few data. The thick curve is the regression for all data.

From Fig. 2 it can seen that the present regression gives a steeper slope than *Donelan* (1990) but almost no difference from *Drennan et al* (2000)

Drag coefficient is a function of wind speed and wave age according to equation (4), (5) and (6). Based on data in Fig. 1, a model of drag coefficient as a function of wind speed, corrected to neutral stability is plotted in Fig. 3. All deep water and fully rough flow data (including $E_1/E_2\geq 0.2$) are used and compared with the model and the result of *Smith* (1980) Except for the youngest wave age group which has too few data, the other two groups are consistent with the model. The curve from *Smith* (1980) agrees with the modeled line for $0.04<u_*/c_0\leq 0.06$.

In Fig. 4, the normalized roughness length is plotted versus inverse wave age for all data with heat flux less than 0.01 mK/s. In order to study the role of the relative size of swell and wind sea (E_1/E_2), data are grouped into four groups according to E_1/E_2. Regression coefficients in each group are listed in Table 1. Except for group 1 that has a more linear trend, a second order polynomial coefficient decreases as E_1/E_2 increases.

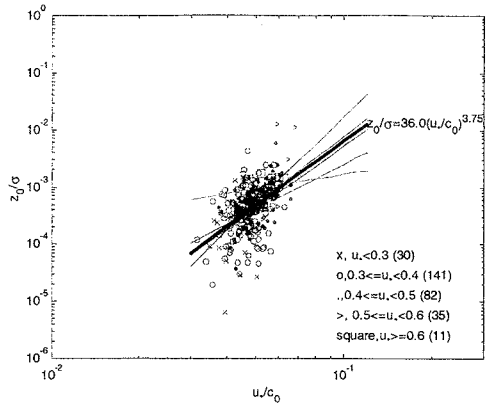

Figure 1: Dimensionless roughness versus inverse wave age for pure wind sea, deep water and rough flow. The data are grouped according to u_*, and a regression is made for each group. The thick line is the mean regression line for the five classes.

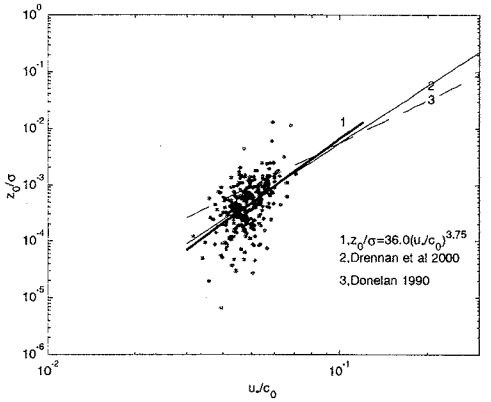

Figure 2: Same data as in Figure 1. The curves are *Donelan* (1990) (3), *Drennan et al* (2000) (2) and the present regression (1).

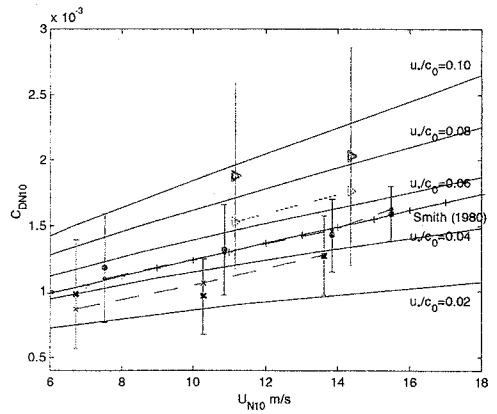

Figure 3: Drag coefficient versus wind speed, both 10m neutral. Data are grouped by inverse wave age, $0.02<u_*/c_0\leq0.04$ (x, 800 points), $0.04<u_*/c_0\leq0.06$ (.,543 points) and $0.06<u_*/c_0\leq0.08$ (>, 13 points), with mean value and the standard deviation, and the dashed line linked symbol represents the expected drag coefficient of each group on its mean u_*/c_0 and U_{10N}. The other curves are *Smith* (1980) (with + in), and the wave age dependent drag coefficient relations resulting from equations (4), (5) and (6).

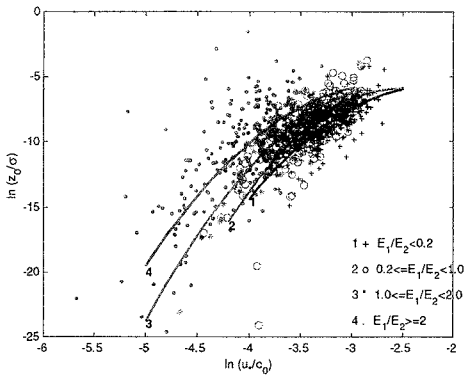

Figure 4: Dimensionless roughness versus inverse wage for data with $|\langle w'\theta'_{10}\rangle| < 0.01$. Data are grouped according to E_1/E_2. The curves are the best fit of second order polynomial of each group.

Table 1: Constants in the best fit curves in relation $\ln(z_0/\sigma)= a \ln^2(u_*/c_0) + b \ln(u_*/c_0) + c$, for the four groups of data in Fig. 4.

Group	Num. of points	Const. a	b	c
1	298	-2.67	-11.75	-18.64
2	254	-3.67	-18.62	-29.47
3	128	-2.94	-14.67	-23.72
4	256	-2.61	-14.06	-24.54

4. Summery

This study demonstrates that over the Baltic Sea there is a wave age dependence of roughness as proposed by earlier studies. This study also shows that the roughness/wave age relation depends on the relative contribution of swell and sea waves.

References

Dobson Fred W., Stuart D. Smith and Robert J. Anderson, *Atmosphere-Ocean* 32 (1), 237-256, 1994

Donelan M. A., *Air-sea interaction, in The Sea:Ocean Engineering Science*, 9, 239-292, 1990

Drennan W., Hans C. Braber, Danièle Hauser and Céline Quentin, On the wave age dependence of wind stress over pure wind seas, Submitted to *the Journal of Geophysical Research*, 2000

Sjöblom Anna and Smedman A.S.,The turbulent kinetic energy budget in the marine atmospheric surface layer, To be submitted to *J. Geophys. Res.* 2001

Smedman A.S., U. Högström, H. Bergström, A. Rutgersson, K.K Kahma and H. Petterson, A case study of air-sea interaction during swell conditions, *J. Geophys. Res.*, 104, 25833-25852, 1999

Smith S.D., Wind stress and heat flux over the ocean in gale force winds, *J. Phys. Oceanogr.*, 10, 709-726, 1980

Vickers D and Mahrt L, Fetch limited Drag coefficients, *Boundary-Layer Meoteorology*, 85: 53-79, 1997

On the forcing of Baltic Sea water and salt exchange

Bo G. Gustafsson and Helén C. Andersson

Department of Oceanography, Earth Sciences Center, Göteborg University, Box 460, SE-405 30 Göteborg, Sweden

1. Introduction

The large Baltic Sea estuary has a hampered exchange with the ocean due to the topographical constriction of the transition area. Understanding the mechanisms controlling the deep-water renewal and possible climatic dependencies are of primary concern in order to understand past and future changes of the Baltic Sea.

The water exchange across the sills is almost exclusively barotropic and vertically homogeneous, and primarily forced by the sea level difference between the Kattegat and the Baltic Sea. The sea level in Kattegat is largely governed by regional winds (*Lass et al.*, 1987), especially during the winter season when they usually are strong. Inflow events, large and saline enough to renew the Baltic deep-water, are also more frequent in the winter than during other seasons (*Matthäus and Franck*, 1992; *Matthäus and Schinke*, 1994). *Matthäus and Schinke* (1994) analyzed typical atmospheric pressure patterns before and during major Baltic inflows. They found that the inflows are associated with a strong meridional air pressure gradient across the North Sea and the stronger the gradient the larger the inflow.

We have used century long time-series to investigate the interrelations between observed air pressure, sea level and salinity in period bands relevant to North Sea - Baltic Sea water and salt exchange. Further a semi-empirical model of the deep-water renewals is developed and evaluated by means of century long observational series of sea level, air-pressure and salinity.

2. Statistical relationships

Daily means of South-North air pressure difference was calculated out of observations from de Bilt, the Netherlands and Oksøy, Norway. We used a daily sea level recordings from Stockholm to represent the mean Baltic sea level and sea level observations from Hornbæk to represent Kattegat sea level. Surface salinity in the Kattegat is taken from daily measurements at Anholt.

More than 70% of the Kattegat sea level variance is explained by oscillations in the South-North pressure difference of periods between 15 and 200 days and the absolute value of the response function is about 2 cm hPa^{-1} (see Fig. 1). For oscillations with periods longer than 35 days, the explained variance is more than 80%. For oscillations with periods longer than about 200 days the explained variance decreases and the sea level is not as clearly dependent on pressure difference oscillations of such long periods. The sea level lags the variations in the air-pressure difference with about 0.7 days for periods of less than 40 days, there after an increase in lag is seen to about 4 days for periods up to 200 days. The fast response and the high explanation factor indicates a strong impact from the east and west wind directions on the sea level due to local and regional set up.

The surface salinity in the Kattegat is statistically highly dependent on the Baltic sea level oscillations (Fig. 2). The explained variance is between 50 to 82% for the period band 30 to 250 days. The interpretation of the small phase lag between the two is that water in the area connecting the Kattegat and the Baltic Sea, oscillates back and forth with the volume changes of the Baltic Sea, causing immediate movements of the horizontal salinity fronts in the Kattegat.

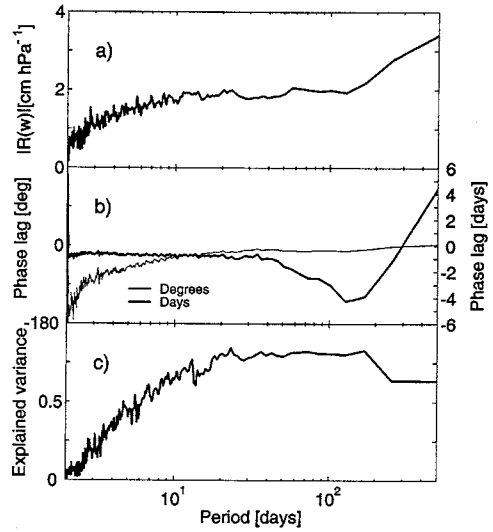

Figure 1: The frequency dependent response of the Kattegat sea level to oscillations in the South-North air pressure difference across the North Sea. The figure shows in (a) the absolute value of the response function, (b) the phase lag between the time series and (c) the explained variance by the frequency dependent linear regression.

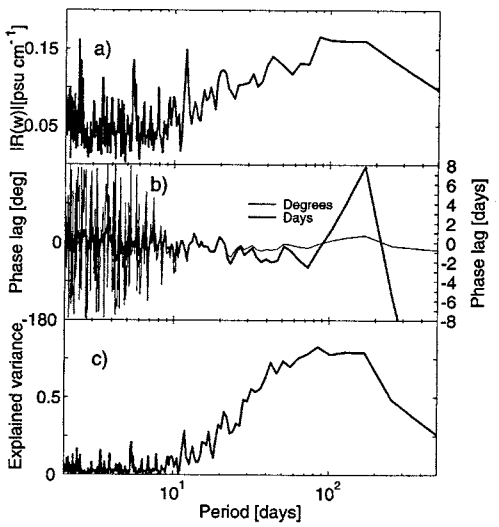

Figure 2: The response of the surface salinity in Kattegat to oscillations in the Baltic sea level. The figure shows in (a) the absolute value of the response function, (b) the phase lag between the time series and (c) the explained variance by the frequency dependent linear regression.

3. Water and salt flux model

The horizontal difference in air pressure is fitted to Kattegat sea level observations by linear regression. The barotropic flow through the narrow straits between the Kattegat and the Baltic proper can be calculated by from the longitudinal barotropic pressure gradient caused by the sea level difference.

We have previously shown the strong co-variation of Baltic sea level and surface salinity at Anholt in Kattegat. We decide that the salinity in Kattegat should be modeled by

$$S_K = c \cdot h + \overline{S_K}$$

where c = 0.2 psu cm^{-1} and $\overline{S_K} = 21$ psu is the mean salinity.

Near the sills, the salinity will not change symmetrically when the water oscillates back and forth. The salinities will gradually increase towards Kattegat salinity during inflows to the Baltic, but more rapidly decrease towards Baltic surface salinity during outflows because of the sharper salinity gradient. To estimate the salinity in the vicinity of the sills, we assume a gradual change towards either Kattegat or Baltic Sea salinity, depending on flow direction.

4. Results

The Baltic sea level computed from the South-North air pressure difference is compared with observed sea level at Stockholm. The explained variance is higher than 80% for oscillations with periods longer than 30 days and the phase error is close to zero. The computed series underestimates the observed variance with 71 cm^2, also primarily originating from the underestimation of long period oscillations.

Sample time-series of observed and modeled salinities at Anholt and the two sills are shown in Fig. 3. The RMS error of the whole time-series 1931-1985 is 2.9 psu, but short-term events occur when the modeled salinity is quite far from what is observed. We think that these events with large discrepancy are due to mixing from occasional storms.

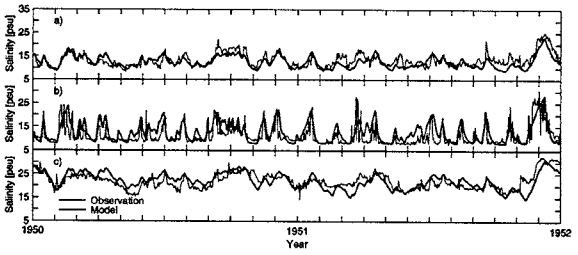

Figure 3: Sample from the time-series of modeled and observed salinity at (a) Darss sill, (b) Drogden sill and (c) Anholt.

The deepest layers of the Baltic Sea can only be renewed if a large volume of water of sufficiently high salinity passes the sills. We used our model to reproduce the variations in the inflow events. We reduced the data set by the requirement that at least 50 km^3 of water with $S > 17$ psu must pass the sills during an inflow. With this condition we are left with 118 inflows during 1902-1998. The integrated salt flux, M, during these inflows is drawn in Fig. 4a. Also shown are annual averaged time-series of salinity and oxygen at 200 m depth in the Baltic proper. The total salt fluxes carried by this selection of inflows vary between 2.38 – 5.32·10^{12} kg and we can already here identify some of the major inflows previously identified by, e.g., *Franck et al.* (1987) and *Fischer and Matthäus* (1996). The salinity of an inflow determines to a large degree its possibility to reach the Baltic deep-water. Therefore we have in Fig. 4b and 4c restricted the integration of the salt flux to water of salinity greater than 17 (M_{17}) and 20 (M_{20}) psu, respectively.

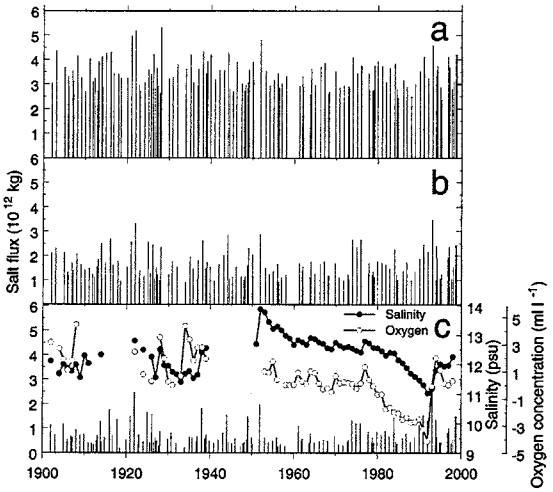

Figure 4: Computations of the integrated salt flux for three different criteria: (a) integration of all salinity ranges (M), (b) integration of salinity of more than 17 psu (M_{17}) and (c) integration of salinity of more than 20 psu (M_{20}).

5. Discussion

The existing models of the vertical circulation of the Baltic Sea presently calculates the water exchange from observed sea levels in Kattegat. Our results will enable these models to simulate the circulation of the Baltic Sea solely from meteorological and hydrological forcing, which can be obtained from regional atmospheric and hydrologic climate models that are already operational.

The inflow model makes it possible to assess the sensitivity of these inflows to climate change directly from regional and global atmospheric scenario simulations. If combined with hydrological forecasts, one can also obtain an approximate development of the average salinity of the Baltic Sea.

References

Fischer, H. And W. Matthäus, The importance of the Drogden Sill in the Sound for major Baltic inflows, *J. Marine. Sys., 9,*137-157, 2000.

Franck, H., W. Matthäus and R. Sammler, Major inflows of saline water into the Baltic Sea during the present century. *Gerlands Beitr. Geophysik 96*, 517–531, 1987.

Lass, H. U., R. Schwabe, W. Matthäus and E. Francke, On the dynamics of water exchange between Baltic and North Sea. *Beitr. Meereskd. 56*, 27-49. 1987.

Matthäus, W. and H. Franck, Characteristics of major Baltic inflows - a statistical analysis. *Cont. Shelf Res., 12*, 1375-1400, 1992.

Matthäus, W. and H. Schinke, Mean atmospheric circulation patterns associated with major Baltic inflows, *D. Hydr. Z., 46,* 321–339, 1994.

Scales of Sea Surface Salinity

Anna Haapaniemi[1], Anniina Kiiltomäki[1], Tuomo Roine[1], Hanna Villa[1], Jari Haapala[1], Antti Lindfors[1], Juha-Markku Leppänen[2]

[1] Department of Geophysics, P.O. BOX 64, FIN-00014 University of Helsinki, Finland
[2] Finnish Institute of Marine Research, P.O. BOX 33, FIN-00931 Helsinki, Finland

1. Introduction

Large horizontal variations of salinity are a typical feature of the Baltic Sea. A general pattern of salinity field is due to the water exchange between the North Sea and the Baltic Sea and advection and mixing of fresh water originating from the large rivers. In this study we have examined horizontal distribution of salinity and temperature based on the unattended flow-through system installed on the ferry running regularly between Helsinki and Lübeck. In addition, measurements have been made in the river Kymijoki estuary with a flow-through system installed on the small boat. Small-scale salinity and temperature measurements have also been made in the Pojo Bay, which is an estuary of the river Mustionjoki and in the Bay of Bothnia by the estuaries of rivers Kemijoki and Oulujoki.

2. Methods and Results

In studies of horizontal distribution of salinity and temperature in the Baltic Sea we have used data of Alga-line program which is an algal monitoring program of *Finnish Institute of Marine Research.* Unattended flow-through system with fluorometer, CT and automated water sampler was set up on a merchant ship *M/S Finnpartner.* Flow-through system has fixed sampling depth of 5m and it collects data every 20 seconds. (*Rantajärvi, E, Leppänen, J-M.* 1994). It traverses Baltic Proper every other day while cruising between Helsinki and Lübeck (*figure 1*).

The salinity and temperature measurements of river Kymijoki estuary were made during the summer 2000 during six different cruises. Each trip covered the same, about 25km long area where the surface water measurements were taken continuously by using a flow-through system with a fixed sampling depth. The location was recorded with a DGPS. This same system was also used in the autumn 2000 when the data from rivers Tornionjoki and Oulujoki were acquired. The data from Pojo Bay has been collected by various methods: with a flow-through system, from regular CTD measurement on several measurement sites and by researching articles concerning this subject. These small-scale salinity variations have been examined in respect of the geographical surroundings of the observation areas and the flow.

Alga-line data shows that greater salinity gardients are found west of Bornholm-island and north of Landsort-Saaremaa line. Salinity anomalies in the western Baltic can easily exceed Darss Sill while travelling east but those usually can't cross the middle part of Arkona Basin. That place seems to be a barrier for many salinity anomalies. Surface water has quite stable salinity there the whole year. On the other hand we found anomalies with lower salinity travelling from Gulf of Finland to Baltic Proper. Horizontal distribution of salinity on two different cruises is shown in *figure 2.*

The small-scale salinity measurements show very clearly the expected shift from fresh to seawater when moving from the river mouth towards the open sea. The shape of the estuary, river flow and weather conditions dictate the behaviour of salinity and temperature on these areas.

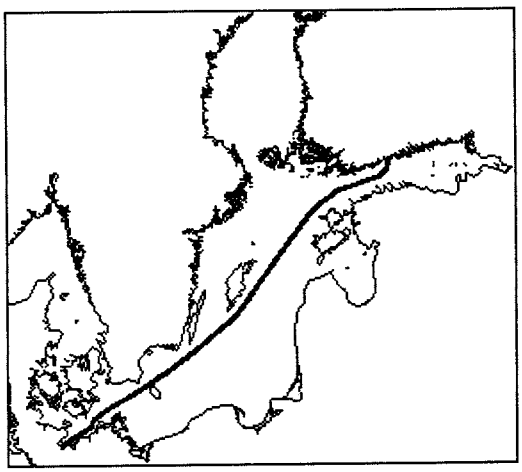

Figure 1: The route of M/S Finnpartner.

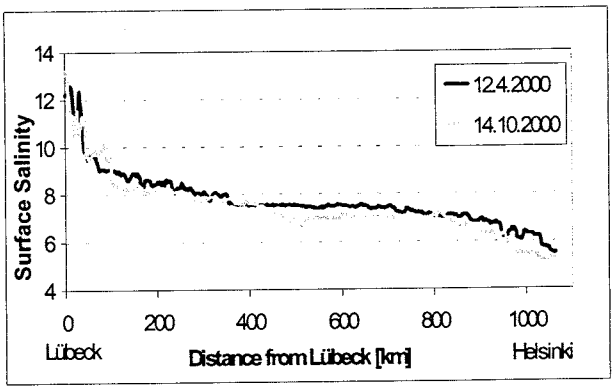

Figure 2: Horizontal distribution of salinity on two cruises.

References

Rantajärvi, E., Leppänen, J.-M. 1994. Unattended algal monitoring on merchant ships in the Baltic Sea. - TemaNord 546:1-60.

Cloud Liquid Water from Combined AMSU and AVHRR Measurements

Heike Hauschildt, Thomas Martin and Andreas Macke

Institute for Marine Research, D-24105 Kiel, Germany

1. Introduction

The atmospheric water plays an important role in the climate system. Catching it's large spatial and temporal variability is a keyproblem in atmospheric research and is currently undertaken in the European project BALTEX CLIWA-NET. While ground based measurements are able to monitor local temporal changes in liquid water, satellite instruments cover large areas with varios spatial resolution. The present work investigates the potential to retrieve cloud liquid water path from a combination of the Advanced Microwave Sounding Unit (AMSU) and the Advanced Very High Resolution Radiometer (AVHRR), both instruments operating on board the NOAA KLM satellite series.

The AMSU measures microwave emission at 20 frequencies between 23.8 GHz and 183.0 GHz divided into two modules. The spatial resolution ranges from 48 km × 48 km at nadir to 79 km × 149 km at the outer beam position. Each scan consists of 30 fields of view (FOV). For the retrieval of liquid water path (LWP) the algorithm of *Grody et al.* (1999) has been applied, using the 23.8 GHz channel and the the liquid water sensitive 31.4 GHz channel.

The AVHRR measures solar reflectance and thermal emission. The spatial resolution ranges from 1 km × 1 km at nadir to 6 km × 2 km at the outer beam positions. Each scan line consists of 2048 FOV. In this study we investigate the GAC-data with a reduced resolution (409 FOV sampled per scan line). A lookup-table based on a cloud radiative transfer model (*Koelemeijer et al.* (1995)) is used to relate solar reflectance at a wavelength of 0.63 µm and viewing/illuminating geometry to the cloud LWP.

The employed AMSU LWP algorithm is restricted to homogeneously emitting surfaces, eg. ocean areas. For the comparison of the two methods an ocean area (subtropic Atlantic ocean) is chosen. Based on the fact that microwave emission is more strongly correlated with LWP than solar reflectance, we asume that AMSU retrieves LWP with a higher confidence in case of homogeneous cloudiness. Therefore, only AMSU measurements under homogeneous cloudy conditions are used in this study. The differences between the two LWPs (LWP(AMSU) – LWP(AVHRR)) are related to the errors of the more indirect AVHRR method. The aim of this work is to calibrate the high resolution AVHRR measurements of LWP with the low resolution but more directly AMSU LWP retrieval.

2. LWP Algorithm

Over ocean surfaces, which provides a uniform cold background due to the low emittance of water, atmospheric water vapour and liquid water increase the measured microwave emission. The variation of the microwave emissivity over land is as high as the variation due to atmospheric water content. Therefore, the LWP over land is difficult to obtain without knowing the exact emissivity of the ground.

To retrieve the LWP one frequency near the water vapour absorption peak (22.235 GHz) and one in the water vapour window (31 GHz), which is sensitive to the liquid water, are choosen (*Kidder and Vonder Haar* (1995)). The algorithm of *Grody et al.* (1999) uses both the 23.8 GHz (ν_1) and the 31.4 GHz (ν_2) AMSU channel.

$$LWP = (a_0 + a_1 (\ln [285 - T_B(\nu_1)]) + a_2 (\ln [285 - T_B(\nu 2)])) \cos\theta \quad (1)$$

$a_0 = 8.240$ $(2.622 - 1.846 \cos\neg) \cos\theta$,

$a_1 = 0.754$ and $a_2 = -2.265$.

The scan angle (limb) correction given in equation (1) is a symmetrical function of the viewing angle. However, the original AMSU data show an asymmetry that appears if the antenna beam position is near the earth's horizon. This is caused by different amounts of cold space radiation recieved by the antenna. This effect is largest in the 31.4 GHz channel. It is corrected with the formula described by *Weng et al.* (1999).

From the AVHRR data the LWP is derived from the 0.63 µm channel only. *Koelemeijer et al.* (1995) prepared a database with atmospheric reflectivity as a function of solar zenith angle, viewing zenith angle, azimut angle, surface albedo and cloud optical thickness. Thus, from the AVHRR measured reflectivity, the actual viewing and illuminating conditions and the surface albedo, the optical thickness τ can be derived. The LWP is assumed to be linearly related to the optical thickness.

$$LWP \cong 2/3\, r_e\, \tau. \quad (2)$$

The effective radius r_e is set to the same value as used in the lookup-table, i.e. 6 µm. We are aware that this assumption may lead to the systematic errors in the LWP retrieval. Future work will account for this deficiency by adding an effective radius retrieval based on the 1.6 µm AVHRR reflectance measurements.

3. Comparison

Figure 1 shows the AMSU LWP for a descending overpass over the Atlantic ocean. Cloud fields are clearly visible. To compare measurements of the two radiometers the high resolution AVHRR measurements have been averaged over the AMSU grid. The contribution of an AVHRR FOV inside the specific AMSU FOV can be estimated with the antenna weighting function.

The AVHRR LWP averaged into the AMSU FOV basically shows the same spatial structure but larger LWP than the AMSU retrieval.

In order to minimize beamfilling errors only complete overcast AMSU measurements are used for the comparison of the two methods. The standard deviation of the AVHRR measurements are taken as a measure of the cloud field inhomogeneity inside the AMSU FOV. For small standard deviations the cloud is considered as homogeneous. To prevent an underestimation in LWP due to scattering by ice particles, a minimum temperature in the 10.3 µm AVHRR channel of 268 K is used. The AVHRR lookup-table covers optical thickness up to a maximum value of 512. In order to prevent errors due to saturation effects caused by this limit, pixels with a higher optical thickness are avoided. The mean LWP from all

AVHRR measurements inside an AMSU FOV is denoted as LWP(AVHRR).

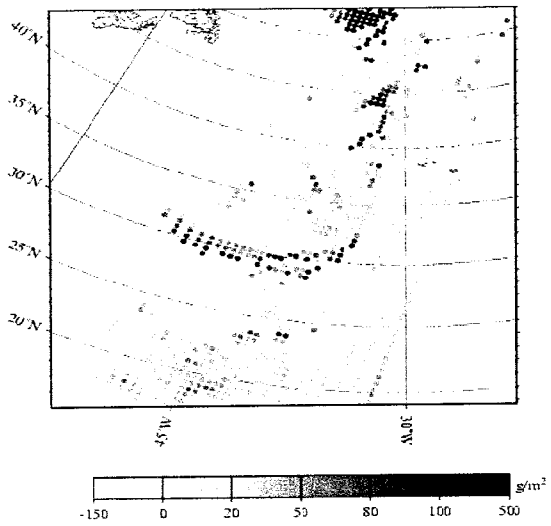

Figure 1: LWP AMSU, 13.06.1999, 10 UTC.

The data are splitt into different cases of inhomogeneity defined as the standard deviation of LWP(AVHRR) inside an AMSU FOV. For each class the distribution of the LWP difference (AMSU – AVHRR) is calculated. For cloud inhomogeneities smaller then 200g/m^2 the shape of the distribution is narrow. This has been used as a threshold to seperate homogeneous from inhomogeneous cases.

In order to obtain a correction term for the LWP(AVHRR) all data are separated both by there cloud inhomogeneity and the LWP(AVHRR). For every 20 g/m^2 interval of LWP(AVHRR) the mean standard deviation is calculated. The results are shown in figure 2.

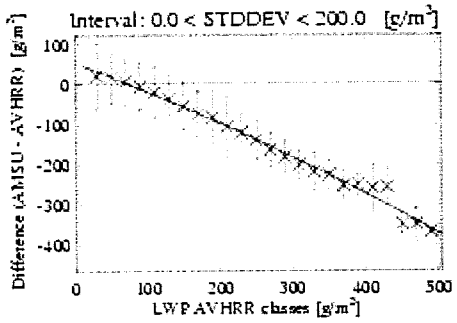

Figure 2: Correction function derived from the statistics over every LWP class for inhomogeneity lower 200 g/m^2.

Equation (3) gives the parameterisation of the difference between LWP AMSU and LWP(AVHRR) for cases with a inhomogeneity less than 200 g/m^2.

$$LWP = a + b\,LWP(AVHRR) + c\,LWP(AVHRR)^2 + d\,LWP(AVHRR)^2 \quad (3)$$

$a = 46.90$, $b = -0.71$, $c = -0.0003$ and $d = -8.28 \times 10^{-8}$

4. Conclusion

AVHRR LWP from th *Koelemeijer et al.* (1995) Lookup-table is significantly larger than LWP retrieved from AMSU measurements based on the Grody algorithm.

For homogeneous AMSU FOV and LWP smaller then 500 g/m^2 it is possible to adjust the AVHRR LWP with the AMSU LWP by means of a simple cubic polynominal.

Given the good agreement between AVHRR LWP and ground based measurements obtained during the measurement campaign CLARA (*Feijt et al.* (1999)) we conclude that the AMSU algorithm strongly underestimates the cloud liquid water path.

Furthermore, comparing the LWP retrieval from the original AMSU algorithm and from MWMOD (*Simmer* (1994)) shows that the Grody algorithm yields considerably smaller LWP for the same brightness temperature (Figure 3).

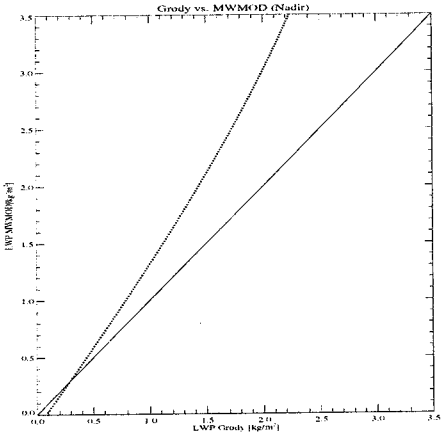

Figure 3: LWP derived from MWMOD compared with LWP from Grody algorithm for the same brightness temperatures.

In order to improve the AVHRR LWP a more sophisticated cloud retrieval scheme including the 1.6 µm channel and surface reflectivity maps will be applied in the future.

References

Feijt, A. Validation of Cloud Parameter Retrieval Methods with Objective Ground Based Measurements, *Phy. And Chem. of the Earth*, Vol.24, No.3, 173 - 176, 1999

Grody, N. Application of AMSU for obtaining hydrological Parameters, *Proceedings of the 6'th Microwave Specialists Meeting in Florence*, 1999

Koelemeijer, R. Optical Properties of Clouds Derived from fully Cloudy AVHRR Pixels, *Beitr. Phys. Atmosph.*, Vol.62, Nr.3, 165 – 171 (1989)

Simmer, C. Satellitenfernerkundung hydrologischer Parameter der Atmosphäre mit Mikrowellen, *Verlag Dr. Korvac*, Hamburg, 1994

Weng, F. Effects of AMSU Cross Track Asymmetry of Brightness Temperature on Retrieval of Atmospheric and Surface Parameter, *Proceedings of the 6'th Microwave Specialists Meeting in Florence*, 1999

One year measurements and simulation of evaporation and precipitation over the Baltic Sea during PEP in BALTEX

Barbara Hennemuth and Daniela Jacob

Max-Planck-Institut für Meteorologie, Bundesstrasse 55, 20146 Hamburg, Germany

1. Introduction

An important part of the water budget of the Baltic Sea is the net precipitation, i.e. precipitation minus evaporation. One of the objectives of PEP in BALTEX (= Pilot study of Evaporation and Precipitation in the Baltic Sea) was the determination of net precipitation over the sea for a one year period by models. The results of different models show great deviations in net precipitation (Smedman et al., 2001). Shortcomings of models in specific details can only be detected by checking the results with observations. The general problem of comparing model values which are representative for the

2. Observational data

Four measuring sites on a transsect over the Baltic Sea from the southwest to the northeast were set up and provided data for at least one and a half year (Zingst (D), Christiansö (DK), Östergarnsholm (SE) and Kopparnäs (FI)). They are located on island or on coasts. Precipitation measurements were performed by Micro Rain Radar and other gauges at three sites. Evaporation was intended to be measured by the correlation method, but difficulties with the fast humidity sensors at two sites (Peters et al., 2001) forced the use of a bulk formulation for latent heat fluxes with sensible heat as quality check. At Zingst which is located on a flat coast the measured sea surface temperature (SST) appears not to be representative for the measuring site and has to be corrected. Direct measurements of latent heat fluxes are available only at Christiansö and Kopparnäs (for several weeks).
Since the sites should represent marine conditions, only onshore wind situations are selected. Table 1 gives an overview of the availability of data.

Table 1: Wind direction sectors with onshore winds and percentage of available onshore measurements for the four PEP sites

Station	sector with onshore wind	percentage of valid data
Christiansö	120°-300°	45
Östergarnsholm	70°-220°	29
Koppernäs	170°-300°	29
Zingst	290°-70°	26

3. Model simulations

The model which is used for simulations of evaporation and precipitation is REMO (bf REgional bf MOdel) (see Jacob and Podzun, 1997). It is a three-dimensional hydrostatic atmospheric model which is based on the Europamodell of Deutscher Wetterdienst (DWD), alternatively running with physical parameterizations of DWD (REMO4.3-DWD) and of ECHAM4 (REMO4.3-EC4) The horizontal resolution is 1/6° (appr. 18 km). The initial and boundary conditions including sea surface temperature (SST) are provided from HIRLAM analyses with a horizontal resolution of 55 km. REMO is alternatively running in a climate or forecast mode.
The latent heat flux is parameterized by

$$E = \rho \cdot C_E \cdot u_z \cdot \Delta q$$

where q_{10} and q_s are specific humidity at 10 m height and at the sea surface, respectively, u_{10} is the horizontal wind speed at 10 m height, ρ is the air density and λ is the specific latent heat of vapourization. The transfer coefficient for water vapour C_E is given by

$$C_E = C_{EN} \cdot f_E\left(\frac{z}{L}, z_0, z_{0H}\right)$$

where C_{EN} is the neutral transfer coefficient and f_E is a stability function which depends on stability z/L and on the roughness lengths z_0 for momentum and z_q or water vapour. In REMO z_0 is determined by

$$z_0 = \frac{\alpha \cdot u_*^2}{g} \qquad \text{(Charnock-formular)}$$

with
$\alpha = 0.0123$ (REMO4.3-DWD, typical for North-Sea conditions)
$\alpha = 0.032$ (REMO4.3-EC4, typical for ocean conditions)
and z_{0H} is determined by

$z_{0H} = \min(z_0, 0.1\text{m})$ (REMO4.3-DWD)

$z_{0H} = z_0 \cdot \exp(2 - 86.276 \cdot z_0^{0.375})$ (REMO4.3-EC4)

The long-term simulation was performed with REMO4.3-DWD and a three-months period was simulated with REMO4.3-EC4.

4. Comparison of simulations and measurements

The comparison of simulated precipitation with single-point measurements is difficult because of the different areal representation. Monthly sums agree in a satisfying manner as is documented by Figure 1 where Micro Rain Radar rainsums are compared with rainsums of REMO for gridboxes over water, over land and an average of 3 water and 3 land gridboxes at Zingst.

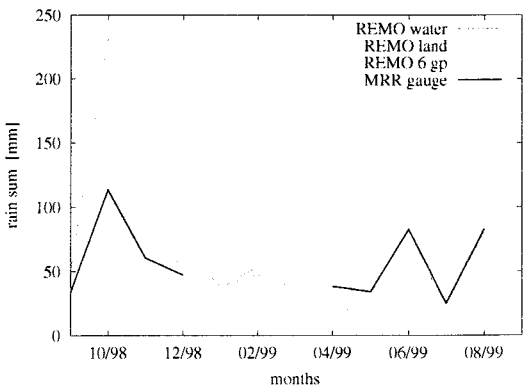

Figure 1: Monthly sums of measured and simulated precipitation at Zingst (for the Micro Rain Radar the winter data are omitted

Simulated and measured latent heat fluxes can only be compared for onshore wind situations and thus not for monthly averages but only for actual values. The factors mainly affecting the quality of model fluxes are the prescribed SST-values and the parameterization scheme.
The comparison of the SST from HIRLAM and the measured SST reveals a hystereris with too high HIRLAM SST in winter and too low HIRLAM SST in summer. The reason is probably that the measured SSTs are influenced by land masses or flat water and react faster and stronder to cooling and heating. Individual deviations of more than 6 K can be found. This effect leads to rather great scatter in comparison of simulated and measured latent heat fluxes.
The parameterization scheme does not appear to have as great an influence as could be expected from the formulation of z_0. Although the models REMO4.3-DWD and REMO4.3-EC4 use different transfer coefficients CE the differences in the heat fluxes are not as great (Figure 2). The reason is a self-adjustment of the models.

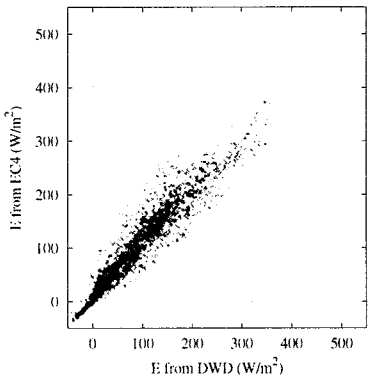

Figure 2: Latent heat fluxes as simulated by REMO4.3-DWD and REMO4.3-EC4 (crosses), together with results from the different parameterization schemes (dots).

Any attempt to improve latent heat fluxes over the Baltic Sea in models should start at periods of great fluxes. Since evaporation is greatest in autumn, the effect in this season will be greatest. Figure 3 reveals some characteristic features of heat flux comparison at measuring sites.

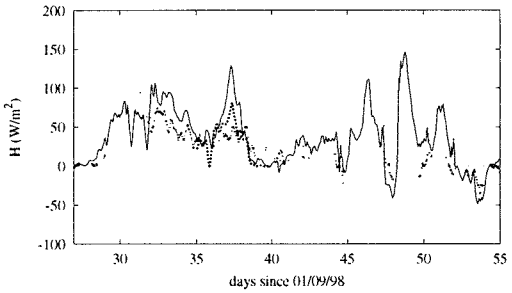

Figure 3: Simulated (solid line) and measured (crosses) sensible heat fluxes at Östergarnsholm for a period in October 1998. The dashed line gives the fluxes with SST fitted to measurements.

The chosen period is characterized by the greatest heat fluxes due to advection of cold and dry air over the relatively warm Baltic Sea. Several events of autumn cold air outbreaks from North, Northeast or East are not captured by measurements because of the limited wind sector (comp. Table 1). The event of 5 - 8 October is recorded at Östergarnsholm and shows that the model overestimates the flux. One reason may be the too strong wind speed dependence of the transfer coefficient of heat as Rutgersson et al. (2001) point out. But more evident is the influence of an uncorrect SST which is prescribed in REMO: while the measured SST decreases in the period of cold air outbreak from 12.4° to 11.8°, the HIRLAM SST remains on the high level of 13.5° which leads to a too great flux. A fit of the model SST in the surroundings of Östergarnsholm to the measured SST reduces the flux substantially.

5. Conclusions and outlook

- The comparison of model results with measured data is problematic due to various conditions (location of measuring site, availability of data, fetch, single point measurement versus gridbox area, insufficient prescribed SST, different parameterization schemes).
- This problem can be reduced by: requirements on measurements: either single point measurements in rather homogeneous areas, e.g. ship/platform, or area average of several single-point measurements on locations typical for the gridbox area.
  For precipitation: radar composites
  requirements on models: for comparsion with single-point measurements the use of a mesoscale model for the inhomogeneous area may be helpful; use of a fully coupled atmosphere - ocean model overcomes the problem of prescribing SST.

Acknowledgements

This work has been performed within PEP in BALTEX, funded by EU, project no. ENV4-CT97-0484. Data have been kindly provided by: Risö National Laboratoy, Roskilde, Denmark, Department of Earth Sciences, Meteorology, Uppsala University, Uppsala, Sweden, Finnish Meteorological Institute, Helsinki, Finland, GKSS Research Center, Geesthacht, Germany. The HIRLAM analyses for initialisation and update of REMO are provided by Swedish Meteorological and Hydrological Institute, Norrköping, Sweden. The help of Ralf Podzun (Model and Data Group, Hamburg, Germany) with all aspects of REMO simulations is gratefully acknowledged.

References

Jacob, D. and R.Podzun Sensitivity studies with the regional climate model REMO. Meteorol.Atmos.Phys. 63, 119-129, 1997.

Peters, G., B.Fischer and H.Münster Eddy covariance measurements with closed-path optical humidity sensors, a feasible concept? J.Atmos.Ocean.Technol., (accepted for publication), 2001.

Rutgersson, A., A. Smedman and A.Omstedt Measured and simulated latent and sensible heat fluxes at two marine sites in the Baltic Sea. sl Boundary-Layer Meteorol., (accepted for publication), 2001.

Smedman, A. (Co-ordinator), T.Andersson, E.Batchvarova, K.Bumke, J.Bösenberg, M.Clemens, B.Fischer, S.-E.Gryning, B.Hennemuth, R.Hyvönen, U.Högström, D.Jacob, C.Johansson, M.Kangas, D.Melas, D.Michelson, A.Omstedt, A.Peltomaa, G.Peters, A.Rutgersson, K.Säntti, B.Tammelin newblock PEP in BALTEX. Final Report. Part I: Summary. newblock Bruxelles, Belgium, 42pp, 2001.

The satellite derived surface radiation budget for BALTEX

Rainer Hollmann[1] and Annegret Gratzki[2]

[1] Institute of Atmospheric Physics, GKSS Research Center, D-21502 Geesthacht, Germany
[2] Deutscher Wetterdienst (DWD), Postfach 100465, D-63004 Offenbach, Germany

1. Abstract

The SAF on Climate Monitoring (CM-SAF) will derive operationally consistent cloud and radiation parameters in high spatial resolution for an area that covers Europe and part of the North Atlantic Ocean in an off-line mode. The availability of the 12 channel instrument SEVIRI and the GERB onboard the MSG satellite, together with the 5 channel AVHRR instrument on board NOAA and METOP satellites provides a unique opportunity to derive consistent cloud and radiation parameters. The cloud and surface radiation products will be based on data from the polar orbiting satellites NOAA and METOP for the northern latitudes, and on data from MSG for the mid latitudes. To reduce inhomogeneities in the transition from mid latitudes to the northern latitudes as much as possible, the same algorithms will be used for both areas.
Here a brief description of the planned surface radiation budget products and the selected algorithms is given.

2. Introduction

With the upcoming new satellite METEOSAT SECOND GENERATION (MSG) with its new and improved instruments GERB (Geostationary Earth Radiation Budget) and SEVIRI (Spinning enhanced visible and infrared imager), it is possible to monitor the environment and the atmosphere in high temporal and spatial resolution. The GERB instrument is specifically designed to derive broadband radiation fluxes at the top of the atmosphere. The 12 channel SEVIRI instrument allows the improved determination of cloud parameters from a geostationary satellite. It not only includes the AVHRR channels, but also additional channels which can be useful for cloud parameter determination (e.g. use of 13.4 µm channel for cloud top height determination). Cloud parameters largely influence the radiation fluxes. An improved cloud detection and cloud parameter generation should improve the determination of surface radiation fluxes.
As a new element of the distributed EUMETSAT ground segment the Deutscher Wetterdienst (DWD) is the host for the Satellite Application Facility on Climate Monitoring (CM-SAF) dedicated to produce consistent climate data sets for a region covering Europe and surrounding areas up to the Arctic. The project has started in 1999 and is at the moment in the algorithm development and implementation phase. After a five year development phase, it turns over into the operational phase of processing products in a routinely manner.
Here in this presentation an overview about the CM-SAF products will be given, but after that the surface radiation budget products will be discussed in more detail. First results and comparisons with surface measurements will be presented.

3. The shortwave surface radiation

For the calculation of the surface incoming shortwave flux (SIS) an algorithm similar to the one developed by Pinker (e.g. *Pinker and Laszlo*, 1992) will be used. The basic idea for the algorithm is that a relationship between the broadband (0.2-4.0 µm) atmospheric transmittance and the reflectance at the top of the atmosphere (TOA) does exist. Once the transmittance is determined from the TOA albedo, the surface irradiance can be computed from the incoming solar flux at the top of the atmosphere and the atmospheric transmittance. With a radiative transfer model, the broadband atmospheric transmittance is calculated once in relationship to the broadband TOA albedo for a variety of atmospheric and surface states. The actual computation of the surface irradiance involves two steps. First the broadband TOA albedo is determined from the satellite measurement. Then the atmospheric transmittance is determined from the TOA albedo together with information on the atmospheric and surface state from the precomputed tables.
Input parameters into the algorithm are the broadband TOA albedo, solar zenith angle, surface albedo, cloud properties as e.g. the cloud optical depth, aerosol and ozone data and the total water vapour content of the atmosphere. The broadband TOA albedo for the area covered by the MSG satellite, the surface albedo and the cloud properties are derived by other groups within the CM-SAF. All other input data are either from climatological data sets (aerosol, ozone) or NWP-data (water vapour). Depending on the availability of appropriate data sets, satellite derived values could be used. To calculate the TOA albedo for the CM-SAF region not covered by the MSG satellite, a narrow-to-broadband conversion of the satellite data and the application of an angular directional model is necessary. In using broadband fluxes at the top of the atmosphere, the algorithm is independent of the satellite instrument and allows for the application to multiple sensors (here MSG/SEVIRI and AVHRR).
The surface net shortwave radiation (SNS) will be calculated from the surface irradiance and the surface albedo. Alternatively, the net shortwave radiation can be derived directly from the TOA reflected flux. From radiative transfer modeling *Li et al.* (1993) established a relationship between the TOA reflected flux and the flux absorbed at the surface which is linear for a fixed solar zenith angle. Sensitivity studies showed that the relationship is independent of the cloud optical thickness and the surface albedo and weakly depending on the sun zenith angle, the amount of water vapour in the atmosphere and the cloud type. It is intended to use the algorithm for automatic quality control. As a preparatory study, the algorithm was applied to data from the Scanner for Radiation Budget (*Hollmann et al.*, 2001).

4. The surface longwave radiation budget

The determination of the surface downward longwave flux (SDL) from satellite radiances is difficult as the atmosphere is only transparent to thermal radiation in the IR window spectral region (8-13µm). Thus, in the other regions, the TOA outgoing longwave radiation is de-coupled from the surface longwave radiation. More than 80% of the clear-sky longwave radiation reaching the surface is emitted within the lowest 500m of the atmosphere. The downward longwave radiation at the surface depends mainly on air temperature and the water

vapour profile of the lower layers of the atmosphere in clear sky conditions. In cloudy cases the fluxes at TOA and surface are entirely de-coupled. Clouds contribute at the surface through the 8-13µm window. The cloud base temperature is the important parameter determining the radiation reaching the surface. It is also difficult to measure from satellites.

For the calculation of the surface downward longwave flux the algorithm described by *Gupta* (1989) and *Gupta et al.* (1992) will be used.

Within the implementation phase of the CM-SAF project, the algorithm was coded and validation with surface measurements has started. The August 1995 was chosen as target month for comparisons with surface measurements. In this first testing phase the Gupta-algorithm was driven by cloud properties (cloud top temperature and cloud flag), derived from ISCCP-DX (*Brest et al.* (1997)) data. The necessary atmospheric profiles of temperature and specific humidity are from ECMWF data.

5. Benefit for BALTEX

The CM-SAF radiation products cover the BALTEX region. They therefore support monitoring of the BALTEX region even beyond the major BALTEX research phase. The CM-SAF development contributes right now to the BALTEX experiment as the August 1995, which was part of the intensive observation period PIDCAP, has been chosen as a target month for comparison with surface observations. The SAF on Climate Monitoring, as a registered BALTEX Data User, is using surface radiation measurements collected at the BALTEX MDC.

6. Status of work

Development work so far has concentrated on the coding and validation of the net shortwave radiation using the Li-Leighton algorithm (*Hollmann et al.*, 2001) and the coding and validation of the longwave fluxes. In this presentation first results and comparisons with surface measurements will be presented.

References

Brest C.L., W.B. Rossow and M.D. Roiter (1997): Update of radiance calibrations for ISCCP. J. Atmos. and Ocean. Tech., 14, 1091-1109.

Gupta, S.K. (1989): A Parameterisation for Longwave Surface Radiation from Sun-Synchronous Satellite Data, J. Climate, 2, 302-315.

Gupta, S.K., W.L. Darnell and A.C. Wilber (1992): A Parameterisation for Longwave Surface Radiation from Satellite Data: Recent Improvements, J. Appl. Meteor., 31, 1361-1367.

Hollmann, R., A. Bodas, A. Gratzki, K. Dammann and R. Stuhlmann, 2001: The Surface Shortwave Net Flux from the Scanner for Radiation Budget (ScaRaB), submitted to Adv. Space Res.

Li, Z., H.G. Leighton, K. Masuda and T. Takashima (1993): Estimation of SW Flux Absorbed at the Surface from TOA Reflected Flux, J. Climate, 6, 317-330.

Pinker, R.T. and I. Laszlo (1992): Modelling Surface Solar Irradiance for Satellite Applications on a Global Scale, J. Appl. Meteor., 31, 194–211.

The Finnish watershed simulation system

Markus Huttunen[1] and Bertel Vehviläinen[2]

[1] Finnish Environment Institute, Helsinki, Finland
[2] P.O. box 140, FIN-00251 Helsinki

Abstract

A watershed simulation and forecasting system is widely used in Finland for simulation of hydrological cycle and for making real-time forecasts. The system is based on watershed model, which is originally the HBV-model, *Bergström* (1992) and *Vehviläinen* (1992). The model simulates the hydrological cycle using standard meteorological data.

The lately developed version of the model simulates the whole land area of Finland, including cross-boundary watersheds, total of 390 000 km2 (Figure 1). The model simulates the area in 1x1 km grid size, which means that the hydrological cycle of each 1x1 km square is simulated. The inputs of the model are precipitation and temperature and the simulated components of hydrological cycle are snow accumulation and melt, soil moisture, evaporation, ground water, runoff and discharges and water levels of main rivers and lakes. In developing the model we have used elevation model for interpolation of precipitation and temperature.

We are planning to use more GIS-data, land-use data and soil type data for improving the accuracy of the spatial variation of the simulated components. The remote sensing data that we are using in the model includes satellite data of snow covered areas and precipitation data from weather radars. In near future we will have data from Luosto weather radar and we have ongoing project in which are developed methods for using ENVISAT data. The main purposes in which the model is used are real time forecasting and simulation of the watersheds in different situations, such as climate change situation.

References

Bergström, S., The HBV Model – its structure and applications, *SMHI Reports Hydrology.* No. 4. 1992.

Vehviläinen, B., Snow cover models in operational watershed forecasting, *Dissertation, Publications of Water and Environment Research Institute.* No. 11. Helsinki 1992.

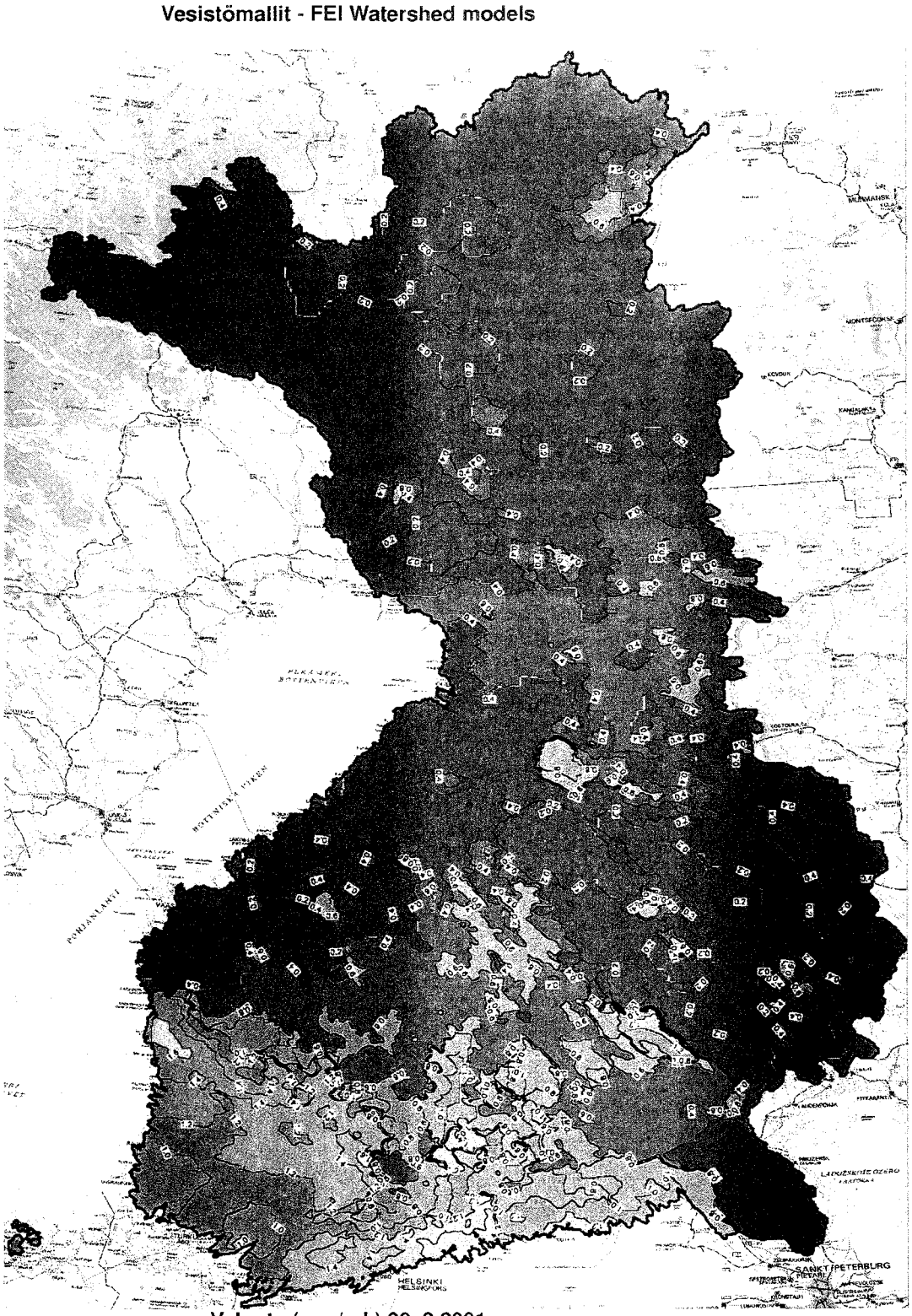

Figure 1: The simulated area and an example of the results.

Comparison of the measured fluxes and the fluxes predicted by HIRLAM at Kopparnäs, Inkoo in Finland

Reijo Hyvönen, Bengt Tammelin and Markku Kangas

Finnish Meteorological Institute

Flux Measurements by Eddy Correlation Method in Kopparnäs

During the period 1998 - 2000 FMI was participating in the EU-project PEP, which was an experimental part of Baltex, measuring turbulent fluxes using fast response hygrometer at coastal site in the Northern part of Gulf of Finland. Combined with weather data for bulk method estimation of fluxes , an extensive data set was gathered for comparison of bulk and turbulent fluxes during summer and autumn in the Gulf of Finland. Good agreement was found between these two methods at the site in most cases.

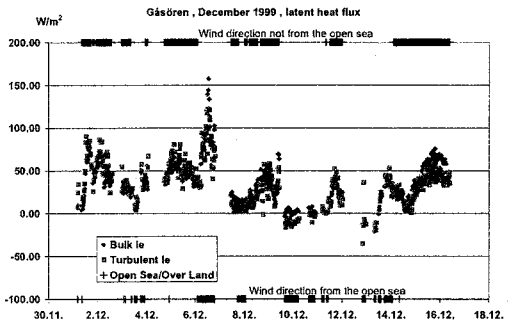

Figure 1: An example of fluxes measured by two methods at Gåsören, Kopparnäs in Inkoo, Finland 'figure'

Comparison of the fluxes by HIRLAM and by direct measurements at Kopparnäs

From 1999 it was possible to get routinely the latent heat flux and the sensible heat flux summations in the coming 6 hours from FMI's HIRLAM version. These values were compared to results by direct method and bulk method measurements in the Kopparnäs area. For on-shore winds the correlations and monthly mean values were mostly in good agreement during the period covered by the measurements.

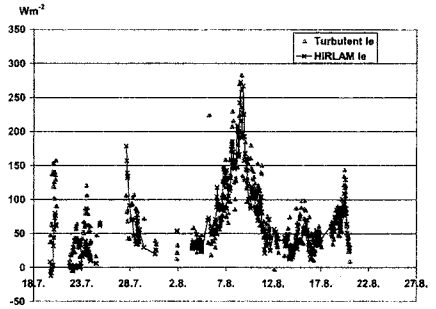

Figure 2: An example of latent heat flux by eddy correlation method and by HIRLAM at Gåsören, Kopparnäs in August 2000.'

References

PEP in Baltex , Publishable Report, Smedman, A-S et al. , Not yet published

The climate of the BALTEX region – regional climate model results

Daniela Jacob

Max-Planck-Institute for Meteorology, Hamburg, Germany

1. Motivation

The climate of the Baltic Sea and its drainage basin is characterised through a relatively mild climate in the South and arctic influences in the North. Low pressure systems are passing the BALTEX region frequently during many months thus leading to a highly variable climate, which in turn is a challenge for regional climate modelling. Simulations on space scales of a few 10 kilometres up to hundreds of kilometres and on time scales of a few hours to decades have to be close to reality in order to describe and model the complete cycles of water and energy budgets in the Baltic Sea region. The comparison of different regional climate simulations within the timeframe of 1980 to 2000 will be used for a first judgement on the accuracy of the regional climate model.

2. Two different physical parameterisation packages – two different climates?

The regional climate model REMO has been used for two long term simulations covering the Baltic Sea region. Re-analyses and analyses data from ECMWF served as lateral boundary conditions for two simulations using a horizontal resolution of 0.5°. Only the parameterisation of the physical processes differ in these simulations. They are implemented in the same dynamical program. The parameterisation packages following the Europa-modell (the former numerical weather prediction model of the German Weather Service, DWD) and one close to the global climate model ECHAM4 /T106 have been applied in two 15 years long simulations.

Investigating the behaviour of two different physical parameterisation packages and their influence of the hydrological cycle in multi-year runs points to the accuracy of the results. Systematic deviations will become visible in the annual cycles and it will be discussed if they do cancel out in the long term mean. Therefore the simulated time series for total precipitation will be compared against each other and observations. The annual and inter-annual variability will be shown.

3. Influence of the horizontal resolution of the climate model

The following questions will be addressed:

- Is there an added value due to higher horizontal resolution?
- Does the different resolution only change the horizontal pattern or does it also influence the climatic mean for the BALTEX area?
- Will single weather events be simulated more realistically?
- Is there an impact of the horizontal resolution on to the calculation of extreme events?
- Is the increase in computer time justified by the value of the additional information?

Results from the global climate model ECHAM4 on a horizontal resolution of T106 (run T106) have been used to drive REMO on 0.5° resolution (run 133) for a period of 10 years. Additionally, the regional climate model REMO has been used for a ten year simulation on 0.16° resolution (run 160) covering a time interval corresponding to the 0.5° resolution (run 141) experiment. The impact of the horizontal resolution on atmospheric quantities like surface pressure, temperature and geopotential will be investigated as well as the fields of precipitation and runoff, which will also be compared to observations.

As a example the percentage of the total precipitation within each intensity class for the land area of the Baltic Sea drainage basin is shown in the Figures below.

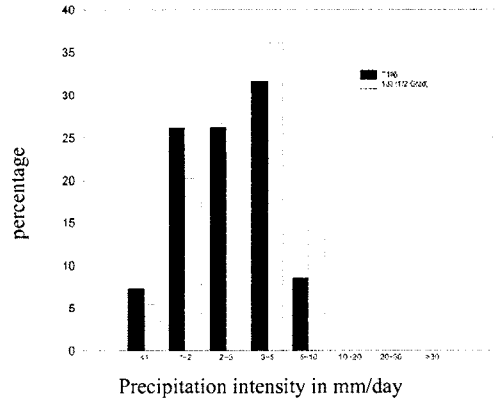

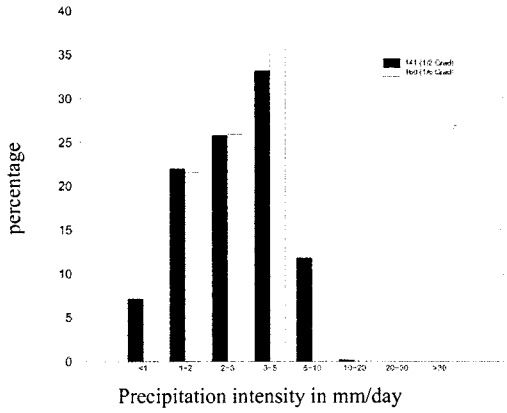

The effect of lakes on the water cycle and inflow of main biogens to the Baltic from the territory of Poland

Jerzy Janczak

Institute of Meteorology and Water Management, Branch of Poznan, 60-594 Poznan, ul. Dabrowskiego 174/176.

Introduction

Poland is a country fairly rich in lakes, though of course they are not as numerous as in Finland or Sweden. A decided majority of them can be found in the north of the country, and all lie in the Baltic drainage basin. Most of them are open lakes, closed lakes can be found in greater numbers only among smaller water bodies. Lakes play a significant role in the flows of rivers and the runoff from Poland. They are also important in the transformation of the main biogens that reach the Baltic. The role of lakes in these processes is not well understood, because there are no balance studies carried out in Poland at a suitable scale. The present article is an attempt at a general assessment of the role of lakes in this respect.

The effect of lakes on river flows

There are more than 7,000 lakes in Poland larger than 1 ha, including 2,913 exceeding 10 ha, *Ja• czak et al.* (1999). Their total area equals about 2,950 km^2, and their capacity, about 18.6 km18^3. The mean annual runoff from Poland for the multi-year period 1951-1990 amounts to some 55 km^3, *Fal et al.* (1997). Lakes exert an influence on river flows primarily in lakeland regions. The mean annual runoff from the lakeland area is about 18 km^3. This concerns the entire region north of the maximum limits of the Last Glaciation, where more than 98% of lakes can be found. Its area covers 94,332 km^2. However, there are also lake-free districts. Lake catchments cover some 48,683 km^2. The runoff from this area amounts to about 9.2 km^3. As can be seen, the lake capacity is almost equal to the runoff from the entire lakeland area, and twice as big as the runoff from lake catchments. One should keep in mind, however, that this is the total capacity which cannot be identified with renewable resources in the yearly cycle. Such resources should be calculated for each lake individually. The effect of lakes on the discharges, especially smaller, rivers that flow through them is obvious. Lakes perform a function similar to impounding reservoirs, diminishing the irregularity of river discharges. In principle, there are no floods in the lakelands. The coefficients of flow irregularity of lakeland rivers are usually below 10 or 20, while those of central Poland are about 50 and in mountain rivers they often exceed 100. There is no agreement, however, on the effect of lakes on runoff. In the few catchments in which this issue has been studied, often conflicting results have been obtained. In some catchments the lakes reduced the runoff mainly owing to increased evaporation from the free water surface, while in others it increased as a result primarily of inflows from the deeper water-bearing horizons.

In the cycle of water and substances, the amount of water flowing through lakes over the course of the year plays a significant role. Such data are available in Poland for very few lakes for which water balances have been calculated. To estimate the amount of water flowing through Polish lakes, three test areas were chosen for which calculations were performed. Water bodies smaller than 10 ha were not taken into consideration. Among larger, those were ignored which had no constant outlet. For lakes for which no direct measurements were available, calculations were made from the isolines of mean specific runoff. The first test area covers 3,552 km^2 and embraces the upper part of the Drw• ca river basin with its 165 lakes of more than 10 ha. The mean annual runoff from this area amounts to about 0.526 km^3, while some 1.152 km^3 of water flow through the individual lakes. This means that the amount of water flowing through the lakes of this area is more than twice (220%) the amount leaving it. The second test area is situated in the Brda river basin. The total area of lake catchments equals 3,364 km^2 there, the mean annual runoff, about 0.626 km^3, and the amount of water flowing through the lakes, 1.544 km^3. In other words, the amount of water flowing through the lakes is almost 250% of that leaving the area. The third test area is much larger, it embraces the lake catchments of the Wielkopolska Lakeland covering some 12,500 km^2. Relatively comprehensive balance-related data are available for this lakeland. There are 522 lakes of more than 10 ha there through which flow 5.6 km^3 of water. The runoff from this area belongs to the lowest in Poland and is equal to about 1.2 km^3. Thus, the amount of water flowing through the lakes constitutes 360% of that flowing out of this area.

In the lakelands a river often flows through several lakes lying in its path. So far it has not been known what part of water leaving Polish lakelands flows through the lakes. The estimates presented above show that probably three times as much, and the figures are almost certainly underestimated, because not all the lakes were counted separately. Smaller lake catchments for which there were no data were combined to form larger ones. It should also be noted that in the Polish lakelands there are no natural lakes lying in the paths of big rivers with a high discharge. They lie in the basins of smaller rivers or in the upper reaches of larger ones, which means that they can greatly modify not only the discharges of such rivers, but also the biogenic load they carry.

The effect of lakes on the transformation of main biogens

Lakes are known to be able either to intercept biogens or to enrich with them the rivers that flow through them *Ja• czak* (1997). It depends on many complex factors which can vary from year to year, especially in the Polish climate in which the distribution and intensity of precipitation in the successive years can be diametrically different. Also significant are temperatures, especially the period and rate of increase in the temperature in spring. This determines the growth of vegetation, which checks rain wash processes in a catchment. An additional factor is the human impact varying from year to year, in particular the quantity and time of spreading fertilisers in the fields and weather-dependent tourist traffic. Besides, some lakes are naturally more predisposed to intercept biogens than others. It depends on their morphometric, hydrological and trophic conditions.

To elucidate the problem, let me describe a few lakes on which I made suitable measurements in the years 1991-2000. They are seven lakes with a considerable water exchange, because only such bodies can be used for the purpose. The mean multi-annual water exchange ranges in them from about 50% for larger lakes to about 200% for smaller ones.

Two lakes are just under 100 ha, the remaining ones are big - 240, 390, 820, and 2,150 ha. On each of them the amounts of in- and outflowing phosphorus and nitrogen were measured, on two for two years, on four for seven years, and on one for three years. In total, for those seven lakes the exchange of water and main biogens was calculated for 35 yearly periods. In 15 cases the incoming amount of phosphorus exceeded the outflowing one, and in 16 cases the outflow was greater than the inflow. In 4 cases the two quantities were about equal. As can be seen, it is rare for the inflow and outflow of phosphorus to achieve a balance. The differences can be very big, up to several tens of per cent, and in smaller catchments, even in excess of 100%. However, it is big lakes that can intercept or produce the largest quantities of phosphorus. In lakes of more than 300 ha the differences between the incoming and outflowing phosphorus even exceed 10 tonnes. Nitrogen presents a similar case. Incoming nitrogen was in surplus in 14 instances, outgoing nitrogen in 17, and the balance was roughly equal in 4 cases. The differences between the inflow and outflow of nitrogen in the larger lakes exceeded 100 tonnes per year. The differences between the inflow and outflow of biogens varied from one year to the next and from lake to lake. The collected observations show that there are lakes which tend to intercept biogens from the catchment, and those in which the biogenic load is enriched in most years. However, this should be treated as a preliminary conclusion, because the number of lakes studied is too small. Such big differences in the loads reaching and leaving lakes may have a significant effect on the total load transported to the Baltic from the territory of Poland. It is estimated that about 50% of the total load of the principal biogens from Poland comes from dispersed-source pollutants. In lakelands this type of supply is definitely dominant. It can be greatly modified by the successive lakes distributed along the flow pathways. Thus, the lower reaches of the big Polish rivers, the Vistula and Oder, which account for about 99% of biogens reaching the Baltic, are nourished by a considerable load from lakes. In the years 1990-1999 the input of phosphorus to the Baltic varied between 11,400 tonnes in 1992 and 15,500 tonnes in 1997, *Environment* (2000), which means that the differences can be as great as 30%. Even wider disproportions are recorded in the case of nitrogen, because they can reach 60%. In those same years 1990-1999 the smallest nitrogen load was transported from Poland to the Baltic in 1990 - 104,400 tonnes, as against the maximum of 254,400 tonnes in 1994. It is hard to tell how big is the influence on these fluctuations of the loads transformed by lakes. In the particular years the influence may change. It would certainly be advisable to carry out a special, more detailed research into the problem, the more so that while efforts to reduce the pollution emitted into the atmosphere have been successful, one cannot say this about the load of the principal biogens introduced *via* rivers into the Baltic. In the other half of the 1990s their amount was bigger than in the early '90s. In the last decades the quality of water in the Polish lakes has deteriorated dramatically. Local government authorities have not enough money for their restoration, or even for measures protecting lake catchments. The first to be liquidated are main point sources of pollution connected with towns and industrial plants. Since, however, such a big load of biogens in Poland comes from dispersed-source pollutants, counter-measures should be taken. They will be hard to implement in the lakelands if no adequate information is available about the effect of lakes on the process of biogen transformation.

References

Fal, B., (Ed.), Bogdanowicz, E., Czernuszenko, W., Dobrzy• ska, I., Koczy• ska, A., Przeplywy charakterystyczne głównych rzek polskich w latach 1951-1990 (Characteristics of river flow in Poland in 1951-199), *Mat. Bad. IMGW,* ser. Hydrol. i Ocean. nr 21. Warszawa 1997.

Janczak, J., (Ed.), Brodzinska, B., Kowalik, A., Sziwa, R. Atlas jezior Polski (The Atlas of Polish Lakes), *Bogucki Wyd. Nauk. Poznan,* Vol. 1- 1996, Vol. 2 – 1997, Vol. 3 – 1999.

Janczak, J. Zmiany jakosci wody jezior na podstawie badan prowadzonych w monitoringu reperowym jezior polskich w latach 1991-1995 (changes in waters quality of lakes on the bases of watemark monitoring studies of Polish lakes in the years 1991-1995), *Bibl. Mon. Srod., PIOS,* Warszawa 1997.

Ochrona Srodowiska 2000, Informacje i opracowania statystyczne, *Główny Urzad Statystyczny,* (Environment 2000, Information and statistical papers, *Central Statistical Office*), Warszawa.

Modelling of water circulation and thermohaline variability in the Southern Baltic by the Princeton Ocean Model

Andrzej Jankowski

Institute of Oceanology of PAS., Powsta• có w Warszawy 55, 81-712 Sopot, Poland,
e-mail: jankowsk@iopan.gda.pl

Results of numerical experiments with an application of the Princeton Ocean Model - code (cf. Blumberg and Mellor, 1987; Mellor, 1993) to investigate circulation and variability of thermohaline fields in the Southern Baltic Sea are presented.
POM is based on a standard formulation of the conservation equations for momentum and mass, utilizing the hydrostatic and the Boussinesq approximation. The model uses Smagorinsky (1963) parameterization for the horizontal mixing (turbulent exchange). To calculate the vertical eddy viscosity and diffusion coefficients a second turbulence closure scheme (Mellor and Yamada, 1974; 1982) is applied.

The model domain (8 ^{o} 50' E - 30 ^{o} 00' E; 53 ^{o} 50' N - 65 ^{o} 50') comprises the whole Baltic Sea with the Gulf of Bothnia, the Gulf of Finland and the Gulf of Riga as well as the Danish Straits and Kattegat and Skagerrak, simplified boundary conditions (radiation type) are applied. Bottom topography of the Baltic Sea used in the model is based on data from Seifert and Kayser (1995).
Two variants of horizonta model resolution are considered - with space step of 10 km and 5 km, respectively. Both model variants with vertical resolution of 24 σ - levels allow to simulate basic features of water movements and hydrology in the Baltic Sea.
Model is forced by realistic wind fields and by heat and salinity fluxes and/or climatological forcings. The river runoff rates are assumed as monthly means.
The three-dimensional fields of the seawater temperature T and its salinity S in August, constructed from the monthly mean (multi - year averaged, climatic) maps presented in Bock's (1971) and Lenz's (1971) atlases, were used in the model runs as initial fields of T, S and as climatological forcings.
The climatological forcings were coupled to the model by means of the so-called method of 'relaxtion towards climatology' (Oey and Chen 1992, Lehmann 1995, Svendsen et al. 1996).
Wind field is estimated from atmospheric surface pressure charts and surface heat fluxes at the sea surface are calculated with standard bulk formulae.
In order to test the capabilities of the model to simulate the characteristic hydrographic features of the the Baltic Sea, the prognostic hindcast calculations were performed for PIDCAP'95 - period.
Model runs, starting with climatological montly means of temperature and salinity were carried out for the period of August to October 1995. For this simulation the model was forced with 3-hourly atmospheric data (pressure, air temperature, specific humidity and the wind - field) derived from the Europa Modell of DWD (supplied by Dr. A. Lehmann from IfM in Kiel).
A comparison of computed and measured temperature and salinity shows (cf. Fig. 1) that the model reproduces the vertical structure of seawater temperature and salinity in a good agreement to the in situ observations. The discrepancy (mean value in the vertical profile) between the calculated and observwd temperature and salinity was equal to 1-2 ^{o} C and 1-2 psu, depending on location of the hydrographic station.
Next prognostic hindcast was performed for September 1989, when an intensive upwelling in some regions along the southern coast of the Baltic was well documented by Malicki and Mi• tus (1994).
In these calculations model was forced by realistic wind fields estimated from atmospheric surface pressure charts taken from (BED, 2000) and by climatological forcings.
Time evolution of the calculated seawater temperature in surface layer reproduced well time history of observed surface temperature at Ko• obrzeg and W• ady• awowo measuring stations.

References

BED, Atmospheric inputs, [in:] The BED database, *http://data.ecology.su.se//Models//bedcontent.htm*, 2000

Blumberg, A. F., Mellor G. L., A description of a three-dimensional coastal ocean circulation model, [in:] Three-Dimensional Coastal ocean Models, edited by N. Heaps, 208 pp., American Geophysical Union , 1987

Bock K.-H. Monatskarten des Salzgehaltes der Ostsee, dargestellt fuer verschiedene Tiefenhorizonte. Dt. hydrogr. Z., Erg.-H. R. B., No.12, Hamburg. 148 pp. , 1971

Lehmann A., A three-dimensional baroclinic eddy-resolving model of the Baltic Sea., Tellus, vol. 47A, No. 5:2, 1013 – 1031, 1995

Lenz W., Monatskarten der Temperatur der Ostsee, dargestellt fuer verschiedene Tiefenhorizonte. Dt. hydrogr. Z., Erg.-H. R. B., No.11, Hamburg, 148 pp. , 1971

Malicki J, Mi• tus M., Climate, [in:] The Baltic Sea Atlas, A. Majewski and Z. Lauer (Eds.), IMGW, Warsaw, 60 - 69, 1994, (in Polish)

Mellor, G. L.,, User's guide for a three-dimensional, primitive equation, numerical ocean model, 35 pp., Prog. in Atmos. and Ocean. Sci, Princeton University, 1993

Mellor G. L., Yamada, T., A hierarchy of turbulence closure models for planetary boundary layers, J. Atmos. Sci., 13, 1791-1806 , 1974

Mellor G. L., Yamada T., 1982, Development of a turbulent closure model for geophysical fluid problems, Rev. Geophys., 20, 851-875 , 1982

Oey, L.-Y., Chen P., A model simulation of circulation in the northeast Atlantic shelves and seas, J. Geophys. Res., 97, 20087-20115 , 1992

Seifert T., Kayser, B., A high resolution spherical grid topography of the Baltic Sea, *Meereswissenschaftliche*

Berichte, No. 9, Institut für Ostseeforschung, Warnemünde, 72-88., 1995

Svendsen E., Berntsen J., Skogen M., • dlandsvik B., Martinsen E., Model simulation of the Skagerrak circulation and hydrography during Skagex, *J. Mar. Syst.*, 8, 219-236, 1996

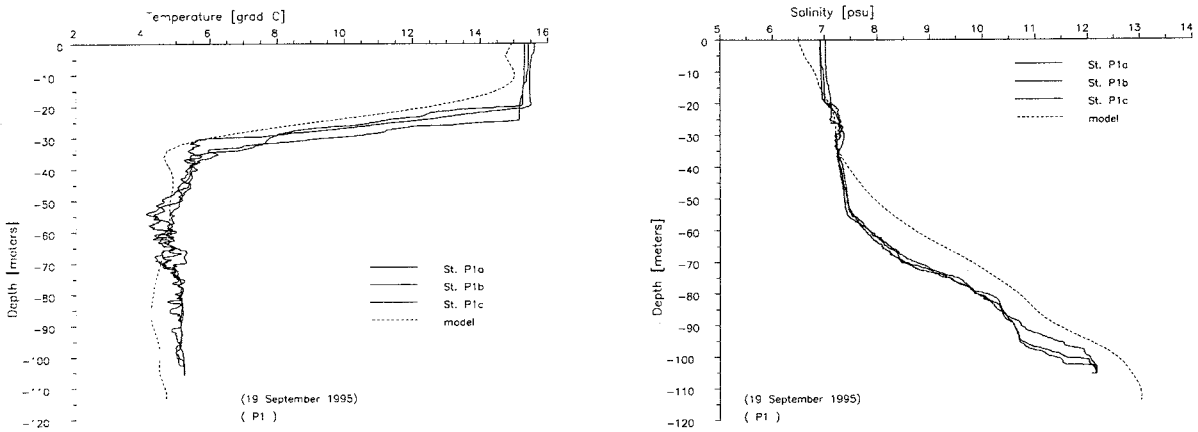

Figure 1: Calculated and measured profiles of sea water temperature (left figure) and salinity (right figure) in vicinity of hydrographic station P1 (Gda• sk Deep)

Influence of the Boundary Layer Height on the Turbulent Structure near the Surface over the Baltic Sea

Cecilia Johansson[1] and Ann-Sofi Smedman[2]

[1] Department of Earth Sciences, Meteorology, Uppsala University
[2] Villav. 16, SE-752 36 Uppsala, Sweden

1. Introduction

A common way to calculate vertical fluxes of momentum, sensible heat and water vapor in models is to use bulk formulations, see equation 1-3.

$$C_D = (u_*/U)^2 = [k(\ln z/z_0 - \psi_m)]^2 \quad (1)$$

$$C_H = \overline{w'\theta'}/U \cdot (T - T_0) = \frac{k^2}{\left(\ln\frac{z}{z_0} - \psi_m\right)\cdot\left(\ln\frac{z}{z_T} - \psi_h\right)} \quad (2)$$

$$C_E = \overline{w'q'}/U \cdot (q - q_0) = \frac{k^2}{\left(\ln\frac{z}{z_0} - \psi_m\right)\cdot\left(\ln\frac{z}{z_{0q}} - \psi_q\right)} \quad (3)$$

The magnitude of the bulk coefficients depends strongly on the stability. Corrections for this are made by using Ψ-functions, which are integrated Φ-functions, see equation 4.

The relations used for the stability corrections are based on measurements, commonly taken over land, and the Monin-Obuhov similarity theory. For example the Φ-functions for momentum is

$$\Phi_m\left(\frac{z}{L}\right) = \frac{kz}{u_*}\frac{\partial U}{\partial z} \quad (4)$$

where L is the Monin-Obukhov length.

Measurements taken in the marine surface layer for unstable conditions show that Φ_m deviate from results over land, se Rutgersson et al (2001). To be able to do a proper correction of the bulk coefficients over the sea, it is important that the Φ_m-function represents sea conditions. This is also of great importance when it comes to estimate the fluxes over the sea.

2. Measurements

Long-term measurements have been made at Östergarnsholm, a small island east of Gotland in the Baltic Sea. The island is very flat and at the southern tip of the island there is a 30-m high tower. The tower has five levels of slow response instrument for wind and temperature and also three levels of turbulence instrument recorded with 20 Hz (Solent Ultrasonic Anemometer 1012R2, Gill instrument). In addition to the long-term measurements, radio soundings have been performed during two spring periods (1997, 2000) and tree autumn experiments (1996, 1998 and 1999). The radio soundings have typically been performed two to four times a day, during daytime.

Data from the tower are used within the wind direction sector 100° to 220°. This assures that the measurements have long fetch over the Baltic Sea and hence the measured quantity on the tower represents over water condition, *Smedman et al. (1999).*

3. The height of the boundary layer

The height of the boundary has been determined from virtual potential temperature profiles from the radio soundings. By using the virtual potential temperature on the tower and from the radio soundings we can assume that an air package, if it follows an adiabatic laps rate, will be able to rise up to the top of the convective boundary layer. Hence the height of the convective boundary layer will be where the temperature from the radio sounding and the temperature at the surface are equal se Figure 1.

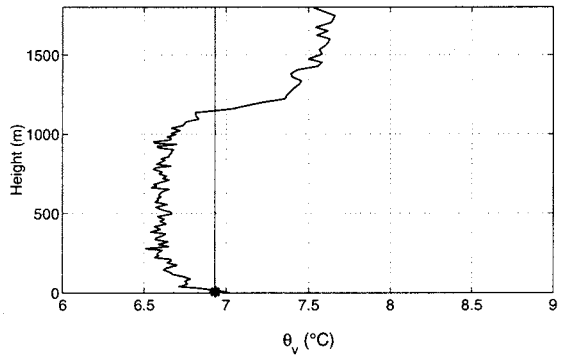

Figure 1: Virtual potential temperature profile from radio sounding made at Östergarnsholm 991020 at 0800 LST. The star is the virtual potential temperature from the tower measurement. The height of the convective boundary layer is the intercept between the two curves. In this case z_i=1150m.

4. Results

The normalized wind gradient over the Baltic Sea decreases much faster with increasing instability, compared to usual over-land values, see Figure 3. It even becomes negative for more unstable conditions. This is due to the effect of swell, which increases the wind speed near the surface, hence the wind gradient becomes negative, Rutgersson et al (2001).

In figure 3 the normalized wind gradient is plotted against z/L and the data are divided into tree groups of z_i/L. The tree groups are 1) 0 >= zi/L> -10, 2) -10 >= zi/L> -20 and 3) -20 >= zi/L. Figure 3 shows Φ_m without swell and Figure 4 with swell. Swell is defined as wave age larger than 1.2, where wave age is $c_0/U_{10}\cos(\theta)$, and θ the difference in direction between the wind and the wave.

From Figure 3 and Figure 4 we see that there is a separation of the tree groups, both in the case without swell and with swell, and especially that the values of group one (the diamonds) falls much faster than the values in group two and tree.

The effect of the boundary layer height, z_i on the non-dimensional wind gradient seems to be more pronounced over the Baltic Sea compared to results from land (Johansson et al. 2001). This can be an effect of the

evolution of the height of the boundary layer. Over the Baltic Sea the height of the convective boundary layer is not varying to much whereas over land the boundary layer evolves during the day and the height becomes approximately constant in the afternoon and then collapse in the evening. Hence the boundary layer over land has a diurnal variation which is much more pronounced then over sea. Another effect could be the fetch, which is more homogeneous over sea compared to the study performed over land.

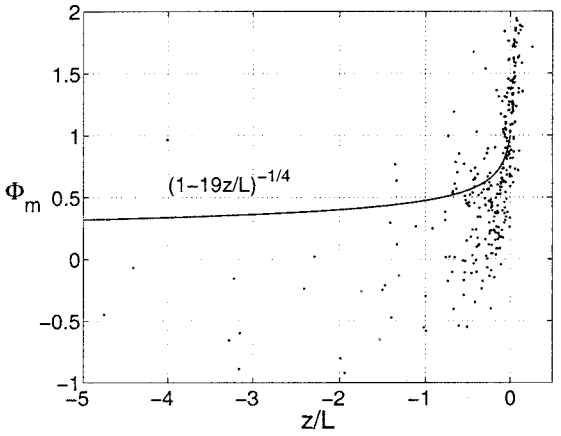

Figure 2: Non-dimensional wind-gradient plotted against z/L. The solid line is from *Högström (1996)*

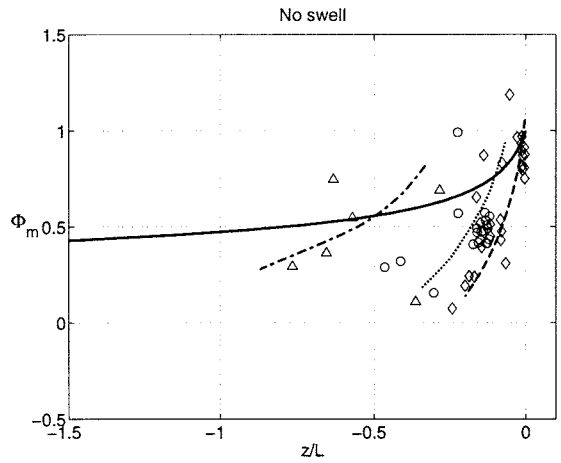

Figure 3: Normalized wind gradient plotted against z/L for data without swell. The data have been separated in three z_i/L groups 1) diamonds 0 >= z_i/L> -10, 2) circles -10 >= z_i/L> -20 and 3) triangles -20 >= z_i/L. The dashed, dotted and dash dotted lines each represent group 1-3 (drawn by eye). The solid line as in figure 2.

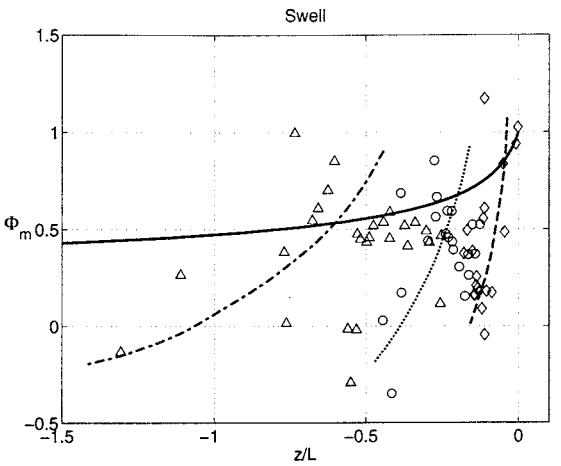

Figure 4: Normalized wind gradient plotted against z/L for data with swell. The data have been separated in three z_i/L groups 1) diamonds 0 >= z_i/L> -10, 2) circles -10 >= z_i/L> -20 and 3) triangles -20 >= z_i/L. The dashed, dotted and dash dotted lines each represent group 1-3 (drawn by eye). The solid line as in figure 2.

5. Conclusions

The non-dimensional wind gradient over the Baltic Sea decreases faster for increasing instability then compared to measurements done over land. It also shows a strong dependence of the height of the boundary layer and the parameter z_i/L.

Since the function for Φ_m are used to correct values of C_D, C_H and C_E in models, it is very important that the function describes conditions over water and not values over land. A further improvement of the Φ_m-function will be to include the parameter z_i/L.

References

Högström, U., Review of some basic characteristics of the atmospheric surface layer, *Boundary–Layer Meteorol.*, 78, 215-246, 1996.

Johansson, C., A. Smedman, U. Högström, J. G. Brasseur, S. Khanna, Critical test of the validity of Monin-Obukhov similarity during convective condition, *accepted for publication in J. Atmos. Sci., 2001*

Rutgersson, A., A. Smedman, U. Högström, The use of conventional stability parameters during swell, accepted for publication in *J. Geophys. Res 2001*

Smedman, A., U. Högström, H. Bergström, A. Rutgersson, K. K. Khama, H. Pettersson, A case study of air-sea interaction during swell conditions, *J. Geophys. Res.*, 104, 25833-25851, 1999.

Water vapour within the BALTEX region obtained from groundbased and spaceborne sensors

Klaus-Peter Johnsen

Institute for Coastal Research, GKSS Research Centre GmbH, D-21502 Geesthacht, Germany

1. Introduction

Water vapour is the most variable of the major components of the atmosphere and a critical element in short term numerical weather prediction (Cucurell et al., 2000). Due to the transfer of energy via its phase changes which drive atmospheric circulations it is important for the energy and hydrological cycles. It is the dominant greenhouse gas.

In order to investigate the energy and water balance over the Baltic Sea and its catchment (BALTEX area), the hydrostatic regional weather forecast model HRM of the German Weather Service (DWD) is validated against groundbased and spaceborne GPS data (GPS/MET and CHAMP) as well as against data of the Halogen Occultation Experiment (HALOE) onboard the Upper Air Research Satellite (UARS).

The US Global Positioning System (GPS) can be used to actively sense properties of the Earth's atmosphere and ionosphere by using groundbased or spaceborne receivers. The signals at both GPS frequencies (L_1=1.57542 GHz and L_2=1.22760 GHz) are delayed and refracted by the gases composing the atmosphere. Due to the permanent dipole moment of atmospheric water vapour it introduces a significant and unique delay (for other components and their influence see e.g. Solheim et al., 1999). Due to the limited space only the groundbased data are presented here.

2. Groundbased GPS data

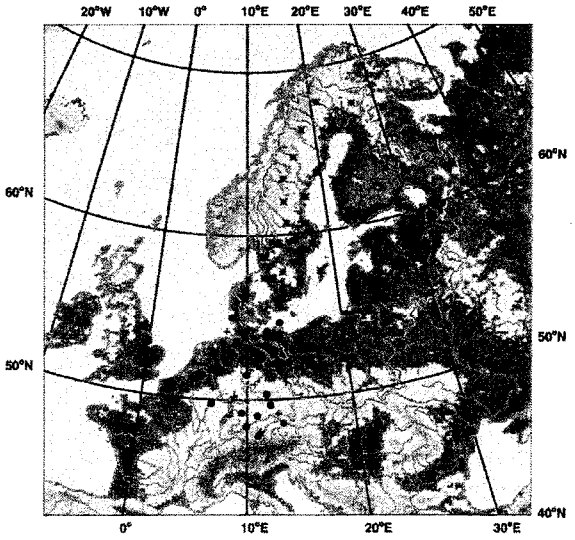

Figure 1: BALTEX area with NEWBALTIC stations (asterisks), SAPOS stations (points) and stations of the DWD (plus symbols).

Within this study two sets of groundbased GPS data are used:

- data of the SWEPOS network obtained from 20 continously operating GPS stations in Sweden and 5 sites in Finland, belonging to the Finnish permanent GPS network (Figure 1) during the PIDCAP period (**P**ilot study for **I**ntensive **D**ata **C**ollection and **A**nalysis of **P**recipitation in the Baltic sea catchment area, August 1 to November 17, 1995). Details about the processing procedure are described e.g. in Emardson et al., 1998.
- GPS zenith path delay data of 16 stations from the SAPOS network (SAtelliten POSitionierdienst) of the German Land Surveying Agencies and 18 stations of the DWD processed by the GeoForschungsZentrum (GFZ) Potsdam are used. They were obtained between 1st of May and 31th of December 2000 within the BALTEX/BRIDGE period (October 1999 to December 2002). The mean atmospheric temperature necessary to derive the IWV is calculated according to Bevis et al. (1992).

3. The HRM model

The weather forecast model HRM used as boundary conditions 6-hourly analyses of the European Centre for Medium-Range Weather Forecast (ECMWF) and for further comparisons 6-hourly analyses (EM3AN) of the Europa-Modell of the German Weather Service (DWD).

The time step was chosen to 90 s. Consecutive 30 h forecast starting each day at 0 UTC were performed. As the coordinate system of the model a rotated latitude/longitude grid was used with a resolution of 0.125° (about 14 km) and 30 vertical layers up to about 25 km height. To obtain the IWV of the model the water vapour is integrated from the height of the GPS receiver up to the uppermost level of the model. The model level of the GPS receiver is calculated from the height of the receiver with the help of the hydrostatic equation. The GPS data were obtained every 5 min., while hourly derived forecasts with the HRM model were compared with one hour mean values of the GPS network.

4. Some Results

Table 1: $IWV_{HRM-GPS}$ - $IWV_{Analysis-GPS}$ is the mean difference between the IWV of the HRM (IWV of the analysis data) and the GPS data. The columns show the different results obtained with ECMWF analysis data or with EM3AN analysis data as initial fields for the HRM model. σ_{HRM} and $\sigma_{Analysis}$ are the standard deviations of the IWV of the HRM model and the analysis compared with the **NEWBALTIC** GPS data, respectively.

Analyses	ECMWF (kg/m^2)	EM3AN (kg/m^2)
$IWV_{HRM-GPS}$	0.74	2.69
$IWV_{Analysis-GPS}$	0.23	2.77
σ_{HRM}	2.555	2.756
$\sigma_{Analysis}$	2.336	2.841

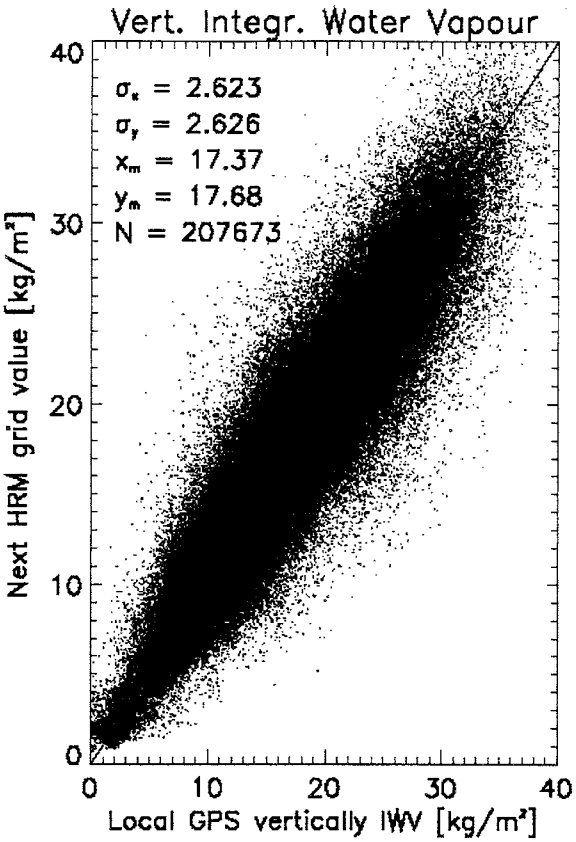

Figure 2: Comparison of the vertically IWV derived from HRM and from the DWD/SAPOS groundbased network between May and December 2000 within the BRIDGE period. x_m and y_m are the mean values of the GPS IWVs and the HRM IWVs, respectively. σ_x and σ_y are the standard deviations between the least square fit and the GPS IWV or HRM IWV, respectively, and N is the number of measurements.

Table 1 shows the differences between the IWV as derived from the HRM model and from the NEWBALTIC GPS data. Altogether 39366 matches were obtained within these roughly 3.5 months of observation period. The columns show the differences when different analysis data are used to initialize the HRM forecast model. The HRM model overestimates slightly the IWV as derived from the GPS data. The differences are larger by using the EM3AN analysis data of the Europa model of the DWD in comparison with use of ECMWF analysis data. The mean differences $IWV_{Analysis}$-IWV_{HRM} are low (e.g. 0.08 kg/m^2 for the EM3AN analysis fields) compared with the difference IWV_{GPS}-IWV_{HRM}. A similar low difference was obtained from the second dataset with 207673 matches at the stations of DWD and SAPOS in Germany (Figure 2). This shows that the mean differences can mainly be explained by the different analysis data.

References

M. Bevis, S. Businger, T.A. Herring, C. Rocken, R.A. Anthes, and R.H. Ware. GPS Meteorology:Remote Sensing of Atmospheric Water Vapor Using the Global Positioning System. *Journal of Geophysical Research*, 97(D14): 15787-15801, 1992.

L. Cucurell, B. Navascues, G. Ruffini, P. Elosegui, A. Rius, and J. Vila. The Use of GPS to Validate NWP Systems:The HIRLAM Model. *Journal of Atmospheric and Oceanic Technology*, 17, 773-787, 2000.

T.R. Emardson, G. Elgered, and J.M. Johansson. Three months of continuous monitoring of atmospheric water vapor with a network of Global Positioning System receivers. *Journal of Geophysical Research*, 103(D2):1807-1820, 1998.

F.S. Solheim, J. Vivekanandan, R.H. Ware, and C. Rocken. Propagation Delays Induced in GPS Signals by Dry Air, Water Vapor, Hydrometeors and Other Particulates. *Journal of Geophysical Research*, 104: 9663-9670, 1999.

The Diurnal Cycle of Clouds and Precipitation.

Colin Jones, Ulrika Willén, Daniel Michelson, and Karl-Göran Karlsson

Rossby Centre, SMHI S601-76 Norrköping, Sweden

1. Motivation

An accurate simulation of the diurnal cycle of cloudiness and precipitation is an important requirement of both Numerical Weather Prediction (NWP) and Climate Models.

Particularly in the summertime there is a clear diurnal cycle in land based precipitation, with a relative maximum in the evening-early night period. This diurnal cycle is convectively driven and results from a sensitive interaction between incoming solar radiation, boundary layer temperature and humidity and atmospheric stability. The timing of precipitation has been a long standing problem in both NWP and Climate modelling.

For NWP it is important that the timing of precipitation is accurately predicted, also the magnitude of precipitation can be sensitive to the amount of instability (or CAPE) the atmosphere is allowed to build up before the onset of convection. In climate prediction an accurate simulation of the diurnal cycle of (convective) precipitation and associated cloudiness is potentially even more important. To simulate cloud-radiation interaction correctly during the summer it is crucial that the cloud fields are phased correctly with the solar cycle. Equally, if a climate model persistently precipitates too early in the day, a significant portion of the precipitation reaching the surface is evaporated the same day. The late evening/nightime precipitation maximum allows a significant fraction of this rain to percolate into the soil, reducing the amount directly lost to evaporation. The result of this systematic error is a well known summertime dry bias in soil moisture in many models.

2. Model and Observational Analysis

Validation of model predictions of the diurnal cycle of cloudiness and precipitation have been hampered by a lack of quality observations, at sufficient temporal frequency. This problem has recently improved over Europe with the introduction of the BALTRAD precipitation data base, where 3 hourly accumulations of precipitation, derived from radar, are available over the Baltic catchment area (Michelson etal. 2000). For clouds, the newly available SCANDIA cloud climatology (Karlsson 1997), derived from AVHRR satellite retrievals, offers 4 samples per day, approximately evenly spaced through the diurnal cycle. Both of these data sets cover the first intensive observing period (CNN1) of the EU Framework 5 project CLIWA-NET. This period covered August and September 2000. Both of these data sets, along with the CNN1 surface observations of clouds and Liquid Water Path, can be used to validate model predictions of the diurnal cycle of clouds and precipitation. In this presentation we analyse the Rossby Centre regional Climate model (RCA) simulation of the diurnal cycle of precipitation and clouds. We concentrate on the CNN1 period over Europe during the summer of year 2000. For this period the RCA has been integrated with ECMWF analysed lateral boundary conditions at a horizontal resolution of 17km. Two vertical resolutions will be analysed, one having considerably higher vertical resolution in the Planetary Boundary Layer. To complement the analysis of CNN1 integrations we also present results describing the diurnal cycle of precipitation simulated by the same RCA model over the United States during the summer of 1993. This integration was part of the PIRCS 1B experiment (Project to Intercompare Regional Climate Simulations, Takle 1999) and concentrated on the intense flood period over the Upper Mississippi Basin. The advantage of combining these two distinct regions is:

1. To determine how universal the physics controlling the diurnal cycle of precipitation and cloudiness are.
2. The strong Solar/Surface forcing over the United States allows for a strong diurnal cycle of convection.
3. An hourly precipitation data base exists for continental USA for model comparison (Higgins 1996)

Figure 1 illustrates the climatological time of maximum precipitation during the diurnal cycle, for the period June10-July31 1993, over the continental United States. The RCA values have been interpolated to the lower resolution of the Observations.

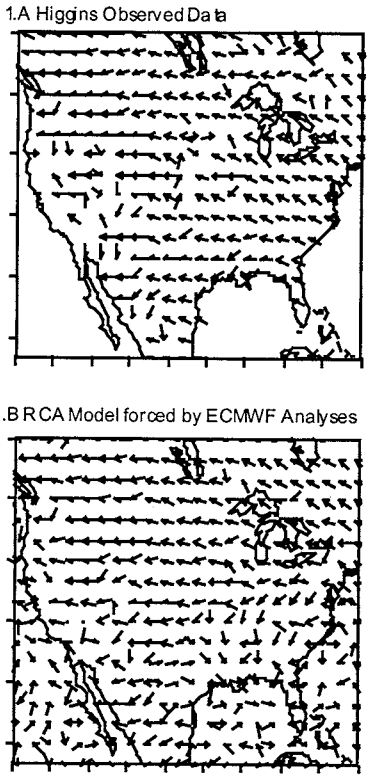

Figure 1: Observed and RCA model predicted time of maximum precipitation during the day, for the period June10-July31 1993. Arrows indicate time of day in 24 hour clock. North=Midnight, East=6am, South=Midday, West=6pm. All times are local time.

Conclusions regarding the quality of the RCA modelled diurnal cycle of precipitation and cloudiness and the

physical processes determining the diurnal cycle will be presented. The importance of a correct diurnal phasing between model moist physics and the solar cycle will be discussed.

References

Higgins R.W, J.E. Janowiak & Y.Yao . A gridded hourly precipitation data base for the United States (1963-1993). *NCEP/Climate Prediction Center Atlas 1, 47pp.*

Karlsson K.G Cloud Climate Investigations in the Noridic Region Using NOAA AVHRR Data. *Theor. Appl. Climatol. Vol.57, 181-195, 1997.*

Michelson D. And Co-authors: Baltex Radar Data Centre Products and their Methodologies. *SMHI Internal Report Series RMK 90 76pp 2000.*

Takle E.S and Co-authors: Project to Intercompare Regional Climate Simulations (PIRCS): Description and initial results. *Journal of Geophysical Research Vol.104, 19443-19462, 1999.*

Acknowledgements:

This work was funded by the EU under the CLIWA-NET project EVK2CT-1999-00007

Changes in Meteorological Parameters in March (Estonia, 1955-1995)

Sirje Keevallik

Tartu Observatory, Tõravere 61602 Estonia

1. Introduction

The threat of global warming has activated investigation of trends in meteorological parameters in different spatial and temporal scales. It is obvious that in case the global warming exists, it does not take place uniformly everywhere and anytime. In Estonia it has been noticed that the weather in late winter and spring has become significantly warmer, whereas there is a slight cooling tendency in autumn. Several investigations show that serious changes in many meteorological parameters have taken place in March. *Tooming* (1996) has investigated temperature regime and snow cover duration at Tõravere (58.35°N, 26.68°E) during a 42-year period of 1953-1994. He has shown that the monthly average air temperature in March has risen by 4 K (probability of significance $P<0.01$) and snow cover duration has decreased by 8.8 days ($P>0.05$). On the other hand, *Keevallik and Russak* (2001) have investigated trends in the low cloudiness during 1955-1995 at 16 meteorological stations of Estonia. It has been shown that the mean monthly amount of low clouds has increased in March by 1.2...3.2 tenths, depending on the station. In the same paper it has been tested that the increase in the amount of low clouds in March is statistically related to the changes in atmospheric circulation. To estimate changes in the atmospheric circulation, the time-series of *Grosswetterlagen* have been used drawn from *Gerstengarbe et al.* (1999). From these time series it can be seen that during 1955-1995 the number of days with the zonal circulation has increased by 7.4 days and the number of days with the meridional circulation has decreased by 9.8 days in March.

In the present paper an extensive analysis has been undertaken to detect changes in the main weather elements in March at Tiirikoja Meteorological Station (58.87°N, 26.95°E) during 1955-1995 and to relate the changes to the trends in the atmospheric circulation.

Several investigations (*Keevallik et al.* 1999, *Post and Tuulik* 1999) have shown that the system of *Grosswetterlagen* is not the best to characterise circulation in Estonia. Therefore, in the present paper the indicator of circulation is the wind vector in the free atmosphere that has been calculated from vertical soundings at Tallinn Aerological Station (59.40°N, 24.60°E).

2. Data

The set of meteorological parameters recorded at Tiirikoja consists of daily mean air temperature, daily precipitation sum, monthly mean amount of low clouds (all for 1955-1995), and number of days with snow cover (for 1962-1995). From the midnight (GMT) vertical soundings at the Tallinn Aerological Station, data for wind speed and direction were drawn at two isobaric levels – 500 hPa and 850 hPa. These data permitted to calculate the zonal (u) and meridional (v) components of wind velocity at both levels and temperature advection at the 850 hPa level. The average values of these parameters are shown in Table 1. It should be reminded that the zonal velocity component u is positive when directed to the east and the meridional component v – when directed to the north.

Table 1: The average values of the observed parameters in March

Parameter	Value
Temperature	-3.3 K
Monthly precipitation	27.3 mm
Amount of low clouds	4.6 tenths
Snow cover duration	24 days
u(850)	4.0 m/s
v(850)	1.0 m/s
u(500)	7.1 m/s
v(500)	-1.2 m/s
Temperature advection	1.0 K/day

3. Trends in the meteorological parameters at Tiirikoja

Linear trends were fitted to time-series of monthly averages of all parameters under consideration during the 41-year period, except the snow cover duration for which data for only 34 years were available. Along the trend lines it was possible to estimate the changes that have taken place during the observation period. These changes and the probability of significance of the respective trend are shown in Table 2.

Table 2: Average changes in the meteorological parameters during 1955-1995 and probability of significance of the trend (P)

Parameter	Change	P
Temperature	5.3 K	0.00
Monthly precipitation	23.5 mm	0.00
Amount of low clouds	2.2 tenths	0.01
Snow cover duration (1962-1995)	-10 days	0.05

The Tiirikoja Meteorological Station is situated on the coast of Lake Peipsi. Therefore, data on the ice cover permitted to conclude that before 1975 the average date was April 10 when the ice started to break on the lake. During the period of 1975-1995 this date was approximately 2 weeks earlier – on March 25.

All these changes indicate that March has become warmer during the last four decades. Additionally, the amount of precipitation has nearly doubled during the same period and the amount of low clouds has increased by 50%.

4. Trends in the winds in the free atmosphere

Keevallik and Rajasalu (2001) have shown that significant increase has taken place in the meridional component of the wind vector at the 500 hPa level above Tallinn. At the beginning of the observation period the component was directed from the north to the south, at the end of the period – from the south to the north. The present investigation shows that significant trends can be observed also in the wind components at the 850 hPa level. Table 3 shows the average wind speed and direction at the beginning and at the end of the observation period calculated along the fitted trend lines.

Table 3: Average wind speed and direction calculated for 1955 and for 1995 along the trend lines

	Speed (m/s)	Direction (Degrees)
850 hPa		
1955	2.7	293
1995	6.3	243
500 hPa		
1955	6.9	311
1995	9.3	257

Table 3 shows that wind speed has increased during the observation period and the average air flow has turned from NWW or NW to SW or SWW.

To investigate the described change in vector magnitude and orientation, new coordinates were introduced by rotating the local Cartesian coordinates by 45° counter-clockwise. The velocity component *u'* in the new coordinates is directed to the north-east and the component *v'* to the north-west. Trends in the velocity components in the new coordinates are expressed much better than in the ordinary local coordinates being 5.1 m/s for *u'(850)* and 7.5 m/s for *u'(500)* during 1955-1995. Both trends are significant at least at the 0.003 level.

5. Relationships between weather elements at Tiirikoja and air flow in the free atmosphere

It is natural to expect that the described changes in the March weather are due to the changes in the average air flow in the free atmosphere above Estonia. To demonstrate this, correlation matrix was calculated between all quantities investigated. As the time series of snow data was shorter, the matrix has been calculated for the period of 1962-1995. Table 4 shows the correlation coefficients that are significant at least at the 0.05-level.

Table 4: Correlation coefficients between different meteorological elements

	Temp	Prec	Cloud	Snow	Adv
Temp	1				
Prec	0.35	1			
Cloud	0.70	0.56	1		
Snow	-0.64			1	
u'(850)	0.71		0.59	-0.37	
v'(850)	-0.34				-0.43
u'(500)	0.56	0.39	0.64		
v'(500)					-0.56

It could be added that the wind vectors at these two levels are tightly interrelated: the correlation coefficient is 0.87 between *u'(850)* and *u'(500)* and 0.90 between *v'(850)* and *v'(500)*.

Table 4 shows that temperature, precipitation and the amount of low clouds are positively interrelated. This situation is quite understandable in late winter conditions when low clouds prevent the boundary layer from radiative cooling. Snow cover is negatively correlated with temperature – when temperature is below normal, snow does not melt.

The most important are correlations detected between the wind components in the free atmosphere and the meteorological elements at the surface. Temperature and low cloudiness are positively correlated with the *u'*-component of the upper-air wind: strong air flow from SW causes high temperature and large amount of low clouds. This can be explained by transportation of relatively warm and humid air masses from the North Atlantic to Estonia. On the other hand, temperature advection is negatively correlated with the *v'*-component of the upper-air wind: increasing air flow component from SE brings about lowering temperature at the 850 hPa level. An interesting feature is that precipitation is significantly correlated with the *u'*-component at the 500 hPa level, but not at the 850 hPa level. This fact can be associated with the common practice of weather forecast where precipitation probability is predicted by baric structures at the 500 hPa level.

6. Conclusions

The analysis shows that changes in the weather conditions in March are related to the changes in the average air flow in the free atmosphere above Estonia. Therefore, the intensity of the air flow from SW can be used at the classification of weather types in this region. This is first of all valid for March. Elaboration of a general classification scheme requires a similar analysis for other months.

References

Gerstengarbe, F.W., Werner, P.C.. Katalog der Grosswetterlagen Europas (1881-1998) nach Paul Hess und Helmuth Brezowsky, Potsdam, Offenbach a.M., 137 pp., 1999.

Keevallik, S., Post, P. and Tuulik, J. European circulation patterns and meteorological situation in Estonia, *Theor. Appl. Climatol.*, Vol.63, 117-127, 1999.

Keevallik, S. and Rajasalu, R. Winds on the 500 hPa isobaric level over Estonia (1953-1998). *Phys. Chem. Earth (B)*, Vol. 26, No 5-6, 425-429, 2001.

Keevallik, S. and Russak, V. Changes in the amount of low clouds in Estonia (1955-1995). *International Journal of Climatology* (accepted).

Post, P. and Tuulik, J. About the relationships between Estonian weather elements and European circulation patterns. *Phys. Chem. Earth (B)*, Vol. 24, 97-102, 1999.

Tooming, H. Changes in surface albedo and air temperature at Tartu, Estonia, *Tellus*, 48A, 722-726, 1996.

Statistical structure of large-scale snow covers extent

Alexander Kislov[1], Lev Kitaev[2], Igor Konstantinov[1]

[1] Moscow States University, Geographical Faculty, 119899, Moscow, GSP-3, Vorobievy Gory
[2] Institute of Geography RAS, 109017, Moscow, Staromonetniy 29

Based on the snow cover data set (developed by Institute of Geography RAS) consisting of the results of routine network measurements of snow cover parameters (1966-1990), the characteristics of its statistical structure were explored. They were used to evaluate how accurate the data from several points locating within the specific territory characterize the spatially-averaged value.
The error of the area averaged value (if there are n stations distributed nearly homogeneously on the area of S) could be given by expression:

$$E(n,S) = \sigma \sqrt{\frac{0{,}23\sqrt{S}}{l_0 n^{3/2}} + \frac{\eta^2}{n}}$$

Here σ is the standard deviation, l_0 is the parameter included into expression for autocorrelative function: $\mu(\rho) = \mu(0) \cdot exp(-\rho/l_0)$, where ρ is a distance; $\eta^2 = (1-\mu(0))/\mu(0)$, $\mu(0)$ is empirically determined by extrapolation : $\mu(\rho) \rightarrow \mu(0)$ when $\rho \rightarrow 0$.

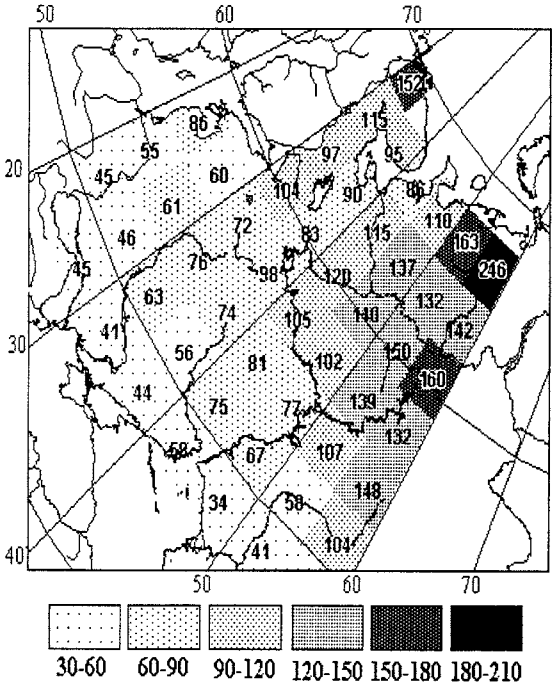

Figure 1: The m ean snow water equivalent in February, mm

The area we study is the territory of the FSU (fig.1). It was shown that for grids 3• 5^0 located within the East European

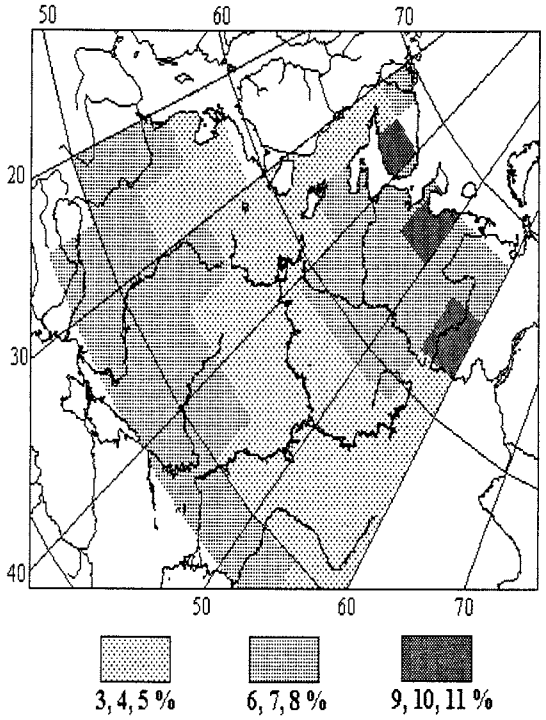

Figure 2: The error of the area averaged value.

Plane the relative uncertainty is ~3-5% in the central part of the region and it is increased as a two times on the north and south parts of the region (fig. 2). It thanks to coarse network on the north and large interannual variability of snow cover on the south.

Acknowledgement

Investigation is supported by Russian Found of Basic Researches (grants 99-05-61572, 98-05-64102) and "Integration" programme.

Spatial peculiarity of the climatic and snow cover parameters fields interannual changes in North Eurasia

Lev Kitaev[1], Viacheslav Razuvaev[2] and Rafael Martuganov[2]

[1] Institute of Geografy RAS, 109017, Moscow, Staromonetniy, 29
[2] ARSRIGMI-WDC, 249020, Obninsk, Koroleva, 6

1. Introduction

The objective of the research is to study interannual changes in the climatic an snow cover parameters fields. The main task is to study temporary changes of the parameters and changes of spatial correlation of their fields. The work has been done with the support of the Russian Fundamental Research Foundation (grant 99-05-65572).

The research is based on the observation data of WMO survey stations for the period of 1936-1995. The study area covers the north of Eurasia within the border of the former USSR. The number of stations is 265-280. They are evenly distributed on the area. The studied parameters include air temperature, precipitation, snow cover depth. The analysis is based on the total amount of precipitation and mean air temperature for the period with durated snow cover (November – March inclusive), as well as on the mean snow cover depth in March taken as the maximal and integral value for the period of snow accumulation.

2. Multi-year changes in the climate and snow cover interaction Next Headline

The whole study area is characterized by a positive trend of snow cover depth (+0.135 cm/year). This corresponds to A.N. Krenke's conclusions concerning snow cover water equivalent in the same area for the period of 1966-1990 (*Krenke et al.*, 2000), and to the conclusions of other researchers for the north of Eurasia and the Arctic (*R.Barry,* 1990; *Fallot J.-M. et all*, 1994]. Trends of snow cover depth in individual large regions of the north of Eurasia are also positive (+0.06 - +0.304 cm/year), except for a slightly negative trend on the Turanskaya Lowland and in Kazakhstan (-0.05 cm/year).

Increase of snow cover depth during the period of 1936-1995 occurs against a background of the positive trends of precipitation and air temperature both in the whole area (+0.59 mm/year and +0.03 degree/year), and in all regions (+0.31 - +1.3 mm/year and +0.02-+0.03 degree/year). The only exception is the north of Siberia where there is a slightly negative temperature trend (0.017 degree/year).

The mentioned trends are essential but not extremal, because its are between minimal and maximal values and not more then standard diviation.

Multi-year growth of snow cover water equivalent in the East-European Plain, their mean values being lower, occurs more slowly in comparison with the Urals, Siberia and Far East, as it is probably accompanied by a more intense climate warming connected with higher entry of warm air from the Atlantic Ocean. In comparison with the west and east of Siberia the snow cover depth in the Far East grows slower, precipitation growth being the highest among all regions and air temperature growth being moderate. Insignificant growth of snow cover water equivalent on the Turanskaya Lowland and in Kazakhstan is due to the minimal, in comparison with the other regions, snow cover water equivalents and warm winters against a background of the continued climate warming.

In a multi-year course of the parameters there is a bend towards the higher growth in the mid 1960s, which is more obvious for snow cover depth and precipitation and less obvious for air temperature. There is a general tendency of precipitations and air temperature synchronism, at the same time them being asynchronous to multi-year snow cover changes (fig1).

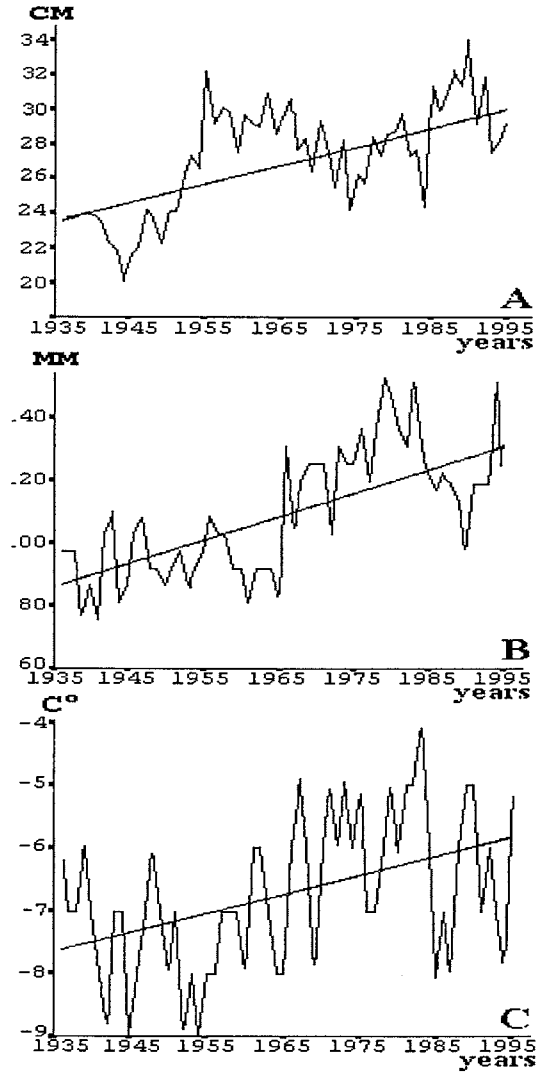

Figure 1: Multi-year changes and trends of snow cover depth (A), precipitation (B) and air temperature (C).

Spatial peculiarities of climate and snow cover interaction

Statistical estimates of interannual interaction of the climatic and snow cover parameters fields give poor results: correlation coefficient of temporal snow cover changes with air temperature and precipitation do not exceed 0.4 and are useful only for estimating general tendencies. To make quantitative estimates of the spatial peculiarities of the climate and snow cover interaction the

obtained meteorological data on air temperature, precipitation and snow cover depth were subdivided into three equivalent graduates, in each case - minimal, mean and maximal values. This allowed formation of the matrixes of the corresponding graduates for snow cover depth – precipitation, and snow cover depth – air temperature. The analysis was held both for the area as a whole, and for individual regions.

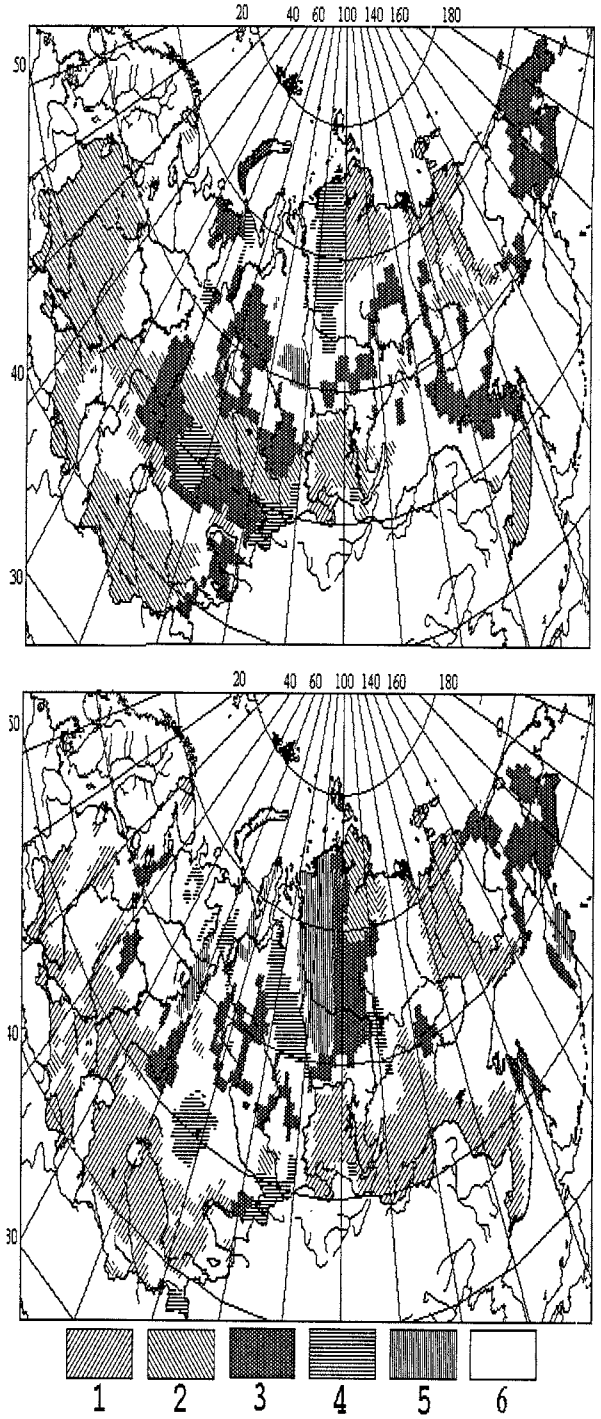

Figure 2: Ratio of fields: snow cover fields (cm) and air temperature (A); snow cover depth (cm) and precipitation (mm) (B).
1 minimum-minimum 4 maximum-minimum
2 minimum-maximum 5 maximum-maximum
3 mean-mean 6 non investigate pairs

It resulted in identification of the spatial peculiarities of interaction between air temperature and precipitation fields with the field of snow cover depth, and their multi-year changes for most representative combinations of the parameters. As an example the results of mean multi-year parameter values processing are given (fig. 2).

The largest areas are occupied by the territories where minimal snow cover water equivalents are formed under minimal precipitation and maximal temperatures, while the extremes of high snow cover water equivalents and low precipitation, and high precipitation and low temperature also occur, but have a non-considerable spatial distribution.

Decrease of areas where minimal snow cover water equivalents are formed under minimal and maximal precipitation and minimal temperatures (trend -0.04 - -0.43 % of area/year) is revealed for the whole study area and for its regions of East-European Plain, Urals, east and west of Siberia. At the same time in those regions the areas where mean snow cover water equivalents are formed under the conditions of mean precipitation and air temperatures (trend +0.002 - +0.40 % of area/year), are increasing. Spatial structure of the snow cover, precipitation and temperature fields interaction is most stable in the north of Siberia and in the Far East. In those regions the areas where formation of mean snow cover water equivalents occur under the condition of mean temperatures and precipitation, are large and hardly changing in time. Spatial structure of the parameters fields interaction is stable on the Turanskaya Lowland and in Kazakhstan.

References

Krenke A.N., Razuvaev V.N., Kitaev L.M., Martuganov R.A., Shakirzyanov R.I. Temporal variability of snow cover period and dimensions at all former USSR and its large regions (1966-1990). *Cryosphere of Earth,* N 4,.35-47, 2000. (In Russian).

Barry R.G. Observational evidence of changes in global snow and ice cover. *Observed climate variations and chande: contribution in support of section 7 of the 1990 IPCC scientific assessment (ed.D.E.Parker).* Cambrige. Cambrige Univ. Press, 1.1 - 1.20, 1990.

Fallot J.-M., Barry R.G., Armstrong R.L. et. al. 20-th century variations in snow cover and climate in Eurasia. *Proceeding of Int. Symposium on the role of the cryosphere in Global Change.* Columbus, Ohio, USA, 11-25 , 1994.

ODRAFLOOD – a flood forecasting system for the Odra drainage basin

Markus Klein[1], Robert Backhaus[2], Ryszard Ewertowski[3], Heinz-Theo Mengelkamp[1], Hilmar Messal[1], Ehrhard Raschke[1] and Zenon Wo• niak[4]

[1] GKSS Research Center Geesthacht, Max-Planck-Str., D-21502 Geesthacht, Germany
[2] DLR German Aerospace Center, Porz-Wahnheide, D-51147 Köln, Germany
[3] MRI Maritime Research Institute/Instytut Morski, ul. Monte Cassino 18A, PL 70-167 Szczecin, Poland
[4] IMGW Institute of Meteorology and Water Management, ul. Parkowa 30, PL 51-616 Wroc• aw, Poland

1. Motivation

In July 1997 two episodes of heavy rainfall in the upper catchment of the Odra river caused severe flooding in the Czech Republic, Poland and some areas in Germany. Hundreds of cities and villages were inundated, more than 100 casualties occurred and vast areas of land were flooded for weeks. The critical situation had to be assessed by the disaster management authorities for taking adequate and effective measures. In case of such a critical flood situation the assessment needs

1. quantitative predictions of water levels and discharges which must be accurate and reliable for as long-term as needed for taking effective measures,
2. a set of rules for the intelligent control of weirs and polders and the resulting impact on the river flow,
3. a knowledge base of consequences of predicted levels and discharges on vulnerable urban and rural areas.

2. Objectives

The ODRAFLOOD project, "Simulation of flood events in the Odra basin with a coupled model system", funded by the German BMBF, develops a multi-scale system that meets various demands of a comprehensive flood forecasting and warning system. The goals of the project are:

- extension of the prediction period and effectiveness of flood forecasts,
- analysis of past flood events,
- scenarios for improving flood mitigation and flood management,
- generation of risk maps for vulnerable areas,
- strategies for refining rules for control and projecting of reservoirs, polders and other constructions,
- provision of basic components (models and scenarios) for the development and implementation of an operational flood forecasting system.

3. System components and first results

The structure of the system refers to the chain of processes converting extreme rainfall and/or snow melt into runoff and river discharge, transforming the flood waves downstream, and inundating local areas. At first, the models are applied and calibrated separately. In the current stage of the project they will be coupled, each model component of larger-scale processes and upper-stream areas delivering boundary conditions for the next component in the model chain.

The rainfall-runoff relationship is modeled with the GKSS model SEROS, which is a combination of the land surface scheme SEWAB (Mengelkamp et al., 2000, 1997; Ruhe et al., 1998) and the large-scale routing scheme (Lohmann et al.. 1996). It is applied for the complete Odra basin covering 120,000 km² on a rotated grid of 1/16 degree (• 7 km) in accordance to the atmospheric regional scale model LM of the German Weather Service DWD. The topographic information of each grid cell is derived from the Hydro1K data set (digital elevation model DEM and "topographic index"), the CORINE land use data base and the FAO soil map. Routing network and sub-catchments of each gauging station are determined from the DEM (fig. 1).

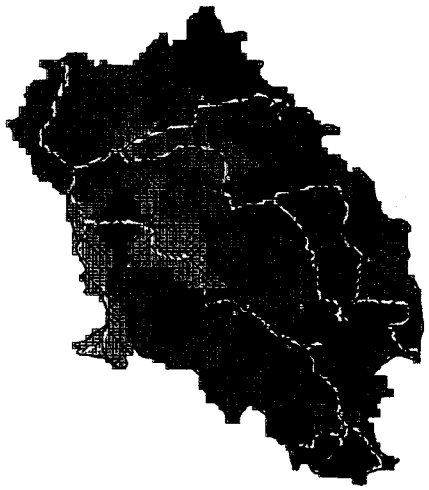

Figure 1: Routing network of the Odra basin on 7 km grid, location of gauging stations and sub-catchments.

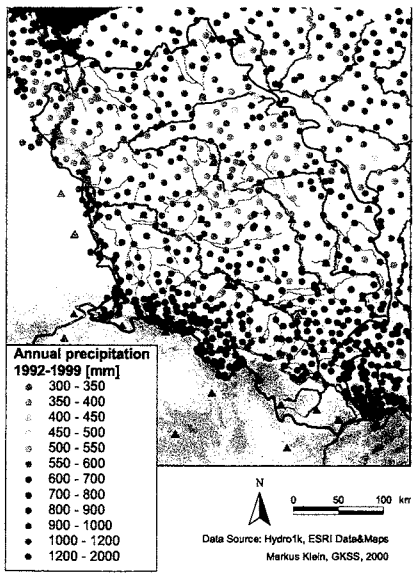

Figure 2: Mean annual precipitation of 650 precipitation stations (circles) and 50 synoptical stations (triangles).

Meteorological forcing data are given by 50 synoptical stations. Additional time series from about 190 climate stations and about 1250 precipitation stations are collected by IMGW for the period of 1991-1999 and saved in the BALTEX meteorological data center at DWD (fig 2). For the preceding years since 1984 the data set is prepared on a less fine spatial resolution. Daily discharges of 29 gauging stations and of 13 reservoirs in the mountainous region are available for 1985 through 1999.

The wave transformation in the Odra river is simulated with the hydrodynamic models of IMGW (for upper and middle Odra) and MRI (for middle and lower Odra). Both models are based on the one-dimensional Saint-Venant equation. River and embankment are characterized by measured cross-sections and typical roughness (Manning) coefficients. The IMGW model is already in operational use for the Polish section between the Czech and the German border (mouth of Lausitzer Neiße/ Nysa • u• ycka). In the lower Odra, flow conditions are much more complex because various types of polders and weirs, tailbacks, wind effects and lateral flows in the channel network of the estuary. These effects are all covered by the MRI hydrodynamic model.

The model TRIM applied by GKSS works as magnifier to the MRI model. The two-dimensional model is based on the Navier-Stokes equation and is feasible for the transient simulation of heavy lateral flows and tailbacks on the main river (Casulli and Cattani, 1994). Fig. 3 shows the reduction of water level in the centered longitudinal section of the river caused by an embankment breach after 2,5 h. The conditions of this scenario are typical for the Odra at the Polish-German border. The model is used for scenarios of embankment breaches and flood plain inundation, for the optimization of control strategies for polders and weirs, and for the evaluation of projected reservoirs and hydrotechnical constructions.

The inundation of urban areas is determined by the complex and small-scale morphology of buildings and terrain. Such kind of high-resolution elevation models are generated for the cities of Wroc• aw and Frankfurt/O./S• ubice (fig. 4). DLR simulates inundation scenarios with the dynamical-statistical model ARCHE and investigates the effect of mobile flood protection walls and similar measures (Braun et al., 1997). Risk maps showing the statistical recurrence times of inundation extents are produced by post-processing the scenarios.

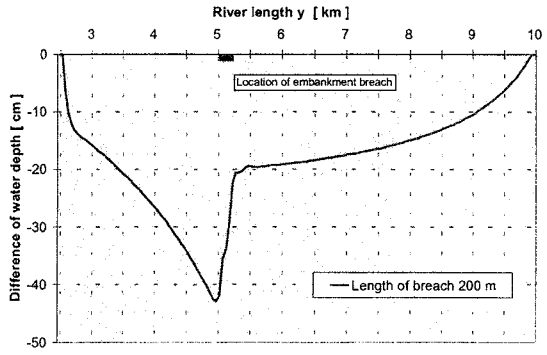

Figure 3: Reduction of water level by embankment breach.

4. Outlook

A large number of applications, analyses and scenarios for flood mitigation and risk assessment is conceivable. The BALTEX community may be interested in one direction of applied research, which is planned for a future stage of ODRAFLOOD after refinement of the hydrologic components and proof of feasibility for flood forecasts.

Figure 4: High-resolution DEM of Frankfurt/O. (partial view).

At the present stage ODRAFLOOD is driven by observed or externally forecasted precipitation data. The reliability of the forecasted precipitation is fundamental for the reliability of the flood forecast. We expect an improvement of the reliability and a prolongation of the flood forecast period of the model chain when SEWAB is directly nested in a numerical weather forecast system. Its nesting in the non-hydrostatic weather model GESIMA was already successfully performed for the upper Odra catchment where the flood originated.

References

Braun, G., S. Ernst, B. Hörsch, S. Weiers, 1997: Hochwasserschutz und -prävention durch räumliche Modellierung. (Flood protection and prevention by spatial modeling) In: *GIS*, Nr. 5/97, Vol. **10**, 10-15

Casulli, V., E. Cattani, 1994: Stability, accuracy and efficiency of a semi-implicit method for three-dimensional shallow water flow. *Computers Math. Applic.* Vol. **27**, No. 4, pp. 99-112.

Lohmann, D., R. Nolte-Holube, E. Raschke, 1996: A large scale horizontal routing model to be coupled to land surface parameterization schemes. *Tellus 48A*, No. **5**, 708-721.

Mengelkamp, H.-T., K. Warrach, C. Ruhe, E. Raschke, 2000: Simulation of runoff and streamflow on local and regional scales, *Meteor. Atmos. Phys.*, **76**, 107-117

Mengelkamp, H.-T., K. Warrach, E. Raschke, 1997: A land surface scheme for atmospheric and hydrologic models: SEWAB (Surface Energy and Water Balance), *GKSS external report,* 97/E69.

Ruhe, C., M. Lobmeyr, H.-T. Mengelkamp, K. Warrach, 1998: Application of a distributed hydrological model to the Odra drainage basin, in: Conference Proceedings of Second Study Conference on BALTEX, Rügen, 25 – 29 May 1998, *BALTEX Secretariat Publication Nr. 11.*

Development and verification of flood forecasting system for St.Petersburg

Konstantin A. Klevanny[1], Valentina P. Gubareva[2], Mohammad S.W. Mostamandi[2], Lidia B. Ozerova[2]

[1] MORZASCHITA Nab. Moiki, 76, 190000 St.Petersburg, Russia
[2] North-West Hydrometeorological Service, 23 linija, 2a, 199106 St.Petersburg, Russia

1. Introduction

Development of an automated and reliable flood forecasting system (FFS) is a current task for St.Petersburg. Storm winds over the Baltic Sea are capable to drive a big volume of water into the shallow head of the Gulf of Finland. It leads to flooding of low lying regions of St.Petersburg, to which refer its central historical parts. Floods cause a significant economic and social damage to the City, sometimes leading to human victims. There were about 300 floods in the City's history and 3 of them were catastrophic. To protect St.Petersburg against floods a Flood Protection Barrier is under construction in Neva Bay but since 1990 it still has openings, which can not be closed in the case of floods. The biggest one is the navigation passage 940 m wide. Numerical simulations, see *Klevanny (1998)*, and observations have shown that with these openings the City is not protected. Therefore, at the present time the FFS is necessary for advance warning of the responsible services and the population. After completion of the Barrier the FFS will serve for management of the Barrier. This paper outlines the results of the development and verification of the FFS, which has an advance time in 36 hours. The work was done in 1999-2000 with the financial support of the Netherlands Ministry of Economic Affairs (grant PSO98/RF/3/10), see *Klevanny et al. (2000)*. The authors express their gratitude to H. Gerritsen of WL|Delft Hydraulics in The Netherlands, H.Dahlin, L.Robertson and M. Andersson of the Swedish Meteorological and Hydrological Institute (SMHI), K.Huber and S.M. Navarra of the Federal Agency for Navigation and Hydrography (Bundesanstalt für Seeschiffahrt und Hydrografie, BSH) in Hamburg and S.K.Belenko of the North-West Hydrometeorological Service of Russia (NWHMS).

2. Baltic Sea Model BSM3

The FFS is based on the 2D numerical model of the Baltic Sea BSM3. The model was developed within the CARDINAL modelling system, which is a system for simulation of currents, water levels and concentrations in arbitrary water domains in 2D and 3D approaches.

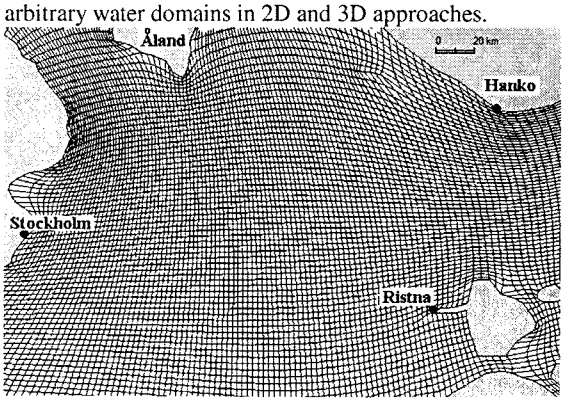

Figure 1: Fragment of the curvilinear grid for the central part of the Baltic Sea in the BSM3 model.

A flexible user interface and the use of boundary-fitted curvilinear co-ordinates make it possible to use the system for solving different complex hydrodynamic and environmental problems. The model grid in BSM3 consists of 30894 active points. The average grid size is about 3 km (**Fig.1**) and the minimum one is in the Barrier openings and equals 270 m.

3. Meteorological forecasts - HIRLAM-22

For testing and validation purposes, forecasted surface wind and atmospheric pressure fields for BSM3 are received from the HIRLAM model, which works operationally at SMHI. The computational domain of HIRLAM covers partly the North Atlantic, the Norwegian Sea, the Greenland Sea, the North Sea and the Baltic Sea, and the bigger part of Europe. The grid size in HIRLAM at present is 22 km (**Fig.2**). Grid consists of 713124 points (31 vertical layer). Each file of HIRLAM output contains data on 20 meteorological parameters for a certain point in time. As these files are rather big it was agreed that SMHI would provide the St.Petersburg FFS with special reduced files with surface wind and atmospheric pressure fields only. These files are loaded in automated regime on the ftp server of SMHI. HIRLAM output is packed in GRIB (Gridded Binary) format. To work with these data, a GRIB decoder and subroutines for their graphical representation were developed in CARDINAL. Comparison with observations shows that forecasts of HIRLAM are rather good.

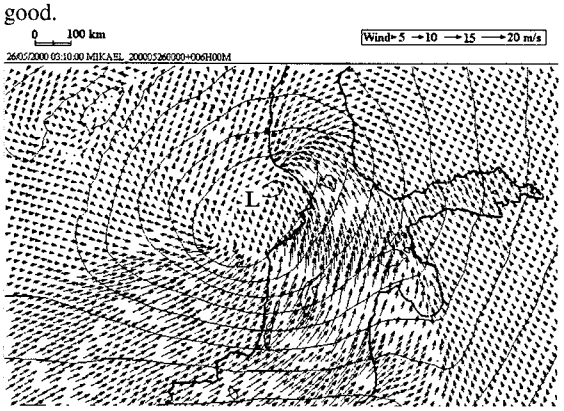

Figure 2: Fragment of HIRLAM forecasted wind and pressure fields for 03 h GMT 26 May 2000.

4. Danish Straits - OPMODEL

Since December 2000 BSM3 receives forecasts of the water exchange between the Baltic and the North Seas through the Danish Straits from BSH, where simulations are made with a large scale model of the Baltic and the North Seas (OPMODEL). This should improve forecast quality, as this water exchange is the basic factor of the water balance of the Baltic Sea. The discharges achieved values above 250 thousand m^3/s. Their daily variability is connected with tides in the North Sea, while long period ones are connected with large scale processes in the North Atlantic. The latter leads to a significant change of mean water level in the Baltic Sea. **Fig. 3** shows a comparison of changes in mean water level and volume of water in the Baltic Sea due to this water exchange with observed time history of water level in St.Petersburg for the same time

period. Changes of mean water level were received by dividing of inflow volume by the Baltic Sea area, which in the BSM3 model equals $3.46 \cdot 10^{11}$ m^2. Between 3.12.2000 and 7.02.2001 the water volume in the Baltic Sea decreased by 133 km^3, that leads to a decrease of mean water level by 38 cm. Comparison with the time history of water level in St.Petersburg shows a good correlation of low water levels in the head of the Gulf of Finland observed in January - February 2001 with the outflow into the North Sea simulated by BSH.

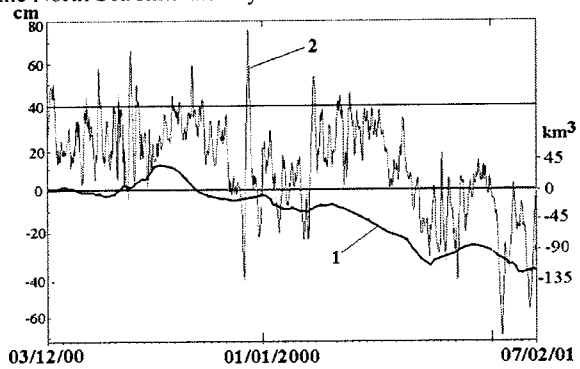

Figure 3: Change of mean water level and water volume in the Baltic Sea due to water exchange through the Danish Straits according to the BSH model (1) and observed water levels in St.Petersburg (station Gorniy Institute) (2) 3.12.2000 -07.02.2001.

5. Performance of the Flood Forecasting System

After the forecasts from SMHI and BSH have been received, the Baltic Sea model BSM3 automatically starts. Simulations are made for the period from 0 h GMT of the current day until 12 h of the next day, i.e. for 36 hours. Water level and current fields, which refer to 0 h of the next day are stored and serve as the initial data for the forecast, which will be made on the next day. The computational time is 10 minutes on the Pentium-III-500 computer. After simulations are done, a one-page report is printed. It contains forecasts of water levels in St.Peterburg in tabular and graphical forms, wind and pressure over the Eastern Gulf of Finland, progressive vector diagram of currents in the central part of Neva Bay and change of mean water level in the Baltic Sea. The whole process is fully automated. Pre-operational forecasts are made in the NWHS since 23 December 1999. During simulations it is possible to view different types of information: fields of wind, pressure, water level, currents in arbitrary scale, time histories of water level in any number of prescribed points and other. The experience obtained during one year of the system work has proved that the organisation of the data loading and processing has a robust character.

6. Results

The root mean square error (RMSE) in forecasted hourly water level values for the period December 1999 - December 2000 (about 9000 values) was 20 cm, mean absolute error was 16 cm, correlation coefficient was 0.73. **Figs. 4, 5** show observed and forecasted time histories of water level in St.Petersburg in May and June 2000. An analysis of observed and HIRLAM-forecasted weather situations was done for 13 cases of significant water level rise. It was revealed that when the wind field over the head of the Gulf of Finland is forecasted accurately, forecasts of water level are, as a rule, also accurate. The most significant errors in water level forecasts were due to errors in wind shifts within Neva Bay.

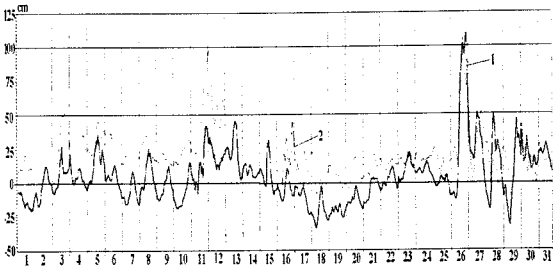

Figure 4: Observed (1) and forecasted (2) water levels in St.Petersburg in May 2000.

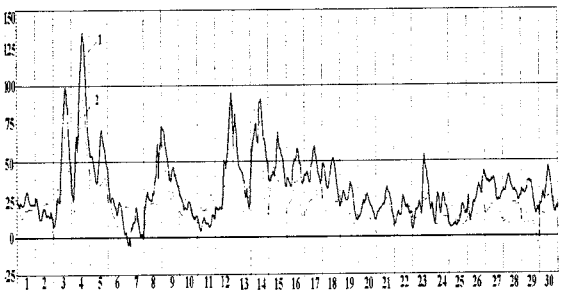

Figure 5: Observed (1) and forecasted (2) water levels in St.Petersburg in June 2000.

7. Conclusions

The developed fully automated flood forecasting system for St.Petersburg gives rather good results, better than all previous methods. There were no floods in St.Petersburg for the validation period considered and verification of the method will continue in 2001. One of the sources of increase of the method accuracy is more adequate description of atmosphere-sea interaction in the Baltic Sea model. It is necessary also to take into account ice cover for winter months and to include in the model the Neva River up to the Ladoga Lake (it will allow to forecast the direction of the currents in the Neva delta). This work is in progress. After some tuning the system could be used for water level forecasts in other points of the Russian coast of the Baltic Sea (new ports of Primorsk, Ust'-Luga, Bukhta Batareinaya, Leningrad Nuclear Power Plant). It also may be used for forecasts of dispersion of pollutants.

References

Klevanny, K.A., Modelling floods for the present state of St.Petersburg Flood Protection Barrier, *Second Study Conference on BALTEX, GKSS*, 1998, 106-108, 1998

Klevanny, K.A., V.P.Gubareva, Flood Early Warning System for St.Petersburg, *Morzaschita, St.Petersburg, Project Report PSO98/F/3/10*, 2000

BALTEX Radar Products and their Accuracies

Jarmo Koistinen[1] and Daniel B. Michelson[2]

[1] Finnish Meteorological Institute, P.O. Box 503, FI-00101 Helsinki, Finland
[2] Swedish Meteorological and Hydrological Institute, SE-601 76 Norrköping, Sweden

From the outset of the BALTEX Main Experiment, the BALTEX Radar Data Centre (BRDC) has been providing datasets for use by research groups both within and outside the BALTEX community (Michelson *et al.*, 2000). These homogenous datasets consist of the following composite products from around 30 radars:

- Radar reflectivity factor every 15 minutes
- Gauge-adjusted accumulated precipitation, 3- and 12-hourly

The spatial resolution of these products is 2×2 km and the common area of radar coverage consists of the majority of the Baltic Sea's catchment area. Almost all the radars are equipped with Doppler capability providing vertical profiles of wind speed, direction and reflectivity every 15 minutes above each radar in vertical slices of 200 m. These products will be briefly presented and described. Changes to the BRDC product flora and dataset format will also be presented.

Alongside the production of BRDC datasets, the BALTEX Working Group on Radar (WGR) has made a number of contributions to the related fields of research. Simple and pragmatic solutions to quality control of conventional products will be illustrated. Also, recent work on normalization of data from a network of heterogeneous radar systems will be highlighted. The reasons behind the discontinuities in a network are usually in the electrical calibration of the systems, in the signal processing and product algorithms, and in the measurement geometry and siting of the radars. Although present in all existing networks, NORDRAD/BALTRAD cooperation has been among the first in creating practical methods to understand, monitor and adjust such heterogeneities. Siting and clutter problems vary among individual radars so much that advantages can be gained if a research application, requiring the best possible accuracy, uses as input radar data only from those radars exhibiting fewer local problems.

One of the difficulties in radar meteorology is in deriving quantitatively accurate precipitation measurements which are valid at the earth's surface. Gauge adjustment has been shown to provide an effective statistical means of achieving this (Michelson and Koistinen, 2000). It will be shown how gauge adjustment removes various sources of bias in the BALTRAD accumulation products. However, to reach acceptable accuracy applying gauge adjustment methods requires large statistical samples. It requires also that gauge estimates are accurate or that they should be corrected. In snowfall, the flow distortion error in gauge observations can be larger than any radar error. The practical implication is that the BALTRAD accumulations are excellent in larger areas for precipitation estimates and for validation of other precipitation data (e.g. those from an NWP model, see presentations elsewhere in this conference by Carl Fortelius and by Colin Jones *et al.*).

When we want to maximize the accuracy of short period precipitation accumulations or the accuracy of instantaneous intensities in small areas or even in the single radar measurement pixels, a gauge adjustment is not accurate enough. It will remove part of the average bias but local errors can still be large. There are three reasons for this:

1. The spatial and temporal representiveness of operational gauge measurements is poor. Radar has much better resolution in detecting *relative* precipitation variations.
2. Even in the case of perfectly co-located gauge and radar measurements, the difference between the two estimates will contain a large noise component due to the different sampling strategies of the two devices (Kitchen and Blackall, 1992). This effect increases as a function of range from a radar.
3. Radar measurements are prone to several sources of measurement error.

A lot of confusion exists over what is the relative importance of each of the above three factors contributing to the difference between the actual precipitation at the surface and the radar sample aloft in a single measurement point. The greater part of the radar meteorological and hydrological research is misleading when trying to point out the essential error factors in the radar measurement itself (3). In addition to the radar system issues, we will show the relative importance of the following meteorological aspects and the possibilities to correct them:

- The vertical profile of reflectivity (VPR)
- The occurrence of rain, sleet, hail, and snow in the measurement volume
- The variability of hydrometeor size distributions, ie. the type of precipitation affecting the relationship between the measured radar reflectivity and the respective precipitation intensity: so-called optimal Z-R relation

The dominating issue in the BALTEX region is that the relatively cold climate of the area generates precipitation structures which introduce other significant measurement problems than those in the mainstream of radar meteorology, namely dealing mostly with severe summer convection in warm climates. It is shown that the VPR dominates other error sources in winter at ranges of 50-250 km from a radar. In the BALTEX WGR, corrections for effects of the VPR (e.g. Vignal *et al.* 2000) are being developed (although the daily gauge adjustment will remove the effect of the average structure of VPR). They show greater promise in preserving local detail in the correction process. Combined with new methods for identifying and treating effects caused by the melting layer (bright band) (Saltikoff *et al.*, 2000, Michelson, 2001), these strategies should lead to more accurate quantitative precipitation measurements with radar. Experiments using such strategies will be presented and discussed. These improvements aim to "perfect" measurements of precipitation with radar. Actually, the existing BALTRAD quality is such that the accumulations can replace traditional gauge observations in a hydrological model. This will be demonstrated with an example applying the Kyrönjoki river model in Finland.

References

Kitchen M. and Blackall R.B., 1992: Representiveness errors in comparisons between radar and gauge measurements of rainfall. *J. Hydrology* Vol 134. pp. 13-33.

Michelson D.B., 2001: Diagnosing Z-R Relations using NWP. *Preprints AMS 30th International Conf. on Radar Meteorol.* 19-24 July, Munich.

Michelson D.B. and Koistinen J., 2000: Gauge-radar network adjustment for the Baltic Sea Experiment. *Phys. Chem. Earth (B).* Vol. 25, Nos. 10-12. pp. 915-920.

Michelson D.B., Andersson T., Koistinen J., Collier C.G., Riedl J., Szturc J., Gjertsen U., Nielsen A. and Overgaard S., 2000: *BALTEX Radar Data Centre Products and their Methodologies.* RMK 90. SMHI, SE-601 76 Norrköping, Sweden. 76 pp.

Saltikoff E., Koistinen J., and Hohti H., 2000: Experience of Real Time Spatial Adjustment of the Z-R Relation According to Water Phase and Hydrometeors. *Phys. Chem. Earth (B).* Vol. 25, Nos. 10-12. pp. 1017-1020.

Vignal B., Galli G., Joss J., and Germann U., 2000: Three Methods to Determine Profiles of Reflectivity from Volumetric Radar Data to Correct Precipitation Estimates. *J. Appl. Meteorol.* Vol. 39, No. 10. pp. 1715-1726.

Analysis of the Heat Budget in the Coastal Area of Hanko Peninsula

Johanna Korhonen, Anniina Kiiltomäki, Irene Suomi, Kaisa Halkola, Jari Haapala

Department of Geophysics, University of Helsinki, Finland, email: johanna.k.korhonen@helsinki.fi

1. Introduction

This study is a part of Baltex/Bridge project course at the Department of Geophysics, University of Helsinki. The course started in autumn 1999 and ends at summer 2001. The project includes lectures, fieldwork and reporting. There have been seven students that participate in this project. We have been divided into two groups. Our group has analysed the heat budget in the coastal area of Hanko peninsula. Also in some extent the whole area of Baltic Sea has been considered.

2. Purpose and Methods

There have been two main goals in this project. The first one is to study energy exchanges between air and sea and the other one is to analyse the heat budget in the sea. Also the atmospheric heat transfer to the area of Baltic Sea has been briefly studied. The time period for analysis is from November 1999 to spring 2001.

Studies on air-sea interaction are mostly based on NCEP/NCAR-data. Also some verifications have been made by comparing NCEP/NCAR-data to Längden lighthouse weather station's measurements. NCEP/NCAR-data is provided by National Center of Environmental Prediction and National Center of Atmospheric Research for free in the Internet. This data is based on global synoptic measurements and weather forecasts made since 1958. The parameters we have used are air temperature, wind, short-wave and longwave radiation fluxes, latent heat flux, and sensible heat flux. From these components we have determined the heat flux to the sea.

Studies on the heat budget of the sea are based on the termistor chain measurements. The termistor chain was deployed near the Längden lighthouse (59° 47′ N, 23° 20′E). It measured temperature profile from surface to 50 meters depth five meters intervals. The seasonal variation of vertical temperature structure has been analysed from these observations. In addition, the heat content of the water mass has been calculated.

References

NCEP Reanalysis data provided by the NOAA-CIRES Climate Diagnostics Center, Boulder, Colorado, USA, from their Web site at http://www.cdc.noaa.gov/

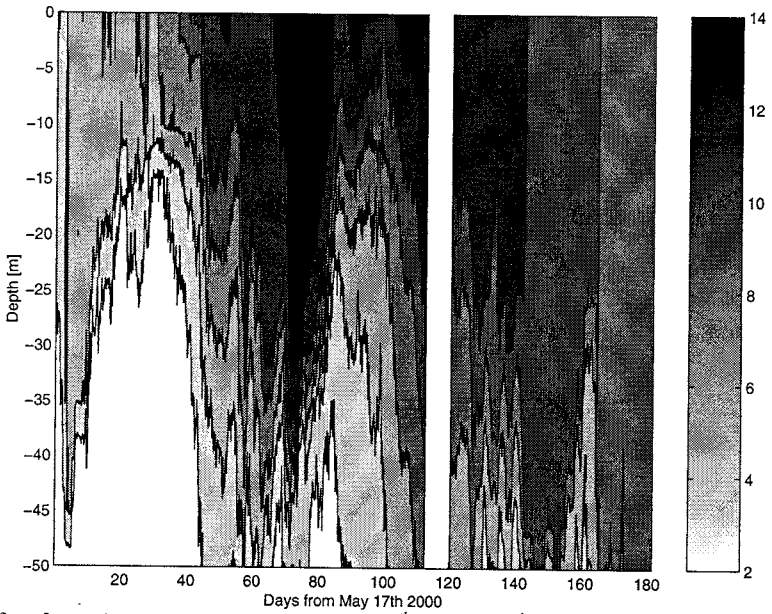

Figure 1: Evolution of surface mixed layer temperature from 17th May to 15th November.

Analysis of marine meteorological observations in Latvia

Janis Kostjukov, Marta Treiliba

Latvian Hydrometeorological Agency, 165, Maskavas Str., Riga, LV-1019, Latvia

1. Introduction

The global temperature is rising. Observations collected over the last century suggest that the average land surface temperature has risen by 0.45-0.6°C and the sea surface has warmed by 0.3-0.6°C. Sea level has risen world-wide approximately by 15-20 cm. Approximately 2-5 cm of the rise result from the melting of glaciers, another 2-7 cm - from the expansion of ocean water due to warmer ocean temperatures. The pumping of ground water and melting of the polar ice sheets may have also added water to the oceans. [2]

Data on the air temperature, sea level, atmospheric pressure and ice days in the port of Riga were processed with an effort to determine trends in the main hydrometeorological elements over the period of operating marine meteorological stations in Latvia.

2. Air temperature

Air temperature observations have shown progressive warming over the territory of Latvia. Comparisons made of the values for the recent 100-year period testify to a more rapid rise in the temperature for the second half of the period. During the first 50 years, annual mean air temperature had become 0.2°C higher on the average, with no influence being observed from the populated areas and the level of economic development. In the second half, however, the effect of industrial areas was evident. The mean annual temperature in Riga has increased nearly by 1°C, with 0.5°C in the rest of the country (Fig. 1).

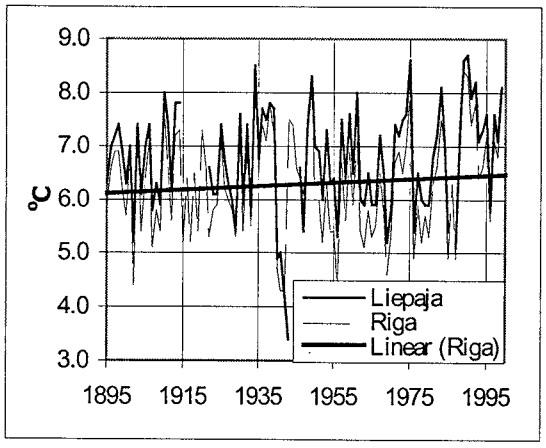

Figure 1: Mean annual air temperature variations in Riga and Liepaja and linear trend

The air temperature amplitude has become narrower. The greatest positive changes have occurred in the winter months, mainly due to rise in temperature at night. Mean annual extreme values have moved closer, with the mean temperature minimum increasing faster than the maximum one.

3. Sea level

Evidence of an increase in the mean sea level was obtained based on an analysis of long annual mean sea level records from tide gauges along the Latvian coast at Daugavgriva (1875-2000) and Liepaja (1865-2000) where round- the-clock readings of water level were made (Fig. 2).

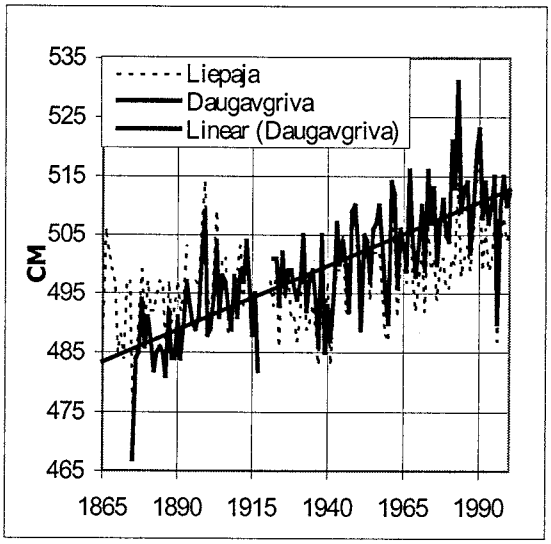

Figure 2: Annually mean sea level changes and linear trend

The investigation is aimed at revealing long-term changes of sea level and determining the rate of the changes employing the tide gauge data [3]. Coefficients for the linear trend equation (A_1) were established to indicate the mean annual rise of sea level and the predicted rate of future mean sea level rise. Complete records of 9 tide gauges for two periods (first - from beginning of the observations until 2000 and second - in 1961-2000) were analysed and positive values of the linear trend coefficients were found, 0.044 cm for Ventspils and 0.2273 cm for Skulte for the first period and 0.0794 cm for Roja and 0.4082 cm for Skulte for the second period (Tab. 1). In the second period, sea levels rise pattern has greatly changed in the last 40 years. Similarly, the atmospheric circulation above the Baltic Sea has become more westerly, thus promoting a more intensive inflow of the oceanic water into the Baltic Sea.

Table 1: Coefficients of linear trend equations for tide gauges on the Latvian coast

Station	1. Period	A1	2. Period	A2
Salacgriva	1929-2000	0.0799	1961-2000	0.1419
Skulte	1940-2000	0.2273		0.4082
Daugavgriva	1875-2000	0.2177		0.1639
Jurmala	1948-2000	0.0806		0.133
Roja	1932-2000	0.0684		0.0794
Kolka	1884-2000	0.066		0.232
Ventspils	1873-2000	0.044		0.211
Pavilosta	1929-2000	0.0972		0.138
Liepaja	1865-2000	0.0669		0.1324

4. Atmospheric pressure

Atmospheric pressure above sea has been decreasing by 0.0187 mb/year in Riga and has been very slowly rising in Liepaja, by 0.0015 mb/year (Fig. 3).

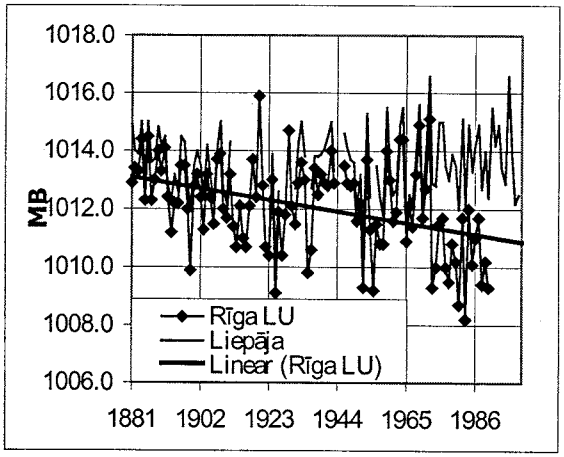

Figure 3: Mean annual atmospheric pressure variation in Riga and Liepaja and linear trend

5. Ice days

Peteris Stakle, Latvian hydrologist, made in 1930 a generalization of ice records (freezing and break-up dates) in the port of Riga, beginning with the winter 1529/30, including those provided in chronicles.

Data for the XVI and XVII century were incomplete (41 and 22 observations, respectively). Since the year 1709, ice observations have been performed nearly regularly. An analysis of the ice break-up dates in the Daugava river near the port of Riga showed that the cycles of early and late break-up alternated fairly irregular. In the XVIII and XIX centuries, the cycles of late break-up were more prolonged. In the XX century, in a more frequent alternation, the periods of late and early break-ups were nearly the same in duration, but break-up occured earlier than in previous centuries.

A graph of distribution of the main characteristics of the sea ice regime - ice days - gives proof to such a conclusion (Fig. 4). The linear trend decreases, and the trend coefficient is 0.5 days per year.

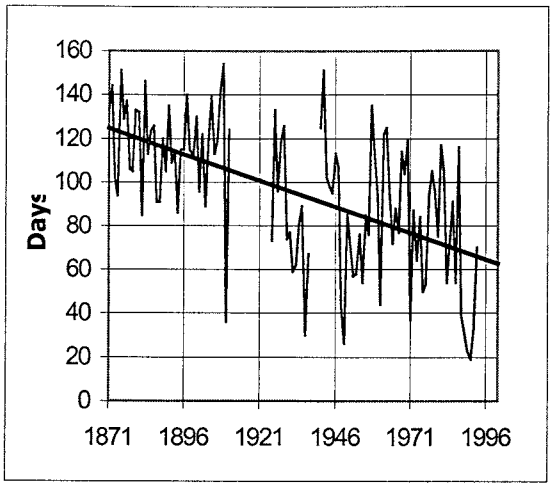

Figure 4: Ice days in the port of Riga and linear trend

6. Conclusion

The changes of meteorological elements and their effects on sea level and ice conditions in the ports of Latvia were studied for a period of around a hundred years. The air temperature observations have shown progressive warming which was more rapid in the second half of the XX century. The atmospheric pressure showed mainly the decreasing tendency. The sea water level along the Latvian coast showed the tendency to significant increase. The increasing air temperature, especially in winter, caused a reduction in the ice cover duration in Latvian ports.

References

Hidrometriskie novērojumi Latvijā līdz 31.X.1929. Finansu ministrija, Jūrniecības departaments, Rīga, 1931.

Titus G., Narayanan V.K. The probability of sea level rise. 1995,Washington.

Zaharcenko E., Klevantsov J., Smirnova A., Kostjukov J. The sea level variability in the Baltic proper and the Gulf of Riga. In: International Geodesy and Geography conference, 12-19 November 1992, Riga.

The Baltic Sea-level events in the system of global change

Eugene Krasnov[1], Larissa Sergejewa[2] and Elena Kostina[3]

[1] Kaliningrad State University, 236041 Kaliningrad, Russia
[2] Baltic Fishing Fleet State Academy, 236029 Kaliningrad, Russia
[3] Institute of Marine Biology, 690041 Vladivostok, Russia

1. Investigation of annual sea-level variations

The trend of averaged annual sea-level variations in the SE Baltic over the period from 1841 to 1950 was estimated by Drs. D. Berenbeim and B. Chuvarenko (1990). In Kronstadt it is amounted to 0.01 cm/year; in Baltiysk - 0.129 cm/year, in Kaliningrad - 0.025 cm/year. Note, that beginning from 1950 there occurred sharper increasing of averaged annual sea-level, therefore we analyze this period individually. Thus, as a first approximation it should be regarded, that averaged annual sea-levels in the vicinity of Kronstadt are not faced with the trend, while subjected to significant inter-layer variations.

On the coastline from Tallinn to Klaipeda, over the period from 1891 to 1950, the elevation of coast (negative trend) occurred at the rate of 0,2-0,5 mm/year, while in the region of Pionersky-Baltiysk the submergence of the coast occurs at the rate of 0,7-1,3 mm/year. Comparing relations between averaged annual sea-levels in 1841-1950 and 1950-1990 we note, that the last period is characterized by stable increased inflow of the North Sea waters.

2. The rapidly rising sea-level and its reasons

Observations and calculation showed that during the ten-year period 1981-1990 there was sudden and considerable rising of the Baltic sea-level (Sergeeva, 1995). For the analysis of long standing fluctuation in southeastern and eastern regions of the Baltic Sea-level during 1900-1990 years in 8 seashore-points (Kronstadt, Tallinn, Kotka, Liepaya, Klaipeda, Pionersky, Baltiysk), were used annual data. The fluctuations of the annual sea-level have synchronous character, the average figure of increasing of the mean levels in southeastern part of the Baltic Sea (Klaipeda, Baltiysk, Kaliningrad) during 1981-1990 years in comparison with previous ten-years period is coming to 11 cm, with 1901-1910 period - to 17 cm.

One of the beast explanations of the sea level rising and increasing of the Baltic Sea water volume may be given by the circulation of the water - balance components. It proposes to produce the equation of the water balance for the Baltic Sea may be done in of the following form: $Z + N + E - V - A = \Delta H$, where

Z - the river flow (including the underground flow)
N - atmospheric precipitation
E - the influx of the North Sea waters
V - water losses for evaporation
A - outflux of the water into the North Sea.

In connection with the rivers levels meaning the average river flow's significance of long standing can be regarded as constant value (not excepting the fluctuation between years) hawing the tendency to decrease. In the water balance budget's part of receipts it comes to 34% for, the atmospheric precipitation's N it comes to 13%. Taking the flow component as Const and taking into account the least influence of the N component with Z we can consider that the main contribution to the Baltic water volume's increasing is making by E component - influx of the North Sea waters into the Baltic that in percentage correlation of the water balance part of receipts is equal to 53%, i.e. the sea water balance is valuing by the A -E difference in the area of Danish straits.

The volume and the intensity of the Danish straits inflow and outflow (E and A components) are closely connected with the special features of atmospheric circulation above the Baltic Sea and the development of cyclonic action above the Atlantic. Consequently, the sea waters volume fluctuation depend on the prevalence of the atmospheric circulation forms above the Baltic Sea which, in it's turn, regulates the development of inflows, outflows and losses. In this case the eastern type of circulation determines the water outflow into the North Sea, meanwhile, increasing of the western forms of atmospheric circulation is facilitating the inflow increasing, the Baltic Sea filling and, consequently, the general trend of rising of the average year levels is observing.

The confirmation of it is the close connection between the average year levels significance's and the number of days with west - direction wind (NW, W, SW) in Kaliningrad. The correlation coefficient of this dependence for number of observations (n=30) is equal 0,76 which makes it possible to come to a conclusion about the reasonable connection between the western form of atmospheric circulation's repetition and the levels fluctuation.

The calculations showed that in accordance with the positive trend of the level the contribution of the western form of atmospheric circulation in the region winds cycle during the present period was rising. Thus from 1951 to 1990 it rised from 39% to 62% (table 1).

Table 1: The western form of atmospheric circulation's in Kaliningrad during 1951-1990 years, % (After L.Sergeeva, 1995)

1951-1960	1961-1970	1971-1980	1981-1990
39	46	49	62

Statistical analysis of synoptically and hydrological materials proved that during 1981-1990 period in southeastern part of the Baltic Sea in comparison with 1951-1960 the number of cases of bringing up a mass of water by storms, the occurrence of which is closely connected with making the cyclonical action more active increases 6 times. As we can see from table 2, it has been rising per ten year periods and came to 5, 10, 12 and 30 events accordingly.

Table 2: Figures of stormy bringing up in the Pregolya river near Kaliningrad for ten-year periods (After L.Sergeeva, 1995)

Level BS, (cm)	Number of stormy			
	1951-1960	1961-1970	1971-1980	1981-1990
95-125	5	9	10	21
126-154			2	6
155-180		1		1
more than 180				2
Total	5	10	12	30

Moreover during the last 10 years not only the number of bringing up was increasing but the obsolete height of the sea level was rising. Thus, if in 1981-90 9 cases of bringing up with height more than 126 cm BS were observed; in 1971-1980 their number was 2, in 1961-1971 - 1, in 1951-1960 years - zero. Besides, in 1981-1990 3 dangerous cases of bringing up with height more than 155 cm BS were fixed and one of them is absolute maximum with height of 188 cm BS (29.01.1983).

In the Baltic Sea isostatistical changing of the level due to the Earth crust's vertical movement is taking place. Thus, it is known from literature that in 1892-1958 the speed of the shore's rising in the north region of the Gulf of Bothnia was about 8-9 mm per year, along the northern shore of the Gulf of Finland - 2-3 mm per year (Hanko, Helsinki). Meanwhile the shores of Sweden (Istad), Denmark (Copenhagen), Germany (Travemunde), Poland (Swinouiste) are immerging. However, the order of isostatical changing of the Baltic Sea level is several times less than observer rising during 1981-1990 years.

Fluctuation of the Baltic Sea level surface and main trend to rise can be considered with sufficient probability as eustatical changing having the connection with the increase of World Ocean level too.

The supposition that during recent ten-year period the trend of the sea level to rise will maintain allows the prediction of probability of the maximum level with 0,01% security, for Kaliningrad it would be more than 200 cm BS. The siminar conclusion was made by Mr. Nezhilovsky saying that in StPetersbourg it's possible to exceed the absolute maximum of the level's height under the circungtances of simultaneous and unidirectional combination of all factors having the influence on the sea level's rising.

3. Sea-level fluctuations in the Baltiysk (Pillau) area

From 1840 to recent days the fluctuation of the sea-level near port Baltiysk have been between - 33 to + 10 cm. Real tendency to increase of sea-level here was established by Drs. N. Lazareva and E. Maximov (1991). Average speed of this process is about 1.4-1.5 mm per year have been observed.

The connection of sea-level rhythmic variations with solar activity cycles (3-4, 11, 22 years) which was discovered by Drs. N. Lazareva and E. Maximov (1991), also will be discussed.

References

Berenbeim, D., Chubarenko, B. Investigation of averaged annual sea-level variations in the South Eastern Baltic. *Materials of the Conference "Ecobaltica - 91".* - Kaliningrad, 107-108, 1991

Sergeeva, L. Increase of the Baltic Sea level: its causes and forecast. *Transactions of Baltic Fleet State Academy "Theory and practice of shipping".* - Kaliningrad, 102-107, 1995

Nezhilovsky, R. Neva River and Neva mouth. *Hydrometeorology Publ. House.* - Leningrad, 108 p., 1981

Lazareva, N., Maximov, E. Sea-level fluctuations in the Baltiysk area. *Proceedings of All-Union Geographical Society*, t. 123, v. 3, 271-275, 1991.

Linkage of snow storage over the FSU territory with the NAO and SOI and its relationship with the Indian monsoon intensity

Alexander Krenke and Lev Kitaev

Institute of Geography, Russian Academy of Sciences. Moscow, 109017, Staromonetny lane 29, e-mail: climate@online .ru

Snow cover interannual changes in the continental scale are compared with some well pronounced features of the global atmospheric circulation - NAO, SOI and the Indian monsoon intensity. The snow data base for the FSU territory (without high mountains) was created for the period 1966 - 1990 (*Kitaev et al., 1997*). It includes snow surveys in the vicinity of about 800 stations. The data for forested and open routs were weighted according to the rate of forestation and then interpolated into the knots of the grid with 2x2 resolution.

As the index of NAO the 5 months (November - March) averages of normalized pressure differences between Iceland and Azores were used. This index grew after 1970 and especially after 1980 (*Hurrel, 1995*) simultaneously with the global warming. That led to the increasing of cyclones activity, precipitation and warming in the northern Europe and to the weakening of Mediterranian cyclones, dry and cold condition in the southern Europe (*Serreze et al., 1997*).

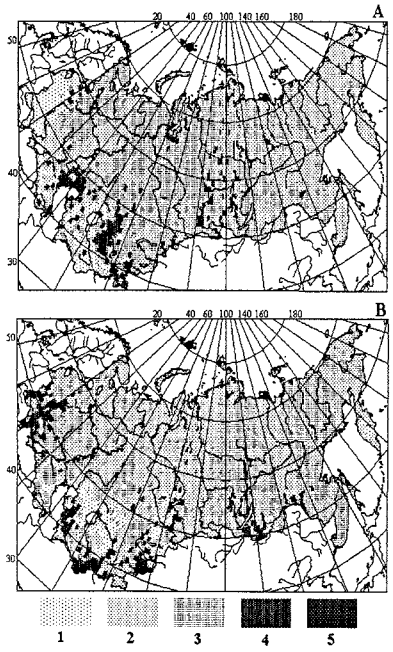

Figure 1: The ratio of the snow storage in the 5 years with maximum NAO (**A**) and 5 years with minimum NAO (**B**) to the average snow storage in the 1966-1990.

1: 0 - 0.75
2: 0.75 - 1.00
3: 1.00 - 1.25
4: 1.25 - 1.75
5: > 1.75

The composite maps of the annual maximum of snow water equivalent for the FSU territory were compiled for 5 years with the maximum and for 5 years with minimum NAO indeces for 1966 - 1990. Snow water equivalent quantities in the grid points were normalysed by the mean for 25 years (Figure 1).

Snow accumulation in the years with high indeces is above normal in the north of the Russian plain and the Ural, and over the West Siberian plain up to Yenisey river. ("diving cyclones"). In the south of Russian plain and in the main part of Kazakhstan the snow accumulation is below normal. The opposite picture reveals in the years with low indeces. To the east of Yenisey river there are no regular differencies. The snow accumulation and the amount of cyclones here depends mostly on the state of Siberian High.

The correlation coefficients between snow water equivalent in different points and NAO indeces were calculated. They appeared to be positive in the north of the Russian plain and over the West Siberian plain and negative in the south of the Russian plain. The correlation of the dates of snow maximums and disappearing is everywhere negative and its significance grew to the west.

South Oscillation Index (SOI) is the air pressure difference between Tahiti island and Darwin (Australia). 4 years with low SOI (El Ninio years) and 4 with the high SOI (La Ninia) years were choosen for the same period (1966 - 1990), and composite maps of snow water equivalent anomalies over the FSU territory were drown. As a whole the snow accumulation in El Ninio years is greater in the south, in the mountaines especially.

In contrast to that in La Ninia years the accumulation is greater in the north. The relation to SOI became significant only in the February - March. That means some months of lag with the El Ninio - La Ninia events. The explanation of this teleconnection is the negative linkage between NAO and El Ninio (*Gushchina and Petrosianz, 1998*).

The intencity of Indian monsoon was determined from the all-India summer season precipitation (*Gadgil, 1995*).

The correlation of these precipitation and previous winter snow water equivalent averaged over the FSU territory is negative and significant. This confirms the theory of snow influence on monsoon through the soil moisture and thus surface temperature. The correlation with the snow water equivalent in the different meridional sectors in the previous and following winters confirms the other theory - the circulation one dealing with the interrelation between monsoon and Rossby waves (*Kripalani and Kulkarni, 1999*). It looks like both mechanisms are taken place in the monsoon - Eurasian snow interrelationship.

The research was accomplished under support of Russian Fund of the Basic Research (RFBR), grant No 99-05-65572.

References

Gudgil S. , 1995. Climate change and agriculture - an Indian perspective. Current Science, 69, 649 - 659.

Gushchina D.Yu. and Petrosianz M.A., 1998. The linkage of sea surface temperature in the equatorial part of the Pacific and wind velocity circulation in the atmospheric Centers of Action. Meteorologia i Hydrologia, No 12, pp. 5 - 22. In Russian.

Hurrell, J.W. , 1995 . Decadal trends in the North Atlantic oscillation: Regional temperatures and precipitation. *Science*. 269, pp 676 - 679.

Kitaev L.M., Krenke A.N., Barabanova E.A. , 1997. Generation and application of snow cover information system in the continental scale. *ADBIS (Advanced Data Base Information Systems) - 96. Proceedings of the 3-th Intern. Workshop. Moscow, Sept. 10 - 13, 1996.* Vol 2., M., pp. 74 - 78.

Kripalani R.H. and Kulkarni A., 1999. Climatology and variability of historical Soviet snow depth data: some new perspectives in snow - Indian monsoon teleconnections. Climate Dynamics , v.15, pp. 475 - 489.

Serreze M.C., Carse F., Barry R.G., Rogers J.C., 1997. Icelandic Low Cyclone Activity: Climatoloial Features, Linkages with the NAO, and Relationships with Recent Changes in the Northern Hemisphere Circulation. *Journal of Climate,* vol.10, No 3, March., pp. 453 - 464.

Retrieval of Aerosol Properties over the Baltic Sea using AVHRR Data

Aleksey Kryvobok

Ukrainian Hydrometeorological Research Institute, Kyiv, Ukraine, UHRI, 37 Nauki str, Kyiv,03028, Ukraine.
Tel:+38 044 2658664; fax:+38 044 2655363, e mail:bel@ozsol.kiev.ua

1. Introduction

The effect of tropospheric aerosols on climate by means of the direct and indirect radiative forcing in local and regional scale is one of the largest remaining uncertainties in climate change studies. Obtaining information about regional distributions of aerosol properties is possible only by use of satellite measurements. The standard one-channel Advanced Very High-Resolution Radiometer (AVHRR) aerosol retrieval algorithm uses 1 channel thus as many limitations [1]. The new two-channel algorithm [2] provides significantly more accurate and less biased retrievals of the aerosol optical thickness then the above mentioned algorithm.

2. Satellite Data

Satellite data were obtained from AVHRR (NOAA) during the summer of 2000 from June to August. The Gulf of Finland was the investigated area, which is shown in fig.1

3. Computational technique.

Reflectances are calculated in channels 1,2 of AVHRR with a multiscattering code based on the scalar version of the discrete-ordinate method [3]. The code takes into account the rough sea surface reflection by means of a modified Kirchoff approximation, water vapour, oxygen and CO_2 absorption by means of the k-distribution technique [4] and multiple scattering by stratospheric and tropospheric aerosols and molecules.

4. Results

The main results of this study are as follows:

1. The two channel algorithm provides more accurate retrievals of aerosol properties over the area;
2. the value of aerosol optical thickness over the coastal zone is larger than those over the sea. As a rule this phenomenon was observed over the whole target area - caused by the influence of anthropogenic factors.

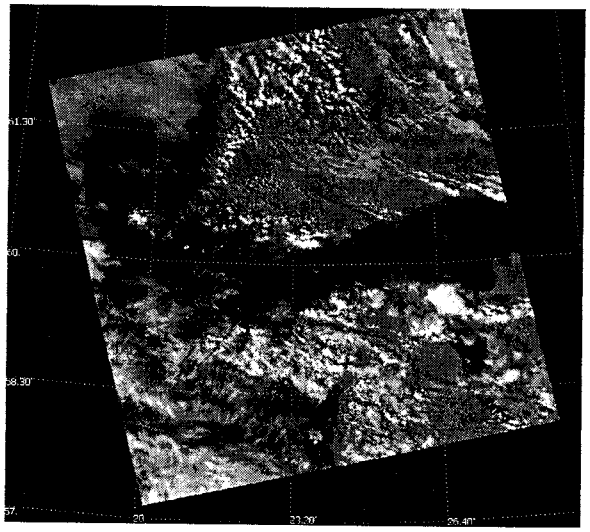

Figure 1: Investigated area in BALTEX region.

References

L.L.Stowe, A.M.Ignatov, R.R.Singh,"Development, validation and potential enhancements to the second-generation operational aerosol product at the National Environmental Satellite, Data and Information Service of the National Oceanic and Atmospheric Administration", J.Geophys.Res. 102, 16,923-16,934 (1997)

M.Mishchenco, I.V.Geogdzhaev, Brian Cairns, William B.Rosssow and A.A.Lacis,"Aerosol retrievals over the ocean by use of channels 1 and 2 AVHRR data:sensivity analysis and preliminary results", J.Applied Optics, vol.38, N36, 7325-7341,(1999)

Kryvobok A.A."Atmospheric correction of Multispectral Satellite Images", Trudy UHRI, vol.246, 41-50.

A.A.Lacis, V.Oinas, "A description of the correlated k-distribution method for modelling non-grey gaseous absorption, thermal emission, and multiple scatterring in vertically inhomogeneous atmosphere", J.Geophys.Res.96,9027-2063.

Estimation of solar radiation for use in environmental science modelling

Leszek Kuchar, Bronislaw Glowicki

Institute of Meteorology and Water Resources, ul. Parkowa 30, PL-51616 Wroclaw (Poland)

1. Introduction

The aim of this study was to determine the accuracy and applicability of a number of existing and newly developed formulae for calculating solar radiation from other weather variables. Records of daily solar radiation measurements are available for few sites and limited series, while other variables like temperature and precipitation from many sites.

2. Data

The data including daily recorded values of solar radiation, maximum and minimum air temperature and precipitation together with values for clear sky radiation (calculated as a function of latitude, day of year, solar angle, and solar constant) obtained from six stations were used for testing several formulae.

3. Methods

Several formulae well known from literature were used to compute solar radiation from data on maximum and minimum temperature, and precipitation for instance *Bristow and Campbell* (1984), *Cengiz et al.* (1981) or *Hunt et al.* (1998). Also a general linear model and selected nonlinear methods were used to predict daily solar radiation. Selection followed examination of the goodness of fit to the data set using Gauss-Newton or Marquardt techniques with a maximum average correlation coefficient criterion and a minimum variation restriction (*SAS*, 1984; *Walpole and Myers*, 1993).
The fitted coefficients from each station in turn were used to estimate solar radiation values for each of the other stations for each day over the full span of data available. Correlation coefficients RR between computed and real values and root mean square errors (RMSE) were then calculated using data from twelve month periods. Overall means and standard deviations were calculated using the available twelve month correlations and RMSE values.
Correlation between the daily solar radiation data measured at each site and that measured at each of the other stations together with RMSE values were also computed for all twelve month periods. Averages and error terms were calculated from twelve month period computations.

4. Results

A summary comparison of all methods used to estimate solar radiation were similar to those obtained by *Supit* (1994), *Reddy* (1987) and *Hunt et al.* (1998). Equation which was proposed by *Hunt at al.* (1998) predicted solar radiation with smallest standard deviation and produced highest average RR for all stations, although in some cases nonlinear equations gave higher values with lack of stability. This lack of stability, as well as the greater difficulty that would be encountered when calculating coefficients for this form of equation in comparison to one that is a simple linear function suggests that it would be best to apply linear rather than more sophisticated nonlinear formula.

References

Bristow C.L., Campbell G.S., On the relationship between incoming solar radiation and daily maximum and minimum temperature, *Agric. For. Meteorol.*31, 159-166, 1984.

Cengiz H.S., Gregory J.M., Sebaugh J.L., Solar radiation prediction from other climatic variables, *Trans. ASAE*, 1981,1269-1272, 1981.

Hunt L.A., Kuchar L., Swanton C.J., Estimation of solar radiation for use in crop modelling, *Agric. For. Meteorol.*, 91, 293-300, 1998.

Reddy S.J., The estimation of global solar radiation and evaporation through precipitation; a note, *Solar Energy* 38, 97-104, 1987.

SAS Institute Inc., *SAS/STAT User's Guide*, Release 6.03 Ed., Cary (NC), 1988.

Supit I., EUR - *Global Radiation*, Luxembourg: Office for Official Publication of the European Communities, Agriculture series, Cat. No.: CL-NA-15745-EN-C, p.194, 1994.

Walpole R.E., Myers R.H., *Probability and Statistics for Engineers and Scientists*, Fifth Ed., MacMillan Publ. Comp., NY, 1993.

Experience with climate simulations in the PIDCAP period with the regional model LM of the Deutscher Wetterdienst

Martin Kücken

Potsdam Institute for Climate Impact Research, Telegrafenberg, P.O. Box 601203, D-14412 Potsdam, Germany

1. Introduction

Since the summer of 1998, a parallel version of a non-hydrostatic local grid-point model (LM) of the German Weather Service (DWD) is available and runs on configurations with up to several hundred processors. *Doms et al.* (1997).

The local model LM is used by DWD for weather forecasts over Germany. One version of the LM was implemented on the IBM RS/6000 SP computer system of the Potsdam Institute for Climate Impact Research (PIK).

Our first simulation runs started with the actual forecast area of the DWD in Europe to study the long time behaviour of the model in space and time. In the case of the BALTEX region, experiments are primarily conducted with a 0.5° horizontal resolution with 20 vertical levels for present-day climate conditions. PIDCAP is the Baltex Pilot Study for Intensive Data Collection and Analysis of Precipitation in the Baltex Sea water catchment region, August to November 1995. For the simulation experiments DWD analyses initial and boundary data (August to October 1995) were used.

Furthermore, three-month climate simulations are performed with higher resolutions of 0.25° and 0.125°.

Near-surface parameters were used to validate the long runs carried out to examine the climatology of the model. The validation is based on the verification of model results against accurate operational analyses data.

A multi-variate statistical technique (Cluster Analysis) is used to allow the validation of different model variables in different model runs simultaneously. Detailed studies of the differences help to identify model errors.

The cluster analysis itself was carried out with the meteorological variables 2m dew point temperature and 2m surface temperature. For each grid point, the mean values for seven days and the accompanying variances of these variables were used.

2. Validation Method

Model validation plays an important role in the development of climate models. The validation encompasses a simple visual comparison, the use of generalising measurement figures (e.g. root mean square error - RMSE) and the application of fully developed statistical methods. The latter often require relatively high calculation time so that they are rarely used for evaluation purposes. Nevertheless, the evaluation of complex correlations can only be done with such complex methods. In order to make progress here, a validation method is developed and used which is based on a multivariate pattern recognition and provides measurement figures for quality evaluation that can be easily interpreted and whose spatial distribution and temporal development serves to derive information on possible sources of error, *Gerstengarbe et al.* (1997, 1999).

The question that should be answered by the method is: How well can a model represent defined complex structures of a climate regime?

In a first step, the validation conditions are defined and the selected parameters are grouped in patterns for a reference field at each grid point of a model area via n time steps by means of a cluster analysis algorithm. It has then to be investigated how far the same parameter combination of the simulated field, i.e. the climate model output, reflects these patterns. This is done by a distance measurement which provides information about the assignment of the grid points to the clusters of the reference field. Thus, one receives a yes/no answer: the simulated value either corresponds with the one of the reference field (the grid point belongs to the same cluster as in the reference field) or the same grid points of the reference field and the simulated field belong to different cluster. In order to specify this yes/no answer, each degree of deviation, standardised to 0;1 (0 - no deviation, 1 - largest deviation with a statistical security of 95%) will be determined in addition.

The numerical value zero indicates that the clusters of these grid points are identical, the numerical value one indicates that the grid points are completely different.

However, numerical values in the transition between zero and one serves as a deviation criterion.

Generally, these numerical values can be used as simple indicators for the shift of model outputs compared to the model patterns identified in operational analyses.

The effectiveness of the method is presented by a comparison of the quality of different regional climate simulation runs.

3. Simulation Results

Table 1 shows the location of our simulation area in the BALTEX region.

Table 1: LM Simulation Area

	Latitude North	Longitude East
Lower left grid point	43.8	3.9
Upper right grid point	68.2	52.2

The next tables show the results of our BALTEX simulation runs.

Table 2 gives a summary of the cluster deviation between the analyses data on the one hand and the first LM version (LM1) and the latest LM version (LM2) on the other hand.

In addition, cluster deviations of simulation runs carried out with the regional climate model REMO of the Max-Planck-Institute for Meteorology Hamburg (MPI), *Jacob et al.* (1997) are presented here.

Two REMO simulation runs were investigated: a simulation run with the physical parameterization of the DWD (REMO1), *Majewski* (1991), and a simulation run with the physical parameterization of the MPI (REMO2).

One can now see the numerical values of cluster deviations for the whole model area for a period of 13 weeks.Here, these values were given as area mean values.

Table 2: Area Mean Values of the Cluster Deviation for Different Regional Model Versions

	LM1	LM2	REMO1	REMO2
Deviation	0.21	0.17	0.34	0.36

There are no remarkable differences between the two REMO scenarios. However, the model with DWD physics is identical with the operational weather forecast model of 1990 and great progress can be seen when comparing this model version with the new DWD versions LM1 and LM2.
Especially in the case of mountain barriers or land/see transitions, the models still need some improvement.
The investigation of the model behaviour depending on time is another approach to check the performance of the model. The question if and how long a model is able to simulate a sequence of well-known real meteorological conditions realistically has the same importance as the question if the models show the same persistence characteristics for the modelling area.
Figure 1 shows the time series of the deviation averaged for the entire area for each week for a period of three months for different regional model versions.

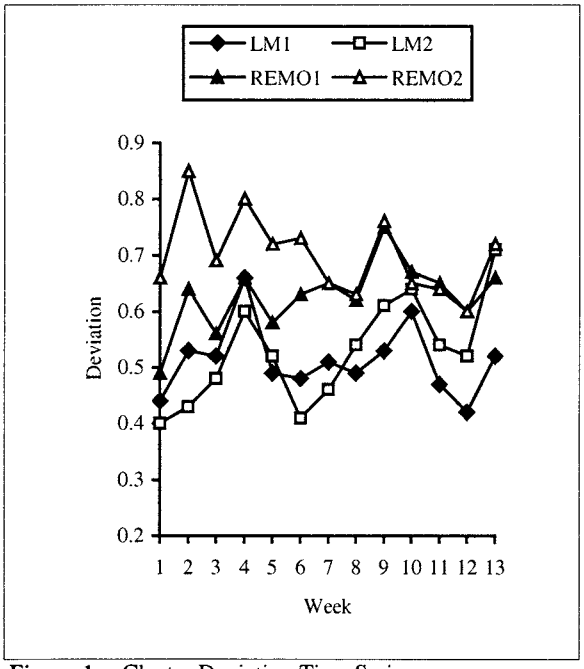

Figure 1: Cluster Deviation Time Series

The analyses data are used as reference field. On the basis of these time series, the temporal dynamics of the individual model can be identified. However, the deviations here are much larger compared to the observations of the entire period with 52 parameters due to the sharper cluster separation which is a consequence of only four existing parameters. At the beginning, the differences between the models are very large but later they are successively getting smaller.
One reason for that could be the increasing influence of the physical parameterization in relation to the model dynamics.
The cluster deviation of the first validation time step is remarkable for all models.
It represents the first seven days of a simulation run that is the range of a weather prediction period. Here, we can also note a quality improvement of the weather prediction models of the DWD. From the climatical point of view, a trend interpretation on the basis of only 13 time series intervals is not useful. The temporal fluctuations of the error that can be observed in all model variants could be caused by different weather conditions.

4. Conclusions

It could be proven that the suggested cluster method is able to evaluate the quality of the spatial and temporal simulation of the climate conditions. The errors remain constant after the calibration period for the investigated model versions, except for some accidental fluctuations. The model result do not "drift off". Differences in the simulations can be easily worked out with the presented method. For a three month prediction period, the new LM of the DWD is able to reproduce the basic weather patterns in space and time. The simulation of the PIDCAP period is a first study case. Long-term simulations for 13 months over Southern America support the results obtained here.

References

Doms, G., Schättler, U., The non-hydrostatic limited-area model LM (Local Model) of DWD – Part I: Scientificdocumentation, Technical Report DWD.

Gerstengarbe, F.-W., Werner, P.C., A Method to Estimate the Statistical Confidence of Cluster Separation, Theor. Appl. Climatolo., 57, 103 – 110, 1997.

Gerstengarbe, F.-W., Werner, P.C., Fraedrich, K., Applying non-hierarchical cluster analysis algorithms to climate classification: Some problems and their solution, Theor.Appl.Climatol., 64, 143-150, 1999.

Jacob, D., Podzun, R., Sensitivity studies with the regional climate model REMO, Meteorology and Atmosphere Physics, 63, 119, 1997.

Majewski, D., The Europa-Modell of the Deutscher Wetterdienst, ECMWF seminar on numerical methods in atmosphere models, Vol. 2, 147 – 191, 1991.

Climate change impacts in the Baltic Sea basin: IPCC TAR perspective

Zbigniew W. Kundzewicz[1,2]

[1] Research Centre of Agricultural and Forest Environment, Polish Academy of Sciences, Bukowska 19, PL- 60-809 Poznan, Poland

[2] Potsdam Institute for Climate Impacts Research (PIK), Telegrafenberg C4, P. O. Box 60 12 03, D-14412 Potsdam, Germany

1. The IPCC Third Assessment Report is there

In May 2001, the Third Assessment Report of the Intergovernmental Panel on Climate Change was published. The volume prepared by the Working Group 2, devoted to impacts, adaptation and vulnerability, consists, among others, of sectorial and regional chapters. Chapter 13, produced by two Coordinating Lead Authors (*Kundzewicz* and *Parry*, 2001), eight Lead Authors, 37 Contributing Authors and two Review Editors, deals with the region of Europe.

2. Disaggregation of the TAR's findings for the Baltic region

An attempt will be made to disaggregate some of the TAR's findings, primarily contained in the European chapter (*Kundzewicz* and *Parry*, 2001), to a sub-region of the Baltic Sea basin. Discussion of climate change impacts within the Baltic region, in the light of the findings of the IPCC TAR is offered, extending to such areas as observed changes in climate, physical and biological systems, and scenarios for the future, water resources, soils, ecosystems, coastal zones, agriculture, forestry, health, insurance, and weather extremes. The European chapter of the IPCC TAR (*Kundzewicz* and *Parry*, 2001) draws extensively from the ACACIA Report of the European Union Project (*Parry*, 2000).

3. Examples of possible climate change impacts in the Baltic region

Studies discussed in (*Kundzewicz* and *Parry*, 2001), deal with observed and projected consequences of regional climate change, in a range of sectors.

Despite the overall warming in the region in the 20th century, in Fennoscandia, cooling in both mean maximum and mean minimum temperature in winter has been observed, but warming in summer. Annual precipitation within the 20th century has increased, particularly in the northern part of the Baltic region, and especially in winter. Changes in timing of the hydrological cycle has been observed and further changes are projected for the future warmer world: delayed river freeze-up and earlier ice break-up, changed flow regimes, high flows coming earlier, shifting from spring towards winter.

Among observed effects in biological systems are: increases in growing season's length, poleward and upward altitudinal range shifts of plants and animals, phenology changes – earlier spring flowering of plants and egg-lying in birds, earlier emergence of insects, earlier arrival and later departure of migratory animals.

Scenario analyses for seasonal (June – July – August and December – January – February) temperature and precipitation in 2020s, 2050s and 2080s, based on a number of GCMs, are presented, following the work of Dr Tim Carter of the Finnish Environmental Institute for the ACACIA Project (*Parry*, 2000).

The Baltic region is likely to experience overall positive agricultural effects, whereas, in some production systems in Central and Eastern Europe, a decrease of productivity can be observed, due to water deficits. Changes in water-limited yield for wheat are likely to be generally positive in the region. The possibility of expansion of grapevine into the Southern part of the Baltic region has been projected.

A significant increase in exposure to coastal flooding is foreseen in the Baltic Coast. By the 2080s, the increase of the number of people experiencing flooding may increase by up to 3000%, and the range of coastal wetland losses can be as high as 84 to 98%. Adaptation costs in the Polish Coast depend largely on the magnitude of the sea-level rise; for a 1 m rise they can be as high as 14.5% of GNP.

Changes in frequency and intensity of extreme events are uncertain. Yet, a number of extreme hydrological events have occurred recently in the region and there are several mechanisms indicating possible increase of the risk in the future.

Occurrence of higher temperatures and more frequent heat waves in Southern Europe may change traditional summer tourist destinations (e. g. the Mediterranean), rendering the Baltic Sea region an even more attractive tourist destination.

4. Adaptive capacity and vulnerability

As in several other regions in mid and high latitudes, a moderate warming can have generally positive aggregate impacts, which can turn negative with a stronger increase in temperature. The regional vulnerability in the Baltic Sea basin is relatively lower than in some other sub-regions of Europe, and in particular, far lower than in the highly vulnerable south. Yet, despite of generally high adaptive capacity, some systems within the sub-region are vulnerable and losses cannot be avoided. For instance, adaptability of biota to a fast climate change is limited, and traditional life style of some societies is in jeopardy.

References:

Kundzewicz, Z. W., M. L. Parry (Coordinating Lead Authors) (2001) Europe. Chapter 13 in: Climate Change 2001. Impacts, adaptation and vulnerability. IPCC WG2 Third Assessment Report, IPCC / Cambridge University Press.

Parry, M. L. (Editor) (2000) Assessment of the Potential Impacts and Adaptations for Climate Change in Europe (ACACIA Report), Jackson Environmental Institute, Norwich, UK.

Dissipation in the Baltic Proper During Winter Stratification

Hans Ulrich Lass[1], Hartmut Prandke[2] and Bengt Liljebladh[3]

[1] IOW, D-18119 Rostock, Germany
[2] ISW, D-17213 Petersdorf, Germany
[3] University of Gothenburg, S-40530 Gothenburg, Sweden

1. Introduction

The dynamics of mixing in the ocean surface boundary layer and in the stratified water column below the mixed layer remains one of the unsolved problems in physical oceanography. The lack of generally valid parameterisations of turbulence and mixing in the ocean implies, for instance, that long-term model simulations of the state of the ocean cannot be trusted. Growing evidence suggests that turbulence in the ocean surface boundary layer are governed by breaking surface waves and vertical motion associated with the gravity wave motion, see e.g. Anis and Moum (1995), and turbulence below the surface mixed layer occur in intermittent patches due to pelagic and benthic disintegration of internal waves that are sub-grid phenomena in most models. The general view has been that the interaction of internal waves supplies the energy for turbulence in the interior of the ocean. This can be quantified in different ways depending on the assumptions made about the wave field and about the nature of the interaction.

The DIAMIX experiments aims at describing the physics behind wind-driven diapycnal mixing below the well mixed surface layer. The Baltic was chosen as study area because of its lack of tides, which should simplify the study of purely wind-driven diapycnal mixing. The experiment is a cooperative undertaking between researchers from institutions in countries surrounding the Baltic Sea. The joined efforts are motivated to cover the temporal and spatial scales associated with the energy cascade from subinertial processes towards internal waves and finally the dissipation of turbulent kinetic energy at scales down to the Kolmogoroff length scale. The chosen 30 by 30 nautical miles survey area is located east of Gotland, see **Figure 1**.

2. Methods and Data

During the Diamix99 cruise vertical profiles of dissipation were made with the MSS profiler. This instrument provides simultaneous microscale temperature and dissipation, as well fine scale temperature and salinity. With respect to the intermittence of marine turbulence, the velocity shear measurements have been made as time series at one position 57° 3.00'N, 19° 11.50'E, see **Figure 1**, in a burst sampling mode. Every hour a burst of 3 profiles was taken from the aft deck of R/V Aranda. The ship was on drift during the dissipation measurements while the main engine and the thrusters were switched off.

The current data come from mooring M1, see **Figure 1**, with two upward looking 300 kHz ADCP mounted near the bottom at 150 m depth and in 70 m depth. The lower ADCP range overlaps the range of the upper one by some bins. This overlapping was used to align the instruments to each other. Due to the generally unfavorable backscatter conditions of the seawater in the Baltic during the winter season, the noise level of the data is higher than usual. This noise was suppressed by forward and backward low pass filtering of the current measurements with a 2nd order Butterworth filter with a cut off period of 5 hours.

Continuous surface meteorological measurements have been performed on board of R/V Aranda.

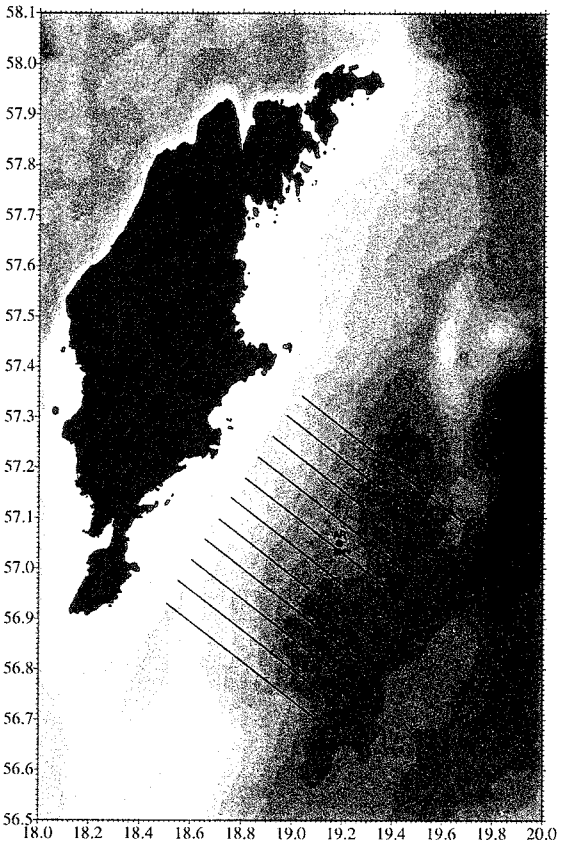

Figure 1: Positions of the dissipation time series measurements on board R/V Aranda (AR) and of the moored ADCP measurements at M1. Towed CTD measurements have been performed along tracks indicated by solid lines.

3. Results

The time series of dissipation is shown in **Figure 2** together with density (sigma-t). High dissipation rates of the order of 10^{-5} W/kg are observed in the upper mixed layer decreasing rapidly with depth to a minimum of the order of 10^{-8} W/kg located approximately at 50 m depth. A secondary maximum of the dissipation rate of approximately 10^{-7} W/kg is located within the halocline.. Below the halocline the dissipation rate is gradually decreasing with depth to about 10^{-9} W/kg at 100 m depth. The downward extension of high dissipation rates in the upper mixed layer is bounded by the varying depths of a weak pycnocline within this layer.

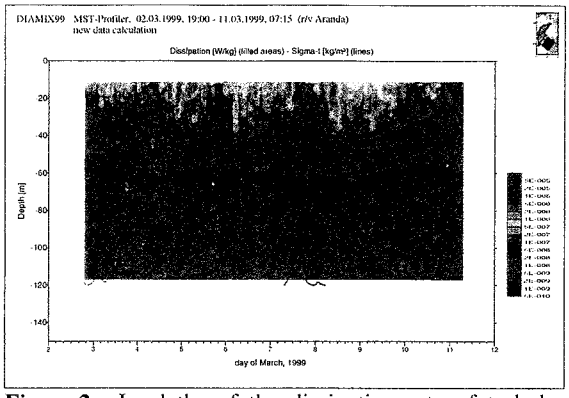

Figure 2: Isopleths of the dissipation rate of turbulent kinetic energy (color code) and density (contour lines), measured from R/V Aranda.

In contrast to dissipation measurements in lakes and calm oceans dissipation in the surface layer scaled not according to the wall layer turbulence but it rather decayed downward as $\varepsilon(z) \propto \exp(kz)$ (k wave number of the surface waves) according to Anis and Moum (1995). The measured dissipated turbulent kinetic energy of the surface layer did not exceed the estimated energy loss by breaking surface waves. These findings support the view that enhanced turbulent kinetic energy is injected by breaking surface waves into the upper few meters and transported downward by fluctuations of the vertical velocity component of the irrotational wave field while dissipation locally balances the divergence of downward transport of kinetic turbulent energy.

Dissipation below the surface layer affected by wind waves turned out to be rather independent from the local wind. This suggests to relate dissipation and internal wave properties, averaged over the whole observation period of about 10 days. The frequencies of the internal waves observed during the DIAMIX99 experiment were all very close to f, the inertial frequency. According to Gargett and Holloway (1984) this suggests the approach $\varepsilon \propto N$ below the surface layer of the Baltic Sea, which was used by Stigebrandt (1987) as well. Since the constant of proportionality has the unit of energy, the approach

$$\varepsilon = \alpha(E_{kin} + E_{pot})N$$

was used, where Ekin and Epot are the averaged profiles of the kinetic and the potential energy of the internal wave field.

Both the amplitude and the eigenfuntion of the first EOF of the horizontal current with periods less than 20 h reflect all the properties of the inertial oscillation. Its contribution to the current field at M1 was subtracted and the averaged profile of kinetic energy was estimated from the remaining current, assumed to represent the internal waves. The potential energy was estimated from the time series of the density profiles measured by the dissipation profiler MSS from R/V Aranda. The parameterisation of the dissipation due to breaking internal waves is shown in **Figure 3** together with the averaged profile of the measured dissipation. The agreement between both below the upper rim of the halocline is quite satisfactory assuming $\alpha=1\times10^{-3}$. That means that about one permille of the internal wave energy is lost per period determined by the local BVF.

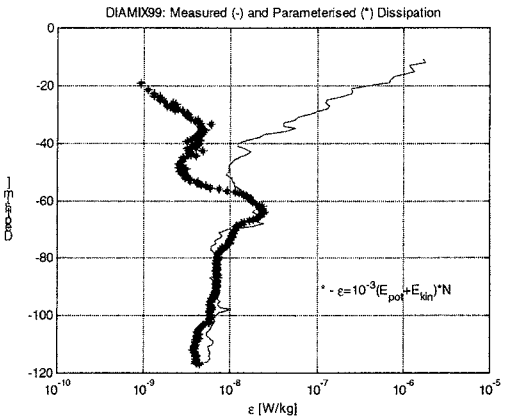

Figure 3: Averaged profiles of measured (full line) and parameterised (*) dissipation during DIAMIX 1999.

The coefficient of diapycnal mixing calculated according to Osborn (1980)

$$K_v = \chi \frac{\varepsilon}{N^2}$$

with χ = 0.2 agree with coefficients estimated by the salt budget method in the Gotland Basin by Matthäus (1990) and Axell (1998).

References

Anis, A. and J. N. Moum, 1995: Surface Wave–Turbulence Interactions: Scaling ε(z) near the Sea Surface. J. Phys. Oceanogr. 25, 9, 2025-2045

Axell, L. B., 1998: On the variability Baltic of Baltic Sea deepwater mixing. J. Geophys. Res. Vol. 103, C10, pp. 21 667-21 682

Gargett, A. E., and G. Holloway (1984): Dissipation and diffusion by internal wave breaking. J. Mar. Res., 42, 15-27

Matthäus, W., 1990: Mixing across the primary Baltic halocline. Beitr. Meereskd., Berlin, 61, 21-31.

Stigebrandt, A., 1987: A model for the vertical circulation of the Baltic Deep Water. J. Phys. Oceanogr., 17, 1772-1785

Baltic Air-Sea-Ice Study (BALTEX- BASIS)

J. Launiainen[1], T. Vihma[1], B. Brümmer[2], D. Etling[3], B. Håkansson[4], A. Omstedt[4], A-S. Smedman[5], and K. Shirasawa[6]

[1] Finnish Institute of Marine Res., POB 33, 00931 Helsinki, Finland
[2] Universität Hamburg, Meteorol. Institut, Bundesstr. 55, D-20146 Hamburg, Germany
[3] Inst. fur Meteor., Univ. Hannover, Herrenhäusstr.2, 30419 Hannover, Germany
[4] Swedish Meteorol. and Hydrol. Institute, 60176 Norrköping, Sweden
[5] Dept. of Meteorology, University of Uppsala, Box 515, S-75120 Uppsala, Sweden
[6] Sea Ice Research Laboratory, Hokkaido University, Mombetsu, Hokkaido 094-0013, Japan

1. Introduction

The Baltic Air-Sea-Ice Study (BASIS) is a process study and process modelling project of BALTEX. The overall objective of the study carried out in 1997-2000 was to create and analyse an experimental data set for verification and optimization of coupled atmosphere-ice-ocean models.

By acting as a thermal insulator and a mechanical cover, the sea ice influences the sea-atmosphere interaction in a dramatic way. Sea ice also has a large climatic importance as a sensitive indicator of a climatic change, and can act as a feedback mechanism for the change. As to the winter navigation, sea ice is of first-rate importance to various Baltic Sea countries. Mathematical modelling is vital for understanding air-ice interaction and weather and predicting the processes affecting the climate and winter navigation, but the models also need verification and optimization by observations. The specific objectives cover investigations of atmospheric boundary layer (ABL), momentum and thermal interaction at the air-ice-sea interfaces, sea ice and its dynamics, the ocean boundary layer (OBL), and the ocean water and heat budget.

2. Experiment

The field campaign in February-March, 1998, formed the central experimental element. Observations were centered in the boundary zone between the open and ice-covered sea in the northern Baltic Sea (Figure 1). The aim was to gather meteorological, sea ice and hydrographic data to quantify the physical processes of energy and mass transfer between the atmosphere, sea ice, and the sea. An ice going *R/V Aranda* served as the central basis and platform in the sea. Airborne measurements were made by both a research aircraft and a helicopter. Several surface meteorological stations and buoys were used. The observations covered atmospheric turbulence, radiation, and clouds. Radiosonde soundings were made at five stations at the coasts of the Gulf of Bothnia. The sea ice was investigated by remote sensing, drifting buoys and surface-based measurements. The ocean boundary layer was studied by various equipment and the ocean boundary layer turbulence was investigated by measuring eddy fluxes below the ice. The experiment and the data are introduced in the BASIS Data Report (Int. BALTEX Secretariat, Publ. No. 14; see Launiainen, 1999).

3. Scientific results

The data-analyses in BASIS concentrated into three main branches: (1) the atmospheric boundary layer, (2) the ice and surface properties and, (3) the ocean boundary layer. Process oriented modelling was made applying the field data as a reference. A compilation of scientific results are presented in the report BALTEX -BASIS, Final Report (Int. BALTEX Secretariat, Publ. No. ; see Launiainen and Vihma, 2001). Various other reports are published or under preparation. Here we summarise the most essential results.

The analyses of atmospheric surface-layer turbulence indicated that the normalized standard deviations of the wind components increased during strong stability, and showed that the wall effect is important for the turbulence structure in the stable surface layer. The analyses of the stable boundary-layer depth agreed with new theoretical predictions.

Profile and turbulence measurements on the sea ice confirmed the validity of the Monin-Obukhov similarity theory, and suggested to a new formula for the ratio of local roughness lengths for momentum and heat. The ratio depends on the local roughness Reynolds number. The analyses further yielded a new formula for the flux-profile relationships in stable stratification. Different methods to determine the ice surface temperature, based on radiation, turbulence and profile measurements, were compared, and the results demonstrated the applicability of a thermodynamic ice model in estimating the surface temperature. The model was also fairly accurate in reproducing the development of the ice and snow temperature profile in conditions of varying weather.

The airborne, land-based, and ice-based observations of the turbulent and radiative fluxes in the atmospheric surface layer showed a good agreement. The study revealed significant spatial and temporal variations in the surface fluxes, which depended on the large-scale weather conditions and on the state of the surface, i.e. open water, compact land-fast sea ice, or broken sea ice. Spatial variability of the aircraft data showed that area-representative fluxes for the whole ice edge zone cannot be derived from land-fast ice stations only.

The aircraft data were applied in parameterizing the turbulent surface fluxes over a broken ice cover. The analyses revealed that in order to get realistic area-averaged fluxes, the roughness lengths for heat and moisture must be 3 to 4 orders of magnitude smaller than the roughness length for momentum. The results based on observation heights of about 30 m are applicable for regional models (e.g. HIRLAM and REMO), because in conditions of stable stratification the lowest model level may often lie above the constant-flux layer, and the flux-divergence should be taken into account as reduced roughness lengths.

The BASIS observations of the ABL were compared with the analyses and 24-h forecasts of the regional model HIRLAM. The rawinsonde sounding data demonstrated that the differences were largest during passages of cold and warm fronts. The differences were largest near the

surface, and the vertical gradients of air temperature and wind speed were smaller in HIRLAM than in the observations. The comparisons based on aircraft observations indicated individual cases in which the surface temperature, wind speed and direction were strongly biased and the latent heat flux was unrealistically large in HIRLAM. In HIRLAM, particularly in the 24-h forecasts, the low-level jets (LLJs) were less common than in the observations. This may have resulted from a boundary-layer parameterization producing too much mixing. A mesoscale modelling study supported this conclusion.

Most of the analyses of the ABL were related to a stable or near-neutral boundary layer. A convective boundary layer was addressed in detail in two cases. In one case, the warm sea surface generated an ice-breeze, a mesoscale circulation resembling the classical land-breeze. The ice-breeze was also reproduced by a numerical model. In the second case a cold-air outbreak from the sea ice to the open sea was documented by an aircraft flight mission and studied by applying two models. In the mesoscale modelling, it was important to take into account the leads among the sea ice, the counter-gradient transport of heat, a forest in an archipelago crossed by the air flow, and the water vapour condensation into ice crystals. In the large-eddy model simulation of the case, the convection was mostly resolved by the model grid.

The analyses of the ice and surface properties concentrated on ice motion, ice and open ocean remote sensing, and snow influence in the ice thickness. The remote sensing and ice drifter data gathered demonstrated how useful a combined data set can be. It provides information on ice kinematics, ice leads and ice concentrations, which are of a great value for coupled air-ice-sea model verification. The ice drifter data show the typical velocity variance found in semi-enclosed basins with seasonal ice cover, whereas the radar image data show closing and opening of leads and where ice deformation takes place.

The study of the wind forcing on the ice drift showed that in the centre of the Gulf of Bothnia the ice drift was highly wind-dependent, and a linear relationship between the wind and drift velocities explained 80% of the drift's variance. Close to the coast, internal ice stresses were important, and the modelling of the ice motion was only successful by using a high-resolution (5 km) model with a realistic ice rheology. In general, an improvement in the model results brought by using an accurate wind stress, depending on the thermal stratification and ice conditions, was comparable to that achieved by raising the grid resolution from 18 to 5 km.

An algorithm for determining sea ice concentration from Radarsat SAR was developed. The algorithm is based on local thresholds, which are partly manually extracted. The algorithm resolves the ice concentration with a resolution of 50 metres, and yielded good results for cases over the Gulf of Bothnia during the BASIS experiment.

The water and heat cycles of the Bothnian Bay were examined on the basis of observations and by using the model PROBE-Baltic. Observed and numerically simulated data from an 18-year period (1981-1998) were analyzed. The results can be summarized as follows. (1) The calculated long-term salinity and temperature structure are stable and in good agreement with observations. (2) The calculated ice concentration and thickness during the BASIS period were quite close to observations. (3) The Bothnian Bay water body heat balance during the BASIS period showed high temporal variation and with major contributions from the sensible heat flux, the latent heat flux and the net long wave radiation from the open water surface. (4) During the BASIS period the solar radiation as well as the heat flow from water to ice cannot be neglected in the heat balance. (5) From the heat balance calculations it was concluded that on long term mean the Bothnian Bay import heat from the Bothnian Sea.

The eddy-flux measurements below the ice revealed interesting features. The momentum flux at the depth of 5 m from the ice bottom was ten times larger than at the depth of 0.5 m, and the heat flux from the water to the ice was very small. Both the findings indicated an existence of a shallow very stable boundary layer just below the ice. This is likely to be related to inflow of river water into the sea below the sea ice. The small water-ice heat flux differs from the basin-scale observations reported above, and demonstrates that spatial differences may be large not only in the ABL but also in the ocean boundary layer.

The BALTEX-BASIS study was financially supported by MAS3-CT97-0117 of the EC.

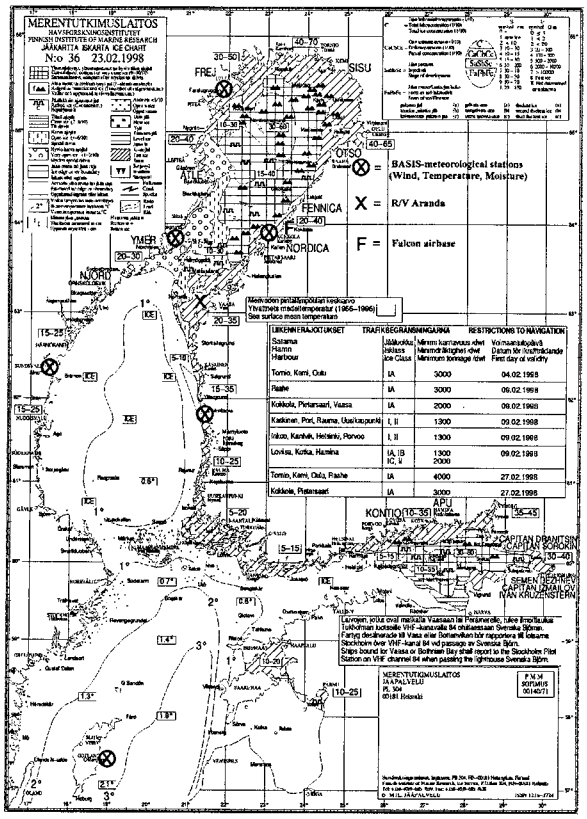

Figure 1: Figure 1. BASIS research area and the sea ice conditions in the northern Baltic Sea. BASIS observation sites marked on a routine sea ice chart of 23 February 1998 (FIMR).

References

Launiainen, Jouko (ed.), BALTEX - BASIS Data Report 1998, *International BALTEX Secretariat Publication,* No. 14, 94 p., 1999.

Launiainen, J., and Vihma, T. (Eds.), BALTEX-BASIS (Baltic Air-Sea-Ice Study), Final Report, *Internat BALTEX Secretariat Publ. No.19* , 2001.

Determination of the Local Turbulent Air-Ice Fluxes in BASIS

Jouko Launiainen, Cheng Bin and Timo Vihma

Finnish Institute of Marine Research, P.O. Box 33, SF-00931, Helsinki Finland

1. Introduction

Accurate determination of the turbulent fluxes and air-ice-ocean coupling and modelling were important goals of the BALTEX-BASIS (Launiainen and Vihma, 2001). In the air-ice coupling, the primary quantities to be studied include the fluxes of momentum, heat and water vapour (latent heat), the radiative fluxes, and the air-ice interfacial (surface) temperature. In this report, determination of turbulent air-ice fluxes and parameterization of air-ice coupling is considered. In more detail, the study has been reported in Launiainen et al. (2001) and Launiainen (2001).

2. Observations and Methods

At the *RV Aranda* Ice Station during BASIS, momentum and sensible heat surface fluxes were measured as eddy-fluxes by a sonic anemometer. Wind and air temperature profile measurements were gathered on a 10 m high profile mast on the sea ice.

From the sonic data the turbulent fluxes of momentum and sensible heat were defined directly as covariances. For comparison, the profile mast measurements allowed us to calculate the momentum and heat flux from profile gradients using the Monin-Obukhov (M-O) similarity theory. The results of the two methods above allow us further to calculate the transfer coefficients of the ordinary bulk aerodynamic formulae, using the similarity theory based flux-profile relationships.

The latent heat was estimated by the bulk aerodynamic method, with the aid of a single-level moisture observation and the surface temperature estimate (yielding the surface saturation humidity) derived from the relationship of the heat flux and temperature profile.

As the third method to determine the turbulent surface fluxes, the one-dimensional multi-layer thermodynamic ice model (Launiainen and Cheng, 1998) was used. In the model, air and snow/ice are coupled by the fluxes and the interface temperature at each time step. For a bulk calculation of the fluxes and the modelled surface temperature, separate single-level meteorological input data were used.

3. Results

Fluxes, drag coefficient

The turbulent fluxes of momentum and sensible heat derived from the sonic anemometer and the profile gradients (level-difference method, LDM) agreed mutually notably well. This methodological good concordance can be realized from Figures 1 and 2. Figure 1 gives the time series of the neutral drag coefficient, known as $C_{DN} = k^2/(\ln z/z_0)^2$ derived from the sonic and LDM method. The results are rather comparable. In Figure 2 is given the time series of the stability parameter, and the both methods yield almost identical results. The consistent stability results, given in terms of z/L, where L is the Obukhov length including the fluxes in the definition, reveal the agreement of the flux results. As to the drag coefficient, neither method showed apparent wind speed dependence. The mean $C_{DN}(10) = 1.28 \times 10^{-3}$ corresponds to a mean aerodynamic roughness length $z_0 = 1.2 \times 10^{-4}$ m. On the contrary, the drag coefficient was distinctly dependent on the wind direction (Figure 3). This was because the upwind roughness of the sea ice varied with the direction, and because the measurement site was located in an archipelago. Our results read $C_{DN}(10) = 1.0$ x 10^{-3} (i.e. aerodynamic roughness $z_0 \cong 3$ x 10^{-5}m) for smooth snow-covered ice, and 1.5 x 10^{-3} ($z_0 \cong 3$ x 10^{-4} m) for deformed ice. By deformed ice we here mean thin Baltic Sea coastal ice of 100% concentration including no ridges and roughness elements higher than 0.3 to 0.6 m. The flux and profile gradient methods agree mutually well even for the dependence of the drag coefficient on wind direction,. As to the third flux determination method, the fluxes (and surface temperature) estimated by the ice model compared well with those derived from the two other methods.

Temperature roughness length, heat transfer coefficient

The measured sensible heat flux, as well as that calculated by the gradient method, allowed us to study the temperature roughness length (z_T) and bulk heat transfer coefficient $C_{HN} = k^2/(\ln z/z_0)(\ln z/z_T)$, calculated from the flux-profile relationships. Unlike the aerodynamic roughness length (z_0) and the drag coefficient (C_{DN}), the z_T results indicated no distinct dependency on the wind direction but on the wind speed. The results indicated z_T to be slightly larger than z_0 for low wind velocities but $z_T < z_0$ for winds higher than 4 - 5 ms^{-1}. As linearized for practical use, our results of z_0/z_T ratio yield

$$\ln(z_0/z_T) = s + a\,V$$

$$C_{HN} = kC_{DN}^{1/2}(\ln z/z_T)^{-1} \cong C_{DN}(1 + C_{DN}^{1/2}k^{-1}(s + aV))^{-1}$$

where s = - 0.80 and $a = 0.15$ for wind speed at a height of 2 m. For a wind referred to 10 m, $a = 0.13$.

For a site with C_{DN} or z_0 known or estimated, the above should give a reasonable estimate of z_T and C_{HN}. The range of our z_0 observations in the analysis was limited from 3×10^{-5} to 9×10^{-4} m, i.e. $C_{DN}(10)$ was from 1.0×10^{-3} to 1.9×10^{-3} and wind speeds from 3 to 17 ms^{-1}. In fact, the z_T and C_{HN} were investigated with respect to a more universal parameter of a roughness Reynolds number ($Re = (z_0 \cdot u_*)\nu^{-1}$) and a comparison indicated our simple formula to agree with the semi-empirical theory by Andreas (1987), within ±5% in the region of conditions of ours.

Universal functions

The universal functions tested for the determination of turbulent fluxes and transfer coefficients by the LDM method and by the ice model yielded results of reasonable agreement with those measured by the sonic anemometer. Strictly however, a detailed analysis of the diabatic eddy-flux-based transfer coefficients with the observed fluxes and the *M-O* similarity theory-based flux-profile relationships suggests the current universal functions for the stable region to suppress the turbulence and transfer coefficients too much. This is to bee seen in Figure 4. For

stability up to $10/L$ = 0.5, the well-known universal functions of Webb (1970) and Holtslag and De Bruin (1988) yield 10 to 12 % lower bulk transfer coefficients than those defined from our data. For $10/L$ = 1 the above difference was 15 to 17 %. Actually, for less stable region up to $10/L$ the both mentioned formulae yield comparable results i.e. $\Psi_M \cong \Psi_H \cong -5z/L$. For a strong stability, our data suggests Ψ_M = -3.5z/L and stability thus to suppress turbulence and the bulk transfer coefficients less than estimated by the above-mentioned universal functions .(Note: Figure 4 is given in terms of $2/L$).

4. Conclusion

The agreement of the gradient-method and coupled air-ice model results with respect to the eddy-flux results supports the validity of the Monin-Obukhov similarity theory. Accordingly, the investigations provided us tools to estimate the local surface fluxes and (skin) surface temperature accurately. New insight of the aerodyamic and temperature roughness lengths, i.e. of the drag coefficient and bulk heat transfer coefficient, were obtained. Finally, for a strong stability our data suggest stability to suppress turbulence and the bulk transfer coefficients less than estimated by the most commonly used universal functions.

References

Andreas, E.L., A theory for the scalar roughness and the scalar transfer coefficient over snow and sea ice. *Boundary-Layer Meteorol.*, **38**, 159-184, 1987.

Launiainen, J., and Vihma, T. (Eds.), BALTEX-BASI (Baltic Air-Sea-Ice Study), Final Report, *International BALTEX Secreteriat Publication,* No. , 2001, (in press).

Launiainen, J., B. Cheng. J. Uotila, and T. Vihma, Turbulent surface fluxes and air-ice coupling in the Baltic-Air-Sea-Ice-Study (BASIS). *Ann. Glaciol.*, **33**, 2001 (in press).

Launiainen, J.,Turbulent fluxes and air-ice coupling in the Baltic Air-Sea-Ice Study, 6th Conference of Polar Meteorology and Oceanography, 14-18 May, 2001, American Meteorological Society, (in press).

Webb, E. K., Profile relationships: the log-linear range and extension to strong stability, *Quart. J. Roy. Meteor. Soc.*, **96**, 67-90, 1970.

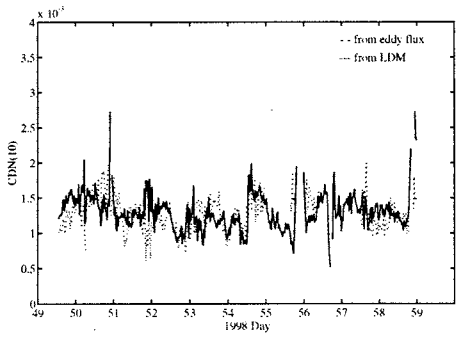

Figure 1: Neutral drag coefficient $C_{DN}(10)$ time series as determined from the eddy flux (dotted) and profile-gradient (continuous line) method during BASIS.

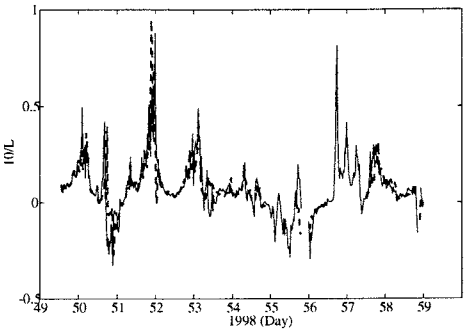

Figure 2: Time series of the stability parameter $10/L$ as calculated from the eddy flux results (broken) and profile gradient method (continuous).

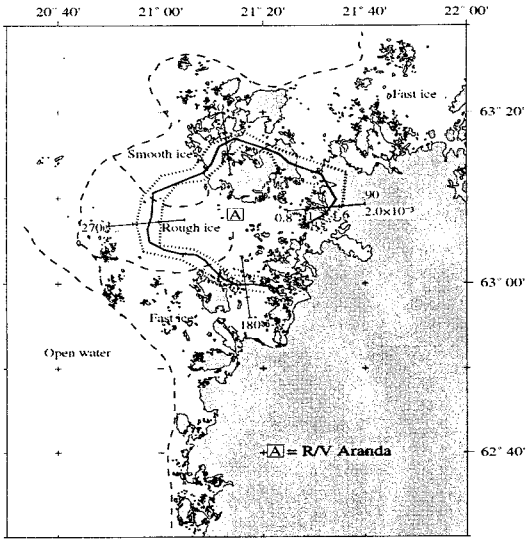

Figure 3: "Aranda" Ice Station area in the northern Baltic Sea during BASIS-98. RV Aranda and eddy flux (Sonic anem.) and profile mast located in point "A". The continuos and dotted curves in the directional plot give the mean and error limit of C_{DN} *(10)*.

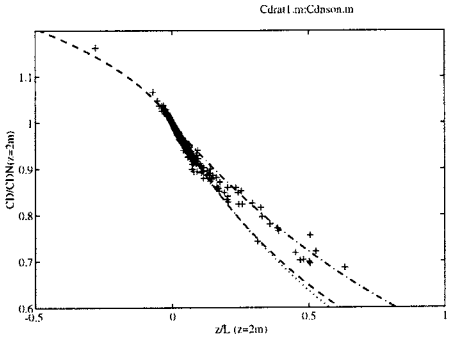

Figure 4: Observed stability dependency of the drag coefficient (crosses; sonic measurements) compared with the estimations calculated by the universal functions of Webb (1970; dotted) and Holtslag and De Bruin (1988; broken). The dash-dot line corresponds to Ψ_M = -3.5 z/L.

Northern Atlantic Forcing Reflections to Sea Ice and Hydrological Conditions in the Northern Seas

Jouko Launiainen, Ari Seinä, Milla Johansson and Pekka Alenius

Finnish Institute of Marine Research, P.O. Box 33, SF-00931, Helsinki Finland

1. Introduction

Understanding and prediction of variations and change in the nature has brought us a profound need to investigate the regional to hemispheric atmospheric and ocean forcing, in order both to find causalities and define processes related. In the northern hemisphere this has been done in terms of NAO and AO forcing. The former (North Atlantic Oscillation Index) is a south-to-north index (of surface pressure difference, most freguently) to be determined from point observations directly. In fact, NAO may be found as a discrete paradigm (Wallace, 2000) of the Arctic Oscillation (AO). The Arctic Oscillation (Thompson and Wallace, 1998) is the first mode of the spatial and temporal global polar pressure field, defined from observations by EOF (empirical orthogonal function) analysis. The forcing index, NAO especially, have been used in studies in the red-hot Third Assessment Report of IPCC (IPCC TAR), to relate the observed hemispheric and regional climate variations to the atmospheric forcing. The both forcing modes exert a strong control on the climate in the northern hemisphere, especially in winter. Generally, a positive phase of AO/NAO result in stronger-than-average (warm) winds from west. The forcing indexes may serve as effective tools in investigation of the long-term variations of climate and climate change. In addition to serve as an obsevational and causal tool, the NAO and AO index estimation are likely to play a central role of verification of the coupled Atmosphere-ocean-land-cryosphere models, which form us the most importat tool in prediction of the climate change.

At FIMR, a study is carried out to study sea ice and hydrographic-hydrological variations related to large scale atmospheric forcing. Results are outlined below. The forcing index used in the examples are of Thompson and Wallace (2000) for AO (updated from http://jisao.washington.edu/data/annularmodes/Data/), and Hurrerll (1995) and Jones et al. (1997) for NAO (updated from www.cru.uea.ac.uk/cru/data/).

2. Results

Variations of sea ice conditions, e.g. the maximum annual sea ice extent and the seasonal ice cover duration in the Baltic Sea was found to be distincly correlated with the NAO/AO. In Figure 1 is given the time serie of the Baltic Sea annual maximum ice cover and the winter-time NAO (December through March). For mutual comparison, the time series are given as normalized anomalies by the mean (mean) and standard deviation (sd), defined as $na(x) = (x - mean(x)) / sd(x)$.

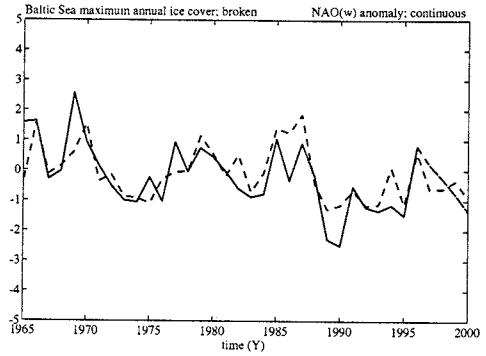

Figure 1: Variation of the maximum seasonal sea ice cover in the Baltic Sea (broken) and the variations of the winter-time NAO in 1965-2000. A vertical unit corresponds to a change in the sea ice coverage of 98 000 km^2. The sea ice data from FIMR. (NAO index given as negative compared to the usual notation.)

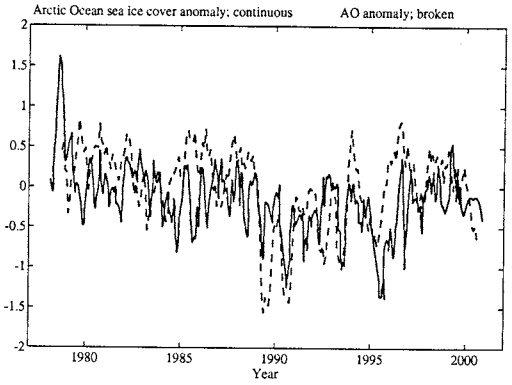

Figure 2: Anomaly of the Arctic sea ice cover (continuous) and AO (broken) in 1978-2000. Monthly AO given as 7 months floating averages. Sea ice data reprocessed from WMO-920 (based on Hadley Centre, The Met. Office; SSMI data HadSST1).

In Figure 2 is given the Arctic Sea Ice anomaly in 1978-2000 with respect to the AO anomaly. The owerall behaviour and most of the peaks in the curves compare well. Additionally, as an interesting characteristics we may see that since 1995, in late 1990s during the warmest years of the global and northern hemisphere temperatures ever recorded, the decline of the Arctic sea ice did not continue but the anomaly merely disappeared towards the end of the decade. The last data from 2000, however, suggest the decline to continue again.

Wang and Ikeda (2000) studied from the historical long-period data the surface air temperature (SAT) and Arctic Sea-Ice Oscillation (ASIO), and found the AO associated ASIO to explane 41 % for the total variance in 1901-1995.

In the long term, the fresh water run-off to the Baltic Sea follows a general similar behavoiur to NAO, allthough e.g. annual peaks are often not too correlated (Figure 3a). Over longer periods, say longer than 7 to 8 years (based on an inspection of frequency band energy content), a similar course is well evident (Figure 3b). In interpretation of run-off versus AO/NAO behaviour we sould note that physically there is no reason to except any dominant causal relation between the forcing and run-off, directly. Additionally, no significant or universal time lag was found between the run-off and AO/NAO. An another study (Launiainen et al. 2001) indicated north Russian rivers, especially Jenisei river, in longer time scales (> 5 y), to reveal a similar trend to AO/NAO.

a)

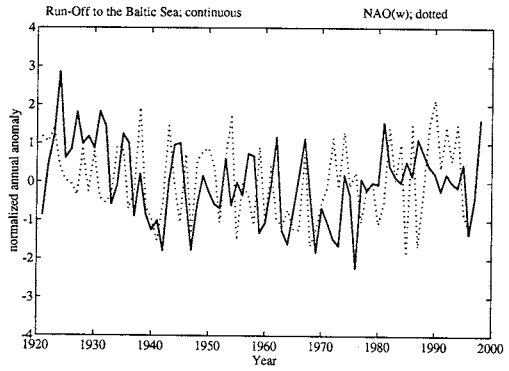

b)

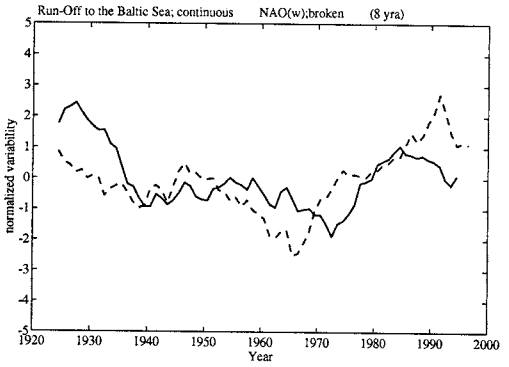

Figure 3: Time serie of the normalized variations of the total fresh water Run-Off to the Baltic Sea (continuous) and of NAO (broken). Annual values given in a and time serie of 8 year floating means in b. Run-Off data (multi-source) from the BALTEX-Hydrological Data Bank (SMHI, Norrköping, Sweden).

In a former study at FIMR, the Baltic sea level variations were found to be related (in positive correlation) to NAO (Johansson et al. 2001).

3. Conclusion

Referring to the above, we may believe that forcing index as AO and NAO are in a causal way related to various physical processes and conditions in the nature. As the conclusion, or rather, as a deduction of practical importance, we may believe that investigation and especially prediction of the atmospheric forcing measures/index offers us a tool for causal studies, model verification, and prediction of the future changes in the hemispheric and regional climate. Unfortunately, the current coupled models cannot yet predict AO/NAO for climate prediction and scenarios quantitatively.

References

Hurrell, J.W., Decadal trends in the North Atlantic Oscillation and relationships to regional temperature and precipitation. *Science*, **269**, 676-679, 1995.

Johansson, M., Boman, H., Kahma, K., and J. Launiainen, Trends in sea level variations in the Baltic Sea, Borealis Environment. 2001 (in press).

Jones, P. D., Jonsson, T., and D.Wheeler, Extension to the North Atlantic Oscillation using early instrumental pressure observations from Gibraltar and South-West Iceland. *Int. J. Climatol.*, **17**, 1433-1450.

Launiainen, J., Johansson, M., Seinä, A., and J. Bareis, Reflections of the Northern Atlantic and Arctic forcing on sea ice and hydrographic conditions in the northern seas. *International Symposium on Climate Change and Variability in the Northern Europe*, 5-6 June, 2001, Turku, Finland (manuscript).

Thompson, D. W. J., and J. .M. Wallace, The Arctic Oscillation signature in the wintertime geopotential height and temperature fields. *Geophys. Res. Lett.*, **25**, No. 9, 1297-1300, 1998.

Thompson, D.W. J., and J. M. Wallace, Annular modes of the extratropical circulation. Part I: Month-to-month variability. *J. Climate*, **13**, 1000-1016, 2000.

Wallace, J.M., North Atlantic Oscillation/annular Mode: Two Paradigms - one phenomenon. *Quart. J. Roy. Meteor. Soc.*, **126**, 791-805, 2000.

Wang, J., and M. Ikeda, Arctic Oscillation and Arctic Sea Ice Oscillation. *Geophys. Res. Lett.*, **27**, No. 9, 1287-1290, 2000.

WMO-920. WMO Statement on The Status of The Global Climate in 2000, WMO, March 2001. 11p.

On the water, heat, salt and sea ice cyle of the Baltic Sea

Andreas Lehmann, Wolfgang Krauss and Hans-Harald Hinrichsen

Institute of Marine Research, Duesternbrooker Weg 20, D-24105 Kiel Germany

1. Introduction

The closing of the water and energy cycle of the Baltic Sea is one of the central aims of Baltex. On the long-term mean the water budget of the Baltic Sea is determined by river runoff, net precipitation (precipitation minus evaporation) and the in- and outflows through the Baltic Sea entrance area (Stigebrandt, 1995), assuming that the mean sea level remains constant, i.e. the ability of the Baltic Sea to store a huge amount of water will be averaged out over the long-term period. For shorter periods (monthly to interannual timescale), the water storage which can be expressed by the variations of the mean sea level plays in important role in budget studies of both the energy and water cycle. On the interannual time scale, the storage can be as high as 100 km^3 (Jacobsen, 1980; Lehmann and Hinrichsen, 2001). Storage variations affect not only the water balance, they also change the heat content of the Baltic Sea. However, on the long-term mean, storage variations will average out and thus the effect on the energy and water budget will become small.

2. Water and energy budget

From a 14-years coupled sea ice-ocean numerical simulation the energy and water budget of the Baltic Sea and the exchange of heat, salt and water with the North Sea as well as within the subbasins of the Baltic Sea has been determined. The sea ice-ocean model is based on a primitive equation ocean model coupled with a dynamic-thermodynamic sea ice model (Lehmann and Hinrichsen, 2000). The coupled model has a horizontal resolution of about 5 km and 41/60 levels in the vertical. The atmospheric forcing has been provided by the SMHI (Swedish Meteorological and Hydrological Institute, Norrkoeping, Sweden) meteorological data base including geostrophic wind, surface pressure, 2-m air temperature, 2-m relative humidity, cloudiness and precipitation, and the river runoff has been taken from a monthly mean runoff data base (Bergstroem and Carlsson, 1994), also compiled by the SMHI. Estimates of the heat exchange with the atmosphere and the water budget determined by precipitation minus evaporation and river runoff and in- and outflows through the entrance area will be given. Results of the analysis of the heat, salt and water cycle will be compared with previously published estimates. The question, whether the Baltic Sea behaves thermodynamically as lake (Omstedt and Rutgersson, 2000) will be addressed. From numerical model simulations it turned out that on average the Baltic Sea exports heat to the North Sea due to the fresh water surplus. If storage variations are negligible, the temperature evolution of the Baltic Sea is in balance with the atmospheric heat and radiation fluxes. On monthly to interannual time scales, variations in the total volume of the Baltic Sea and thus in the total heat content have to be considered when relating the heat exchange with the temperature evolution in the Baltic Sea.

References

Bergstroem, S. and B. Carlsson, River runoff to the Baltic Sea: 1950-1990, Ambio, 23, (4-5), 280-287, 1994.

Jacobsen, T.S., Sea water exchange of the Baltic - measurements and methods. In: The Belt Project. National Agency of Environmental Protection, Denmark, ISBN 87-503-3532-4, 107 pp., 1980.

Lehmann, A. and H.-H. Hinrichsen, On the thermohaline variability of the Baltic Sea. J. Mar. Sys., Vol. 25/3-4, 333-357, 2000.

Lehmann, A. and H.-H. Hinrichsen, The Importance of water storage variations for water balance studies of the Baltic Sea. Phys. Chem. Earth, B, Vol.26, No. 5-6, 383-389, 2001.

Omstedt, A. and A. Rutgersson, Closing the water and heat cycles of the Baltic Sea. Meterol. Z., Vol. 9, No. 1, 59-66, 2000.

Stigebrandt, A., The vertical large-scale circulation of the Baltic Sea. In First study conference on BALTEX. Conference Proccedings, Editor, A. Omstedt. Int. BALTEX Secretariat Pub. Ser. No. 3, 28-47, 1995.

Meteorological Data Centre of BALTEX (BMDC)

Angela Lehmann, Kirsten Zimmermann

Deutscher Wetterdienst, BALTEX Data Centre, P.O. Box 100465, D-Offenbach, Germany

1. Introduction

The poster of the Meteorological Data Centre for BALTEX (BMDC) will inform about the work of the Data Centre.
The BMDC is operated by the German Meteorological Service (Deutscher Wetterdienst) as a part of the Business Area of Research and Development, Department of Climate and Environment. The BMDC is mainly a service centre which supplies project related meteorological data of the **Ba**ltic Sea **C**atchment **A**rea "***BACAR***" and the **Ba**ltic Sea **M**odel **A**rea "***BAMAR***" to national and international institutions participating in the BALTEX research project. Therefore a perfect data management is necessary.

2. The BMDC

Synoptic and ***aerological data*** from the whole ***BAMAR*** are of highest interest for model development and model run in BALTEX. All data are routinely observed in the meteorological networks of the countries on the basis of WMO regulations and distributed in real-time (rt) via the Global Telecommunication System (GTS). The BMDC stores them in the ***BAMAR*** archive using the routine services of the DWD.
Since August 1995 Belarus, Denmark, Estonia, Finland, Germany, Latvia, Lithuania, Poland, Russia and Sweden (BACAR countries) supply ***BALTEX relevant meteorological data***, for example precipitation, snow depth and radiation, which normally are not exchanged internationally. The data are available since August 1995. Recently the BMDC gets also data from the Czech Republic and Slovakia of which only small parts belong to the ***BACAR***.
The data pass through a preprocessing procedure at the BMDC which includes a Minimum Quality Check (MQC) for correctness and completeness of metainformation for data and station identification, number and order of observations, and the data are reformatted into fixed BALTEX formats. After this procedure the data are stored in the ***BACAR*** *archive.*
The BMDC offers besides ***precipitation data*** which are corrected for the systematic measurement error and analysed at the University of Veterinary Medicine Vienna. Additionally to the non-real-time data of the regular meteorological networks the BMDC manages ***precipitation data*** which are measured on ferries running between Lübeck and Helsinki. Data supplier is the Institute of Marine Research (Institut für Meereskunde) of the University of Kiel.

3. Use of Data

BALTEX data will be passed only to registered BALTEX data users. Confirmation as BALTEX data users will be done by members of the BALTEX SSG, as has been decided on the 4th meeting of the BALTEX SSG (June 1996, Sopot, Poland).
Information on the registration procedure are given at the Internet pages of the GKSS Research Centre:
http:// w3.gkss.de/baltex/user.html.
A registered BALTEX data user may request data at the BALTEX MDC. After having signed a Data License Agreement, confirming the rules and conditions of data use, the user will get data on an appropriate medium (DAT tape, diskette) or via data line (ftp or Internet).

References

Lehmann, A., K. Zimmermann, C. Graute, D. Stein , Meteorol. Data Centre for BALTEX, STATUS REPORT No. 4, Oct. 2000

Impacts of cloud and turbulence schemes on integrated water vapor: comparison between GPS measurements and model predictions.

Geert Lenderink, and Erik van Meijgaard

Royal Netherlands Meteorological Institute, 3730 AE De Bilt, The Netherlands, email: lenderin@knmi.nl

1. Introduction

Structures in atmospheric (vertically) Integrated Water Vapor (IWV) strongly reflect the dynamics of the atmosphere. This is, for example, clearly visible in the developing and maturing stage of an extra-tropical cyclone with bands of high and low IWV curving into the center of the cyclone.

Global positioning systems (GPS) provide point measurements of IWV. However, in regions with sufficient high coverage of GPS information about the spatial structure can be obtained by comparing the measurements from different GPS stations located close to each other.

In this abstract we will describe a case study to illustrate the potential of this approach by examining the mean characteristics of a frontal system (e.g., gradient, mean value, phase) as it passes different stations. In this approach we have evaluated the impact of changes in the model physics (one version with ECHAM4 physics and one with revised physics) on the structure of IWV in a regional atmospheric model. In more detail, we studied spatial structures in IWV for three cyclones (Isemer, 1996) during the PIDCAP (Pilot Study for Intensive Data Collection and Analysis conducted from August to November 1995) observational campaign. Result of Monika (2-5 okt) are presented here; other results are presented in Lenderink and van Meijgaard (2001) (Herafter LM2001). We used data of GPS stations in Sweden and Finland as described in Emardson et al. (1998).

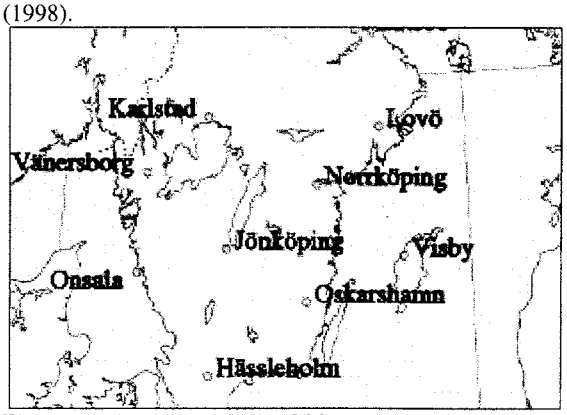

Figure 1: Location of the GPS stations (redrawn from Emardson et al 1998).

2. Model and Physics

We used the KNMI Regional Atmospheric Climate Model (RACMO) for our study. We operated on the standard grid used for the PIDCAP model intercomparison (1/6 x 1/6 degree, 24 hybrid levels). Boundary fields (updated every 6 hours) and initialization were taken from ECMWF analysis fields.

The "standard" version of RACMO uses the ECHAM4 physics package. In addition, we performed runs with a "revised" physics package with modifications in the cloud and turbulence physics. These modifications are designed to make the cloud and turbulence scheme physically more consistent, in particular for boundary layer clouds (for details LM2001). The modifications are motivated by the strong numerical sensitivities of the cloud scheme and the instability of the turbulence scheme for low wind shear in the ECHAM4 reference versions (Lenderink et al 2000).

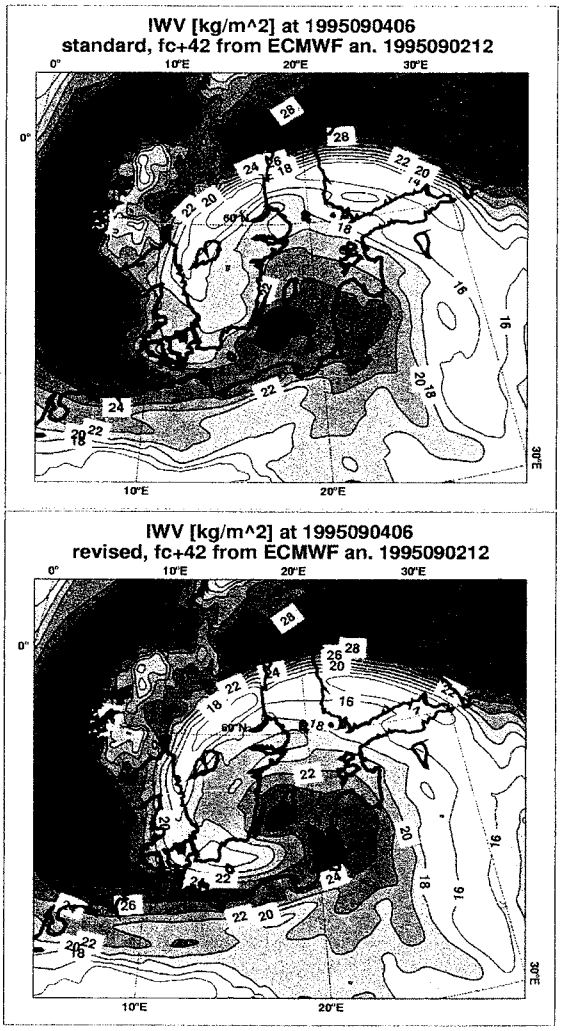

Figure 2: Predictions of IWV for both model versions.

3. Results.

We used data of seven GPS stations in the southern part of Sweden (Emardson et al., 1998) close to the path of the cyclone (ordered from east to west): VISBy, NORRköping, OSKArshamn, JÖNKöping, KARLstad, VÄNErsborg, ONSAla (see Fig. 1). Two 60-h integrations (with standard and revised physics) were initiated from 2 Sep 12 UTC.

In general, the development of the cyclone turned out to be quite similar for both model versions. Differences, for example, in surface pressure are small. The positioning of the centre of the cyclone is nearly correct at 06 UTC on 4 September (fc+42) but the predicted pressure in the center

of the cyclone (located near the southeastern corner of the Swedish coast) is about 6 hPa low. The most striking difference in model performance is the presence of finer-scale structures in IWV with the revised physics. To illustrate this we show IWV at 4 September 06 UTC in Fig. 2. In the run with the revised physics the development of the curved structure with bands of high and low humidity curving into the center of the low is much more pronounced than in the run with the standard physics.

We now focus on the passage of the band with low values of IWV over South Sweden. Both model versions predict a band of low IWV propagating to the north-west. Looking at the GPS station data in Fig. 3 it shows that a minimum can be found in the IWV measurements of all stations. Considering the eastern GPS stations, VISB, NORR and JONK, the propagation of this dry band can be identified from the consecutive minima for these stations. During the north-westward propagation the observed minima become deeper, indicating that the air was drying out. Station OSKA has a more flat minimum, indicating that it is only touched by the southern edge of the band. More to the (north-)west (ONSA, KARL and VANE) the minimum values in GPS time series start to diverge more.

In Fig. 3 we also compared the GPS station data directly with model data for the selected stations. For the standard physics, the successive minima for the eastern stations VISB, NORR and JONK are reasonably well represented. On the downside, the minima occur 1-2 hours late, the shapes of curves near the minima are somewhat flat, and the value of the minima are somewhat high (approx. 1 kg/m^2). The run misses the minimum for OSKA. The model fails to predict realistic minima for the more western stations, KARL, ONSA and VANE. On the other hand, the range of predicted minima for these stations is reasonably well predicted (between 15.2 and 18.0 kg/m^2). For the revised physics, the predictions for VISB, NORR, JONK are improved. The timing of the minima is better, the shape of the curves is somewhat steeper, and the values for the minima become lower - all in better agreement with the GPS data. Furthermore, the model predicts a flat minimum for OSKA, although still not very convincing. For the western points the situation is comparable to the run with standard physics. The range of the minima for these stations (between 13.9 and 17.1 kg/m^2) and their timing seem to be somewhat better than with the standard physics.

4. Conclusions

We studied structures in model predicted IWV for Monika (2-5 Sep 1995). Two model versions with differences in the model physics package were compared: standard ECHAM4, and ECHAM4 with revised cloud and turbulence physics. With the revised physics more pronounced IWV structures are predicted. The model predictions were compared to measurements from GPS stations in Sweden.

By combining data of different GPS stations we identified the passage of a dry band in the GPS data of 7 stations, and compared this to the model output. Based on this qualitative comparison, it turns out that the model with the revised physics provides a better representation of 1) the shape of the minimum (sharpness), 2) the minimum value, and 3) the timing of the minimum better than the model with the standard physics package. More results can be found in LM2001.

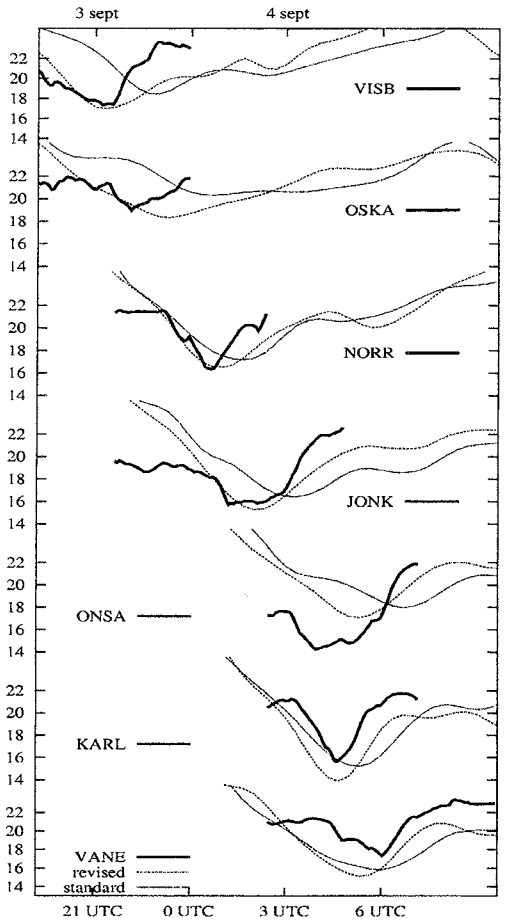

Figure 3: GPS IWV measurements (solid) and model predictions (dashed lines) for seven stations in Sweden.

References

Emardson, T.R., G. Elgered, and J.M. Johansson, 1998: Three months of continuous monitoring of atmospheric water vapor with a network of Global Positioning System receivers. *J. Geophys. Res.*,**103**, 1807-1820.

Isemer, H.-J., 1996: Weather Patterns and Selected Precipitation. Records in the PIDCAP period, August to November 1995. A Preliminary Overview. GKSS-Forschungszentrum Geesthachtpp. 92.

Lenderink, G. and E. van Meijgaard, 2001: Impacts of cloud and turbulence schemes on integrated water vapor: comparison between model predictions and GPS measurements. *Meteorology and Atm. Phys*, in press.

Lenderink, G., E. van Meijgaard and A.A.M. Holtslag, 2000: Evaluation of the ECHAM4 cloud-turbulence scheme for Stratocumulus, *Meteorologische Zeitschrift*, **9**, 41-47.

Acknowledgements

We thank Harald Bouma and Gunnar Elgered from Chalmers University of Technology for providing the GPS station data and Fig. 1. Part of this work is done within the NewBaltic2 project sponsored by the EU under contract number ENV4-CT97-0626.

Energy and Water Balance of the Baltic Sea Derived from Merchant Ship Observations

Ralf Lindau

Meteorologisches Institut der Universität Bonn, Auf dem Hügel 20, D-53121 Bonn, Germany

1. Introduction

The investigation of the Baltic Sea energy and water balance is a major objective of BALTEX. Meteorological observations onboard of Voluntary Observing Ships provide data to determine the mean climatological state and the seasonal and interannual variability of the entire set of involved surface fluxes: the precipitation, the latent and sensible heat fluxes and the net surface fluxes for short and longwave radiation. Using individual reports of COADS (Comprehensive Ocean Atmosphere Data Set) these five components are calculated on a time scale of monthly means for the period 1980 to 1995. Basic parameters as wind speed and wet bulb temperatures are corrected due to known measurement biases following Lindau (2000). Effects of sea ice are estimated by using the monthly ice coverage from GISST data.

For longtime periods the mean amount of P-E should be small compared to its two constituent components, since the average water outflow through the Danish Belts is comparable to the Baltic Sea river runoff. But no sharp constraint is known for P-E. Therefore, we considered additionally the energy bugdet at sea surface which contains one component of the water budget, the evaporation. The energy budget of the quasi-enclosed Baltic Sea is known to be almost completely balanced, thus providing a useful constraint for the consistency of the derived air-sea fluxes.

2. Data Treatment

The first problem in calculating these quantities is the inhomogeneous data distribution. Most reports are concentrated along narrow ship routes. Thus, the simple avarage of all available observations does not necessarily represent the mean conditions in the Baltic Sea.

Therefore, we distribute the information with an exponential distance-dependent function into the area, reaching a weight of 1/e at 111 km. Compared to this value the correlation length of the considered parameters (on monthly scale) is much greater, lying in the order of 1000 km. Thus, smoothing effects of the applied technique remain limited. Nevertheless, fully covered fields are obtained. After the procedure the data density e.g. in January ranges between 40 observations per tenth degree grid box in the southern Baltic Proper and 4 observations in the Bothnian Sea.

3. Precipitation

Following the basic ideas of Tucker (1961), we derived a simple rain algorithm which needs as input not more than the present weather code ww and the specific humidity, both observed routinely on merchant ships. For the decision whether it rains at all, the present weather code is very reliable, whereas rain intensity is estimated by the additional humidity information. For the derivation of the algorithm we calibrated the weather and humidity observations of 24 years from four light vessels in the German Bight against the wind corrected daily rain measurements carried out aboard these ships. In a second step the quality of the obtained rain algorithm is checked by its application on independent COADS data. For monthly means a correlation of 0.85 is obtained, for the climatic annual cycle even one of 0.96 (fig.1).

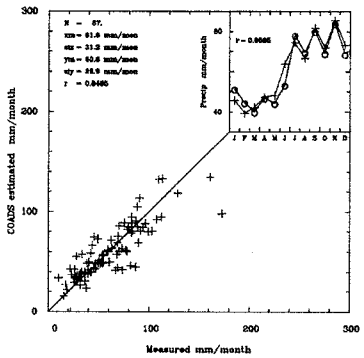

Figure 1: Calibration of rain estimates from COADS against measurements on Light vessels

However, for principle reasons rain observations are difficult to validate, since available measurements themselves are not beyond any question. Thus, before using the rain algorithm in the Baltic Sea, we tested it with global data by comparing its results to the evaporation. For a 14-years period mean P-E was estimated to about -300 mm/a. This amount can easily be balanced by the fraction of ocean (20%) where no ship observations are available. In these areas, mainly the Southern ocean, P-E is probabely positive. Additionally, the worldwide river runoff or, looking from the atmospheric point of view, the mean water vapour export from ocean to land causes a negative marine P-E. After these encouraging results from global application the rain algorithm is used to estimate the precipitation over the Baltic Sea (fig.2a).

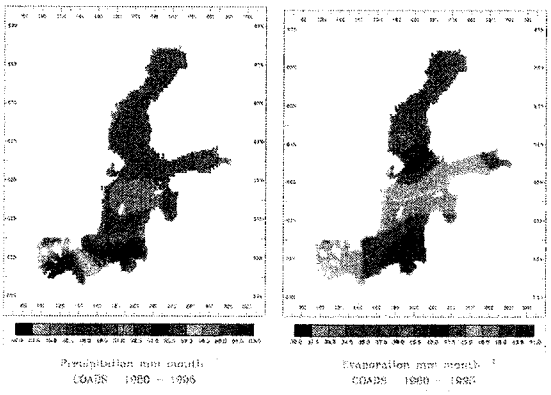

Figure 2: a) Precipitation and b) evaporation in Baltic Sea from COADS for 1980 to 1995

We found highest precipitation at the German coast and a minimum in the central Baltic Sea. Spatial mean of the considered 16-years period amounts to 50 mm/month.

4. Effects of Sea Ice on Heat Fluxes

Concerning the other four fluxes, further problems occur in the Baltic Sea due to sea ice which changes albedo and

surface temperature and influences in this way the air sea fluxes. Monthly mean ice concentrations with a spatial resolution of 1° by 1° are available from the GISST data set, mean ice thickness is estimated by an empirical function of sea surface temperature. Using these ice information we calculated the energy fluxes seperately for those parts of the Baltic Sea which are ice covered.

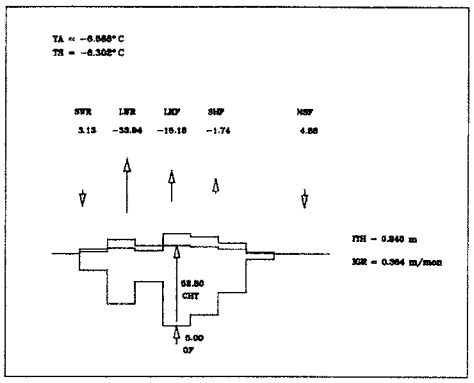

Figure 3: Applied ice correction scheme. Example shows the mean conditions in January

We applied a model of seven ice thickness classes (Maykut & Untersteiner, 1971) covered by a possible snow layer (Fig.3). The idea is to find an equilibrium temperature of the ice surface, so that the four atmospheric fluxes and the conductive heat flux through the ice are in balance. If that is not possible at temperatures below 0°C, the surplus of surface energy is used for melting. Applying this procedure to the individual observations, we found e.g. for January a mean ice temperature of -6.3°C whereas the mean reported air temperature for that month is -6.6°C. A latent heat flux of 15 Wm^{-2} results. Although the sum of atmospheric fluxes cools the ice surface, melting occurs due to strong convective fluxes through the relative thin ice of in average 24 cm. The oceanic flux at the bottom of the ice is considered to be constant at 5 Wm^{-2}, so that the freezing at the bottom prevails the surface melting. For the considered month of January a mean ice growth of 36 cm per month results.

5. Results

Using the above described ice correction scheme, an annual mean evaporation of about 45 mm/month is calculated, strongest in the S-E-part and decreasing to NW (fig 2b). Together with precipitation it shows that the Baltic Sea gains water from the atmosphere in its northern and its southern part and loses water in the central part (fig.5a). The total average is 5 mm/month, approximately 10% of both components.

A view on the annual cycle shows an increase of both components during the year from spring to autumn. P minus E remains nearly balanced almost throughout the year, but reaches considerable positive values in spring and early summer, when rain is already increasing but evaporation is still low due to the relative cold sea temperature. Individual monthly means of P-E show an increase of variability since 1980 (fig.4).

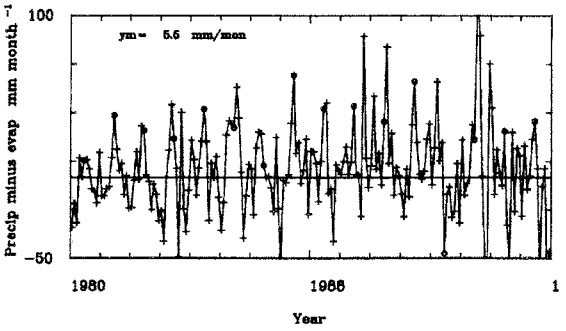

Figure 4: Time series of mean E-P in the Baltic Sea

The derived net energy flux, consisting of the ice corrected radiative and turbulent fluxes at sea surface, is giving a total mean of about 1 Wm^{-2} for the entire Baltic Sea. Thus, the energy balance is nearly closed. Spatial distribution shows, not surprisingly, an energy gain in the south-western part, while the north-eastern parts, especially the Bothnian Bay, lose energy in the annual mean. The mean annual cycle (Fig.5b) shows the commonly known variation in shortwave radiation, while the variability of the other three fluxes remains subdominant. Consequently, strong differences in the net energy flux between summer and winter of more than 300 Wm^{-2} occur.

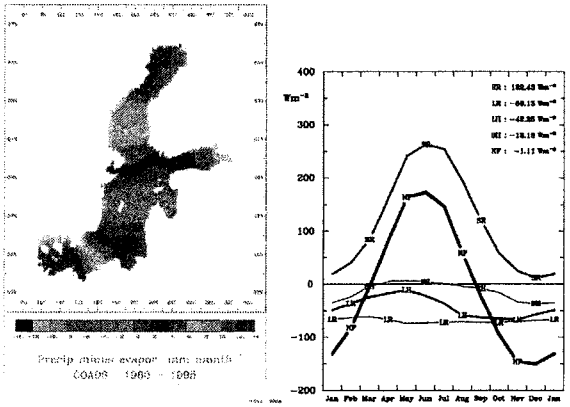

Figure 5: a) Geographical distribution of mean E-P (left), and b) mean annual cycle of the surface energy fluxes (right) both for the period 1980 to 1995.

References

Lindau, R., 2000: *Climate Atlas of the Atlantic Ocean derived from COADS* , Springer Verlag Heidelberg, 448pp.

Tucker, G.B., 1961: Precipitation over the North Atlantic, *Quart. J. Roy. Meteor. Soc.*, **87**, 147-158.

Maykut, G.A. and N. Untersteiner, 1971:, Some results from a time-dependent thermodynamical model of sea ice, *J. Geophys. Res.*, **76**, 1550-1575.

Using physical process models to force biogeochemical models

Torbjörn Lindkvist, Helma Lindow and Jörgen Sahlberg

Swedish Meteorological and Hydrological Institute, SMHI, SE-60176, Norrköping, Sweden

A new system is being developed in collaboration between SMHI and the Swedish Environmental Agency using the HOME concept. HOME stands for Hydrology, Oceanography and Meteorology for the Environment. The idea is to combine observations and mathematical models to describe the transport of water and substances for the whole hydrological cycle in drainage areas and sea areas. The first phase is focused on water flows and nutrients. The system is going to be set up on a national and a regional scale. The aim is to apply the system backward in time, real-time, short time forecasts and for scenarios of the future for different developments of climate and emissions. A preliminary real-time version has been set up for the Baltic Sea and its drainage area. Another application has been set up for an archipelago area in south-east Sweden for 1985-98. Knowledge of transport and mixing of water are essential for the success of the biogeochemical modelling.

One fundamental idea is to identify and specify water-planning objects common to all actors. This means specifying water dividers that form standard drainage areas of a maximum size, lakes, watercourses and their segmentation and coastal water areas such as bays and coastalstreches. With this standards we have a common base for communication with all actors involved and data can be stored coupled to this uniquely identified water areas.

The coastal water is composed by water from large areas and you have to look at the whole upstream drainage area and the open sea to be able to manage the coastal water. Observation data and geographical data are necessary but not enough to produce the decision support information that we need. We can not observe the concentration and flow of water and substances with enough resolution in time and space. We need to use mathematical model tools. The models have to be coherent in terms of variables, space and time. The processes involved have very short time steps and have to come down to hours and even less for some areas and variables mainly due to the sun radiation variation. When made available to the normal user all data is transformed to weekly averages.

Thermal and Hydrological studies lead over the BALTEX region with the Canadian regional Climate Model.

Virginie Lorant[1], Norman McFarlane[1] and René Laprise[2]

[1] Canadian Centre for Climate Modelling and Analysis, University of Victoria, P.O. Box 1700 STN CSC Victoria, B. C., V8W 2Y2.
[2] Université du Québec à Montréal, Quebec, Canada.

1. The Canadian Regional Climate Model

The CRCM is a non hydrostatic, limited-area, nested atmospheric model developed at 'Université du Québec à Montréal (UQAM) to carry out regional climate studies. Its dynamic core is derived from the mesoscale non hydrostatic community model developed at the Cooperative Centre for Research in Mesometeorology (CCRM), described by *Tanguay, Robert and Laprise* (1990) and *Caya and Laprise* (1998). An earlier version of this model included the physical processes package of the second generation atmospheric general circulation model of the Canadian Centre for Climate Modelling and Analysis (CCCma). That version of the CRCM has been used extensively for regional climate simulations. Although this version of the CRCM is able to simulate realistic regional details, some deficiencies have been identified by Laprise et al (1998), regarding the atmospheric and surface moisture budget, due in part to the simplified land surface scheme.

2. The second generation of Land surface scheme

The version of the physical package employed by this study is that of the recently established third generation AGCM of the CCCma. This new version includes the much more physically complete Canadian Land Surface Scheme (CLASS) first documented by Verseghy(1991), and Verseghy et al (1993). This land surface scheme includes three soil layers and a separate and more complex treatment of vegetation, soil and snow cover. Temperature is carried as prognostic variable as well as liquid and frozen water. Energy fluxes are computed for each "vegetation-soil-snow" subarea as a function of surface temperature. The soil albedo varies according to texture and moisture content. Additional snow albedo and density vary with time according to a simple exponential decay function. More recently a new formulation for evaluation of surface fluxes of heat, moisture, and momentum following Abdella and Mc Farlane (1996) has also been included. A complete description of this most recent version of CLASS is given in Verseghy (2000). The treatment of boundary layer processes in the new version is similar to that of the previous one. However the moist convective adjustment scheme used in the previous version has been replaced by the penetrative convection scheme of Zhang and McFarlane (1995). A newer version of the radiation scheme is also included. This newer radiation scheme includes 4 bands in the solar, 7 bands for terrestrial radiation, and a revised formulation of the water vapor continuum. The treatment of clouds in the new version is similar to that of the earlier version.

3. Experimental design

The computational domain is centered over the Baltic sea. Figure 1 shows the topographic height over the 101*101 grid point domain used for this study. Horizontal grid spacing is fixed at 45 km. In the vertical 29 Gal-Chen scaled-height layers are used with about 10 under 850 hPa. Such high vertical resolution combined with the new land surface scheme and the penetrative convection scheme should give a much more realistic simulation of the moisture and thermal budget of the surface and atmosphere.

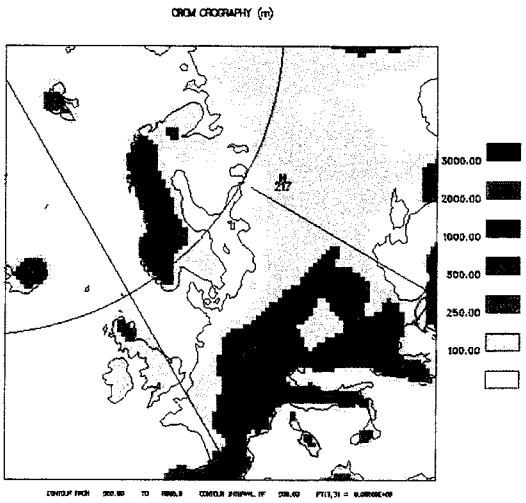

Figure 1: CRCM-Baltex Domain. 101*101 grid point, 45km grid spacing.

A two year simulation, including the PIDCAP period has been conducted in the configuration described above. The 19 month simulation run before the PIDCAP period has assessed as a reasonable spin up period to reach the soil equilibrium according to the "CCCma GCM -AMIP2-17year average" simulation the initialization data has come from.

Over the PIDCAP period, which extends from beginning of August 1995 to the end of November 1995, two simulations are performed. In the first one time–dependent lateral boundary conditions are supplied to the CRCM by the ECMWF analyses, while the NCEP reanalyses are used in the second simulation.

The purpose of the present study is to show how the CRCM behaves and downscale the large scale information provided at its boundary. It also deal with the CRCM ability to retain the large scale patterns. Furthermore, comparison with observation provided by the Baltex Meteorological Data Centre will indicate how regional characteristics are reproduced. Particular interest will be paid to the thermal and moisture budget, especially near the surface and in the boundary layer.

References

ECMWF: European Centre for Medium-Range Weather Forecast

NCEP: National Centre for Environmental Prediction

PIDCAP pilot study for Intensive Data Collection and Analysis of Precipitation.

Abdella, K., N.A. McFarlane, Parameterization of the surface-layer exchange coefficient for atmospheric models. , *Boundary-Layer meteorological*, Vol.80, No.1, 223-248, 1996.

Caya, D., and R. Laprise, A Semi-Implicite Semi-Lagrangian Regional Climate Model :The Canadian RCM. *Monthly Weather Review*, Vol. 127, 341-362,1999.

Laprise, R., et al., Climate and Climate change in Western Canada as Simulated by the Canadian Regional Climate Model., *Ocean-Atmosphere*, Vol.,XXXVI, No.2,1998.

Tanguay, M., A. Robert and R. Laprise, A semi-implicite semi-Lagrangian fully compressible regional forecast model. *Monthly Weather Review*, Vol. 118,1970-1980,1990.

Verseghy, D.L. "CLASS - a Canadian land surface scheme for GCMs - I. Soil model", *Int. J. Climatol.* 11: 111-143, 1991.

Verseghy, D.L., N.A. McFarlane and M. Lazare, "CLASS - a Canadian land surface scheme for GCMs - II. Vegetation model and coupled runs", *Int. J. Climatol.* 13: 347-370,1993.

Verseghy, D.L., "The Canadian Land Surface Scheme (CLASS): its history and future", *Atmosphere-Ocean*, special issue,2000.

Zhang, G. J., and N. McFarlane, Sensitivity of Climate Simulations to the Parameterization of cumulus Convection in the Canadian Climate Centre General Circulation Model, *Atmophere-Ocean*, Vol. 33, 407-446, 1995.

Modelling of Snow Influence on Land Fast Ice Thickness

Maria Lundin[1] and Anders Omstedt[2]

[1] SMHI, Nya Varvet 31, SE-427 71 Västra Frölunda, Sweden.
[2] SMHI, SE-601 76 Norrköping and Department of Oceanography, Earth Science Centre, SE-40530 Göteborg, Sweden.

1. Introduction

The Baltic Sea is a semi-enclosed sea located in the seasonal sea ice zone. An ice cover, typically less than one metre thick, forms and melts every year. Meteorological conditions have a pronounced effect on the sea ice, which acts as a thermal insulator and influences the air-sea exchange of energy, water and momentum.

The Baltic Sea Experiment (BALTEX) explore, models and quantifies the main physical processes that control the energy and water exchange within the Baltic Sea and its drainage area. In the sub-project BASIS, the Baltic Air-Sea-Ice Study *Launiainen and Vihma* (2001), meteorological, sea ice and hydrographic data have been gathered to quantify the physical processes of energy and mass transfer between the atmosphere, the sea ice and the sea. In the experimental stage of BASIS, the field campaign carried out at different places in the area of Gulf of Bothnia in February-March, 1998 formed the central element.

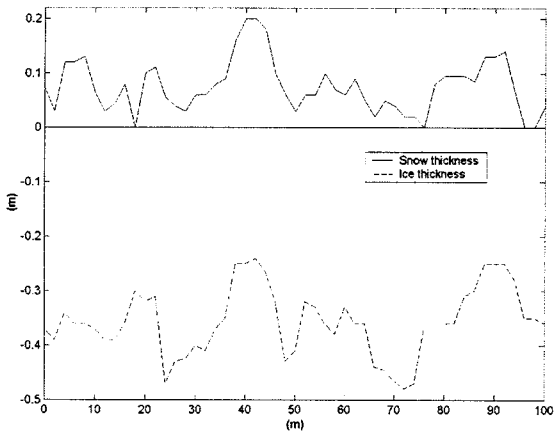

Figure 1: Snow and land fast sea ice thickness along 100 m from February 19.

During the BASIS field campaign snow and ice thickness, showing high variation, see Figure 1, were measured in land fast ice in the Northern Quark between Bothnian Sea and Bothnian Bay *Lundin et al.* (1999). The area is characterised by shallow water and smooth sea ice surface. Due to the smooth ice surface the rough ice bottom found in the data was unexpected. The snow and ice thickness measurements were made every second metre along a line of hundred metres at nine occasions between 19 February and 6 March 1998. The ice thickness of 19 February in Figure 1 shows high negative correlation to the snow thickness, which varies due to snow dunes formed by the wind. Later during the measuring period there was a melting period and the correlation between ice and snow thickness was lost.

The rough ice bottom could be due to rafting in the early freezing period, but ice cores from the area show mainly undisturbed columnar ice with a snow-ice layer on top. Also the smooth ice surface points towards the hypothesis that relatively stationary snow dunes has caused the uneven ice growth. Therefore this study aims to investigate to what degree the snow cover causes the ice thickness variations. In order to investigate the influence of snow on the fast ice thickness, a one-dimensional ice model with snow cover and snow-ice was applied.

2. Method

A one-dimensional ice model was used which describes the ice growth through thermodynamic growth *Omstedt et al.* (1996), snow-ice formation and sun radiation when melting.

Due to the small water depth in the modelled near shore area, the water column was assumed well mixed at temperature of freezing and the heat flux from below was assumed zero. Also the sun radiation part was assumed zero in the early winter period and during the ice growth period. The following expression was used to describe the ice thickness.

$$dh_i = \frac{k_i k_s}{k_i h_s + k_s h_i} \cdot \frac{(T_f - T_{surf})}{\rho_i L} dt + \left(\frac{h_i \rho_i + h_s \rho_s}{\rho_w} - h_i\right)$$

where the fist term describes the thermodynamic growth of ice and the last term describes snow-ice formation. Snow-ice forms when the snow thickness h_s increases the pressure on the ice, making sea water pour up through brine channels or cracks in the ice and a slush layer is created. In the model this layer is assumed to freeze instantaneously into so called snow-ice.

In order to get the date of freezing, a turbulent model was applied using the equation solver PROBE (PROgram for Boundary layers in the Environment) *Svensson* (1998). When the water column reach the freezing temperature the ice growth started.

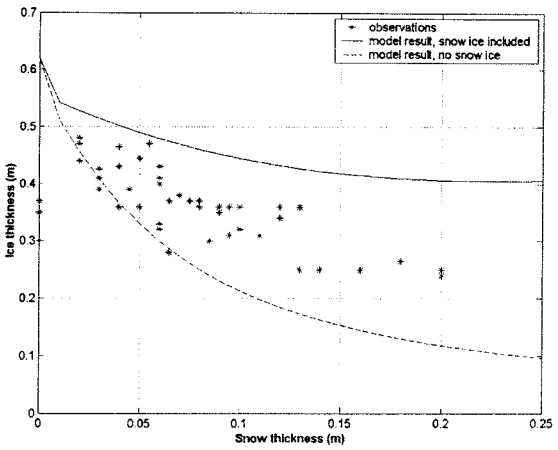

Figure 2: Modelled and observed ice thickness after -290 °C-days, with and without snow-ice formation, as a function of snow thickness.

3. Results

In order to investigate how much the snow depth influences the ice growth on local scale, the snow thickness was varied in order to simulate the effect of snow dunes. The result is shown in Figure 2 where the modelled ice thickness after -290 °C-days is plotted as a function of snow thickness. The number -290 °C-days corresponds to February 19, 1998 where also the verification data are taken. The hypothesis that the snow layer affects the uneven ice growth is verified in Figure 2, where the isolating characteristics of snow is indicated in the lower line, while the snow-ice effect is indicated by the upper line. The figure shows that a change of 0.1 m in snow gives a change of ice thickness by 0.1 m. It can be seen that the measured ice thickness is between the model results including snow-ice formation and the model results from thermodynamic growth only. This indicates that on a small area the ice growth is controlled to a large degree by the snow thermodynamics, whereas the snow-ice formation has a smaller influence, probably due to snow-ice formation on a larger area. Snow-ice formation is dependent on the mean snow thickness over a larger area, which in this case gives a small snow-ice contribution to the measured data but not as large as it should be if the whole area had the same snow thickness.

Modelled ice thickness including snow-ice formation based on weather and snow history, determined from the mesoscale analyses system MESAN *Häggmark et al.* (2000) and weather mast data from the BASIS experiment *Vihma et al.* (1999) are shown in Figure 3. The analysed period runs from June 1997 until May 1998 and simulates the BASIS experimental area with land fast ice around the experimental location in the Northern Quark. The observations represent mean snow and ice thickness along the 100-meter line measured during BASIS winter experiment. The snow-ice limit, representing the minimum snow depth for snow-ice formation, is shown by a dotted line in the diagram. The snow-ice limit is sensitive to the snow density, which varies between near zero up to 600 kg/m^3. In this study snow mean density is set to 300 kg/m^3 according to measurements from the BASIS experiment and earlier field measurements *Lundin et al.* (1999) and *Saloranta* (1999).

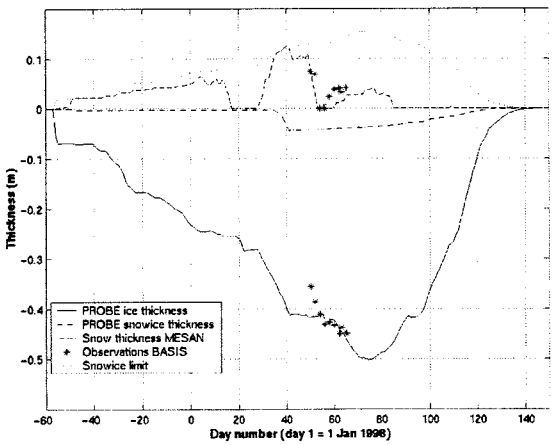

Figure 3: Modelled land fast ice, snow-ice and snow thickness from June 1997 – May 1998.

The model result shows good agreement to measured mean ice thickness during the main part of the BASIS experiment period, indicating that snow-ice formation depends on mean snow and ice thickness over a large area. The difference between the model and the first two observed values could be due locally variations in snow fall leading to snow-ice formation at different dates.

4. Conclusions

The thickness of land fast ice was modelled in order to investigate the snow influence on ice growth. The conclusions from the paper are summarised in the following points:

- From measurements made during the BASIS winter experiment it was found that snow covered land fast ice could have a rough bottom with quite large thickness variations even though the ice surface looks smooth.
- By setting up a thermodynamic ice model including snow-ice formation, it was found that the thickness variations found in the land fast ice partly can be explained by the isolating characteristics of the snow cover and partly by the snow-ice formation.
- The mean ice thickness of land fast ice is well described by the ice model used in this paper. It is shown that the snow ice formation depends on the mean snow thickness over a large ice area rather than local variations.

References

Häggmark, L., K.I Ivarsson,, S. Gollvik and P.O. Olofsson (2000) Mesan, an operational mesoscale analysis system, *Tellus*, 52A, 2-20, 2000.

Launiainen, J., and T. Vihma (Eds.) (2001) *BALTEX-BASIS (Baltic Air-Sea-Ice Study), Final Report*, International BALTEX Secretariat Publication No. (in press)

Lundin, M., M. Moberg, B. Håkansson and M. Granskog, (1999) Ground, air and satellite data obtained during BASIS field experiment by SMHI, in; Launiainen, J, (editor), *BALTEX-BASIS Data Report 1998*, Int. BALTEX Secretariat Publ. No. 14, Geesthacht, Germany, 94 pp.

Leppäranta, M (1993) A Review of Analytical Models of Sea-Ice Growth, *Atmosphere-Ocean*, 13(1), 123-138.

Omstedt, A., and L. Nyberg (1996) Response of Baltic See ice to seasonal, interannual forcing and climate change, *Tellus*, 48A, 644-662.

Saloranta, T.M. (1999) Modeling the evolution of snow, snow-ice and ice in the Baltic Sea, *Tellus*, 52A, 93-108.

Svensson, U. (1998) PROBE Program fro Boundary Layers in the Environment System description and Manual, *Reports Oceanography SMHI*, 24.

Vihma, T., J. Uotila, B. Cheng, T. Purokoski, P. Kosloff, J. Launiainen, and C. Schrum (1999) Marine meteorological, sea ice and oceanographic observations by the Finnish Institute of Marine Research, in; Launiainen, J, (editor), *BALTEX-BASIS Data Report* 1998,Int. BALTEX Secretariat Publ. No. 14, Geesthacht, Germany, 94 pp.

On the analysis of the Baltic Sea Level interannual variability

Valery Malinin, Alexei Nekrasov, Svetlana Gordeeva

Russian State Hydrometeorological University, 195196, Malookhtinsky Pr., 98, St. Petersburg, Russia

In this presentation the interannual variability in the Baltic Sea level is considered together with its possible causes.
It would appear reasonable that the interannual changes in the Baltic Sea level can be separated into two main parts: (1) long-period (background) variations due to relevant variations in the level of the North Atlantic, and (2) short-period (regional) oscillations related with changeability of the Baltic Sea water balance components and other regional factors. Observational data from 28 shore stations have been used covering a period of 103 years (1892-1994). In Figure 1 the interannual changes in level averaged for 28 stations are shown where a negative trend measuring –0.6 mm/yr is clearly seen with its contribution to the total variance exceeding 60%. The nature of this trend is discussed with focusing on two main factors: the global ocean level rise and the effect of the Baltic shore tectonic movements which can be estimated, according to *Baltic Sea* (1992), as +0.9 and –1.5 mm/yr, correspondingly.

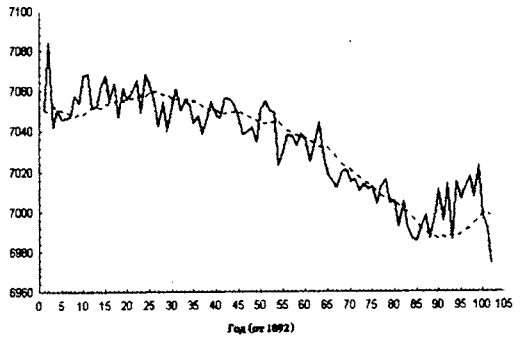

Figure 1: Interannual changes in Baltic Sea level averaged for 28 stations.

After subtracting the trend from the data matrix, the latter was decomposed into 'principal components' with a very fast converging procedure. As a result, the following representation of the Baltic Sea level time variations has been given:

$$h(t) = T(t) + A_1(t) + A_2(t) + \Sigma A_j(t)$$

with $h(t)$ – sea level averaged for stations data, $T(t)$ – sea-level trend component, $A_1(t)$ and $A_2(t)$ – first and second principal components contributing, correspondingly, 76% and 8% in the variance of initial (trend removed) data field, and $\Sigma A_j(t)$ – the sum of remaining (much less significant) components describing together about 16% of the initial variance.
The geographic distribution of first and second principal components loading is given in Figures 2a and 2b. The considerable homogenity of A_1-loading can be seen in contrast with A_2-loading, which shows an opposition between the northern and southern parts of the Baltic Sea.
The analysis of temporal variability characteristics of principal components showed that in $A_1(t)$ the constituents with periods 4.5 and 3.6 years play a considerable role while in $A_2(t)$ the small-scale nonregular oscillations are predominant.

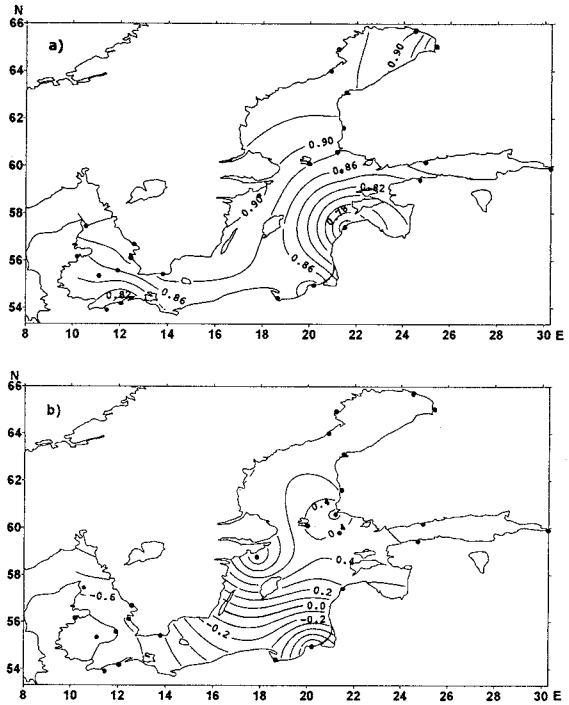

Figure 2: Geographic distribution of first (a) and second (b) principal components loading.

Regression models were proposed for describing the basic properties of principal components. It was found that the most significant predictors for $A_1(t)$ are the index of the North Atlantic Oscillation, Icelandic Depression pressure, water exchange through the Danish Straits and some other, less significant, factors. For $A_2(t)$ the most significant predictors were found to be the characteristics of water balance.

References

Baltic Sea. *Hydrometeorology and hydrochemistry of the seas of USSR*, Vol. 2. St. Petersburg, Hydrometeoizdat, 450, 1992 (*in Russian*)

Gordeeva, S., V. Malinin. On the interannual changeability of the Baltic Sea water balance components. *Contemporary problems of hydrometeorology.* Collection of papers St. Petersburg, 64-80, 1999 (*in Russian).*

The effect and influence of the Northern cyclogenesis on the Ethiopian weather

Meklit Mekre Mandefro

National Meteorological Service Agency Addis Ababa, Ethiopia, P.O. Box 1090, e-mail: m_meklit@hotmail.com

During the short rainy season from mid February to late May, Ethiopian weather is characterized by the frequent passage of mid latitude westerly trough associated with easterly waves enhancing the moisture influx from the northern Indian Ocean, especially Arabian Sea.

As seen from global model charts and satellite images for those days of the year, great importance is the deepening and intensification of low pressure or depression over Mediterranean area extending its trough axis along 40° E at the time of the short rainy period

Some of these westerly troughs have a phase velocity, which is westward relative to the mean flow and may thus freely propagate into the tropics. In such case, the energy flux entering the tropics from middle latitudes may act simultaneously with in suit energy generation in the tropics. The resulting interaction, which is reflected in satellite pictures in the form of huge cloud clusters extending from horse latitude to the tropical belt has been studied.

The paper briefly discussed the relevant charts depicting the mid latitude troughs extending from the cyclogenesis of Mediterranean region and easterly waves during short rainy period of Ethiopia.

The paper also attempted to discusses the failure of the short rainy season held under the cold episode La Niña condition of the year 1998, 1999 and the year 2000.

The paper concluded by certifying the influence of the mid latitude trough to the Ethiopian weather in the short rainy season.

Using a 30GHz Radiometer and GPS to measure atmospheric liquid water

Lorenz Martin and Christian Mätzler

Institute of Applied Physics, University of Bern, Sidlerstrasse 5, CH-3012 Bern, Switzerland, email: lorenz.martin@mw.iap.unibe.ch

1. Introduction

Microwave radiometry is a very useful method to determine the integrated liquid water content (ILW) and the water vapor content (IWV) of the atmosphere. With measurements of the atmospheric brightness temperature near the 22.235 GHz water vapor line and in the atmospheric window around 30 GHz, the ILW and IWV can be computed with a simple linear algorithm (Janssen (1993), Chapter 4).

The Global Positioning System (GPS) provides another way to measure the IWV of the atmosphere. Because of the atmospheric gases, the GPS signals are delayed on their way from the satellites to the earth. Extracting the part of the delay due to water vapour allows for the calculation of the IWV (Bevis et al. (1992)).

With a combination of both methods, the GPS measurement of the IWV can replace the information from the lower radiometer frequency.

2. Method

In our investigations we tested this possibility with model calculations. Temperature and humidity profiles from radiosoundings and estimated liquid water profiles served as database. With the Millimeter-Wave Propagation Model (MPM93) by Liebe et al. (1993) and radiative transfer, the brightness temperatures and the delay were computed. A linear combination of the brightness temperature at 30GHz and the wet delay was used to calculate the ILW and compare this value with the integrated liquid water profiles.

3. Results

The ILW from the integrated liquid water profiles and the calculated ILW are in very good accordance (see Fig. 1). This is valid for the whole considered period of three years (2200 soundings) and for all amounts of liquid water.

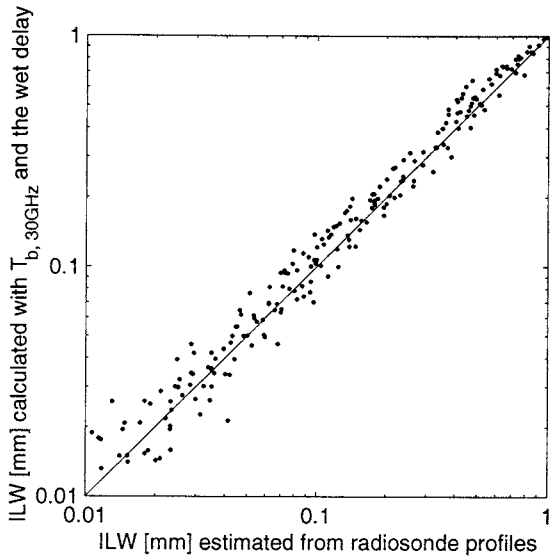

Figure 1: The integrated liquid water content (ILW) estimated from radiosoundings against ILW calculated with the brightness temperature at 30GHz and the wet delay.

4. Outlook

The next step to be presented at the conference is to apply this method to the data of the CNN I campaign of the CLIWANET project, where the 22.235GHz channel of our radiometer failed. As we have a collocated GPS receiver, the wet delay measurements can replace the missing radiometer channel. Additional data from an infrared sensor could enhance the quality of the measurement of the ILW.

References

Bevis, Michael, Steven Businger, Thomas A. Herring, Christian Rocken, Richard A. Anthes, Randolph H. Ware GPS Meteorology: Remote Sensing of Atmospheric Water Vapor Using the Global Positioning System, Journal of Geophysical Research, Vol. 97, No. D14, 15'787-15'801, 1992

Janssen, Michael A. (Editor) Atmospheric Remote Sensing by Microwave Radiometry, Wiley 1993, New York

Liebe, H. J., G. A. Hufford, M. G. Cotton Propagation Modeling of Moist Air and Suspended Water/Ice Particles at Frequencies Below 1'000GHz, Proceedings of AGARD 52nd Specialists' Meeting of the Electromagnetic Wave Propagation Panel, Mallorca, 1993

The circulation of the Baltic Sea and its communication with the North Atlantic - a large scale and high-resolution modeling approach.

Wieslaw Maslowski[1], Waldemar Walczowski[1,2], and Douglas C. Marble[1]

[1] Department of Oceanography, Naval Postgraduate School, Monterey, CA 93943, USA
[2] Institute of Oceanology, Polish Academy of Sciences, Sopot 81-712, Poland

1. Introduction

General circulation models (GCMs) have become a powerful tool for investigating local, basin-wide, and global ocean dynamics and climate variability. In fact, such models are an important component of environmental prediction and climate change studies. Over the last few decades, GCMs have made significant advancements in (i) representation of physical processes controlling the ocean dynamics and its variability at a wide range of spatial and temporal scales and (ii) in use of modern high performance computers to solve complex oceanographic problems (Semtner, 1995). Limited-domain or regional models have increased their spatial resolution from 0(100 km) to 0(10 km) or more. This has allowed for more adequate representation of marginal or semi-enclosed seas, such as the Baltic Sea. In addition, higher resolution provides means of studying processes controlling communication between such regions and the large-scale ocean circulation.

2. Model Description

To address some of the U.S. Navy requirements of predictive operational oceanography in the ice-covered Northern Hemisphere oceans, a new regional coupled ocean and sea ice model has been developed at the Naval Postgraduate School (www.oc.nps.navy.mil/~pips3). This model is called the Polar Ice Prediction System (PIPS) 3.0 and it will replace the earlier version of the operational model (PIPS 2.0). Its domain (Figure 1) extends from the North Pacific (at ~ 30 °N) through the Arctic Ocean and the Nordic Seas into the North Atlantic (to ~45°N), including the Baltic Sea. The model uses a 1/12° (or ~ 9 km) and 45-level grid. In the vertical direction, the upper 100 meters in the ocean are resolved by eleven layers and the upper 500 meters by nineteen layers. Such a resolution allows accurate representation of continental shelves, shallow marginal seas, and other bathymetric features important for communication between local and large scales. This research is an extension of our previous ice-ocean modeling effort using a 1/6° and 32-level grid (Maslowski et al., 2000, Maslowski et al., 2001, Zhang et al., 1999, <www.oc.nps.navy.mil/sbi>). The coupled model adapts the Los Alamos National Laboratory (LANL) Parallel Ocean Program (POP) (Maltrud et al., 1998) with a free-surface approach and a dynamic-thermodynamic sea ice model with a Lagrangian formulation of the sea ice thickness distribution (Bitz and Lipscomb, 1999). In its final phase the PIPS 3.0 will produce daily forecasts of sea ice and oceanic conditions for the entire model domain, including the Baltic Sea. Results of this high resolution model may contribute toward realization of some of the goals of the Baltic Sea Experiment (BALTEX) program.

During the 27-year spinup integration, the model has been forced with the daily-averaged annual cycle of climatological atmospheric fields derived from the European

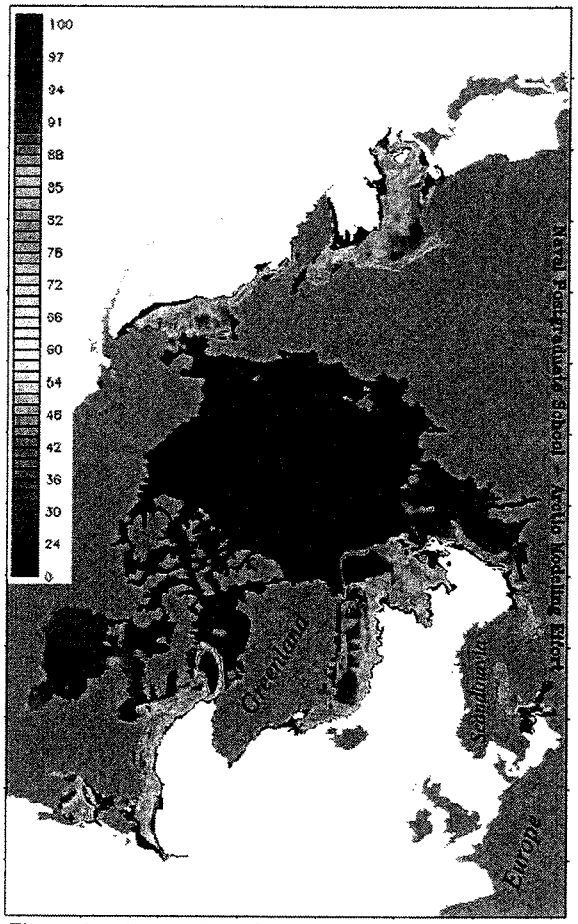

Figure 1: A snapshot of sea ice concentration (%) from March of spinup year 22 of the Polar Ice Prediction System (PIPS) 3.0 model. The full model domain is shown.

Centre for Medium-range Weather Forecasts (ECMWF) 1979-1993 reanalysis. Forcing fields include: 10-meter winds, sea surface pressure, temperature, and dewpoint, and long-wave and short-wave radiation In addition, the ocean surface (0-5 m) temperature and salinity fields are restored with a 30-day timescale to monthly mean climatology values derived from the University of Washington Polar Science Center Hydrographic Climatology data set (PHC, Steele et al., 2000). The PHC is a combination of the World Ocean Atlas (Antonov et al., 1998, Boyer et al., 1998) with the regional Arctic Ocean Atlas (EWG, 1997 and 1998). Some marginal seas, such as the Baltic Sea may require further improvements of the existing climatologies. Data sets available from the Baltex Program could provide alternative climatology fields for that region.

3. Model Results

Model output from the spinup include monthly-averaged 3-dimensional fields of temperature, salinity, and velocity and daily snapshots of selected 2-dimensional fields at

several vertical levels. Results from this integration represent mean or climatological conditions. In Figure 2, the monthly mean distribution of temperature and velocity fields at depth 0-10 m is shown in August of spinup year 27. Within the limits of

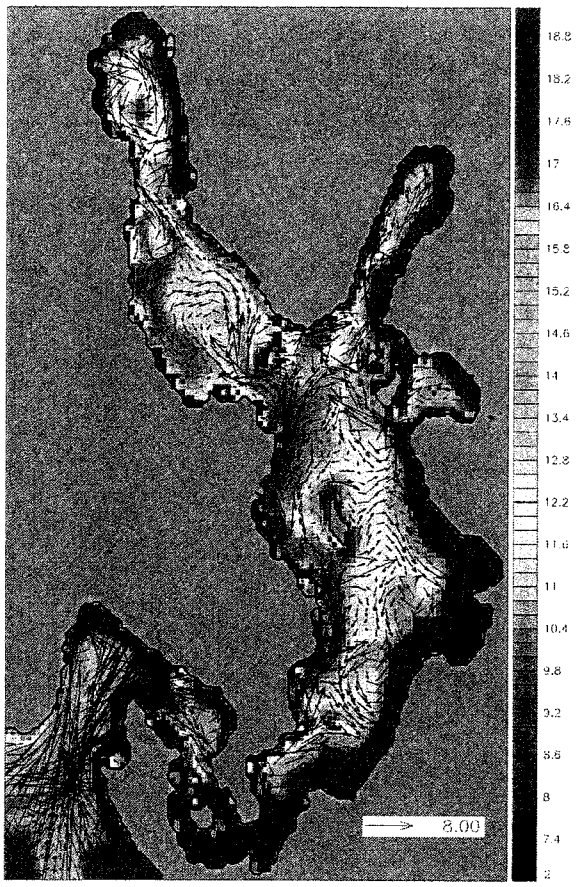

Figure 2: The August monthly mean temperature (°C) and velocity (cm/s) fields at depth 0-10 m from year 27 of model spinup. Every 2nd velocity vector shown.

spatial resolution, the model realistically represents general circulation in the Baltic Sea. It complements other higher resolution studies of the water and ice circulation in the region. More importantly, it provides information about communication of this enclosed sea via the Danish Straits with the North Sea and the North Atlantic. In addition to predicting ice extent and thickness in the Northern Hemisphere (Figure 1), this model can provide oceanic and sea ice boundary conditions for other local models, e.g. operational weather forecasting models of the Baltic Sea.

Examples of available ocean and sea ice model output for the Baltic Sea are presented. Mass and property fluxes between the region and the large-scale ocean to the west are calculated to determine their role in establishing local hydrographic conditions.

References

Antonov, J.L., S. Levitus, T.P. Boyer, M.E. Conkright, T.D. P'Brien, and C. Stephens, 1998 World Ocean Atlas 1998 Vol 1: Temperature of the Atlantic Ocean, NOAA Atlas NESDIS 27, U.S. Government Printing Office, Washington D.C.

Bitz, C.M. and W.H. Lipscomb, 1999: An energy-conserving thermodynamic model of sea ice, J. Geophys. Res., 104, 15,669-15677.

Boyer, T.P,. S. Levitus, J.I. Antonov, M.E. Conkright, T.D. P'Brien, and C. Stephens, 1998: World Ocean Atlas 1998 Vol. 4: Salinity of the Atlantic Ocean, NOAA Atlas NESDIS 30, U.S. Government Printing Office, Washington D.C.

Environmental Working Group (EWG), 1997: Joint U.S.-Russian Atlas of the Arctic Ocean for the Winter Period [CD-ROM], Natl. Snow and Ice Data Cent., Boulder, Colorado.

Environmental Working Group (EWG), 1997: Joint U.S.-Russian Atlas of the Arctic Ocean for the Summer Period [CD-ROM], Natl. Snow and Ice Data Cent., Boulder, Colorado.

Maltrud, M.E., R.D. Smith, A.J. Semtner, and R.C. Malone, 1998: Global Eddy-resolving Ocean Simulations Driven by 1985-95 Atmospheric Fields, J. Geophys. Res., 103, 30825-30853.

Maslowski, W., B. Newton, P. Schlosser, A.J. Semtner, and D.G. Martinson, 2000: Modeling Recent Climate Variability in the Arctic Ocean, Geophys. Res. Lett., Vol. 27, No. 22, pp. 3743-3746.

Maslowski, W., D.C. Marble, W. Walczowski, A.J. Semtner, 2001: On Large Scale Shifts in the Arctic Ocean and Sea Ice Conditions during 1979-1998, Annals of Glaciology, in press.

Semtner, A.J., 1995: Modeling Ocean Circulation, Science, 269, 1379-1385.

Steele, M., R. Morley, and W. Ermold, 2001: Polar Science Center Hydrographic Climatology (PHC) – A Global Ocean Hydrography with a High Quality Arctic Ocean, in press, J. Clim.

Zhang, Y., W. Maslowski, and A.J. Semtner: Impacts of mesoscale ocean currents on sea ice in high resolution Arctic ice and Ocean simulation, J. Geophys. Res., 104(C8), 18,409-18,429, 1999.

Simulated water and heat cycles of the Baltic Sea using a 3D coupled ice-ocean model

H.E. Markus Meier

Swedish Meteorological and Hydrological Institute, Rossby Centre, S - 601 76 Norrköping, Sweden

1. Introduction

The Baltic Sea is one of the world's largest brackish water sea areas with hampered water exchange to the world ocean.

The semi-enclosed character supports studies on water and heat cycles using either observations, regional atmosphere models, Baltic Sea models or even coupled atmosphere-ice-ocean models. Within the Swedish Regional Climate Modeling Program, SWECLIM, a 3D coupled ice-ocean model for the Baltic Sea has been developed to simulate physical processes on time scales of hours to decades. This model is the Rossby Centre Ocean model (RCO) which has open boundary conditions in the northern Kattegat. Results of 13-year simulations (1980-93) are used to calculate the water and heat cycles of the Baltic Sea. Recently, also the coupling with a regional atmosphere model, i.e., the Rossby Centre Atmosphere model (RCA), has been performed. The technical basis for the coupling is given by the OASIS coupler.

The first study of this kind utilizing a horizontal integrated model of 13 boxes has been performed by *Omstedt and Rutgersson* (2000). They found that in a long-term mean the Baltic Sea is almost thermodynamically closed like a lake. The dominating fluxes, as annual means, are the sensible heat, the latent heat, the net long wave radiation, the solar radiation to the open water and the heat flux between water and ice. In water and heat cycle studies for the BALTEX program, the response of the salinity and heat content of the Baltic Sea are important parameters to study when evaluating and improving the atmosphere, ocean and river runoff models. An overview of recent research achievements of the BALTEX research program is given by *Bengtsson* (2001).

2. Model description

RCO is a further development of the OCCAM version (Ocean Circulation Climate Advanced Modeling Project at the James Rennel Division, Southampton Oceanography Center, Southampton, UK) of the widely used Bryan-Cox-Semtner primitive equation model with a free surface (*Webb et al.*, 1997). OCCAM includes improved vertical and horizontal advection schemes, harmonic horizontal viscosity and diffusivity and a third order polynomial approximation

of the equation of state, as set by the Joint Panel on Oceanographic Tables and Standards (UNESCO). The conservation equations of momentum, mass, potential temperature and salinity are discretized in spherical co-ordinates horizontally on the Arakawa-B-grid and vertically in non-uniform geopotential levels.

Open boundary conditions as developed by *Stevens* (1990) are implemented. Hourly sea level data from tide gauge data at Ringhals (Sweden) and climatological mean temperature and salinity profiles from observations at the open sea montoring station P2 in the northern Kattegat are used.

The model depths are based on realistic bottom topography data (*Seifert and Kayser*, 1995). RCO makes use of 41 levels with layer thicknesses from 3 m close to the surface to 12 m near the bottom. The maximum depth in RCO is only 250 m to avoid small time steps. Two different horizontal resolutions are used: 2 and 6 nautical miles.

For the calculation of initial temperature and salinity fields the model domain has been divided into 14 boxes. The borders have been chosen according to topographic features which determine the hydrography of the sub-basins. Profiles from the SHARK (Svenskt HavsARKiv) data base (Swedish Oceanographic Data Center at the Swedish Meteorological and Hydrological Institute, SMHI) have been selected to compile initial conditions for May 1980.

The atmospheric forcing is developed at SMHI and based on three hourly gridded observations of sea level pressure, geostrophic wind components, 2 m air temperature, 2 m relative humidity and total cloud cover. In addition, at 06 and 18 UTC also 12 hourly accumulated precipitation is used. Data from all available synoptic stations (about 700 to 800) covering the whole Baltic Sea drainage basin are interpolated on a one degree regular horizontal grid. A two-dimensional univariate optimum interpolation scheme is used. As only geostrophic wind fields are available, a boundary layer parameterization is utilized to calculate wind speeds in 10 m height (*Bumke et al.*, 1998). Standard bulk formulae are used to calculate sea surface fluxes of wind stress, sensible and latent heat, long wave and short wave incoming radiation.

The river runoff data have been taken from the BALTEX Hydrological Data Center at SMHI. The monthly data do not only represent the inflow by major rivers, but the runoff through coastal segments including estimated smaller runoff ways (*Bergström and Carlsson* , 1994). In RCO the 29 most important coastal segments are considered.

As mixing plays a dominant role for an estuary like the Baltic Sea, a sophisticated two-equation turbulence model of the k-ε type (cf. *Rodi,* 1980) is used with corrected dissipation term, flux boundary conditions to include the effect of a turbulence enhanced layer due to breaking surface gravity waves and a parameterization for breaking of internal waves.

The ocean model in RCO is coupled with a Hibler-type (*Hibler*, 1979) two-level (open water and ice) dynamic-thermodynamic sea ice model. An elastic-viscous-plastic rheology is used (*Hunke and Dukowicz*, 1997). The ice thermodynamics are based on Semtner's 3-layer model (*Semtner*, 1976).

For a more detailed model description of RCO, the reader is referred to *Meier et al.* (1999), *Meier* (2000) and *Meier et al.* (2001). Results of 13-year hind cast simulations for the period May 1980 to December 1993 have been compared with observations by *Meier* (1999) and *Meier* (2001). A performance analysis of the multiprocessor model is given by *Meier and Faxen* (2001).

3. Model validation

Sea surface temperatures (SST's) are compared to observations from 9 monitoring stations for the period 1980-93. The agreement is regarded as good. The rms

error is increasing from Anholt East in Kattegat (1°C) to F9 in the Bothnian Bay (1.7°C). The monthly mean SST error is
within the range of −1°C and 1°C. Independently of the used heat flux package the mean SST error has a clear seasonal cycle with overestimated SST's in summer and underestimated SST's in winter. Obviously, this is the consequence of the atmospheric forcing data set which includes mainly land stations.
Simulated sea ice extent, ice thickness and snow thickness at the monitoring station Kemi in the Bothnian Bay are in good correspondence with observations. The mean error of maximum ice extent is $15*10^9$ m^2 (model overestimation of about 8%) and the rms error is $39*10^9$ m^2. The model simulation shows also high skill for the date, when the maximum ice extent occurred.
Compared with climatological data for the eastern Gotland Basin monthly mean short wave radiation is somewhat underestimated. Obviously, this is compensated in summer by an overestimation of long wave incoming radiation due to overestimated total cloud coverage in the atmospheric forcing data set.
Simulated salt content is evaluated using monitoring data.

4. Results

Model results are used to calculate annual and seasonal mean water and heat budgets of the Baltic Sea. For example horizontal distributions of annual and seasonal mean net heat fluxes are shown. Several sensitivity experiments have been performed to estimate model uncertainties concerning heat flux parameterizations, atmospheric forcing, mixing parameterizations and horizontal resolution.
The Baltic Sea gains heat at the sea surface of about 1 W/m^2 in the long-term mean. This heat is transported through the Danish Straits out of the system. Short wave radiation, long wave radiation, sensible and latent heat amount to 90, -45, -12 and −32 W/m^2, respectively (positive values indicate heat fluxes into ice or ocean). These results agree very well with results by *Omstedt and Rutgersson* (2000).
It is shown that horizontally averaged annual mean heat fluxes are relatively insensitive. Sensitivity experiments with low performance concerning SST's can reproduce these numbers as well.

5. Conclusions

- In 13-year simulations SST, sea ice cover and stratification are simulated realistically.
- Due to the high variability of the system multi-year runs are necessary to calculate water and heat cycles of the Baltic Sea.
- The largest uncertainty in the heat cycle is related to the radiative fluxes.
- The Baltic Sea heat cycle is almost closed.
- Horizontally averaged annual mean heat fluxes cannot be used to evaluate ocean models.

References

Bengtsson, L., The energy and water cycle of the Baltic Sea – Overview of recent research achievements of the BALTEX programme, submitted to *Meteorol. and Atmos. Phys.*, 2001.

Bergström, S., and B. Carlsson, River runoff to the Baltic Sea: 1950-1990, *Ambio*, 23, 280-287, 1994.

Bumke, K., U. Karger, L. Hasse, and K. Niekamp, Evaporation over the Baltic Sea as an example of a semi-enclosed sea, *Contr. Atmos. Phys.*, 71, 249-261, 1998.

Hibler, W.D., A dynamic thermodynamic sea ice model, *J. Phys. Oceanogr.*, 9, 817-846, 1979.

Hunke, E.C., and J.K. Dukowicz, An elastic-viscous-plastic model for sea ice dynamics, *J. Phys. Oceanogr.*, 27, 1849-1867, 1997.

Meier, H.E.M., First results of multi-year simulations using a 3D Baltic Sea model, Reports Oceanography No. 27, Swedish Meteorological and Hydrological Institute, S-60176 Norrköping, Sweden, 48 pp, 1999.

Meier, H.E.M., The use of the k-ε turbulence model within the Rossby Centre regional ocean climate model: parameterization development and results, Reports Oceanography No. 28, Swedish Meteorological and Hydrological Institute, S-60176 Norrköping, Sweden, 81 pp, 2000.

Meier, H.E.M., The first Rossby Centre regional climate scenario for the Baltic Sea using a 3D coupled ice-ocean model, Reports Meteorology and Climatology No. 95, Swedish Meteorological and Hydrological Institute, S-60176 Norrköping, Sweden, 63 pp, 2001.

Meier, H.E.M., and T. Faxen , Performance analysis of a multiprocessor coupled ice-ocean model for the Baltic Sea, submitted, 2001.

Meier, H.E.M., R. Döscher, A.C. Coward, J. Nycander, and K. Döös, RCO – Rossby Centre regional Ocean climate model: model description (version 1.0) and first results from the hindcast period 1992/93, Reports Oceanography No. 26, Swedish Meteorological and Hydrological Institute, S-60176 Norrköping, Sweden, 102 pp, 1999.

Meier, H.E.M., R. Döscher, and T. Faxen, A multiprocessor coupled ice-ocean model for the Baltic Sea, submitted, 2001.

Omstedt, A., and A. Rutgersson, Closing the water and heat cycles of the Baltic Sea, *Meteorologische Zeitschrift*, Vol. 9, No. 1, 55-66, 2000.

Rodi, W., Turbulence models and their application in hydraulics – a state-of-the-art review, Int. Assoc. for Hydraul. Res., Delft, Netherlands, 104 pp, 1980.

Seifert, T., and B. Kayser, A high resolution spherical grid topography of the Baltic Sea, Meereswiss. Ber. Warnemünde, 9, 73-88, 1995.

Semtner, A.J., A model for the thermodynamic growth of sea ice in numerical investigations of climate, *J. Phys. Oceanogr.*, 6, 379-389, 1976.

Stevens, D.P., On open boundary conditions for three dimensional primitive equation ocean circulation models, *Geophys. Astrophys. Fluid Dynamics*, 51, 103-133, 1990.

Webb, D.J., A.C. Coward, B.A. de Cuevas, and C.S. Richmond, A multiprocessor ocean circulation model using message passing, *J. Atmos. Oceanic Technol.*, 14, 175-183, 1997.

On the Representation of Clouds in the regional atmospheric Model HRM

Insa Meinke, Burkhardt Rockel, Rainer Hollmann and Ehrhard Raschke

GKSS Research Center, D-21502 Geesthacht, Germany

1. Introduction

A common problem of numerical atmospheric models is the poor representation of clouds. The radiation budget and the water cycle show a strong sensitivity to cloud processes. As these are the most significant components of weather and climate generating processes their sensitivity to clouds indicates the importance of an accurate cloud parametrization scheme in numerical atmospheric models for correct weather forecasts and reliable climate studies. In connection with BALTEX this study is on the validation of the cloud parametrization scheme in the regional atmospheric model HRM (High Resolution Model). For this validation satellite data from the International Satellite Cloud Climatology Project (ISCCP) are used. The objective is the identification of model errors due to clouds as a basis for improvements within the cloud parametrization scheme of the model.

2. Data

The investigation area maintain the Baltic Sea and its catchment area, North- and Central Europe and the eastern part of the North Atlantic (Figure 1 left). Within BALTEX several extensive observation periods are planned and carried out in combination with modeling activities. The investigation period of this study is connected with PIDCAP (Pilot Study for Intensive Data Collection and Analysis of Precipitation) from August to October 1995.

For PIDCAP model calculations are carried out by the regional atmospheric model HRM (High Resolution Model) which has the same physics as the global forecast model "GME" of the German Weather Service (DWD). Its prognostic variables are surface pressure, temperature, water vapour, cloud water and horizontal wind components. The parametrizations of the model related to cloud processes are the mass flux convection scheme after Tiedke (1989) and the delta-two-stream radiation scheme after Ritter and Geleyn (1992). The grid scale precipitation is included in the parameterized cloud microphysics. Driven by analyses of the German Weather Service (DWD) the model is operated in forecast mode. It is started each day of the studying period at 00 UTC with a forecast length of 30 hours. In this way the model state is forced to stay close to the real weather situation. In combination with the high spatial resolution of 1/8° this is an important prerequisite for a model validation in high resolution scales in time and space.

The satellite data used for the comparison with model outputs are a data product of ISCCP (Rossow et al. 1996). The objective of ISCCP is the development of a global cloud climatology from satellite data. The DX data set maintain various cloud properties as cloud cover, cloud water path, cloud optical thickness, cloud top pressure and cloud top temperature. Due to its high horizontal and temporal resolution (30 x 30 km^2 (sampled pixel) and 3 h respectively) as well as the full coverage of the investigation area the data are well suited for a validation of the high resolution model.

3. Results

In general the HRM simulated total cloud cover has larger values than the ISCCP satellite derived total cloud cover. A spatial comparison of mean total cloud cover differences over the whole period from August until October 1995 shows that there are no significant spatial variations. The mean difference between simulated (HRM) minus satellite derived (ISCCP) total cloud cover from August to October 1995 is about 4 %. Temporal comparisons of area means show that the differences increase with time. The spatial comparison of monthly means (August, September, October 1995) shows that this increase with time is only present over land.

In contrast to the total cloud cover the simulated cloud water path has lower values than the satellite derived cloud water path. The mean difference between HRM simulated minus satellite derived (ISCCP) cloud water path from August until October 1995 is about -200 g/m^2. No significant differences between land and water has been recognized.

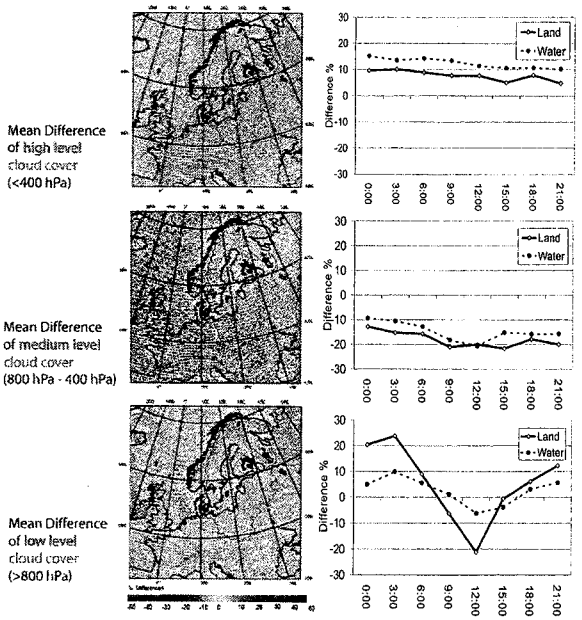

Figure 1: Left: Mean differences (August - October 1995) between simulated and satellite derived cloud cover (HRM minus ISCCP) in the low, medium and high level.
Right: Mean daily variation of differences (area means HRM minus ISCCP, August – October 1995) in the low, medium and high cloud level over land and over water.

In this context the investigation of the vertical cloud structure might be important (Figure 1). The simulated values of high level and low level cloud cover are about 10 % larger than the ISCCP satellite derived cloud cover in these levels. But the simulated cloud cover in the medium level has about 5 % - 25 % smaller values than the satellite derived cloud cover (Figure 1, left).

To identify any structures within the temporal and spatial variations the diurnal cycle of simulated and satellite derived cloud cover has been compared over land and over water separately. Figure 1 (right) shows mean diurnal variations of cloud cover differences (HRM minus ISCCP) in the low, medium and high cloud level. While cloud cover differences in the medium and high level have only small diurnal variations a significant diurnal cycle has been found within the cloud cover differences in the low level over land. This is the result of a significant diurnal cycle of the mean low level cloud cover from ISCCP especially over land which is in contrast to the nearly missing diurnal cycle of HRM simulated low level cloud cover over land. This might be connected with uncertainties within the mass flux convection scheme after Tiedtke (1989). Otherwise there might be also problems within the cloud detection algorithm of ISCCP detecting low clouds over land. However the strong diurnal cycle of low level cloud cover over land detected by ISCCP were also found in other investigations (Crains 1995, Rossow 1999). Validations with other measurements confirm the correctness of these findings.

These results and further investigations will localize weaknesses in the cloud parametrization scheme as basis for improvements in the representation of clouds in the regional atmospheric model HRM.

References

Crains, B. Diurnal variations of cloud from ISCCP data, *Atmospheric Research* No. 37,.133-146, 1995

Rossow, B. and Schiffer, A. Advances in Understanding Clouds from ISCCP. In: Bul. Am. Met. Soc., Vol. 80, No. 11, p.2261-2287, 1999

Rossow, W.B., A.W. Walker, D.E. Beuschel, and M.D. Roiter International Satellite Cloud Climatology Project (ISCCP) - Documentation of New Cloud Datasets. *WMO/TD-No. 737, World Meteorological Organization*, 115 pp. 1996

Ritter, B and J.F. Geleyn A comprehensive radiation scheme for numerical weather prediction models with potential applications in climate simulations, *Mon. Wea. Rev.*, No. 120, 303-325, 1992

Tiedtke, M. A comprehensive mass flux scheme for cumulus parameterization in large-scale models, *Mon. Wea. Rev.*, No. 117, 1779-1800, 1989

Characteristics of the atmospheric surface layer over the Baltic Sea

Antonios Niros, Timo Vihma and Jouko Launiainen

Finnish Institute of Marine Research, P.O. Box 33, FIN-00931 Helsinki, Finland

1. Introduction

The atmospheric boundary layer (ABL) over the Baltic Sea has been studied experimentally mostly on the basis of coastal and archipelago stations and airborne measurements. The influence of the Baltic Sea on the ABL brings a challenge for the modelling community.

The objective of this study is to analyse the data set recorded by the R/V Aranda automatic weather station in the Baltic Sea in from 1991 to 1999. We analyse the wind, temperature and humidity data, and estimate the atmospheric surface layer stratification parameters and turbulent fluxes of sensible and latent heat. The statistics of the observed and calculated quantities are studied with an attention in the seasonal, diurnal and spatial variations, as well as in the interdependency between various quantities.

2. Observations

The *R/V Aranda* has an automatic ship weather station (MILOS 200, Vaisala Co.) with sensors for the wind speed and direction, air temperature, air relative humidity, atmospheric pressure, sea surface temperature, and downwelling solar radiation. The observation height is 19 m for the wind speed and 14 m for the other meteorological quantities. In general, the following type of data are registered: hourly mean value, instantaneous value and the maximum and minimum values during the hour.

The data set from the period of 1991-1999 includes about 50000 hourly mean values of each quantity, and the spatial and seasonal distributions of the observations are shown in Figure 1. For the analyses, the Baltic Sea was divided into 8 sub-basins as shown in Figure 1. During the period from 1991 through 1999, R/V Aranda was in harbour for 46% of the time and outside of the Baltic Sea for 12% of the time, and those data are not included in the analyses. The data sets from the Danish Straits, Åland Sea, Gulf of Riga, and Archipelago Sea were much smaller than those from the larger sub-basins, and are thus not always representative enough. In addition to the direct observations, we calculated turbulent surface fluxes, stratification parameters, and wind gust factor. We further analysed the geostrophic winds.

3. Results

The mean annual cycles of the air and sea surface temperature, temperature difference, air specific humidity, and the saturation specific humidity corresponding to the surface temperature are shown in Figure 2. The monthly means and their standard deviations are shown. All round the year, except late spring and early summer (from May to June), the monthly mean sea surface temperature is higher than the air temperature. The monthly mean surface specific humidity is, on the average, always higher than the air specific humidity.

The standard deviations are in general larger for the air than for surface temperature, but during the later warming period of the sea (in June and July) the standard deviation is larger for the sea surface temperature. This seems to be related to its large basin-scale spatial variability. The same holds for the specific humidity. The air temperature has its largest standard deviation in winter and autumn, while the air specific humidity is most variable during summer and autumn.

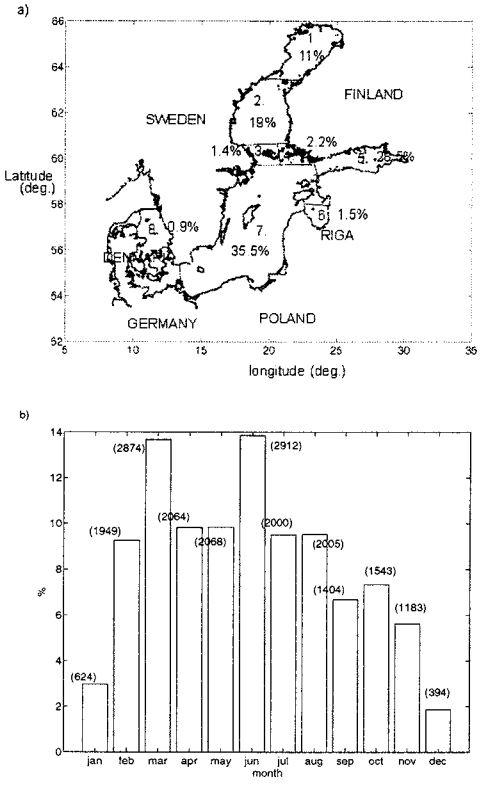

Figure 1: (a) Spatial and (b) seasonal distribution of the R/V Aranda marine meteorological data in the Baltic Sea. The total number of observations (hourly means) for each month from 1991 to 1999 is shown above the bars.

This is partly related to the low saturation humidities in winter. The air temperature has a larger diurnal cycle than the sea surface temperature, and the sensible heat flux and the Bowen ratio also show a clear diurnal cycle, while mean diurnal variation is less evident for the latent heat flux. (Figure 3).

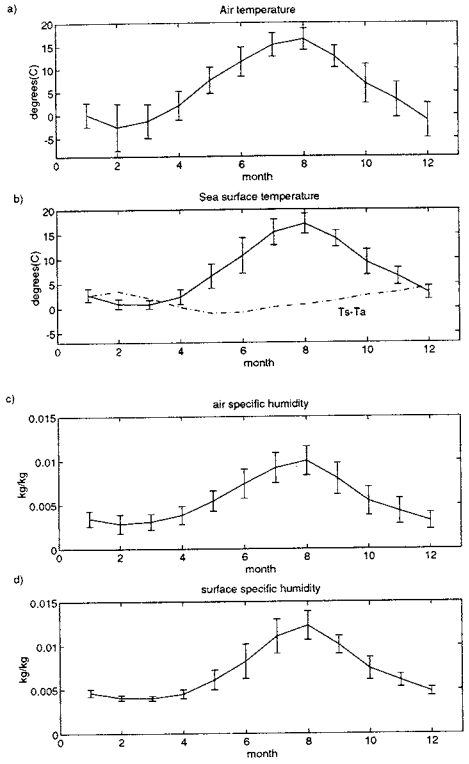

Figure 2: Monthly means and standard deviations of (a) air temperature, (b) sea surface temperature, (c) air specific humidity, and (d) surface specific humidity. The sea surface air temperature difference is added in (b).

In general, the differences between various sub-basins are small or moderate. The shape and morphology of the sub-basin has, however, a distinct effect on the wind direction (Figure 4), as previously found by Launiainen and Laurila (1984).

The air and surface temperature have a high mutual correlation (r= 0.91). The sensible and latent heat fluxes depend more on the air than the surface temperature while the wind effect on fluxes is at its strongest in summer. The gust factor decreases with increasing wind speed and has an apparent relationship with the Richardson number. The maximum wind is linearly related to the mean wind roughly approximated by a gust factor of 1.3.

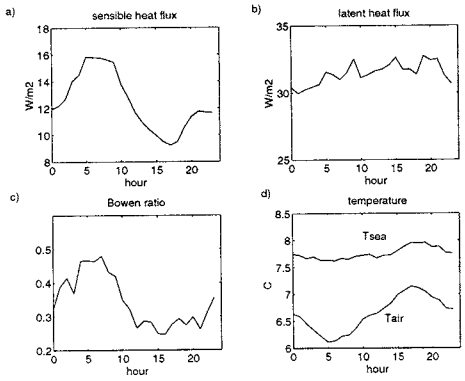

Figure 3: Diurnal cycles of (a) sensible heat flux, (b) latent heat flux, (c) Bowen ratio and (d) air and sea surface temperature.

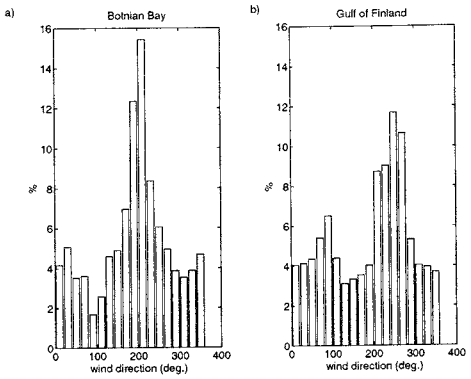

Figure 4: Distribution of wind direction in (a) Botnian Bay and (b) Gulf of Finland.

4. Conclusions

The air temperature, sea surface temperature, air specific humidity, wind speed, and the wind speed variance show a clear annual cycle. The maximum wind speed can be estimated from the mean wind speed by using a linear expression, and the distribution of the mean and maximum wind is well approximated by the Weibull theoretical distribution function. The gust factor decreses with increasing wind speed and is apparently related to the stability. An upward sensible heat flux prevailed in autumn and winter, while the latent heat flux was usually upwards during all seasons. In general, the differences between the various sub-basins were small or moderate. The air-surface temperature difference depends more on the air than the surface temperature.

References

Launiainen, J., T. Laurila. Marine wind characteristics in the Northern Baltic Sea, *Finnish Marine Research*, N:o 250, 52-86, 1984.

Selection of representative stations by means of a cluster analysis for the BAMAR region in the PIDCAP period

Hermann Oesterle

Potsdam Institute for Climate Impact Research (PIK), Telegrafenberg, P.O. Box 601203, 14412 Potsdam, Germany

1. Introduction

It is more advisable to use real data for comparative validation of models with different resolution than grid data from objective analyses. For the purposes of such investigation, it is desirable to have a set of stations which represent all climatic zones of each sub-region. The cluster analysis procedure allows to select representative stations for these zones. Synoptic data were used to identify such stations for the BAMAR region in the PIDCAP period (01.08.1995 - 30.11.1995). Mean values of daily minimum and maximum air temperature and daily precipitation were computed for the PIDCAP period using verified data. Computations were made for stations with data availability of more than 67%.

2. Cluster analysis procedure

A cluster analysis procedure was used as described in Lund (1963) and others such as (Oesterle and Shapovalova (1974), Oesterle and Enke (1994), Werner et al. (2001)). The essence of this analysis is as follows:
For each pair of objects, in our situation for each pair of stations, $\mathbf{X}_m$ and $\mathbf{X}_l$, the difference between the objects is computed according to the formula

$$d(X_m - X_l) = \sum_{i=1}^{n} (X_{mi} - X_{li})$$

where **n** is the objects' dimensionality, $(\mathbf{X}_{mi}-\mathbf{X}_{li})=0$ if the value is not larger than the threshold value $\mathbf{db}_i$, and $(\mathbf{X}_{mi}-\mathbf{X}_{li})=1$ if the value is larger than $\mathbf{db}_i$ which is given for each component describing the vector. Thus we have normalized values for different components of the vector.
As a result, we have a matrix of distances $\mathbf{d}_{ml}$. The algorithm includes a threshold value which describes a hyposphere around each object, and the number of objects which are included in the hyposphere (number of "neighbours") are defined to be the rank. The revised object which has the highest rank is declared to be the standard object for the first cluster. In the next step, the standard object and its "neighbours" will be deleted from the matrix, and the procedure will be repeated for the remaining objects. The procedure will be stopped if it is not possible to find more than 2 "neighbours".
After the selection of standard objects, all other objects are classified according to the minimum-distance to them. This second step is necessary because in the first step any object was included by the previous cluster although they were nearer to other standard objects.
In a next step, the classification will be improved.
Therefore, mean values were computed for each component in each cluster, and all objects are exposed to the classification on the principle of the minimum-distance to these "mean standard objects" or "cluster centroids". Stations with a minimum distance to the cluster centroids were selected as representative stations (standard stations) for each cluster.

3. Classification results

From 1560 stations available, 950 stations were used for which it was possible to compute mean values for the entire time period (see figure 1). Other station had less than 67% of complete data to compute mean values for temperature and precipitation.

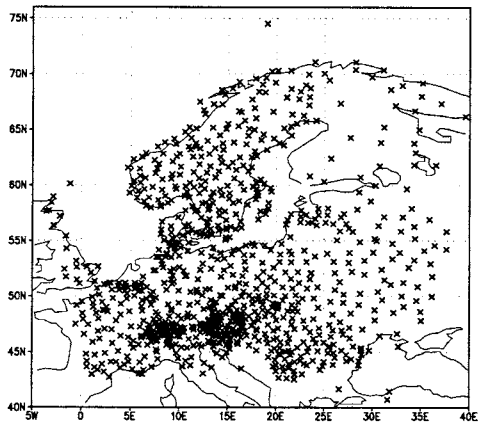

Figure 1: 950 stations (x) with temperature and precipitation data of sufficient quality used in the cluster analysis for the PIDCAP period

These stations were put through classification procedure. The mean values of minimum and maximum air temperature, mean daily precipitation for the time period and latitudes and longitudes of the stations are the parameters that were used to describe the stations. Co-ordinates of the stations were used to select representative stations for each sub-region.
In the experiments, the threshold value $\mathbf{db}_i$ was 2° K for temperature, 1 mm for precipitation and 5° for co-ordinates. First, a classification was done on the basis of temperature only. In this case 21 clusters were selected for all regions. On the basis of temperature and co-ordinates, 57 clusters were selected, and on the basis of temperature, precipitation and co-ordinates, the most complete classification of 83 clusters was obtained (see figure 2).
The highest number of clusters was selected for the mountains (Alps) and coastal-mountains (Norway) regions. In the window 45-50°N and 5-20°O (~Alps) 28 clusters were selected as an example, whereas in its neighbouring, rather flat sub-region between 50-55°N and 5-20°O, only 5 clusters were selected.
In the analysis, the variation of values of the standard stations in the Alpine sub-region is:
- for maximum temperature - from 5.6 °C (WMO-number 6780, elev. 1828 m) to 23.4 °C (WMO-number 16088, elev. 97 m) ;

- for minimum temperature - from 0.8 °C (WMO-number 6780, elev. 1828 m) to 13.7 °C (WMO-number 16088, elev. 97 m);
- for precipitation - from 42 mm/month (WMO-number 16061, elev. 710 m) to 165 mm/month (WMO-number 6702, elev. 1675 m).

In the second sub-region with a less structured orography, these differences are less substantial:

- for maximum temperature - from 16.2 °C (WMO-number 10558, elev. 630 m) to 19.9 °C (WMO-number 12415, elev. 124 m);
- for minimum temperature - from 9.0 °C (WMO-number 12230, elev. 73 m) to 13.7 °C (WMO-number 10113, elev. 13 m);
- for precipitation - from 18 mm/month (WMO-number 12415, elev. 124 m) to 57 mm/month (WMO-number 10558, elev. 630 m).

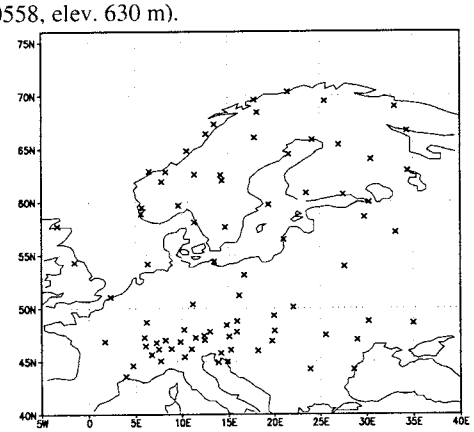

Figure 2: 83 standard stations (x) were selected for the classification using temperature, precipitation and co-ordinates of stations.

4. Conclusion

The approach allows to select stations from a large number of stations which are typical for regions with different meteorological regimes. These stations have basic information available for describing temperature and precipitation fields and can be considered as representative stations used for validation of different models. All these stations were used for validation of the LM-model at PIK.

References

Lund, I.A., Map-pattern classification by statistical methods, *J.Appl.Met.*,Vol. 2, N. 1, 56-65, 1963.

Oesterle, H., Shapovalova, V., Study of some climatological characteristics of precipitation in Central Asia for short-term weather forecasting, *SANIGMI-Report,* N. 11 (92), 54-66, 1974.

Oesterle, H., Enke, W., Zeitreihenanalyse von Temperatur und Niederschlag der letzten 100 Jahre für ausgewählte Stationen in Osteuropa, *PIK-Report*, No.1, 202-203, 1994.

Werner, P.-C., Gerstengarbe, F.-W., Fraedrich, K., Oesterle, H., A climate change signal in the north Atlantic / European sector, *Theoretical and Applied Climatology*, (in press).

A simple parameterization of atmospheric precipitable water vapor in Tallinn, Estonia

Oleg Okulov, Hanno Ohvril and Rigel Kivi

Institute of Environmental Physics, University of Tartu, Ülikooli 18, 50090 Tartu, Estonia

1. Introduction

Knowledge on the amount of water vapor in a unit area vertical column of the atmosphere – atmospheric precipitable water vapor or simply precipitable water W (in cm of liquid water) – is an important input of hydrological, energetic and radiation models.

In this work we have studied the correlation between atmospheric precipitable water and surface-level water vapor pressure in Tallinn, Estonia, during 1999 and 2000. Our aim was to express precipitable water W (cm) in terms of partial pressure of water vapor e (millibars).

2. Database

The Tallinn Aerological Station (59.48 N, 24.60 E; 37 m above sea level) is situated on the western boundary of Tallinn, Estonia. The station has used Vaisala Oy radiosondes RS80 since 1993 and sondes RS90 since March 2000. Sondes are launched at 12 and 24 UTC.

Sounding data for years 1999 and 2000 are accessible for public use in the HTML tabular format at WWW site of the University of Wyoming. Each sounding profile is represented with 15–30 levels up to 9 km. Because we further needed the data on precipitable water for solar radiation modeling, we have used only daytime sounding profiles during 1999–2000 (12:00 UTC = 13:38:24 Local Mean Time in Tallinn).

Each sounding profile actually contains more than 100 levels of measurements up to 22 km. In order to evaluate the applicability of the limited use of sounding levels for the calculation of W (15–30 levels instead of more than 100), we have compared detailed calculations with the limited ones. The average difference was about 2 % (Fig. 1). This uncertainty is comparable to the error of device (Jauhiainen, Antikainen, 1995).

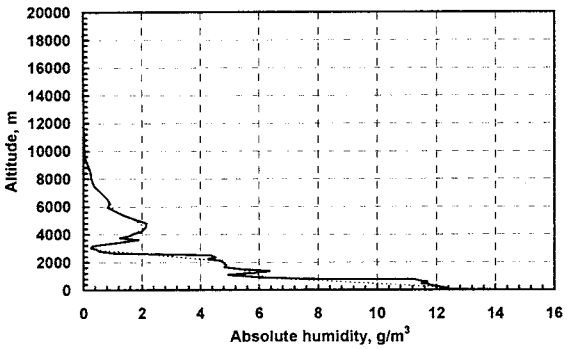

Figure 1: Vertical humidity profiles in Tallinn on July 12, 1999. Solid line corresponds to 113 sounding levels, dotted line to 22 sounding levels.

Analysis of full profiles of humidity for Tallinn showed that 90 % of total humidity is concentrated below 5 km and 95 % below 8.5 km. Last facts justified use of the limited Web dataset instead of full profiles.

The NOAA-14 Environmental Satellites images in AVHRR channel 4 (thermal, from the Web archive of the Dundee Satellite Receiving Station, Dundee University) helped us to select the clear sky conditions about 12 ± 3 UTC.

3. Analysis and results

Figure 2 presents a scatter plot of atmospheric precipitable water W (cm) versus surface partial pressure of water vapor e (millibars) for all available days (clear and cloudy) in Tallinn during 1999–2000.

Minimal values of precipitable water, W ≈ 0.2 cm, correspond to an extremely dry winter atmosphere while a humid summer atmosphere may contain almost 4 cm.

Coefficient of cross-correlation between values of W and partial pressure of water vapor e, r = 0.9, indicates a tense connection between these terms. Beside linear, we have verified, using the least squares method, power, logarithmic, exponential and polynomial approximation of the relation between W and e.

It is also visually evident that the linear approximation presents an acceptable matching of the experimental data (Fig. 2). Equation for the linear regression is:

$$W = 0.147\, e + 0.039. \quad (1)$$

Analysis of this linear regression by the criterion of the Student has shown that the straight line (1) secures statistical significance better than 99 %.

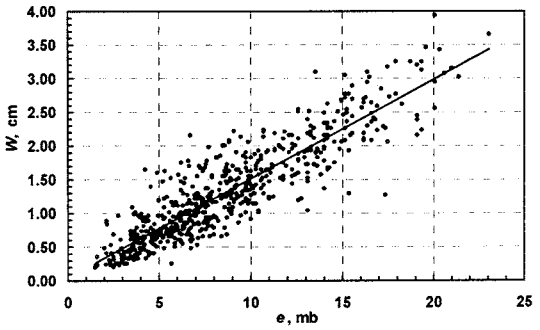

Figure 2: Scatter plot of precipitable water *W* (cm) versus surface partial pressure of water vapor *e* (mb), for all available 12:00 UTC profiles (all clear sky and cloudy sky cases) in Tallinn in 1999–2000.

Sorting clear sky cases (circles on Fig. 3) from the cloudy cases (points on Fig. 3), we obtain two linear regressions:

$$W = 0.1329\, e + 0.019, \quad (2)$$

for clear sky and

$$W = 0.1506\, e + 0.099, \quad (3)$$

for cloudy sky situations.

The values of precipitable water at clear sky conditions are evidently smaller, compared with cloudy sky conditions. In Tallinn during 1999–2000, the average values of W at clear sky, calculated by Eqn (2), form 89 % of the total mean expressed by Eqn (1) and 85 % of the particular mean at cloudy sky expressed by Eqn (3).

These ratios probably depend on the dominant type of a cloud cover, the profile of temperature, synoptic activity, etc. According to *Hoyt* (1978, *Iqbal* 1983), precipitable

water on a cloudless day is 81% of the mean USA conditions (clear + cloudy sky cases).

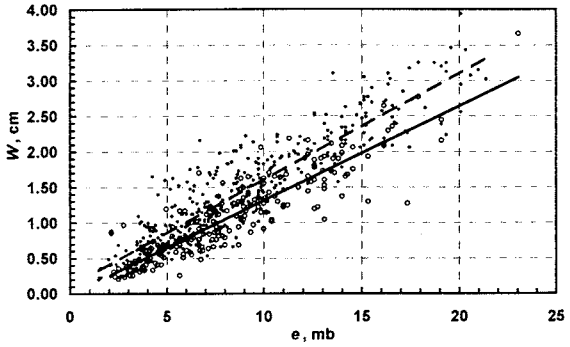

Figure 3: Precipitable water W (cm) versus surface partial pressure of water vapor e (cm) in Tallinn during 1999–2000. Circles and solid line correspond to clear sky profiles, points and dotted line – to cloudy sky profiles.

Figure 4 presents the monthly means of precipitable water W in Tallinn according to all 12 UTC data in 1999–2000. Solid line is calculated directly from radiosondes' data and dotted line – indirectly, using parameterization (1) for each sounding.

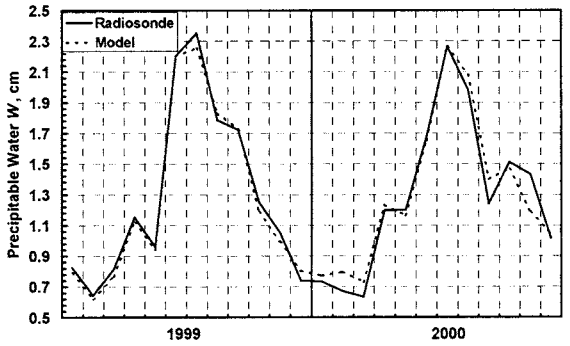

Figure 4: Time series of monthly average precipitable water W in Tallinn 1999–2000 according to all 12 UTC values. Solid line – direct calculations from radiosondes' data, dotted line – indirect calculations from parameterizaton (1).

Maximal differences between the monthly means of precipitable water obtained respectively by direct and indirect method can be found in November 2000 (2.3 mm) and in February 2000 (1.7 mm).

The average difference in the monthly means is only 0.6 mm of liquid water. Consequently, the derived parameterization is adequate to represent interannual variability of precipitable water in Tallinn.

The monthly average of precipitable water varies with season. During cold months (December–March) the atmosphere is the the driest (W < 8 mm). During warm months (June–August) column of precipitable water is higher than 1.7 cm and reaches maximal values of 2.2–2.3 cm values in the warmest month of July. It can be concluded from Fig. 4 that the precipitable water during summer time in Tallinn is about three times as high as during the winter time.

Difference, $\Delta W = 0.43$ cm, between September 1999 and September 2000 indicates the variability of the monthly means in different years.

4. Conclusions

Analysis of more than 600 sounding profiles during 1999–2000 for Tallinn, Estonia, shows that a single value of precipitable water in Tallinn varies from about $W = 0.2$ to 4 cm, and monthly average from about $W = 0.7$ to 2.3 cm.

High correlation between the amount of precipitable water W (cm) and surface water vapor pressure e (millibars) has been revealed.

This high correlation allowed to derive linear regression (1) for the parameterization of precipitable water through surface water vapor pressure.

For the further study of the attenuation of direct solar beam, a parameterization formula (2) for clear sky conditions has been developed.

Acknowledgements

This work was supported by national grant No. 4140 of the Estonian Science Foundation and by international scholarship of the World Federation of Scientists.

The University of Wyoming made initial data for this research accessible.

References

Hoyt, D., V. A model for the calculation of solar global insolation. *Sol. Energy* 21(1), 27–35, 1978

Iqbal, M. An introduction to solar radiation. *Academic Press Canada*, 90–95, 1983

http://www-das.uwyo.edu/upperair/eu.html

http://www.sat.dundee.ac.uk/

Jauhiainen, H., Antikainen, V. Vaisala's new RS90 family of radiosondes, *Vaisala News*, No. 136, 9–12, 1995

Evapotranspiration and transpiration of a forested Upper Volga catchment: field measurements and model simulations

Alexander Oltchev[1], Jan Cermak[2], Alexander Tishenko[3] and Gode Gravenhorst[1]

[1] Institute of Bioclimatology, University of Göttingen D-37077 Göttingen, Germany
[2] Institute of Forest Ecology, Mendel University of Agriculture and Forestry, 61300, Brno, Czech Republic
[3] Twer State University, 170002, Tver, Russia

1. Introduction

The energy and water budgets of a forested Upper Volga's catchment area in Russia were quantified using different experimental and modelling approaches within the frameworks of the "Volgaforest" project (IC15-CT98-0120). The main goals of this project were to evaluate a possible response of the water regime of boreal forest ecosystems at the Volga source area on climatic and land-use changes, and to estimate a possible feedback of water budget changes on forest conditions. The selected catchment area (about 3410 km^2 between 56°20'-57°20'N, 32°00'-33°20'E) of the Upper Volga (flows into the Caspian Sea) is located close to sources of other large European rivers: Dnepr (flows into the Black Sea), Daugava and Neva (flow into the Baltic Sea). The landscape of the Upper Volga area is relatively flat with many small rives, streams, lakes and bogs. Coniferous and mixed coniferous-broadleaf forests cover about 75% of the catchment area.

2. Methods

The experimental site for measurements of the of energy, H_2O- and CO_2-fluxes was selected and established in the mixed forest (represented by spruce, birch, aspen and alder trees) near the small town Peno about 30 km from Volga source and about 20 km from source of Daugava. Field measurements included:

- meteorological measurements of the air and soil temperatures, air humidity, wind speed and wind direction, net radiation, incoming and reflected solar radiation, precipitation rate, soil water content (since December 1999);
- eddy covariance measurements of momentum, sensible heat, H_2O and CO_2 fluxes between the forest canopy and the atmosphere (since July 2000) (*Ibrom et al.*, 1998);
- measurements of forest transpiration (overstorey, understorey) using sap-flow technique (since June 1999) (*Cermak et al.*, 1999);
- Forest inventory.

Results of these field measurements were used:

- to quantify in a long-term perspective the principal components of energy, water and carbon budgets,
- to improve and validate different scale models, and
- to find out what are the important processes controlling the energy and water exchange on ecosystem and tree scales.

In order to describe the land surface – atmosphere interaction and to quantify the spatial and temporal variability of energy and water fluxes, a vertically structured SVAT-Regio model was developed and applied to the Upper Volga catchment area. This model allows to describe vertical energy-, H_2O-, CO_2-exchanges, internal canopy microclimate, water uptake, and partitioning the fluxes within the forest canopy (soil, understorey and overstorey) in local and in regional scales (*Oltchev et al.*, 1996, 1998). As input parameters the SVAT-Regio model uses:

- the mean daily or hourly meteorological data (air temperature, relative humidity, wind speed, precipitation, global solar radiation (cloud amount)) measured at meteorological stations located inside and around the catchment area;
- digital maps of relief, land-use, vegetation and soil;
- biophysical data for different vegetation and soil types.

The modelling procedure consists of three steps. In the first step, the meteorological data from different meteorological stations are interpolated to individual grid cells (assumed to be uniform) to which the entire study area is divided. A dimension of each grid cell can vary from 100m × 100m to 10km × 10km. In the second step, for each grid cell the different output parameters and fluxes (e.g. micro-climatic conditions, energy, H_2O and CO_2 fluxes) are sequentially simulated with a temporal resolution of 1 hour. Model assumes that the land surface and vegetation within each grid cell is spatially uniform, but can be represented by different vegetation forms (tree species). Finally, modelled parameters and fluxes are scaled up to the entire area. Results can be presented in tables, graphs and maps.

3. Results

Results of the field measurements at the established experimental forest site show a large temporal variability of energy and water fluxes. In the diurnal pattern in summer the sensible heat flux usually significantly exceeds the latent heat fluxes. Bowen ratios range during the day usually from 1.2 to 2.2. In rainy days the Bowen ratio is significantly smaller (between 0.6 and 1.1). Daily transpiration decreased when trees suffered partial drought in 1999 and also when they suffered by lack of soil air during the wet year 2000. Broadleaf trees transpired about 10-20% more then coniferous trees during summer months, but naturally did not transpire when they have no foliage in spring and in late autumn, while coniferous species can transpire over the whole year under the demand of sufficient evaporation when the soil is not frozen. Under conditions of high underground water table in poorly aerated soils tree roots evidently suffered by *hypoxia*. Roots of all species cannot grow in deep (mostly wet) soil layers, although some species are more resistant to *hypoxia* (e.g. aspen) and others are more sensitive (e.g. spruce). This must result in decreasing anchoring ability of root systems, thus lowering mechanical stability of forests. In addition, functional stability of trees can also be easily impaired, when root growth and their absorption ability is blocked by lack of oxygen during wet years.

Comparisons of modelled and measured fluxes show that the developed model can adequately describe diurnal, seasonal and annual variability of energy and water exchanges, canopy microclimate, and soil and plant hydrolo-

gy of non-uniform land surface (represented by different vegetation species) in local and regional scales.

Results of numerous modelling experiments show that a spatial variability of energy and water fluxes is mainly influenced by local hydro-meteorological conditions (e.g. air temperature, solar radiation, precipitation, soil water content) and depend also on relief, land surface and vegetation properties. Minimal spatial variability of evapotranspiration (up to ±10%) was observed for rainy days and maximal (up to ±40%) for days with sunny and dry weather conditions. Relief, land surface and vegetation generally influenced energy and water budgets via land surface properties to absorb and reflect solar radiation and via natural variability of physiological properties of different vegetation types to transport water from the soil through the plants into the atmosphere.

The contribution of understorey vegetation and soil surface evaporation to total forest evapotranspiration reaches maximum in the early spring. During the summer it does generally not exceed 10% (maximum about 30% for sparse mixed forest canopy) of the total forest evapotranspiration. It generally depends on tree density, tree species composition and soil moisture conditions.

In order to estimate the dependence of regional evapotranspiration on spatial resolution of model grid cells several modelling estimations with the SVAT-Regio model of the evapotranspiration and transpiration were made for summer periods from 1994 to 1999. For model experiments a different spatial model resolution (gradually decreasing from maximal grid resolution 200 m × 200 m to minimal - 10 km × 10 km) was used. For each grid cell the hourly, daily and monthly values of different components of energy, water and carbon budgets were estimated.

Modelling results show that decreasing the spatial grid resolution of the model (from 500m × 500m to - 10km × 10km) results in significant changes of daily and hourly evapotranspiration (up to 24%) and in an insignificant decrease (up to 6%) of the monthly and total summer evapotranspiration rates. The sensitivity of such evapotranspiration changes increases gradually while decreasing the size of considered catchment area and depends on depends on relief heterogeneity and actual composition of different vegetation and soil types.

As it was already emphasised the "Volgaforest" project was focused on investigation only of the Upper Volga catchment. The relief, hydrography, vegetation and soils of selected catchment are rather typical and representative for all areas of Valday Hills. So, it can be expected that the response functions of water flows on environmental changes at the Upper Volga area can have similar features and can be representatively used for the neighbouring catchments (such as Daugava, Neva and Dnepr) also beginning at Valday Hills.

This project was supported by the European Commission within the framework of the INCO-COPERNICUS research program (Grant IC15-CT98-0120)

References

Cermak, J., E. Cienciala, J. Kucera, A. Lindroth, E. Bednarova, Individual variation of sap flow rate in large pine and spruce trees and stand transpiration: A pilot study at the central Nopex site. *Journal of Hydrology*, No.168, 17-27, 1995

Ibrom, A., C. Schütz, T. Tworek, K. Morgenstern, A. Oltchev, M. Falk, J. Constantin, G. Gravenhorst, Eddy-correlation measurements of fluxes of CO_2 and H_2O above a spruce forest. *Journal Physics and Chemistry of the Earth*, Vol. 21 (5-6), 409-414, 1996

Oltchev, A., J. Constantin, G. Gravenhorst, A. Ibrom, J. Heimann, J. Schmidt, M. Falk, K. Morgenstern, I. Richter, N. Vygodskaya, Application of a Six-Layer SVAT model for simulation of evapotranspiration and water uptake in a spruce forest. *Journal Physics and Chemistry of the Earth*, Vol. 21 (3), 195-199, 1996

Oltchev, A., A. Ibrom, H. Kreilein, G. Gravenhorst, Evaluation of the response of a spruce forest on climatic changes: results of modelling experiments. *Journal Physics and Chemistry of the Earth*, Vol. 24 (1-2), 103-110, 1999

The role of the large gulfs of the Baltic Sea in the water and heat cycling

Anders Omstedt[1,2], Lars Axell[2] and Anna Rutgersson[2]

[1] Department of Oceanography, Earth Science Centre, SE-40530 Göteborg, Sweden.
[2] SMHI, SE-601 76 Norrköping, Sweden.

1. Introduction

Most of the river runoff and net precipitation to the Baltic Sea is supplied to the large gulfs (Gulf of Bothnia, Gulf of Finland and Gulf of Riga). They also represent sea areas that are strongly influenced by sea ice. The freshwater input to the gulfs is mixed with seawater and enters the Baltic proper as low-saline surface water. The deepwater renewal takes place through sinking surface water from the Baltic proper entering the gulfs as dense bottom currents. The river runoff, the atmosphere-ocean interaction, the vertical and frontal mixing, and the strait flow exchange between the different sub-basins mainly control the water and heat cycling within the Baltic Sea. The aim of the present presentation is to discuss the role of the large Gulfs in the water and heat cycling by using Baltic Sea modeling.

2. Baltic Sea model, forcing and validation

The Baltic Sea model used is the PROBE-Baltic model (*Omstedt and Nyberg*, 1996), forced by observed river-runoff and gridded meteorological data. Observed vertical profiles of temperature, salinity and maximum seasonal ice extent data are the main sources in the validation (*Omstedt and Axell*, 1998, 2001). However, also observed turbulent atmosphere-ocean fluxes as well as precipitation have been investigated (*Rutgersson et al.*, 2001a,b).

3. Water cycle

The in- and outflows, river runoff, and net precipitation mainly control the water balance of the Baltic Sea and the large gulfs. The different components, based upon observed and 18 years modeled data (1981-1998), are listed in Table 1. As can be noticed in the table the largest fluxes are associated with the in- and outflows. By comparing the freshwater inflow to the large gulfs with that of the total Baltic Sea we can estimate that about 80% of the total river runoff and 85% of the net precipitation enter the large gulfs, which thus represents the major source of fresh water to the Baltic Sea.

Table 1: Mean water balance for the Baltic Sea (the Belt Sea and the Kattegat excluded) averaged over an 18-year period. The Archipelago and the Åland Sea are included in the Bothnian Sea calculations. Unit 10^3 m^3 s^{-1}. The flows are denoted by: River runoff ($\mathbf{Q_f}$), net precipitation (**P-E**), inflow ($\mathbf{Q_{in}}$), outflow ($\mathbf{Q_{out}}$) and **Storage change**.

Sea area	Q_f	P - E	Q_{in}	Q_{out}	Storage change
Baltic Sea	15.12	1.53	39.96	57.08	-0.47
Bothnian Bay	3.46	0.29	12.80	16.60	-0.05
Gulf of Bothnia	6.72	0.97	61.98	69.79	-0.12
Gulf of Finland	3.84	0.25	11.85	15.98	-0.04
Gulf of Riga	1.20	0.09	4.80	6.12	-0.03

4. Heat cycle

The heat transports through the straits can be calculated by considering the closure heat equation for the different sub-basins (*Omstedt and Rutgersson*, 2000, *Omstedt et al., 1997*). In Table 2, the long-term mean values of the fluxes for an 18-year period (1981-1998) are given. The main balance is between sun radiation to the open sea surface and the sum of sensible and latent heat fluxes and net long wave radiation. The heat-flux from water to ice also plays an important role. On the average, the Baltic Sea and the Bothnian Sea gain heat, whereas the Bothnian Bay, Gulf of Finland and Gulf of Riga loose heat to the atmosphere. The heat loss to the atmosphere in the Bothnian Bay needs to be compensated by the heat transport through the Northern Quark Strait and equal to 6 Wm^{-2}. Meanwhile, the Bothnian Sea gains 3 Wm^{-2} over an area of about twice the Bothnian Bay. Hence, the heat loss in the Bothnian Bay can be compensated through advection from the Bothnian Sea. The calculation also indicates that both the Gulf of Finland and Gulf of Riga need to import heat from the Baltic proper. However, the whole Baltic Sea water body is in almost balance with the atmosphere and the net heat exchange through the Baltic entrance area is small.

Table 2: Mean heat balance of the Baltic Sea (the Belt Sea and the Kattegat excluded) averaged over an 18-year period. The fluxes are positive when going from the water to the atmosphere. Unit: Wm^{-2}.The fluxes are denoted as: Sensible heat (F_h), latent heat (F_e), net long-wave radiation (F_l), sun radiation to the open water surface (F_{so}), sun radiation through ice (F_{si}), heat flow from water to ice (F_{wi}) and net heat loss $F_{loss}=(1-A_i)((F_{so}+F_h+F_e+F_l)+ A_i(F_{si}+ F_{wi})$.

Sea area	F_h	F_e	F_l	F_{so}	F_{wi}	F_{si}	F_{loss}
Baltic Sea	9	37	37	-88	4	-0	-1
Bothnian Sea	5	24	32	-74	10	-0	-3
Bothnian Bay	10	25	30	-66	7	-0	6
Gulf of Finland	12	31	32	-77	5	-0	3
Gulf of Riga	11	40	36	-87	2	-0	2

5. Discussion

From the previous sections it is clear that the large gulfs of the Baltic Sea play a major role in the water and heat cycling. These sub-basins are also the least investigated areas in the Baltic Sea with strong influence from surrounding land area. The uncertainties in estimating the individual terms in the water and heat cycling are probably quite large. Several processes are purely resolved or parameterized. In the meteorological forcing of ocean and hydrological models, synoptic station values without horizontal interpolations or coarse meteorological gridded databases or model re-analysis with coarse resolution are often used (SMHI 1^0x1^0, ERA, NCEP). These databases do not resolve the geometry of the Baltic Sea in a proper manner and the data are often too much influenced by land. The development of re-analyzed meteorological data sets with high horizontal resolution (at least 22 km) has begun within the BALTEX/Bridge experiment. Still only short periods are available but in the future high-resolution meteorological data will become important information for the understanding of water and heat cycling in the region.
Also a deeper understanding of the dynamics and modeling of many different processes are still needed, such as wind and wave interaction, precipitation and evaporation over the Baltic Sea, up- and downwelling, frontal and vertical mixing, as well as heat fluxes over sea ice. All these aspects are important research areas within BALTEX.

6. Conclusions

The introduction of ocean modeling into the BALTEX research has considerably improved our possibilities to analyze the water and heat cycling. In this presentation we focus on the role of the large gulfs (the Gulf of Bothnia, Finland and Riga) in the water and heat cycling. The main conclusions are:

- The large gulfs of the Baltic Sea receive the major input of river runoff and net precipitation to the Baltic Sea. This fresh water is mixed in the large gulfs and enters the Baltic proper as baroclinically controlled currents.
- The Baltic Sea is almost in local thermodynamic balance with the atmosphere but redistribute heat within its sub-basins. The Bothnian Bay, Gulf of Finland and Gulf of Riga loose heat, while the Bothnian Sea gain heat calculated as long-term means.

References

Omstedt, A. and L., Axell (1998). Modeling the seasonal, inter annual and long-term variations of salinity and temperature in the Baltic proper. Tellus, 50A, 637-652.

Omstedt, A. and L.B., Axell, 2001. Modeling the variations of Salinity and Temperature in the Large Gulfs of the Baltic Sea. Submitted.

Omstedt, A. and A., Rutgersson (2000). Closing the water and heat cycles of the Baltic Sea. Meteorol. Z., 9, 57-64.

Omstedt, A. and L., Nyberg (1996). Response of Baltic Sea ice to seasonal, inter annual forcing and to climate change. Tellus, 48 A, No. 5, 644-662

Omstedt, A., Meuller, L., and L., Nyberg (1997). Inter-annual, seasonal and regional variations of precipitation and evaporation over the Baltic Sea. Ambio, 26, No. 8, 484-492

Rutgersson, A., Smedman, A.-S., and A., Omstedt (2001). Measured and simulated latent and sensible heat fluxes at two marine sites in the Baltic Sea. Boundary Layer Meteorology, in press.

Rutgersson, A., Bumke, K., Clemens, M., Foltescu, V., Michelson, D., and A., Omstedt (2001). Precipitation estimates over the Baltic Sea: present state of the art. Submitted to Nordic Hydrology.

Characteristic of marine aerosol over the beach

Tomasz Petelski and Maria Chomka

Polish Academy of Sciences, Institute of Oceanology, Powstancow Warszawy 55, 81-712 Sopot, Poland,
e-mail: petelski@iopan.gda.pl

1. Introduction

The sea aerosol effects nearly every physical process taking place in the atmospheric marine boundary layer *(Garbalewski 1999)*, therefore there is a strong connection between beach ecology and the sea aerosol. As transport of sea aerosols considerably affect the magnitude of heat fluxes *(Petelski 1996)* and also humidity fluxes *(Petelski and Chomka 1996)*, it plays an important role in creating the beach microclimate. The sea aerosol fluxes equally affect the beach environment through transport of pollutants. Therefore the aerosol fluxes are a very efficient mechanism of transfer of any pollutants from the sea to the atmosphere and further to the land. Data regarding concentration and special distribution of sea salt in the air over the beach are presented in the paper.

2. Results

The data were collected during two cycles of experiments, namely BAEX and TABEX. The presented findings refer to the sea salt, which is the best tracer, of the size of 1 to10μm, which corresponds to sea aerosol droplets of the size of 4 to 40 μm. Vertical profiles of sea salt concentration in the air over the beach are disscused. For all the profiles the maximum concentration of sea salt is at the height of 3m. This maximum occurs probably as a result of the transformation of the boundary layer characteristic in the coastal zone of the sea *(Panin et al. 1994)*. The aerosol gradient above that maximum is characteristic for the breaker zone. Its big values testify the intensive emission from the coastal zone, which was proved on the grounds of aerosol balance calculations over that zone *(Petelski and Chomka 1996)*. Advection fluxes calculated for those profiles take values from 50μg/m^{2}s to 600 μg/m^{2}s. The maximum values of the flux occur at the height of 3 m and reach 700 μg/m^{2}s, that is around 80 g/m^{2}s of sea water. This massive transport is carried mainly by the droplets in the size range 8 to 20 μm. The high concentration of the sea salt appears as far as 22 m from the seashore. Further at the distance 22 m ÷ 32 m from the seashore there is a considerable gradient of the level of the sea salt concentration. Further from the seashore the decrease of the concentration is much lower. At 82 m from the shore the concentration is several times smaller. The concentration also decreases: on the shore the concentration ranges from 6 to 40 μg/m^3 but at the distance of 82 m the value of concentration ranges from 1.5 to 4 μg/m^3. This is because big particles of the sea salt fall out. A change in size distribution related to the distance from the sea is observed too. No salt particles bigger than 10 μm were observed beyond 82 m from the shore. The measurements presented indicate massive transport of the sea aerosol over the beach, even during moderate winds it reaches 250μg/m^{2}s. The greatest amounts of the aerosol are transported at the height of about 3m above the sea level where the advection flux reaches 700 μg/m^{2}s.

The zone of intensive falling out of the aerosol is as wide as about 30m over the land, and particles smaller than 10μm are carried further over the land.

The findings on aerosol mass transfer can be useful when determining the pollutants' transfer from the sea to the shore. The structure of the boundary level over the beach is not well known yet. Our findings should be supported by a greater number of measurements. A rather modest equipment did not allow to carry out simultaneous measurements of vertical gradients of aerosol at different distances from the seashore. Further investigations of the structure of the boundary layer in the coastal zone are planned.

References

Chomka M., T. Petelski, 1997, Modelling of the sea aerosol emission by the coastal zone. *Oceanologia*, no. 39 (3), 211-225.

Garbalewski Cz., 1999, Fizyka Aerozolowej Aktywności Morza. I.O.PAN Rozprawy i monografie 12 pp.203.

Monahan E.C., 1968, Sea spray as a function of low elevation wind speed. *J. Geophys. Res.* 73, 1127-1137.

Panin G.N., A. Raabe, S. V. Krivitskii, A.Yu. Benilov and S. Marinov, 1994, Small-scale interaction between a water body and the atmosphere in the shore zone. *Water Resources*, Vol.21, no1, 54-62.

Petelski T., 1996, Emission of Sea Sprays and Heat Exchange between the Sea and Atmosphere, *Water Resources* Vol.23 No 2 , 145-148.

Petelski T., M. Chomka, 1996a, Marine aerosol fluxes in the coastal zone - BAEX experimental data. *Oceanologia*, 38 (4), 469-484.

Petelski T., M. Chomka, 1996, The role of sea spray emission in the mass exchange in the coastal zone, *Atmospheric Physics*, 18, No 1, 35-39.

Petelski T., M. Chomka, 2000, Sea salt emission from the coastal zone, *Oceanologia*, 42 (4), 399-410.

DIAMIX: Pycnocline-slope interaction and mesoscale structures observed in Polish DIAMIX data.

Jan Piechura, Agnieszka Beszczyńska-Möller and Robert Osiński

Institute of Oceanology PAS, Powst. Warszawy 55, 81-712 Sopot, Poland, e-mail: piechura@iopan.gda.pl

During winter 1999 and summer 2000 DIAMIX's experiments high resolution measurements of tempera-ture and salinity on the north-western slope of the Gotland Deep were made. Towed CTD probe was used and vertical TS record was made every 100-200 meters. Vertical profiles of currents with the ship-mounted ADCP were recorded at the same time.

Numerous cases of wave-like disturbances of thermocline with 10-20 km in length and about 10 m amplitude were observed during winter experiment. Disturbance of the main flow along the slope by mesoscale structure were recorded as well.

The eddy-like structure was nearly symmetric and was about 15 km in diameter and reached down to 140 m depth; it moved in SSW direction with speed about 4-5 cm/s. Other smaller eddies were observed as well. Bottom topography is considered as the most probably cause of flow instability and eddies.

Summer experiment data show strong coastal upwelling, caused by south-western winds during 3 days before experiment. Isotherms at the seasonal thermocline arose over 20 m climbing on the slope and salinity distribution revealed upwelling as well.

Processes in the contact zone of thermocline/halocline and bottom slope are also discussed.

HIRLAM verification over the Baltic Sea

Roberta Pirazzini[1], Timo Vihma[1], Jouko Launiainen[1] and Priit Tisler[2]

[1] Finnish Institute of Marine Research, P.O. Box 33, FIN-00931 Helsinki, Finland
[2] Finnish Meteorological Institute, P.O. Box 503, FIN-00101 Helsinki, Finland

1. Introduction

The operational atmospheric model HIRLAM serves at the basis for weather forecasts in several European countries. In this study, the accuracy and quality of the HIRLAM analyses and forecasts has been verified over the sea ice and open Baltic Sea far from the coasts. The verification is mostly based on rawinsonde sounding data that were not assimilated into HIRLAM. In addition to that data, weather mast data from an ice station, as well as ship weather station data were used in the comparison. The objective of the comparisons was, in particular, to study the applicability and accuracy of HIRLAM data as a forcing for marine models.

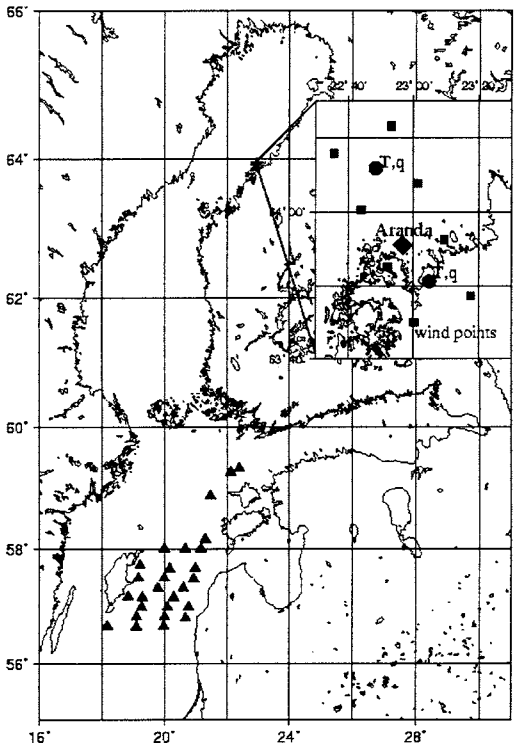

Figure 1: Location of R/V Aranda at the time of the radiosounding launching in March 1999 (star) and October 1999 (triangles). On the right, the area of March location has been zoomed to show the HIRLAM grid points used in the comparison: circles are the wind grid points, squares the mass grid points, and the diamond is the position of R/V Aranda.

2. Model and Observations

The analyses and 6 h and 48 h forecasts of the HIRLAM version 4.6.2, implemented into operational use at the Finnish Meteorological Institute in autumn 1999, were compared with R/V Aranda observations. The comparisons were made for two regions (Figure 1) and periods: over sea ice close to Kokkola, from 18 to 26 March, 1999, and in the Baltic Proper east and north-east of Gotland, from 11 to 18 October, 1999. The 48 h forecasts were available only for the October comparisons. The data of the fine mesh suite runs of HIRLAM 4.6.2 with horizontal resolution of 0.2 degrees were used. For the winter comparisons over the sea ice, the HIRLAM values were taken from the grid points over land and sea nearest to the R/V Aranda location (63.97 N, 22.95 E). The distance from the ship position to the land grid point was 17.6 km, and to the sea grid point 24.5 km. The wind speed and direction were calculated to the mass grid points. During the autumn comparisons over the open sea, R/V Aranda was cruising in the Baltic Proper (Figure 1). The HIRLAM values were quadratically interpolated to the ship location. For comparison, HIRLAM values were also taken from the nearest grid point (the grid point and the distance from the ship varied). There were no sighificant differences between the interpolated and nearest grid point values.
In comparing the results, the time-averaged vertical profiles were calculated using the geopotential height as a vertical coordinate, and the lowest 3 km were studied.

3. Comparison Over Sea Ice in March

In March 1999, the verification of HIRLAM was based on measurements in a coastal sea-ice zone. The most interesting results were that the minimum 2 m and surface temperature, occurring at night and associated with surface-based inversions, were delayed and too weak in HIRLAM (Figure 2).

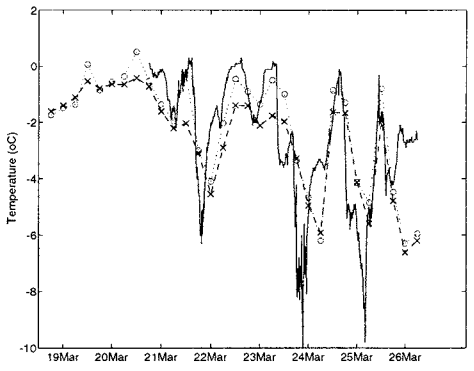

Figure 2: Time series of temperature at 2 m: mast temperature (continuous line), and HIRLAM temperature over land (circles with dotted line) and sea (x-mark with dashed line).

Secondly, the boundary layer in HIRLAM was too moist before the occurrence of the coldest night temperatures. This may have too much reduced the longwave cooling of the surface in the model. Since a good agreement was found between the HIRLAM cloud detection and the visual cloud observations, a possible cause for the HIRLAM underestimation of the surface inversion could arise from HIRLAM problems in the turbulence flux parameterization in very stable conditions. On the other

hand, other possible sources of errors could be in the HIRLAM radiation transfer algorithm in cloud free atmosphere, or in the determination of the HIRLAM boundary conditions (i.e. sea ice and snow temperatures). More work should be done in order to verify these various possibilities.

The wind speed and direction were described well in the HIRLAM analyses and 6 h forecasts. In general, in all considered comparisons there was not much difference between the values obtained for the nearest land and sea grid points. This is partly due to the small thermal differences between the snow-covered land and frozen sea.

4. Comparison Over Open Sea in October

In October 1999, the verification was based on measurements in the open sea mostly far from the coasts. It was observed that the lowest 1 km was too humid in HIRLAM (Figure 3) and that the wind speeds were mostly 1 to 2 m s^{-1} too low, except in the lowermost 100 m, where they were too high (Figure 4).

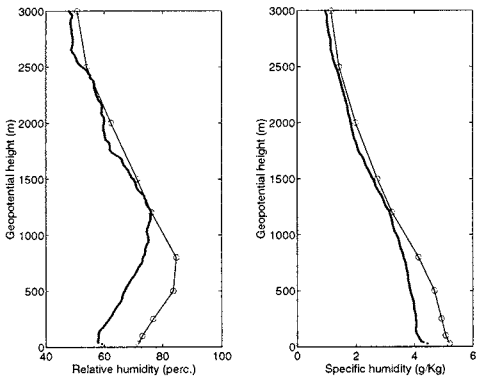

Figure 3: Mean humidity profiles from radiosounding data (continuous line) and HIRLAM analyses (circles).

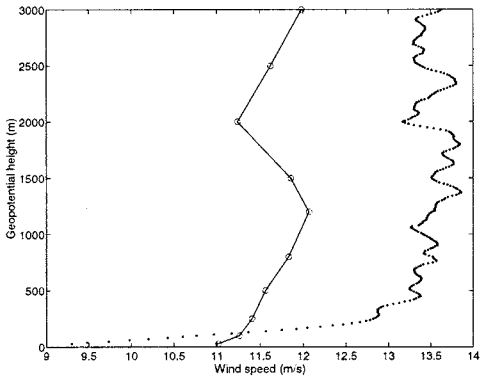

Figure 4: Mean wind speed profiles from radiosounding data (points) and HIRLAM 48 hours forecasts (circles).

The mean temperature profiles were accurate within 0.5 K. With respect to the vertical profiles of wind, air temperature and humidity, the analyses and 6 and 48 h forecasts were almost equally good. The HIRLAM 6 and 48 hours forecast fluxes of sensible and latent heat were compared with the surface fluxes calculated from the ship weather station data applying the bulk-method. Because of the different observation heights of the wind speed (19 m) and air temperature and humidity (14 m), an iterative flux-profile scheme was applied (*Launiainen and Vihma*, 1990). The comparison showed a rather low correlation between the HIRLAM values and the observations. The HIRLAM fluxes were strongly affected by the surface temperature used in the model, and that differed from the observed one, in particular in the 48 hours forecasts (Figure 5). These results point out the importance to get reliable sea surface temperatures into HIRLAM, in order to obtain a realistic prediction of the air-sea interaction and the atmospheric boundary layer processes.

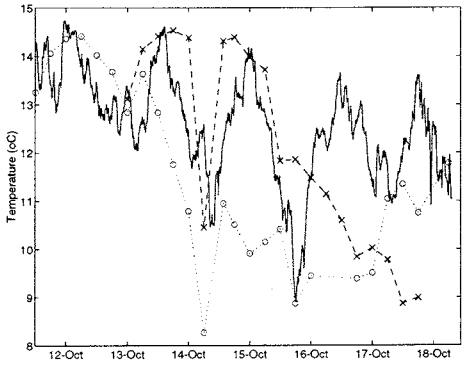

Figure 5: Time series of sea surface temperature from Aranda weather station (continuous line), HIRLAM 6 h forecast (circles with dotted line) and HIRLAM 48 h forecast (x-mark with dashed line).

5. Conclusions

The value of this HIRLAM verification is related to the following points of view: (1) the data are obtained from sea ice and open ocean, where no regular observations exist, (2) detailed vertical profiles were available, not only data from the standard pressure levels, and (3) the data were independent, not assimilated to HIRLAM.

In general, the HIRLAM temperature profiles agreed well with the observations. The largest discrepancies between the model and the data concerned the surface temperature in cases of strong surface inversion over the sea-ice, and the humidity and wind profiles in the lowest kilometer of the atmosphere above the open sea. In addition to that, the sea surface temperature introduced in the model as a boundary parameter often differed from the observations causing errors in the latent and sensible heat fluxes. The results obtained from this study indicate that further work with coupled air-ice and air-sea models is relevant in order to study the problems that the HIRLAM model showed in the present comparisons.

References

Launiainen, J. and T. Vihma, Derivation of turbulent surface fluxes – an iterative flux-profile method allowing arbitrary observing heights. *Environmental Software*, 5, 113-124, 1990.

Circulation weather types and their influence on the meteorological regime in Estonia

Piia Post, Janno Tuulik and Valdur Truija

University of Tartu, Department of Environmantal Physics, Ülikooli 18, 51014 Tartu, Estonia

1. Introduction

An objective classification scheme of the atmospheric circulation is presented for the time period 1968-1997, where daily circulation is described through the strenght, direction and vorticity of the geostrophic flow at the sea level and at higher isobaric levels. The synoptic characteristics during the basic circulation types are discussed as well as the amount of precipitation and daily temperature associated with each type.

The analysis revealed that the most common circulation types in the new classification are anticyclonic (A) and cyclonic (C), that are good in relationship with the meteorological parameters. The variability of daily temperature and precipitation inside the precipitation types is high. Therefore the ways were searched to reduce it.

2. The classification of weather types

The scheme of *Jenkinson and Collison* (1977) has been introduced for the Baltic Sea area. From daily mean sea level pressure data on a 5° latitude and 10° longitude grid the following air flow indices are derived: (1) the direction of the flow; (2) the strength of the flow and (3) the total shear vorticity. The latter is the measure of the rotation of the atmosphere and is positive, if there is a low pressure area (cyclone) and negative for a high pressure area (anticyclone). The values of these three indices determine the weather type of the considered day. There are 27 types: anticyclonic (A), cyclonic (C), 8 directional types, 16 hybrid types and one type denoted as undefined (U). We have modified this Jenkinson classification for the grid, what is centered at 60 N, 22.5E. The scheme was used for the sea level pressures, but also for the 500 hPa geopotentional heights from NCEP/NCAR daily Reanalysis for the period 1968-1997.

Table 1: The occurrence frequencies of circulation weather types (in per cent) for sea level and 500 hPa level (in parenthesis) during time period 1968-1997.

Synoptic types			
A	C	U	
19.3 (17.5)	14.6 (15.1)	0.7 (0.4)	
Directional types			
N	O	S	W
4.5 (4.3)	2.3 (0.6)	5.5 (3.6)	7.9 (11.3)
NO	SO	SW	NW
2.7 (1.1)	2.4 (0.9)	8.7 (9.5)	5.6 (9.5)
Hybrid types			
AN	AO	AS	AW
1.6 (1.4)	1.1 (0.3)	1.9 (1.3)	2.7 (3.8)
CN	CO	CS	CW
1.5 (1.3)	0.8 (0.3)	1.4 (1.3)	2.5 (3.3)
ANO	ASO	ASW	ANW
1.3 (0.4)	1.3 (0.3)	2.7 (2.7)	1.9 (3.6)
CNO	CSO	CSW	CNW
1.0 (0.4)	0.6 (0.3)	2.4 (2.8)	1.4 (2.9)

The occurrence frequencies of weather types for both levels are presented in Table 1. The classification

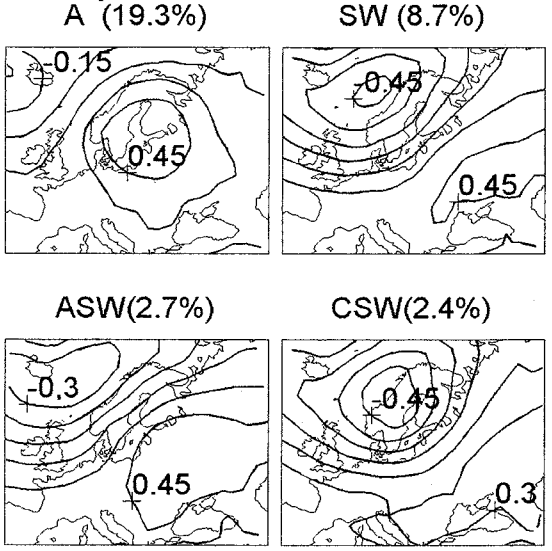

Figure 1: Mean sea level pressures for some weather types from daily values for 1968-1997. To reduce the influence of very high and low pressures, the fields are normalized: to the highest value of the region is assigned 1 and to the lowest −1, therefore are the units relative. The highest and lowest pressure areas are marked with a "+" and the isolines are drawn after every 0.15.

supports the fact that at the 500 hPa level the western flow is stronger than at the sea level. The thresholds to distinguish between directional, hybrid and synoptic types are chosen on the basis of standard deviation of air flow indices for both levels.

In Figure 1 some examples of the fields of sea level normalized air pressure for classified types are presented. In the case of synoptic types the anticyclone (A) or cyclone (C) sits in the middle of the area. In case of directional types the air flow is determined by the pair of cyclone and anticyclone (SW in the Figure 1). At the time of hybrid types the air pressure distribution is similar to the respective directional one, only the very center of the region is more influenced by the anticyclone (ASW) or cyclone (CSW).

3. The influence of weather types to the daily temperature and precipitation

To investigate the influence of atmospheric circulation to the meteorological regime daily average temperatures, precipitation sums and the proportion of rainy days (precipitation occurrence) were calculated for Pärnu for the distinct weather types over the period 1968-1997. Pärnu (58.37 N, 24.50 E) is situated at the eastern coast of the Baltic Sea. To understand the capability of the classification to describe the variability of the local

(Pärnu) temperature and precipitation, the dispersion analysis could be used. We have calculated the mean-squared-error skill scores (*Buishand and Brandsma*, 1997). what show how much of the variability of the

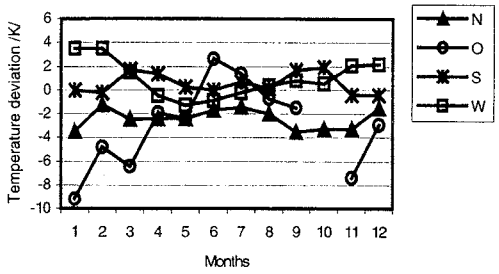

Figure 2: Annual cycles of daily temperature in Pärnu for directional weather types at the 500 hPa level: N-north, O-east, S-south, W-west. There has been no eastern type during Octobers during the period 1968-1997.

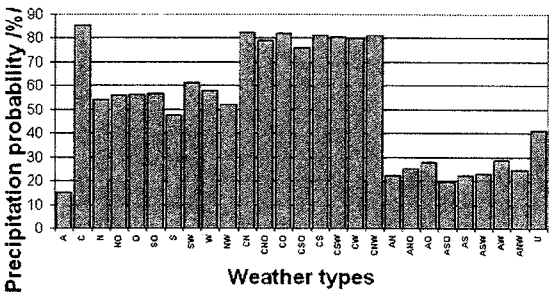

Figure 3: Daily precipitation occurrence probabilities (per cent) in Pärnu for different weather types 1968-1997.

temperature and precipitation is determined by the changing of weather types. The skill score gives the proportion of explained variance and is the square of the multiple correlation coefficient. The magnitude of the skill score is determined by the squared deviations of the individual values from monthly averages. In Table 2 are introduced the seasonal mean and the annual skill scores. Temperature is described better by the 500 hPa classification and precipitation by the sea level one. The reason is intuitively understandable. A daily temperature of the local area is directly connected with large-scale air masses, which motions are more correlated with 500 hPa

Table 2: Mean-squared-error skill scores (per cent) for the predicted daily values in the verification period (1968-1997) in Pärnu for both classifications: SLP (sea level pressure) and 500 hPa geopotentials one.

Parameter	Temperature		Precipitation amount		Precipitation occurence	
Classifi-cation	SLP	500 hPa	SLP	500 hPa	SLP	500 hPa
Winter	29.3	17.1	28.5	18.0	26.2	22.0
Spring	15.9	33.9	22.3	15.8	29.6	26.6
Summer	17.1	46.4	17.2	13.6	28.3	28.5
Autumn	23.2	22.1	27.7	18.6	31.1	30.1
Year	21.3	30.0	23.9	16.5	28.8	26.8

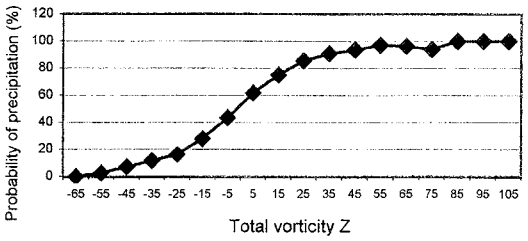

Figure 4: Dependence of the precipitation occurrence in Pärnu on the total shear vorticity Z for all days during the time period 1968-1997. Each unit of Z is equivalent to 0.004 times the Coriolis parameter at 60°N.

than SLP geostrophic wind fields (due to friction close to heterogeneous surface). Precipitation processes otherwise, are more related with surface conditions.

Figure 2. shows that four main directional types (N, S, W, O) have clear annual cycles of the temperature deviation. This is valid also for the cyclonic and anticyclonic type. But at the time of hybrid types the annual cycle depends more if the directional and the synoptic type have the annual cycle in the same phase or not. It means that the variability of temperature depends on the vorticity and also of the direction of the flow. From Figure 3 could be seen that the precipitation probability is well correlated to the vorticity of the weather type. Cyclonic types give precipitation more frequently than the anticyclonic ones. There is also analysed a relation between total shear vorticity and precipitation probability independently of weather types (Figure 4), which is symmetric and convinces well average behaviour of cyclonicity.

4. Conclusions

Development of the new circulation weather type classification for Baltic Sea area is needed to analyse more precisely regional atmospheric circulation. Using here simple physical models, like geostrophic wind approximation, gives direct physical meaning of each class and chance to classify the atmospheric circulation with reasonable number of classes.

Classification of Jenkinson and Collison (1977) has justified itself already, because its simple introduction to the Baltic Sea region has given better relationships with meteorological parameters than German Weather Service's Grosswetterlagen.

The next task will be to improve the classification with the aim of decreasing of the variation of meteorological elements within the weather types, trying at first to give physical meaning to the classification criteria.

References

Jenkinson, A. F. and Collison, F. P. An initial climatology of gales over the North Sea. *Synoptic Climatology Branch Memorandum* No. 62, Meteorological Office, Bracknell. 1977.

Buishand, T. A. and Brandsma T. Comparison of circulation classification schemes for predicting temperature and precipitaion is he Netherlands. *Int. J. Clim.* Vol 17, 875-889, 1997.

Had the "project" BALTEX so far met its original objectives ?

Ehrhard Raschke, Jens Meywerk, Burkhardt Rockel

GKSS Research Center, 21502 Geesthacht, Germany

1. Introduction

The Baltic Sea Experiment (BALTEX) had been defined with its major objectives during the years 1992 to 1994 to develop and validate numerical models coupling the atmosphere with the vegetated land surface and the Baltic Sea, to relate energy and water cycles in the BALTEX area to anomalies of the global circulation in the atmosphere and ocean, and to transfer developed models to other geographic regions. After more than 6 years of active research a first assessment of this project should be performed.

2. The Project

Preparatory scientific work within BALTEX started in different groups in Finland, Sweden, Denmark and Germany already in 1992. The organization of the project could be developed later, when funding could be secured to support a secretariat and its activities and to support in particular the collection of observations of precipitation and runoff from stations, which are not regularly reported in the worldwide GTS of WMO. This latter activity enabled all other countries on the Eastern shore of the Baltic Sea to participate actively in BALTEX.

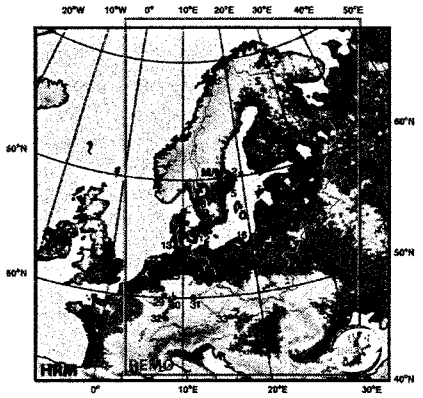

Figure 1: Model domain (red rectangular borders) for the BALTEX region. The numbers indicate locations of partners.

The BALTEX area covers the entire discharge basin of the Baltic Sea, as shown in Fig. 1. Three data centers have been installed at national weather and oceanographic services.

During an earlier data collection event (PIDCAP: Precipitation Intensive Data Collection and Analysis Period, Aug. to Oct. 1995) a rather complete data set on precipitation, runoff and other parameters could be collected from observations made during the months September, October and November 1995, which is still used in model development and validation.

The scientific strategy of BALTEX is steadily reviewed in the BALTEX Science Steering Group (BSSG), whose members come from all countries and cover the three prime disciplines, involved in this work: atmospheric sciences, oceanography and hydrology. Close relations were established to the other Continental Scale Experiments of the GEWEX, which follow similar goals.

In the beginning several working groups had been established to define specific problem (e.g.: required process studies, radar network, modeling, etc.) and encourage scientists to participate in this long lasting experiment. Particular attention has been paid to the model validation and coupling, to specific field experiments over land and over sea and to the radar network over the entire area.

The project received never a funding from a central organization, but individual components of it were supported by various national funds and in several projects by the European Union.

3. Status and Future

BALTEX is concentrating its efforts now in collecting data, both observational and modeling, during a period of about 2 years (BRIDGE) to meet the 3 scientific objectives mentioned above. This period will end in fall 2002 and overlaps with a similar world wide effort of the GEWEX (CEOP: Coordinated Enhanced Observational Period), which provides also data for the validation of satellite products. A major period for analyses will afterwards last to about the year 2005.

About 50 groups from 14 European nations declared their interest in contributing to the BALTEX research goals or using the BALTEX data. They receive their support from national sources; some are part in EU-funded projects (e.g.: CLIWA-NET).

BRIDGE consists of two major components. Enhanced , mostly operational observations dominate the baseline components covering the entire period. Up to 5 Enhanced Observational Periods (EOP) had been planned for specific problems, such as the cloud-aerosol and radiation interaction, investigated in the European project CLIWA-NET. Others will concentrate on oceanographic and in particular sea ice studies and on water and energy exchanges over vegetated areas, respectively.

Prime attention in the next years will be paid to the investigation of the water and energy budget of this region and its relation to global scale circulation anomalies in the atmosphere and ocean. Also a climatology of the entire region covering a longer period of several decades should be established.

Atmospheric models of the German and Scandinavian weather services have been modified for BALTEX and are now subject of improvement of their internal physics packages and in particular of their lower boundaries (vegetated land surfaces, lakes and the Baltic Sea). This coupling is now full interactive. Various process-oriented field studies have been performed at major stations in Germany, Sweden and Finland to improve the simulation of areal evapotranspiration. Many validation studies, also with GPS data (see Fig. 2), have been made.

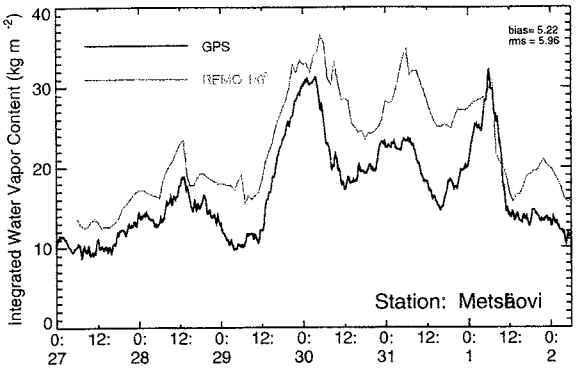

Figure 2: Total atmospheric water vapor content. Comparison between model and GPS data, at station Metsahovi (Sweden).

Also first measurements of sea ice dynamics and ist effects on the air-sea interaction had been obtained in the Gulf of Bothnia. Along a transect in the Baltic Proper the near bottom transport of salty , nutrient- and oxygen-rich water could be measured, which penetrates occasionally from the Kattegat into the Baltic Sea.

So far only one time series of the continental water supply into the Baltic sea exists, based on a model for the total runoff from each major river basin. Further climate studies (2. objective) are still missing. Only a preliminary model study of the water end energy budget of the entire area, based on PIDCAP data, has been made with a regional model. See Fig. 3.

Particular attention is paid to the correction of all precipitation measurements during the PIDCAP period. Satellite data of clouds (ISCCP) and of the radiation budget were used in several model validations.

Considerable improvements had been achieved in the modeling of water and energy exchanges within the top soil layers and between them and the atmosphere. They lead also to improvements of the distributed modeling of the runoff within different river basins.

Rare attempts have been made to meet the 3. Objective, which indeed is a general request for all GEWEX Continental Scale Experiments. Only an individual cooperation existed with a team of the Mackenzie-River basin to exchange model and to analyze data of the planetary radiation budget over both areas.

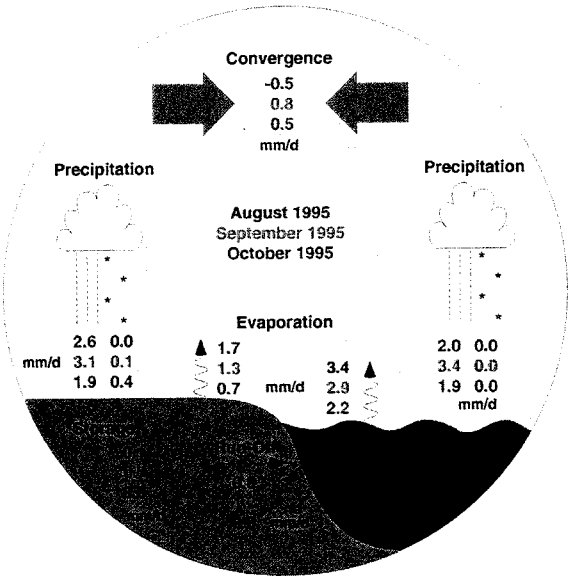

Figure 3: Water budget of the BALTEX area during the PIDCAP period in 1995.

4. Conclusive Remarks

In summary we can state, that the past work within the frame of BALTEX gained considerable interest by new teams from almost all BALTEX states and others in Europe and resulted in many excellent studies. Intensive model validation work was overrun by the implementation of new model generations by the weather services requiring new validations. But a first complete interactive simulation of the circulation over and within the Baltic Sea could demonstrate an improvement of wind forecasts. The hydro-meteorological model work lead to projects for the development of flood forecasting systems, demonstrating a first immediate use of BALTEX results.

References (selected):

Bergstroem, S. and B. Carlsson, 1994: River runoff to the Baltic sea: 1950-1990. *Ambio,***23,** 280-287.

Hagedorn R., A. Lehmann, D. Jacob, 2000: A coupled high resolution atmosphere-ocean model for the Baltic region. *Meteorol. Z.,* **9,** 7-20.

Launiainen J., and T. Vihma, 2001: BALTEX-BASIS (Baltic Air-Sea-Ice Study), Final Report, Int.BALTEX Secret., in press

Omstedt A., and A. Rutgersson, 2000: Closing the water and heat cycles of the Baltic Sea, *Meteor. Z.,* **9,** 57-66.

Raschke E., J. Meywerk, K. Warrach and 36 coauthors, 2001: BALTEX (Baltic Sea Experiment): A European Contribution to Investigate the Energy and Water Cycles over a large Drainage Basin. *Submitted*

Regional Climatic Modelling to Forecast Extreme Events for the Rhine Basin

K.-G. Richter[1], D. Jacob[2], C.-J. Lenz[2], M. Ebel[1], Karl Ludwig,[1]

[1] Beratender Ingenieur Wasserwirtschaft-Wasserbau, Herrenstr. 14, 76133 Karlsruhe.
[2] Max-Planck-Institut für Meteorologie, Bundesstraße 55, 20146 Hamburg

The forecast of extreme hydrometeorological events has been improved significantly during the last ten years. But there still exists a deficit in praxis according to the detailed analysis and forecast of extreme hydrometeorological rainfall runoff events. By coupling the atmospheric circulation model REMO (Regional Model) with the hydrological model LARSIM (Large Area Runoff Simulation Model) the quality of forecast of extreme hydrometeorological events can be improved significantly.
The model area of the atmospheric model covers a region between 0 and 30 degree East and 45 to 75 degree North with a horizontal grid mesh size of 1/6 degree. REMO is a regional hydrostatic, numerical circulation model to calculate the three-dimensional atmospheric fields of the wind vector, temperature, humidity and precipitation. The hydrological model area covers the Rhine basin from Switzerland to the German-Dutch (gauge Lobbith) border. The grid size is consistent to the grid size of the atmospheric model. LARSIM is a conceptual physically based continuous model describing the water cycle. Beside the runoff generation in the area and the translation and retention in river channels, LARSIM includes the processes of interception, evapotranspiration and water storage in soils and aquifers. Snow accumulation and snow melt can be considered as well as artificial influences.
The coupling of the models is done by two steps. In the first step the meteorological parameters are calculated with the atmospheric model REMO. The model results for precipitation, temperature, relative humidity, wind velocity and radiation are used as input for the hydrological model LARSIM to calculate floods. In the presentation this method as well as simulation results are shown for recent flood events in the Rhine basin (3/1988,12/1993 and 1/1995). In the next step the atmospheric model REMO and the hydrological model LARSIM are coupled directly by using a common hydrological model for the vertical water transport in the soil.

The area-averaged precipitation calculated with REMO corresponds to the measured area average of precipitation in larger sub basins quite well, but on some days a time delay in the calculated precipitation can be seen. The quality of the flood-simulations (with meteorological input from REMO results) with the hydrological model LARSIM strongly depends on the reliability of the meteorological input. For gauges with larger areas the calculated and measured floods are corresponding well, if there is no time delay in the calculated precipitation.
Coupling the atmospheric model REMO and the hydrological model LARSIM directly, only a small change in the model results for precipitation and river discharge is expected in the case of a 20-day simulation period for a flooding event. For long-term and/or climatological simulations a stronger response of the model results to the direct coupling can be expected.

Prognosis of maximum snow water equivalent changes in Lithuania

Egidijus Rimkus

Department of Hydrology and Climatology, Vilnius University, Ciurlionio21/27, 2009 Vilnius, Lithuania

1. Data and methods

Maximum snow water equivalent is one of the main factors that determine spring flood discharges. Prognosis of already mentioned index's mean values also helps to provide changes in hydrological and agriclimatic regime of territory. According to contemporary climate model outputs it is possible to directly foresee some meteorological parameters (air temperature, precipitation, cloudiness and etc.). Regression links between parameters can be used for forecasting of changes of others

A permanent snow cover usually occurs in the second part of December, maximum depth of snow cover – in the third ten-day period of the February. Water snow equivalent is a function of snow depth: correlation coefficient in Lithuania reaches - 0,83 and spatial distribution of both characteristics is very similar. Snow depth and snow water equivalent reach maximum means during the same ten-days period in greater part of Lithuania (Figure 1). Only in seacoast region snow water equivalent reach maximum mean at first ten-days period of the ablation.

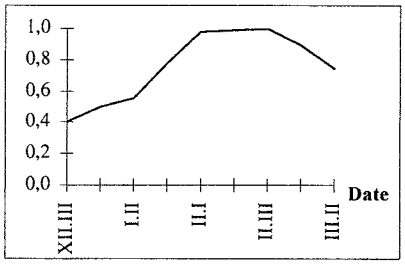

Figure 1: Mean change of snow water equivalent during cold season in Lithuania.

Due to this reasons solely climate conditions of accumulation period (January - February) were analyzed in this work. Inhomogeneous phasal composition of precipitation (especially in seacoast region) and differences in number of days with thaws at different years determine rather weak correlation between amount of precipitation in accumulation period and maximum snow depth. Relationship between complex parameter $p^2 \times t$ (where p – precipitation amount (mm) and t – mean air temperature (°C) during accumulation period) and maximum snow depth much more close than in case mentioned above. The forecast of snow water equivalent based on regression equations with complex parameter was made. It is very important to correctly determine character of relationship since linear regression can't be often used in analysis of meteorological parameters, that changes are limited; as well as other parameters can affect nature of relationship (for instance 0 °C for snow cover parameters). Relationships between complex parameter of accumulation period and maximum snow cover depth were approximated by exponential type of regression. If mean air temperature of accumulation period was close to 0 °C, changes of maximum snow water equivalent size would not be significant. Probability of permanent snow cover formation is likely to decrease in this case. Due to this reason maximum value of parameter can be achieved very often within one synoptic process. Such processes usually are separated by thaws periods when snow cover may disappear.

Outputs of Global Climate Models experiments from five modeling centers (HadCM2 (United Kingdom); ECHAM4 (Germany); CGCM 1 (Canada); GFDL-R15 (USA); CSIRO-Mk2 (Australia)) were used in this work (The IPCC data distribution center, 2000). All outputs based on increasing greenhouse gas (equivalent CO_2) and sulphate aerosols 1% per year after 1990. On the other hand data from global monitoring station in Mauna Lao (Hawaii) show only 0,4% increase of CO_2 per year during the last decade of XXth century. Strive for comparing outputs of GCM experiment made in the UK Hadley Center for Climate Prediction and Research that based on increasing greenhouse gas (equivalent CO_2) and sulphate aerosols 0,5 % per year was analyzed too.

Due to differences of outputs generalization level (different spatial resolution and grid point location) air temperature and precipitation data from nearest grid points were used for snow water equivalent changes prediction in Lithuania (Figure 2). Regional peculiarities of climate change tendencies in different parts of Lithuania don't reflect in GCM outputs, so data from one nearest grid point can be used for all territory.

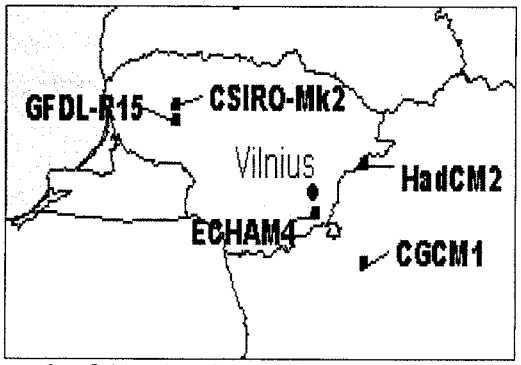

Figure 2: Grid points from different GCM experiments outputs which date used for climate change prediction in Lithuania.

If regression link between meteorological parameters is exponential (for instance: between air temperature and probability of permanent snow cover formation) regional peculiarites become very clear while mean of predictor crosses some phisical limit. In case of regression link between meteorological parameters is linear regional peculiarities of analyzed parameters tendencies do not reveal at all and location of izolines in both maps of predicant and predictor is the same. In this case dispersion around regresion line is absent. Due to this reason only absolute mean size and dimension is different in forecasting maps of different meteorological parameters.

Despite of differences of means sizes, character of predicted air temperature change in XXIth century in Lithuania is similar to most outputs of GCM experiments. It is expected that the air temperature will increase especially rapidly in cold period of the year (November – March). It does coincide with current climate change tendencies in Lithuania. Outputs of HadCM2 (United Kingdom) experiment are slightly different. Outputs of

this model show the smallest changes of air temperature in Lithuania: expected rise of mean air temperature is 0,2 °C/ decade in first part and 0,4 °C/ decade in the second part of XXIth century (even air temperature rise (about 0,35 °C/ decade) is predicted in outputs of other climate modeling centers). More rapid rise of warm season air temperature (in comparison with cold period) is another peculiarity of this model prediction.

Analyzed GCM outputs present rather different forecasts for changes of precipitation amount in XXIth century in Lithuania. Only single feature is general for all outputs: precipitation amount will be higher at the end of XXIth century. On another hand, rate and character of predicted changes is very different.

Some seasonal aspects of changes of precipitation amount can be revealed after summarizing of GCM outputs. It is expected that precipitation amount of cold season of year will rise more rapidly than in warm season. The highest grow rate of this parameter is predicted in March; the lowest – in the second part of summer and in the beginning of autumn. Current climate change tendencies in Lithuania will remain in future: difference between precipitation amount in cold and warm season will be smaller. It means that continental features of Lithuanian climate will become weaker.

It is expected, that air temperature during accumulation period will increase by 0,3 °C/decade in the beginning, 0,6 °C/decade – in the middle and 0,4 °C/decade in the end of XXIth century. Precipitation amount will rise by 2 mm per accumulation period in every decade of this century.

Forecast of snow water equivalent in Lithuanian territory based on this prediction was made. Two cases were analyzed: 1) the mean temperature of accumulation period will rise by 1,5 °C, precipitation amount – by 8 mm (it is expected around 2040 year); 2) the mean temperature will rise by 3,0 °C, precipitation amount – by 14 mm (it is expected around 2065 year).

2. Results

Maximum snow depth in Lithuanian territory will decrease significantly during air temperature rise in accumulation period. Snow water equivalent will also decrease because snow density will not change: the higher temperature of solid precipitation and more often cases of mixed precipitation will be compensated by shorter period of accumulation (during that time intensive processes of snow cover densification are going on).

Maximum snow water equivalent was in average 40 mm in Lithuania territory in 1961-1990 years. The highest mean determined in Zemaiciai upland (60 mm), the lowest in Southwestern part of Lithuania (21 mm). If changes in accumulation period will be the same as forecasted regional features of spatial distribution remain but range of dispersion decreases (from 39 mm in 1961-1990 years to 26 mm in 2065 year). Average maximum snow water equivalent will decrease to 34 mm, when weather temperature as well as precipitation increases accordingly 1,5 °C and 8 mm. Average maximum snow water equivalent will decrease to 28 mm, when weather temperature increases 3 °C and precipitation increases 14 mm.

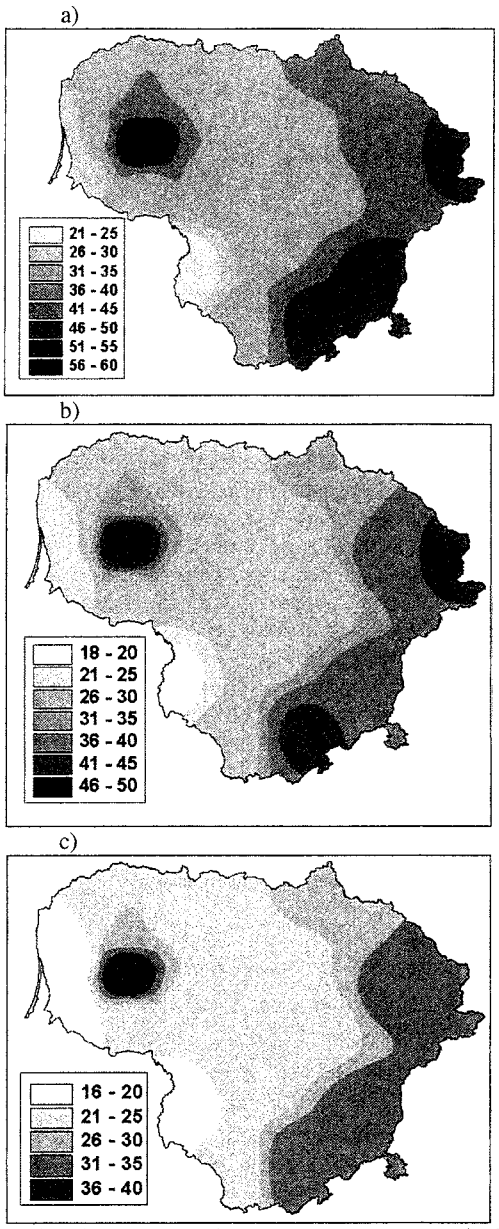

Figure 3: Average maximum snow water equivalent (mm) in Lithuania in 1961-1990 (a), when average temperature increases 1,5°C and amount of precipitation - 8 mm during snow accumulation period (b), ΔT – 3 °C; ΔP – 14 mm (c).

Such changes will also predetermine character of nutrition of Lithuania rivers. If nutrition by melting snow in the annual runoff of Lithuania rivers came to 31 %, in 1961-1990, according to future forecasts snow nutrition would come to 26 % in 2040 and 21 % in 2065. Character of annual hydrograph of rivers, influenced by snow nutrition will be mostly changed.

Reference

The IPCC data distribution center, *GCM experiments*, 2000

NCEP-DOE Reanalysis Global Water and Energy Budgets for the GHP CSEs

John Roads[1], M. Kanamitsu[2] and R. Stewart[3]

[1] Scripps Institution of Oceanography, UCSD, 0224, La Jolla, California 92093
[2] National Center for Environmental Protection, NCEP, Camp Springs, MD,
[3] Climate Research Branch, Meteorological Service of Canada, Downsview, Ontario, Canada

Abstract

During the past several years, many continental-scale experiments (CSEs) have started to develop regional hydroclimatological datasets and studies. A common objective of the CSEs is to understand how well we can close water and energy cycles from observations and models. By closing a budget, we really mean determining how accurately we can observe, simulate and predict relevant processes. To provide a global background for these regional experiments, we describe here vertically integrated global and regional water and energy budgets from the NCEP-DOE reanalysis II (NCEPRII). There are of course still problems with global reanalyses, which are especially noticeable at regional scales, and another one of the goals of the CSEs is to examine the global reanalysis at regional scales in order to understand what improvements are needed and might be obtained with regional observations and analyses. As shall be shown, maintaining the NCEPRII reanalysis close to observations requires some nudging and this nudging is an important component of the budget.

Still, to first order we can discern important mechanisms in the reanalysis. For example, water and energy cycles can be characterized by temperature. Water vapor, precipitation, evaporation and moisture convergence increase with increasing temperature. Surface water decreases with temperature and surface runoff is bimodal with temperature, in part because much runoff occurs near melting temperatures as well as in tropical rivers. Moisture convergence also has two preferred modes because during winter net increases in moisture convergence are stored in the snow pack and inactive surface layer until spring melt and during summer moisture convergence contributes to the monsoon rainfall. Some of these general characteristics are caused by regional differences; midlatitude hydrologic cycles are different from monsoon hydrologic cycles. A monsoon hydrologic cycle shows increased precipitation, evaporation, moisture convergence, runoff, with increasing temperature. A midlatitude hydrologic cycle shows increased precipitation, evaporation, but decreased moisture convergence, runoff, and surface water. Again, the surface water stored during the winter is important for maintaining the summertime precipitation in midlatitudes.

Water budget of cyclones and their contribution to the freshwater supply in the Baltic Sea catchment area: A case study

Burkhardt Rockel[1] and Ute Karstens[2]

[1] GKSS Research Centre, D-21502 Geesthacht, Germany
[2] Max-Planck-Institute for Biogeochemistry, Jena, Germany

1. Introduction

One major source for the freshwater supply in the Baltic Sea catchment are extra-tropical cyclones.
During the PIDCAP (BALTEX Pilot study for Intensive Data Collection and Analysis of Precipitation) period, August to November 1995, several cyclones crossed the Baltic Sea catchment causing extensive rainfall over different parts of the area. The development and life cycle of of three of these cyclones is investigated with respect to selected components of the energy and water cycle. Model simulations with the regional atmospheric model REMO are compared with observations including precipitation and satellite measurements.
The version of the regional model REMO used at GKSS contains the physical parameterisations of the German Weather Service and additionally includes cloud ice as a prognostic variable. The model is operated in the forecast mode, i.e. consecutive 30 h forecasts starting each day at 0 UTC were performed. The model runs with 1/6° horizontal resolution on a rotated latitude-longitude grid with 24 vertical levels. The initial and boundary values were provided by the Danish Meteorological Institute (DMI). The soil fields (except SST) were only used as initial conditions for 1 August and the soil model was run continously afterwards. Hourly outputs of the REMO simulation were stored and are the basis of this study.

2. The Case Study

Figure 1 shows the development of three cyclones during the period 28 August to 5 September 1995. These cyclones caused extensive rainfall in most parts of the BALTEX region (Isemer, 1996). The first of these cyclones (named "Kerstin") developed during 28 August at the southern boundary of the polar air mass over Northern Italy. It quickly moved northeast- and northward across Poland. Its centre was located near the Bay of Riga on 30 August and dissolved over the Finnish Bay one day later. "Kerstin" developed into a violent Baltic Sea storm with enhanced precipitation in the central and southeastern BALTEX region. The second surface cyclone (named "Liane") developed at the Black Sea coast and moved northward during 30 - 31 August. It again caused heavy rainfall especially ver the eastern BALTEX region. "Liane" weakened over western Poland and dissolved on 2 September. The third surface cyclone (named "Monika") also moved from the Black Sea coast northward during 1 September. It intensified remarkably on 3 – 4 September over the Baltic Sea and left the BALTEX region westward over the North Sea on 6 September. Heavy, in some parts even extensive precipitation occurred with this cyclone in most of the southern and mid BALTEX region.
At the station Kaliningrad the influence of all three cyclones is visible in the measurements of surface pressure as well as in the reanalyses and model results. REMO reproduce the temporal variation very well. However, in the results of REMO the effect of the daily restart is obvious, especially on 29 August when the model drastically overestimates the strength of the development.

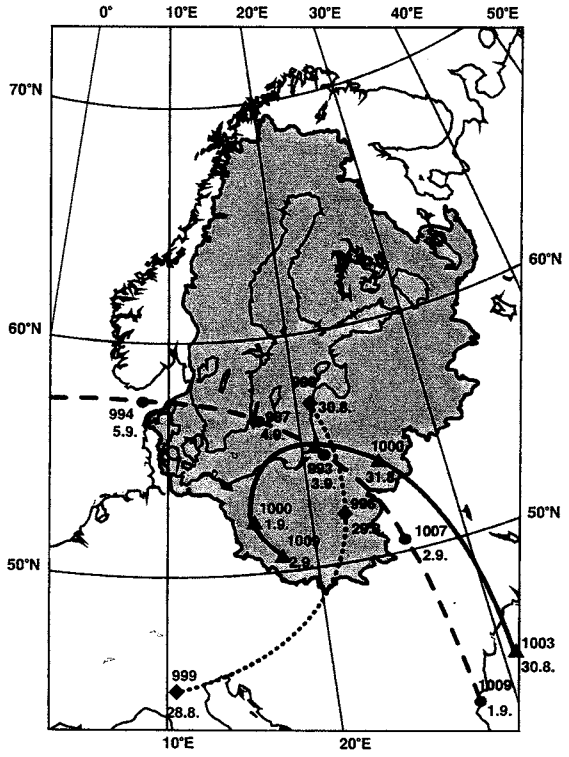

Figure 1: Tracks of the cyclones "Kerstin" (dotted line), "Liane" (dashed line), and "Monika" (solid line). The grey shades area is the Baltic Sea catchment. The numbers besides the symbols show the date (at 00 UTC) and the reduced surface pressure.

Precipitation results for this period from REMO are compared with rain gauge measurements. A large scale correction of wind induced errors and evaporation and wetting loss has been applied to the precipitation measurements. This correction has increased the precipitation amount by ~8%. REMO reproduce the temporal variation of the area mean precipitation and reproduces the precipitation amount on the days with maximum cyclonic activity (28-29 Aug., 31 Aug., 3 Sept.), see top of figure 2. A comparison of total cloud cover and cloud water path means with data derived from NOAA/AVHRR measurements (see figure 2) shows that REMO produces higher cloud cover values than the satellite data. The cloud water paths, however, are very similar. The reason for this may be an overestimation of thin high cirrus in REMO.
The precipitation results mentioned are daily means averaged over the Baltic Sea catchment. To get information about the amount of precipitation that is transported into the Baltic Sea catchement and then released over the catchment we have to observe the following points:

1. Only the precipitation related with the cyclone has to be taken into account.
2. Instead of daily sums, the precipitation on the track of the cyclones has to be summed up. To put through points one and two a method for tracking the cyclones has to be applied.
3. To put through points one and two a method for tracking the cyclones has to be applied.

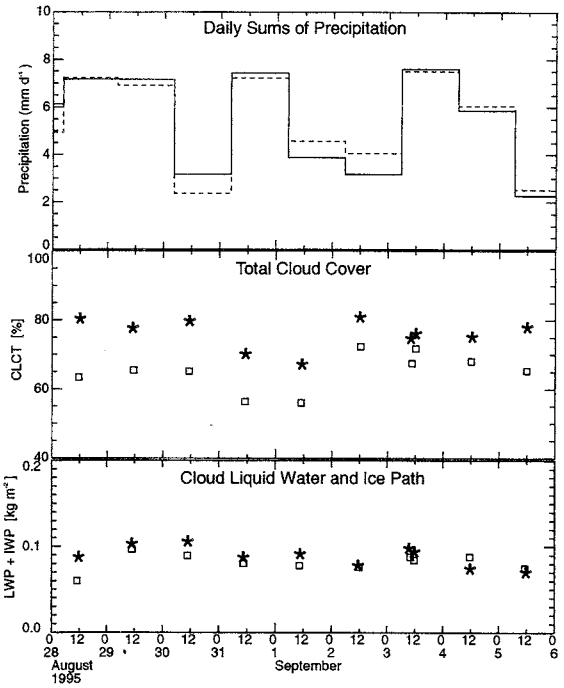

Figure 2: From top to bottom: daily sums of precipitation, cloud cover and sum of cloud liquid and ice water path averaged over the Baltic Sea catchment. Dashed and solid lines show precipitation values from model results and measurements, respectively. In the lower two pictures asterisks stand for model results and open squares for measurements. Precipitation measurements are from precipitation stations, cloud parameters are derived from NOAA/AVHRR data.

Rockel and Karstens (2001) have described a first approach how to do this. They stated that the best way to get the precipitation related to a cyclone would be to identify the exact precipitation pattern of the cyclone. They, however, use a more easily applicable approach were a circle of 500km radius with centre point at the centre of the cyclone is defined. The precipitation is then averaged over this circle and summed up hourly. The centre point of the circle moves with the cyclone. Thus its position has to be defined again for each output step of the model, i.e. hourly in this study. To do this automatically one would need a tracking algorithm. There are a few publications on this, but for this case study it was easier to track the cyclones by manually investigating the data than to implement these algorithms.

The same method was used to investigate the temporal evolution of the water budget of cyclones. It was investigated how precipitation, liquid and ice water of clouds change during the life cycle of the cyclones.

Acknowlegements:

The meteorological weather centres provided us with precipitation and synop data.

The work was partly funded by the EU under contract no. ENV4-CT97 (NEWBALTIC II).

References

Rockel, B, and U. Karstens, Development of the water budget for three extra-tropical cyclones with intense rainfall over Europe, *Meteorol. Phys.*,in print,2001

Isemer, H.-J., Weather patterns and selected precipitation records in the PIDCAP period, August to November 1995. A preliminary Overview, GKSS-Forschungszentrum Geesthacht, GKSS 96/E/55, pp. 92, 1996.

Runoff changes by river regulation and North Atlantic Oscillation - do they influence the deep water conditions in the Baltic Sea?

Raimund Rödel

Institute of Geography, University of Greifswald, Jahnstr. 16, D-17489 Greifswald, Germany
e-mail: roedel@uni-greifswald.de

1. Introduction

The natural runoff regimes in the Baltic Drainage Basin range from lowland hydrographs with floods in early spring to mountain hydrographs with flood-peaks in early summer. The hydrographs in the southern lowlands are influenced by eastward decreasing cyclonal precipitation. In the northern mountain regions snow melt influenced hydrographs can be found. All these typical runoff regimes were described in several articles by Gottschalk and Krasovskaia (*Krasovskaia, Arnell & Gottschalk* (1994)).

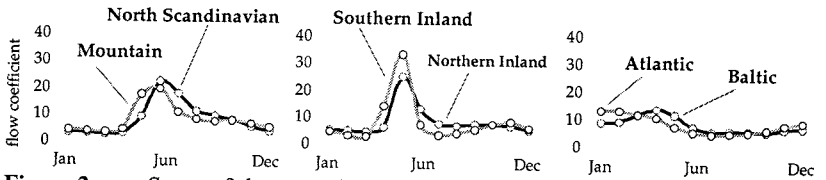

Figure 3: Some of the natural runoff regimes in the Baltic catchment

If more fresh water leaves the Baltic Sea, the inflow of salt water over the Kattegat becomes more difficult. In this case, river regulation may be one reason that Major Baltic Inflows (MBI) do not occur in the last decades of the 20th century (*Matthäus & Schinke* (1998 & 1999)).

2. Hydrograph changes by river regulation - a time dependent view

The answer to a correlation between MBI and influence of river regulation requires a synchronous view to man made runoff changes and further climatic fluctuations like the North Atlantic Oscillation (NAO).

For this the yearly hydrographs of all dam influenced Baltic basins were classified into natural regime types and the equalized anthropogenic regime year by year. The underlying concept of such a hydrographic classification was a cluster analysis with linkage between groups and cosinus as similarity measure (*Haines, Finlayson & McMahon* (1988)).

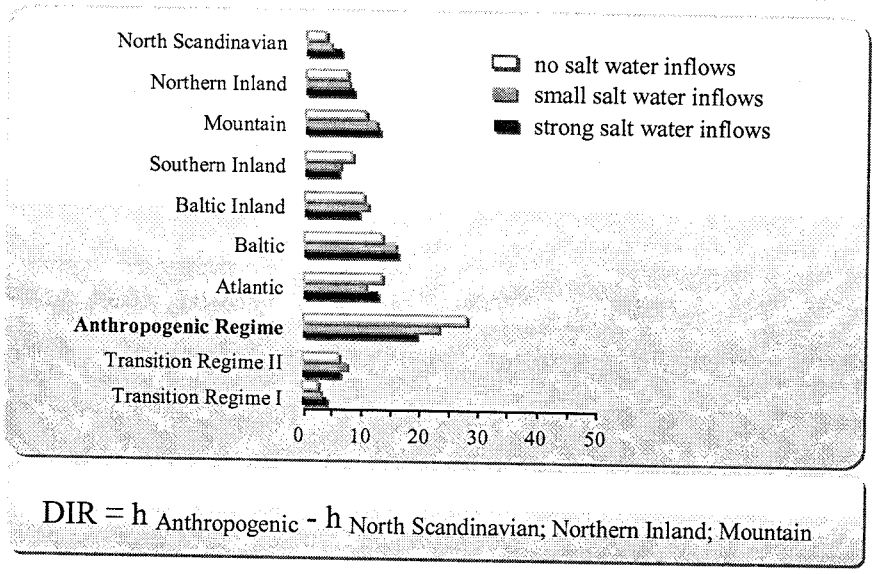

Figure 2. relative frequency of runoff regimes in years with and without salt water inflows - formulation of a Dam Influenced Regime -Index (DIR) for the runoff into the Baltic Sea

According to the findings in non regulated rivers the natural regimes switch between different hydrograph types very often. This switching is more frequently in precipitation-influenced than in snow melt-influenced hydrographs. Regulation stabilize these switching of regimes. Additional in more regulated rivers the equalized anthropogenic regime can be found in most years.
Dependent on intensity of river regulation and reservoir management in several dam influenced basins the relative frequencies of natural hydrographs decline and the frequency of the anthropogenic hydrograph increases. So that a yearly index of dam influenced runoff can be formulated like in Figure 2.

The natural seasonal distribution of monthly flows has been changed dramatically since the 1960s - 1970s by river regulation. About 240 dams with heights more than 15 m are registered around the Baltic Sea by the International Commission on Large Dams (*ICOLD* (1984 & 1998)). Especially in the northern part of the Baltic basin spring-floods are smoothed and winter-runoff is increased in case of hydro-power generation. The resulting anthropogenic hydrograph nearly shows equal runoff in all months of one year. Today, after regulation, about 7% more water flows into the Baltic Sea during wintertime.

3. Salt water inflows and dam influenced runoff - a synchronous view

A pattern of man made and climatic runoff changes seems to explain the salt water inflows into the Baltic Sea. The North Atlantic Oscillation (NAO), a climatic fluctuation, pretends better conditions for Major Baltic Inflows in time of negative NAO-Index.. Thats why winter precipitation and especially winter runoff in

Scandinavia is lower when NAO-Index is lower (*Hurrel (*1995) and see Figure 3).
To sum up, Figure 4 points out assumed correlations between MBI, North Atlantic Oscillation and dam influenced runoff into the Baltic Sea. The North Atlantic Oscillation determines more predominantly in- or outflow conditions into the Baltic Sea. But reservoir management in the dam influenced basins strengthens an existing disfavour for salt water inflows. This situation can be more obvious when winter runoff increases because of global warming.

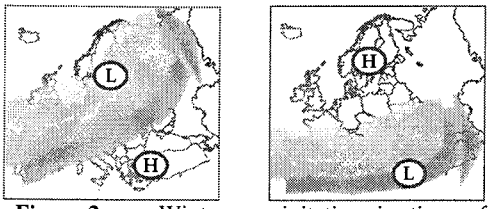

Figure 3: Winter precipitation in time of positive (left) and negative (right) NAO-Index.

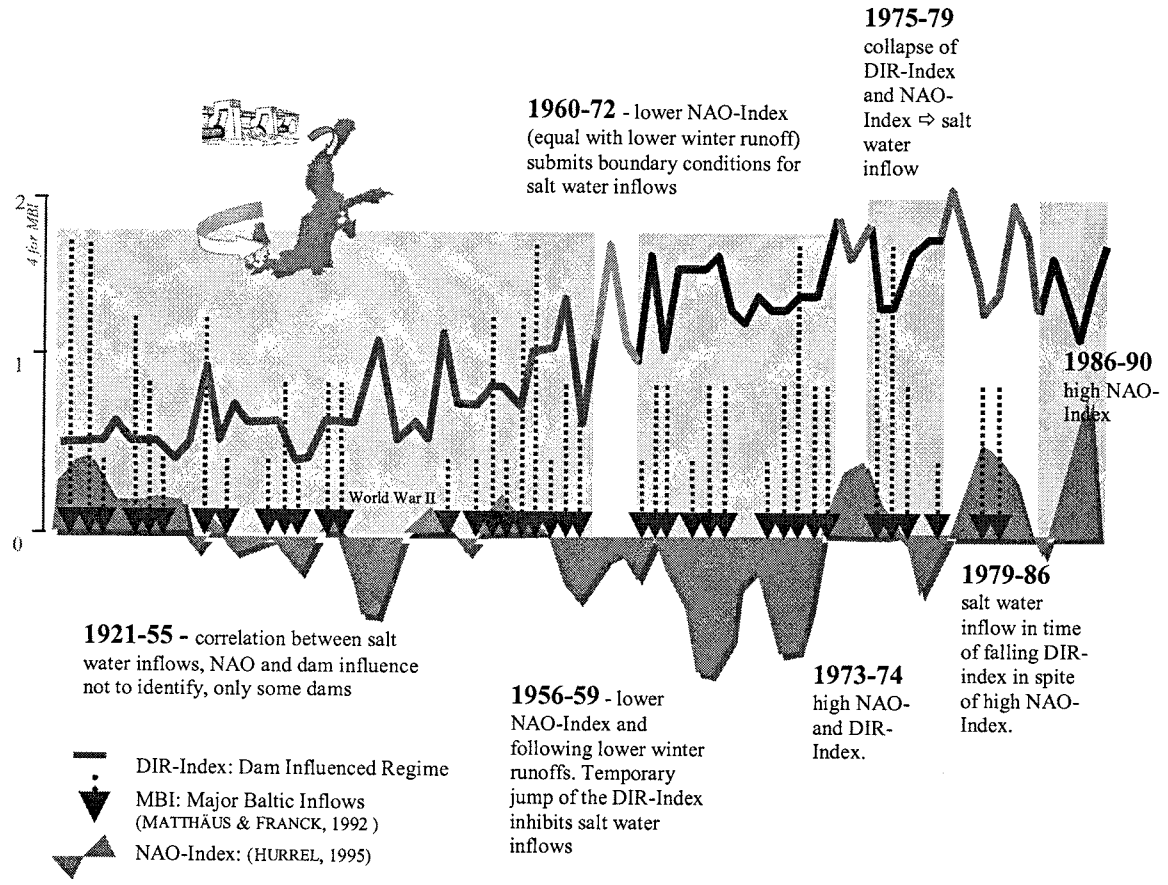

Figure 4. Dam Influenced runoff Regimes (DIR), the North Atlantic Oscillation (NAO) and their effects on the salt water inflows into the Baltic Sea

References

ICOLD, World Register of Dams, Paris, 1984 & 1998

Haines, A. T., B. L. Finlayson & T. A. McMahon, A global classification of river regimes. In: *Appl. Geogr. 8*, p. 255-272, 1988

Hurrell, J. W., Decadal Trends in the North Atlantic Oscillation Regional Temperatures and Precipitation. In: *Science* 269, p. 676--679, 1995

Krasovskaia, I., Arnell, N. W. & L. Gottschalk, Flow regimes in northern and western Europe: development and application of procedures for classifying flow regimes. In: Seuna, P., A. Gustard, N. W. Arnell & G. A. Cole (Eds.), FRIEND: *Flow Regimes from International Experimental and Network Data*, Vol. 221, IAHS, pp. 185-193, 1994

Matthäus, W. & H. Schinke, The influence of river runoff on deep water conditions of the Baltic Sea. In: *Hydrobiologia* 393, pp 1-10, 1999

Rödel, R., Die Auswirkungen des historischen Talsperrenbaus auf die Zuflußverhältnisse der Ostsee. Diss. Univ. Greifswald, 2000

Schinke, H. & W. Matthäus, On the cause of major Baltic inflows – an analysis of long time series. In: Continental Shelf Research 18, pp. 67-97, 1998

The effect of swell on air-sea exchange in the Baltic Sea

Anna Rutgersson[1,2], Ulf Högström[1], and Ann-Sofi Smedman[1]

[1] Department of Earth Sciences, Meteorology, Uppsala University, Uppsala, Sweden
[2] Swedish Meteorological and Hydrological Institute (SMHI), Norrköping, Sweden

1. Introduction

Swell are waves travelling faster than the wind. In the open ocean, swell is more or less omnipresent and often omnidirectional. It originates in areas with strong winds but can travel over thousands of kilometers with very little attenuation. Thus, swell observed at a given position in the open ocean at a given occasion can have any direction quite independently of the local wind direction.

Up till recently, the study of swell has received much less attention than wind waves, and its properties are hence less well known. In recent years several studies have, however, highlighted intriguing features of the effect of swell on the turbulent exchange of momentum, sensible heat and water vapor at the air-sea interface, *Smedman et al.* (1999), *Rutgersson et al.* and others.

The Baltic Sea differs from the open ocean in an important respect, the size being small in relation to the size of typical synoptic disturbances which may give rise to swell. This means that usually there is not more than one, well-defined source of swell present at a given time in the Baltic Sea, and that the direction of swell at a certain site is likely to be more or less unidirectional.

Data from several years of measurements of concurrent atmospheric data and wave data from the site Östergarnsholm east of Gotland (see Section 2) have been used for the studies presented here. It is found that swell occurs as often as 40% of the time at this site. Very often the swell comes from a southerly direction. As winds from this sector are common, a situation with swell and wind having roughly the same direction is typical for this site. The studies presented here represent such, rather well defined conditions.

2. Site and measurements

Östergarnsholm is a low island with no trees, situated about 4 km east of Gotland. On the southernmost tip of the island, a 30 m tower has been erected, with its base only about 1 m above mean water level. The tower is instrumented with Solent sonic anemometers at 9, 16 and 25 m above the ground and slow response, 'profile' sensors for wind and temperature at 5 levels. Wave height and direction is obtained from a Waverider buoy (run and owned by the Finnish Institute for Marine Research) anchored about 4 km to the South-south-east of the tower at a water depth of 36 m. Measurements started in 1995 and have run semi-continuously since then.

The measurements at the tower represent open sea conditions with very long fetch (> 100 km) for the sector from North-east over South to South-west. As shown from the 'flux footprint' calculation in *Smedman et al.* (1999), the measurements on the tower are likely not to be influenced by limited water depth outside the island.

3. Effects of swell on the momentum flux

In numerical models the exchange of momentum at the surface of the sea is usually expressed in terms of the drag coefficient C_D, defined as

$$C_D = u_*^2 / u_{10}^2 \qquad (1),$$

where u_* is the friction velocity and u_{10} the wind speed at 10 m height. Figure 1a shows, for *unstable conditions*, C_D plotted against the stability parameter z/L, where z is height above the water surface and L is the Monin-Obukhov length:

$$L = -\frac{u_*^3 T_0}{kg\overline{w'\theta_v'}} \qquad (2),$$

with T_0 mean temperature of the surface layer (K), k = von Karman's constant, g = acceleration of gravity and $\overline{w'\theta_v'}$ the buoyancy flux. The filled symbols represent measurements during swell, open symbols non-swell. The full line is the corresponding standard formulation used in most models. It is seen that the momentum flux observed with swell is very much lower than expected. As shown by *Smedman et al.* (1994) and others, the momentum flux during wind-following swell is sometimes even directed upwards from the ocean instead of, as usually observed, downwards.

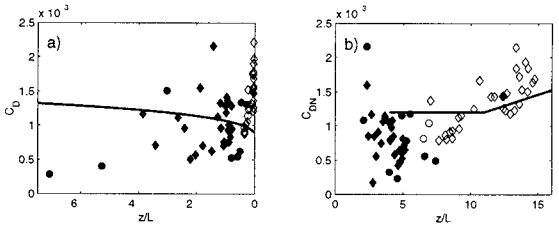

Figure 1: Drag coefficient during unstable conditions, a) C_D as a function of z/L; the line was calculated from standard expressions; b) neutral drag coefficient calculated with standard ϕ_m-functions, plotted as a function of 10 m wind speed; the solid line is based on an often used expression. From *Rutgersson et al.* (2001).

In Figure 1b C_D has been reduced to its value at neutrality (z/L = 0), denoted C_{DN}, with the aid of standard Monin-Obukhov expressions, and plotted against u_{10}. The full line is an often used expression. Also in this graph it is clear that the swell data are very much lower than expected. This is, however, not surprising, considering that the dimensionless wind gradient expressions

$$\phi_m(z/L) = \frac{kz}{u_*}\frac{\partial u}{\partial z}$$

observed during swell (not shown here) differ considerably from what is otherwise observed and used in reducing C_D to C_{DN}. A characteristic observed feature during swell in unstable conditions is the occurrence of a low level (< 10 m) wind maximum – a wave-driven wind - which gives negative values for ϕ_m within an appreciable part of the surface layer. Monin-Obukhov similarity is thus not valid during these conditions.

In *stable conditions*, i.e. when z/L > 0, the observed ϕ_m-curves agree much better with what is otherwise observed (not shown here), but nevertheless, C_D is only half its

value during non-swell conditions. *Rutgersson et al.* (2001) observe such conditions for u_{10} as high as 8 m s^{-1}.

4. Exchange of sensible heat and water vapor

The turbulent exchange of sensible heat, H is derived in numerical models with a bulk formulation similar to that for the exchange of momentum:

$$H = \rho \overline{w'\theta'} = C_H u_{10}(\theta_{10} - \theta_s) \qquad (3),$$

where ρ is air density, C_H the bulk exchange coefficient, θ_{10} potential temperature at 10 m and θ_s surface temperature.

Figure 2 presents data for C_H plotted against z/L for *unstable* conditions ($z/L < 0$). The measurements show that C_H is only about 10 % lower in the mean than expected from standard expressions (the thin line) during swell. Note, that swell occurs over a very wide stability range, $-8 < z/L < 0$, whereas non-swell conditions, represented by the thick line, is obtained only for $z/L > -0.5$. As noted in Section 3, the friction velocity is strongly reduced during swell conditions and, as seen from the definition of the Monin-Obukhov length, Eq. (2), this will result in a strong reduction in $-L$ and correspondingly large values of $-z/L$ even for a comparatively small heat flux.

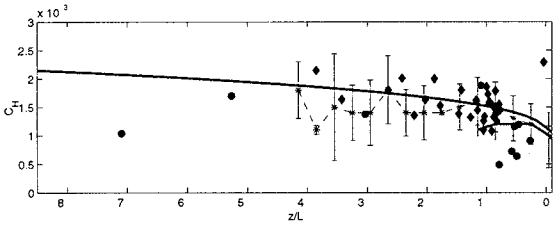

Figure 2: C_H plotted as a function of z/L for unstable conditions. Filled symbols represent measurements during swell conditions. The thin solid line has been derived with $C_{HN} = 1.1 \cdot 10^{-3}$ and standard ϕ_h - functions. Dashed lines connects averages over z/L intervals using all available swell data for 1995 – 1998 in the range $-4.5 < z/L < 0$. Thick solid line is average of all data from the same time period *without* swell. From *Rutgersson et al.* (2001).

Figure 3 shows C_H for *stable conditions* as a function z/L. Again the thin line has been derived from standard expressions. The observational swell data are found to be approximately constant $\approx 0.5 \cdot 10^{-3}$ over the stability interval $0 < z/L < 1.5$, decreasing probably for higher z/L. Also the data for non-swell conditions, the short thick line, indicates that $C_H \approx 0.5 \cdot 10^{-3}$ for near-neutral stable conditions, rather than about $1.1 \cdot 10^{-3}$ as traditionally thought. This lower value is supported by other recent studies. Thus, there is a near-discontinuity of C_H at $z/L = 0$. This is probably caused by a feedback effect: stable stratification reduces turbulence, which reduces the waves, which reduces friction further etc. This interpretation is in agreement with the finding reported in Section 3 that, during stable conditions, C_D is found to be only about half of what is usually assumed in spite of the fact that ϕ agrees with what is found over land, indicating that the roughness length is being reduced over sea in stable air by this feedback effect.

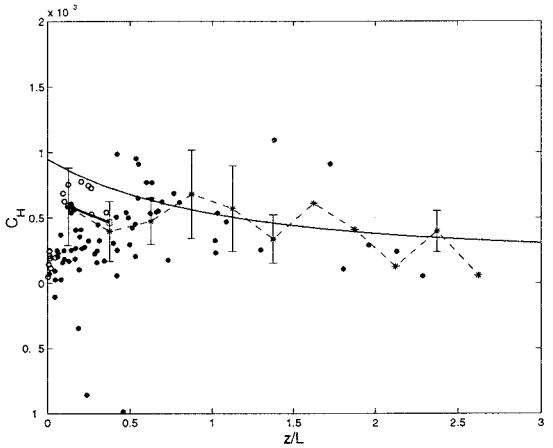

Figure 3: C_H for stable conditions plotted against z/L. Notations as in Figure 2. From *Rutgersson et al.* (2001).

The results obtained for the flux of sensible heat appears to be equally valid for the corresponding exchange of water vapor, but the experimental data are still relatively scarce.

5. Conclusions

Analysis of several years worth of measurement at Östergarnsholm shows that swell occurs as often as 40 % of the time in the Baltic Sea. As the source of swell is in most cases located in a well defined geographical area of the Balic, uni-directional swell is often found. At Östergarnsholm, the swell has often approximately the same direction as the local wind. The results given here all represent such conditions.

The exchange of momentum at the water surface is strongly influenced by swell. This results in a much reduced bulk exchange coefficient, C_D. Often a wind maximum is found below 10 m (a wave-driven wind), invalidating Monin-Obukhov similarity.

The exchange of sensible heat and water vapor is also affected by swell but not as much as in the case of momentum. At slightly and moderately stable conditions, the bulk coefficient C_H is found to be virtually constant at $0.5 \cdot 10^{-3}$, also during non-swell.

References

Rutgersson, A., A. Smedman and U. Högström, The use of conventional stability parameters during swell. *J.Geophys. Res.*, accepted.

Smedman, A., U. Högström, H. Bergström, A. Rutgersson, K.K. Kahma and H. Pettersson, A case-study of air-sea interaction during swell conditions. *J.Geophys. Res., 104,* 25,833-25,851, 1999.

Smedman, A., M. Tjernström and U. Högström, The near-neutral marine atmospheric boundary layer with no surface shearing stress: A case study. *J. Atm. Sci., 51,*3399-3411, 1994.

Net precipitation over the Baltic Sea during present and future climate conditions

Anna Rutgersson[1], Anders Omstedt[1,2] and Jouni Räisänen[1]

[1] SMHI, SE-601 76 Norrköping, Sweden.
[2] Department of Oceanography, Earth Science Centre, SE-405 30 Göteborg, Sweden.

1. Introduction

The net precipitation over the Baltic Sea together with the fresh water inflows due to river runoff and the in- and outflows through the Baltic Sea entrance area are the main components in the hydrological cycle of the Baltic Sea *(Omstedt and Rutgersson, 2000)*. We study the net precipitation using an ocean model. This method constraints the water budget to be consistent in the ocean basin and enables verification using observed salinity. The ocean model is forced with an atmospheric database with certain uncertainties and the sensitivity of the forcing data is here investigated for an 18-year period. The 18-year period is too short to give a 'climate estimate' for net precipitation and in order to get an extended period the net precipitation is related to river runoff and maximum ice extent for the last 100 years. The purpose of the present work is to present a realistic climate estimate of net precipitation valid for the 20th century. This value is then used to validate estimates from climate model simulations during present and future climate conditions. Further details concerning this investigation can be found in *Rutgersson et al. (2001c)*.

2. The Baltic Sea model

The Baltic Sea model used is the PROBE-Baltic model (*Omstedt and Nyberg*, 1996), forced by observed river-runoff and a gridded meteorological database. The database SMHI(1x1)° covers the Baltic Sea with a grid of (1x1)° grid squares and uses all available synoptic weather stations in the area. Estimated errors in the gridded meteorological database (*Rutgersson et al., 2001a, b*) are used as starting point for a sensitivity analysis of the forcing of the system. Sea surface temperature and maximum ice extent are used to validate the ocean model.

3. Net precipitation during present climate conditions

The Baltic Sea model is used for the period 1981-1998 and several simulations are made: a reference simulation with forcing directly from the SMHI(1x1)° database, and sensitivity runs with an increase in temperature of 1 degree (T+1), an increase in humidity by 1gkg^{-1} (q+1), a decrease in wind speed by 1 ms^{-1}(U-1), a decrease in cloudiness of 10% (0.9cl) and an increase in precipitation of 10% (1.1P). The resulting 18-year mean valuess in precipitation, evaporation and net precipitation are shown in Table 1.

Table 1: Averages for the 18-year period of the sensitivity tests. The reference case uses the gridded meteorological database. For the reference case ± one standard deviation of the interannual variability is given.

	reference	T+1	q+1	U-1	0.9cl	1.1P
P(mm)	596±60	596	596	596	596	655
E(mm)	467±55	499	301	446	485	467
P-E(mm)	129±84	97	295	150	111	189
P-E (m^3s^{-1})	1526±994	1147	3500	1774	1313	2238

The largest effect is found when changing humidity and precipitation. The upper limit of the sensitivity study gives probably a significant overestimation and it is likely that the upper limit for net precipitation is significantly below 3000 m^3s^{-1}. This is due to the fact that an error in net precipitation of 2000 m^3s^{-1}, changes the salinity with about 1 permille and gives unrealistic salinity profiles. The reference simulation agrees well with measured salinity profiles (*Omstedt and Axell, 1998*)
The average seasonal cycle for the investigated 18 years is shown in Figure 1.

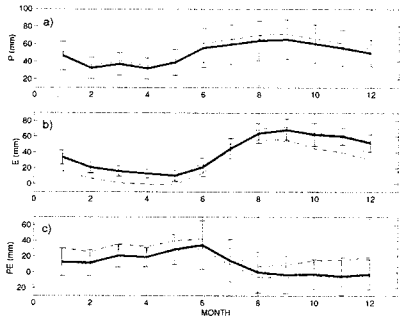

Figure 1: Monthly mean values of (a) precipitation, (b) evaporation and (c) net precipitation for 18 years. The shaded area represents the estimated uncertainty range using different meteorological forcing. The thick solid line is the reference version, and bars represent ± one standard deviation of the interannual variability for each month.

On a larger scale the net precipitation over the Baltic Sea is related to the net precipitation over the entire Baltic Sea drainage basin (the river runoff). The large-scale atmospheric circulation and major weather systems result in similar precipitation patterns and qualitatively the same temperature anomalies over land and sea. As sea ice significantly reduces evaporation over sea *(Omstedt et al. 1997)* it is also of importance. Based on monthly mean distribution of total river runoff to the Baltic Sea, and maximum ice extent a relation between net precipitation (P-E) river runoff (Q_f) and maximum ice extent (A_{ice}) is obtained:

$$P - E = aQ_f + bA_{ice} + c \left(m^3 s^{-1}\right)$$

where a=0.50406, b=4.395 and c=-6830. This can give a rough estimate of net precipitation for periods where we have no data, other than river runoff and ice extent. Using this method for the period 1901 to 1998 give a climate value of net precipitation valid for the 20th century, $(P-E)_{climate}$=1157±864 m^3s^{-1}. This value is lower than the value obtained for the earlier investigated 18 years, indicating that these years were relatively wet (Figure 2).

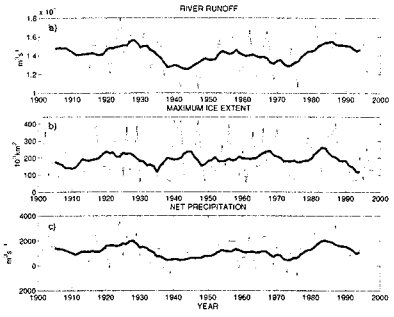

Figure 2: a) River runoff and b) maximum ice extent from measured data, and c) net precipitation from Equation 1 for the 1901 to 1998 period. Thin lines show the annual values and thick lines show the 10-year running mean.

4. Net precipitation in regional climate model simulations

To investigate possible future changes in the net precipitation, two regional climate change experiments are studied. These experiments were made with the version RCA1 of the Rossby Centre regional climate model for northern and central Europe (*Rummukainen et al. 2001*), using 44 km horizontal resolution and boundary data from two climate models: HadCM2 and ECHAM4. The two RCA1 experiments (RCA-H and RCA-E respectively) consist of a 10-year simulation representing the present day climate and a 10-year scenario run with 100-150% higher green-house-gas concentrations. The results for the present day climate are shown in Table 2.

Table 2: Average of precipitation, evaporation and net precipitation from the control simulations with the RCA model with two different forcing models. Also shown are the value from the reference Baltic Sea model using the gridded data base and the estimated 20th century value using the relation between net precipitation, river runoff and ice.

	20th century	Reference 18 years	RCA-H ctr	RCA-E ctr
P(mm)		596	629	783
E(mm)		467	323	300
P-E(mm)	98	129	306	483
P-E (m^3s^{-1})	1157	1526	3603	5687

The net precipitation in the RCA simulations is much above the reference value, due to both high precipitation and low evaporation. The low evaporation can be explained by a too low sea surface temperature giving less efficient evaporation in combination with a larger ice cover and by too humid layer close to the surface damping the evaporation. High precipitation in northern Europe is a common feature also in global climate models *(Räisänen, 2000)*.

The precipitation increases in both simulations for a changed climate (Table 3). Due to the warming there is also an increase in evaporation which is smaller. The total change in net precipitation for a changed climate is according to these simulations relatively small which indicates that an increase in precipitation could more or less be compensated by increased evaporation.

Table 3: Mean values of precipitation, evaporation and net precipitation from the RCA1 model with the two different forcings for higher greenhouse-gas concentration. The differences between control and scenario runs are shown in parenthesis.

	RCA-H scn	RCA-E scn
P(mm)	735(106)	857(74)
E(mm)	360(37)	366(66)
P-E(mm)	375(69)	491(8)
P-E(m^3s^{-1})	4416(813)	5781(94)

5. Conclusions

- Considering uncertainties in meteorological forcing and the constraints imposed by realistic salinity stratification, we conclude from our model simulations that the Baltic Sea net precipitation for the period 1981-1998 was between 1100 and 2500 m^3s^{-1}. This period was relatively wet, and a realistic value representative for the 20th century is 1500±1000m^3s^{-1}.
- There are significant interannual as well as seasonal variations in the net precipitation..
- Two simulations with the climate model RCA1 show too large annual values of net precipitation over sea as well as a too small seasonal cycle.
- For a changed climate (with increased green-house-gases) the two climate models showed a relatively small change in net precipitation due to compensating effects in precipitation and evaporation.

References

Omstedt, A. and L., Axell (1998). Modeling the seasonal, inter annual and long-term variations of salinity and temperature in the Baltic proper. Tellus, 50A, 637-652.

Omstedt, A. and A., Rutgersson (2000). Closing the water and heat cycles of the Baltic Sea. Meteorol. Z., 9, 57-64.

Omstedt, A. and L., Nyberg (1996). Response of Baltic Sea ice to seasonal, inter annual forcing and to climate change. Tellus, 48 A, No. 5, 644-662

Omstedt, A., Meuller, L., and L., Nyberg (1997). Inter-annual, seasonal and regional variations of precipitation and evaporation over the Baltic Sea. Ambio, 26, No. 8, 484-492

Rummukainen, M., Räisänen, J, Bringfelt, B., Ullerstig, A., Omstedt, A., Willen, U., Hansson, U., and C. Jones (2001). A regional climate model for northern Europe – model description and results from the downscaling of two GCM control simulations. Climate Dynamics in press.

Rutgersson, A., Smedman, A.-S., and A., Omstedt (2001a). Measured and simulated latent and sensible heat fluxes at two marine sites in the Baltic Sea. Boundary Layer Meteorology, 99, 53-84.

Rutgersson, A., Bumke, K., Clemens, M., Foltescu, V., Michelson, D., and A., Omstedt (2001b). Precipitation estimates over the Baltic Sea: present state of the art. Submitted to Nordic Hydrology.

Rutgersson, A., Omstedt, A. And J. Räisänen (2001c) Net precipitation over the Baltic Sea during present and future climate conditions. Submitted.

Räisänen, J. (2000) CO_2-induced climate change in northern Europe: Comparison of 12 CMIP2 experiments. RMK 87, SMHI, SE-601 76 Norrköping, Sweden, 59 pp.

Comparison of HIRLAM predicted soil moisture with observed data in Estonia

Triin Saue[1] and Jüri Kadaja[1], Simo Järvenoja[2]
[1] Estonian Meteorological and Hydrological Institute, Rävala 8, Tallinn 10143, Estonia
[2] Finnish Meteorological Institute, P.O.B 503, Helsinki 00101, Finland

1. Introduction

Estonian Meteorological and Hydrological Institute (EMHI) carries out soil moisture observations in a quite large amount giving good possibilities for evaluation of model predicted data. The aim of the present work is to compare soil moisture values forecast by the HIRLAM surface scheme with the ones achieved from the agrometeorological observations.

2. Data

Data of 486 soil moisture observations for the period from April to September 1999 were used in this work, each made for 5 depth layers (0-10, 10-20, 20-30, 30-40 and 40-50 cm). Observations include different stations, fields, and crops.

The model soil moisture data are from the operational forecasts carried out at Finnish Meteorological Institute (FMI). The HIRLAM 2.5 version with some upgrades was used at that time in the operations, and the simple three-layer surface scheme was used (Källen, 1996). In the calculations the area including Estonian territory was divided into 17 x 17 squares, each corresponding to one HIRLAM grid square of 22 km x 22 km. For each square the soil moisture was computed - for two upper-most layers - the surface layer 0-7.2 cm and the deeper layer 7.2-50.4 cm.

To compare these two kind of data, several modifications have been made. As the model and observations give the soil moisture data for different soil layers, there was a need to carry these data into the layers of the same depth. At first the observation results of soil moisture were transferred into two groups - one for surface layer (0-10 cm), other for summarised deeper layer (10-50 cm). Then the surface layer's observation data were carried from a 10 cm layer into 7.2 cm layer and restricted to 20 mm, as such limit exists for model data. For deeper soil layer the observation results were calculated into 42.8 cm layer, the final result was reduced to 7.2 cm layer and limited to 20 mm. To match the series geographically the model data were interpolated into observation points.

3. Results

Differences between model predictions and observations were evaluated using coefficient of correlation, reliability and accuracy between data series. To evaluate the temporal and spatial aspects on the results the grouping of the data was used based on different criteria.

The results from the whole selection show that correlation exists between model prognoses and observed values of soil moisture. The correlation coefficients 0,57 for the surface layer and 0,59 for the deeper layer prove the 99% reliability *(Figure 1)*. The model accuracy is better in the case of higher observed soil moisture values. Great over-prediction exists if measured soil moisture is low. It can be concluded that model is not able to predict as low soil moisture values as they actually decrease. Faint under-prediction occurs, when soil moisture is close to the maximum values.

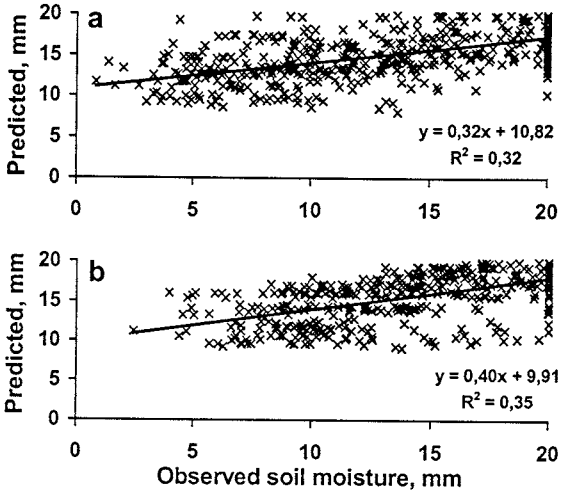

Figure 1: Comparison of observed and predicted soil moisture values for surface layer (a) and deeper layer (b).

Reliability is accounted by the value of mean error and in most cases it is positive for both layers. It means that in average model calculates higher values for soil moisture if compared with observed values. Mean deviation from observations is 2,4 mm for the surface layer and 1,4 mm for the deeper layer. The most likely the reason for positive deviation is the over-predicting of the low soil moisture values. The mean error is positive for lower observed moisture and falls below zero for higher values *(Figure 2)*. The best reliability of forecasts appears near the observed soil moisture values of 15 mm.

The accuracy, as described by the mean absolute error, is 3,8 mm for the surface layer and 3,1 mm for the deeper layer.

To evaluate the spatial aspect (territorial connection) the correlation coefficients were calculated over the whole territory at a certain time intervals. Months and observation days were used. The results indicate that the model takes the territorial differences into the consideration relatively poorly, as in most cases there is no reliable correlation between data. The best connection between predicted and observed data occurs in September for the surface layer, reliable correlation appears also in July for deeper layer and in June for both layers. As indicated by mean error, forecasted soil moisture was less reliable in June-July. Reliability was higher in August and September. In September the mean error is negative - model has under-predicted the moisture values, for other months appears over-prediction. The course of accuracy, presented by mean absolute error is comparable with the one of reliability. The worst accuracy occurs in summer (June-July-August), when the soil moisture is low; its best values were found in May.

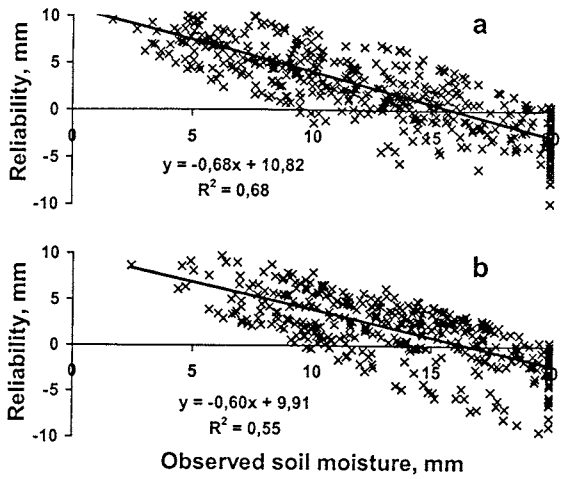

Figure 2: Dependence of mean error of soil moisture prediction on the value of observed soil moisture for surface layer (a) and for deeper layer (b).

To estimate the forecasted soil moisture from the temporal point of view time series of soil moisture were carried out for the whole observation period at the same place. The aim was to clarify if the model forecasts seasonal variations of soil moisture. Grouping by stations gives high correlation for most cases, except Vinni, where its reliability was 95% for surface layer.

Some specific signs could be mentioned for several stations. At Võru the reliability and accuracy are extremely low, but the correlation is good. Model has expressed correctly the time fluctuations but strongly (5-10 mm) over-predicted the soil moisture values. The reason could be the soil type - at Võru light sandy and sandy loam soils prevail and they are not calculated dry enough by the model. Mean error is negative for both layers at Pärnu station - model has calculated too low soil moisture values. It is probably conditioned by the fact that at Pärnu subsoil water lies near the surface and soil is continuously damper than could be counted by the water balance. The best results were got at Viljandi as for correlation as well as for reliability. At Vinni the correlation is relatively lower, but reliability is staying high anyway.

In addition to stations the time series were compared for concrete observation fields. For deeper soil layer the analysis of fields gave in most cases better result compared with stations, for the surface layer there was not great differences.

Consequently, model can calculate time fluctuation well, but does not consider spatial variability.

The comparison of soil moisture under different crops (potato, winter and summer cereals, grassland) and in different soil types has been treated as they count territorial aspect as well as temporal. Correlation on 99% reliability is approached for every crop. Higher correlation coefficient, better reliability and accuracy appear for grassland, worse values for winter crop. Comparison of different soil types differentiates between light (sand and sandy loam), medium (sandy silt loam) and heavy soils (clay loam and clay). The correlation is the better the heavier the soil is, staying on 99% reliable for all cases. Reliability and accuracy are worse for light and heavy soils, better for medium soils.

4. Conclusions

1. In general a reliable correlation exists between model predicted and observed soil moisture values.
2. For whole selection the mean error is positive - model generally predicts higher values for soil moisture than it really is.
3. In the region of low measured soil moisture values a heavy over-prediction exists. Slight under-prediction occurs when observed soil moisture value is near to the maximum value.
4. HIRLAM describes well the temporal variations of soil moisture during the vegetation period.
5. Territorial correlation between predicted and observed soil moisture is not good.

It could be concluded that differences in soil types and properties not taken into account in model determine most of the differences between predicted and observed data over the territory.

References

Källen, 1996. HIRLAM Documentation Manual. System 2.5. Available from SMHI, Norrköking, Sweden..

Broken sea ice and its effects on the parameterization of atmospheric heat fluxes as determined by aircraft measurements over the Gulf of Bothnia

David Schröder[1], Timo Vihma[2], Burghard Brümmer[1] and Agathe Kerber[1]

[1] Meteorological Instiute, University of Hamburg, Bundesstrasse 55, D-20146 Hamburg, Germany
[2] Finnish Instiute of Marine Research, P.O. Box 33, FIN-00931 Helsinki, Finland

1. Introduction

The proper knowledge of sea ice is essential for the parameterization of turbulent surface fluxes. Aircraft measurements during BASIS (Baltex Air-Sea-Ice Study) 1998 and BASIS/BALTIMOS 2001 at levels between 10 and 30 m height allow to determine the properties of sea ice (concentration, surface temperature, and albedo) and the turbulent fluxes of momentum and heat over broken sea ice. Ice concentration was calculated from both infrared surface temperature and albedo. The relation between surface temperature and albedo as well as the variation of the turbulent fluxes with respect to surface temperature and albedo are discussed. Furthermore, applying the Monin-Obukhov similarity theory, the roughness lengths and the corresponding bulk transfer coefficients for momentum and heat are calculated from the measurements. Their magnitudes and their dependence on ice concentration are presented.

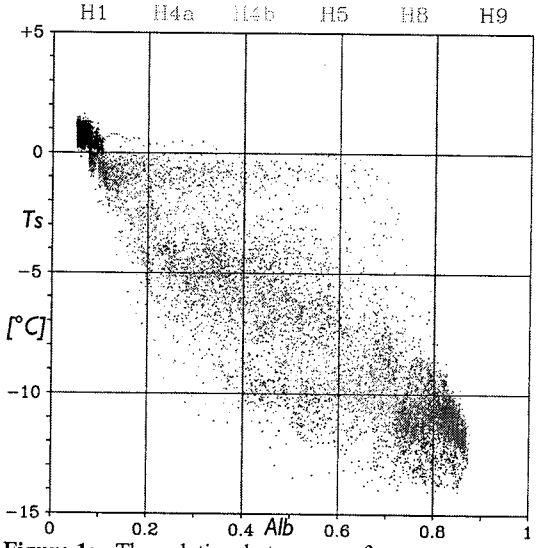

Figure 1: The relation between surface temperature and albedo of broken sea ice as determined by aircraft on 5 March 1998 in example.

2. Surface temperature and albedo of sea ice

Based on the aircraft measurements there is a linear relation between surface temperature and albedo in the sense that surface temperature is lower when albedo is higher. The gradient depends on the actual flow situation. An example is shown in Figure 1 for a cold off-ice air flow on 5 March 1998. There is a remarkable amount of "grey ice" with albedo values between the two extremes: open water (about 0.1) and white ice (about 0.8). Is is obvious that the ice concentration estimated on the basis of surface temperature results in higher values than ice concentration estimated on the basis of albedo (assuming that an intermediate albedo is a mixture of white ice and open water). On the other hand, the more correct ice concentration based on surface temperature does not help any further if it would be interpreted as ice consisting of only one ice class e.g. white ice. The question arises if e.g. the heat flux over an area completely covered with grey ice is the same as over an area covered partly by open water and white ice but with the same albedo as the grey ice area. From a satellite image this cannot be distinguished.

3. Heat flux as function of surface temperature and albedo

The turbulent surface fluxes of latent and sensible heat were classified with respect to surface temperature and albedo. By calculating the ice concentration from surface temperature and by using one ice class, the heat fluxes are underestimated. Heat fluxes over a grey ice area are smaller than over a mixed area of open water and white ice of same mean surface temperature and albedo.

4. Roughness lengths and transfer coefficients

The effective roughness lengths and corresponding transfer coefficients for momentum, heat, and moisture over broken sea ice were calculated for horizontal intervals 20 km long. The 20-km intervals are shifted by 1km. The calculations were based on the parameter aggregation method applying Monin-Obukhov theory and the universal stability functions. The results show that the mean effective roughness length for heat ($z_T = 3 \cdot 10^{-8}$ m) is 4 orders of magnitude smaller than that for momentum ($z_0 = 3 \cdot 10^{-4}$ m). The corresponding neutral transfer coefficients are $C_{HN} = 0.9 \cdot 10^{-3}$ and $C_{DN} = 1.6 \cdot 10^{-3}$. The ratio $\ln(z_0)/\ln(z_T)$ is presented as a function of ice conentration n_{ice} (separately for surface temperature and albedo). The best regression curve is e.g.: $\ln(z_0)/\ln(z_T) = 1.4 - 2.6 \cdot n_{ice} + 1.7 \cdot (n_{ice})^2$ for n_{ice} based on suface temperature.

5. Sensitivity of turbulent fluxes to roughness length

To investigate the influence of the roughness lengths on the turbulent fluxes, comparisons between the measured and parameterized sensible heat fluxes are presented. In Figure 2a, H is parameterized according to *Launiainen and Vihma* (1990) applying the universal functions, setting z_0 to 10^{-3} m, and calculating z_T as a function of z_0 and the roughness Reynolds number Re (*Andreas*, 1987). The comparison shows that H is generally overestimated by a factor of approximately two. The root-mean-square error (RMSE) is 24 Wm^{-2}, and the observed fluxes vary between −30 and +90 Wm^{-2}. In Figure 2b, the above mentioned new functional form for z_T depending on z_0 and ice concentration is applied. The RMSE is reduced to 15 Wm^{-2}, and a good agreement is reached for the whole range of values. The comparison shows that the roughness lengths have a large effect on the surface heat fluxes. A significantly smaller z_T than z_0, as previously observed over heterogeneous land surfaces, is necessary to

realistically parameterize the heat fluxes over broken sea ice.

6. Discussion

The properties of sea ice in the ice edge zone show a high degree of variability. The albedo values cover the whole range from 0.2 to 0.85. Heat fluxes over a grey ice area are smaller than over a mixed area of open water and white ice of same mean surface temperature and albedo. A proper sea ice classification depending on objective and resolution of the used model remains a problem.

Our calculated ratios of the effective roughness lengths (z_0/z_T ~ 1000) and of the corresponding transfer coefficients (C_{DN}/C_{HN} ~ 1.8) for a broken sea ice cover are approximately in agreement with several observational results obtained for heterogeneous land surfaces, being closest to those of *Beljaars and Holtslag* (1991). This is reasonable, because from the point of view of the surface temperature distribution, a mixture of sea ice and leads often resembles heterogeneous land surfaces more than a compact ice cover.

A comparison between measured and parameterized fluxes using different roughness lengths shows that (1) commonly used parameterization techniques strongly overestimate the surface heat fluxes over broken sea ice and (2) realistic heat fluxes can be parameterized using significantly smaller values for z_T than for z_0. Our experimental functional form leads to good results concerning the sensible heat flux. The proposed formula is applicable for use in numerical models, if the ice concentration is known (e.g. form SSM/I satellite data).

References

Andreas, E. L.:1987, 'A theory for the scalar roughness and the scalar transfer coefficients over snow and sea ice, *Bound.-Layer Meteorol.* **38**, 159-184.

Beljaars, A. C. M. and Holtslag, A. A. M.: 1991, 'Flux parameterization over land surfaces for atmospheric models, *J. Appl. Meteorol.* **30,** 327-341.

Brümmer, B., Schröder, D., Launiainen, J., Vihma, T., Smedman, A., and Magnusson, M.: 2001, Temporal and spatial variability of surface fluxes over the ice edge zone in the northern Baltic Sea, *J. of Geophys. Res.*, submitted

Launiainen, J. and Vihma, T.: 1990, 'Derivation of turbulent surface fluxes - an iterative flux-profile method allowing arbitrary observing heights, *Environmental Software* **5**, 113-124.

Vihma, T., Schröder, D., Kerber A., and Brümmer, B.: 2001, On the parameterization of turbulent surface fluxes over broken sea ice, *BALTEX-BASIS Final Report*, J. Launiainen (edt.), in press.

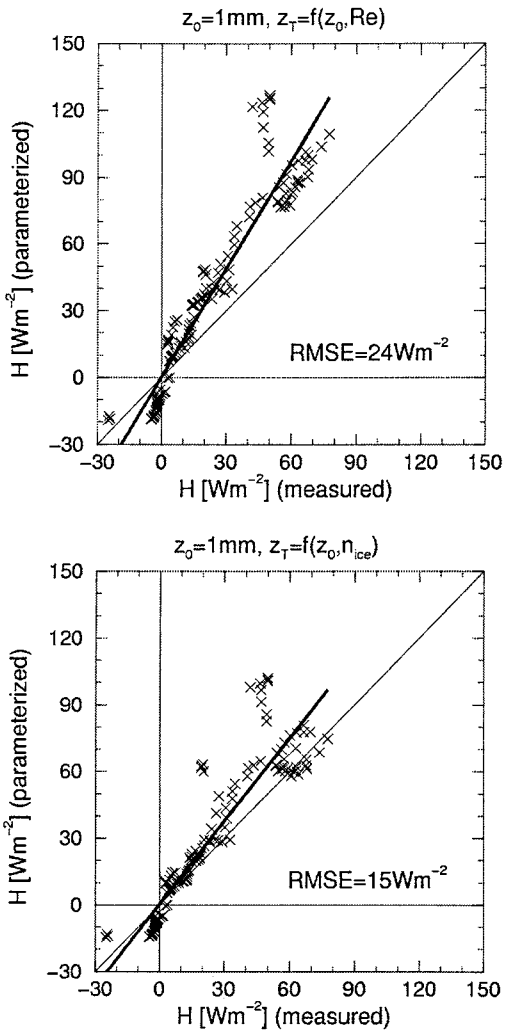

Figure 2: Comparison between measured and parameterized sensible heat flux H based on 20km-averages. In Figure a (top), z_T is determined as a function of z_0 and the Reynolds number Re (*Andreas*, 1987), whereas in Figure b (bottom) our functional form for $z_T = f(z_0, n_{ice})$ is applied.

Relationship between Frequency of Circulation Patterns (according to Classifications by Wangenheim-Girs and Hess-Brezowsky) and Weather Fluctuations in Europe

Mait Sepp, Jaak Jaagus

Department of Geography, University of Tartu, Vanemuise 46, 51014 Tartu, Estonia

1. Introduction

Atmospheric circulation is a leading factor that determines climate variability in Europe. Many authors have analysed relationship between the intensity of westerlies on the North Atlantic and winter air temperature on the continent. Atmospheric circulation can be characterised using circulation indices or circulation types. The most popular circulation index - the North Atlantic Oscillation index - is an important measure of intensity of westerlies on the North Atlantic.

There have been developed a variety of classifications for atmospheric circulation. The majority of them are composed for single countries or limited regions. But some of them are based on circulation types over large territories and even over the whole hemisphere. Two circulation classifications most suitable for the territory of Europe are taken into analysis in this study. Circulation macrotypes worked out by Wangenheim and Girs (Arctic and Antarctic Institute, St. Petersburg) have the highest correlation with climate variability in the Northern and Eastern Europe while circulation groups by Hess and Brezowsky (Grosswetterlagen) are mostly designed for the Central Europe.

The objective of this study is to analyse geographical distribution of correlation between frequencies of circulation patterns according to Wangenheim-Girs and by Hess-Brezowsky, and air temperature and precipitation fields in Europe. Areas with maximum correlation are determined. Main peculiarities of atmospheric circulation that influence on formation of air temperature and precipitation fields are discussed.

2. Data and methods

Monthly and seasonal frequencies of circulation macrotypes W, E and C by Wangenheim-Girs, and of zonal (Z), half-meridional (HM) and meridional (M) circulation groups by Hess-Brezowsky are used to characterise circulation conditions over Europe. Climate variability is expressed using 5x5 degree gridded values on monthly sea-level pressure, air temperature and precipitation in sector between 35°N and 75°N, and 30°W and 60°E covering the territory of Europe. The gridded data are obtained from the Global Climatological Dataset created by the Climatic Research Unit, University of East Anglia, UK.

Frequencies of the circulation patterns are correlated with the climatic variables in every grid cell during the study period 1900-1998. Correlation fields are drawn using kriging for interpolation, and a great number of correlation maps are analysed. On a base of the correlation maps, general regularities concerning the influence of atmospheric circulation on formation of temperature and precipitation patterns in Europe are formulated.

3. Results

The aim of analysing correlation fields between sea-level pressure and frequencies of circulation patterns is to get a better understanding on the essence and meaning of single circulation patterns. Mostly, they are determined using 500 hPa geopotential fields. Correlating them with sea-level pressure fields enables to connect them with synoptic processes. The highest correlation between frequencies of circulation pattern and sea-level pressure is typical for winter season. Certain similarities between these two classifications can be found. Circulation types W and Z are positively correlated with air pressure in the Southern Europe, and negatively correlated with pressure in the Northern Europe (Figure 1). At the same time, patterns E and M have an opposite location of the correlation areas (Figure 2). Macrotype C corresponds to high pressure in the Western Europe and low under the East European plain (Figure 3).

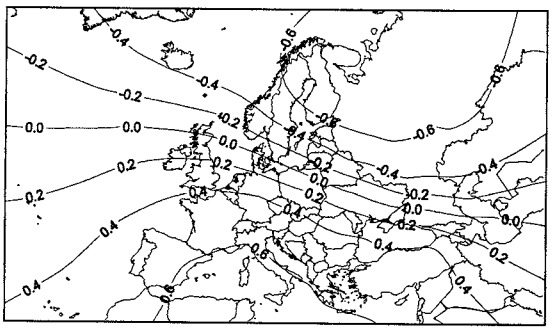

Figure 1: Correlation between sea-level pressure and frequency of circulation macrotype W in winter.

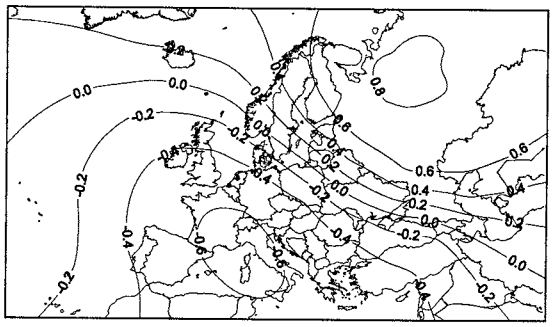

Figure 2: Correlation between sea-level pressure and frequency of circulation macrotype E in winter.

Relationship between atmospheric circulation and air temperature in winter and summer is of opposite sign in the most parts of Central and Northern Europe (Figures 3 and 4). Prevailing western flow (circulation types W and Z) is positively correlated with temperature in winter and negatively correlated in summer. Areas of maximum correlation in winter are located in Central Russia (W) and in Central Europe (Z). In summer, the highest negative correlation is met in southern Scandinavia, in the Baltic Sea region and under the British Isles (Z).

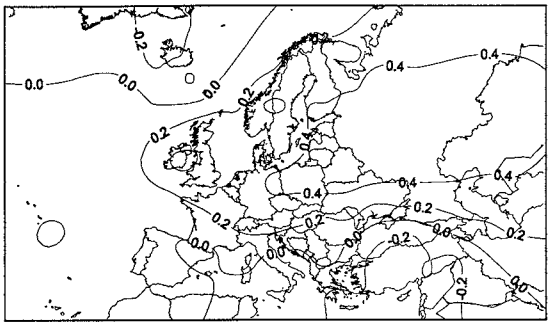

Figure 3: Correlation between air temperature and frequency of circulation macrotype W in winter.

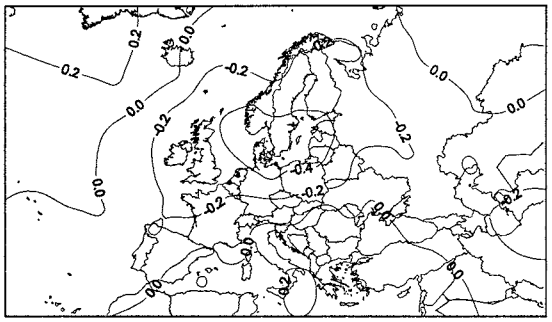

Figure 4: Correlation between air temperature and frequency of circulation macrotype W in summer.

Meridional circulation patterns E and M have negative correlation with temperature in winter and positive correlation in summer. In case of macrotype E, the area with the highest negative correlation in winter is situated in the Southern Russia and the area with maximum positive correlation embraces the Northwestern Russia, Finland and Estonia. Meridional circulation group by Hess-Brezowsky has the highest negative correlation with winter mean temperature in the Central Europe and has no correlation with temperature in summer. Circulation macrotype C that corresponds to northerly winds in Eastern Europe is mostly negatively correlated with air temperature.

Correlation patterns between atmospheric circulation types and precipitation are much more complicated. Correlation depends very much on orography, location of windward and leeward slopes of mountains. This dynamic effect is the most important factor in formation of precipitation pattern in Europe. As a rule, zonal circulation is positively correlated with precipitation in the Northern Europe and negatively correlated in the southern one. Thereby, maximum correlation is typical for windward, i.e. western slopes of the Scottish Highland and of the Scandinavian Mountains. A significant correlation between frequency of the W pattern and precipitation is observed also in Finland, Estonia and Northern Russia (Figure 5). At the same time, there is no correlation on the leeward sides of the mountains, in the Eastern Scotland and in the eastern coasts of Sweden. This type of correlation fields is characteristic for winter as well as for summer precipitation.

Zonal circulation type Z according to the German classification has even higher correlation with precipitation with maximum in Great Britain, Northern Germany, Southern Scandinavia and in the Baltic region.

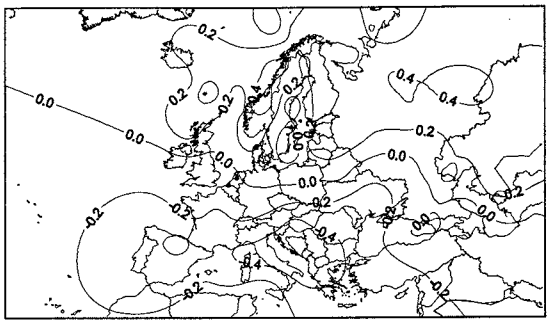

Figure 5: Correlation between precipitation and frequency of circulation macrotype W in winter.

Circulation macrotype E is followed by precipitation in the Southern Europe and on the eastern coast of Sweden, and by no rainfall on the Norwegian coast (leeward side) and in Russia. Macrotype C is mostly associated with dry weather in the Northern part of Europe.

The meridional circulation group by Hess-Brezowsky has a highly significant positive correlation (above 0.4) in the Mediterranean and negative correlation in the Northern Europe. The highest correlation is characteristic for winter.

4. Conclusions

Atmospheric circulation patterns are rather densely correlated with weather fluctuations in Europe. Frequency of circulation macro-types by Wangenheim-Girs has higher correlation with air temperature and precipitation in the Northern and Eastern Europe while circulation groups by Hess-Brezowsky better describe climate variability in the Central Europe. Western circulation (types W and Z) causes mild weather in winter and clouds, rainfall and lower temperature in summer in Central and Northern Europe. At the same time, it is dry in the Mediterranean. Meridional circulation includes airflow from directions between north, east and south. Usually, meridional circulation is positively correlated with summer temperature and negatively correlated with winter temperature. It is connected with below normal precipitation in the most of the Northern and Central Europe and above normal precipitation in the Mediterranean. Circulation types are positively correlated with precipitation on windward coastal regions and slopes of mountains, and negatively correlated with precipitation on the leeward side of mountains. This correlation pattern is clearly expressed on the Scandinavian Peninsula, for example.

Acknowledgements

This study is financed by the Estonian Science Foundation (grant No. 4347).

The Baltic sea catchment climate patterns simulated by the AMIP II GCMs.

Igor Shkolnik, Valentin Meleshko and Veronika Govorkova

Voeikov Main Geophysical Observatory, 7 Karbyshev str., 194021 St Petersburg, Russia

The skill of current GCMs to realistically simulate climate is a stumbling-block for regional climate modelling when a limited area model is nested into and driven by a GCM to reproduce statistical ensemble of the mesoscale and the global scale circulations. Particularly, as indicated in numerous studies the simulated regional climate strongly depends on how well the driving global model reproduces the atmospheric circulation properties over the separate region. The AMIP II provides an opportunity to figure out the current GCMs ability to be adequate while portraying the regional scale climate patterns. Since the AMIP I (see *Gates*, 1992) had completed the global models have undergone tremendous development both in increasing their resolution and improving physical parameterizations. In this study we evaluate the performance capabilities of the GCMs to reproduce climate over the Baltic sea catchment area using data set of the AMIP II 17 years climate simulations. For this area the analysis of the precipitation, the evaporation, the runoff, the snow mass, the surface air temperature, the cloudiness, the radiation properties, and some other has been conducted. The following 10 models that include various resolutions and physical packages are considered and their data compared against observation: **CCSR**, **CNRM**, **DNM**, **ECMW**, **JMA**, **NCAR**, **NCEP**, **PNNL**, **UGAM**, and **UKMO**. All the models uniformly treat the observed SST data.

The seasonal cycles of the computed characteristics reveal scattering of the modelling results. The departures of the modelling data from those observed tend to be independent of the model's resolution. The magnitude of the modeled cycles is reproduced by most of the models except that for the snow mass, the evaporation, and the cloudiness. The smaller range of the modelling differences can be found for the computed surface air temperature and some radiation properties which are reproduced by the models as compared to observation. Some models compute the annual mean runoff close to corresponding observational estimates. The model's mean runoff departure from that observed is less than 10%.

References

Gates, W.L., 1992. AMIP The atmospheric model intercomparison project. *Bull. Amer. Meteor. Soc.*, 73, 1962-1970

Radiative Flux Divergence Profiles from MSG

Oliver Sievers

GKSS Research Centre, Institute for Coastal Research, 21502 Geesthacht, Germany

1. Introduction

Vertical divergence of radiative flux is one of several reasons for dynamical forcing in the atmosphere. The knowledge of this parameter is important for better understanding of dynamical processes such as cloud formation. Furthermore the internal forcing of current models such as REMO has to be validated. It is necessary to use satellite information to derive atmospheric heating (and cooling) rates produced by radiation divergences over larger areas.

In section 2 some information about the new Meteosat system is given, the basic idea of resolving an aspect between atmosphere and radiation follows in section 3, and section 4 shows some highlights.

2. MSG

The next generation of Meteosat satellites (Meteosat Second Generation, MSG) will give us the unique chance of imaging the earth' surface with high temporal (15 minutes) and spatial (3x3 km^2) resolution. MSG will carry the narrowband instrument SEVIRI (Spinning Enhanced Visible and Infra-Red Imager) that will measure the radiation in 12 channels between 0.6 and 13.4 µm.

The three channels of former Meteosat satellites will be changed in the following manner. The former visible channel (0.5-0.9 µm) will be replaced by three channels with center wavelengths at 0.6, 0.8 and 1,6 µm and an additional high resolution channel (HRV) between 0.6 and 0.8 µm with a spatial resolution of 1x1 km^2. Two water vapour channels (WV) at 6.2 and 7.3 µm will replace the former WV channel at 6.4 µm, and 8 infrared channels (3.8, 8.7, 9.7, 10.8, 12.0 and 13.4 µm) take the place of the former 11.5 µm channel.

Besides, the broadband instrument GERB (Geostationary Earth Radiation Budget) will measure the outgoing radiance in the wavebands 0.32 µm – 4.0 µm (SW) and 0.32 µm – 30 µm (total), with a pixel size of about 50x50 km^2 at nadir. The accuracy will be better than 1% for SW and better than 0.5% for the LW channel. This offers the possibility to examine the radiation budget with a high temporal resolution over a large area.

The first of at least three MSG satellites is planned to be launched in January 2002.

3. Method

Several estimates of divergence values have been published before (e.g. Cox and Griffith, 1979a,b). It has been found that the main cause for vertical radiation divergences are clouds (see figs. 1,2). Depending on cloud geometry and microphysics, net radiation differences between two layers may vary from appr. −100 W/m^2 to +100W/m^2 with the largest values at top and bottom of the clouds. Using a vertical resolution of 1000 m, these differences correspond with net flux divergences of ±0.1 W/m^3.

To derive an interrelation between the flux profile and the outgoing radiance it is necessary to create a data set including several variations of cloud geometry, microphysics and atmospheric condition. This data set was created using the radiative transfer model Streamer (Key and Schweiger, 1998). Streamer allows the user to vary many variables describing the current state of the atmosphere.

Such examinations of cloud type variations have been done (for example) by Chen *et al.* (2000), often using the ISCCP data set (Schiffer and Rossow, 1983). The target in earlier investigations was (nearly) always to derive information about the vertical structure of the cloud, using not only satellites but rawinsondes (Wang and Rossow, 1995) or a combination of several instruments (Wang *et al.*, 1999).

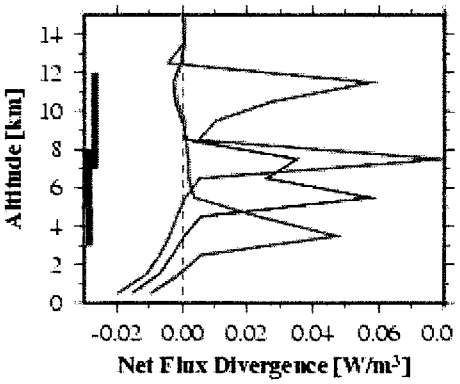

Figure 1: Net flux Divergence for three types of clouds with different geometry (cloud top and thickness). The vertical extension is shown by the colored rectangles at the left.

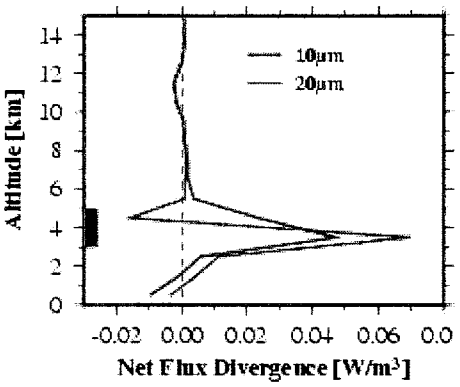

Figure 2: Net flux divergence for two clouds, with different mean particle size, but same vertical extension.

A main restriction of Streamer is the fact that clouds are plane-parallel, i.e. horizontally homogeneous. Real clouds are never homogeneous, and the influence of such inhomogeneities has been the topic of several examinations (Davies, 1978; Galinsky and Ramanathan, 1998; Várnai, 2000). To investigate the 3 dimensional effects, a Monte Carlo model which has been developed at the University of Kiel was used at the institute.

4. Results

Clouds have a major influence on radiative flux divergences. Fig. 1 shows the net divergence profiles for water clouds with an effective radius of 10 µm for different cloud tops and geometrical thickness. At the top and the bottom of the clouds large positive net divergences (corresponding with a strong warming) are noticeable. For the lowest cloud (red), the vertical resolution of the Streamer model is not high enough to show both peaks. Net flux divergence grows with increasing altitude of the cloud, but as shown in Fig. 2, the sign of the radiative flux divergence at the top of the cloud may change to a net cooling when doubling the effective radii of the cloud droplets (blue line). This exhibits the importance of variing all parameters while creating the data set.

The influence of horizontal and vertical inhomogeinities to the upwelling flux above the cloud is shown in fig. 3. The clouds used for the calculation consist of two layers, each 500 m thick. The blue line represents a vertically homogeneous, but horizontally inhomogeneous cloud, while the red one represents a horizontally homogeneous (integrated over both layers, but inhomogeneous in each layer) but vertically inhomogeneous cloud. If the horizontal scale is much larger than the vertical scale (i,e, the cloud has a large aspect ratio) the vertical inhomogeneities dominate the deviation from the homogeneous cloud. Only for clouds with an inhomogeneity aspect ratio of less than 10 an effect in upwelling flux, depending on the horizontal scale, is noticeable.

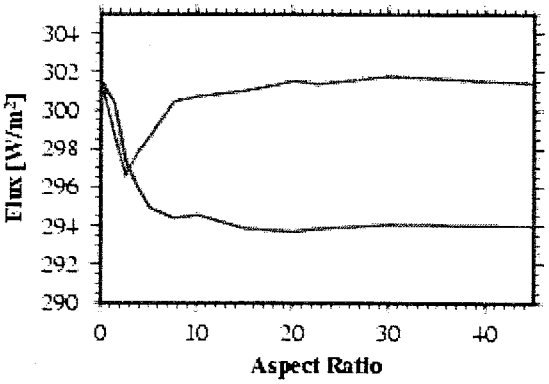

Figure 3: Upwelling radiation flux, depending on horizontal scale of inhomogeneity; the red line represents a vertically and horizontally inhomogeneous cloud, the blue line a horizontally inhonogeneous one only. The sun zenith angle is 60 degree.

References

Chen, T., Rossow, W.B., Zhang, Y., Radiative Effects of Cloud-Type Variations, *Journal of Climate*, Vol. 13, 264-285, 2000

Cox, S.K., Griffith, K.T., Estimates of Radiative Divergence during Phase III of the GARP Atlantic Tropical Experiment: Part I. Methodology, *Journal of the Atmospheric Sciences*, Vol. 36, 576-585, 1979a

Cox, S.K., Griffith, K.T., Estimates of Radiative Divergence during Phase III of the GARP Atlantic Tropical Experiment: Part II. Analysis of Phase III Results, *Journal of the Atmospheric Sciences*, Vol. 36, 586-601, 1979b

Davies, R., The Effect of Finite Geometry on the Three-Dimensional Transfer of Solar Irradiance in Clouds, *Journal of the Atmospheric Sciences*, Vol. 35, 1712-1725, 1978

Galinsky, V.L., Ramanathan, V., 3D Radiative Transfer in Weakly Inhomogeneous Medium. Part I: Diffusive Approximation, *Journal of the Atmospheric Sciences*, Vol. 55, 2946-2959, 1998

Key, J., Schweiger, A.J., Tools for atmospheric radiative transfer: Streamer and FluxNet, *Computers and Geosciences*, Vol. 24, No.5, 443-451, 1998

Schiffer, R.A., Rossow, W.B., The International Satellite Cloud Climatology Project (ISCCP): The First Project of the World Climate Research Programme, *Bulletin of the American Meteorological Society*, Vol. 64, No.7, 779-784, 1983

Várnai, T., Influence of Three-Dimensional Radiative Effects on the Spatial Distribution of Shortwave Cloud Reflection, *Journal of the Atmospheric Sciences*, Vol. 57, 216-229, 2000

Wang, J., Rossow, W.B., Determination of Cloud Vertical Structure from Upper-Air Observations, *Journal of Applied Meteorology*, Vol. 34, 2243- 2258, 1995

Wang, J., Rossow, W.B., Uttal, T., Rozendaal, M., Variability of Cloud Vertical Structure during ASTEX Observed from a Combination of Rawinsonde, Radar, Ceilometer, and Satellite, *Monthly Weather Review*, Vol. 127, 2484-2502, 1999

The Turbulent Kinetic Energy Budget over the Baltic Sea

Anna Sjöblom and Ann-Sofi Smedman

Department of Earth Sciences, Meteorology, Uppsala University, Villav. 16, SE-752 36 Uppsala, Sweden

1. Introduction

Air-sea interaction has not got as much attention as flux measurements over land, mainly because it is much more difficult to measure over sea than over land. Ships and buoys usually have to be used, and since they move it is very difficult to perform accurate measurements. Measurements on ships and buoys are also very sensitive to flow distortion.

The inertial dissipation is a method that has been used for about 30 years to estimate the fluxes over sea. There are several advantages with this method, for example, only measurements in the inertial subrange are needed, and these high frequency fluctuations can easily be separated from the disturbances caused by the movements of for example a ship at lower frequencies. It is also clear that this method is superior to the direct covariance method in regions of severe flow distortion.

The turbulent kinetic energy (TKE) budget plays an important role in the inertial dissipation method, and it has not been as thoroughly investigated over sea as over land. The normalized TKE-budget in stationary and homogeneous conditions is defined as

$$\underbrace{\frac{kz}{u_*}\frac{\partial \overline{u}}{\partial z}}_{\text{(PN)}} - \underbrace{\frac{kz}{u_*^3}\frac{g}{T_v}\overline{w'\theta_v'}}_{\text{(BN)}} + \underbrace{\frac{kz}{u_*^3}\frac{\partial}{\partial z}\frac{\overline{w'e'^2}}{2}}_{\text{(TtN)}} + \underbrace{\frac{kz}{u_*^3}\frac{1}{\rho}\frac{\partial \overline{p'w'}}{\partial z}}_{\text{(TpN)}} + \underbrace{\frac{kz}{u_*^3}\varepsilon}_{\text{(DN)}} = 0 \quad (1)$$

where PN is the mechanical production, BN the buoyancy, TtN the turbulent transport, TpN the pressure transport and DN the dissipation.

The terms have to be correctly parameterized when using the inertial dissipation method, and it is common to assume that the sum of the transport terms is small. Therefore they are most often neglected, at least in near neutral conditions (e.g. *Fairall and Larsen,* 1986).

It is not completely understood how the different terms in the TKE-budget responds to different wave conditions, even though several studies have been made of the influence of swell on the turbulent characteristics (e.g. *Smedman et al.*, 1999).

In this study, the TKE-budget and the influence of waves have been analyzed using long term measurements over the Baltic Sea.

2. Measurements

The measurements were performed at the small island of Östergarnsholm, outside Gotland, in the middle of the Baltic Sea. A 30 m tower is erected at the southern most tip, with turbulence measurements at three levels and slow response measurements (wind speed, wind direction and temperature) at five levels. The flux footprint for Östergarnsholm shows that it resembles open sea for most conditions in the undisturbed sector with long over water fetch (*Smedman et al.,* 1999).

In addition to these instruments, a wave rider buoy (run and owned by the Finnish Institute for Marine Research) is deployed 5 km south-east of Östergarnsholm.

Mechanical production, buoyancy and the turbulent transport were determined directly from the measurements, and the dissipation was computed from the inertial subrange of velocity spectra. The pressure transport term was determined as a residual. The Kolmogorov constant used is 0.52, in accordance with *Högström* (1996).

Only measurements with an undisturbed over water fetch was used, leaving more than 2000 30 minutes averages, where more than 1000 also contain wave information.

3. Waves

One way to describe how well developed the wave field is, is to use the so called wave age, defined as $c_0/(U_{10}\cos\theta)$, where c_0 is the phase velocity at the peak of the spectrum, U_{10} the wind speed at 10 m, and θ the angle between wind- and wave direction.

The peak of the spectrum is defined as the highest peak in the wave spectrum, with no consideration taken to the number of peaks, i.e. if there is more than one peak, it is more or less random which one is taken as the highest. Wave spectra with more than one peak are not uncommon in the Baltic Sea.

Swell, that is waves travelling faster than the wind, is here defined as $c_0/(U_{10}\cos\theta)>1.2$. Since the Baltic Sea is semi-enclosed, swell will not be able to travel a long way before it reaches land, which is in contrast to the open ocean where swell can travel very long distances, and from several directions. Most of the swell encountered at Östergarnsholm is produced at the southern part of the Baltic Sea and then transported northwards.

4. Results

The different terms in the TKE-budget were investigated according to stability, wave age and wind speed. The results are defined so that a positive value indicates a gain in energy and a negative value a loss. All the terms are normalized according to Equation (1) and bin-averaged in two dimensions. In this study, only measurements from the lowest level of turbulence measurements (approximately 10 m above sea level) will be presented.

As discussed above, it is common to assume that the sum of the transport terms are small, i.e. to assume that production equals dissipation. However, as showed in Figure 1, where the imbalance is plotted as a function of wave age and stability, this is very seldom the case.

Only values close to neutral are showed here, so it is perhaps difficult to see a large stability dependence on the imbalance. The largest imbalance is found for stable conditions and swell, and the imbalance will be larger for both more stable and more unstable conditions (not showed here).

Figure 1 shows that the imbalance clearly depends on the wave age. For very young waves, $c_0/(U_{10}\cos\theta)<0.5$, and neutral conditions, the production exceeds the dissipation, probably due to the fact that energy is helping to build up the waves rather than being dissipated into heat. This is in accordance with *Edson and Fairall* (1998), who found that production was exceeding dissipation for slightly unstable conditions.

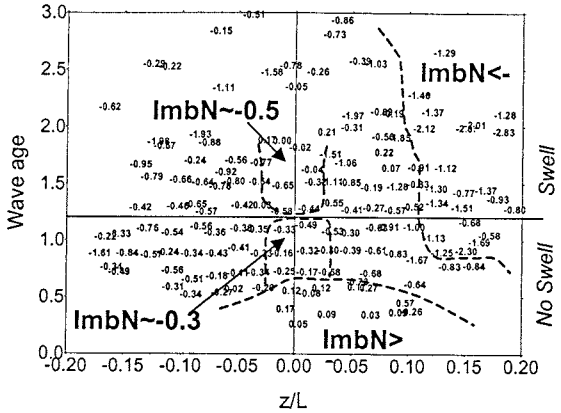

Figure 1: Normalized imbalance, ImbN (normalized production – normalized dissipation) as a function of wave age ($c_0/(U_{10}\cos\theta)$) and stability (z/L).

For swell $c_0/(U_{10}\cos\theta)>1.2$, the dissipation is much larger than the production.

The waves seem to be "saturated" between $0.5<c_0/(U_{10}\cos\theta)<1.2$, i.e. neither growing, nor decaying. The value of the imbalance in this wave age range is approximately –0.30 (dissipation exceeding production), which is close to what has been found over land (e.g. *Högström*, 1996).

The same type of structure for the imbalance as in Figure 1 can also be seen in Figure 2, where the imbalance is plotted as a function of wind speed and stability.

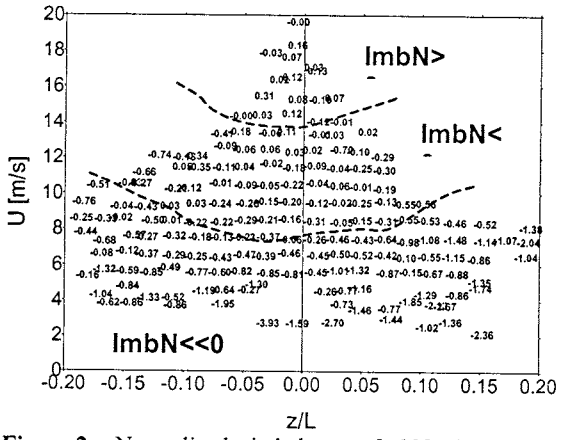

Figure 2: Normalized imbalance, ImbN (normalized production – normalized dissipation) as a function of wave age $c_0/(U_{10}\cos\theta)$ and wind speed (U).

For low wind speeds (U<~8 ms^{-1}), which is also associated with swell is the dissipation much larger than the production. At U~14 ms^{-1} the imbalance changes sign, and the production becomes larger than the dissipation. The positive imbalance found for high wind speeds resembles the small wave ages in Figure 1.

What is then responsible for the imbalance between production and dissipation? The turbulent transport is even though some scatter (not showed here), small for all conditions encountered in this study (not showed here), and will therefore give very little contribution to the imbalance.

The pressure transport is however not negligible (Figure 3), and will not be balanced by the very small turbulent transport.

The values of the pressure transport is almost the same as for the imbalance (Figure 1), but with opposite signs.

For small wave ages is the pressure transport positive, and for swell it is quite large negative. And for moderate wave ages, the pressure transport resembles what has been found over land (*Högström*, 1996).

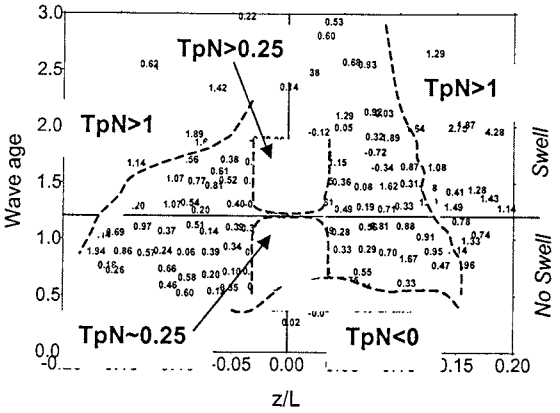

Figure 3: Normalized pressure transport, TpN, as a function of wave age ($c_0/(U_{10}\cos\theta)$) and stability (z/L).

5. Conclusions

This study has shown that the transport terms in the TKE-budget are not negligible, and that the different terms in the budget depend not only on stability, which has been previously suggested, but also on wave age and to some degree wind speed.

The imbalance between production and dissipation origins mainly from the pressure transport. The reason for this is probably due to so called "inactive turbulence", where energy is being transported down to the surface from higher levels without interacting with the "ordinary" turbulence (e.g. *Smedman et al.*, 1999).

The use of the "classical" inertial dissipation method, where the transport terms are assumed small and most often neglected, is questionable during swell conditions since the imbalance between production and dissipation is very large. For "saturated" waves and "moderate" wind speeds, the sea surface seem to resemble a land surface, and there should the same corrections as suggested over land be valid over sea, to compensate for the imbalance.

References

Edson, J. B., Fairall, C. W., Similarity relationships in the marine atmospheric surface layer for terms in the TKE and scalar variance budgets, *J. Atm. Sci.*, 55, 2311-2328, 1998.

Fairall, C. W., S. E. Larsen, Inertial-dissipation methods and turbulent fluxes at the air-ocean interface, *Boundary–Layer Meteorol.*, 34, 287-301, 1986.

Högström, U., Review of some basic characteristics of the atmospheric surface layer, *Boundary–Layer Meteorol.*, 78, 215-246, 1996.

Smedman, A., U. Högström, H. Bergström, A. Rutgersson, K. K. Khama, H. Pettersson, A case study of air-sea interaction during swell conditions, *J. Geophys. Res.*, 104, 25833-25851, 1999.

Monitoring of Emergencies in the Western Dvina Transboundary River Basin.

Ivan Skuratovich[1], Vladimir Korneev[2]

[1] State Committee on Hydrometeorology Republic of Belarus
[2] Central Research Institute for Complex Development of Water Resources (The Ministry of Natural Resources and Environmental Protection of the Republic of Belarus)

The Western Dvina river is one of the main transboundary rivers of the Europe. The overall length of the river of 1005 kms, 325 kms from them flow through the territory of Russia, 328 kms - through the territory of Belarus, 352 kms - through the territory of Latvia.
Catchment area of the river basin is about 87900 km^2, 21 % from them is disposed on the territory of Russia, 37,8 % - on the territory of Belarus, 28,1 % - on the territory of Latvia, 13,1 % - on the territory of Lithuania and Estonia.
The river plays the main role in economic activity of the people, which one live in the river basin. There are approximately 254 thousand inhabitants of Russia, 0,7 million inhabitants of Belarus and 1,4 million. inhabitants of Latvia. On the territory of Latvia on the Western Dvina/ Daugava river the water reservoirs of the Hydroelectric Power Station of Pliavinas, Kegumas and Riga cities are situated.
The main tributaries of the Western Dvina which related to the territory of Belarus are: Obol, Polota, Usviacha, Drysa, Kasplia, Luchosa, Ulla, Ushacha, Disna, Druika (see table 1.)

Table 1: Characteristics of the Western Dvina Tributaries

Name of tributary	Length (km)	Catchment area (km^2)	Average annual discharge (m^3/s)
Obol	148	2690	19,4
Polota	93	651	4,8
Usviacha	100	2340	15,9
Drysa	183	6420	45,6
Kasplia	136	5410	35
Luchosa	90	3510	21,4
Ulla	123	4090	25,4
Ushacha	118	1150	8,0
Disna	178	8180	52,4
Druika	52	1050	6,8

State Committee on Hydrometeorology Republic of Belarus make measuring procedure of the quantitative and qualitative parameters of water of the Western Dvina river and its tributaries base on the set of hydrological and hydrochemical observations. The hydrological points make standard measuring technique of hydrological regime (daily observations of water level and water discharge - in applicable points). In the Western Dvina river basin are situated 11 hydrological points of observations (see fig.1) :
Western Dvina (Suraj, Vitebsk, Ulla, Polotsk, Verchnedvinsk);
Obol (Obol) ;
Polota (Iankovo);
Drysa (Demechy (closed since 07.2000), Dernovichy);
Luchosa (Luchosa);
Ulla (Bocheykovo);
Disna (Sharkovchina)

The sample on hydrochemical points are make 12 time per year for Western Dvina and 7 time per year for its tributaries. In the Western Dvina river basin are situated 10 hydrochemical points of observations (see fig 1) :
Western Dvina (Suraj, Vitebsk, Polotsk, Novopolotsk, Verchnedvinsk);
Obol (Obol)) ;
Polota (Polotsk);
Ushacha (Novopolotsk));
Ulla (Chashniky);
Disna (Sharkovchyna).

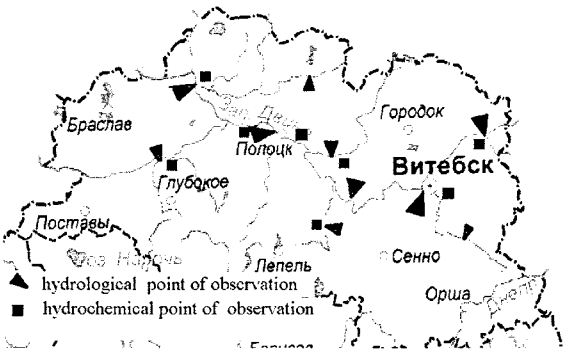

Figure 1: Location of hydrochemical and hydrological observatories in the western Dvina River basin.

On the basis of the National System of Monitoring of Environment in the Republic of Belarus the system of local monitoring of sewage disposal at the enterprises are developing. Tacking into account this system at the enterprises 2 times per month are conducted measuring procedure of the quantitative and qualitative parameters of sewage's. The information is representing in territorial center of monitoring of the Vitebsk Regional Committee of Natural Resources and Environmental Protection. The Vitebsk Regional Committee is defines the list of the priority enterprises for procedure of local monitoring of sewage's.
Base on the State Water Cadastre Information (1999 y.) priority parameters of water quality of the river of Belarus are:
nitrogen ammonia,
nitrogen nitrate,
manganese,
petroleum.
Maximum concentration of petroleum - 14 of Maximum Admissible Concentration (MAC) - is fixed on the Ushacha river downstream of Novopolotsk, manganese (25MAC) on the Western Dvina river downstream of Novopolotsk.
General describing of the situation of water quality in the Western Dvina river Basin :
quality of water in Western Dvina is characterized by the heightened contents of manganese and other metals,

downstream, of Novopolotsk - heightened contents of petroleum;
in the river of Ulla the exceeds of MAC on copper, Zincum, petroleum are observed;
in the river of Polota the exceeds of MAC on heavy metals and petroleum are observed;
in the river of Ushacha the exceeds of MAC on heavy metals, nitrogen ammonia, nitrogen nitrate and petroleum are observed;
in the river of Disna the exceeds of MAC on coppers, zinc, manganese, phenols and petroleum are observed;
in the river of Obol the exceeds of MAC on heavy metals, nitrogen ammonia and petroleum are observed.
The major emergencies on large water objects in the Western Dvina river basin take place extremely seldom, thus the measuring procedure of emergency discharges take place not always. The largest fixed accident on transboundary water objects of Belarus is the accident in 1990r. The main result of this failure - the emergency discharge of several tens tons of cyanides in the Western Dvina river. The surge of emergency pollution's has reached territory of Latvia and has caused major damage both territory of Belarus and Latvia. In 2001y there was emergency in Western Dvina of fair quantity of sewage's from sewage refining system of Vitebsk.
The emergency input of cyanides has taken place 3.11.1990. Measuring of passing of an emergency wave surge of concentration of cyanides has taken place only on the territory of Latvia - in points of cities Daugavpils and Eckabpils. Eckabpils is disposed downstream. Data's of measuring in points of Eckabpils exceeded the applicable measuring in points of Daugavpils approximately in three times. Tacking into account results of measuring in point of Daugavpils and using the hydrodynamic model of moving water and pollution in the river basin the calculated total discharge of cyanides is about 17.7 tons.
For modeling of pollution's transboundary transfer in Western Dvina the hydrodynamic model was developed which include the detailing information about river basin from Novopolotsk to board with Latvia [1]. For this purpose the following activities was made :
the digitization of the map of Western Dvina river and neighboring territory was made;
the collecting of the geometrical and hydraulic information about cross-sections of the Western Dvina river (including local coordinates and coefficients of roughness) was made;
tacking into account observations of the State Committee on Hydrometeorology the graphs of water discharge and water level on the boarder of river - section was made;
After mathematical model and its calibration model was decided many different numerical experiments was made using different values of arguments : summary discharge and regime of cyanides load etc.)
The analysis of the numerical experiment outcomes has shown, that the mathematical model adequately reacts to variation of arguments of emergency pollution's load in river and takes into account other factors on which ecological situations in the Western Dvina river basin depends (see a fig. 2).

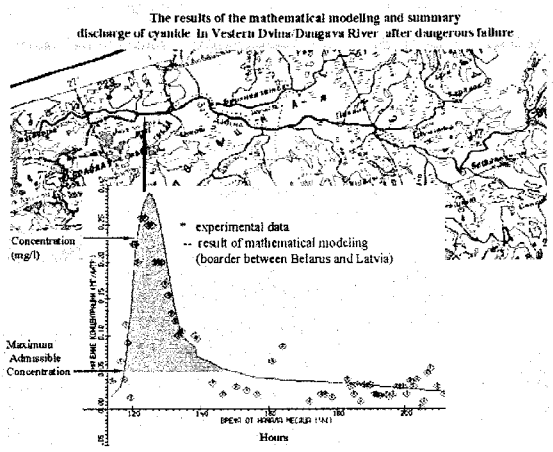

Figure 2: Explanation see text

References :

A. Stankevich, V.Korneev, P. Afanasiev. Mathematical model of forecasting pollution transfer in water object of industrial area. Thesis's of the reports. The 9th Stockholm Water Symposium. 9-12 August 1999. (English)

Summary of the results obtained in the PEP in BALTEX experiment

Ann-Sofi Smedman[1],Tage Andersson[3], Ekaterina Batchvarova[2], Karl Bumke[6], Jens Bösenberg[3], Marco Clemens[6], Bernd Fischer[3], Sven-Erik Gryning [2], Barbara Hennemuth[3], Reijo Hyvönen[4], Ulf Högström[1], Daniela Jacob[3], Cecilia Johansson[1], Markku Kangas[4], Dimitrios Melas[1], Daniel B. Michelson[5], Anders Omstedt[5], Aulis Peltomaa[4], Gerhard Peters[3], Anna Rutgersson[1,5], Kristiina Säntti[4], Bengt Tammelin[4]

[1] Department of Earth Sciences, Meteorology, Uppsala University, Uppsala, Sweden
[2] Risö National Laboratory, Roskilde, Denmark
[3] Max-Planck Institute, Hamburg, Germany
[4] Finish Meteorological Institute, Helsinki, Finland
[5] Swedish Meteorological and Hydrological Institute, Norrköping, Sweden
[6] Institut für Meereskunde, University of Kiel, Kiel, Germany

Conclusions

The objectives and goals of the project PEP in BALTEX have been successfully carried out.

Measurements at four well-exposed sites on islands and peninsulas around the Baltic Proper have provided a unique set of turbulent flux data for water vapour and sensible heat over the Baltic Sea, covering all parts of the year. A four weeks cruise with research vessel R/V Heincke during the Concentrated Field Effort provided additional flux data away from land. These data have all been extensively used for testing models of various types, as outlined below.

Radar techniques for measuring precipitation have been substantially improved as a result of work within PEP in BALTEX. The new algorithms developed for accurate precipitation retrieval are now implemented in the BALTRAD project, which includes simultaneous operation of 29 radars within the BALTEX area. BALTRAD is now fully operational and will provide reliable precipitation estimates for the Baltic Sea.

A Micro-Rain-Radar system was installed at three of the sites and were shown, for the first time, to operate satisfactorily over an extended period of time in the field, giving detailed and useful information about the vertical profile of rain. The instrument is capable of recording even very low intensity rain events. Preliminary results indicate that the sum of these low intensity rain events may be appreciable. As such low rain rates, due to wetting problems are likely to be partially lost with conventional rain gauge sampling, it is possible that this result may have implications for the budget calculations of net precipitation.

Two *regional scale weather forecast model*s, HIRLAM (a Swedish version and a Finnish version, with different flux parameterization schemes) and REMO _DWD, one *meso-scale model*, the MIUU model, one *oceanographic model*, PROBE-Baltic, and two *models based on interpolation* of 1) synoptic data and radar data (MESAN) and 2) synoptic data and data from merchant ships (here called ship/IfM model) were tested against the turbulent flux measurements for evaporation and against measurements with the specially designed ship rain gauge (SRG) onboard merchant ships, travelling between Lübeck and Helsinki, for precipitation.

The *precipitation tests* reveal that the regional scale models and MESAN give higher precipitation – by some 20 percent – than is deduced from the ship measurements.

As *evaporation* is determined in all models with so called bulk formulas, basic tests were first conducted to check the performance of current bulk formulations. For unstable stratification most data indicate that unbiased results are obtained with a constant value for the neutral coefficient $C_{eN} \approx 1.1\times10^{-3}$. For stable stratification, it was shown that the value of the coefficient C_e is about half of that previously assumed, so that water vapour flux is reduced by the same amount during stable stratification, which occurs during several months per year in some parts of the Baltic Sea.

When testing evaporation predictions from regional scale models etc., the flux parameterization scheme is only one factor which determines the result. In the case of the Swedish HIRLAM model, tests against flux measurements showed that the model overpredicted evaporation strongly. This overprediction was shown to be partly related to the flux formulation. After changing the parameterization in accordance with the above results, overprediction was significantly but not completely removed. Comparison of predictions with the different models against flux measurements gives a result which varies to some degree between the models and between the tests for which the sites were conducted. Interestingly, the models seem to make best agreement with the measurements from the site Kopparnäs. This site differs from the other sites in an important respect. Here islands are situated at the lateral sides of the relatively narrow open sea sector in such a manner that strong swells will never occur at the measuring site (K. Kahma, private communication). On all the other sites, strong swells are known to occur. In a special study within this project it was shown that swell can have strong influence on the exchange process. This is not included in any of the models and can, no doubt, explain some of the scatter and differences in the flux-comparison plots.

Estimates of evaporation, E and precipitation, P for the entire Baltic Proper for a 12 month period were made with several models. It was shown that the variation during the year of these two variables and of $(P\text{-}E)$ for all the predictions follow each other well. But when it comes to the overall sums, there are still important differences, in particular in $(P\text{-}E)$, where the values range from 57 mm/year for the REMO_DWD model to 250 mm/year with the Swedish HIRLAM model. Analysis of the prediction of precipitation and evaporation with the different models discussed above show that each estimate may have individual systematic errors as large as 20 percent. As mean precipitation is about 700 mm/year and mean evaporation about 550 mm/year, this implies that the error in $(P\text{-}E)$ in individual estimates may very well amount to as much as 100 mm/year. A best estimate of $(P\text{-}E)$ for the 12 months period studied here is 150 ± 50 Wm^{-2}. But the yearly mean of this quantity is likely to

vary considerably from one year to another. This is substantiated by simulations with the PROBE-Baltic model for a 18 years period, which gave 95 mm/year for the 12 months period studied here and 32 mm/year as an average for 18 years.

It is clear that PEP in BALTEX has given a very substantial contribution to the knowledge of the precipitation and evaporation regime over the Baltic Sea. Nevertheless, it is also evident that much remains to be done. The project has thus highlighted how difficult it is, even with the extensive and sophisticated methods employed here, to get an accurate estimate of the net precipitation over the Baltic Proper for a one year period. This uncertainty is highly relevant not only in the special BALTEX context but also in the wider context of climate change studies globally, as it gives an indication of how uncertain energy and water balance estimates over the ocean really are.

Forecast in Baltic coastal region in Poland in mesoscale model

Katarzyna Starosta

Interdisciplinary Centre for Mathematical and Computational Modeling Warsaw University, Institute of Meteorology and Water Management, Podlena 61, 01 - 673 Warsaw, Poland

Abstract

When interpreting forecasts at the land-sea border line one should consider many factors connected with surface variety. The model surface is logically divided into sea and land points. Averaging a dataset of fractional land cover over the model grid squares creates the mask. Those grid squares which have less than 50 % land in them are assigned to be sea points, the remainder land. If a grid square is assigned to be land then the amount of land is set to be 100%, coastal effects are not allowed for in the current version of the model .The important element is surface characteristics. A layer of seaice may cover the sea. In the land vegetation and soil type needs be to define. The land be covered with snow and the moisture content the soil also need to be known. One of the most important fields is the sea surface temperature (SST). The SST will modify the local climate near the coasts. Current work in the UKMO operational models involves using high resolution satellite data to create a high resolution SST analysis on the mesoscale model grid. The orography is also a very important element in the model. Distribution of these elements at the coastal region of Polish Baltic Sea was analysed. Moreover, the verification of data derived from the model covering the period from April 2000 to March 2001 was made Quality of 48-hour mesoscale forecast of UMPL model (Unified Model from Poland) was estimated through intercomparison of forecast results to near surface weather parameters observed at synoptic station. Verification was made in 12-hour intervals for precipitation, extreme temperatures, atmospheric pressure, wind speed and wind direction. To estimate precipitation a broad range of indexes is used supported by contingency tables. For the remaining elements mean error and mean

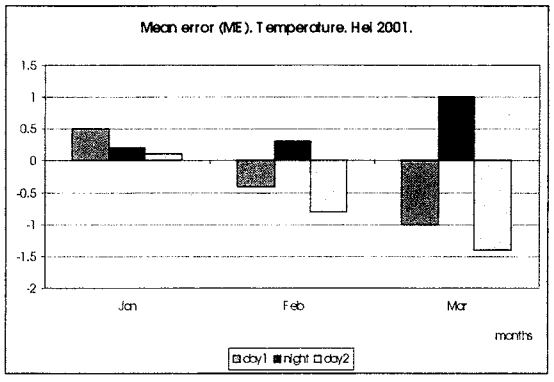

square error have been determined.

The four points on the background field grid surrounded the observation are used for interpolation with the weight inversely proportional to squared distance knots to station. Errors are greatly dependent on station location.
Non-typical location of Hel station contributes to bigger differences between observation and interpolated forecast. For interpolation from grid point to the station an information was used on either land or sea location of given point and with eliminating from calculation sea

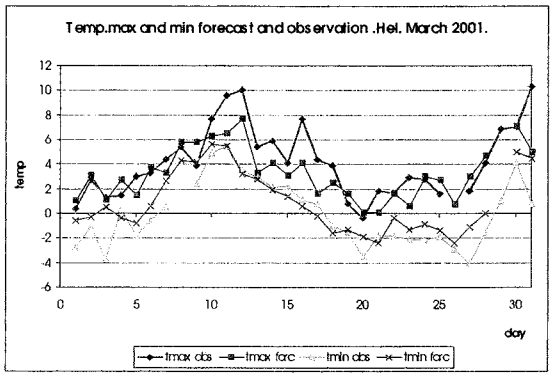

points. For this station instead of interpolation the values of the closest grid point were introduced. As a result Hel station is distinguished itself by bigger errors than stations located up-country.

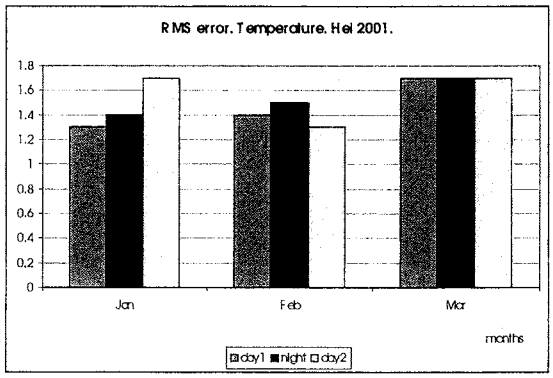

References.

LAM Newsletter Report of the 21st EWGLAM Meeting and 6th SRNWP Network Meeting 11-15 October 1999. Slovak Hydrometeorological Institute . February 2000.

Aplication and verification of ECMWF products in Member States and Co-operating States. Report 1998

An update on the Mackenzie GEWEX study

R. E. Stewart

Climate Research Branch, Meteorological Service of Canada, Downsview, Ontario, Canada

The Mackenzie River basin of northwestern Canada covers about 20% of the country's land mass and the discharge from this region represents the largest North American source of fresh water for the Arctic Ocean. There is a very dramatic annual cycle of surface temperature over this region with monthly average temperatures typically reaching -25 or -30°C during the winter, whereas these average values reach 15°C during the summer. There are correspondingly large pronounced annual cycles of other critical variables such as water vapour, precipitation, snowcover, and discharge. The Mackenzie basin is also experiencing some of the greatest warming in the world. This is occurring in particular during the cold season and is characterized by decadel warming rates of up to 2°C. However, this warming trend is very non-linear. It is characterized by large interannual variations that have increased in magnitude over the last two decades, beginning in the mid-70s.

The Mackenzie GEWEX Study (MAGS) is focusing on the atmospheric, surface and hydrological processes that are occurring over this region. It has brought together about 50 researchers from government and the university community to address these issues. Significant progress is being made through a number of activities:

- A large number of special atmospheric, surface and hydrological observations were made during the 1998-99 Canadian GEWEX Enhanced Study (CAGES). This water year dataset is acting as a key focal point for many research activities.
- A number of special datasets are being prepared for distribution that are focused on specific observational sites and particular phenomena as well as on CAGES.
- Process studies are continuing on a host of phenomena that occur within the basin. These include, for example, the flow of moisture over the Rocky Mountains into the basin, lee cyclogenesis, recycling of water within the basin, cloud-climate interactions, snowpack development and evolution, snow melt, ice jams, lake evaporation, land surface evapotranspiration and sub-surface storage.
- Tests are being made of the ability of the Canadian Regional Climate Model and the Canadian Meteorological Centre's GEM (Global Environmental Multiscale) Model to replicate the observed climate of the basin. In this sense, MAGS is acting as a premier Canadian activity for developing benchmarks for such models.
- The behaviour of the basin's climate as a whole is being better appreciated. The large scale environment obviously dictates many aspects of the basin's climate but local feedbacks involving water and energy processes certainly modify this. In particular, local processes control much of the "efficiency" at which the large scale moisture is converted into precipitation and discharge.
- Preparations are being made to test our diagnostic and modelling capabilities over the adjacent Saskatchewan River basin of the Canadian Prairies. These tests will take advantage of the special Coordinated Enhanced Observing Period (CEOP) to be available after 2003.
- Interactions with local communities are occurring. Meetings are being held with or presentations are being made to, for example, schools, Aboriginal communities and local governments. Such groups are very concerned with their changing climate. Right now, for example, the levels of some of the largest lakes are at record lows and this is causing problems with transportation and hydro-electric generation.

Many of the processes associated with the regional climate of the Mackenzie basin are felt to be applicable to the Baltic Sea region. Both regions span similar latitude bands and both are located on the western edge of a continent and are therefore subject to the effects of major storm tracks. Cryospheric processes are important for both areas. To a certain degree, the climate of each region is subject to the effects of local water bodies although, in the case of BALTEX, there is one dominating large inland sea whereas, in the case of MAGS, there are three large lakes and an enormous number of small ones.

In summary, MAGS is steadily making progress towards better understanding and simulating the variable climate of the Mackenzie River basin. Stronger interactions with BALTEX would undoubtedly help both projects to realize their goals.

DIAMIX – The experiment and some preliminary results

Anders Stigebrandt

Oceanography, Earth Sciences Center, Göteborg University, Box 460, SE-40350 Göteborg, Sweden

1. Introduction

The deepwater of the Baltic is contained in deepwater pools. To model the evolution of the vertical stratification in the Baltic on time-scales comparable to or longer than the residence time of water, it is necessary to model the vertical advection and mixing correctly. This is of crucial importance, for e.g. modelling the biogeochemical states of the Baltic because nutrient turnover and benthic nutrient sinks depend strongly on oxygen concentration. Vertical or diapycnal mixing takes place both in the dense bottom currents and in the deepwater pools. The magnitude and characteristics of vertical advection depends both on the flow through the entrance straits (the Belts and Öresund) and mixing, entrainment and detrainment performed by thin dense gravity-forced bottom currents. These transport the new deepwater to the deepwater pools of the Baltic.

At the start of DIAMIX, the magnitude of vertical mixing in the deepwater pools had been estimated from observations taken during so-called stagnant periods, i.e. periods lacking inflow of new deepwater, using the budget method, e.g. *Matthäus* (1990). Vertical mixing in both deepwater pools and dense bottom currents had also been estimated from 20-years-long model simulations using a 1-D ocean model, see *Stigebrandt* (1987). The vertical diffusivity κ in the deepwater pools seemed to be well described by the following relationship

$$\kappa = \alpha \cdot N^{-1} \qquad (1)$$

provided the intensity factor α was set to $2 \cdot 10^{-7}$ ($m^2 s^{-2}$).

The main goal of DIAMIX is to develop improved parameterisations of vertical mixing in deepwater pools based on increased understanding of the physical processes. The strategy to achieve this goal is to first investigate and rank the processes responsible for the mixing. Since tides are exceedingly weak in the Baltic, the mixing processes should ultimately be wind-driven. We will try to describe the paths of wind energy, from the introduction into the surface layer to dissipation in the deepwater. Several processes bringing energy from the surface layer to deepwater were of course known before DIAMIX but their importance in the Baltic were unknown. For instance, how great is the energy transfer from inertial currents, caused by the time-dependent response of the surface layer to wind changes, to near inertial internal waves beneath the surface layer? How much energy is radiated to the deepwater during geostrophic adjustment of coastal currents to variations of converging/diverging Ekman transports?

In DIAMIX we intend to estimate the distribution of kinetic and potential energy in an experimental area extending from the shoreline to the maximum depth of a deep basin. In this way, the experiment should cover scales ranging in space from the size of the experimental area and in time from the length of the experiment down to the spatial and temporal scales of molecular dissipation and diapycnal mixing. To cover seasonal variations we have done a summer experiment with a seasonal, essentially thermal stratification in the surface layers, and a winter experiment when the water was almost homogeneous down to the halocline at about 60 m depth.

Besides more traditional descriptions of experimental data in terms of coastal dynamics, mixed layer dynamics, internal waves and mixing, an evaluation of the distribution of kinetic and potential energy on all space and time scales down to dissipation scales has been aimed at. This will include the quantification of the transfer of energy between different scales of motion. Knowledge of the meteorological forcing, including buoyancy fluxes through the sea surface is a pre-requisite for the analysis. Finally, parameterisations will be developed for diapycnal mixing as function of e.g. wind speed and air-sea buoyancy fluxes (meteorological forcing), stratification, horizontal and vertical distances to the sea bottom and possibly other important factors yet to be identified.

This talk, given on behalf of the DIAMIX Group, will give an overview of DIAMIX and briefly present some results.

2. Field measurements

The chosen area bordering the Southeast Coast of Gotland was considered appropriate for DIAMIX. Here the bottom slope is typical of the Baltic Proper and the area includes parts of East Gotland Basin, one of the major Baltic Sea basins. The experimental area is about 30 by 30 nautical miles (Fig. 1).

Two pilot experiments were conducted in the springs of 1997 and 1998 to fine-tune the observational scheme with the given instrumentation. Thereafter we have conducted the two main experiments, a winter experiment in 1999 and a summer experiment in 2000. All experiment lasted about 2 weeks. Three ships have participated in all the DIAMIX experiments, namely Aranda (FIMR, Helsinki), Skagerak (OI, Göteborg) and Oceania (IOPAS, Sopot). A. v. Humboldt (IOW, Warnemünde) participated in all except the final summer experiment.

To get a description of the actual large-scale fields of density and currents, we made continuous CTD (Conductivity- Temperature-Depth) and ADCP (Acoustic Doppler Current Profiler) measurements along the 30 nautical miles long transects perpendicular to the coast. Vessel-mounted ADCP and vertically undulating vehicles carrying CTD's have been used for this. The distance between transects is 3 nautical miles. Each ship was able to cover about four transects a day. Unfortunately, it turned out that the ship-borne ADCP measurements have a lot of scatter why it was hard to make quantitative estimates. During the main winter and summer expeditions, R/V Aranda was used as a non-anchored platform in an almost fixed position for CTD profiling and profiling of turbulent dissipation, in bursts of five profiles per hour, from the sea surface to the sea bed. A second profiler for microstructure was used in the final summer experiment to observe dissipation just above the bottom around the halocline. At the start of each experiment, moorings with current meters (mostly ADCP's) and CT (Conductivity-Temperature)-sensors were deployed in the experimental area for studies of the frequency domain.

3. Some preliminary results

The halocline was unusually deep during the pilot experiment in 1997. In later experiments the halocline was situated at more normal depths (60 m). The current records from the moored rigs always got strong contributions from

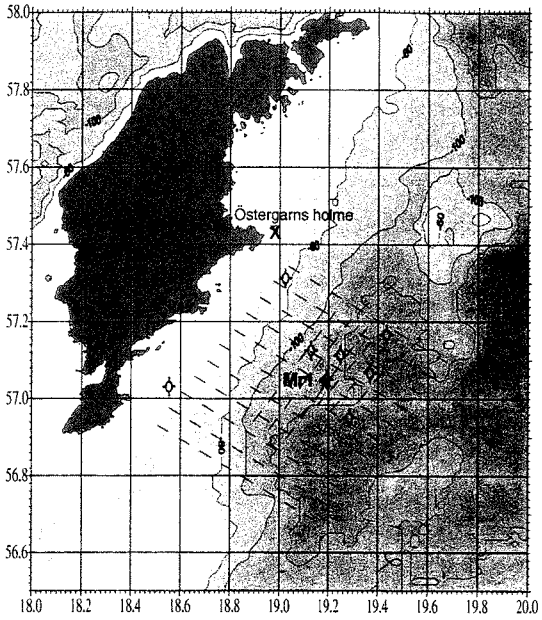

Figure 1: The experimental area of DIAMIX

inertial and slightly super-inertial frequencies. Inertial currents in the surface layers seemed to be generated by the local wind. When passing the uppermost pycnocline, inertial currents shifted phase by 180 degrees, cf. Fig. 2.

The mean dissipation measured under winter conditions (Lass, Prandke and Liljebladh, 2001) seems to be less than the dissipation calculated from the diffusivity estimated by tuning long-term model runs against field data. A preliminary analysis of dissipation data from the summer experiment shows that at around the depth of the halocline dissipation was an order of magnitude greater close to the sea bed than in the open deep sea (Aranda profiles). There seems to be a vigorous dynamic activity along the bottoms. This has been studied in particular by IOPAS.

The energy transfer to deeper layers by internal waves, probably generated by baroclinic wave drag acting on inertial currents in the surface layer, was calculated by Liljebladh and Stigebrandt (2001). They calibrated their model using DIAMIX data and run it thereafter for two years. As an average only about 0.35 mW m^{-2} seems to be radiated into the deepwater by internal waves. This is only about 20-40% of the energy needed for turbulent dissipation and work against the buoyancy forces connected to diapycnal mixing as estimated from long-term model tuning.

Transect data show the presence of anticyclonic baroclinic eddies in the halocline during all experiments. In the winter experiment there were also cyclonic baroclinic eddies, characterised by a marked thinning of the pycnocline. Dissipation increased when eddies were present at the site of dissipation measurements.

DIAMIX has acted as a primer for focused research on mixing processes in the Baltic. In this work, analysis of historical data and modelling have been important. The budget method was carefully applied to data obtained under stagnant conditions in the Baltic proper by *Axell* (1998). His results largely confirm the validity of Eq. (1) for the East Gotland Basin but with a relatively large seasonal variation of α, with maximum in winter and minimum in summer in pace with the wind over the Baltic. Furthermore, he also found that α is a factor of ten greater in the narrow Landsort Deep. Later Axell (2001) developed a mixing parameterisation that explicitly included the forcing by wind. He tested this formulation using an 1-D ocean model and found that the N-dependence suggested in Eq. (1) actually is the one that best fits data.

The DIAMIX data sets will also be quite useful for testing ocean circulation models with respect to, e.g. meso-scale dynamics. Circulation models are instrumental for the interpretation of motions on larger spatial scales in the experiment.

References

Axell, L., On the variability of Baltic Sea deepwater mixing, *J. Geophysical Research*, Vol.103, 21, 21667-21682, 1998

Axell, L., Turbulent mixing in the ocean with application to Baltic Sea modeling. PhD Thesis, *Dept. of Oceanography, Earth Sciences Centre, Göteborg university,* A66, 2001

Lass, H.U., H. Prandke and B. Liljebladh, Dissipation in the Baltic proper during winter stratification, 2001 (submitted)

Liljebladh, B. and A. Stigebrandt, The contribution from the surface layer via internal waves to the energetics of deepwater mixing in the Baltic, 2001 (submitted)

Matthäus, Mixing across the primary Baltic halocline, *Beitr. Meereskd*, 61, 21-31, 1990

Stigebrandt, A., A model for the vertical circulation of the Baltic deep water. *J. Phys. Oceanogr.*, Vol.17, No.10, 1772-1785, 1987.

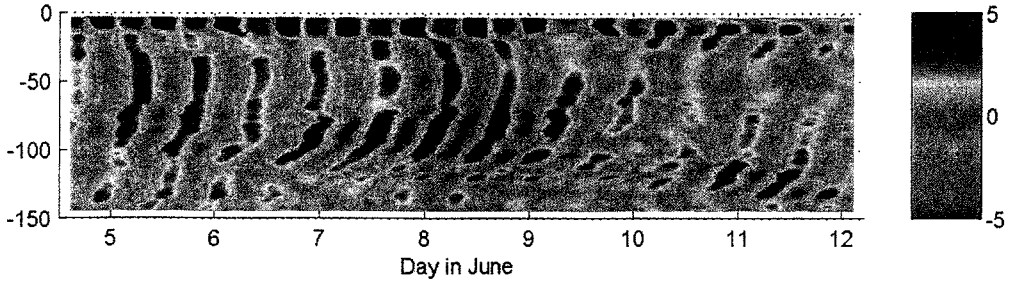

Figure 2: Currents in the inertial band, spring 1998

Heat anomalies are driven by freshwater fluxes in the shivering Baltic

Tapani Stipa

Institute of Marine Research, 00931 Helsinki, Finland

1. Introduction

The existence of a density maximum in a saline water body results in dynamics that is counterintuitive to most oceanographers. Here the fact that the effect of heat gradients on density gradients is almost negligible in this regime is underlined. The free variation of temperature on isopycnals emerges as a null-space solution to the density-spice -space. The name of "shiver" is suggested for this null-space solution.

The Baltic Sea is a major occupant of this very peculiar part of the oceanic temperature and salinity range. Measurements from the Baltic are used to illustrate the overwhelming dynamic importance of salinity gradients in shivering oceanic environments.

2. Isopycnal gradients of salt and temperature

For hydrostatic, baroclinic, incompressible and mechanically unforced processes, density gradients drive the motion. The relative importance of temperature and salinity on the dynamics is then a result of their effect on the density gradients:

$$\rho^{-1}\nabla\rho = \rho^{-1}\frac{\partial\rho}{\partial T}\nabla T + \rho^{-1}\frac{\partial\rho}{\partial s}\nabla s \equiv -\alpha\nabla T + \beta\nabla s$$

Along isopycnals, density gradients are by definition zero: $\rho^{-1}\nabla\rho\cdot\mathbf{e}_\rho \equiv 0$, where $\mathbf{e}_\rho$ is any vector on the tangent isopycnal plane. For the sake of concreteness, we may define it as $e_\rho = (\nabla\rho)^0 \times \mathbf{\Omega}^0$, where $(\nabla\rho)^0 = \nabla\rho\left|\nabla\rho\right|^{-1}$ and $\mathbf{\Omega}$ is the rotation vector of the Earth.

Veronis [1972] realized that two different quantities can be combined from two variables, and introduced $\tau = \alpha\, dT + \beta\, ds$, which was later termed spice by Munk [1981]. Now we have a complete set of equations for isopycnal variations of temperature and salinity,

$$\rho^{-1}\nabla\rho\cdot\mathbf{e}_\rho = -\alpha\nabla T\cdot\mathbf{e}_\rho + \beta\nabla s\cdot\mathbf{e}_\rho \equiv 0 \qquad (1)$$

$$\alpha\nabla T\cdot\mathbf{e}_\rho + \beta\nabla s\cdot\mathbf{e}_\rho = \tau_\rho \qquad (2)$$

What seems to have escaped attention, however, is the existence a of a "null space" solution when α passes through zero at T_ρ. Then, Eq. (1) gives $\beta\nabla s\cdot\mathbf{e}_\rho = 0$, which in turn renders spice in Equation (2) zero.

Isopycnals, and therefore the dynamics, are completely determined by salinity gradients in this solution. For small disturbances $T' = T - T_\rho$, $\nabla T'\cdot\mathbf{e}_\rho$ is free to vary on isopycnals: a linearisation around T_ρ yields $\alpha = 0$ and Equations (1)-(2) reduce to $\rho^{-1}\nabla\rho\cdot\mathbf{e}_\rho = \beta\nabla s\cdot\mathbf{e}_\rho = \tau_\rho = 0$.

The original argument of Veronis [1972] for introducing spice to fully utilize information in the T and s fields loses its meaning, because temperature fluctuations get entirely decoupled from density fluctuations. In fact, the role of spice as a container of (T, s)-information unrelated to density is taken by temperature.

Since the importance of isopycnal salinity variance decreases also in cold oceanic waters (e.g. the Arctic and Antarctic waters) in favor of isopycnal temperature variance, the latter might more appropriately be termed "shiver".

3. Observations of shiver

The Baltic Sea lies in a unique part of the oceanic temperature and salinity range; in its present state it is the world's largest brackish water body whose bulk cools annually to or below T_ρ. This results from the low, horizontally homogeneous salinity of the Baltic Sea as compared to many other estuaries: the surface salinity ranges mostly between 5 and 10 psu.

In addition, tidal stirring, which imposes a short time scale for stratification over many shelves, is virtually absent. The maximum amplitude of Baltic tides is about 10 cm. The absence of tides makes it possible to observe persistent patterns of shiver, frequently associated with fresh coastal currents that create salinity gradients.

One such current is the Finnish Coastal Current (FICC), originating mostly from the River Neva discharging at St. Petersburg (approx. 60°N, 30°E). The freshwater discharge of the river maintains a rather narrow front, where velocities up to 30 cm/s have been observed (T. Stipa, unpublished material). The current is observed to flow along the northern shore of the Gulf for prolonged periods during calm weather [Stipa, 1999].

Measurements of the FICC were made in April-June, 1993, at the entrance to the Gulf of Finland. The DGPS-positioned measurements were made from a charted trawler at 1 nautical mile intervals with a SIS 100Plus CTD sonde. One section was completed in 5 hours. The accuracy of the measurements was checked to be within 0.05 psu of salinometer-determined water sample salinity.

The transects shown in Figure 1 clearly show that rather sharp isopycnal temperature contrasts are observed in this front. The temperature contrasts, however, do not have a large density signal--in fact, the isotherms are almost vertical and orthogonal to isopycnals in the front. This is a consequence of shiver: small temperature variations around T_ρ are a free parameter on isopycnals, as discussed in Section 2.

Vertical isotherms would be flattened out with a timescale of the local inertial period if temperature would have an influence on density, i.e. it would be dynamically active. Hence, the steep isotherms in the transects are a strong empirical indication for the dynamic insignificance of temperature.

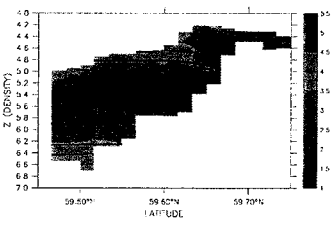

(a) temperature (degrees C)

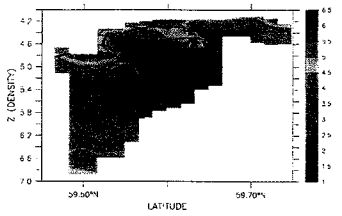

(b) temperature (degrees C)

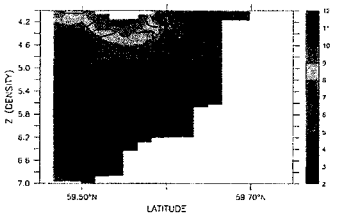

(c) temperature (degrees C)

Figure 1: Shivering fronts from the northern Baltic Sea during the onset of seasonal stratification. In situ temperature is filled and overlaid with contours of salinity. a) April 29, 1993, b) May 5, 1993, c) May 19, 1993. T_p surfaces coincide with salinity surfaces with $T_p = 2.9°C$ at $s = 5.4$ psu and $T_p = 2.3°C$ at $s = 7.6$ psu . In (c) the temperature has already increased enough to generate non-zero spiciness at the cost of shiver, as seen in the upward tilt of isohalines in the front.

As a further verification, Figure 2 shows a cross transect from the Gulf of Riga. The second largest river in the Baltic, Daugava, discharges to the southern part of the Gulf, generating horizontal salinity gradients. Isopycnals are determined by salinity here as well, with temperature an essentially free parameter.

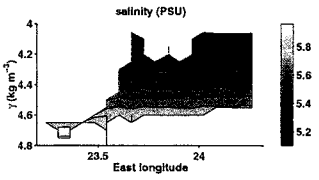

(a)

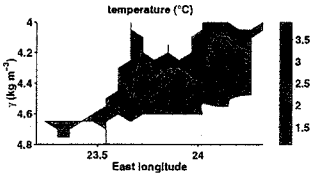

(b)

Figure 2: A transect across the Gulf of Riga, April 22, 1995 drawn in density coordinates ($\gamma = \rho - 1000\ \mathrm{kgm^{-3}}$; data from Stipa et al. [1999]). The bottom of the gulf is almost flat at 40-50 m. Salinity (a) and temperature in (b) show that isopycnals coincide with isohalines, whereas in lakes isopycnals trivially coincide with isotherms. In the ocean mixed layer, both temperature and salinity vary in a largely compensating manner [Rudnick and Ferrari, 1999].

4. Discussion and conclusions

The existence of an apparently previously undocumented property of ocean thermodynamics is derived theoretically and shown to exist in observations. Shiver, as the free variation of temperature on isopycnals is called here, is a unique property of cold, brackish waters. Mathematically, it arises as a null-space solution in the equations of density and spice when they are linearised around the temperature of maximum density. Phenomenologically, it is combination of spice in the ocean and the thermal bar in freshwater lakes. Its behaviour, however, is not directly deducible from either spice or the thermal bar.

The experimental data show that temperature fluctuations may indeed be orthogonal to the density field, as suggested by the teory. The thermal bar in lakes has also almost vertical isotherms. The horizontal density gradients, however, vanish near the thermal bar because of vanishing α, whereas in shivering seas horizontal density gradients may and do exist, due to salinity.

Purely shivering dynamics result in the somewhat odd consequence that heat anomalies are passively transported by salinity anomalies. Since salinity anomalies are determined by oceanic freshwater sources and sinks, it is solely the external freshwater fluxes that drive the oceanic transport of heat in cold, brackish areas. This relationship may have implications for example for rapid changes in the thermohaline circulation that are driven by high latitudes.

Acknowledgements

This study would not have been possible without a consistent financial support from Maj and Tor Nessling Foundation and the University of Helsinki funds. Capt. Sture Berndtsson is acknowledged for the cruises on board M/S Jette. Logistic support for the observations was provided by Tvärminne Zoological Station, University of Helsinki. Dr. Timo Tamminen arranged the funding and participated in the measurements when the author was too sick.

References

Munk, W., Internal waves and small-scale processes, in Evolution of Physical Oceanography, edited by B. A. Warren and C. Wunsch, pp. 264-291, Massachusetts Institute of Technology, 1981.

Rudnick, D. L., and R. Ferrari, Compensation of horizontal temperature and salinity gradients in the ocean mixed layer, Science, 283, 526-529, 1999.

Stipa, T., Instabilities and along-shore variability in the Finnish coastal current, in 4th workshop on physical processes in natural waters, 13-17 september 1999 Roosta, Estonia, vol. 10 of Report series, pp. 62-66, Estonian Marine Institute, Tallinn, 1999, ISSN 1406-023X ISBN 9985-9058-9-X.

Stipa, T., T. Tamminen, and J. Seppälä, On the creation and maintenance of stratification in the Gulf of Riga, Journal of Marine Systems, 23, 27-49, 1999.

Veronis, G., On properties of seawater defined by temperature, salinity, and pressure, J. Mar. Res., 30, 227-255, 1972.

Towards Operational Real-Time Estimation of Total Atmospheric Delay

Borys Stoew and Per Jarlemark

Onsala Space Observatory, Chalmers University of Technology, S-43992 Onsala, Sweden

1. Prerequisites

The Swedish network of geodetic Global Positioning System (GPS) receivers SWEPOS routinely acquires data which are used to produce estimates of the total atmospheric propagation delay. An earlier developed processing strategy allows for the delivery of estimates of atmospheric parameters every 15 s with a typical delay of 3 s, based on the use of broadcast satellite orbits. The first experiments with the new setup of the Kalman filter algorithm were conducted with data from 8 of the GPS sites shown in Fig.1.

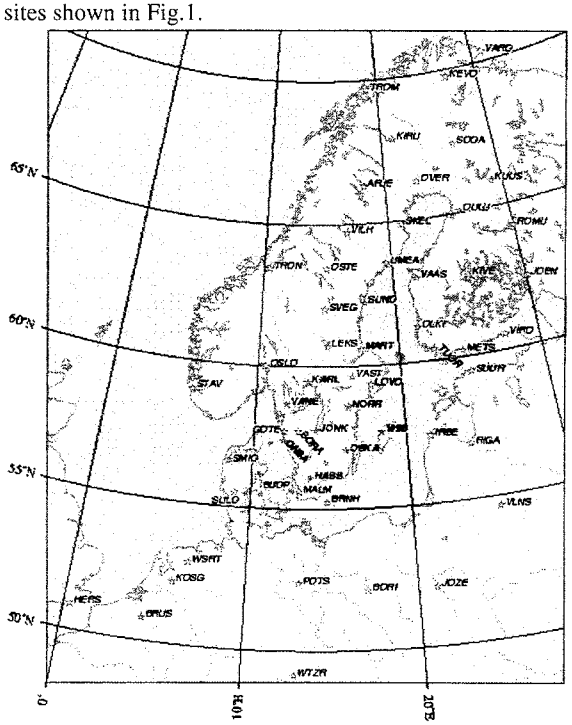

Figure 1: The GPS network used in BALTEX. The GPS sites used for the real-time atmospheric filtering were Hässleholm, Jönköping, Karlstad, Norrköping, Onsala, Oskarshamn, Vänersborg and Visby.

The early results were encouraging and showed root-mean-square differences in the total delay of the order of 0.03 m (*Stoew et al.*, 2001) when the real-time solution and the solution using the Final IGS orbits (*Beutler et al.*, 1996) were compared. An example of the time series for the GPS site at Jönköping produced by the experimental real-time filter is shown in Fig.2. These initial results call for the investigation of the limiting number of sites and computational delays in terms of used software as the goal is to include all the sites in the SWEPOS network.

2. Implications to operational meteorology

The developments of real-time estimation of atmospheric parameters with GPS may be of interest to the numerical weather prediction community, especially as efforts are made towards assimilation of Integrated Water Vapour (IWV) related data with higher temporal resolution.
Algorithms for deriving IWV (*Emardson et al., 1998*) usually require knowledge of the pressure and temperature

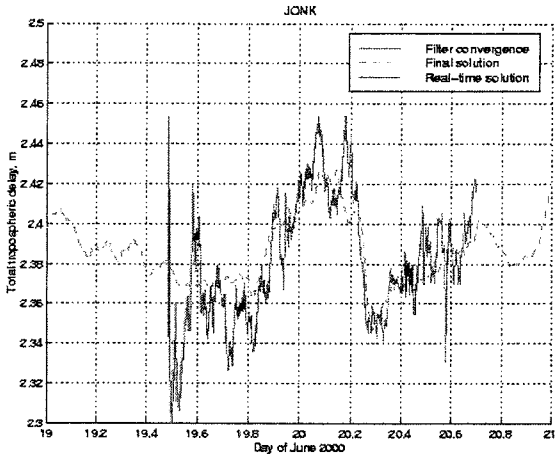

Figure 2: An example for the station at Jönköping (JONK). The initial three hour long period of the run of the real-time Kalman loop allows for the convergence from the a-priori setup of the filter towards its steady state. After converging, the real-time solution (solid lines) approximately matches the Final solution using IGS orbits (dashed lines).

fields which may introduce unnecessary latency in the calculation of the results at the GPS processing center. An alternative is the direct use of the total atmospheric propagation delay in the assimilation process at the meteorological institute. With this in mind one may investigate the limitations of matrix computation algorithms and computer performance. With the use of portable software which performs the real-time processing, the best configuration can be utilized on virtually any computer. We investigate the compromises between the computational speed and data quality. We present the impact of changing the rate at which estimates are produced with various set-ups in comparison to the set-up in the initial experiment, and the optimum GPS solution using the Final IGS orbits.

References

Brown, R.G. and P. Hwang. *Introduction to Random Signals and Applied Kalman Filtering.* John Wiley & Sons, 1997.

Emardson, T.R., G. Elgered and J.M. Johansson. Three months of continuous monitoring of atmospheric water vapor with a network of Global Positioning System receivers, *J. Geophys. Res.*, Vol. 103, 1807-1820, 1998.

Stoew, B., P. Jarlemark, J. Johansson and G. Elgered. Real-Time Processing of GPS Data Delivered by SWEPOS, *Physics and Chemistry of the Earth*, In press, 2001.

Beutler, G., I.I. Mueller and R.E. Neilan, The International GPS Service for Geodynamics (IGS): The story, in *GPS Trends in Precise Terrestrial, Airborne, and Spaceborne Applications*, vol. 115, 3-13, Springer-Verlag, New York, 1996.

What is the Arctic Oscillation, and why do we care?

David Thompson

Department of Atmospheric Sciences, Colorado State University, Fort Collins, CO, USA

The Arctic Oscillation (AO; also known as the North Atlantic Oscillation) is the leading pattern of large scale climate variability in the Northern Hemisphere extratropical circulation. In this talk I will present an overview of the AO, its climate impacts over Northern Europe, and its signature in global climate. In the process, I will attempt to provide a global perspective of climate variability in the Baltic Sea region.

The AO, like its Southern Hemisphere counterpart, is characterized by a seesaw in zonal wind anomalies along ~35° and ~55° latitude accompanied by displacements of atmospheric mass between the polar cap and the surrounding zonal ring centered ~ 45°. Although its amplitude is largest in the Northern Hemisphere extratropics, the AO has a distinct signature in both the tropics and even the subtropics of the Southern Hemisphere.

The AO strongly impacts climate throughout the Northern Hemisphere. For example, its high index polarity (i.e., anomalously strong zonal flow along ~55°N) is marked by higher than average surface temperatures throughout much of the Northern Hemisphere midlatitudes, lower than normal stratospheric ozone, and an increased frequency of severe storms over both the North Atlantic and North Pacific stormtracks. Over the Baltic Sea region, the high index polarity of the AO is marked by warmer than average surface temperatures, an increased frequency of occurrence of high wind events, and increased precipitation. The AO exhibits variability on week-to-week, month-to-month, and seasonal-to-interannual timescales. It has also exhibited a systematic trend over the past few decades that is clearly reflected in climate change throughout the hemisphere. In fact, during the Northern Hemisphere winter months, virtually all of the strengthening of the zonal flow from the surface to the lower stratosphere, about 40% of the recent warming of the Northern Hemisphere continents, and ~1/3 of the observed ozone losses since the late 1970s are linearly congruent with the recent trend in the AO. This same trend has also contributed to much of the observed warming and increases in precipitation that have occurred over Northern Europe during this same period. That the trend in the AO could be a response to anthropogenic forcing is suggested by the fact that it is unprecedented in the historical record, and that similar trends have been noted in GCM simulations run with increasing concentrations of greenhouse gases and depletion of stratospheric ozone.

Atmospheric Circulation Indices for Estonia and their Correlation with Climatic Fluctuations

Oliver Tomingas

Institute of Geography, Tartu University, Vanemuise 46, 510 14, Tartu, Estonia

1. Introduction

Atmospheric circulation is an important factor that has a direct impact on climate variability. Weather fluctuations in Estonia are closely associated to atmospheric circulation, especially in wintertime, when strong westerlies from the Atlantic brings warm and moist air to the continent. There have been made several attempts to describe atmospheric circulation in Estonia. These efforts mainly concentrated to the analysis of a linkage between large-scale atmospheric circulation classifications and weather situation in Estonia. However, large-scale classifications are not always suitable for smaller regions that are not situated in the territory of particular classification. It was indicated that there is a need for a numeric characteristic that would describe the air circulation over Estonian territory.

The objective of this study is to compose circulation indices (zonal and meridional) for Estonia, to analyse relationship between these indices and weather fluctuations in Estonia, and to estimate trends in time series of the circulation indices and climatic variables.

2. Data and methods

Gridded data of daily sea-level pressure for the Northern Hemisphere for the period 1881-1997 were used to calculate circulation indices for Estonia. This averaged air pressure data superfile was obtained from the U.K. Meteorological Office. Size of the grid box is 5 degrees in latitude and 10 degrees in longitude. Pressure data of eight grid cells surrounding Estonia was used for index calculations (Figure 1). Geographical coordinates of the center points of the grid boxes are: a) 62.5°N, 15°E, b) 62.5°N, 25°E, c) 62.5°N, 35°E, d) 57.5°N, 15°E, e) 57.5°N, 35°E, f) 52.5°N, 15°E, g) 52.5°N, 25°E, h) 52.5°N, 35°E.

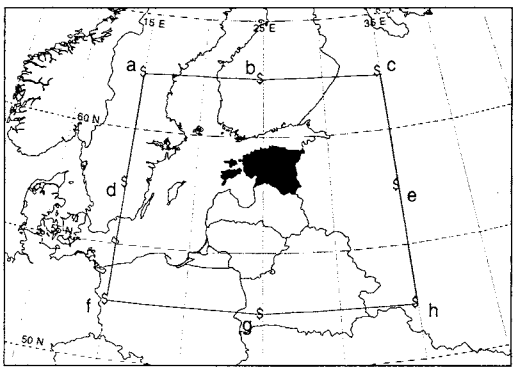

Figure 1: Central points of the selected grid boxes.

Air pressure values at the three northern grid cells were averaged, to get values for the north. By the same way, values at the southern, eastern and western sides were calculated. Pressure data at each of the four sides were standardized by division of monthly (or seasonal) pressure anomalies by standard deviation. Zonal circulation index is calculated as a difference between standardized sea level pressure values at the southern and northern sides. It means that positive values of the index express higher than normal westerly circulation. Meridional circulation index is found as difference between standardised pressure at eastern and western sides from Estonia. Positive values correspond to southerly airflow and negative values to northerly one. As a result, a database of monthly and seasonal circulation indices (zonal and meridional) is created for the territory of Estonia.

Monthly and seasonal air temperature data from 8 Estonian stations (Pakri, Pärnu, Viljandi, Vilsandi, Tartu, Tallinn, Ristna and Sõrve), precipitation data from 4 stations (Pärnu, Tartu and Kuusiku and Türi) and snow cover data as well as sunshine duration from Tartu during 1946-1997 are used in this study. Monthly and seasonal (averaged value for three months) data of air temperature, precipitation, snow cover duration and duration of sunshine are correlated with monthly and seasonal values of the circulation indices. Correlation is considered to be significant on $p<0.05$ level. Trends in time series of circulation indices and climatic variables in Estonia are analysed and compared.

3. Correlation between circulation indices and climatic variables in Estonia

Correlation between air temperature in Estonia and zonal as well as meridional circulation indices varies significantly between different months and seasons. Air temperature is positively correlated with zonal circulation index during the period from September to March (maximum correlation in Ristna 0.816 in December), and has no significant correlation from April to August (Figure 2). Meridional index has positive correlation with air temperature from April to September (the highest correlation in September) and no significant correlation in winter. However, averaged winter temperatures (December-February) are in most of the 8 used stations in significant negative correlation with meridional circulation index. This can be explained with an important role of the Atlantic Ocean in winter. As most of the warm air in winter comes with westerlies, zonal index is more connected to temperature fluctuations. Meridional index, that describes meridional air movement, does not have any influence. In summer the situation is different. Zonal airflow loses its role, as temperature difference between ocean and continent decreases and meridional airflow becomes more crucial factor for air temperature fluctuations. April and September as transition months have much higher correlation with meridional index than other months of the warm season. In summer, temperature contrasts diminish and correlation weakens.

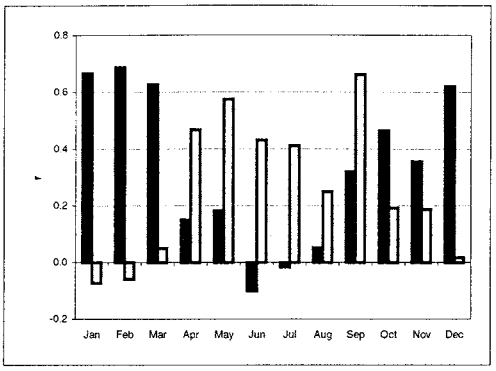

Figure 2: Correlation between circulation indices and monthly mean air temperature in Tartu (black coloumns show correlation with zonal indices and white ones with meridional indices).

Correlation between precipitation and zonal circulation index in winter months is statistically significant only for two stations in the Western Estonia in February and during the whole winter season (DJF). Precipitation data have no significant correlation with meridional atmospheric circulation index. Sunshine duration in Tartu is in significant positive correlation with zonal index only in April (r = 0.42), September (r = 0.48), October (r = 0.32) and autumn (r = 0.42). Meridional index was in negative correlation with sunshine duration in December (r = -0.50). Correlation between snow cover duration in Tartu and zonal index is negative from January to March (maximum in February r = -0.62). Correlation between snow cover data and meridional index is not statistically significant.

4. Comparison of trends in circulation indices and climatic variables

During the period 1946-1997, statistically significant increasing trends are determined for March (slope 0.074) and spring (0.034). A remarkable trend in September is negative (-0.026), but not significant. In Pärnu, Sõrve, Vilsandi and Viljandi statistically significant trends are observed also in March and in spring. For other months, trend is not significant but negative trends for September and December are present in all selected stations. Increasing trends for January and February as well as for the whole winter is rather impressive (slopes 0.04-0.06) but not statistically significant. This can be referred to as a result of recent climate warming. Slope of snow cover duration in Tartu was –0.24 that is also connected with warming in winter.

Although there are some upward trends in Estonian wintertime precipitation, this cannot be obvious impact of intensified zonal circulation, because data of precipitation is regionally very different.

Using regression analysis, trends are calculated also for atmospheric circulation indices. It allows analysing if changes in mean atmospheric circulation are related to recent trends in climatic variables. During the period 1946-1997, zonal circulation index has a statistically significant increasing trend in February (Figure 3) and in winter, and downward trend in April, June, September and summer season. In case of meridional circulation index, a statistically significant positive trend is present only in March (Figure 4). It means that airflow from south has intensified in March during 1946-1999. It can have a linkage to a warming trend that has been observed in March.

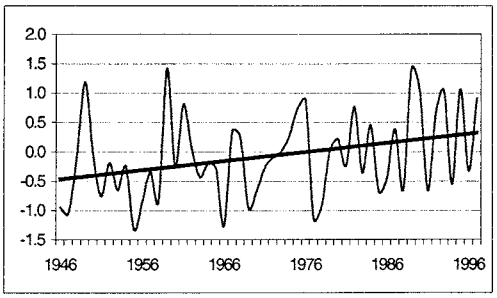

Figure 3: Zonal circulation index in February and linear trend (slope 0.016)

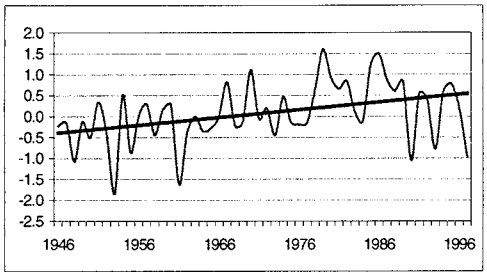

Figure 4: Meridional circulation index in March and linear trend (slope 0.018)

5. Conclusions

Developed monthly atmospheric circulation indices can be used as simple numeric characteristics of atmospheric circulation in Estonia. The highest correlation between circulation indices and climatic variables is observed with air temperature. This relationship is significantly different during warm and cold half-year. Other variables are not so dependent on atmospheric circulation. Comparison of trends between weather characteristics in Estonia and atmospheric circulation indices brought out that in some months changes in climatic variables can be directly associated with changes in circulation.

Acknowledgements

The author is thankful to Dr. Jim Arnott from U.K. Meteorological Office for kindly offering data from the global sea-level pressure superfiles. This study is financed by the Estonian Science Foundation (grant No. 4347).

Relationships among the ice extent on the Baltic Sea, the snowcover in surrounding areas, and the temperature

Heino Tooming[1] and Sirje Keevallik[2]

[1] Estonian Meteorological and Hydrological Institute, Rävala 8, Tallinn 10143, Estonia
[2] Tartu Observatory, 61602 Tõravere, Estonia

1. Introduction

The snow and ice covers show substantial inter-annual variability *Haapala, Leppäranta* (1997), *Tooming, Kadaja* (1998, 1999, 2000). In order to completely understand the climate system, these variations must be understood. The Baltic Sea ice climate has been traditionally approached by time-series analysis *Seinä, Palosuo* (1993), *Tarand* (1993), *Isemer* (1998). Sea ice conditions have been regarded as an indicator of the severity of the winter season. In warm winters the ice on the Baltic Sea and snow cover in surrounding areas are absent. In cold winters the Baltic Sea is covered with ice. In both cases the weather conditions may be quite different in surrounding areas of the Baltic Sea. Above all snow cover is an integrator of weather and indicator of climate *Tooming* (1997). The presence or absence of snow plays an important role in affecting surface albedo, radiation budget, air temperature, and warmth index, *Groisman et al.* (1994), *Keevallik* (2001), *Keevallik, Tooming* (1996). *Chaoimh* (1998) has shown using satellite-derived monthly snow-cover data and station temperature anomalies that a direct relationship exists between maximum annual snow-cover extent in Europe and April temperature in the Baltic and Central Europe region. Correlation coefficients were generally in the range of 0.4-0.7. The authors have analysed a similar problem on the basis of ISCCP data for the whole Northern Hemisphere *Keevallik, Tooming* (1996). The correlation of snow cover extent with the warmth index up to June was established in regions where the year-to-year variations in snow cover extent were substantial. *Keevallik* (2001) has calculated lag correlations between snow cover and temperature over large areas around the Baltic Sea. It has been shown that for the northern part of the BALTEX region, the influence of March snow cover on the temperature regime in April is significant and exceeds the influence of the temperature of the preceding month. It was found that the surface conditions (the duration of snow cover and the warmth index) are in correlation with the duration of the sea ice *Tooming, Kadaja* (1998).

The aim of the present work is to explain the impact of the air temperature on the sea ice maximum extent on the Baltic Sea and on the snow cover extent in surrounding areas and their impacts on the temperature anomalies in the following spring months. The possibility to use the early predicted sea ice maximum extent on the Baltic Sea as a predictor of temperature anomalies in surrounding areas in spring months is studied.

2. Material and method

In the present paper we analyse relationships between sea ice extent on the Baltic Sea, monthly average temperature and snow cover extent in six squares of 5 degrees latitude by 10 degrees longitude around the Baltic Sea. The six squares can be called:

1) Germany (50-55° N, 10-20° E), **2)** South Sweden (55-60° N, 10-20° E), **3)** North Sweden (60-65° N, 10-20° E), **4)** Poland and Lithuania (50-55° N, 20-30° E), **5)** Estonia and Latvia (55-60° N, 20-30° E), **6)** Finland (60-65° N, 20-30° E). The data of the sea ice extent on the Baltic Sea have been drawn from the paper by *Seinä and Palosuo* (1993). Snow data have been obtained from the digitised archive of snow cover data prepared on the basis of Weekly Snow and Ice Charts of the National Earth Satellite Service (NESS) for the period 1972-1990. Temperature deviations from average values have been used for the analysis of the relationships among ice extent in the Baltic Sea, snow cover, and temperature anomalies in surrounding areas.

3. Results

Ice and temperature

It is obvious that air temperature has a strong impact on the maximum extent of the ice cover on the Baltic Sea. The correlation coefficients between air temperature anomalies in areas surrounding the Baltic Sea and the maximum extent of sea ice on the Baltic Sea are statistically significant everywhere exceeding 0.01 or 0.05 significance levels in winter months. These correlation coefficients are maximal in January and February and the highest in North and South Sweden where r = -0.88...0.91 (Figure 1).

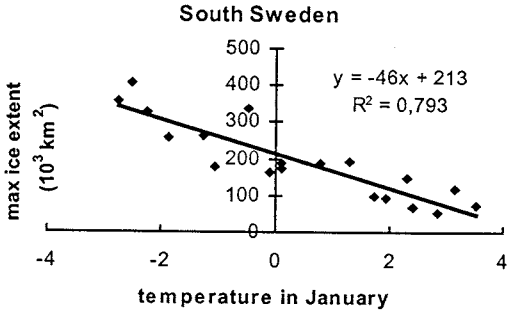

Figure 1: Dependence of the maximum ice extent on the Baltic Sea on temperature deviation in January (the prediction equation for the maximum ice extent)

Consequently, the ice maximum extent on the Baltic Sea may be predicted already in January. On the other hand, the temperature anomalies in March and April are in close correlation with the maximum ice extent and, therefore, may be predicted already in January The relationships between the maximal extent of sea ice and the air temperature anomalies in South Sweden continue until the end of May (r = -0.68). Consequently, in this region sea ice has a substantial after-effect on the heat accumulation during the spring period (Fig 2).

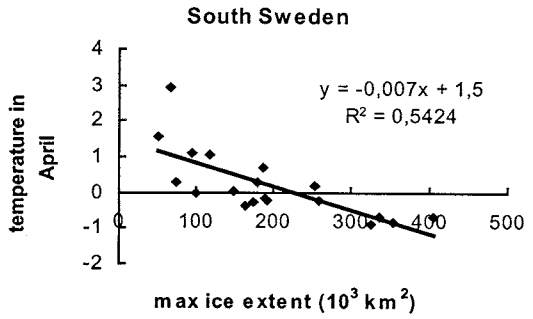

Figure 2: Dependence of the temperature deviation in April on maximum ice extent (the prediction equation for temperature deviation in April)

Similar effects with high correlation coefficients exist in North Sweden. Significant relationships between air temperature anomalies and ice cover extent on the Baltic Sea with after-effects continuing until May can be followed in Finland (r = -0.42...0.56). In the remaining regions under consideration the after-effect of sea ice to the temperature can be detected mostly only until April. Consequently, temperature determines the maximum extent of sea ice and in turn, the extent of sea ice has an after-effect on the heat accumulation in surrounding areas in late winter and spring.

Snow and temperature

Snow cover extent around the Baltic Sea is negatively correlated with the air temperature of the respective month, except in January in Finland and North Sweden. The highest is this dependence during snowmelt in March and April.

It is normal to expect that temperature is the primary factor to influence the formation of ice and snow cover. But in late winter and/or early spring the roles change - the late ice and snow cover interrupts the heat accumulation near the surface. In warm years the reduced sea ice and snow cover extent contribute to the rise of temperature in areas around the Baltic Sea.

4. Conclusions

Besides the cyclonic activity connected with the North Atlantic, ice cover maximum extent and snow cover have an impact on heat accumulation near the surface around the Baltic Sea. The extending sea ice in cold winters causes the inertia in the snow cover duration and cold springs. In case of warm winter, the extent of ice is limited and snow melts early.

The ice maximum extent on the Baltic Sea is a better predictor than the snow cover for the April and May temperature anomalies in some surrounding areas (South and North Sweden). The temperature in April and May may be predicted already in January because the relationships between the January temperature around the Baltic Sea and maximum ice extent on the Baltic Sea are close and correlation coefficients are large (between 0.74 and 0.91). In some cases the temperature deviation of the preceding months is a good predictor for the temperature of the following months.

References

Una Ni, Chaoimh. European snow cover at its influence on spring and summer temperatures. *The Geographical Journ.*, 164, 1, 41-54, 1998

Groisman, P. Ya., Karl, T. R., Knight, R. W. Observed impact of snow cover on the heat balance and the rise of continental spring temperatures. *Science,* 263, 198-200, 1994

Haapala, J., Leppäranta. The Baltic Sea ice season in changing climate. *Boreal Environment Research* 2, 93-108, 1997

Isemer, H.-J. Sea ice concentration at the Baltic Proper - A digital 1° data set for 1964 to 1995. Proc. of Second Study Conference on BALTEX, Juliusruh, Island of Rügen, Germany, 25-29 May 1998, International BALTEX Secretariat, Publication No 11, 78-79, 1998

Keevallik, S. Relationships between temperature and snow cover in spring. In: *IRS2000. Current Problems in Atmospheric Radiation.* Eds. Yu. Timofeev and W. Smith. A. Deepak Publishing (accepted). 2001

Keevallik, S., Tooming, H. Relationships between surface albedo and spring heat accumulation. *Tellus 48 A*, No 5, 727-732, 1996

Seinä, A., Palosuo, E. The classification of the maximum annual extent of ice cover in the Baltic Sea 1720-1992. Meri, 20, 2-20, 1993

Tarand, A. The Tallinn time serie of break-up as climate indicator. Proc. 1st Workshop on the Baltic Sea Ice Climate, Tvärminne, Finland, 24-26 August, 1993. Department of Geophysics, University of Helsinki, Report Series in Geophysics 27,91-93, 1993

Tooming, H. Surface albedo as an indicator of climate. Pamietnik Pulawski, Prace IUNG, Pulawy, Zeszyt 110, 43-58, 1997

Tooming, H., Kadaja, J. Surface thermal forcing and sea ice condition. 2nd European Conference on Applied Climatology 19 to 23 October, Central Institute for Meteorologie and Geodynamics, Vienna, Austria, Österreichische Beiträge zu Meteorologie und Geophysik, Nr. 23, Publ. Nr. 392, CD-ROM, 1998

Tooming, H., Kadaja, J. Snow cover and surface albedo in Estonia. *Meteorol. Zeitschrift*, N. F. 9, Nr. 2, 97-102, 2000

Snow cover depth and water equivalent in Estonia

Heino Tooming and Jüri Kadaja

Estonian Meteorological and Hydrological Institute, Rävala 8, Tallinn 10143, Estonia

1. Introduction

Snow cover duration and surface albedo are integrators of weather conditions and indicators of climate changes *Tooming* (1997). Snow depth, density and water equivalent or water storage are of primary importance for hydrological purposes particularly in early spring runoff and water budget predictions *Tooming, Kadaja* (2000). The snow depth in Estonia is earlier studied by *Letzmann* (1921) and by *Kirde* (1939) for time interval 1923-1935.
In the present paper the distribution of snow cover depth, density and water equivalent over Estonian territory are described. The trends in snow cover depth and water equivalent over the time span 1962-1995 are also studied.

2. Methods

Snow cover depth

Snow cover depth is measured on the territory of meteorological stations and posts and on the routes. In the paper the measurements from 1962 to 1995 are used for stations and posts and data up to 1997 for routes. Field routes have the length of 1000-2000 meters in open areas inside the forests - 500 m. The depth of snow cover is measured after every 10 meters.

Density of snow

Snow density is measured with snow-gauge in ten points in the field route and in 5-7 points in the forest simultaneously with snow depth measurements.

Calculation of snow cover water equivalent

The water equivalent is the depth of water layer in millimetres, which originates in the surface when snow cover melts completely. Snow cover water equivalent can be found by multiplication of snow cover depth and snow density. In this paper the maps for monthly maximum snow water equivalent are presented. The calculation of water equivalent was carried out separately for every measurement date using the maps of snow depth and density. The values of these fields were multiplied in every gridpoint. For composing the maximum monthly water equivalent maps, the maximum values were found in every gridpoint, covering all the maps of this month. Further analysis was done on the basis of the monthly maximum water equivalent.

3. Results

Snow cover depth in Estonia

In Estonia the first snow appears usually in November (Table). In rare years it happens in October. In November the snow depth has its maximum in Pandivere and Haanja uplands about 3 cm. On the western coastal areas and islands the snow cover depth as an average is only 1 cm. The isoline of 2 cm snow depth halving the Estonian territory is directed from North to South.
In February snow cover depth has its maximum in Estonia on the upland Haanja and Pandivere, as measured at meteorological stations respectively 26 and 24 cm (Fig. 1).

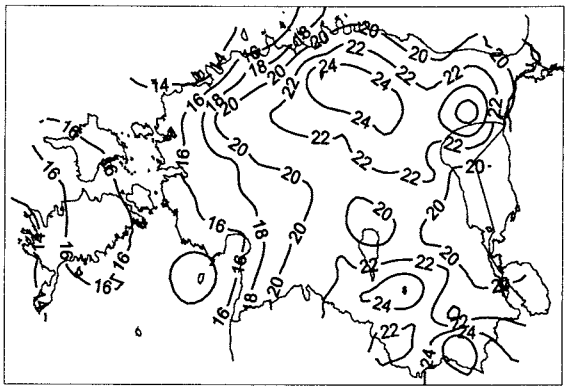

Figure 1: Average snow cover depth (cm) in meteorological stations and posts in February between 1962-1995.

Table 1: Snow cover depth in different locations in Estonia

	Nov	Dec	Jan	Feb	Mar	Apr
Met. Stations and posts						
Pandivere upland	3	12	18	24	24	4
Haanja upland	3	10	18	26	24	4
Insular and coastal areas	1-2	4-6	10-12	14-16	12-14	0-2
Field routes						
Pandivere upland	3	11	16	22	20	2
Haanja upland	3	13	22	31	24	4
Insular and coastal areas	1-2	5-7	8-12	13-16	8-11	< 1
Forest routes						
Pandivere upland	2	12	20	28	23	6
Haanja upland	2	12	22	31	29	7
Insular and coastal areas	1-2	9-11	14-16	21-23	17-20	2-3

In some years (1966, 1989) snow cover depth reached 50-60 cm, in some locations 76-77 cm. On the Western coast of Estonia and on islands the snow cover depth is in an interval 14-16 cm.
In March the character of isolines over Estonian territory is similar to the previous months. However the snow cover depth decreases 2-4 cm.
The snow cover depth based on route measurements in the field is mostly 1-3 cm lower than in the observation areas of meteorological stations and posts (Table).
Route measurements in the forests show that until December snow cover depth in the forest is thinner than in the fields. From January snow cover depth in the forest is deeper than in the fields (Table). Snow cover depth reaches the maximum of 18-24 cm in the forests in March, later than in the fields since snow melts slowly in the

forest. Snow cover in the forests in April is on an average 2-5 cm deeper than in the fields.

Snow cover density

The average density of snow cover has small differences over Estonian territory. The average of maximum 260 kg/m^3 snow density in the fields was observed in March. The mean snow cover density in the forests from November until April is lower than in the fields - snow in the forest is sheltered from the winds and is therefore more fluffy. Snow cover density has the maximum in the forest 250-260 kg/m^3 in April. Trends in snow cover density are mostly not significant.

Snow cover water equivalent

The maximum of mean snow cover water equivalent both in the forests and in the fields occurs in February and particularly (Fig. 2 - 3) in March and is in the interval of 40-90 mm in the fields and 50-80 mm in the forests. . In some years (1966, 1982) the snow cover water equivalent in the fields reached the value 206 and 174 mm, in forests up to 207 and 173 mm in some locations. In April the water equivalent in the forest is higher than in the fields, while in other months snow cover water equivalent is greater in the fields than in the forests. Consequently, forests store more snowmelt water for the vegetation period than fields.

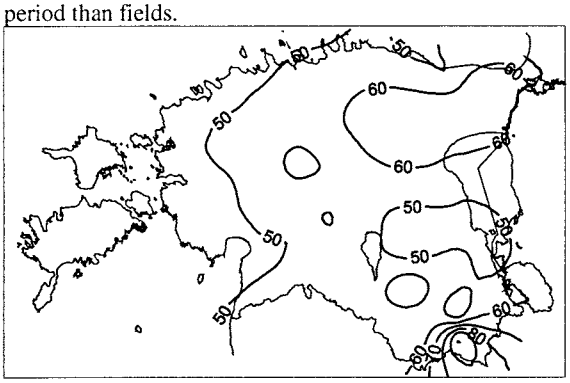

Figure 2: Snow cover maximum water equivalent in fields (mm) in February between 1962-1997 on the basis of route measurements.

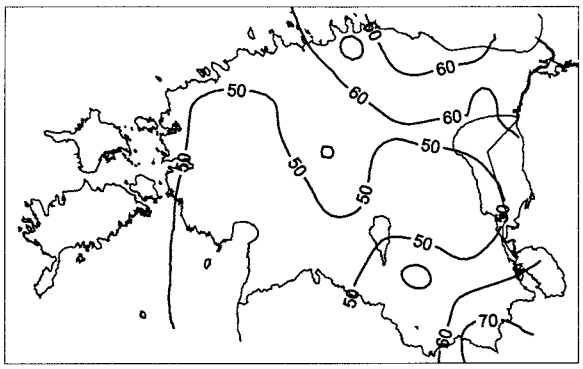

Figure 3: Snow cover maximum water equivalent in forests (mm) in February between 1962-1997 on the basis of route measurements.

4. Conclusions

Snow cover depth and water equivalent are quite variable over Estonia. The depth of snow and water equivalent are greatest in the upland areas. The temperature, presence or absence of the sea ice cover and its duration has a primary impact on the snow depth and water equivalent besides the cyclonic activity connected mostly with the North Atlantic *Tooming, Kadaja* (1998). We found negative linear trends of snow cover depth and its water equivalent in all months with snow cover except November. Maximum negative trends up to -0.5-0.6 cm per annum were detected in the Estonian uplands for February and March. In other areas in Estonia, the negative trend of snow cover depth is not so high. Considering our results, the climate in the winter half of year on Estonia is turned warmer and somewhat more maritime in continental areas.

Acknowledgement

The authors acknowledge the Estonian Science Foundation for the support.

References

Kirde, K. Andmeid Eesti kliimast. Tartu. 1939.

Letzmann, J. Die Höhe der Schneedecke im Ostbaltischen Gebiet. Acta Comm. Univ. Dorpat, A III, 65 p. 1921.

Tooming, H. Surface albedo as an indicator of climate. Pamietnik Pulawski. IUNG, Zeszyt 110, Pulawy, 43-58, 1997.

Tooming, H. and Kadaja, J. Surface thermal forcing and sea ice conditions. European Conference on Applied Climatology 19 to 23 October 1998, Vienna, Austria. Österreichische Beiträge zu Meteorologie und Geophysik, Nr 19. ZAMG, Vienna, Austria, CD-ROM.

Tooming, H. and Kadaja, J. Snow cover and surface albedo in Estonia. *Meteorol. Zeitschrift* N. F. 9, N° 2, 97-102, 2000.

Simulation of bottom water inflow in the Cetntral Baltic.

Valeriy Tsarev

Russian State Hydrometeorological Institute, 98, Malookhtinsky Ave., 195196, St.Petersburg, Russia,
e-mail: tsarev@sici.ru

Possible features of bottom flow from the Stolp Channel into the Cenral Baltic are investigated by numerical simulation. A set of the model governing equations involves tree-dimensional non-stationary non-linear equations of motion for the horizontal and vertical directions (Tsarev V.). It also includes equations of mass and salinity conservation and equation of the state. Equations of motion and mass conservation are transformed with the method of vector potential to three-dimensional equations of vector vorticity, vector and scalar potentials. Resulting currents velocity $\mathbf{u}$ is assumed as a sum of potential $\mathbf{u}_p$ l and rotor $\mathbf{u}_r$ components. $\mathbf{u}_p$ and $\mathbf{u}_r$ are found from scalar φ and vector ψ potentials accordingly.

$\mathbf{u}_p = \nabla\cdot\varphi$; $\mathbf{u}_r = \nabla\times\psi$.

φ is obtained from equation $\nabla^2\varphi = 0$. ψ is connected with vorticity by equation $\nabla^2\psi = -\Omega$. Ω is calculated from equation of vorticity

$$\frac{\partial\Omega}{\partial t} + (\mathbf{u}\cdot\nabla)\Omega - (\Omega\cdot\nabla)\mathbf{u} - f_z\frac{\partial\mathbf{u}}{\partial z} - k_z\frac{\partial^2\Omega}{\partial z^2} - k_l\nabla_l^2\Omega = g\times\nabla\rho.$$

For calculation of water salinity and density the following equations are used

$$\frac{fs}{ft} + u\frac{fs}{fx} + v\frac{fs}{fy} + w\frac{fs}{fz} = k_z\frac{f^2s}{fz^2} + k_l\ ^2s$$

$$\rho = \rho_0 + \alpha_s s$$

u, v, w are velocity components along coordinate axes x, y, z; ρ_0, ρ are standard and real sea water density respectively; s is salinity; k_z, k_l are coefficiens of vertical and horizontal eddy viscosity ,k_s,k_l are coefficients of vertical and horizontal diffusivity respectively; α_s is a coefficient of the saline contribution to density; g is gravitational acceleration; f is the Coriolis coefficient.

The accounts were carried out for rectangular area located in the central part of the Baltic sea, including the Gotland and Gdansk Deeps (fig. 1a). That was reflected in used depths distribution (fig. 1b). The lateral border was considered as solid except for its small part in area of the Stolp Channel , through which occurs bottom water inflow.As initial condition the homogeneous salinity distribution equal 10‰ and zero initial vortisity were set. On liquid border the salinity was 16‰. The salinity on the free surface during all period of accounts was kept equal to 10‰ The vertical and horizontal viscosity coefficients were accepted equal $k_z = 10^{-4}$ м^{2}с$^{-1}$, $k_l = 10$ м^{2}с$^{-1}$. The vertical and horizontal diffusivity were as follows $k_{sz} = 10^{-5}$ м^{2}с$^{-1}$, $k_{sl} = 10$ м^{2}с$^{-1}$. The domain was covered by 25x59x30 grid with 30 levels in vertical direction. The spatial steps was 5 kms. In a vertical direction first ten steps from the bottom were 2 м, and above equaled (H-20м) /19, where H bottom depth in meters.

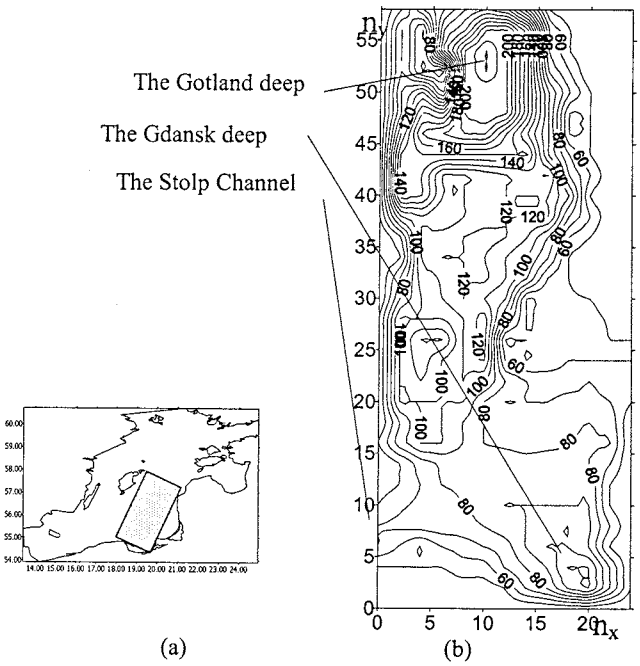

(a) (b)

Figure 1: Model area location(a) and bottom depth distribution(b). (n_x, n_y –grid nodes numbers along x and y axises)

From the model run inflowing saline bottom water moves along right sea slope. In some days the bottom water reaches the bottom area, separating the Gotland and Gdansk Deeps (fig. 2a). Here the bottom flow divides into two branches. The right branch deviates to the Gdansk Deep, spreading along its right slope. In 10 days it reaches the the most deep depth of the Gdansk Deeep and partially passes to its opposite slope. The left branch goes to the Gotland Deep reaching its maximal depths approximately in month. Next forty days the bottom salinity distribution doesn't change sufficiently and is characterized by the bottom water storage in the Gotland Deep (fig.2b). Main bottom water flow is found over the right Gotland Deep bottom slop (fig.5). . The direction of the bottom water currents (fig.3) follows the main isobaths. The flow velocity and width are depended on the bottom inclination. Over area with high bottom inclination its width decreases but velocity increases. The maximum velocity is marked near the Stolp Channel where it reaches 60 cm s^{-1}. In upper layer the opposite directed currents (fig. 4) are formed, which velocity is in some times lower then in the bottom one. Close results are obtained by Zhurbas V. (Zhurbas V and others,2000).

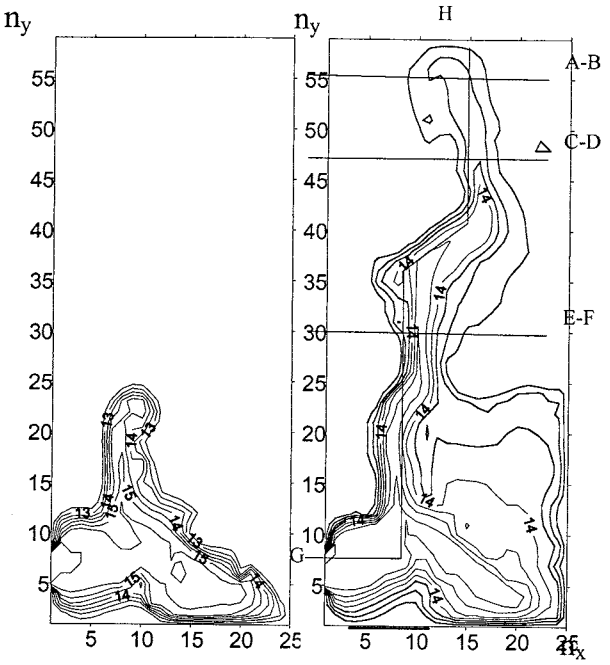

Figure 2: Bottom salinity distribution calculated in 10 (a) and 70 (b) days.

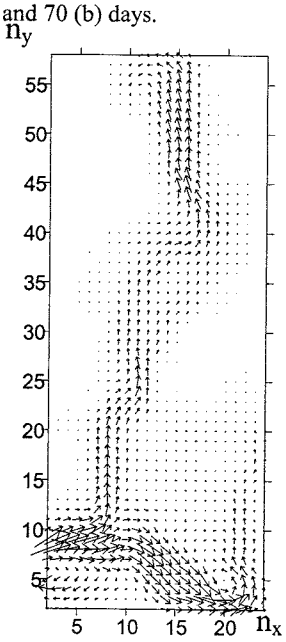

Figure 3: Calculated in 70 days bottom currents velocity distribution

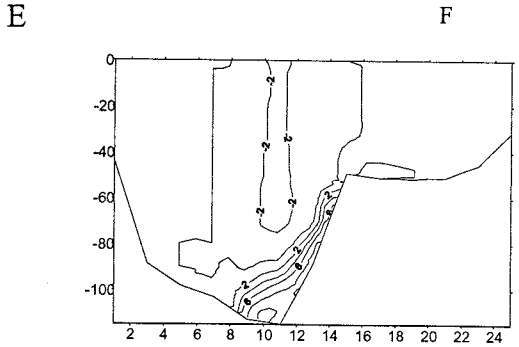

Figure 4: Calculated in 70 days longitudinal currents velocity component distribution at section E-F

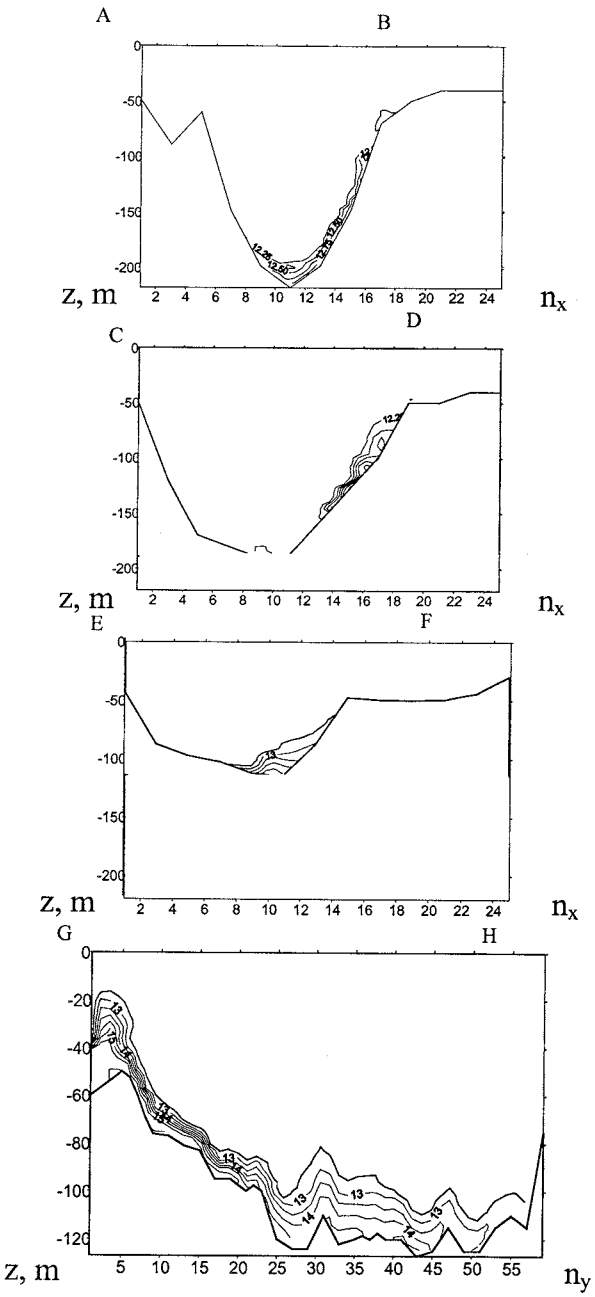

Figure 5: Computed across and longitudinal sectional salinity distribution.

Reference

Zhurbas V.M., Oh L.S., Paka V.T. Generation of deep water cyclonic eddies in the Estern Gotland Basin following major Baltic inflows: Numerical experiments *Journal of Marine Systems*, 2000, submitted.

Tsarev V.Evolution of bottom lens based on numerical simulation *Oceanologia*, 2000, V.40. N.6. P.833-839.(in Russian)

Test of a number of modifications to the ECMWF land surface scheme using the Torne/Kalix Pilps2E experiment

Bart van den Hurk[1] and Pedro Viterbo[2]

[1] Royal Netherlands Meteorological Institute, PO Box 201, 3730 AE De Bilt, The Netherlands
[2] European Centre for Medium-range Weather Forecasts, Reading, Berkshire RG2 9AX, UK

1. Introduction

A recent experiment in the context of the Project for Intercomparison of Land Surface Parameterization Schemes (PILPS) was devoted to the model performance under Arctic conditions in the Torne/Kalix river basins, in the North of Sweden and Finland. In this PILPS study, labeled PILPS2E, approximately 20 modelling groups submitted results of simulated surface fluxes, soil moisture content and temperature, snow properties and hydrological components of an area covering 58000 km^2 for a 10 year period (1989-1998) (*WCRP*, 1999).

Among the participating models were two versions of the recently developed ECMWF land surface scheme. This ECMWF scheme is a tiled version of the well-known scheme by *Viterbo and Beljaars* (1995). The tiled version has demonstrated to yield a major improvement for the simulation of snow development in boreal forest areas, where the positioning of the snow under the canopy layer inhibited an excessive snow evaporation (*Van den Hurk et al*, 2000). However, a number of issues related to processes affecting exposed snow and high-frequency runoff events were not addressed during the development of this new ECMWF scheme. Therefore, another version of the ECMWF scheme was submitted to the PILPS2E project in which a small number of modifications was incorporated. This alternative ECMWF scheme is labeled MECMWF hereafter, and briefly described below.

2. Modifications to the ECMWF scheme

Compared to the operational ECMWF land surface scheme the following modifications are included in MECMWF:

1. Surface runoff is no longer dependent on the saturation of the entire upper soil layer, but subgrid saturation is explicitly parameterized as function of soil moisture content and orographic variability, following the approach by *Dümenil and Todini* (1992).
2. Sublimation of snow on bare ground and low vegetation is limited by imposing a surface roughness length which reduces as the snow pack covers the individual low vegetation and rocks.
3. The soil hydraulic characistics are parameterized using the so-called *Van Genuchten* equations instead of the widely used scheme of *Clapp and Hornberger*.
4. The ageing of the snow albedo is delayed when the snow temperature is very low.

These four changes have the effect of:

- Reducing the snow sublimation of exposed snow, mainly by an increase of the aerodynamic resistance. This causes an increase of the depth of the snow pack at the end of the winter/spring season.
- Increasing the surface runoff during periods of snow melt and precipitation. This changes the temporal signature of the total runoff from a gradual evolution with little peaks to a more periodic event driven runoff generation.

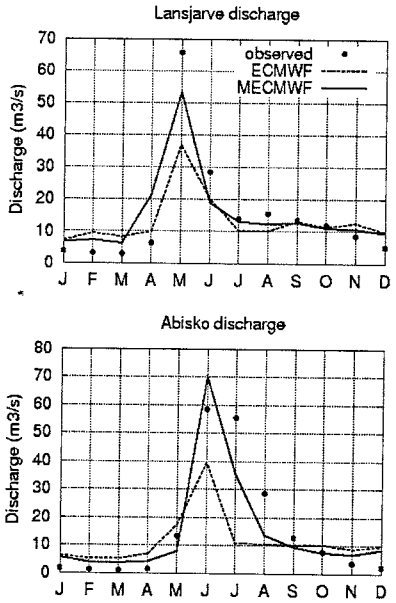

We have used the PILPS2E experiment to evaluate the impact of these changes on the performance of the ECMWF land surface model.

Figure 1: simulated and observed discharge from the Lansjarve calibration basin (top) and the Abisko basin (bottom).

3. Comparison of simulated discharge with observations from small sub-catchments.

As part of the PILPS2E project, discharge data from two small catchments were provided to the participants in order to allow a calibration of the participating models.

One basin, Ovre Abiskojokk, is located in the mountainous North-Western area in the basement, with little vegetation and steep orographic gradients. Ovre Lansjarve is a basin in the Eastern lower region in the basin, where forest vegetation and relatively small orographic differences are present.

The ECMWF and MECMWF models are not calibrated specifically using discharge observations from these

catchments, but rather a priori estimates of necessary coefficients have been used.
Figure 1 shows the average annual cycle of the modeled and observed discharge from the mountainous "Abisko" catchment, as well as the flat "Lansjarve" basin. It is clearly demonstrated that the MECMWF model results in a stronger spring melt peak generated by the melting snow from the area, in correspondence to the observed discharge volumes.
For both catchments, the ECMWF predicted spring melt peak is too low, and too little runoff is generated in the period following the peak. This implies that the amount of snow that is accumulated prior to melt in ECMWF is less than in MECMWF, as a result of stronger sublimation (see below). A preliminary analysis of the PILPS results showed that, averaged over the entire Torne/Kalix basin, the ECMWF simulation did not produce a noticeable spring melt peak at all. The contribution of the areas where, as shown in Figure 1, a spring melt peak is produced is probably very small compared to the basin area (results not shown).

4. Annually averaged hydrological budget

The modifications to the runoff have a minor impact on the annually averaged partitioning of precipitation over evaporation and runoff. Since precipitation is a prescribed forcing, and evaporation is basically energy limited rather than moisture limited in this area, the runoff formulation can only affect the timing of the runoff and the seasonal cycle of the soilwater deficit.
On the other hand, formulation of the sublimation of snow may result in considerable shifts in the annual water balance, as it affects the partitioning of snowfall over sublimation and melt.
Estimates of total runoff were available for the period 1989-1998 from a long term simulation of a hydrological model calibrated to the river discharge at a number of locations in the area. Observed evaporation was obtained using the forcing precipitation, assuming a negligible change of soil moisture storage over the 10 year period.
Figure 2 clearly demonstrates the considerable impact of the modifications to the snow treatment incorporated in the MECMWF simulations. Averaged over the 10 year period, the total evaporation is reduced by nearly 25% (from ± 400 mm/year to 300 mm/year). Within the limitations of the method to derive evaporation loss from available data, the change to the snow treatment results in a clearly improved correspondence to the observations.
Since in MECMWF more runoff is generated as surface runoff, also the relative contribution of surface runoff to the total runoff has increased, from 19% to 40%. Observations of this ratio are not present, but the analysis shown in the previous section supports the relatively high contribution of fast responding surface runoff to the total discharge from the catchment.

Figure 2: 10-year (1989-1998) averaged water budget of the Torne/Kalix river basin. Shown are model values for evaporation, surface runoff and baseflow runoff, and the best estimate of runoff from the catchment. Observed evaporation is inferred from this runoff estimate and the imposed precipitation.

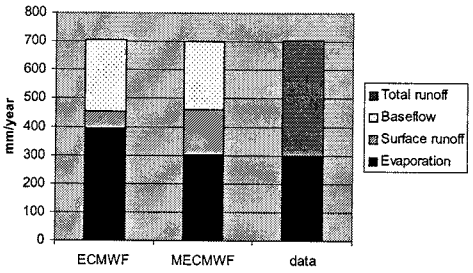

5. Discussion

The changes in the runoff formulation and the treatment of the exposed snow pack appear to have a beneficial impact on the annual partitioning of precipitation over evaporation and runoff. Snow sublimation plays an important role in this partitioning in the study area.
The generation of surface runoff using a variable infiltration capacity method, using a priori estimates of calibration coefficients, appears to improve the temporal dynamics of the runoff simulations. On site calibration may be used to improve this dynamics, but this will hardly affect the annual partitioning of the precipitation.
The PILPS2E experiments (and its precessors) appear a very useful platform for evaluating and developing land surface parameterization schemes used in large scale applications.

References

Dümenil, L. and E. Todini, 1992: *A rainfall-runoff scheme for use in the Hamburg climate model*; in: Adv. Theor. Hydrology, J.P. O'Kane (Ed.); European Geoph. Soc. Series on Hydrological Sciences, Vol. 1, Elsevier Science Publishers, Amsterdam, pp. 129-157.

Van den Hurk, B.J.J.M., P. Viterbo, A.C.M. Beljaars and A.K. Betts, 2000: Offline validation of the ERA40 surface scheme; ECMWF TechMemo 295 (to be submitted to *J.Climate*)

Viterbo, P. and A.C.M. Beljaars, 1995: An improved land surface parametrization scheme in the ECMWF model and its validation; *J.Climate* **8**, 2716-2748.

WCRP, 1999: Report on the hydrology inter-comparison planning meeting Koblenz, 27-29 March 1999; WCRP Informal report 12/1999.

Acknowledgements

The work described here would have been impossible without the support from the PILPS2E coordination committee, in particular Dennis Lettenmaier and Laura Bowling.

A comprehensive model intercomparison study investigating the water and energy cycle during the Baltex-PIDCAP period.

Bart van den Hurk[1], Jacob, D.[2], Andræ, U., Elgered, G., Fortelius, C., Graham, L.P., Jackson, S.D., Karstens, U., Köpken, Chr., Lindau, R., Podzun, R., Rockel, B., Rubel, F., Sass, B.H., Smith, R.N.B., Yang, X.

[1] Royal Netherlands Meteorological Institute, PO Box 201, 3730 AE De Bilt, The Netherlands
[2] Max-Planck-Institute for Meteorology, Hamburg, Germany

1. Context and description of the experiment

In order to assess the variability between models used for simulation of the atmospheric water and energy cycles in the Baltic Sea catchment area, a comprehensive model intercomparison experiment was carried out. During this experiment, a suite of eight regional atmospheric model systems - used for regional climate studies and numerical weather prediction - were operated on a common grid and forced by common sea surface temperatures and lateral atmospheric analyses. A special Baltex reanalysis archive, produced at the Danish Meteorological Institute DMI, was used for this purpose. Apart from a few exceptions, horizontal and vertical resolution was identical for all models at 1/6° × 1/6° and 24 vertical levels, respectively. The models were initialized at 1 August 1995, and a three-month period (until 1 November 1995) was analysed. The model systems fell apart in three main categories: atmospheric analysis systems, routine short term forecasts initialised from an interpolated analysis, and climate mode integrations without update of the model interior during the course of the experiment. Table 1 briefly lists the participating model systems and the category they belong to.

The study is extensively described in a paper by *Jacob et al* (2001). Here, only a limited number of highlights is presented. We will address the correspondence between models in their simulation of land surface hydrology (precipitation, evaporation, runoff) and the simulation of processes associated with clouds and radiation.

2. Land surface hydrology

The simulation period was characterised by a dry warm spell until 23 August 1995, followed by a series of well-developed cyclones and associated precipitation from 24 August onwards. Precipitation and surface radiation were significantly different in these two sub-periods, and so is the land surface hydrology. Therefore, the simulations of late summer/early autumn land surface hydrology by each of the models is summarized in Figure 1, in which a distinction between the early dry and later wet periods is made. Also shown are an estimate of precipitation over land using the analysis of *Rubel (1998)*, and catchment discharge generated by a calibrated hydrological model HBV-Baltic (*Graham, 1999*), both shown as "obs". In the warm period, precipitation is usually less than the sum of evaporation and runoff, and the soil water reservoir is depleted. In the later period, soil moisture recharge is usually simulated by the models.

Table 1: Summary of participating model systems. (References can be found in *Jacob et al (2001)).*

Model acronym	Operating institute	System type	Remarks	References
DMI-CSE	DMI, Denmark	Analysis	0.4° resolution, nested in ECMWF analysis	*Sass and Yang, 1997*
DWD-BM	DWD, Offenbach	Analysis	1/6° 30 level assimilation using nudging	*Majewski, 1991*
REMO-GKSS	GKSS, Geesthacht	Forecast	Sequence of 30hrs forecasts	*Majewski, 1991*
RACMO	KNMI, Netherlands	Climate mode	HIRLAM + ECHAM4 physics + ECMWF surface scheme	*Christensen et al, 1996*
REMO-EC4	MPI, Hamburg	Climate mode	REMO + ECHAM4 physics	*Roeckner et al, 1996*
REMO-DWD	MPI, Hamburg	Climate mode	REMO + DWD physics	*Jacob and Podzun, 1997*
SMHI	SMHI, Sweden	Climate mode	HIRLAM physics	*Källen, 1996*
UKMO	The MetOffice, UK	Climate mode	Unified Model	*Cullen, 1993*

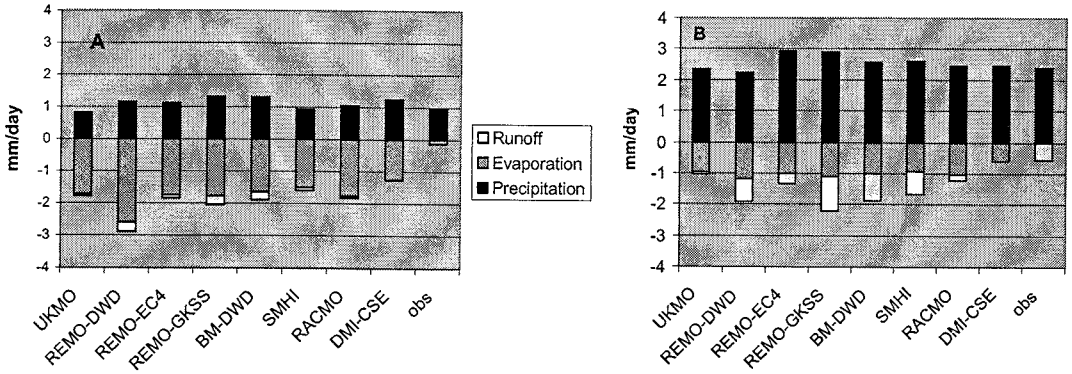

Figure 1: Average daily precipitation, evaporation and runoff over the catchment land area for the first 23 days (A) and remaining days (B) of the simulation period. Observations of evaporation, and runoff from DMI-CSE were not available.

The increase in average daily precipitation from about 1 mm/day to approximately 2.5 mm/day later in the simulation period is clearly picked up by all models. Also shown is a pronounced reduction of land surface evaporation, from approximately 1.8 mm/day to slightly more than 1 mm/day. Where runoff plays a minor role in the warm subperiod for most models, it becomes increasingly important later in the season.

In the warm period precipitation above land is overestimated by most models compared to the analysis of *Rubel (1998)*, and also in the wet spell overestimation of precipitation is the rule rather than exception. Anomalous evaporation in the dry period, as shown by REMO-DWD, appeared a result of an inconsistently high initial soil moisture content. Also the low evaporation calculated by DMI-CSE appeared related to soil water. These anomalies still bear a signature in the later wetter part of the season.

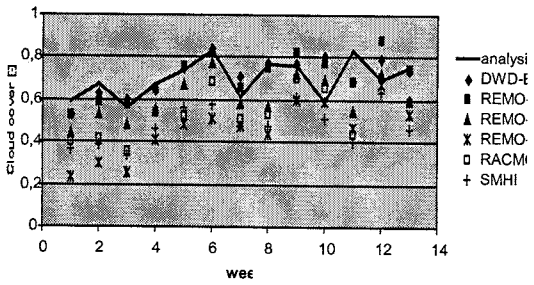

Figure 2: weekly averaged total cloud cover from the DWD analysis and the models shown.

Consistent with simulations by HBV-Baltic most models generate little runoff in the dry period. However, as precipitation intensifies runoff occurs more frequently in HBV-Baltic, but this is not represented by UKMO and RACMO. Differences in the physical parameterization of runoff are the main reasons for these differences.

3. Clouds and radiation.

Observations of downward radiation were available at four ground stations in the simulation domain. An analysis of total cloud cover was prepared by DWD, based on a combination of METEOSAT and ground based observations.

Figure 2 shows weekly averaged total cloud cover simulated at 12 UTC from most models and the DWD analysis. The models operating in forecast or analysis mode (DWD-BM and REMO-GKSS) are shown to have a significantly higher total cloud cover, closer to the analysis. Models using the ECHAM4 physics in climate mode (RACMO and REMO-EC4) have considerably less cloud cover.

However, simulations of surface shortwave radiation are not linearly related to the cloud cover bias. Table 2 shows the mean bias of downward radiation at the surface averaged over the four observation points and over the entire simulation period. In spite of the systematic underprediction of cloud cover by both REMO-EC4 and RACMO, the former overestimates surface radiation whereas the latter underpredicts it. The study has given rise to sensitivity analyses addressing cloud radiative properties, liquid water content and clear sky absorption. Also, problems with cloud cover in e.g. REMO-EC4 were diagnosed after this experiment was completed.

Table 2: Mean bias (W/m^2) of downward shortwave radiation at four ground stations.

Model	Mean bias
DWD-BM	-10.2
REMO-GKSS	+2.0
REMO-DWD	-10.8
REMO-EC4	+11.5
RACMO	-25.0
SMHI	+13.4

References

Graham, L.P., 1999. Modeling runoff to the Baltic Sea. *Ambio* **28**, 328-334.

Jacob, D. (and CoAuthors), 2001. A comprehensive modelintercomparison study investigating the water budget during the BALTEX-PIDCAP period; *Meteorol.Atm.Phys.*, submitted.

Rubel, F., 1998. PIDCAP- Ground truth precipitation atlas; *Oesterreichische Beitrage zu Meteorologie und Geophysik*, **18**, 76pp.

The BALTEX BRIDGE Cloud Liquid Water Network Project: CLIWA-NET

André van Lammeren and the CLIWA-NET project team

Royal Netherlands Meteorological Institute, PO Box 201, 3730 AE De Bilt, The Netherlands.

1. Introduction

On average, more than 60% of the Earth's surface is covered by clouds. Clouds strongly affect atmospheric radiative fluxes and heating rates. However, cloud processes are still not well understood and the representation of clouds remains one of the greatest sources of uncertainty in present day climate models. The CLIWA-NET project aims to contribute to a better cloud representation in atmospheric models by an advanced observational program and improved parameterisations.

Within the CLIWA-NET project a prototype of a European cloud observing system will be established by co-ordinating the use of existing, ground-based passive microwave radiometers and profiling instruments. The data from the ground-based remote sensing instruments will be used to improve the satellite-based estimates of cloud water content. New procedures will be developed to fully exploit this synergy.

CLIWA-NET focuses on observations of cloud liquid water and vertical structures, and the evaluation and improvement of model parameterisations. The specific CLIWA-NET objectives are:

- Implementation of a prototype of a European Cloud Observation Network
- Objective evaluation of atmospheric models for weather forecasting and climate
- Improvement of the parameterisation of cloud processes, with a focus on vertically integrated cloud liquid water and vertical structure of clouds
- Design of a "low cost" microwave radiometer in co-operation with industry (SME)
- Development of an adequate observing system for the detection of icing conditions for aircraft
- Contribution to BALTEX/BRIDGE.

In this paper an overview of the CLIWA-NET project is given. In section 2 the observational plan is described, the next section briefly describes the modelling work within the project. The design of a low cost micro-wave radiometer is described in section 4 and we will end with some concluding remarks.

2. Observational Plan

Within CLIWA-NET observations are taken during three campaigns. These campaigns are co-ordinated with the BALTEX BRIDGE Enhanced Observational Periods (EOP).

Within the CLIWA-NET Network (CNN) in total 12 stations within a European network contributed. CNN was operated in August/September 2000 (CNN I) and in April/May 2001 (CNN II). At the ground based stations routine cloud remote sensing measurements were made for the full two month periods. At every station a microwave radiometer was present. A full description of the ground based network can be found in *Crewell et al.* (2001).

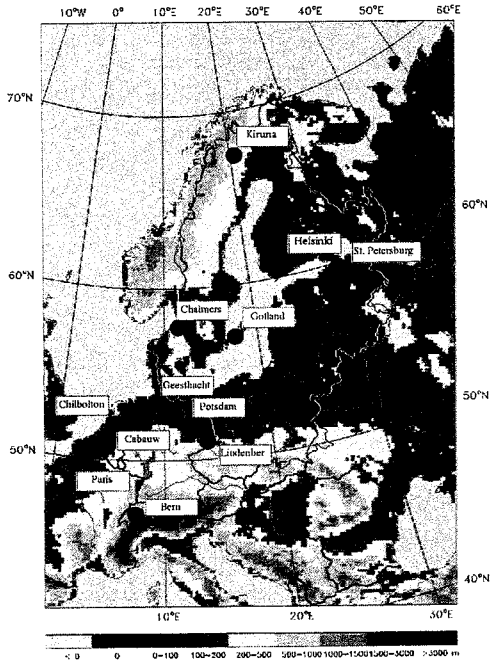

Figure 1: The CLIWA-NET network. The purple line indicates the BALTIC catchment area.

The BALTEX BRIDGE Cloud campaign (BBC) is organised in August/September 2001. During the first two weeks of August a microwave radiometer calibration campaign will be organised at Cabauw (The Netherlands). Seven microwave radiometers from the CNN network will participate. This intercomparison will provide detailed information on the reliability of the observations during the CNN campaigns.

After the intercomparison the instruments are distributed over a local network of five stations around Cabauw in the Netherlands (see Figure 2). At each station microwave radiometer measurements will be combined with lidar ceilometer, IR-radiometer and pyranometer measurements. At the central facility in Cabauw an extensive set of remote sensing instruments will be installed. See table 1.

In September three aircraft will take in-situ and radiation measurements over the BBC network. The aircraft and part of the ground based remote sensing instruments are funded from other projects (e.g. 4D-Clouds, CAATER) or are individual contributions from the participants.

During both CNN and the BBC campaigns the ground based measurements are complemented by satellite observations from Meteosat, NOAA/AVHRR and AMSU. All ground-based instruments are operated around the day-time overpasses of the NOAA satellites. Outside these intervals the data is taken continuously as much as possible.

More information on the analysis of the satellite measurements is given in *Feijt et al.* (2001).

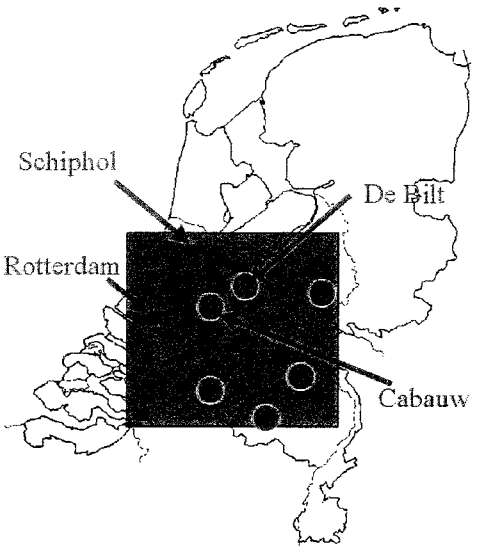

Figure 2: Map of the BBC Network. The red dots indicate the stations where a microwave radiometer will be installed. The grey area has a typical size of 120x120 km^2. The aircraft will be located at Rotterdam Airport.

3. Modelling

The retrieved CLIWA-NET data-sets will be used for an objective evaluation of the performance of state-of-the-art cloud parameterisation schemes in atmospheric models (*Meijgaard and Mathieu*, 2001). The focus will be on liquid water path (LWP) and vertical structure of cloud amount and cloud water. Three lines of research will be pursued:

- Evaluation of cloud related output from several leading European atmospheric models (ECMWF, HIRLAM, DWD-LM and RACMO).
- Investigation of the sensitivity of model cloud parameters to the employed horizontal grid spacing in the meso-scale range from (1-10 km)
- To develop/improve/test cloud parameterisations and underlying assumptions.

4. Implementation

The cost and complexity of the available microwave radiometers presently hamper the implementation of an operational network. For this reason, the design of a low-cost operational microwave radiometer by a commercial company is included in this project. A first design indicates that the commercial price of such a system may be reduced by a factor 3 to 4.

5. Concluding Remarks

A full description of the CLIWA-NET project and latest results can be found at the CLIWA-NET web site: www.knmi.nl/samenw/cliwa-net.

The CLIWA-NET project is carried out under the BALTEX umbrella.

Table 1: Overview of the ground-based instruments participating in the BBC campaign

Radars	1.2 GHz windprofiler + RASS (KNMI) 3 GHz radar TARA (TUDelft) 35 GHz radar (KNMI) 94 GHz radar MIRACLE (GKSS) 94 GHz radar (IfT Leipzig), test
Lidars	1064nm, 532 nm backscatter lidar (RIVM) CT75K ceilometer (KNMI) LD40 ceilometer (KNMI)
Micro wave	22 channel MICCY (UBonn) 89, 157, 183 GHZ MARSS (UKMO) During microwave intercomparison also: 24, 37 GHz (CETP) 24, 31 GHz (DWD) 21, 31 GHz (Chalmers) 21, 32 GHz (UBern) 13, 22, 37, 89 GHz (St. Petersburg)
Rad-iation	SW in & out, SW direct & diffuse, LW in & out (KNMI) Oxygen-A band spectrometers (UHeidelberg) IR radiometer (KNMI) Albedometer (IfT Leipzig) Sunphotometer (IfT Leipzig) radiation (TUD)

Meteo	Cabauw meteo tower, 2 – 200 m	temperature dew point temperature wind direction wind speed
	Tethered balloon (Univ. Utrecht), 0 - 1.4 km	temperature pressure RH wind
	Radio soundings De Bilt (KNMI): 0,6,12,18 UTC Cabauw (National Army): 3,9,15,21 UTC	temperature pressure RH wind direction wind speed

Other	Digital video camera (KNMI)

References

Crewell, S., M. Drusch, U. Löhnert, C. Simmer and A. Van Lammeren, Cloud Observations from the Ground -Based CLIWA-NET Network I (CNNI) during BRIDGE EOPI. *This conference.*

Feijt,A., R. Dlhopolsky, D. Jolivet and R. Roebeling, Quantitative Cloud Analysis using AVHRR for CLIWA-NET. *This conference.*

Meijgaard, E. van, and A. Mathieu, Analysis of model predicted liquid water path with observations from CLIWA-NET. *This conference.*

Analysis of model predicted liquid water path using observations from CLIWA-NET

Erik van Meijgaard and Anne Mathieu

Royal Netherlands Meteorological Institute, PO Box 201, NL-3730 AE De Bilt, The Netherlands

1. Introduction

Cloud condensate is a crucial parameter in the representation of cloud induced processes. The vertical distribution of cloud liquid water and ice and the vertically integrated amount strongly affect the balance of solar and terrestrial radiation in the atmosphere. The in-situ cloud content controls the size and rate at which condensate is converted into precipitation. Despite its relevance in atmospheric processes reliable observations of cloud content were until recently only available from aircraft measurements mostly operated within dedicated field campaigns. With the advance of remote sensing instruments like microwave radiometers and cloud radars it becomes feasible to observe cloud parameters more systematically and perform long-term monitoring. Recently the EU-funded project CLIWA-NET (Cloud Liquid Water Network) has been initiated to implement a prototype of a European cloud observational. System. The aim is to demonstrate the usefulness of integrating remote-sensed observations from existing ground-based stations with satellite data in producing spatial distributions of cloud parameters with high temporal resolution. An overview of the CLIWA-NET project can be found in *Van Lammeren et al.* (2001). An extensive description of the ground-based network is presented by *Crewell et al.* (2001).

An important objective of CLIWA-NET is to carry out a quantitative evaluation of cloud parameters provided by atmospheric models used in weather forecasting and climate prediction. In this contribution we focus on vertically integrated liquid water or liquid water path (LWP). Integrated water vapour (IWV) is used to detect changes in air mass mostly related to the passages of frontal systems. We present first results of a comparison with the level-1a compilation of ground-based observations of LWP taken during the first CLIWA-NET campaign (CNN I) in August/September 2000. This type of analysis was pioneered by *Mace at al.* (1998), who looked at the occurrence of hydrometeors.

Four European institutes are participating in the evaluation of model predicted cloud parameters. ECMWF with the global forecast model operated at an effective horizontal resolution of 55 km and with 60 layers in the vertical, DWD with the recently developed Lokal Modell (LM) operated in non-hydrostatic mode at a resolution of 7 km and with 35 layers in the vertical, the Rossby Center with a climate version of HIRLAM, here referred to as RCA, and KNMI with a regional version of the ECHAM4 GCM. The latter two are operated in as much an identical fashion as possible, i.e. they share the same domain, the horizontal resolution is 18 km, the number of model layers is 24, and both are driven from the lateral boundaries by the same set of ECMWF analyses. The output from all models refers to a 12 to 36 hour window taken from each daily forecast initiated at 12:00 UTC. Further details on the model set up can be found at the CLIWA-NET web site: www.knmi.nl/samenw/cliwa-net.

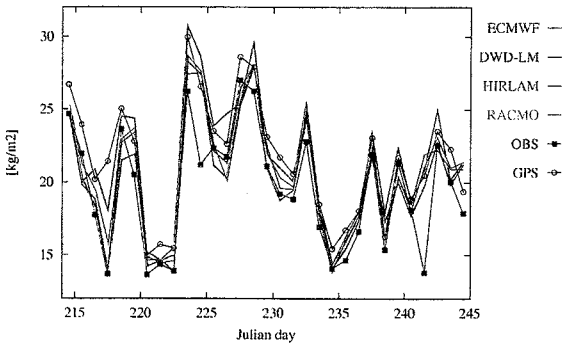

Figure 1: Daily average values of IWV for Onsala Space Observatory during August 2000. Observations are inferred from the microwave radiometer instrument (OBS) and from GPS.

2. Comparison of time series

IWV and LWP have been inferred from microwave radiometer measurements and are compared to the equivalent model parameters. Figure 1 shows the daily average values during August 2000 of observed and model predicted IWV for Onsala Space Observatory in Sweden.(57.4 N, 11.9 E). The daily variations of IWV are strongly controlled by synoptical systems, which in general are quite well captured by large-scale atmospheric models. At Onsala, GPS-measurements provide a second estimate for observed IWV, independent from the microwave radiometer measurements. Figure 1 shows that the two observed curves are very well aligned with the exception of a few days. The Figure furthermore shows that the GPS inferred value is systematically larger than the radiometer inferred value. It is not a priori obvious which of the two observed values provides a better estimate in an absolute sense.

Similarly, Figure 2 shows the observed and model predicted daily averaged values of LWP for Onsala, where observations have been inferred from microwave radiometer measurements. It is pointed out, however, that a sensible inference of observed LWP can only be

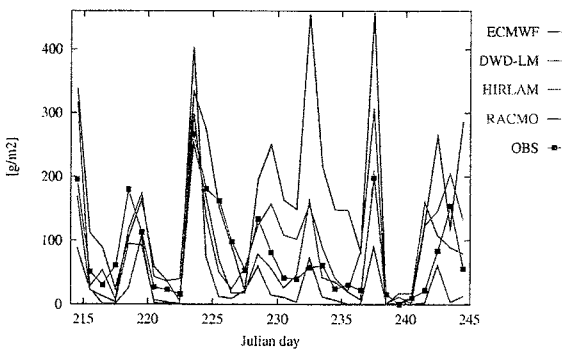

Figure 2: Daily average values of observed and model predicted LWP for Onsala during August 2000.

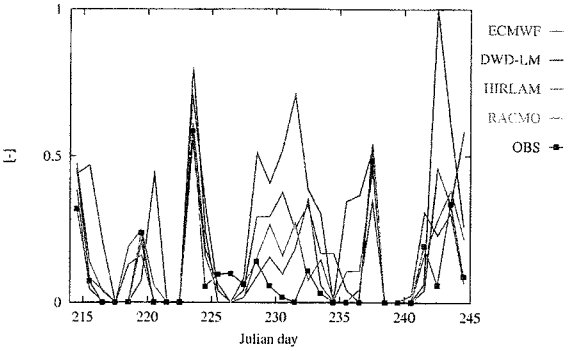

Figure 3: Frequency of occurrence of precipitation at Onsala during August 2000.

performed in the absence of precipitation. In the present analysis, the observed values of LWP are therefore labeled missing in the event of rain, which implies that the shown values of observed LWP in Fig. 2 likely provide a lower limit. The model predicted LWP values, on the other hand, are unconditioned.

Thus, information on the occurrence of precipitation is essential to the interpretation of observed LWP. Figure 3 shows the frequency of rainfall for Onsala during August 2000 both inferred from observations and predicted by the models. The observed values have been analyzed from a infrared radiometer, positioned next to the microwave radiometer and equipped with a precipitation detector. The model curves refer to model precipitation rates of at least 0.1 mm/hour. Figure 3 clearly shows the occurrence of a few days with ongoing precipitation, some of them quite well captured by the models when analyzed per day. However, in general the events of precipitation in the models do not match sufficiently precise with the observations to use the observed occurrence of precipitation as a mask in order to condition the model predicted LWP to non-precipitative events. To merge the information in the Figures 2 and 3 we have therefore confined the model predicted LWP to events with model predicted precipitation rates less than the above mentioned limit. The result is shown in Figure 4.

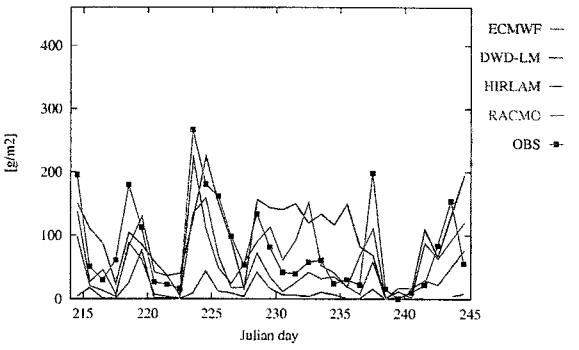

Figure 4: Like Figure 2, but model predicted curves refer to non-precipitative events.

Compared to Figure 2 the model predicted values have indeed reduced significantly. In general, LWP values predicted by ECMWF, HIRLAM and RACMO compare reasonably well in size with the observed amounts, ECMWF and RACMO tending to be on the high side, and HIRLAM tending to be on the low side. DWD, however, is too low in LWP, and on the other hand too high in frequency of precipitation, indicating that cloud condensate in this model is very quickly released as precipitation.

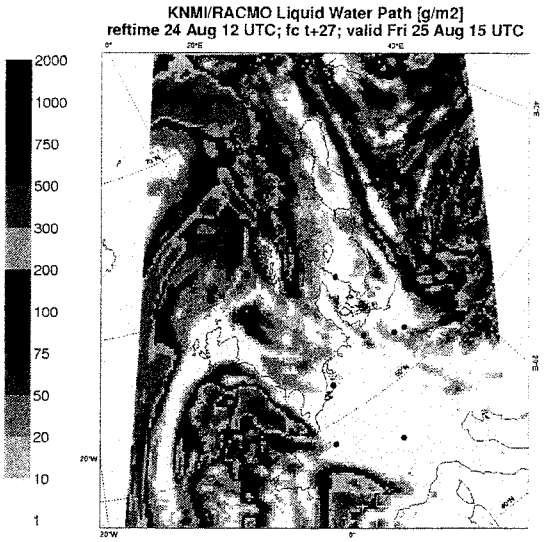

Figure 5: Model predicted LWP-field. Map indicates the CLIWA-NET integration domain of HIRLAM and RACMO. Red squares indicate the CLIWA-NET sites.

3. Spatial distribution of Liquid Water Path

During the CNN campaigns satellite observations inferred from NOAA/AVHRR and AMSU will be used to derive spatial distributions of LWP calibrated with ground-based inferred values. The proposed methodolgy is described by Feijt et al. (2001), however an application for an event within CNNI is not yet available. Figure 5 shows the instantaneous spatial distribution of LWP predicted by RACMO. For this particular day, Onsala reported nearly cloud free conditions. Clearly visible are the large-scale features related cyclones and frontal systems over various parts of Europe and the Eastern Atlantic. The largest values are found over the UK and could be associated with significant convective activity in the model. In reality, the system was positioned slightly further west, just missing the site of Chilbolton (UK).

References

Crewell, S., M. Drusch, U. Löhnert, C. Simmer, and A. van Lammeren: Cloud observations from the ground-based CLIWA-NET Network 1 (CNN1) during BRDIGE EOP1 *This conference.*

Feijt, A., R. Dhlopolsky, D. Jolivet, and R. Roebeling: Quantitative cloud analysis using AVHRR for CLIWA-NET. *This conference.*

Mace, G.G., C. Jakob, and K.P.Moran, 1998: Validation of hydrometeor occurrence predicted by the ECMWF model using millimeter wave radar data; *Geophys. Res. Lett.* 25, 1645-1648.

Van Lammeren and the CLIWA-NET project team: The BALTEX BRIDGE Cloud Liquid Water Network Project. *This conference.*

Acknowledgements:

We like to thank Colin Jones and Ulrika Willén (SMHI), Günther Doms (DWD), and Adrian Tompkins (ECMWF) for making available the model output. Part of this work is done within the CLIWA-NET project sponsored by the EU under contract number EVK2CT-1999-00007.

Model predicted cloud amount and cloud vertical structure compared with ground-based observations from the KNMI Cloud Detection System

Erik van Meijgaard[1], Ulf Andræ[2], and Burkhardt Rockel[3]

[1] Royal Netherlands Meteorological Institute (KNMI), PO Box 201, NL-3730 AE De Bilt, The Netherlands
[2] Swedish Meteorological and Hydrological Institute (SMHI), S-60176 Norrköping, Sweden
[3] GKSS-Forschungszentrum Geesthacht GmbH, Postfach 1160, D-21494 Geesthacht, Germany

1. Introduction

Model predicted cloud parameters are directly compared with cloud observations analysed with the KNMI Cloud Detection System (CDS). The CDS comprised a network of ground-based instruments combined with satellite retrievals covering a 100x100 km^2 area in the Netherlands and has continuously been operated in 1995 and 1996 (*Van Lammeren et al., 2000*). Output from three regional model systems is considered, i.e. the Regional Model REMO, the High Resolution Limited Area Model HIRLAM, and the Regional Atmospheric Climate Model RACMO. This paper focuses on the ground-based component of a study which was recently completed within the framework of the EU-project NEWBALTIC II (*Bengtsson, 2000*). A detailed description of this contribution, including the satellite component, can be found in *Van Meijgaard et al., 2001*. It examines a 10-day period, 27 August to 5 September, hereafter referred to as *D10*. These days were part of the PIDCAP observational campaign defined within BALTEX. Synoptically, *D10* could be characterised by the development of three cyclones over Central Europe, named Kerstin, Liane, and Monika. each of them moving in the direction of the Baltic Sea, causing marked events of precipitation, and affecting the atmospheric conditions in the BALTEX region, including the Netherlands.

2. Observations

The ten ground-based stations in the CDS were equipped with an infrared radiometer and a Lidar ceilometer, independently used to measure the cloud base temperature and height, respectively. Moreover, at most sites routine synoptic observations were made on an hourly basis.

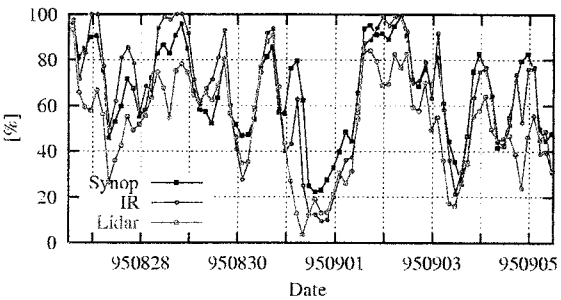

Figure 1: Time series of observed total cloud cover.

Figure 1 shows that, in general, the Lidar total cloud cover presents the lowest estimate. This is consistent with the notion that the employed ceilometers were insensitive to clouds above 4 km. The total cloud cover inferred from the IR radiometer network is close to the synoptical estimate, with time average values in the order of 65%.

The Lidar inferred vertical distribution of clouds is obtained by averaging the measured cloud base height values in space and time. For a single Lidar, measurements of cloud base height have been processed in 1-minute intervals. Similarly, the IR measurements are collected in a temperature-time distribution. The basic information from a single IR radiometer consists of a maximum (minimum) temperature, the corresponding number of events in a 5°C-interval below (above) this temperature, the averaged sky temperature, and the possible onset of precipitation, all stored after processing a 10-minute interval. The measured brightness temperatures are corrected for clear-sky atmospheric contributions, mainly coming from water vapour. This is done using temperature and humidity information from the De Bilt radio sonde available at 6-hour intervals. The methodology and underlying concepts are described in detail in *Van Meijgaard et al., 2000*. In the event of precipitation the IR radiometer measurements are supplied with Lidar measurements. This combined data set includes nearly all possible cloud occurrences - the exception being optically thin cirrus - assuming that precipitation is strongly correlated with cloud base height within the Lidar probing range. During *D10* it was raining at about 15% of the time.

3. Model Evaluation

The set-up in which the regional atmospheric models are configured is unified as much as possible. The models are operated with a horizontal resolution (1/6°x1/6°) and on a vertical mesh with 24 layers. They share the same integration domain. Initialisation and boundary relaxation are made from ECMWF analyses, available at 6-hour intervals. Surface characteristics like orography, land sea mask, and SST are prescribed from a common database. All integrations are carried out in forecast mode. Initialisation is from daily analyses verifying at 12:00 UTC and a 10-day sequence of 12-36 hour forecasts is then used to exactly match the time frame.

The diurnal cycle components of total and low-level (below 4 km) cloud cover are shown in Figure 2. This way of presentation readily gives an impression on the model performance relative to the observations. The diurnal variations in observed cloud amount inferred from both instruments appear to be rather small, with a tendency of higher (lower) values in the early morning (evening). This constancy probably reflects that the weather during *D10* was dominated by large-scale synoptic systems rather than by locally driven convection. The model predictions of cloud cover compare reasonably well with the observed amounts, with the REMO-results generally on the high side for total cloud cover, and slightly on the low side for low-level cloud cover. The HIRLAM-curves contain short-term variations even after averaging over 10 days. These result from large variations in model cloud cover per grid point across the CDS-region which have not been entirely averaged out.

To generate a model quantity that is compatible to the observations the model vertical profiles of the grid-box mean cloud fraction are transformed into a vertical profile

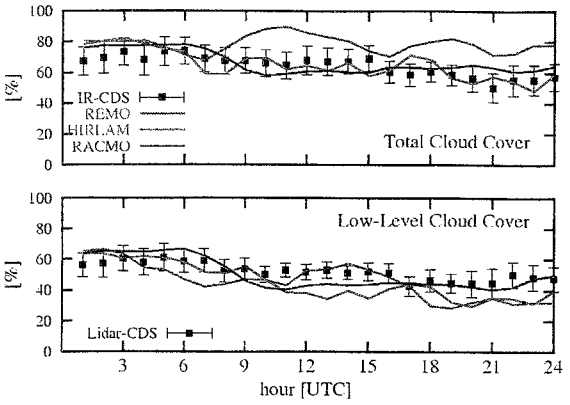

Figure 2: Diurnal cycle of total and low-level cloud cover from observations and model predictions.

of cloud cover seen from the ground. For this, maximum-random cloud overlap is assumed. The results are shown in Figure 3. It clearly demonstrates that all three model predictions tend to overestimate the amount of cloud cover at low altitude between 1000 hPa and 850 hPa, even when compared with the pure Lidar observed profile. When compared with the IR-results, the reverse statement seems to hold for the pressure range between 800 and 500 hPa, but it must be noted that the occurrence of optically thin water clouds will result in a slight overestimation of observed height of the meteorological cloud base. With one of the models (RACMO) this effect is mimicked by composing the cloud cover from the effective cloud fraction in which optically thin clouds are replaced by optically thick clouds with reduced cloud fraction. This is done consistent with the cloud optical properties used by the model. The effect of this modification is remarkably modest, showing that the RACMO model has virtually no optically thin water clouds. This might be different for the other two models, but it turned out not feasible to verify this on the basis of the available model output.

4. Conclusion

Concerning cloud amount, the two instrumental estimates yield different results, but the differences can be understood. However, the status for determining the vertical cloud structure is less conclusive. The network of IR radiometers yields a vertical profile of cloud cover, which is surprisingly linear with height. Hence, according to the IR radiometers clouds are rather evenly distributed in the troposphere. However, it should be realised that any deviation from opacity results in an underestimation of thermodynamic cloud temperature. This is likely to occur frequently for upper-tropospheric clouds, but also low-level clouds may be optically thin. Here, we can make use of the Lidar inferred cloud base height, which is virtually insensitive to the cloud emissivity, to distinct optically thin and thick clouds.

Assessing the performance of the models has shown that they reasonably well predict the cloud amount. In terms of vertical cloud structure all models depart in the same direction from the distribution inferred from the IR radiometers, in particular in the lower troposphere the models have more clouds than observed. This conclusion remains valid when compared with the Lidar observed profile. It seems also consistent with the finding (discussed in *Van Meijgaard, 2001*) that all three models tend to underestimate the boundary layer depth and overpredict the relative humidity in the boundary layer.

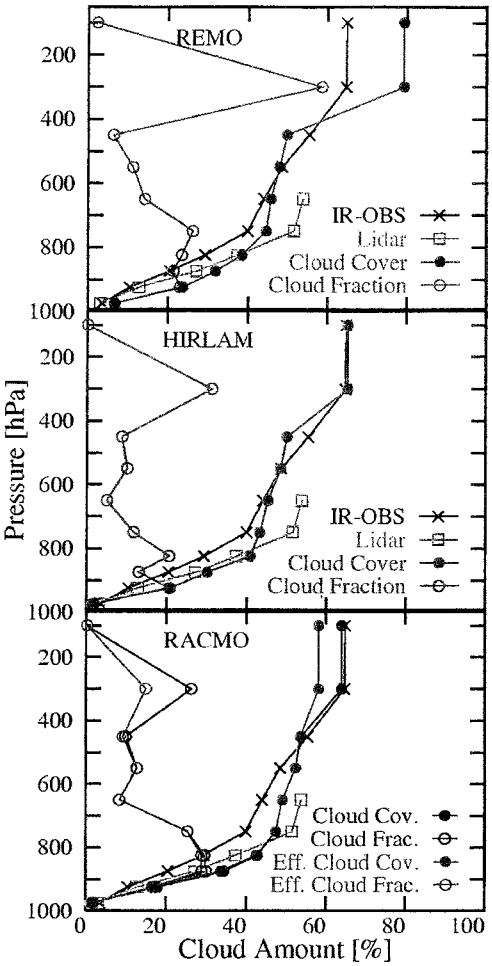

Figure 3: Vertical profiles of cloud cover.

References

Bengtsson, L.(Ed.), 2000: Numerical studies of the energy and water cycle in the Baltic region NEWBALTIC II; Final report covering the period 1/4/1998-31/3/2000 (Contract number ENV4-CT97-0626), 204 pp [Available from Max-Planck-Institute for Meteorology, Bundesstrasse 55,D-20146, Hamburg, F.R. Germany.]

Meijgaard, E. van, J.A. Konings, A.J. Feijt, and A.C.A.P van Lammeren, 2000: Comparison of model predicted cloud cover profiles with observations from ground and satellite. *Meteorol. Z.*, **9**, 21-31

Meijgaard, E. van, U. Andræ, and B. Rockel, 2001: Comparison of model predicted cloud parameters and surface radiative fluxes with observations on the 100 km scale. Submitted to *Meteoro. Atmos. Phys.*

Van Lammeren, A.C.A.P., A.J. Feijt, J.A. Konings, E. van Meijgaard, A.P. van Ulden, 2000: Combination of ground-based and satellite cloud observations on a routine basis. *Meteorol. Z.*, **9**, 125-134

Acknowledgements:

The first author likes to thank André van Lammeren (KNMI) for valuable discussions on the interpretation of the ground-based measurements. Part of the work is done within the NewBaltic2 project sponsored by the EU under contract number ENV4-CT97-0626.

Case Studies of On-Ice and Off-Ice Air Flows Over the Baltic Sea

Timo Vihma[1] and Burghard Brümmer[2]

[1] Finnish Institute of Marine Research, P.O. Box 33, 00931 Helsinki, Finland
[2] Meteorologisches Institut, Univärsität Hamburg, Bundesstraße 55, D-20146 Hamburg, Germany

1. Introduction

The Baltic Sea influences the overlying atmospheric boundary layer (ABL) via the turbulent and radiative surface fluxes, and the degree of influence depends on the state of the surface (open water or sea ice of various thickness and concentration) and on the origin of the flow (off-land, off-ice, off-sea). Off-ice winds bring cold air from the sea ice over the open ocean, where a convective boundary layer develops. In the reverse situation, on-ice winds bring warm and moist air over the ice, where downward turbulent fluxes consequently take place. In this report, two cases of on-ice and off-ice airflow characterizing the extreme weather conditions over the northern Baltic Sea are analyzed. We present aircraft observations on the ABL modification. A two-dimensional mesoscale model is then applied to simulate the observed modification and to study the sensitivity of the modification on fetch characteristics and turbulence parameterizations.

2. Observations and the Model

The data were gathered by the German Falcon research aircraft over the ice-covered and open part of the Gulf of Bothnia during the BASIS experiment. Two cases, that on 27 February, 1998, in a warm on-ice airflow situation, and that on 5 March, 1998, in a cold off-ice air flow situation, are presented here (Figure 1). The flight patterns were arranged along the mean wind direction, and consisted of vertical profiles in the lowest 1-3 km and of horizontal flight legs at different levels. The horizontal legs were arranged as vertical stacks perpendicular to the wind direction.

The ABL flow in the ice edge zone over the Gulf of Bothnia was simulated using a two-dimensional hydrostatic ABL model developed in the University of Helsinki, Department of Meteorology. The equations of the model dry dynamics are as given in Alestalo and Savijärvi (1985), but the physical parameterizations are as in Savijärvi (1997). For the present simulations, we improved the description of turbulence by applying a non-local closure with a parameterization for the counter-gradient transport of heat and moisture in convective conditions.

3. Modelling of On-Ice Flow on 27 February, 1998

On 27 February an extensive low produced a south to south-westerly flow over the Gulf of Bothnia. This day was characterized by weak temperature differences between the ice and the water surface. The air mass modification over a total distance of 190 km in the ice edge zone was rather small. The stable boundary layer was about 250 m high, and characterized by large wind shear and a pronounced low-level jet (around 20 m/s) at its top.

The model domain included a 40 km patch of land surface followed by 380 km of open water, and 140 km of sea ice. The upwind boundary conditions for temperature and humidity were taken from the MESAN fields, and the initial inflow wind profile was set as an Ekman-Taylor spiral. The model was then run for 12 h to reach a steady state. The first simulations were made by forcing the flow by a geostrophic wind constant in height. Then the baroclinicity was taken

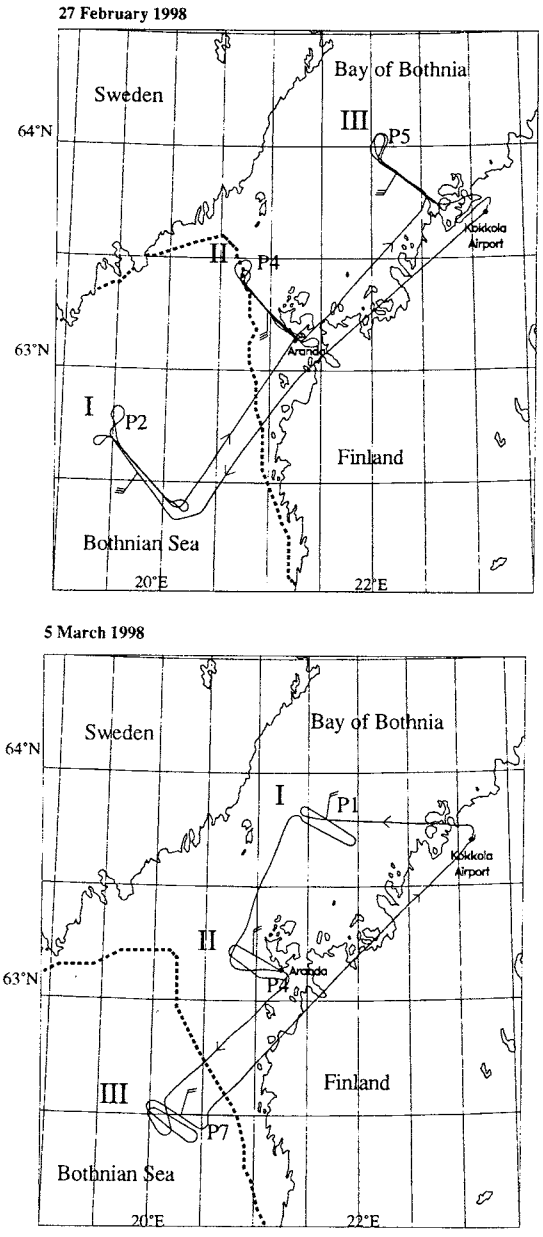

Figure 1: Flight patterns of the Falcon research aircraft on 27 February and 5 March 1998. Locations of vertical stacks (I-III) and profiles (P1-P7) and the ice edge (dashed line) are marked.

into account by estimating the air temperature gradient on the basis of the rawinsonde sounding data from six stations around the Gulf of Bothnia. The resulting wind profiles included an low-level jet (LLJ) (Figure 2) that fitted the observations reasonably well. We see that the

baroclinicity explains the shape of the wind profile above the stable boundary layer, but the LLJ is also generated without the baroclinic effect, and this seems to be related to intertial oscillations in space. In the model results, the LLJ is clearly a spatial feature: it is stationary, it does not exist over the upwind land surface, and it is most pronounced 500 km downwind of the coast, which corresponds to a distance covered in half of the inertial cycle. It was essential to use an upper limit for the mixing length that was about 10% of the ABL height, and a strong stability-dependence of the transfer coefficients in the interior of the ABL (not at the surface) produced the best results.

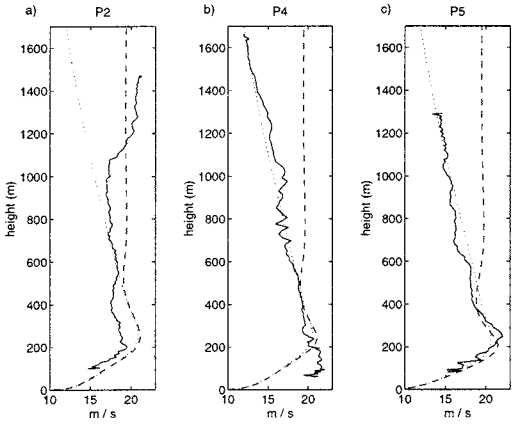

Figure 2: Observed (continuous lines) and modelled wind speed profiles at (a) 95 km upwind of the ice edge, (b) the ice edge, and (c) 95 km downwind over the ice during the on-ice flow on 27 February, 1998. The barotropic model results are show as dashed lines, and the baroclinic ones as dotted lines.

4. Modelling of the Off-Ice Flow on 5 March, 1998

On 5 March the wind was from the north over the Gulf of Bothnia. The air temperatures were between -10 and -15°C. The mean surface temperature over ice was -11°C, while the water surface temperature was about 0.7°C. The boundary layer was unstably stratified both over the ice (weakly) and over the water (strongly). The air temperature and the depth of the boundary layer increased downwind.

This case was modelled applying inflow vertical profiles of wind speed, air temperature, and humidity over ice as observed by the aircraft over the ice at site P1 (Figures 1 and 3). The flow was forced by the observed geostrophic wind of 8 m s^{-1} at a height of 3 km. The subgrid-scale ice concentration was set according to the Falcon data and the FIMR and SMHI ice charts. Below the air-mass trajectory from P1 to P4 there were a few islands covered by pine and spruce forest, and hence their roughness length and energy balance were different from those of the sea ice. We therefore developed a subroutine to calculate the energy balance of the forest. In addition to the liquid water cloud droplets, ice crystals were observed over almost the entire experimental area. The saturation specific humidity was therefore calculated in the model as an average of the saturation humidities with respect to water and ice.

The observed and modelled vertical profiles of the air temperature and specific humidity are shown in Figure 3. We see that, in the lowest 300 m, the air mass is already heated by about 1.5°C over the fractured ice cover and the forest between P1 and P4, and this heating is rather well reproduced by the model. Still more warming, about 3°C, takes place from P4 to P7, and this the model reproduces well. The air humidity profiles are also good, except that the air above the ABL is a somewhat too dry at P5. The modelled vertical fluxes at different levels at stacks I, II, and III agreed reasonably well with the observed ones. Sensitivity tests were made simulating the case (1) without the forest, (2) without leads, and (3) with the air saturation humidity calculated with respect to water only.

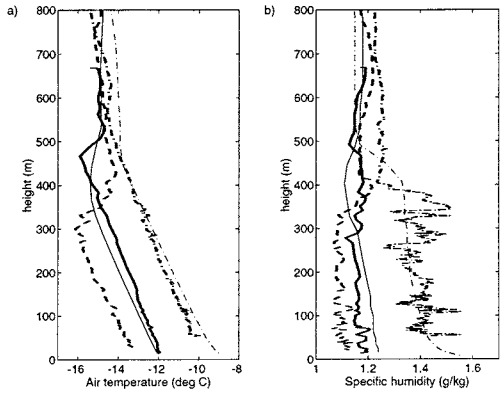

Figure 3: Observed (thick lines) and modelled (thin lines) vertical profiles of (a) air temperature, and (b) specific humidity at P1 (dashed line, observed profile used as the model inflow boundary condition), P4 (solid lines), and P7 (dot-dashed lines) during the off-ice flow on 5 March, 1998. See Figure 2 for the locations of P1, P4, and P7.

5. Conclusions

In the on-ice flow case, the wind field showed a low-level jet that was most pronounced over the ice. In the model, the jet was associated with inertial oscillations, while baroclinicity explained the overall shape of the wind profile above the boundary layer. The inertial mechanism is a spatial analogy to the classical nocturnal jet development in time, and is in agreement with the observations of Smedman et al. (1993) over the open Baltic Sea in spring and summer. Although the observed jet was most pronounced over the ice, the modelling suggests that the jet was not generated by the ice edge but by the coastline, where a much more drastic change in the surface roughness and thermal stratification took place.

In the off-ice flow case, it was important to take into account four topics to reach realistic results. These were (1) recognition of the effect of the forest on the surface energy balance in the archipelago, (2) parameterization of the heat and moisture fluxes from the subgrid-scale leads within the sea ice, (3) recognition of the presence of ice crystals in the parameterization of the air saturation humidity, and (4) the parameterization of counter-gradient transport of heat.

References

Alestalo, M., and H. Savijärvi, Mesoscale circulations in a hydrostatic model: coastal convergence and orographic lifting, *Tellus* 37A, 156-162, 1985.

Savijärvi, H., Diurnal winds around Lake Tanganyika,

Quart. J. Roy. Meteorol. Soc. 123, 901-918, 1997.

Smedman, A.-S., M. Tjernström, and U. Högström,

Analysis of the turbulence structure of a marine low-level jet, *Bound.-Layer Meteorol.* 66, 105-126, 1993.

Long-term variations inflow to the Gulf of Finland from the Neva River basin and the Lake Ladoga role in its control

Valery Vuglinsky and Sergei Zhuravin

State Hydrological Institute, 23, Second Line, St.Petersburg, 199053, Russia

Introduction

Mean annual freshwater runoff to the Baltic Sea from the territory of Russia is at approximately 86 km^3 per year. It is about 20% of the total freshwater runoff of 450 km^3 to the Baltic Sea from land areas of the entire Baltic Sea basin (*Bergstrom and Graham*, 1998). Main part of this inflow is forming in the Neva River basin (at approximately 90% of total inflow), which area within Russia is 283000 km^2. Substantial part of the Neva River basin (56000 km^2) is in the territory of Finland. Area of the Neva River basin itself is small: it is only 1.8% from the area of "large Neva" basin. More than 48 thousand rivers flowing within "large Neva" basin are discharging as a result to the largest European lakes – Lake Ladoga and Lake Onega joined by the Svir River. Thus, main volume of the river runoff accumulates by the Lake Ladoga and discharges to the Gulf of Finland by the Neva River, which in other words is a big transit river system controlled by the Lake Ladoga. It would be useful to remind that mean annual runoff of the Neva River is only about 9% (79.4 km^3) from the average Lake Ladoga volume (908 km^3). Analysis of the lake water balance components variations and their influence to the Neva River flow regimes was carried out to consider features of water circulation in the system. This study was also undertaken to improve understanding of mechanisms the Neva River flow control by the Lake Ladoga for the development of corresponding block of the "Hydrograph" model adopting to the Neva River flow modeling.

Results of the Neva River runoff and Lake Ladoga regimes analysis

Results of the study are the following. The long-term variations the Neva River runoff is small: variation coefficient (C_v) of mean annual discharges for the period 1859-2000 is 0.16. Slight trend to runoff decrease for this period is observed. The spectrum function of this series exceeds confidential limit of white noise substantially that means the signal component is predominant. At the same time general runoff increase evident for the past fifty years. The periodogramm of the Neva River annual runoff shows that periods of 6, 11 and 33 years have the most contribution in it variability, and the period of 33 years (in average) is predominant. The smoothed average curve of interannual runoff confirms this conclusion (Fig.1). Expected changes in the Neva River behaviour did not occur under the climate long-term variability since previous study (*Vuglinsky and Zhuravin*, 1998) and runoff recession brunch observed.

Analysis shows close correspondence of the Neva River annual runoff variations and annual variations of the Lake Ladoga mean annual water level (Fig.1). At the same time there is some difference of these two characteristics range for the wet and dry periods.

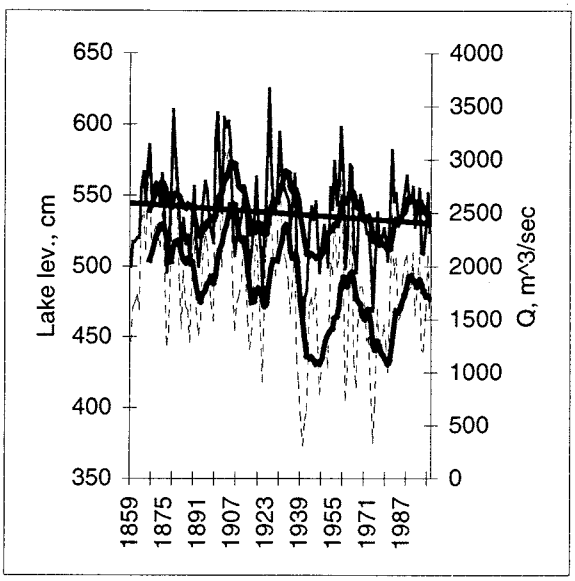

Figure 1: Variations of the Neva River mean annual discharges (solid line) and the Lake Ladoga mean annual water levels (broken line).

It means that despite close relationship of the Neva River runoff and the Lake Ladoga water level (Fig.2) hydrological model should take into account these features of water circulation in the system Lake Ladoga – Neva River.

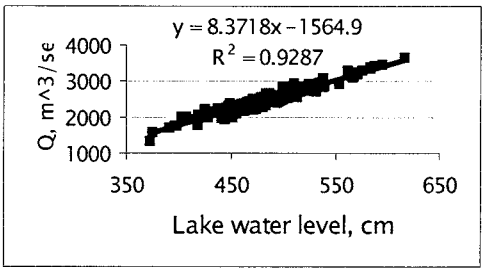

Figure 2: The Neva River mean annual discharges and the Lake Ladoga mean annual water level relationship.

Mean annual Lake Ladoga water level depends of the water storage in the lake. The storage, in its turn, depends of the regime of water circulation in the land area of the lake basin (inflow) and water recharge and discharge to/from the lake itself. The surface inflow to the Lake Ladoga is predominant in the lake storage formation. It ranges from 50 to 107 km^3 per year. Contribution of precipitation falling to the lake surface is rather small (2.9-13.3 km^3 per year) as well as evaporation from the lake surface (4.8-10.9 km^3 per year). These water balance components have opposite trends during last decades: precipitation increases slightly, while evaporation slightly decreases (*Gronskaya*, 2000). Values of the lake water

balance components for typical years are shown in the Table 1.

Table 1: Lake Ladoga water balance components (km^3) for typical years.

Yrs.	In-flow	Prec.	Out-flow	Evp.	Stor.
1962 (wet)	107	11.5	91.3	5.39	21.7
1941 (dry)	50	2.9	48.5	6.8	-2.84
Mean annual for 1932 - 1995	73.2	8.65	74.6	6.88	-0.15

This data shows the Lake Ladoga may accumulate up to 30% of mean annual Neva River runoff or, on the contrary, may drawdoun its storage that resulting to the Neva River not linear for these events.

These results confirm close relationship of the Lake Ladoga storage, its water level and the Neva River runoff. Year cycle of water circulation in the Lake Ladoga and its influence to the Neva River hydrograph formation is considered too.

Special interest of the study was related to the current climate situation and its influence to possible further changes in the surface inflow to the Lake Ladoga and corresponding Neva River runoff. The analysis of Vangengeim-Girs atmospheric circulation indices was carried out (*Girs*, 1974). It shown that currently there is no significant trends in changes of atmospheric circulation. North – South atmospheric transfer is still predominant in average for the area. At the same time some changes occur and western atmospheric transfer began dominate during winter and transfer seasons. It has resulted to precipitation increase. In combination with some evaporation decrease it resulted to small and middle rivers runoff increase in southern and western parts of the "Large Neva" basin up to 10-20% for the past 25-30 years.

Conclusions

1. The Lake Ladoga control of the Neva River runoff resulting to its small interannual variations (C_v=0.16) and dependence of the lake water level ranging.
2. Character of the Lake Ladoga mean annual level and Neva River runoff relationship may changes during dry and wet periods despite its close correlation (R=0.97).
3. Inflow is predominant component in the Lake Ladoga water storage formation, while precipitation on the lake water table and evaporation from the lake play insignificant role in its formation.
4. Analysis of the Ladoga Lake water balance have to play key role in the development of corresponding block of the "Hydrograph" model adopting to the Neva River flow modeling as well as its testing and verification.

References

Bergstrom, S., Graham, L.P., The Baltic drainage basin – a focus for interdisciplinary research, *NHP Report No.4*, Vol.1, 3-12, 1998

Vuglinsky, V.S., Zhuravin, S.A., The estimation of river inflow into the Baltic Sea – provision with information, peculiarities of forming, variability, Second Study Conference on BALTEX, *Conference Proc.*, International BALTEX Secretariat, Publ. No.11, 231, 1998

Gronskaya, T.P, Lake districts of North – Western Russia: identification of subregions based on analysis of hydrological data, *Freshwater Biology*, 43, 385-390, 2000

Girs, A.A., Macro-circulation method of the long-term meteorological forecasts, *Gidrometeoizdat*, 487, 1974 (in Russian)

Analysis of two approaches of topographically controlled runoff simulation as in the land surface model SEWAB

Kirsten Warrach[1], Marc Stieglitz[2] and Heinz-Theo Mengelkamp[3]

[1] Max-Planck-Institute for Meteorology, Bundesstr. 55, D- 20146 Hamburg, Germany
[2] Lamont Doherty Earth Observatory, Route 9W, Palisades, NY 10964, USA
[3] GKSS Research Centre, Max-Panck-Str., D-21502 Geesthacht, Germany

1. Introduction

A critical deficiency in standard GCM-based LSMs, is the neglect of an explicit treatment for spatial variability in soil moisture, though heterogeneity can have a strong impact on surface energy and water budgets. Recently, there has been substantial progress with respect to the modelling topographic control over surface hydrologic processes. Two approaches to improving simulated runoff have become especially popular. A VIC, or variable infiltration capacity approach, implicitly accounts for the impact that topography has on surface infiltration (e.g. *Wood et al.*, 1992). The second approach, TOPMODEL explicitly uses topographic information to determine catchment soil moisture heterogeneity and the impact this heterogeneity has on runoff generation (e.g. *Stieglitz et al.*, 1997). Because neither approach needs to explicitly track surface or subsurface flow within a catchment, they represent computationally efficient ways to represent hydrologic processes within the context of regional and global modeling.

2. Topographically controlled runoff

The land surface model SEWAB (Surface Energy and Water Balance) is a one-dimensional SVAT scheme solving the coupled surface energy and water balance equations and the vertical heat and water fluxes within the soil column (*Mengelkamp et al.*, 1999, *Warrach et al.*, 2001a). In its original version SEWAB only calculated runoff as free drainage from its lowest modelled soil layer and as infiltration and saturation excess runoff. The advantage of such a simple and common approach is that no calibration of baseflow parameters is necessary. The disadvantage is that this scheme often yields a poor runoff simulation. This study demonstrates the advantages and disadvantages of using a VIC-type approach, a TOPMODEL-type approach, and for completeness, the original SEWAB approach.

3. Results

We show that the primary weakness of VIC is in the simulation of surface runoff, presumably due to a poor representation of the expansion and contraction of lowland saturated zones. TOPMODEL, which explicitly relies on topographic information, does much better on this count. However, when VIC is used in combination with a fast and slow baseflow term, it seems to better reproduce the snowmelt recession curve. A main drawback of the modified VIC approach, especially for regional and global application, is that with 4 free parameters, significantly more model calibration is required. TOPMODEL, on the other hand, only requires extensive pre-processing of topographic data, although issues as to the resolution of the data used become relevant. A detailed description and discussion of the study and the results is given by *Warrach et al.* (2001b).

References

Mengelkamp., H.-T., K. Warrach, E. Raschke, SEWAB - a parameterization of the Surface Energy and Water Balance for atmospheric and hydrologic models, *Advances in Water Resources*, Vol. 23, 165-175, 1999

Stieglitz, M., D. Rind, J. Famiglietti, C. Rosenzweig, An efficient approach to modeling the topographic control of surface hydrology for regional and global climate modeling, *Journal of Climate*, Vol. 10, 118-137, 1997

Warrach, K., H.-T. Mengelkamp, E. Raschke, Treatment of frozen soil and snow cover in the land surface model SEWAB, *Theoretical and Applied Climatology*, in print, 2001a

Warrach, K., M. Stieglitz, H.-T. Mengelkamp, E.. Raschke, Advantages of a topographically controlled runoff simulation as in the land surface model SEWAB., *Journal of Hydrometeorology*, submitted, 2001b

Wood, E. F., D. P. Lettenmaier, V. G. Zartarian, A land-surface hydrology parameterization with subgrid variability for general circulation models. *Journal of Geophysical Research*, Vol. 97, 2717-2728, 1992

The impact of cloud-radiation interactions on the radiative surface fluxes for a coupled Atmosphere-Ocean regional model

Ulrika Willén, Colin Jones, Ralf Döscher and Ulf Hansson

Rossby Centre, Swedish Meteorological and Hydrological Institute, S-60176 Norrköping, Sweden

1. Introduction

Clouds play a major role in modulating the solar and terrestrial radiation fields. Due to the inherent problem of modeling clouds and the lack of adequate observations for validation, they are a large source of uncertainty when simulating the present climate and for predicting any future climate change.

Cloud-radiation interaction has been identified as a major factor in explaining the difference in sensitivity to greenhouse gas increases between different climate models *Lee et al.* (1997). A small change in the cloud or radiation parameterizations, which affects the cloud fraction, the vertical distribution of clouds, the cloud overlap, the cloud water content or phase, can make a drastic change to the vertical distribution of the radiative heating and cooling of the atmosphere and the distribution of radiative fluxes at the surface.

A coupled atmosphere-ocean model system is being developed at the Rossby Centre. For such a system the atmospheric surface radiative fluxes are crucial in determining the sea surface temperatures (SST's) and the development of ice, the ice extent and the length of the ice season.

2. Models and Results

The Rossby Centre Atmospheric model, RCA, *Rummukainen et al* (2001) has been coupled to the Rossby Centre three dimensional ocean model, RCO, *Meier et al.* (1999). Simulations for present day climate with ECMWF Re-Analysis data at the boundaries of RCA have been made for a period September 1988 to August 1989. The first results gave too cold SST's and more ice compared with observations and ocean only runs forced by observed fluxes. The coupling and the results for RCO are presented by Döescher et al. also at this BALTEX conference.

Validation of the monthly surface short-wave (SW) radiative flux with observations from a solar radiation network of 12 stations operated by SMHI, *Persson* (2000) showed a negative bias of up to 30 W/m**2 in spring, Figure 1. A similar bias signal could also be seen for the top of the atmosphere (TOA) net SW flux averaged over the Nordic region when compared with satellite observations from the ERBE data set, Figure 2. This indicated that the atmosphere was reflecting too much. Separation into cloudy and clear-sky fluxes showed that the cloud albedo was too high and therefore not enough radiation was transmitted through the clouds to the surface.

The transmission is affected by the amount of cloud water and the cloud fraction. These variables are difficult to verify but attempts have been made to compare with existing data sets and more validation will take place in the EU Framework 5 project CLIWA-NET. In order to investigate the sensitivity of the radiation scheme to the cloud fields a number of changes were made in the cloud and radiation parameterizations, which lead to an improved SW balance reducing the biases as shown by the curves marked 'changed' in the figures. Re-running the coupled system with the improved SW surface fluxes gave somewhat better SST and reduced the too long ice season in the control run.

The long-wave (LW) flux is more difficult to verify since there are fewer and less accurate surface measurements available. In the wintertime the LW flux constitute the primary term in the surface energy balance and it greatly affects the ice development. Comparing the RCA fluxes with 3 surface stations showed an underestimation of the downwelling LW flux by 20-30 W/m**2 throughout the year. This LW bias is also consistent with a small but negative temperature bias seen in the atmosphere. A number of possible changes to the cloud and radiation scheme have been tested. The impact of the different model changes on the LW and SW surface fluxes and the SST's will be discussed.

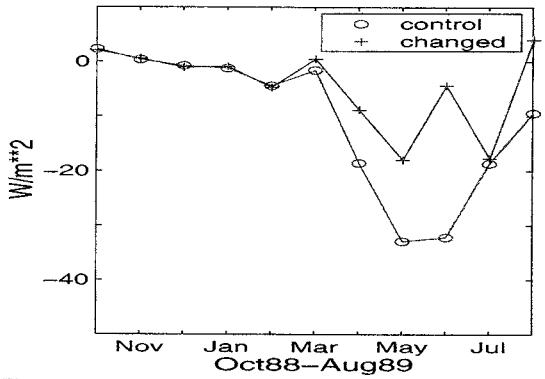

Figure 1: The SW surface bias, RCA-Observations.

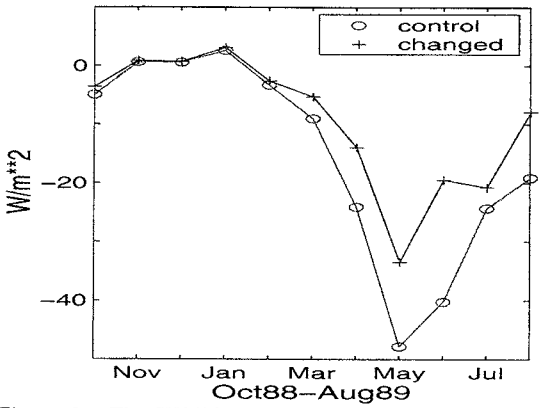

Figure 2: The SW TOA net flux bias, RCA-ERBE.

References

Lee, J. Cloud Radiation Forcings and Feedbacks: General Circulation Model Tests and Observational Validation, *J. Climate*, Vol.10, No.1, 2479-2496, 1997

Persson, T, Measurements of Solar Radiation in Sweden 1983-1998. *SMHI Reports Meteorology and Climatology*, 89, 74pp, 2000

Rummukainen, M., J. Räisänen, B. Bringfelt, A. Ullerstig, A. Omstedt, U. Willén U. Hansson, C. Jones, A regional climate model for northern Europe: model

description and results from the downscaling of two GCM control simulations, *Climate Dyn.*, Vol.13, No.17, 339-359, 2001

Meier, M., R. Döscher, A. Coward, J. Nycander, K. Döös, The first Rossby Centre regional climate scenario for the Baltic Sea using a 3D coupled ice-ocean model, *SMHI Reports Oceanography*, 26, 102pp, 2000

Acknowledgements:

This work was funded by the EU under the CLIWA-NET project EVK2CT-1999-00007

Some results of studies on dynamics of variations of hydrological conditions in the Oder Estuary.

Bernard Wisniewski, Halina Kowalewska-Kalkowska, Tomasz Wolski

Physical Oceanography Lab., University of Szczecin, ul. Wąska 13, 71-415 Szczecin, Poland,
e-mail: halkalk@sus.univ.szczecin.pl

The Oder Estuary is a very complicated hydrological system of water flows with great dynamics of variations of hydrological conditions. They result first of all from the Baltic sea level variability and fast reaction of that system on those changes. Weather conditions have a great influence on hydrological conditions of the estuary as well.

The Oder River flows into the Pomeranian Bay, situated at the southern coasts of the Baltic Sea, through a branched system of water flows and prior transformation of waters in the Szczecin Lagoon. An important navigation and transport route is passed across the estuary. It connects the southern part of Poland with the Baltic Sea. Therefore the proper functioning of hydrological and meteorological protection system is of great importance in the Oder Estuary. Among institutions busy with that system different surveying networks operate such as Institute of Meteorology and Water Management and Marine Board. IMWM gives regularly announcements to marine infrastructure institutions (forecasts and analyses), which include atmospheric pressure situation, velocities and directions of wind, state of bays and lagoons, air temperature and visibility as well as storm warnings. Independently on weather announcements given by IMWM the Harbour Master's Office in Szczecin carries out a 24-hour monitoring of weather and hydrological conditions along the fairway Szczecin – Świnoujście using the radar system of ship traffic control so-called VTS (Vessel Traffic Service), running since January 2000. The system was designed to improve safety, navigation efficiency and environment protection along all the navigation channel. Operators of the system have the continuous TV monitoring of course of meteorological and hydrological conditions like winds, currents, water level, wave height, water temperature and salinity, ice phenomena, air temperature, visibility, air pressure and relative humidity. That monitoring allows to correct navigational conditions for each ship on the fairway.

Independently Physical Oceanography Laboratory carries out studies (measurements and analyses) on weather and hydrological factors having an influence on navigation as well as work of ports in the region of the Oder Estuary. It co-operates with other institutions busy with those tasks. First of all the attention is focused on the analysis of dynamics and structure of currents as well as water physical fields in the region of estuary.

Test measurements of currents in 15 measuring points of the Szczecin Lagoon showed its complicated and diverse character. The results of measurements proved earlier conclusions of studies carried out by Majewski (1980), Robakiewicz (1993). However in the present study there were measured relatively significant velocities of currents at the bottom (about 25 cm/s) in comparison to the results of earlier investigations (about 5 cm/s) for stable atmospheric conditions (velocity of wind less than 5 m/s). From the present work it was possible to draw conclusion that under convenient weather conditions predominating in September and at the beginning of October 1999 the position of the measuring point has a great impact on the distribution of current velocities. Some points characterise the central part of the lagoon, the others the Old Świna and reservoirs situated near its mouth. The depth of measuring point and bottom topography in its neighbourhood were other important factors influencing the current distribution as well. It confirms the scale of difficulty in proper interpretation of the distribution of currents of the Szczecin Lagoon.

Circulation conditions as well as local winds, generating advection and convection movements of waters, have a great impact on spreading out of the Oder waters in the Pomeranian Bay. They modify interdependent relations between the Lower Oder discharge, water level differences in the region of the Szczecin Lagoon and salinity of coastal waters of the Pomeranian Bay having an influence on the lag of maximum correlation and on its strength. When the circulation from north to west sector was coming the inflow of fresh waters to the region of Międzyzdroje followed faster and the relations were more statistically significant. It is the results of the fact that winds coming from south sector (SE–S–SW) have the tendency of taking out waters of the Świna Strait directly towards the open waters of the Pomeranian Bay, using also the deepened gutter of the fairway. On the other hand winds coming from W–NW–N slow down especially surface water layers flowing from the Świna Strait, pushing them down towards the coasts and causing their flow to the east through the shallow coastal zone of the bay along the coasts of the Wolin Island.

Circulation conditions modify also relations between temperature of coastal waters of the Pomeranian Bay and temperature of air masses and water temperature of the Lower Oder. The influence of river temperature on sea temperature was increased during inflows of air masses from western sector (the highest for NW). The effect of air temperature was increased during the periods under air circulation coming from north to east directions (the strongest for NE).

References

Majewski A, Zalew Szczeciński, Wyd. Komunikacji i Lacznosci, Warszawa, 1980

Robakiewicz , W. (ed.), Warunki hydrodynamiczne Zalewu Szczecinskiego i Ciesnin laczacych Zalew z Zatoka Pomorska, Wyd. IBW PAN, Gdansk, 1993

The use of satellite data for climatological applications: The SAF on Climate Monitoring

H. Woick[1], S. Dewitte[6] , A. Gratzki[1], P. Hechler[1] , R. Hollmann[4] , K.-G. Karlsson[2], V. Laine[5], P. Löwe[7] , H. Nitsche[1], R. Roebeling[3], M. Werscheck[1], G. Wollenweber[1]

[1] Deutscher Wetterdienst (DWD), Frankfurter Strasse 135, D - 63067 Offenbach am Main, Germany
[2] Swedish Meteorological and Hydrological Institute (SMHI), Folksborgsvaegen 1, S - 60176 Norrköping, Sweden
[3] Royal Netherlands Meteorological Institute (KNMI), Postbus 201, NL - 3730 AE DeBilt, The Netherlands
[4] GKSS Research Centre Geesthacht, Max-Planck-Strasse, 21502 Geesthacht, Germany
[5] Finnish Meteorological Institute (FMI), P.O. Box 503, 00101 Helsinki 10, Finland
[6] Royal Meteorological Institute of Belgium (RMIB), 3, Av. Circulaire, B - 1180 Bruxelles, Belgium
[7] Bundesamt für Seeschiffahrt und Hydrographie (BSH), Bernhard-Nocht-Str. 78, D - 20359 Hamburg, Germany

1. Aim

As the evolution of the climate system is a growing concern of mankind the systematic investigation of its basic mechanisms represents a main focus of scientific interest. In this respect homogeneous and comparable data sets are required representing key factors of the system. Data must be measured operationally in a continuous long-term manner covering all dimensions. Satellite data are –in combination with in-situ data and model output- particularly suitable for this task.
The Satellite Application Facility (SAF) on Climate Monitoring is addressed to the high-quality long-term monitoring of the climate system's state and variability, partly on the regional level. It supports the analysis and diagnosis of climate parameters in order to detect and understand changes in the climate system. The SAF furthermore serves the modelling of the atmospheric system as well as planning and management purposes.

2. Background

EUMETSAT, the European Organisation for the Exploitation of Meteorological Satellites, enhanced its Convention to include support to climate change studies. EUMETSAT's METEOSAT Second Generation (MSG) and European Polar System (EPS) programmes will provide essential data for climate monitoring activities. As a new element of the distributed EUMETSAT ground segment, the SAF on Climate Monitoring will form the basis for the operational long term monitoring of the climate system. The SAF comprises a 5 years common project effort based on the know-how of the partner institutes from Finland, Sweden, The Netherlands, Belgium and Germany. Hosted by DWD the development work started in 1999.

3. Products

The SAF on Climate Monitoring presently focuses on three areas:

- determination of consistent parameters of cloud and radiation suitable for regional climate applications
- Global Ocean State Estimate: Dynamical extrapolation of sea surface observations into the global ocean interior
- Validation and merging of satellite derived water vapour information.

Cloud and Radiation:
The SAF on Climate Monitoring fills a gap in providing consistent data sets of cloud and radiation budget parameters for an area which covers Europe (including parts of the North Atlantic Ocean). The spatial resolution will be 15 km (except components of the radiation budget at the top of the atmosphere where a spatial resolution of 50 – 70 km is envisaged). Besides surface- and top of the atmosphere radiation budget components (including albedo), several cloud parameters, such as fractional cloud cover, cloud classification, cloud top temperature and height and others will be derived.

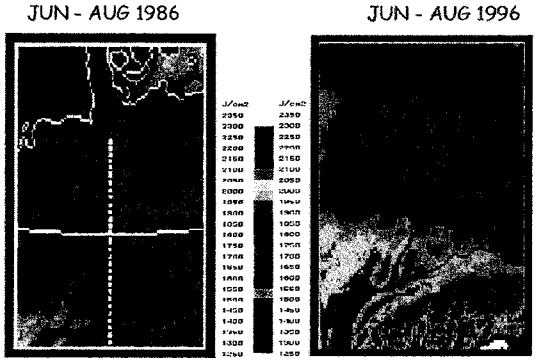

Figure 1: Downward Surface Short-wave Radiation over Germany

Global Ocean State Estimate:
Dynamical extrapolation of sea surface observations into the global ocean interior ocean assumes the central role in the planet's climate system on behalf of its immense capacity to store and redistribute water, heat and radiatively active trace substances. Climate monitoring and predictions therefore require the continued assessment of the state of the interior ocean. By merging data from remote sensing facilities with numerical models of the global ocean circulation the SAF on Climate Monitoring will generate an estimate of the state of the global ocean circulation at monthly time intervals. This estimate includes sea-ice extent, temperatures and salinities of the ocean interior as well as circulation velocities.

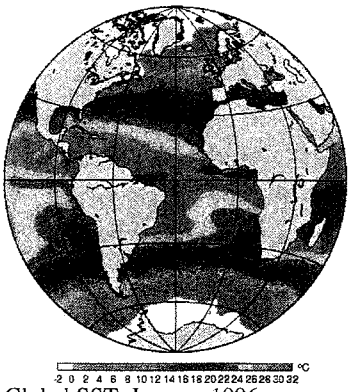

Figure 2: Global SST, January 1996

Water Vapour in the Atmosphere:
Water vapour in the atmosphere is for several reasons of special interest in climatology: as a greenhouse gas, as a component in the water cycle and because of the latent heat and its role in atmospheric dynamics. The SAF on Climate Monitoring will contribute merged and gridded daily data sets of total precipitable water as well as layer precipitable water (3 layers) based on operational level-2.0 satellite products and validated with in-situ observations as well as ground-based remote sensing data. With an initial spatial resolution of 100 km x 100 km the products cover Europe and parts of the North Atlantic.

Figure 3: Total precipitable Water over Europe, 26.12.99

References

Woick, H., et al. 2001: The Satellite Application Facility on Climate Monitoring, submitted to Adv. Space Res.

SAF Training Workshop- Climate Monitoring, November 2000, Dresden, Germany
http://www.dwd.de/research/eve_ann.htm

Comparison between various formulae for sea surface net infrared radiation flux and a new empirical formula for southern Baltic region

Slawomir B. Wozniak[1], Tomasz Zapadka[2] and Bogdan Wozniak[1,2]

[1] Institute of Oceanology, Polish Academy of Sciences, Powstanców Warszawy 55, PL-81-712 Sopot, Poland
[2] Institute of Physics, Pomeranian Pedagogical Academy, Arciszewskiego 22 B, PL-76-200, Slupsk, Poland

Abstract

This paper discusses problems in estimation of the sea surface net infrared radiation flux basing on easily measurable hydrometeorological quantities (temperatures of sea and air, air humidity and cloudiness). The comparison between empirical data and existing formulae is presented. Additionally a new improved formula for the southern Baltic region is introduced.

1. Introduction

In the literature there are several practical algorithms for estimating the net infrared radiation flux for climate modelling purposes (*Fung et al.* (1984) and papers cited there, *Bignami et al.* (1995), *Woźniak et al.* (2000), see also *Timofeyev* (1983), *Trenberth* (1992)). The aim of this paper is to compare these formulae with empirical data based on *in situ* measurements made in the southern Baltic, and to present a new and more accurate formula.

2. Presentation of the physical problem

The net IR radiation flux of a sea surface is the difference between thermal radiation from the sea to the atmosphere $IR^{\uparrow}$ and thermal radiation from the atmosphere to the sea $IR^{\downarrow}$ (see *e.g. Dera* (1992)).

Mostly it is assumed that the sea (or earth surface) radiates almost in the same way as a black body, i.e. according to Stefan-Boltzmann law, or more precisely, as a grey body whose total emissivity is ε :

$$IR^{\uparrow} = \varepsilon\sigma T_s^4 \tag{1}$$

where ε is estimated to be between 0.9 and 1, and $\sigma = 5.7\times10^{-8}\,\mathrm{Wm^{-2}K^{-4}}$ is the Stefan-Boltzman constant (see *e.g. Garbuny* (1965)), T_s is an absolute temperature of the water surface.

The second part of effective radiation is the infrared flux emitted by the atmosphere to the sea. To describe this flux, using easily measurable quantities, empirical formulae are applied. Generally, for the clear sky conditions the following equation can be given:

$$IR^{\downarrow} = \varepsilon\sigma T_a^4\left(A + Be^{C}\right), \tag{2}$$

where e is near surface vapour pressure (in milibars), T_a is an absolute temperature of the air, A,B and C are empirically determined coefficients.

If the sky is cloudy, the formula is more complicated. Clouds increase the IR flux reaching the surface, since they are better absorbers of radiation than a clear atmosphere: they are thus better emitters too. This flux is influenced by cloud cover, the type of clouds and their distribution, and the place of the observation. The most common and simple way of taking clouds into account is adding a correction factor, which depends on only one meteorological parameter *i.e.* cloudiness N, measured on a scale from 0 to 1.

In the literature one can find different empirical formulae for the net infrared radiation flux $IR\uparrow\downarrow$given as a function of easily measurable meteorological quantities. Such formulae based on the above scheme, where presented by:

-*Brunt* (1932) (cit. by *Fung et al.* (1984))

$$IR^{\uparrow\downarrow} = \varepsilon\sigma T^4\left(0{,}39 - 0{,}05e^{1/2}\right)\left(1 - 0{,}8N\right), \tag{3}$$

-*Anderson* (1952) (cit. by *Fung et al.* (1984))

$$IR^{\uparrow\downarrow} = \varepsilon\sigma\left(T_s^4 - T_a^4\left(0{,}74 + 0{,}0049\,e\right)\right)\left(1 - 0{,}8N\right), \tag{4}$$

-*Berliand and Berliand* (1952) (cit. by *Fung et al.* (1984))

$$IR^{\uparrow\downarrow} = \varepsilon\sigma T_a^4\left(0{,}39 - 0{,}05e^{1/2}\right)\left(1 - 0{,}8N\right) + 4\varepsilon\sigma T_a^3\left(T_s - T_a\right), \tag{5}$$

-*Efimova* (1961) (cit. by *Fung et al.* (1984))

$$IR^{\uparrow\downarrow} = \varepsilon\sigma T_a^4\left(0{,}254 - 0{,}00495e\right)\left(1 - 0{,}8N\right), \tag{6}$$

-*Swinbank* (1963) (cit. by *Fung et al.* (1984))

$$IR^{\uparrow\downarrow} = \varepsilon\sigma\left(T^4 - 9{,}36\times10^{-6}T_a^6\right)\left(1 - 0{,}8N\right), \tag{7}$$

-*Clark et al.* (1974) (cit. by *Fung et al.* (1984))

$$IR^{\uparrow\downarrow} = \varepsilon\sigma T_s^4\left(0{,}39 - 0{,}05e^{1/2}\right)\left(1 - 0{,}69N^2\right) + 4\varepsilon\sigma T_s^3\left(T_s - T_a\right), \tag{8}$$

-*Bunker* (1976) (cit. by *Fung et al.* (1984))

$$IR^{\uparrow\downarrow} = 0{,}22\cdot\left(\varepsilon\sigma T_a^4\left(11{,}7 - 0{,}23e\right)\left(1 - 0{,}8N\right)\right) + 4\varepsilon T_a^3\left(T_s - T_a\right), \tag{9}$$

-*Hastenrath and Lamb* (1978) (cit. by *Fung et al.* (1984))

$$IR^{\uparrow\downarrow} = \varepsilon\sigma T_s^4\left(0{,}39 - 0{,}056q^{1/2}\right)\left(1 - 0{,}53N^2\right) + 4\varepsilon\sigma T_s^3\left(T_s - T_a\right), \tag{10}$$

(in this case authors used the specific humidity q instead of water vapour pressure e),

-*Bignami et al.* (1995)

$$IR^{\uparrow\downarrow} = \varepsilon\sigma T_s^4 - \left(\in\sigma T_a^4\left(0{,}653 - 0{,}00535e\right)\right)\left(1 + 0{,}1762N^2\right), \tag{11}$$

-*Woźniak et al.* (2000)

$$IR^{\uparrow\downarrow} = \varepsilon\sigma T_s^4\left(0{,}39 - 0{,}0077e\right)\left(1 - 0{,}75N^2\right) + 4\varepsilon\sigma T_s^3\left(T_s - T_a\right). \tag{12}$$

The formulae (3)-(10) were obtained for land environments and the last two for marine environments. Since the existing formulae differ one from another in both their analytical form and the selection of empirical coefficients, it is important to assess their applicability to the estimation of the infrared energy budget of marine basins in different regions and for different seasons.

3. Empirical material

The following empirical material collected during 8 cruises of *r/v Oceania* (PAS) (June 1999 - October 2000) served to test the formulae presented above: values of $IR\uparrow$ and $IR\downarrow$ (measured using Kipp&Zonen pyrgeometers and averaged over 10-minute intervals, which corresponded to times of weather observation), temperatures of air and water surface, near surface vapour pressure and the overall cloudiness estimated by the observer. Over 500 points were obtained in this way (including over 200 for clear sky condition) (for detailed descriptions of methods see *Zapadka and Woźniak* (2000), *Zapadka et al.* (2001)).

4. Results

Testing the formulae involved comparing the predicted value $IR\uparrow\downarrow_{model}$ (according to equations. (3)-(12)) with the empirical data $IR\uparrow\downarrow_{real}$ obtained as described above. The discrepancies between the results are presented on the basis of an analysis of statistical and systematic errors and correlation coefficient (see Table 1).

As it can be seen, most of the formulae discussed here are in poor agreement with the empirical data, and so they cannot be applied in unmodified form to the southern Baltic Sea area.

Table 1: The systematic and statistical errors of formulae, and correlation coefficient

References	Systemaical error $\langle\varepsilon\rangle$ [Wm^{-2}]	Statistical error σ_ε [Wm^{-2}]	Correlation coefficient r
Brunt (1932)	-24.4	22.3	0.73
Anderson (1952)	-27.9	21.9	0.74
Berliand and Berliand (1952)	-23.2	22.0	0.74
Efimova (1961)	-30.4	22.7	0.71
Swinbank (1963)	-19.0	22.8	0.73
Clark et al. (1974)	-14.2	21.0	0.76
Bunker (1976)	-24.9	22.1	0.73
Hastenrath and Lamb (1978)	41.7	23.6	0.75
Bignami et al. (1995)	6.4	21.2	0.76
Woźniak et al. (2000)	2.8	21.8	0.78

where: $\varepsilon = IR^{\uparrow\downarrow}_{model} - IR^{\uparrow\downarrow}_{real}$, $\langle\varepsilon\rangle$-arithmetic mean of errors (systematic error), σ_ε-standard deviation of errors (statistical error), correlation coefficient:

$$r = \frac{\left\langle IR^{\uparrow\downarrow}_{real} \cdot IR^{\uparrow\downarrow}_{model} \right\rangle - \left\langle IR^{\uparrow\downarrow}_{real} \right\rangle \cdot \left\langle IR^{\uparrow\downarrow}_{model} \right\rangle}{\sigma_{real} \cdot \sigma_{model}}.$$

5. A new formula

Based on collected empirical material and using a non-linear approximation technique a new formula has been found (see *Zapadka et al.* (2001)):

$$IR^{\uparrow\downarrow} = 0.98\sigma T_s^4 - \sigma T_a^4 (0.732(1-\exp(-0.476e)) \quad (13)$$
$$(1-0.067N+0.301N^2))$$

The correlation between experimental data and those calculated by the new formula and the histogram of errors is compared in Fig.1. The systematic error of this approximation is reduced to 0.9 Wm^{-2}, the statistical error is 19,9 Wm^{-2}, and the correlation coefficient equals 0.79.

6. Conclusions

The results of analysis show that the majority of existing formulae obtained for land environments (equation (3)-(10)) are inappropriate for estimation of net infrared radiation flux over the southern Baltic due to high values of systematical error. The last three formulae obtained for marine environments (eq. (11), (12) and (13)) are more useful for the southern Baltic region, especially the last one proposed by the authors. However, all analysed formulae suffer from significant statistical error. In order to obtain more precise results the net infrared radiation flux should be estimated with use of more appropriate environmental parameters describing type and distribution of clouds.

Figure 1: Comparison between modelled and measured

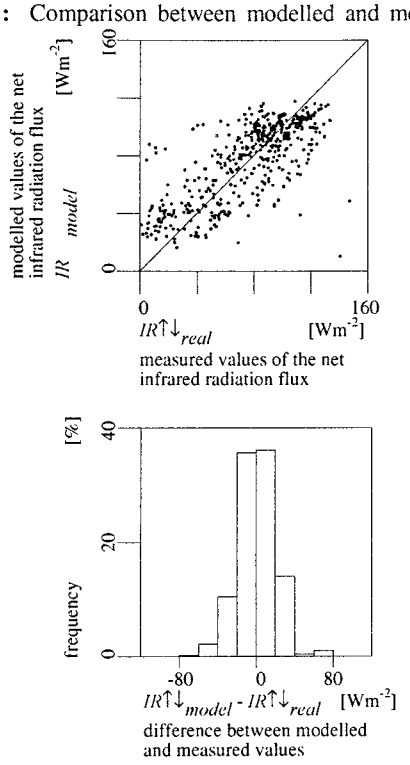

values of net infrared radiation fluxes and error histogram for proposed new formula.

References

Bignami F., Marullo S., Santoleri R., Schiano M.E., Longwave radiation budget in Mediterranean Sea, *J.Geophys. Res.*, 100 (C2), 2501-2514, 1995

Dera J., Marine Physics, Elsevier Sci. Publ., Amsterdam, 516 pp, 1992

Fung I.Y., Harrison D.E., Lacis A.A., On the variability of the net longwave radiation at the ocean surface, *Reviews of Geophysics and Space Physics*, 22(2), 177-193, 1984

Garbuny M., Optical physics, Academic Press, New York - London, 466 pp, 1965

Timofeyev N.A., Radiation regime of the ocean, (in Russian), Nauk. Dumka, Kiev, 247 pp, 1983

Trenberth K.E. [ed], Climate system modelling, Cambridge University Press, 1992

Wozniak B., Rozwadowska A., Kaczmarek S., Wozniak S.B., Ostrowska M., Seasonal variability of the solar radiation flux and its utilisation in the South Baltic, *ICES Cooperative Research Reports*, (in press), 2000

Zapadka T., Wozniak S. B., Preliminary comparison between various models of the long-wave radiation budget of the sea and experimental data from the Baltic Sea, *Oceanologia*, 42(3), 359-369, 2000

Zapadka T., Wozniak S.B., Wozniak B., A simple formula for Baltic Sea surface net infrared radiation flux, *Oceanologia*, (in submission), 2001

Regionalisation of extreme precipitation distribution on area of Poland

Zenon Wozniak, Irena Otop

Institute of Meteorology and Water Management, Branch in Wroclaw ul. Parkowa 30, 51-616 Wroclaw, Poland

1. Introduction

This paper deals with the extreme daily precipitation amounts on area of Poland and automatically takes under consideration the topographical relief features. It is also taken to account as second main factor the distance from Baltic coastal line and monthly/seasonal variability of extreme precipitation events.

The aim of the study was to learn more about regional differences in causes for flooding occurrences and next for developing quantitative parameterization of measurements information from meteorological radars.

In recent years same research was done on the number of days with precipitation exceeding specific amounts as *Førland et al.* (1998b), *Heino et al.* (1999) and *Hostýnek et al.* (1999). Heino did not found any long term changes but it is supposed that his treshold, that comprised all days with precipitation exceeding 10 mm only, was to low.

From older Polish work made by *Cebulak* (1982) has been learned that for determining the climatic and flood prone changes of extreme precipitation amounts on area of Poland it will be better to chose higher tresholds. For finding the best specific amounts it was taken from probability curves of maximum daily rainfalls counted by *Cebulak* (1982) for the stations on area with Polish maximal amounts of precipitation (The Tatra Mts.)

2. Methods and data

It was decided that, for the needs of our case, the tresholds (in mm for 24 hours) will be amounts computed by *Cebulak* (1982) for probabilities of: 95%, 75%, 20%, 10% and 5% i.e. with average maximum daily precipitation of 30, 50, 80, 100 and 120 mm respectively.

The presented analyse is based on data (amounts of daily precipitation) from area of Poland within ten years period (1991-2000) and from available set of about 1250 measurement stations. At first the processing comprised selection from data sets all the days with amount of precipitation with the highest probability of occurence i.e. 95% $\geq$ 30mm. In next steps were selected days with other tresholds amounts: $\geq$ 50, $\geq$ 80, $\geq$ 100 and $\geq$ 120 mm. Areal processing of the extreme precipitation amounts, parted for respective tresholds, comprise of preparing maps with use SURFER programme and simple kriging interpolation. After processing the data on annual base were also prepared the maps of extreme precipitation pattern in summer and winter hydrological half years and separately maps for selected precipitation prone months. The analoque study was done in pre informative times period (1960-1970) with one treshold $\geq$ 50 mm only by *Morozowska* (1975). In the presented paper have been compared, for instance, the results of above study with map of relevant $\geq$ 50 mm treshold produced during our study. The map was based also on ten-year period but thirty years after the first one and processed with help of new generation computers.

3. Results

The last decade (1991-2000) was very interesting and specific one for analysing extreme precipitation spatial pattern due to two periods (in one month) of extraordinary flood events in Poland. The floods of July, 1997 along the Odra River were triggered by two periods of extremely heavy rainfall in large areas of the upper and middle parts of Odra catchment. The precipitation centres correspond well to the mountains areas.

The work presented here uses the relief to improve the regionalisation of the extreme rainfall intensity distributions. Considering that topographical information becomes more and more easily accessible in numerical form, the method can bring an additional application for DEM-s in the hydrology and better use of radars information. Flooding in the summer months is usually triggered by heavy rainfall falling on already moistened ground and resulting from low pressure system moving from the Adriatic through Hungary to Poland (the so-called Vb regular track of atmospheric circulation pattern). In principal rain-producing mechanism is orographic lifting of oceanic humid air and thus high rainfall intensities could be explained by topographical enhancement of air vertical motion.

From a meteorological point of view orographic rainfall mechanism may be interpreted in several ways: simple forced ascendant motion, lee-wave effect, seeder-feeder effect, wind drift and others that highlight the complexity of the phenomena. Due to numerous intervening factors, in mountains areas, rainfall gradients may or may not strongly correlated to the altitude and even local crests have an imput on the rainfall parameters. Precaution must be taken when using the estimation regarding slopes opposite to prevailing wind direction. On the hilly terrain (as moraine belts) is need to take into account very local effects of the relief. The important factor is also origin of extreme precipitation: from convective rain cells (thunderstorms) or from cyclonic frontal storms.

It appears that the most rain prone areas are those directly facing the northern or north-western slopes (sometimes north-eastern, as in Klodzko Valley in 1998 yr.).

In study done by first author about 20 years ago on the area of Sudety Mts. (unpublished) was stated that the extreme daily precipitation amounts were mostly restricted to stations located in the end of valleys and passes between mountain ridges open to north. Those general observations were confirmed during recent study.

Our maps and experience shows that by using good measuring radars and maps with quantity information (isohyets) and spatial information about extreme precipitation on mountainous area, in certain conditions, may be obtained more information not only qualitative but also quantitative, in time close to real one.

Referring to *Heino* (2000) statement: "periods of high 1-day precipitation values seem to coincide well with hot summers" agree generally with our results.

The general pattern of extreme precipitation amounts on area of Poland (like the overall precipitation amounts) are composed of several parallel belts. The first one with the highest extreme precipitation is located on mountainous southern most areas and next high one in piedmont areas. Lower extreme precipitation are in the middle belt of Polish lowlands. Additionally on the north, along the coast

of Baltic Sea, is located secondary belt of higher precipitation connected with postglacial moraine hills (up to 329 m a.s.l.) and probably with close range to the Sea itself.

References

Cebulak, E., Maximum daily rainfalls in The River Basin of Dunajec, *Przeglad Geofizyczny (Geoph. Review)*, Vol. 27, No. 1-2, 109-119, 1982

Førland E., H. Alexandersson, A. Drebs, I. Hanssen-Bauer, H. Vedin, O.E. Tveito, Trends in maximum 1-day precipitation in the Nordic Region, *DNMI-Report DNMI-Report 14/98,* Klima, 55, 1998

Heino R., R. Brázdil, E. Førland, H. Tuomenvirta, H. Alexandersson, M. Beniston, C. Pfister, M. Rebetez, G. Rosenhagen, S. Rösner, J. Wibig, Progress in the study of climatic extremes in Northern and Central Europe, *Climatic Change*, 42, 151-181, 1999

Heino R., Changes of climate extremes – fact or fiction?, *Prace Geograficzne (Geograph. Studies)*, No. 108, 143-147, 2000

Hostýnek, Z. Lepka, V. Sosna, Processing of N-year precipitation of annual and monthly maxima of daily precipitation amounts in western Bohemia, *Meteorologicke zprávy*, 52, 1999.

Morozowska I., Heavy precipitation (50 mm and more during 24 hours) in Poland in 1961-1970, *Przeglad Geofizyczny (Geoph. Review)*, Vol. 20 (28), No. 4, 329-335, 1975

Generation of deep water cyclonic eddies in the Eastern Gotland Basin following major Baltic inflows: Numerical experiments

Victor Zhurbas[1] and Vadim Paka[2]

[1] Shirshov Institute of Oceanology, 117851 Moscow, Russia, zhurbas@sio.rssi.ru
[2] Atlantic Branch of Shirshov Institute of Oceanology, 23600 Kaliningrad, Russia, paka@ioran.gazinter.net

Zhurbas and Paka (1997, 1999) reported data of closely spaced CTD profiling which was carried out in the Eastern Gotland Basin in April 1993 within 3 months after the 1993 major Baltic inflow. A few tens of miles to south-south-west of the Gotland Deep, they found a mesoscale cyclonic eddy in the permanent halocline (Fig.1).

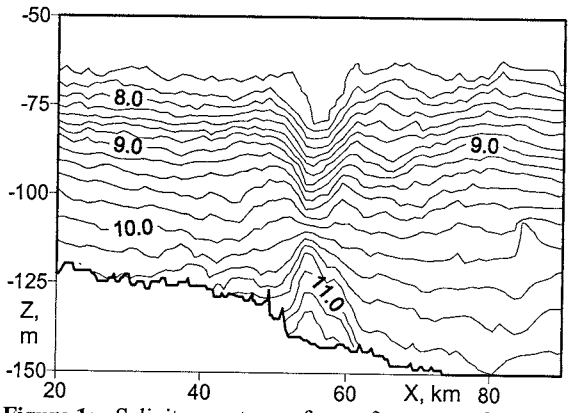

Figure 1: Salinity contours for a fragment of closely spaced CTD transect in the Eastern Gotland Basin with a mesoscale cyclone in the permanent halocline.

Being undetectable on the sea surface both in thermohaline fields and dynamical topography, the cyclone transferred highly saline water of the inflow origin towards the Gotland Deep. Lateral periphery of the cyclone was filled with thermohaline intrusions with numerous temperature inversions that may be thought as a complementary mechanism responsible for deep water ventilation in the Eastern Gotland Basin. More common and well-known mechanism of deep water renewal is believed to be the near bottom intrusion of highly saline, inflow water overturned in the basin and propagated along the sloping seabed, filling up deepest layers of the basin.

The objective of this study is to develop a numerical circulation model capable to simulate properly mesoscale dynamical features observed in the Eastern Gotland Basin by major inflows, such as cyclonic eddies in the permanent halocline and the near bottom intrusion carrying highly saline water of the inflow origin.

A primitive equation, free surface, hydrostatic, σ-coordinate 3D model by Blumberg and Mellor (1980) known under abbreviation of POM has been used.

All runs are performed with a major part of the Baltic Sea closed in the west at 12°E and at the narrowest section of the Sound, in the east at 22°24′E, and in the north at 60°20′N, that is, just at the entrances to the North Sea and gulfs of Riga, Finland, and Bothnia. Results are depicted and analyzed only for the Eastern Gotland and Gdansk basins which are expected to be not influenced considerably by the introduced artificial shorelines. Similar reduction of the model area has been used by Krauss and Brügge (1991).

The grid step is chosen at 4′ and 2′ along x and y axes (that is, about 4.0 km and 3.7 km, respectively). In total, the grid dimension is 157×191×30 along the x, y, and z axes, respectively.

The initial conditions simulate the real thermohaline stratification of February-March 1993 when the Arkona and Bornholm basins and partially the Stolpe Furrow were already filled with the inflow water, while the Eastern Gotland and Gdansk basins still contained the old water of pre-inflow stratification. Model runs with a constant northerly and easterly wind forcing were performed.

Figs. 2-4 present vectors of currents in the upper layer of permanent halocline and salinity contours in the bottom layer for northerly wind acting over a period of 12, 35, and 62 days, respectively.

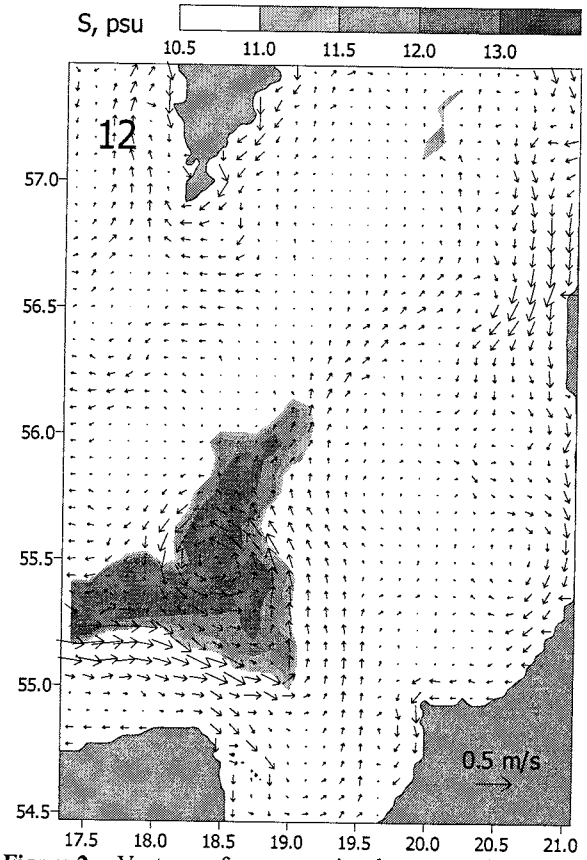

Figure 2: Vectors of currents in the upper layer of halocline and salinity contours in the bottom layer for northerly wind acting over a period T=12 days. The vectors are depicted for every other grid node.

Entering the Eastern Gotland Basin from the Stolpe Furrow, the bottom intrusion of high salinity water splits in two: one goes northeast towards the Gotland Deep, and second moves southeast towards the Gulf of Gdansk.

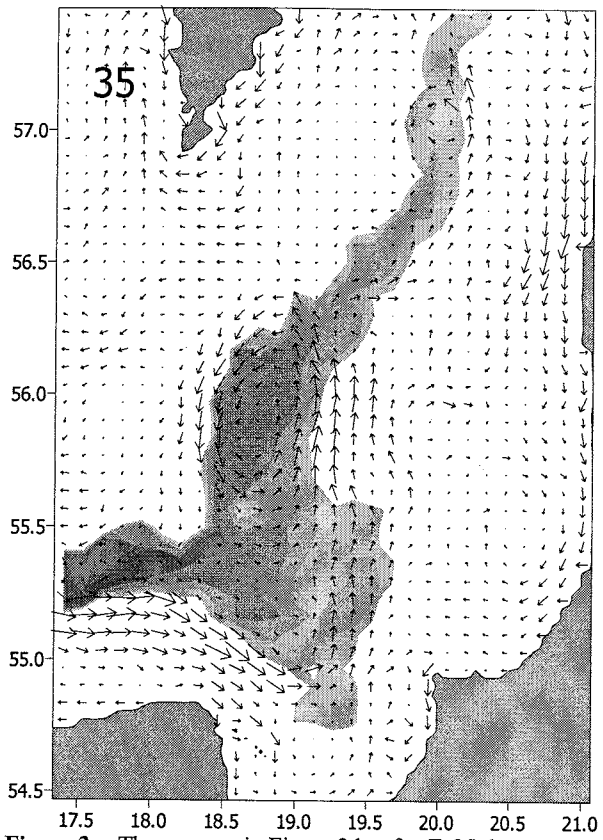

Figure 3: The same as in Figure 2 but for T=35 days.

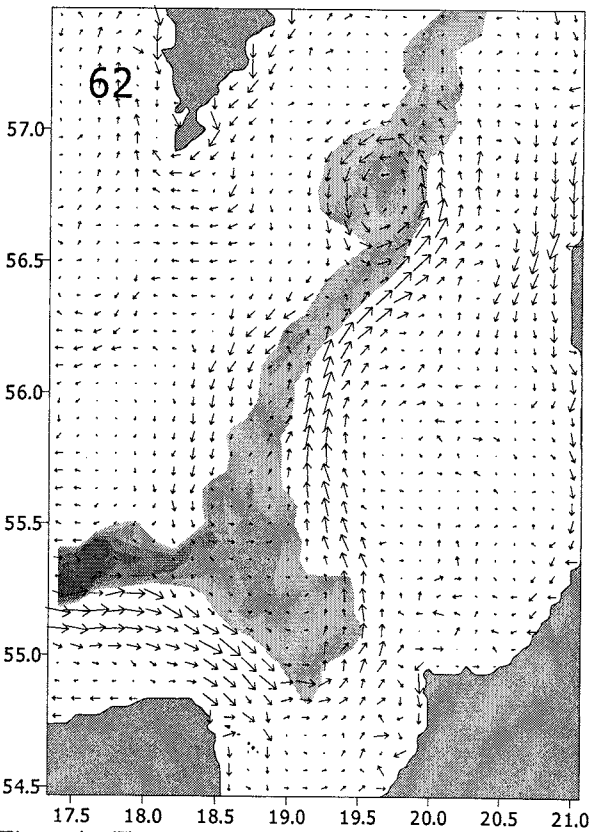

Figure 4: The same as in Figure 2 but for T=62 days.

A mesoscale cyclonic eddy carrying the inflow water is generated at the Stolpe Furrow outlet and then transferred towards the Gotland Deep (Cyclone 1). Cyclone 1 is clearly seen in all figures 2 to 4. The tip of bottom intrusion moves towards the Gotland Deep three times faster than Cyclone 1 does (0.13 m/s versus 0.04 m/s), so that these two phenomena may be considered as relatively independent mechanisms responsible for deep water renewal. One more mesoscale cyclonic eddy (Cyclone 2) carrying the inflow water is generated in the southern vicinity of the Gotland Deep above the bottom intrusion propagating over the sloping seabed (see Figure 3). Horizontal size of Cyclone 2 is much smaller than that of Cyclone 1.

Salinity contours and meridional velocity for zonal transect across Cyclone 2 are shown in Figure 5.

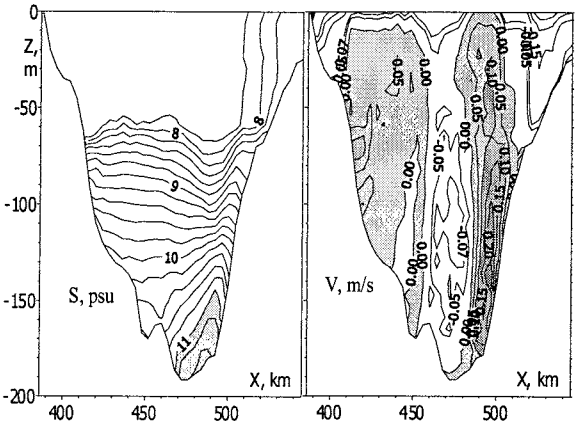

Figure 5: Salinity contours and meridional velocity for zonal transect at 57°N and T=35 days.

The symmetrical double-concave shape of salinity/density disturbance in Cyclone 2 resembles well the themohaline signature of cyclonic eddy observed in the Eastern Gotland Basin in April 1993 following the major inflow event (cf. figs. 1 and 5). It is also seen from Figure 5 that deep water Cyclone 2 has no salinity signature and a weak velocity signature on the sea surface.

Generation of cyclones rather than anticyclones in the course of inflow water propagation is physically explained using the law of potential vorticity conservation.

References

Blumberg, A. F., G. L. Mellor. A coastal ocean numerical model. In: Mathematical Modelling of Estuarine Physics, Proc. Int. Symp., Hamburg, Aug. 1978, ed. by J. Sunderman and K.-P. Holtz, pp. 203-214, Springer-Verlag, Berlin, 1980.

Krauss, W., B. Brügge. Wind-produced water exchange between the deep basins of the Baltic Sea, *J. Phys. Oceanogr.*, Vol. 21, 373-394, 1991.

Zhurbas, V. M., V. T. Paka. Mesoscale thermohaline variability in the Eastern Gotland Basin following the 1993 major Baltic inflow, *J. Geophys. Res.*, Vol. 102, No. C9, 20,917-20,926, 1997.

Zhurbas, V. M., V. T. Paka. What drives thermohaline intrusions in the Baltic Sea?, *J. Mar. Sys.*, Vol. 21, 229-241, 1999.

Use of the hydrological modelling for the regulation of the complex water management systems

Ansis Zīverts, Inese Jauja un Atis Plūme

Latvia University of Agriculture, Akadēmijas Str. 19, LV-3001 Jelgava, Latvija

1. Introduction

The detailed research in the fields of meteorology and hydrology was carried out in the frame of the BALTEX program (Raschke E. et. al., 2001). Based on that the hydrological models were further developed. They allow to simulate and forecast discharges in the rivers with the limited amount of the discharge measurements. Aiviekste river basin (one of the largest tributaries of the Daugava River) was used as the test basin for the evaluation of the model performance used for the regulation of the complex water management system. The results show that hydrological models with meteorological forcing data can be efficiently used for the management of the water management systems.

2. The test basin

Aiviekste River basin covers 9130 km^2. Lubana Lake is situated in the center of the Aiviekste River basin. Lubana Lake is surrounded by approximately 100 km^2 large lowland where the land surface elevations are changing within the few meters.

During the last 75 years the large hydrotechnical structures were built in the Lubana Wetland. The main works were done in two steps:

- during the period from 1926 - 1937 the lowering of the water level in the Lubana Lake were carried out. That was done by straightening and deepening the river-bed of the Aiviekste River of 76 km length.
- during the period from 1956 - 1985 the Meiranu canal was diggen out, as well as protection dams, two regulated gates and several polders were constructed.

The hydrotechnical structures constructed during the second step allowed to restore the previous water level in the Lubana Lake - reservoir which was before 1926. As the result from contructing the hydrotechnical structures the Lubana Wetland was divided into the three parts where water exchange is regulated by two gates (Fig.1). Meiranu Canal now is the second outlet from the Lubana Wetland.

This water management system allows to regulate the water level in the Lubana Lake - reservoir and to some extent also the water levels and discharges in the Aiviekste River and Meiranu Canal. The task of the management agency is to estimate and apply the optimum water regulation regime through the gates. The mathematical models can be used very efficiently for the estimation of the optimum water regulation in the gates.

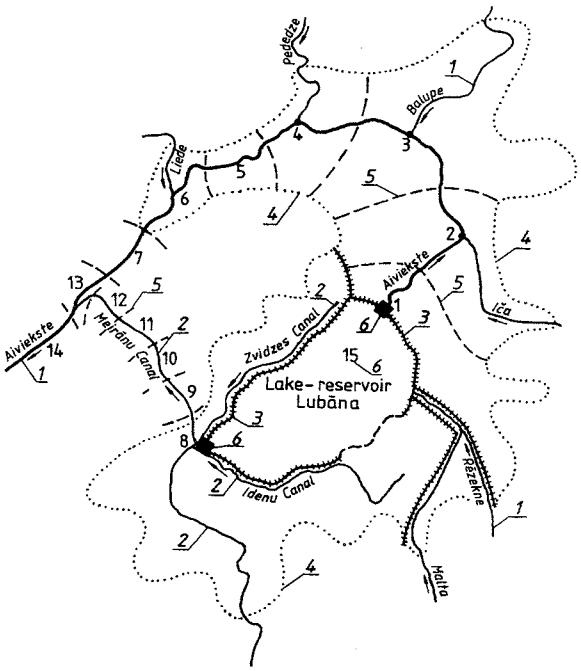

Figure 1: Scheme of the Lubana lowland: 1- rivers; 2 – canals; 3 – levees; 4 – initially submerged area; 5 – borders of computation reaches; 6 – gates.

3. Mathematical models and data used for the modelling

There are two mathematical models used in this study:

- The conceptual hydrological model METQ98 *(Ziverts A. and I.Jauja, 1999)* were used to simulate inflow to the Lubana Wetland (from Rezekne and Malta, Ica, Balupe, Pededze, Liede Rivers and Meiranu Canal basins).
- The hydraulic water flow model based on the discretisations of the Saint-Venant equations (Ziverts A., 1982). For the simulation of the unsteady flow the Meiranu Canal, Aiviekste River bed and flood plains are divided into the 15 computational reaches. Lubana Lake-reservoir is the 15th computational reach (Fig.1.)

There are several versions of the hydraulic model used in this study with the options to regulate the degree of the opening of both water gates - they can be either opened, closed or partly opened.

The meteorological forcing data (daily mean air temperature, air moisture and precipitation) is used in the model METQ98. The water level observations in Lubana Lake (since 1985) are used for the evaluation of the performance of the models.

4. Results

There is no records about the water outlet through the regulation gates since 1985. It was possible to restore the regulation regime through the gates by the development of the approximation routine and comparing the simulated and observed water level in Lubana Lake - reservoir (called "actual" water level). As it is shown at the Fig.2. the simulated water levels in the Lubana Lake - reservoir completely match the "actual" water levels (except four cases in May 1986, 1988, October 1990 and January 1993). Also the simulated and observed discharges in the gauging station Aiviekste-Aiviekstes HPP shows the good coincidence. Based on that the models were used to analyze several possible past and future regimes.

For example, the hypothetical water level in the Lubana Lake (green line in the Fig.2.) and Aiviekste River were simulated in case if protection dams and regulation gate would not be constructed at the outflow of the Aiviekste River from the Lubana Lake. As it is shown in the Fig.2. the water level fluctuations considerably reduced due to the water level regulation since May, 1985. Water level fluctuations reduced for more than 1.5 m. By using the coupled hydrological and hydraulic models it is also possible to simulate various water level regulation schemes and choose the optimal one.

In this study the meteorological observations are used as the forcing data to the models, however the coupled hydrological and hydraulic models are very well possible to use in the forecasting mode - use the meteorological forecasts as the forcing data for the model system and simulate the regulation regime of the lake-reservoir system.

Use of the coupled meteorological and hydrological model systems for the regulation of the complex water management systems is one of the applications of the results from the BALTEX program.

References

Raschke,E., Warrach, K., Meywerk, J., et.al. BALTEX (Baltic Sea Experiment): A European Contribution to Investigate the Energy and Water Cycle over a Large Drainage Basin, *Bulletin of AMS, 2001,* (submitted)

Ziverts, A., Jauja,I. Mathematical Model of Hydrological Processes METQ98 and its Applications, *Nordic Hydrology, 30 (2), 1999, 109-128.*

Ziverts, A. Simple model of the unsteady water flow calculation in complex channel systems. Water Resources, 1982, No2, pp. 89-98 (in Russian)

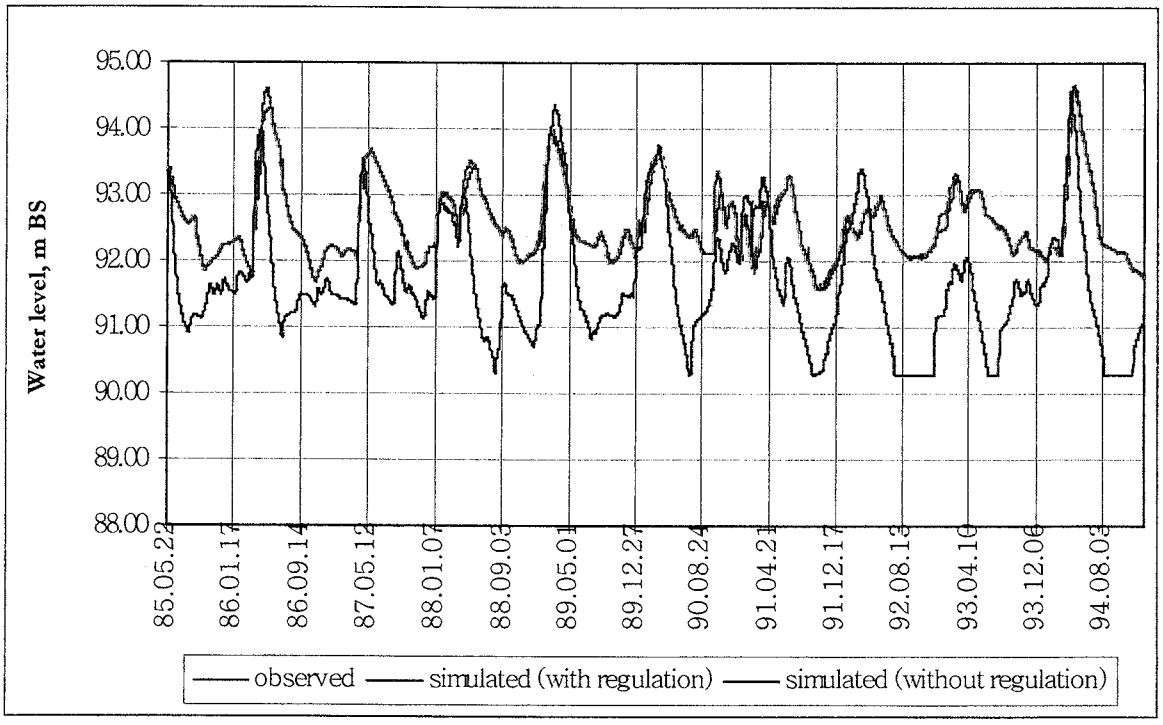

Figure 2: Water level in the Lubana lake – reservoir (computation reach No.15)

International BALTEX Secretariat Publication Series

No. 1: Minutes of First Meeting of the BALTEX Science Steering Group at GKSS Research Center in Geesthacht, Germany, 16-17 May, 1994. August 1994

No. 2: Baltic Sea Experiment BALTEX – Initial Implementation Plan. March 1995, 84 pages

No. 3: First Study Conference on BALTEX, Visby, Sweden, August 28 – September 1, 1995. Conference Proceedings. Editor: A. Omstedt, SMHI Norrköping, Sweden. August 1995, 190 pages

No. 4: Minutes of Second Meeting of the BALTEX Science Steering Group at Finnish Institute of Marine Research in Helsinki, Finland, 25-27 January, 1995. October 1995

No. 5: Minutes of Third Meeting of the BALTEX Science Steering Group at Strand Hotel in Visby, Sweden, September 2, 1995. March 1996

No. 6: BALTEX Radar Research – A Plan for Future Action. October 1996, 46 pages

No. 7: Minutes of Fourth Meeting of the BALTEX Science Steering Group at Institute of Oceanology PAS in Sopot, Poland, 3-5 June, 1996. February 1997

No. 8: *Hydrological, Oceanic and Atmospheric Experience from BALTEX.* Extended Abstracts of the XXII EGS Assembly, Vienna, Austria, 21-25 April, 1997. Editors: M. Alestalo and H.-J. Isemer. August 1997, 172 pages

No. 9: The Main BALTEX Experiment 1999-2001 – ***BRIDGE.*** Strategic Plan. October 1997, 78 pages

No. 10: Minutes of Fifth Meeting of the BALTEX Science Steering Group at Latvian Hydrometeorological Agency in Riga, Latvia, 14-16 April, 1997. January 1998

No. 11: Second Study Conference on BALTEX, Juliusruh, Island of Rügen, Germany, 25-29 May 1998. Conference Proceedings. Editors: E. Raschke and H.-J. Isemer. May 1998, 251 pages

No. 12: Minutes of 7th Meeting of the BALTEX Science Steering Group at Hotel Aquamaris in Juliusruh, Island of RÜGEN, Germany, 26 May 1998. November 1998

No. 13: Minutes of 6th Meeting of the BALTEX Science Steering Group at Danish Meteorological Institute in Copenhagen, Denmark, 2-4 March 1998. January 1999

No. 14: BALTEX – BASIS Data Report 1998. Editor: Jouko Launiainen March 1999, 96 pages

No. 15: Minutes of 8th Meeting of the Science Steering Group at Stockholm University in Stockholm, Sweden, 8-10 December 1998, May 1999

No. 16: Minutes of 9th Meeting of the BALTEX Science Steering Group at Finnish Meteorological Institute in Helsinki, Finland, 19-20 May 1999

No. 17: Parameterization of surface fluxes, atmospheric planetary boundary layer and ocean mixed layer turbulence for BRIDGE – What can we learn from field experiments? Editor: Nils Gustafsson, April 2000

No. 18: Minutes of the 10th Session of the BALTEX Science Steering Group in Warsaw, Poland, 7-9 February 2000, April 2000

No. 19: BALTEX-BASIS: Final Report, Editors: Jouko Launiainen and Timo Vihma, May 2001

No. 20: Third Study Conference on BALTEX, Mariehamn, Island of Åland, Finland, 2-6 July 2001, Conference Proceedings. Editor: Jens Meywerk, 264 pages.

Copies are available upon request from the International BALTEX Secretariat.